PORTLAND CEMENT **pca** ASSOCIATION
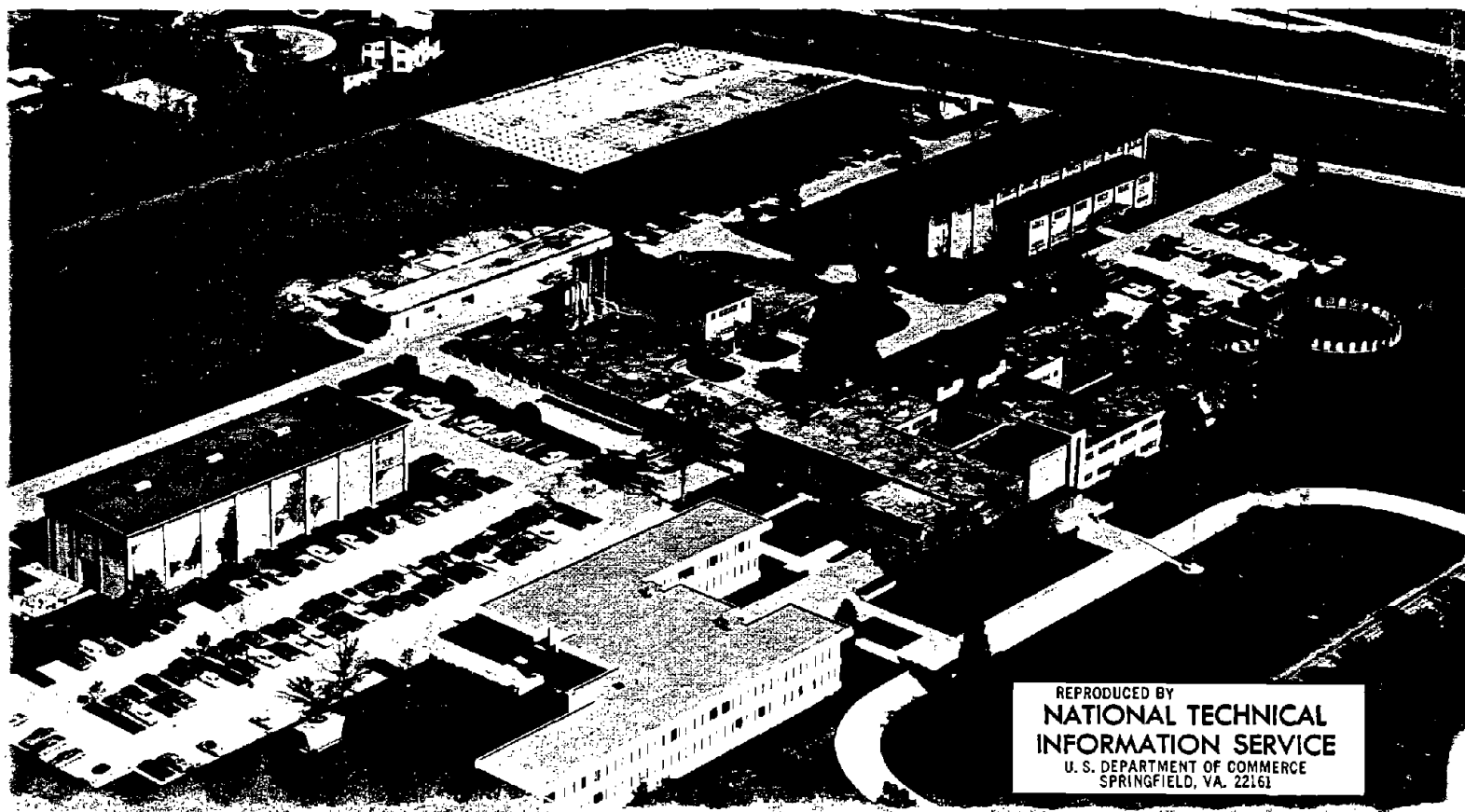
Research and Development
Construction Technology Laboratories

EARTHQUAKE RESISTANT STRUCTURAL WALLS -
TESTS OF ISOLATED WALLS

BIBLIOGRAPHIC DATA SHEET	1. Report No. NSF/RA-760815	2.	3. Recipient's Accession No. PB-271 467

4. Title and Subtitle	5. Report Date
Earthquake Resistant Structural Walls-Tests of Isolated Walls; Appendix A - Experimental Program; Appendix B- Test Results	November 1976
	6.

7. Author(s) R. G. Oesterle, A. E. Fiorato, L. S. Johal, J. E. Carpenter, H. G. Russell, and W. G. Corley	8. Performing Organization Rept. No. PCA R/D Ser.1571

9. Performing Organization Name and Address	10. Project/Task/Work Unit No.
Portland Cement Association Old Orchard Road, Skokie, Ill. 60076	
	11. Contract/Grant No. NSF-RANN GI-43880

12. Sponsoring Organization Name and Address	13. Type of Report & Period Covered
National Science Foundation Research Applied to National Needs Washington, D.C. 20550	final report (1974-1976)
	14.

15. Supplementary Notes

This is part of a series of reports; the reports on the Analytical Investigation of this project will be forthcoming about mid-July, 1977.

16. Abstracts   The behavior of structural walls for use in earthquake resistant buildings is being studied experimentally. Isolated reinforced concrete walls are being subjected to reversing, in plane, lateral loads. The overall objective is to develop designs to insure adequate inelastic performance. This report describes the test program and the results from the first nine wall tests. Variables included shape of the wall cross section, amount of flexural reinforcement, and the use of confined boundary elements. One wall was subjected to monotonic loads and one wall was repaired and retested. Results show the behavior of the wall is governed by the level of shear stress. However, significant inelastic performance was obtained in a wall subjected to a shear stress of $8.8\sqrt{f'_c}$. The use of stiff confined boundary elements significantly increased inelastic performance of the walls.

17. Key Words and Document Analysis.   17a. Descriptors

concrete structures
earthquake resistant structures
walls
tests
bend properties
shear properties
yield strength
ultimate strength
plastic deformation

ductility
damping capacity

17b. Identifiers/Open-Ended Terms

structural walls
shear walls
concrete (reinforced)
buildings

17c. COSATI Field/Group   1313, 2012

18. Availability Statement No restriction on distribution. Available from National Technical Information Service, Springfield, Va.22161 A-II	19. Security Class (This Report) UNCLASSIFIED	21. No. of Pages 321
	20. Security Class (This Page UNCLASSIFIED	22. Price PC A14-A01

FORM NTIS-35 (REV. 10-73)   ENDORSED BY ANSI AND UNESCO.   THIS FORM MAY BE REPRODUCED   USCOMM-DC 8265-P74

Report to
NATIONAL SCIENCE FOUNDATION
(RANN)
Grant No. GI-43880

EARTHQUAKE RESISTANT STRUCTURAL WALLS -
TESTS OF ISOLATED WALLS

By: R. G. Oesterle, A. E. Fiorato, L. S. Johal,
J. E. Carpenter, H. G. Russell and W. G. Corley

Date: November 1976

Submitted by
RESEARCH AND DEVELOPMENT
CONSTRUCTION TECHNOLOGY LABORATORIES
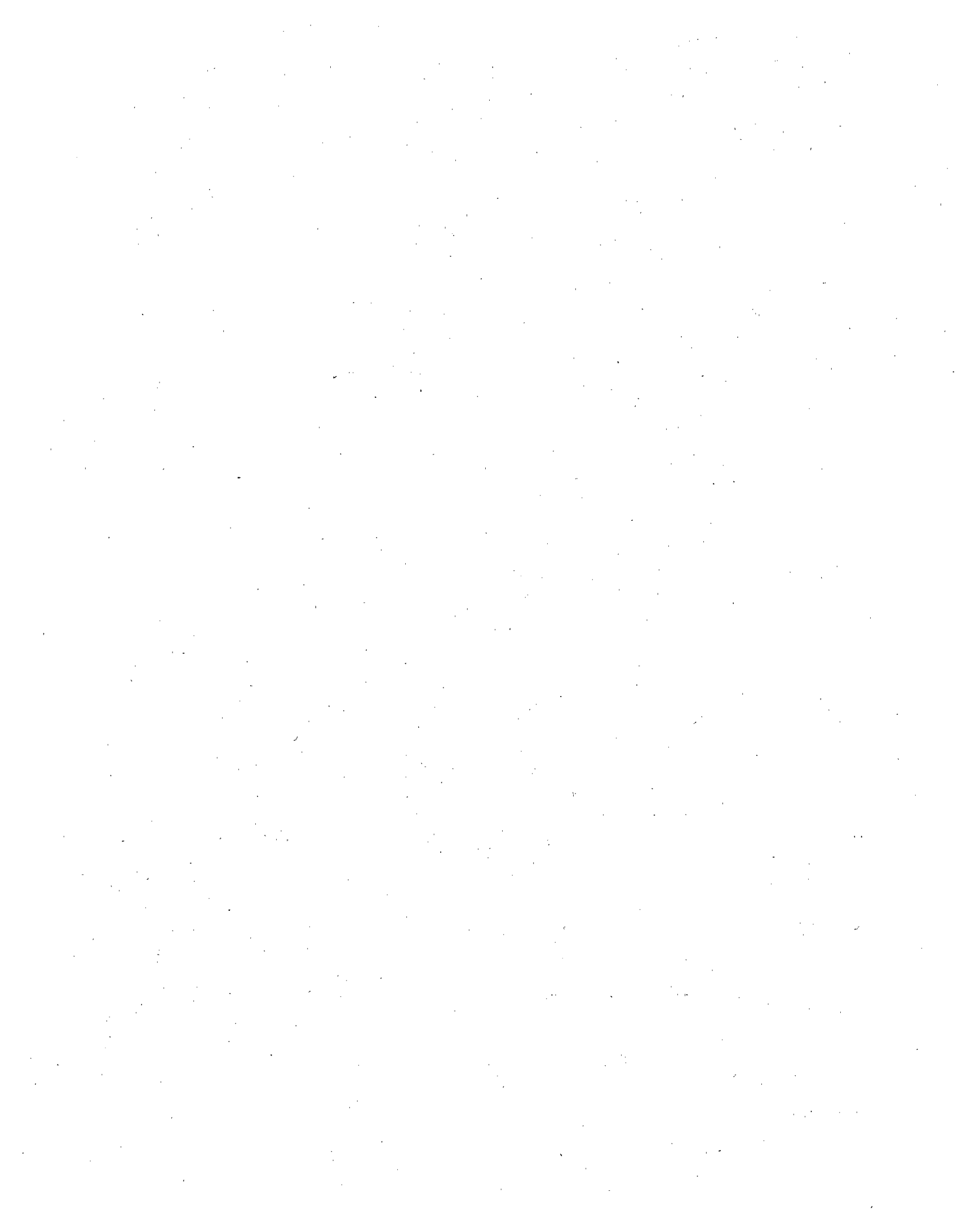PORTLAND CEMENT ASSOCIATION
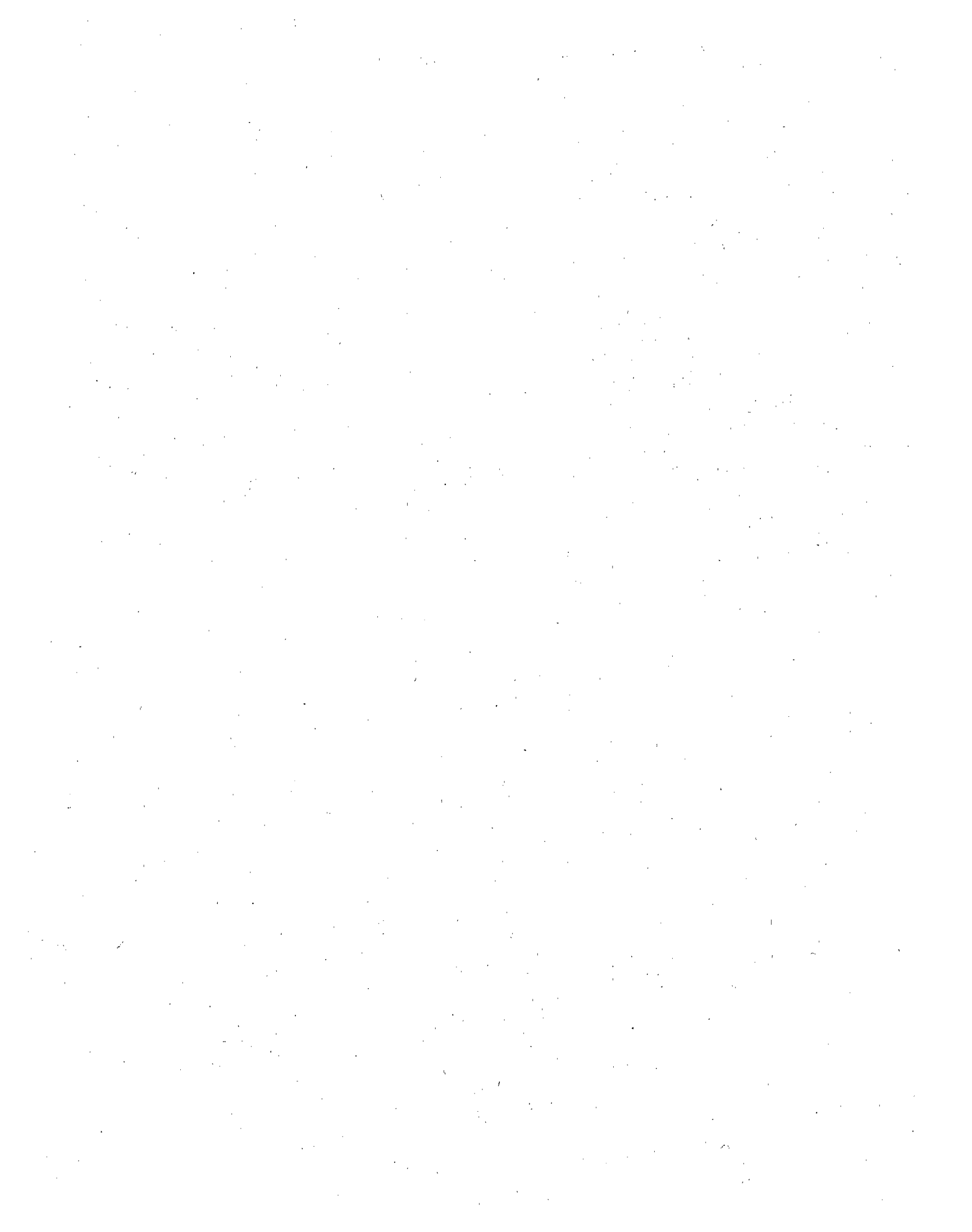Old Orchard Road
Skokie, Illinois 60076

TABLE OF CONTENTS

TABLE OF CONTENTS (Continued)

EARTHQUAKE RESISTANT STRUCTURAL WALLS -

TESTS OF ISOLATED WALLS

by

R. G. Oesterle, A. E. Fiorato, L. S. Johal, J. E. Carpenter

H. G. Russell and W. G. Corley*

INTRODUCTION

It has been observed in recent earthquakes that structural walls used as lateral bracing in multistory buildings can significantly enhance performance under seismic loading.[1] However, there is a lack of information on the strength and deformation capabilities of structural wall systems. To help provide some of the needed data, the Portland Cement Association is conducting a combined experimental and analytical investigation to develop design criteria for reinforced concrete structural walls in earthquake resistant buildings. The primary purpose of this investigation is to determine the ductility, energy dissipation and strength of the walls.

As part of this experimental program, reversing loads are being applied to isolated walls. Currently, tests of nine wall specimens have been completed. This report presents the results of these nine tests. Observed behavior of the isolated walls is described and a summary of the test results is presented. Conclusions from the tests are given.

*Respectively, Structural Engineer, Senior Structural Engineer, Associate Structural Engineer, Former Principal Structural Engineer and Manager, Structural Development Section; Director, Engineering Development Department, Portland Cement Association, Skokie, Illinois.

A detailed description of the experimental program is included in Appendix A. Detailed descriptions of each test and the resulting data are included in Appendix B.

Further conclusions concerning strength and deformation characteristics, and ductility and energy dissipation capacities will be reported in future papers.[2,3]

OBJECTIVES AND SCOPE

The objectives of the experimental investigation are:

1. To determine load-deformation characteristics for a wide range of configurations of wall specimens. This information is being used in the inelastic dynamic analyses.[4]

2. To determine ductilities and energy dissipation capacities of walls subjected to reversing loads.

3. To determine flexural and shear strengths of walls subjected to reversing loads, and to compare these strengths with the strengths under monotonic loading.

4. To determine means of increasing the energy dissipation capacity of walls where required.

5. To develop design procedures to insure adequate strength and energy dissipation capacity in reinforced concrete structural walls used in earthquake resistant buildings.

OUTLINE OF EXPERIMENTAL PROGRAM

To attain the objectives, an experimental program was developed to investigate the behavior of large isolated reinforced concrete walls. Appendix A contains a detailed description of the experimental program. Only a brief description of the program is given here.

The isolated walls represent an element of a structural wall system. Test specimens are approximately 1/3-scale representations of full-size walls, although no specific prototype walls were modeled. Controlled variables included in the first nine tests were the shape of the wall cross section, the amount of main flexural reinforcement and the amount of hoop reinforcement around the main flexural reinforcement. In addition, one wall was subjected to monotonic loading and one wall was repaired and retested. Table 1 provides a summary of test specimen details.

Dimensions of the test specimens are shown in Fig. 1. Flanged, barbell, and rectangular cross sections have been investigated. Nominal cross sectional dimensions of these sections are shown in Fig. 2.

In proportioning the walls, the design moment was calculated following procedures in the ACI Building Code.[5] Strain hardening of the steel was neglected. Horizontal shear reinforcement was provided so that the calculated design moment would be developed. Shear reinforcement was provided to satisfy the ACI Building Code.[5] Design yield stress of the steel was 60 ksi (414 MPa) and design concrete strength was 6000 psi (41.4 MPa).

Fig. 1 Nominal Dimensions of Test Specimen with Rectangular Cross Section
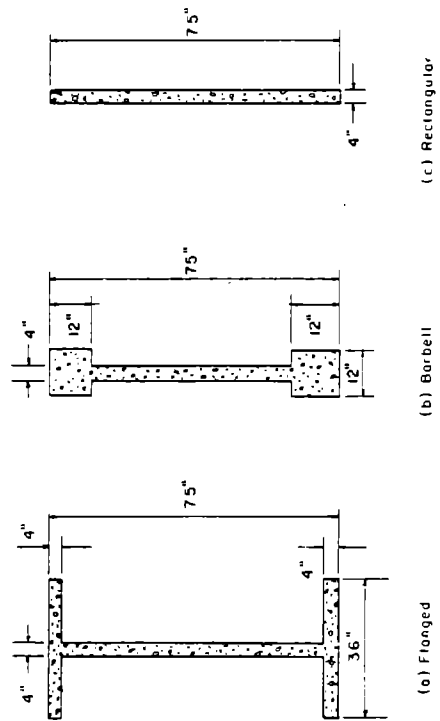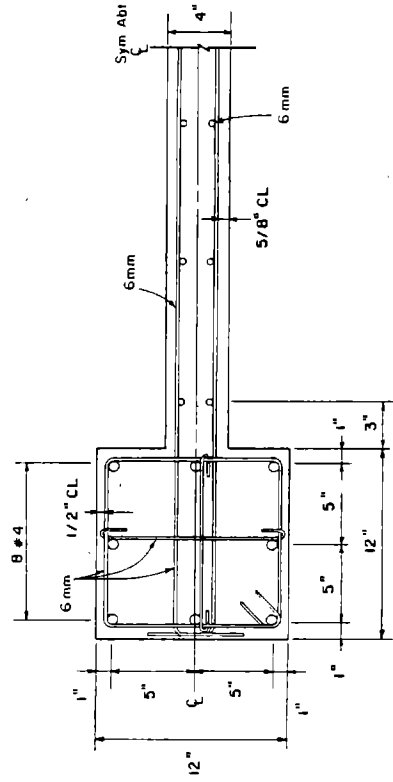
Fig. 3 Cross Section of Specimen B1

TABLE 1 - SUMMARY OF TEST SPECIMENS

Specimen	Shape	Reinforcement (%)			
		ρ_f	ρ_h	ρ_n	ρ_s
R1		1.47	0.31	0.25	--
R2		4.00	0.31	0.25	2.07
B1		1.11	0.31	0.29	--
B3		1.11	0.31	0.29	1.28
B4(1)		1.11	0.31	0.29	1.28
B2		3.67	0.63	0.29	--
B5		3.67	0.63	0.29	1.35
B5R(2)		3.67	0.63	0.29	1.35
F1		3.89	0.71	0.30	--

(1) Monotonic loading
(2) Repaired specimen

where:

ρ_f = ratio of main flexural reinforcement area to gross concrete area of boundary element.

ρ_h = ratio of horizontal shear reinforcement area to gross concrete area of a vertical section of wall web.

ρ_n = ratio of vertical web reinforcement area to gross concrete area of a horizontal section of wall web.

ρ_s = ratio of effective volume of confinement reinforcement to the volume of core in accordance with Eq. A.4 of ACI 318-71.(5)

1'-0" = 0.305 m
1" = 25.4 mm

(a) Flanged   (b) Barbell   (c) Rectangular

Fig. 2 Nominal Cross-Sectional Dimensions of Test Specimens

The test specimens were constructed in six vertical lifts. Figure 3 shows the reinforcing details used in one of the walls. Specimens B3, R2, B4, and B5 were constructed with confinement reinforcement in the lower 6 ft (1.83 m) of the boundary elements. For rectangular sections, the "boundary element" was taken to extend 7.5 in. (190 mm) from each end of the wall.

Specimen B5R was a retest of Specimen B5. Following the test of B5, damaged web concrete was removed up to a height of about 9 ft (2.74 m). New web concrete was cast in three lifts. The columns were repaired with a surface coating of neat cement paste.

The apparatus for testing the walls is shown in Fig. 4. Each specimen was loaded as a vertical cantilever with forces applied through the top slab. The test specimens were loaded in a series of increments. Each increment consisted of three complete reversed cycles. About three increments of force were applied prior to initial yielding. Subsequent to initial yielding, loading was controlled by deflections in 1 in. (25 mm) increments.

Free vibration tests were conducted at selected stages as the number and magnitude of loading increments applied to the specimen increased. These tests were carried out to determine the frequency and damping characteristics of the walls.
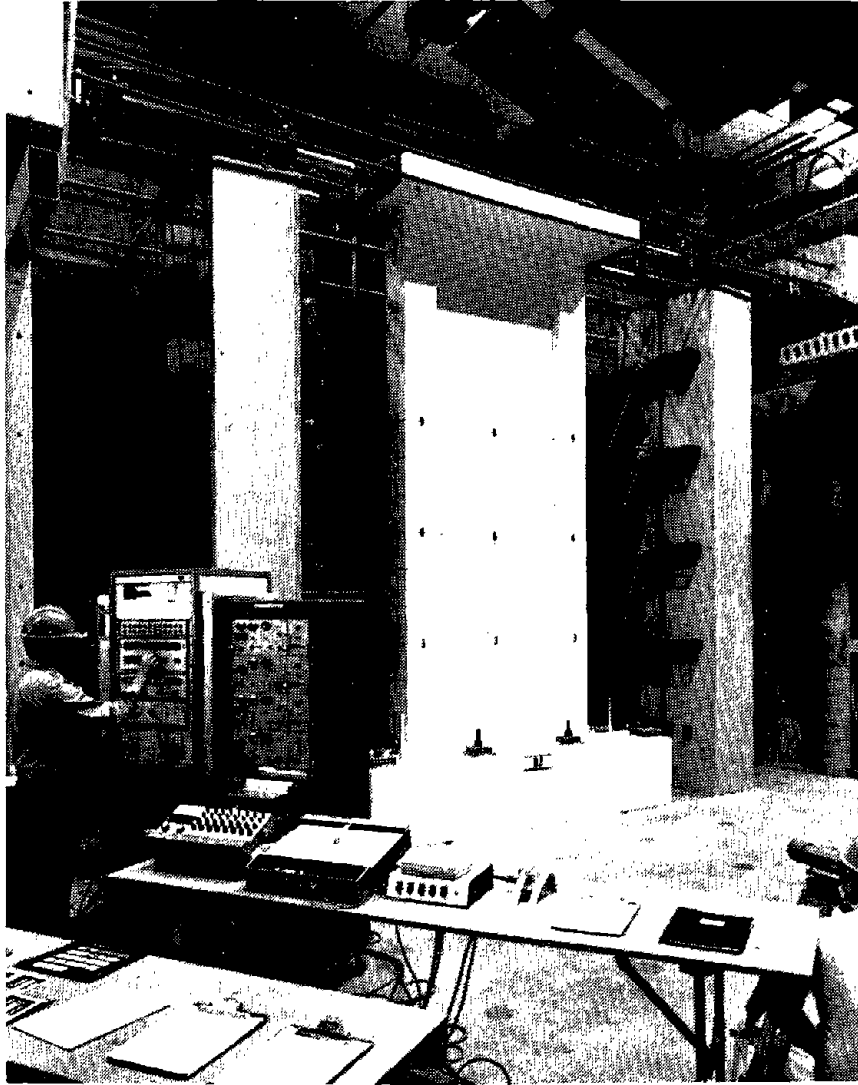
Fig. 4   Test Specimen and Test Apparatus

Controlled variables included in a second series of tests presently being carried out are concrete strength, axial load and the amount of horizontal shear reinforcement. A description of these tests is not included in this report.

OBSERVED BEHAVIOR

Introduction

In general, the performance of the specimens can be divided into two types of behavior with some general observations common to both. The two types of behavior were distinguished by the magnitude of applied shear stresses.

General Observations

As shown in Table 2, the maximum observed load in all specimens subjected to reversing loads exceeded the ACI design strength for either flexure or shear. However, observed strengths were somewhat lower than the flexural strengths calculated using measured material properties including strain hardening in the reinforcement. With the exception of monotonically loaded Specimen B4, the maximum observed load for each specimen varied from 77% to 91% of the calculated flexural strengths.

Table 3 shows a summary of deformation results for the nine test specimens. The following definitions are used in Table 3.

A loading increment consists of three complete reversed cycles at a specific maximum load or top deflection.

A stable loading increment is an increment in which the specimen sustained at least 80% of the previous maximum observed load in all three cycles.

A stable cycle is a cycle within a stable loading increment.

TABLE 2 SPECIMEN STRENGTHS

Specimen	Confined Boundary Element	ACI Design Flexure kips	ACI Design Flexure $\sqrt{f'_c}$ [1]	ACI Design Shear kips	ACI Design Shear $\sqrt{f'_c}$	First Yield Load Calculated [3] kips	First Yield Load Calculated [3] $\sqrt{f'_c}$	First Yield Load Observed kips	First Yield Load Observed $\sqrt{f'_c}$	First Yield Load Obs./Calc	Maximum Load Calculated [3] kips	Maximum Load Calculated [3] $\sqrt{f'_c}$	Maximum Load Observed kips	Maximum Load Observed $\sqrt{f'_c}$	Maximum Load Obs./Calc	Maximum Load Obs./ACI [4]	Failure Mode [5]
R1	No	18	0.9	82[2]	4.2	17.7	0.9	20.1	1.0	1.14	29.1	1.5	26.6	1.4	0.91	1.48	F
R2	Yes	35	1.8	82[2]	4.2	32.4	1.6	37.0	1.9	1.14	57.3	2.9	48.7	2.5	0.85	1.39	F
B1	No	46	2.2	82[2]	3.9	40.2	1.9	45.1	2.1	1.12	72.1	3.4	61.0	2.9	0.85	1.33	F
B3	Yes	46	2.3	82[2]	4.1	39.9	2.0	45.2	2.3	1.13	73.4	3.7	62.0	3.1	0.84	1.35	F
B4	Yes	46	2.4	82[2]	4.2	40.3	2.1	45.3	2.3	1.12	74.3	3.8	75.3	3.9	1.01	1.64	F
B2	No	129	6.1	127	6.0	110.8	5.2	119.8	5.7	1.08	170.9	8.1	152.8	7.2	0.89	1.18	WC
B5	Yes	129	6.6	127	6.5	118.4	6.1	112.3	5.8	0.95	213.7	11.0	171.3	8.8	0.80	1.33	WC
B5R	Yes	129	6.8	127	6.7	118.4	6.3	--	--	--	213.7	11.5	167.8	8.9	0.79	1.30	WC
F1	No	145	8.1	140	7.8	144.2	8.0	150.6	8.4	1.04	242.6	13.5	187.9	10.5	0.77	1.30	WC

(1) Shear stress $v = \dfrac{V}{0.8 \varrho_w b \sqrt{f'_c}}$ (psi)

(2) Shear reinforcement governed by maximum bar spacing
(3) From analysis based on strain compatibility using measured material properties including strain hardening of reinforcement
(4) ACI taken as the lower of flexure or shear design strength
(5) F = Flexure, WC = Web Crushing
(6) 1 kip = 4.448 kN, $1.0\sqrt{f'_c}$ (psi) = $0.08304\sqrt{f'_c}$ (MPa)

TABLE 3 DEFORMATION RESULTS

Specimen	Last Stable Top Deflection Increment (in.)	Top Deflection At Full Yield (in.)	No. of Stable Inelastic Cycles	Rotation, $\theta_3^{(1)}$ At Full Yield (rad.)	Max. Observed Rotation[2] $\theta_3^{(1)}$(rad.)	Max. Observed Shear Distort.[2] $\gamma_3^{(3)}$, (rad.)	Max. Slip[2] At CJ1 (in.)
R1	± 3	+0.53	12	0.00302	-0.01860	-0.00971	-0.164
R2	± 4	+0.85	12	0.00457	-0.01981	-0.01969	-0.304
B1	± 4	+0.70	12	0.00420	-0.02323	-0.01782	-0.197
B3	± 7	+0.70	21	0.00401	+0.02762	-0.04811	+0.100[7]
B4[5]	+12.5	+0.80	--	0.00465	+0.06295	+0.03396	+0.145
B2	± 4	+1.00	9	0.00517	-0.01610	-0.02242	+0.170
B5	± 4	+1.10	9	0.00645	-0.01708	-0.01842	+0.110
B5R	± 5	+2.50[6]	9	0.01187[6]	+0.02038	-0.02369	+0.192
F1	± 2	+1.00	6	0.00339	-0.00932	-0.00800	-0.103

(1) θ_3 = Rotation of the horizontal section approximately 74 in. (1.88 m) above the base block

(2) Maximum measured during the last stable deflection increment

(3) γ_3 = Average shear distortion in a zone from the base to a level approximately 74 in. (1.88 m) above the base block

(4) CJ1 = Construction joint at the base of the wall

(5) Monotonic test

(6) Measured yield deformation at yield load level in test B5

(7) Gage failed in cycle 31 at ±5 in. increment

(8) 1 in. = 25.4 mm

An inelastic cycle is a complete reversed load cycle in which both the load and the top deflection exceeded the first yield level.

First yield level is the first load and deflection at which a yield strain was measured in the boundary element tensile reinforcement.

Full yield level is the load and deflection at which all of the main tensile reinforcement in the boundary element yielded.

As shown in Table 3, all specimens exhibited substantial inelastic deformation capabilities, even those designed without any special details for reversed loading. The minimum number of stable inelastic cycles was 6 for Specimen F1. The maximum nominal shear stress in F1 was $10.5\sqrt{f'_c}$ ($0.87\sqrt{f'_c}$, MPa). The maximum number of stable inelastic cycles was 21 for Specimen B3 with a maximum nominal shear stress of $3.1\sqrt{f'_c}$ ($0.26\sqrt{f'_c}$, MPa).

Yielding of both horizontal and vertical steel occurred up to the 6-ft (1.83 m) level in all specimens. In most specimens yielding of the vertical steel extended to the 9-ft (2.74 m) level. However, primary damage in the specimens was limited to the lower 3 ft (0.91 m).

In all specimens, "pinching" of the load-deformation loops and shear stiffness degradation was noticeably greater in the lower 3 ft region.

As the specimens were cycled at later load increments, the stiffness of the wall continually degraded until a large

load reduction occurred. The final failure always occurred at or below the 3 ft (0.91 m) level. The observed behavior varied according to the magnitude of applied shear stress as discussed below.

Walls Subjected to Low Nominal Shear Stress

As shown in Table 2, four specimens were subjected to maximum nominal shear stresses at or below $3.1\sqrt{f_c'}$ ($0.26\sqrt{f_c'}$, MPa). Their behavior is distinguished from that of walls subjected to high nominal shear stress by the crack pattern and a flexural failure mode.

For walls with low nominal shear stress, cracks started as horizontal flexural cracks in the boundary element, usually at level where horizontal reinforcement was located. Closely spaced confinement hoops caused these cracks to be finely distributed. The horizontal cracks progressed into coarsely distributed inclined cracks in the web. The cracks crossed the web until they intercepted a crack from the previous loading in the opposite direction. By the time the yield increment was reached the cracks had segmented the web into large pieces with several predominantly horizontal cracks completely traversing the lower 3 ft (0.91 m) of the wall. These cracks sliced the lower wall region into several horizontal layers as illustrated in Fig. 5. Because the loading was always applied in the same direction first, the cracks were usually somewhat more angular and jagged on the right side of the wall.

-13-
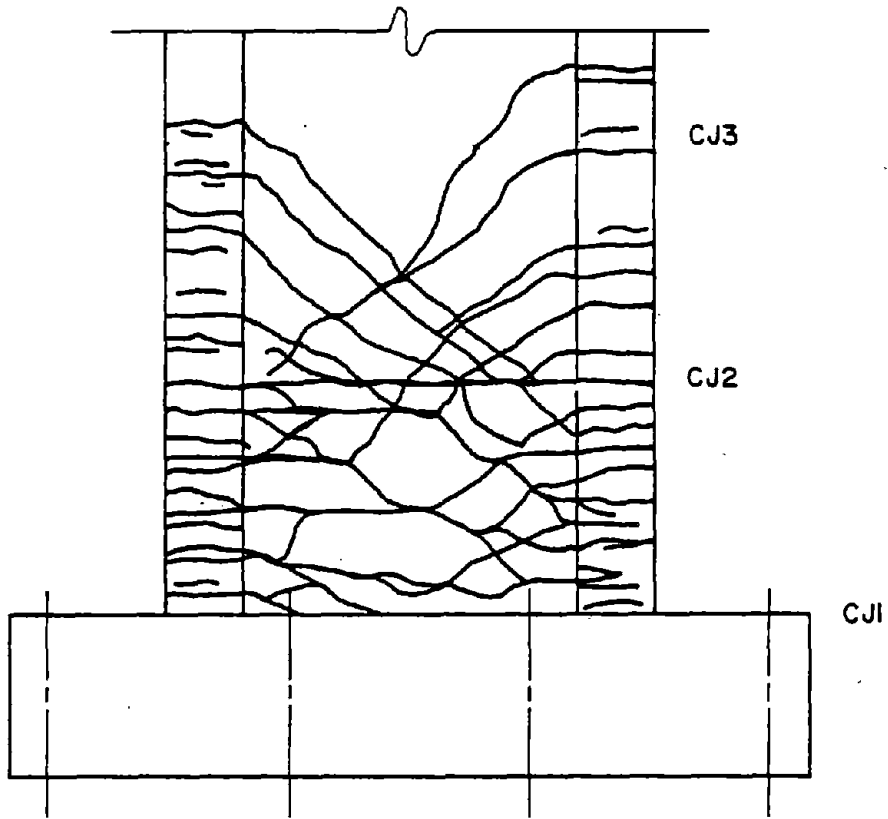
Fig. 5 Crack Pattern in Lower Portion of Specimen B3
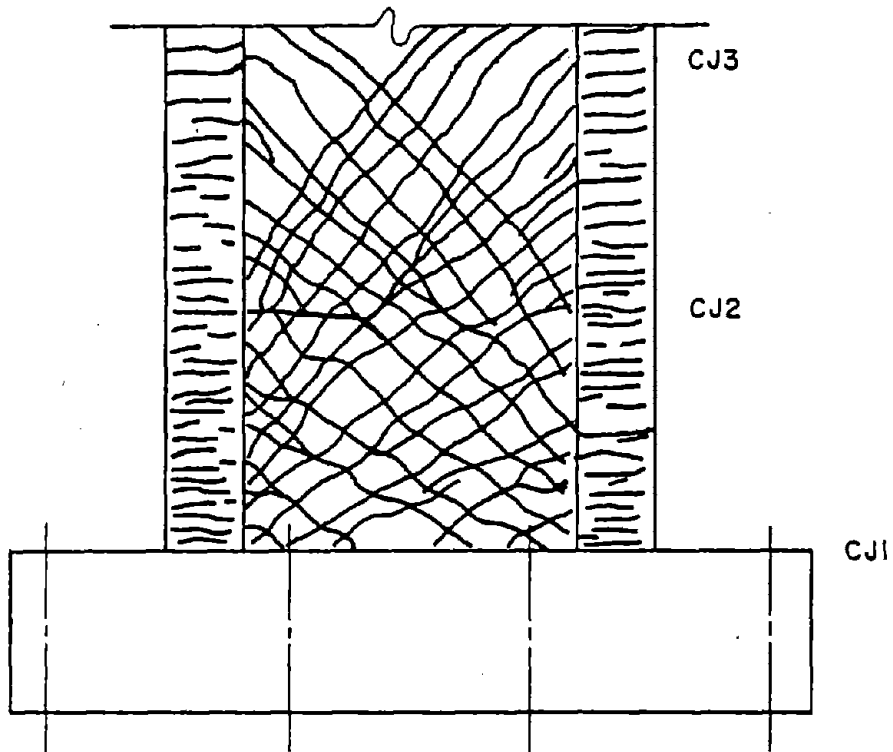
Fig. 6 Crack Pattern in Lower Portion of Specimen B5

Due to the horizontal nature of the cracks very little truss action developed. Only a small amount of horizontal steel crossed the cracks where they were inclined. Therefore, after yield, shear was predominantly transferred by interface shear and dowel action in the boundary elements. A shear stiffness reduction occurred as the number of applied inelastic cycles increased. However, at low shear stresses, this mode of shear transfer was adequate to maintain the strength of the wall until the test was terminated by fracture of the main flexural reinforcement.

In Specimens R1, B1, and B3, the loss of strength was due to damage to the boundary elements by alternate tensile yielding and compressive buckling of the main tensile reinforcement. This steel buckling was accompanied by loss of concrete not contained by the reinforcement. Buckling of the vertical steel was followed, after several cycles, by bar fracture. One or two bars fractured at a time. A load reduction accompanied each fracture.

The confinement hoops at 1-1/3 in. (33.9 mm) on center in Specimen B3 did not significantly increase the strength or the maximum rotation as compared to B1. However, the hoops maintained the integrity of the boundary elements by delaying bar buckling and containing the concrete core. Although a large number of inelastic cycles were sustained, bar buckling did occur.

In Specimen R2, the first load reduction was associated with a large out of plane displacement of the compression

zone. Initially, no lateral support of the wall was provided.
As inelastic cycles were applied, a continually increasing
out of plane displacement of the compression zone was
observed. The test was stopped after 10 inelastic cycles
and lateral support was added 3 ft (0.91 m) above the base.
The test was then continued. During the 14th inelastic
cycle, a large out of plane displacement of the compression
zone was observed within the lower 3 ft of the wall.
Shortly after this cycle, flexural reinforcement fractured
near the base of the wall.

The out of plane displacement of the compression zone
was caused by alternate tensile yielding of the flexural
reinforcement. As the specimen was loaded beyond yield in
one direction and then unloaded, permanent deformations
remained in the tension steel. As the load was reversed,
the compression zone was supported across numerous cracks
only by the steel. This steel had sustained several pre-
vious inelastic strain reversals. Therefore, the section
stiffness of the compression zone for axial load was
decreased considerably and an out of plane displacement
resulted. The fact that lateral support was not present
during a major portion of the test probably led to premature
strength loss in Specimen R2.

Walls Subjected to High Nominal Shear Stress

As shown in Table 2, four specimens were subjected to
maximum nominal shear stresses greater than $7.0\sqrt{f'_c}$ (0.58
$\sqrt{f'_c}$, MPa). The crack pattern that developed in these

specimens is illustrated in Fig. 6. Closely spaced flexural cracks were first observed in the boundary elements. When they reached the web, the cracks became inclined with a steeper angle than those in the specimens with low shear stress. The direction of these cracks was not altered by cracks caused by forces from the opposite direction. The inclined cracks crisscrossed the web forming relatively symmetrical compression strut systems for each direction of loading. Each compression strut was segmented into parallelogram shaped pieces of concrete. The crack pattern along any horizontal plane was sawtooth shaped.

The angle of the inclined cracks was affected by the stiffness of the boundary element. A flexible boundary element in Specimen F1 caused the crack pattern to converge toward a small area in the web near the base of the wall.

After a loading increment in which yielding of the flexural steel occurred, upon reversing the load, the shear was initially resisted by dowel action in the boundary elements. However, as the web cracks closed, the compression struts aided in resisting shear. This truss action provided a stiffer system than that in the specimens with low nominal shear stress.

As can be seen in Table 3, after approximately the same number of inelastic cycles, the maximum shear distortion in B2 and B5 was of the same order of magnitude as those in R2 and B1. However, the nominal shear stresses were approximately 3 times higher in B2 and B5.

As the specimens were repeatedly cycled in the
inelastic range, the surfaces of the concrete segments in
the struts were subjected to abrasion. Loss of concrete
caused by abrasion increased shear deformations and reduced
the compressive strength of the struts.

In all four specimens, web crushing occurred at the end
of the test. The web crushing was associated with deterio-
ration of the struts along cracks transverse to the thrust
line of the strut. Loss of load capacity at web crushing
was sudden.

In Specimen B2, without confinement, the boundary
elements deteriorated prior to web crushing. Several bars
buckled and concrete was lost from the core of the columns
as loads were cycled. In the last load cycle, the boundary
elements in B2 were about to shear through near the base
when the web crushing occurred.

In Specimen B5, confinement hoops prevented bar buck-
ling and loss of material from the boundary elements. They
also reinforced the boundary elements for shear. Confine-
ment allowed Specimen B5 to sustain 1 more inelastic cycle
at a higher deflection increment than Specimen B2. There-
fore, the maximum measured load was higher in B5. However,
through the first 9 inelastic cycles, the load-deformation
characteristics in B2 and B5 were very similar. The maximum
rotation in B5 was slightly higher and the shear distortion
and construction joint slip slightly lower. Specimen B5 was
repairable simply by replacing the damaged web concrete.

The maximum shear stress sustained in these four walls indicates that the concrete contributed to the shear strength. Even assuming the horizontal reinforcement stressed to an ultimate 100 ksi, the concrete contribution was at _least_ from $0.5\sqrt{f'_c}$ to $1.3\sqrt{f'_c}$ ($0.04\sqrt{f'_c}$ to $0.11\sqrt{f'_c}$, MPa). A more reasonable estimate, based on reinforcement stresses of 75 ksi, would be that the concrete contribution varied from $2\sqrt{f'_c}$ to $3\sqrt{f'_c}$ ($0.17\sqrt{f'_c}$ to $0.25\sqrt{f'_c}$, MPa).

SUMMARY OF TEST RESULTS

Load-Top Deflection Relationships

Load versus deflection envelopes for all specimens are shown in Fig. 7. The deflection is that at the top of the specimen. The envelope for each curve was obtained by passing lines through the peak points of each new maximum loading cycle.

Moment-Rotation Relationships

Moment versus rotation envelopes for all specimens are shown in Fig. 8.

As observed by other investigators,[6,7,8] alternate tensile yielding of the reinforcing steel causes a "growth" in the hinging region. As a specimen was loaded beyond yield in one direction and then unloaded, permanent deformations remained in the tension steel. As the specimen was loaded in the opposite direction, prior to crack closure, only the reinforcement was effective in resisting moment. This steel section had a lower stiffness than the combined concrete-steel section. As the cracks closed the stiffness increased. This accounts for "pinching" observed in the moment-rotation loops. An example of "pinched" loops is shown in Fig. 9.

After several load reversals, the cracks in the compression side appeared to stay open. They were, in fact, closed near the outer compression face and were riding on the debris in the cracks.
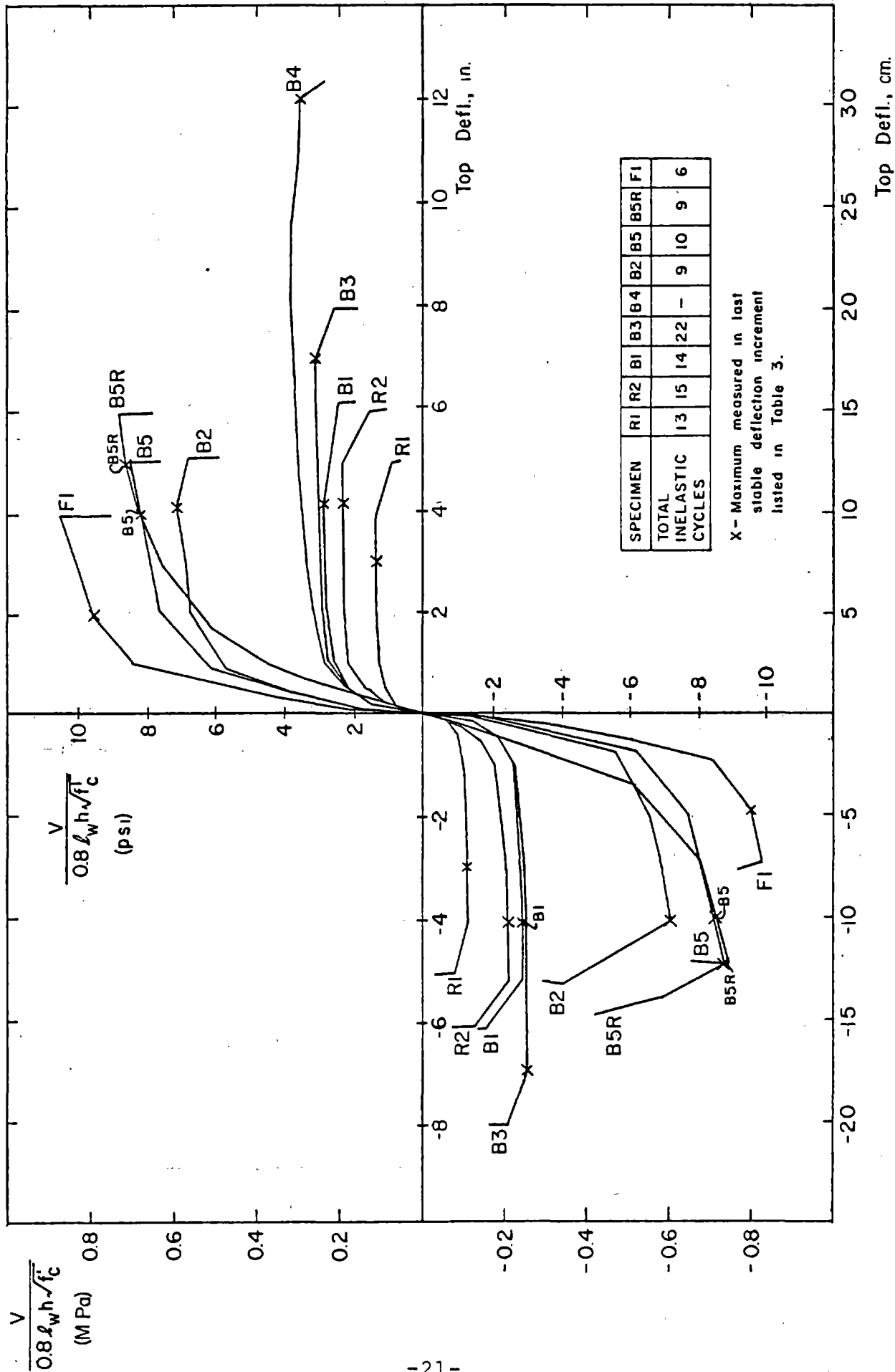
Fig. 7 Load versus Top Deflection Envelopes

SPECIMEN	RI	R2	BI	B3	B4	B2	B5	B5R	FI
TOTAL INELASTIC CYCLES	13	15	14	22	–		9	10	9	9	6

X – Maximum measured in last stable deflection increment listed in Table 3.

-21-
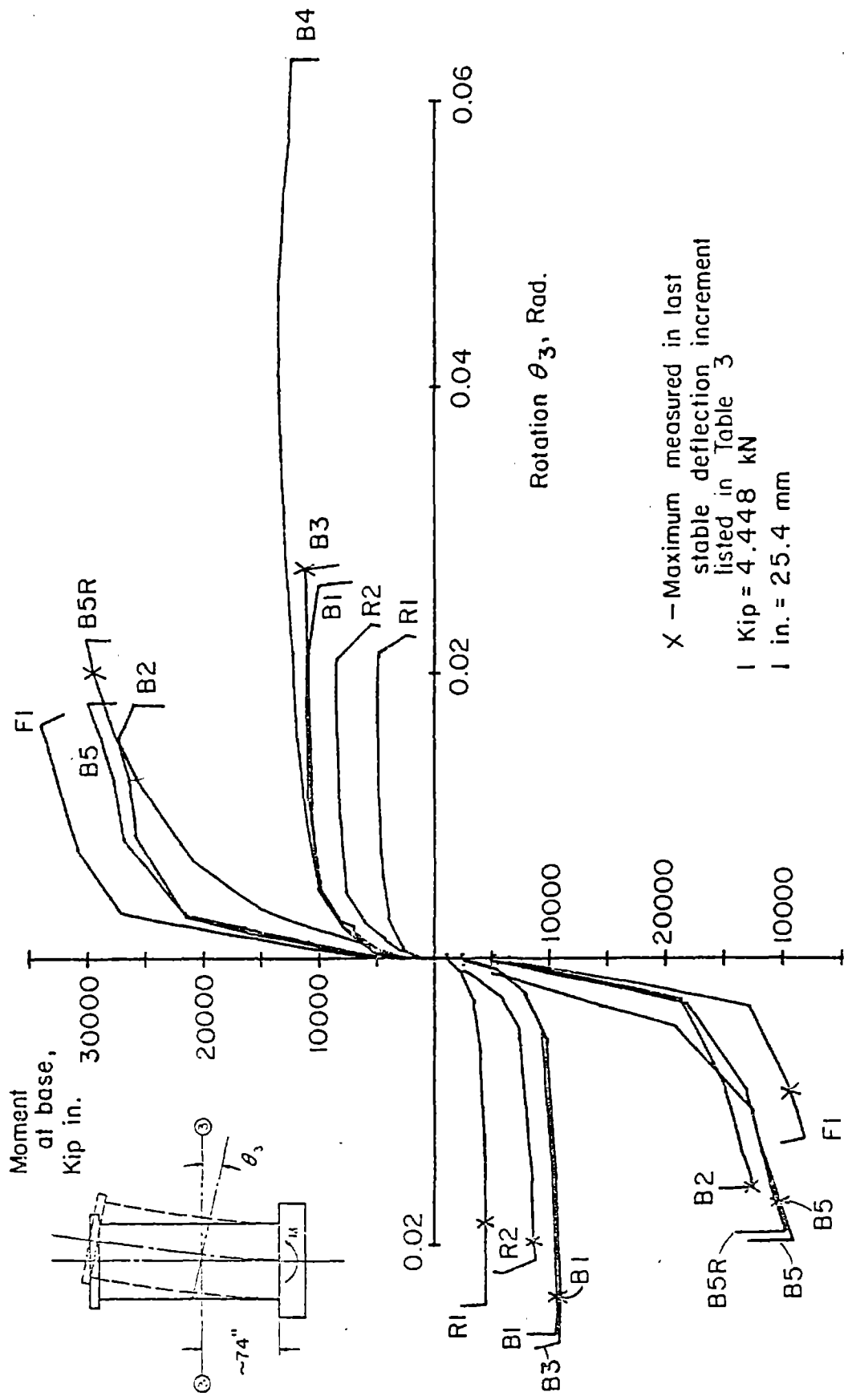
Fig. 8 Moment versus Rotation Envelopes
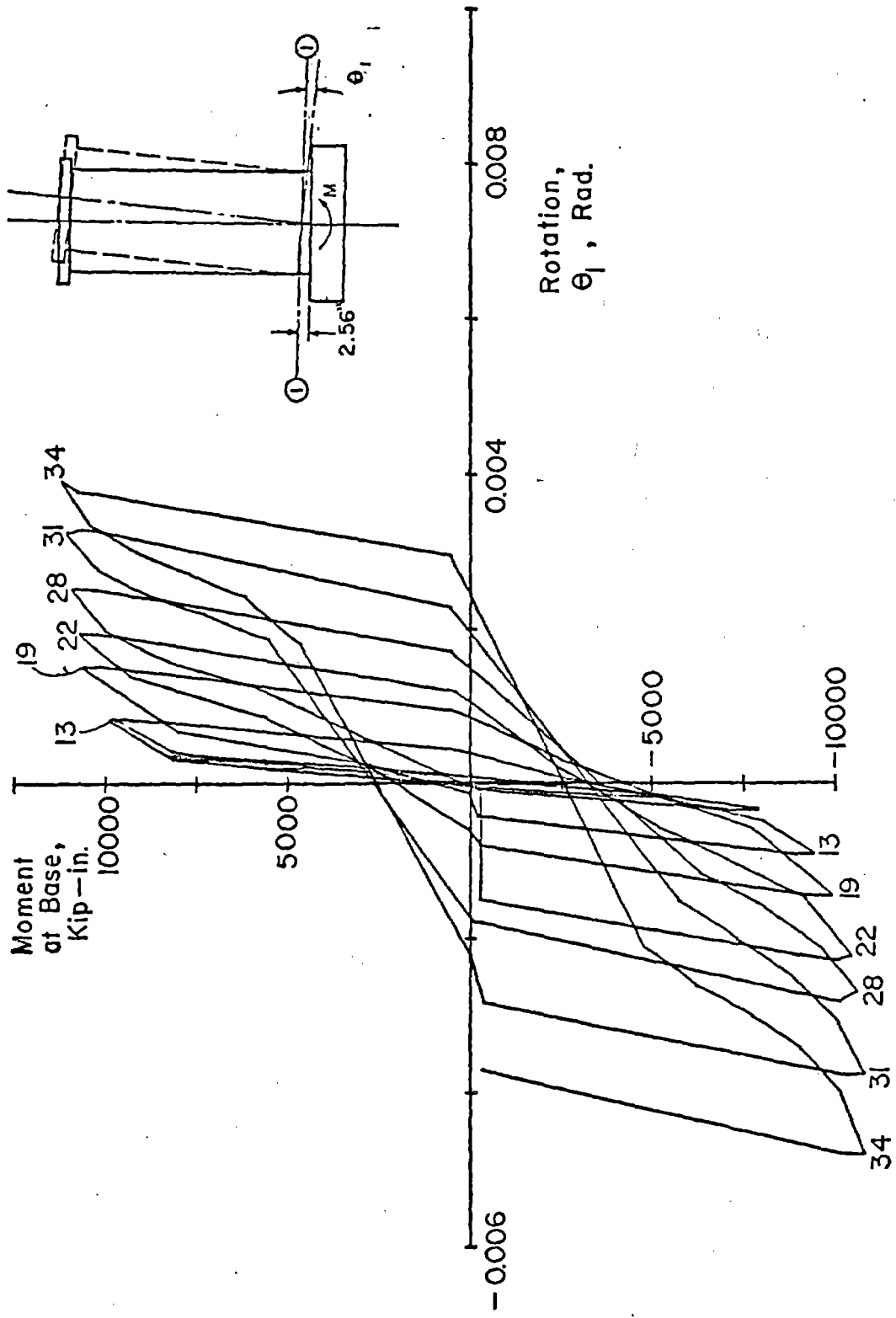
Fig. 9 Example of "pinching" in Moment-Rotation Loops

As shown in Fig. 8, the envelopes for the cyclically loaded Specimens B1 and B3 exhibit a lower rate of "strain hardening" than the monotonically loaded Specimen B4. Increased "growth" with increased inelastic deflections partially accounts for the reduced rate of "strain hardening". The growth permitted increasing amounts of rotation to occur before the cracks closed. With the cracks open, the section was less stiff than the combined steel-concrete section. Therefore, higher rotations were attained without appreciable increase in load. The rate of "strain hardening" is also affected by:

1. Loss of compression material from abrasion and crushing.

2. The effect of load reversal on the stress-strain relationship of the steel.

A comparison of the envelopes for Specimens B3 and B4 in Fig. 8 indicates maximum rotations are less when reversed loads are applied. Similar comparisons are presented with the data for each specimen in Appendix B. A calculated value for the maximum monotonic rotation is used.

As shown by the test results in Appendix B, the monotonic moment-rotation relationship is not "the" envelope for cyclic moment-rotation relationships. It is an upper limit.

Shear-Distortion Relationship

Load versus shear distortion envelopes for all specimens are shown in Fig. 10. The envelopes indicate that a shear "yielding" occurred in each specimen during the same load
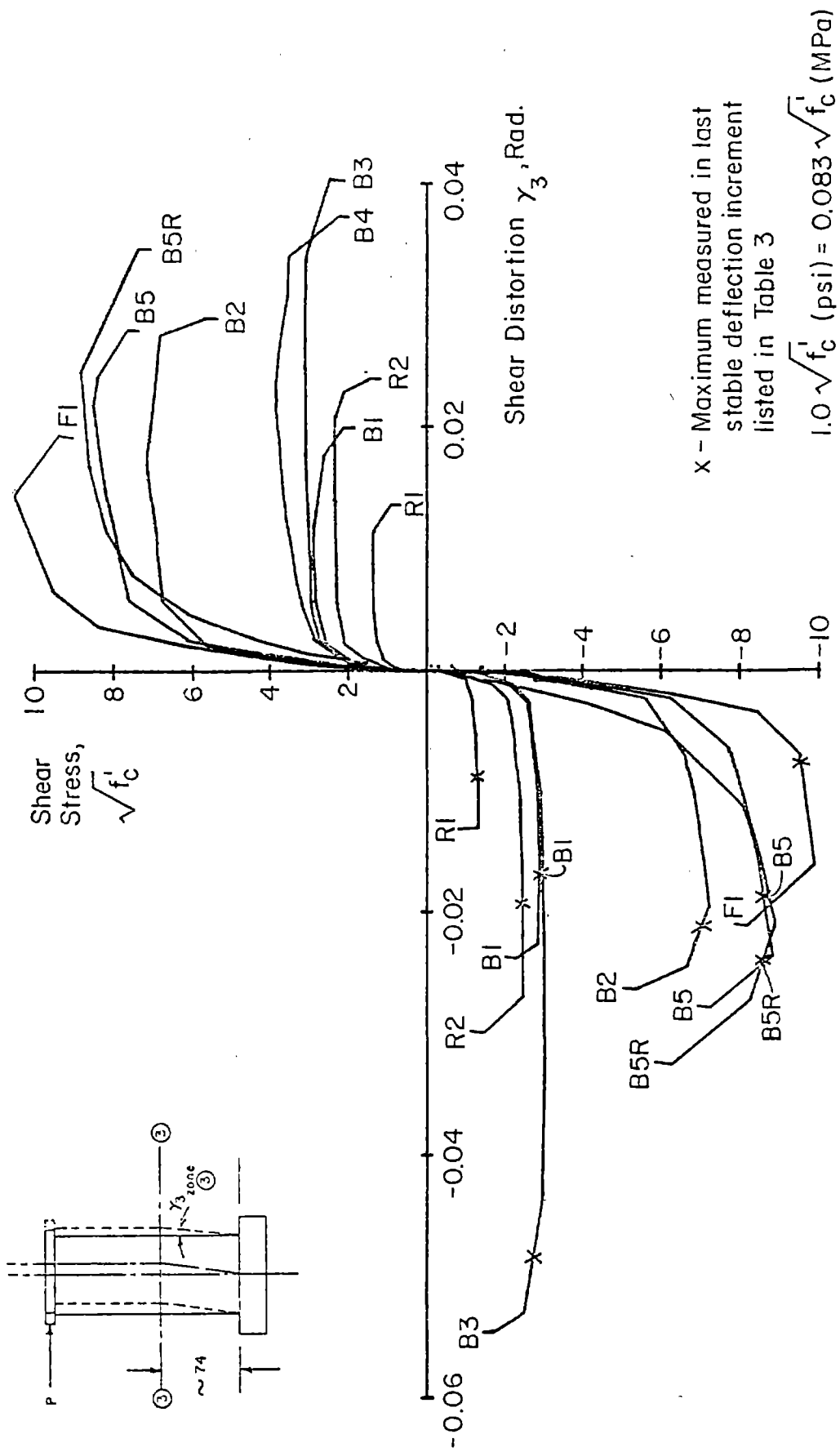
Fig. 10 Shear-Distortion Envelopes

stages that flexural yielding occurred. Shear "yielding" is defined as a large increase in shear distortion corresponding to a small increase in load. This shear "yielding" was observed in all the specimens including the specimens over-reinforced for shear and the monotonically loaded Specimen B4. Yielding of the horizontal reinforcement did not necessarily coincide with "yielding" observed in the shear-distortion data.

Shear "yielding" could be partially attributed to loss of aggregate interlock and a reduction in the dowel stiffness of the tension boundary element as the cracks widened. However, this "yielding" was also partially caused by large horizontal strains accompanying the large vertical strains from flexural yielding across inclined cracks. A component of the rotation across inclined cracks was contained in the measured shear distortions.

In addition to the "yielding" described above, a reduction of shear stiffness occurred in the specimens subjected to cyclic loading. This has also been observed by other investigators.[5,6,7] It was attributed to alternate tensile yielding of the reinforcing steel. As the specimen was loaded beyond yield in one direction and then unloaded, permanent deformations remained in the tension steel. As the specimen was loaded in the opposite direction the shear was transferred predominantly by dowel action prior to crack closure. This dowel action had a relatively low stiffness. As the cracks closed, interface shear transfer plus some

truss action increased the shear stiffness. The load then increased with significantly less shear deformation. This resulted in "pinching" of the shear-distortion loops as shown in Fig. 11.

As a wall was repeatedly cycled in the inelastic range, abrasion due to the interface shear transfer occurred in the hinging region cracks. At increasingly larger deflection increments, plastic deformations remaining in the steel after peak loads were larger. Therefore, increased shear distortions occurred with just dowel action transferring the shear before the cracks closed. As a result, increasingly larger shear deformations occurred in each new cycle.

Shear-Construction Joint Slip Relationship

Load versus base construction joint slip envelopes for all specimens are shown in Fig. 12. As seen in this figure, the slip at the base construction joint was approximately the same order of magnitude for all specimens. However, for equivalent applied shear stress and number of inelastic cycles, the rectangular specimens exhibited significantly more slip than the other cross sections. This slip did not affect the final failure mode for the rectangular specimens.

The performance of two specimens was affected by the behavior of construction joints. In the test of Specimen B5, deterioration of a portion of the joint at the 3-ft level caused by improper construction methods may have precipitated early web crushing. In the test of Specimen B5R, a sliding-crushing failure in the joint at the 3-ft

-27-
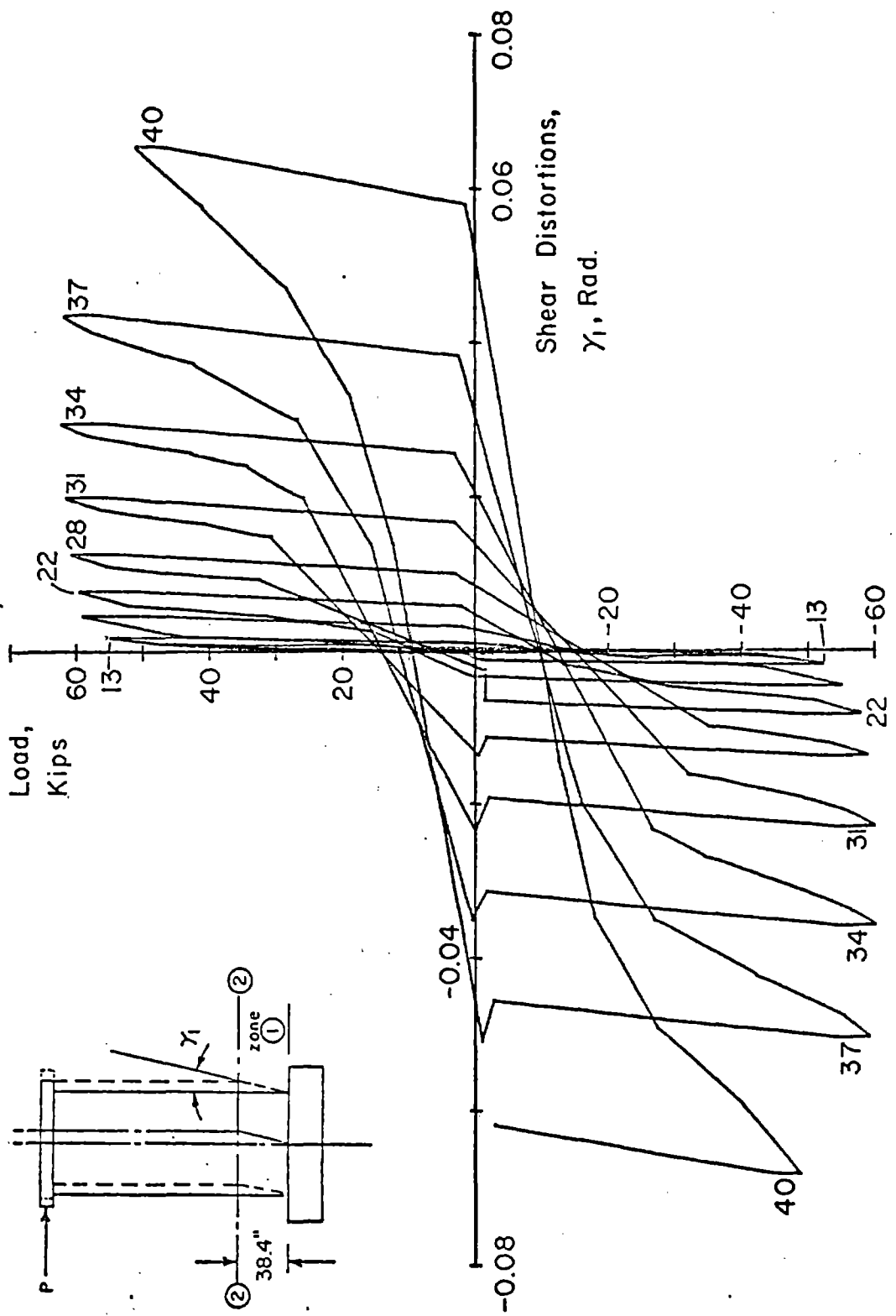
Fig. 11 Example of "pinching" in Shear-Distortion Loops
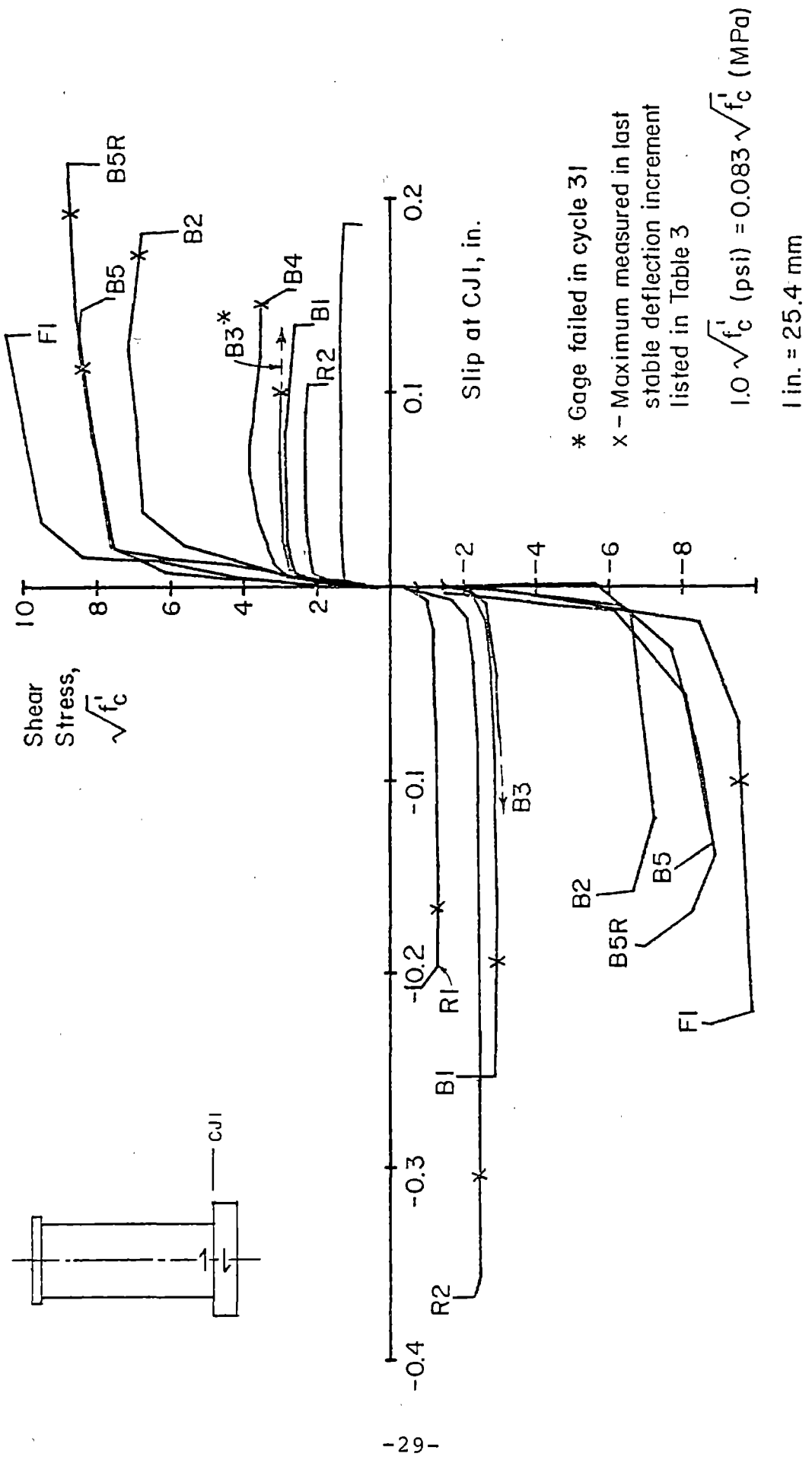
Fig. 12 Load versus Base Construction Joint Slip Envelopes

level was the final failure mode. This failure was probably precipitated by the reduced dowel action resistance of the boundary elements across this joint. Dowel action of the columns in B5R was reduced by large cracks resulting from the large number of inelastic cycles sustained through the B5 and B5R tests.

The data presented for each specimen in Appendix B showed that slip at the base construction joint remained a relatively constant percentage of the shear deflections in the lower 3-ft (0.91 m) zone. This percentage was higher in the rectangular shaped specimens and lower in the barbell shaped specimens. The barbell shape with confinement hoops in the boundary elements exhibited the least slip as a portion of the total deformation.

Ductility

The ductility of a structure is commonly used as a measure of its inelastic deformation capacity. Ductility is often defined as the ratio of a specified deformation at a particular load to that at yield. The use of ductility ratios in seismic design implies certain limitations that are discussed by Paulay and Uzumeri.[9]

Figure 13 shows the cumulative top deflection ductility ratio[10,11] versus load for each specimen. The full yield deflection was used to calculate the ductilities. From the inset in Fig. 13, it is apparent that the ductility ratio is very sensitive to the definition of the yield deflection.
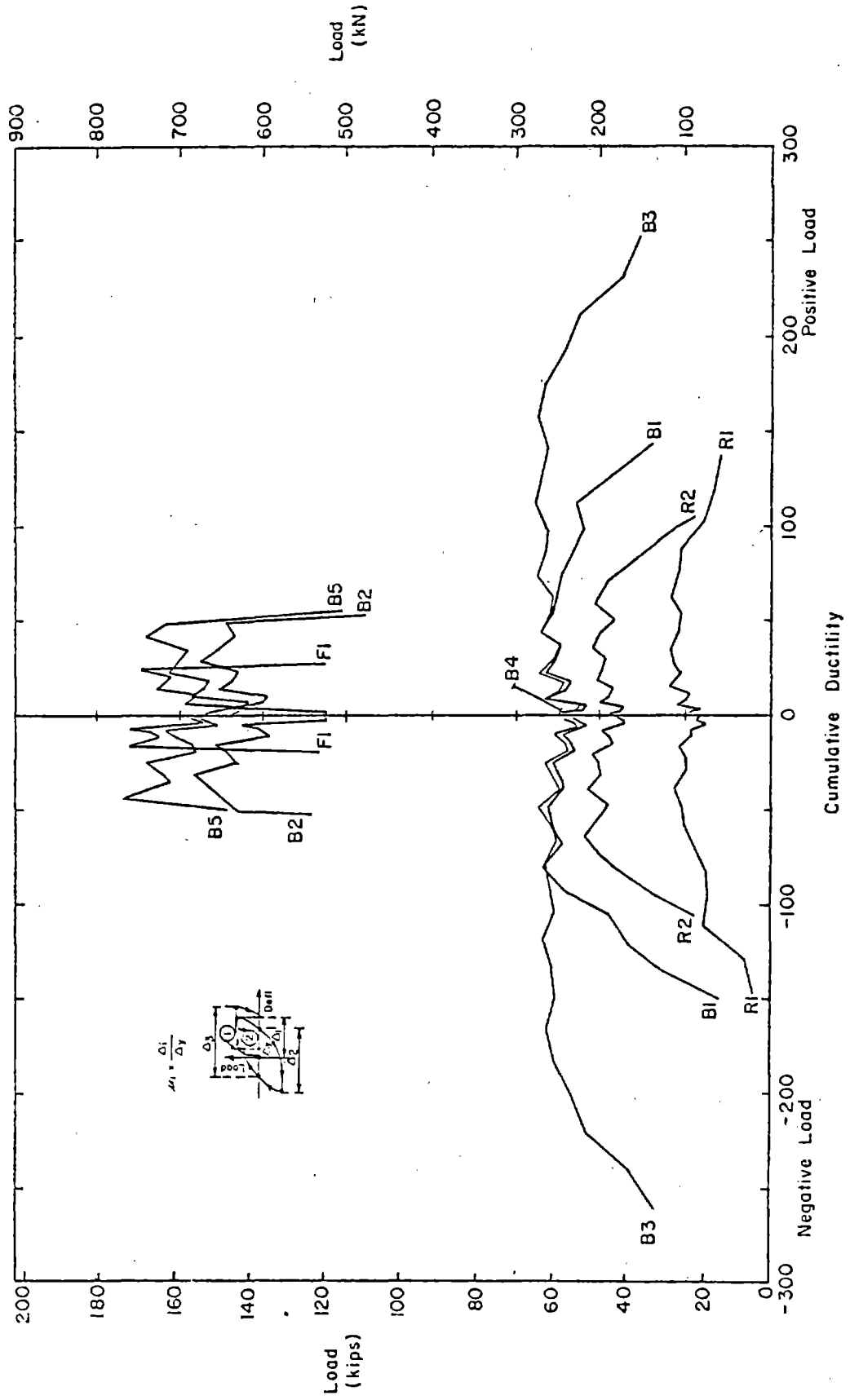
Fig. 13 Load versus Cumulative Top Displacement Ductility

Comparison of Specimens Bl and B3 in Fig. 13 shows a beneficial effects of confinement reinforcement on the top deflection ductility for walls that failed in the flexural mode. However, a comparison of moment-rotation envelopes in Fig. 8 shows that confinement reinforcement had little effect on rotational ductility for Specimens Bl and B3.

For walls that failed in shear, B2 and B5, no increase in ductility as a result of confinement hoops was observed.

Figure 13 indicates the larger top deflection ductilities obtained for all walls subjected to low shear. However, even the walls subjected to high shear exhibited significant ductility capacities. In any case, the ductility must be evaluated in terms of what is required as well as what can be attained.

Energy Dissipation

The energy dissipation capacity of a structure may also be used to evaluate the inelastic performance under reversing loads. The optimum performance would be a maximum amount of energy absorbed with a corresponding minimum amount of deformation. The load-deformation loops should be as open or as full as possible. A measure of the energy dissipation capacity should not only relate the amount of energy absorbed to the amount of energy input, it should relate the energy absorbed to the level of deformations.

Figures 14 and 15 present the energy dissipation data for each of the specimens. In these figures, the cumulative energy absorbed is presented as a percentage of cumulative
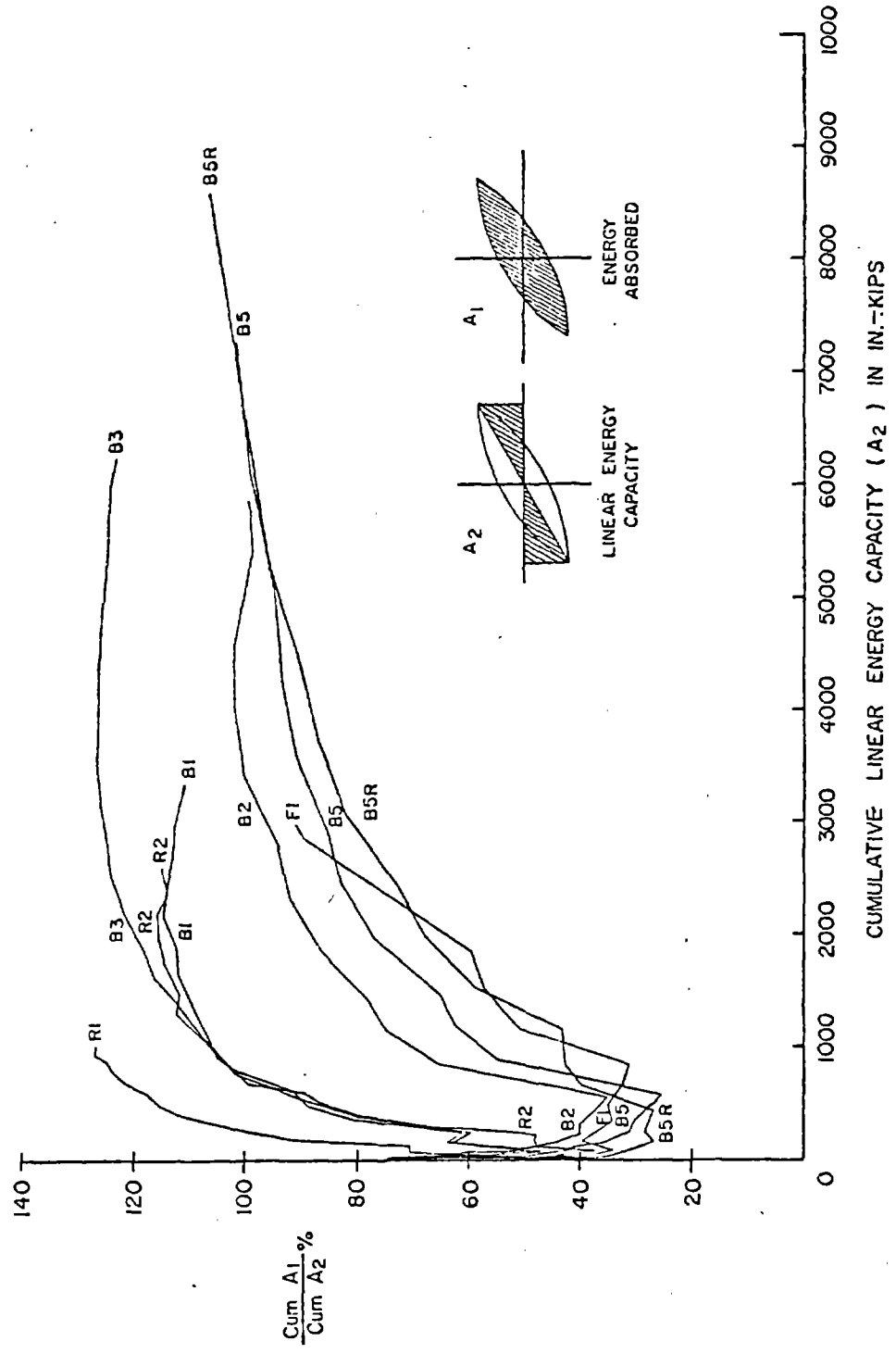
Fig. 14   Absorbed Energy versus Cumulative Linear Energy Capacity.
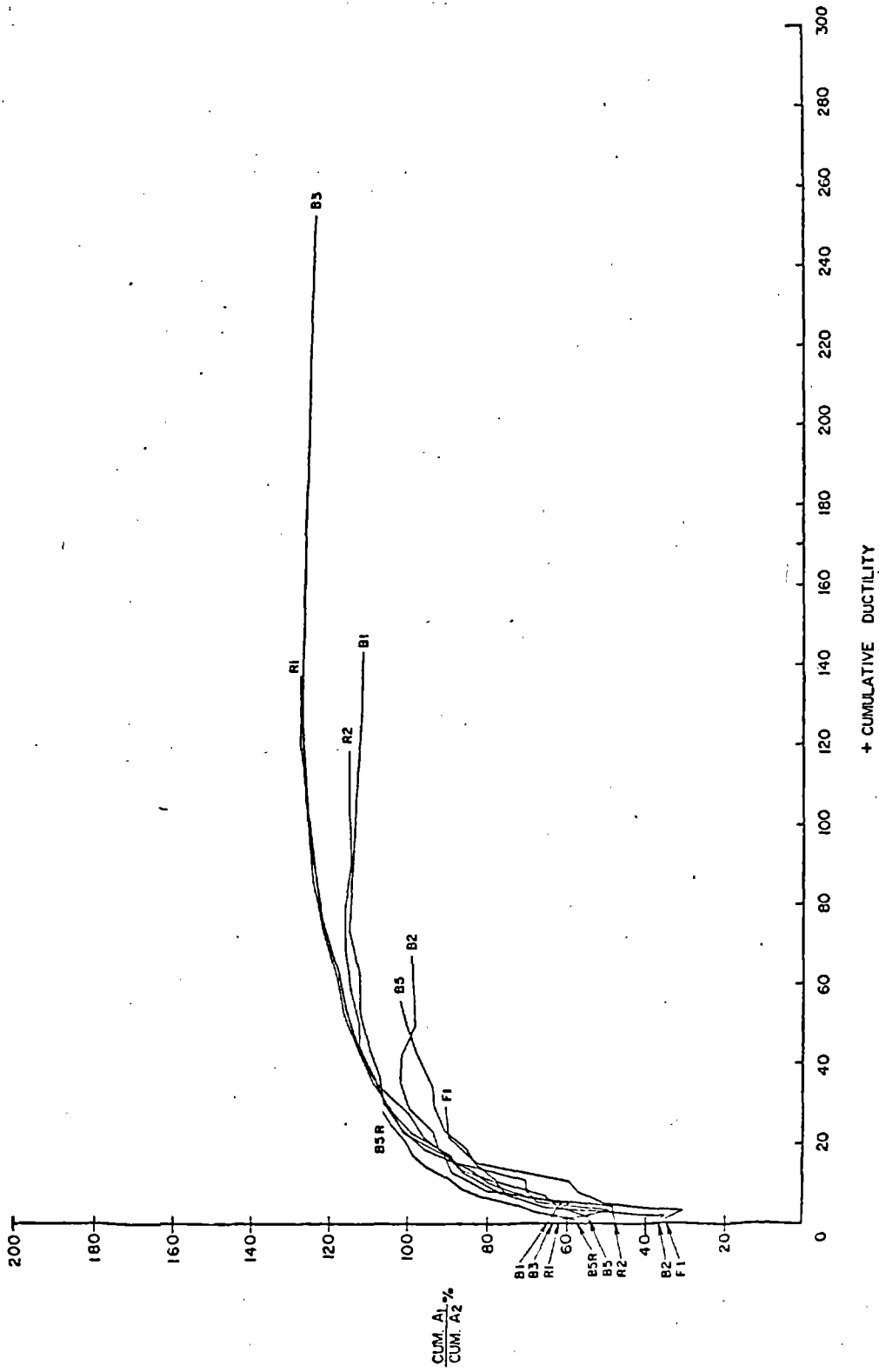
Fig. 15 Absorbed Energy versus Cumulative Top Displacement Ductility

linear energy capacity.[12] This is defined in the insets
in Fig. 14. This relationship includes a measure of the
stiffness of the specimens.

Figure 14 shows the cumulative percentage of absorbed
energy related to the cumulative linear energy capacity.
The walls subjected to low shear absorbed a larger per-
centage of the cumulative linear energy capacity than did
the walls subjected to high shear. This is expected due to
the lower yield loads and deformations in the specimens
subjected to a low nominal shear stress.

Figure 15 shows the cumulative percentage of absorbed
energy related to the cumulative top displacement ductility.
The difference between the low and high shear specimens is
not as obvious as in Fig. 14 and this difference may not be
significant. As with ductility, the energy dissipation
capacity must be evaluated in terms of what is required as
well as what can be attained.

Repaired Specimen

The reparied specimen strength and deformation capabil-
ities in the inelastic range were similar to the original
specimen.

Free Vibration Tests

The following observations are made on the results of
the free vibration tests.

1. Frequency measured prior to the application of
    lateral load ranged from 64% to 82% of the

frequency calculated based on uncracked section properties.

2. The measured frequency decreased by an average factor of 2.2 from the inital tests to the tests carried out after application of lateral load cycles near the flexural yield load. For the same conditions, the average damping coefficient changed from 3.4% to 8.5% of critical.

3. In general smaller amplitude hammer tests gave higher frequencies and lower damping coefficients than "initial displacement-sudden release" tests.

CONCLUSIONS

The following conclusions are based on the results of the experimental program.

1. Structural walls designed according to the 1971 ACI Building Code[5] without special details for seismic load will attain the ACI flexure and shear design strengths. Also, they possess significant inelastic deformation capacity when subjected to reversing loads.

2. For walls subjected to low shear stresses ($v_{max} \leq 3.0 \sqrt{f_c'}$).

   2.1 Flexural bar buckling and loss of compression concrete are the limiting factors in the inelastic performance. However, a significant number of inelastic cycles can be sustained prior to occurrence of bar buckling.

   2.2 Large out of plane displacement of the compression zone may limit inelastic performance of rectangular shaped walls.

   2.3 Construction joints will perform adequately if made following minimum standard practice of roughening and cleaning the surface to remove laitance and loose particles. The amount of shear displacement that occurs across cracks at construction joint locations is not any larger than that which occurs across cracks at other locations.

3. For walls subjected to high shear stresses ($v_{max} > 7\sqrt{f'_c}$).

   3.1 Web shear distress is the limiting factor in the inelastic performance. However, even in a wall stressed to $8.8\sqrt{f'_c}$, a significant number of inelastic cycles can be sustained prior to loss of strength.

   3.2 A construction joint made using minimum standard practice and located at the base of the wall does not influence the strength of the specimen. The presence of a straight, horizontal construction joint within the hinging region of a wall subjected to high shear stresses may limit the inelastic performance.

4. The use of stiff boundary elements increases the inelastic performance of structural walls. Boundary elements behave as large dowels decreasing shear distortions and construction joint slip.

5. The use of confinement reinforcement in the boundary elements within the hinging region of a structural wall significantly increases the inelastic performance.

   5.1 Confinement hoops maintain the integrity of the boundary elements by delaying bar buckling and containing or confining the concrete core.

5.2 Confinement hoops increase the stiffness of the boundary element against slip across construction joints.

5.3 Confinement reinforcement limits the extent of damage to the boundary elements. There-fore, the wall is easier to repair.

5.4 Confinement reinforcement increases the shear capacity of the boundary elements.

5.5 High concrete compressive strains may be generated in the boundary elements of a structural wall with a high percentage of flexural steel. Confinement steel provided in accordance with the 1971 ACI[5] or 1976[13] UBC Building Code was adequate to maintain the compressive strength of the boundary elements of the specimens tested.

5.6 Designing confinement reinforcement based on a criteria to increase the useable concrete strain may not be necessary for a wall with a low percentage of flexural steel. Design criteria should also be based on spacing to prevent or delay inelastic bar buckling and to contain the concrete core.

6. Displacements due to shear distortions are a significant portion of the total lateral inelastic displacements in structural walls subjected to reversed loads.

ACKNOWLEDGMENTS

REFERENCES

1. Fintel, M., "Ductile Shear Walls in Earthquake Resistant Multistory Buildings," ACI Journal, Proceedings, Vol. 71, No. 6, June 1974, pp. 296-305.

2. Fiorato, A.E.; Oesterle, R.G. and Corley, W.G., "Earthquake Resistant Structural Walls - Strength and Deformation Characteristics of Isolated Walls," To be Published.

3. Fiorato, A.E.; Oesterle, R.G. and Corley, W.G., "Earthquake Resistant Structural Walls - Ductility of Isolated Walls," To be published.

4. Fintel, M., etal, "Structural Walls in Earthquake Resistant Structures - Dynamic Analysis of Isolated Structural Walls," PCA Report to NSF-RANN, December 1976.

5. ACI Committee 318, Building Code Requirements For Reinforced Concrete, ACI Standard 318-71, American Concrete Institute, Detroit, 1971 78 pp.

6. Brown, R.H. and Jirsa, J.O., "Shear Transfer of Reinforced Concrete Beams Under Reversed Loading," Shear in Reinforced Concrete, Vol. 1, Publication SP-42, American Concrete Institute, Detroit, 1974, pp. 347-357.

7. Paulay, T. and Binney, J.R., "Diagonally Reinforced Coupling Beams of Shear Walls," Shear in Reinforced Concrete, Vol. 2, Publication SP-42, American Concrete Institute, Detroit, 1974, pp. 579-598.

8. Bertero, V.V.; Popov, E.P. and Wang T.Y., "Hysteretic Behavior of Reinforced Concrete Flexural Members with Special Web Reinforcement," EERC Report No. 74-9, University of California, Berkeley, August 1974, 126 pp.

9. Paulay, T. and Uzumeri, M., "A Critical Review of the Seismic Design Provisions for Ductile Shear Walls of the Canadian Code and Commentary," Canadian Journal of Civil Engineering, Vol. 2, No. 4, 1975, pp. 592-601.

10. Hanson, N.W. and Conner, H.W., "Seismic Resistance of Reinforced Concrete Beam-Column Joints," Journal of the Structural Division, ASCE, Vol. 93, ST5, October 1967, pp. 533-560.

11. Paulay, T. and Santhakumar, A.R., "Ductile Behavior of Coupled Shear Walls," Journal of the Structural Division, ASCE, Vol. 102, ST1, January 1976, pp. 93-108.

12. Freeman, S.A., "Testing Wall Panels for Earthquake Response," ASCE/FMD Specialty Conference, Dynamic Response of Structures, UCLA, Los Angeles, March 1976, pp. 342-351.

13. International Conference of Building Officials, Uniform Building Code, 1976 Edition, Whittier, California, 1976, pp. 2626.

14. ACI Committee 315, Manual of Standard Practice For Detailing Reinforced Concrete Structures, ACI Standard 315-74, American Concrete Institute, Detroit, 1974, 167 pp.

15. ACI Committee 301, Specifications for Structural Concrete for Buildings, ACI Standard 301-72, American Concrete Institute, Detroit, 1972, 36 pp.

16. Ghosh, S.K., "A Computer Program for the Analysis of Slender Structural Wall Sections Under Monotonic Loading," Supplement No. 2 of PCA Interim Report to NSF-RANN, August 1975, 99 pp.

17. Kent, D.C. and Park, R., "Flexural Members with Confined Concrete," Proc. of ASCE, Journal of Structural Division, ST7, July 1971, pp. 1969-1990.

18. Corley, W.G., "Rotational Capacity of Reinforced Concrete Beams," Journal of the Structural Division, ASCE, Vol. 92, ST5, October 1966, pp. 121-146.

19. Kaar, P.H.; Fiorato, A.E.; Carpenter, J.E. and Corley, W.G., "Earthquake Resistant Structural Walls - Concrete Confined by Rectangular Hoops," PCA Report to NSF-RANN, December 1976.

20. Bachmann, H., "Influence of Shear and Bond on Rotational Capacity of Reinforced Concrete Beams," Publications, International Association for Bridge and Structural Engineering, Vol. 30, Part II, Zurich, 1970, pp. 11-28.

21. Park, R. and Paulay, T., "Reinforced Concrete Structures," John Wiley and Sones, Inc., New York, 1975, pp. 307-309.

22. Mattock, A.H., Discussion of "Rotational Capacity of Reinforced Concrete Beams," by W.G. Corley, Proc. of ASCE, Journal of Structural Division, Vol. 93, ST2, April 1967, pp. 519-522.

NOTATION

A_{sh} = Area of transverse hoop bar (one leg)

E_c = Modulus of elasticity of concrete

f'_c = Compressive strength of standard 6x12-in. (152x305 mm) concrete cylinders

f_r = Modulus of rupture of concrete

f_y = Yield strength of reinforcement

f_{su} = Tensile strength of reinforcement

h = Wall thickness

ℓ_h = Maximum unsupported length of rectangular hoop

ℓ_w = Horizontal length of wall

s_h = Center-to-center spacing of hoops

V = Shear force

v = Nominal shear stress = $\dfrac{V}{0.8\ell_w h}$

v_{max} = Maximum nominal shear stress

Δ_{CJ1} = Slip at the base construction joint

$\Delta\gamma_1$ = Shear deflection at the 3-ft level

γ_1 = Average shear distortion in Zone 1, from 0 to 3-ft (0.91 m) level

γ_2 = Average shear distortion in Zone 2, from 3-ft to 6-ft (0.91 m to 1.83 m) level

γ_3 = Average shear distortion in Zone 3, from 0 to 6-ft (1.83 m) level

ε_c = Strain in concrete at the outer compression faces at the base of the wall

ε_u = Ultimate compressive strain for concrete

-43-

θ_1 = Rotation of the horizontal section approximately 3 in. (76.2 mm) above the base block

θ_2 = Rotation of the horizontal section approximately 38 in. (0.97 m) above the base block

θ_3 = Rotation of the horizontal section approximately 74 in. (1.88 m) above the base block .

ρ_f = Ratio of main flexural reinforcement area to the gross concrete area of the boundary element. For rectangular sections, the boundary element was taken to extend $0.1\, \ell_w$ from each end of the wall

ρ_h = Ratio of horizontal shear reinforcement area to the gross concrete area of a vertical section of the wall web

ρ_n = Ratio of vertical reinforcement area to the gross concrete area of a horizontal section of the wall web

ρ_s = Ratio of effective volume of confinement reinforcement to total volume of core = $\dfrac{2A_{sh}}{\ell_h s_h}$

APPENDIX A - EXPERIMENTAL PROGRAM

Test Specimens

Detailed descriptions of the geometry and design of the nine specimens are given in this section. In addition, material properties and construction procedures are described.

Description

The overall dimensions of the test specimens are shown in Fig. A-1 and A-2. Height of the wall, from the top of the base block to the center of the top slab, is 15 ft (4.57 m). The horizontal length of the wall is 6 ft 3 in. (1.91 m) and its web thickness is 4 in. (102 mm).

Three different wall cross-sections have been tested. These are flanged, barbell and rectangular sections. The nominal cross-sectional dimensions of the three sections are shown in Fig. A-2.

The 2x4x10-ft base block shown in Fig. A-1 was used to secure the specimens to the laboratory floor during testing. The slab on top of the wall, also shown in Fig. A-1 was used to transfer loads to the test specimen. Both the base block and the top slab were designed to ensure that no premature termination of the test would occur because of the failure of the loading or supporting elements.

Design

Vertical Reinforcement. The first step in the design of the test specimens was to select a nominal percentage of
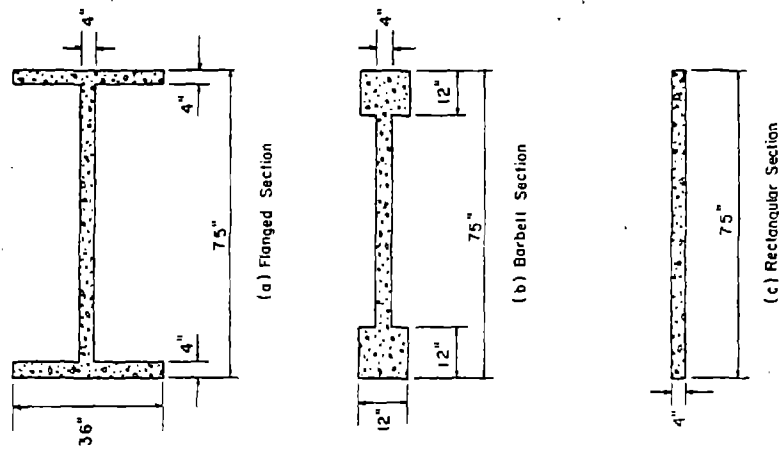
Fig. A-2   Nominal Cross-Sectional
Dimensions of Test Specimens
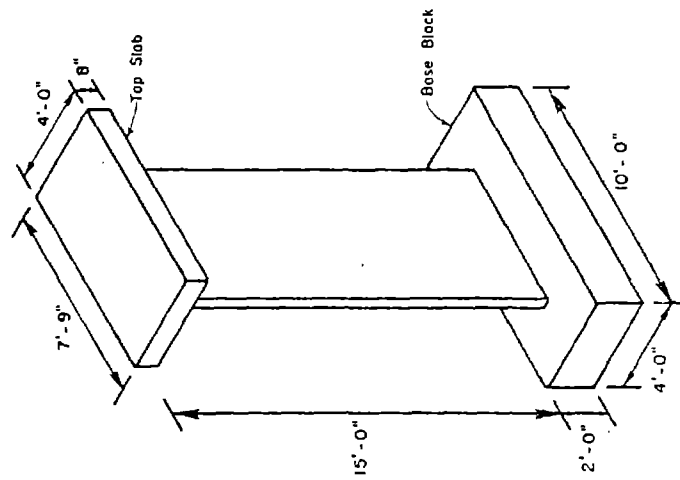
(1 in.=25.4mm)

Fig. A-1   Nominal Dimensions of Test Specimens

(1 in.=25.4mm)

A-2

main flexural reinforcement. This was either 1% or 4% based on the area of the boundary element. For rectangular sections, the "boundary element" was taken to extend 7.5 in. (191 mm) from each end of the wall. The percentages of flexural reinforcement were chosen to give section moment capacities corresponding to both low and high nominal shear stresses.

Nominal vertical web reinforcement provided in the walls was 0.25% of the gross concrete area of the horizontal wall section. This is the minimum amount permitted by the 1971 ACI Building Code.[5] Once the nominal vertical reinforcement percentages were selected, bar sizes and locations were determined based on modeling and construction requirements.

The moment capacity of the section was calculated according to Section 10.2 of the 1971 ACI Building Code.[5] Design yield stress of the steel was taken as 60,000 psi (414 MPa) and design concrete strength was taken as 6000 psi (41.4 MPa). Strain hardening of the steel, according to ACI Code assumptions, was neglected in calculating the moment capacity.

The vertical reinforcement was continuous from the base block to the bottom of the top slab. The vertical bars were lap spliced with the top slab bars in the top 32 in. (0.81 m) of the wall.

Horizontal Reinforcement. Horizontal shear reinforcement was designed to develop the calculated ACI moment capacity. The shear design was made according to Section

11.16 of the 1971 ACI Building Code.[5] However, ACI
minimum reinforcement requirements governed in the low
moment capacity specimens.

The horizontal reinforcement was placed at a constant
spacing over the height of the wall.

Boundary Element Horizontal Reinforcement. Two designs
were used for horizontal steel in the boundary elements.
The first design, used for unconfined specimens, provided
ordinary column ties designed as lateral reinforcement
according to Section 7.12 of the 1971 ACI Building Code.[5]

The second design, used for confined specimens, pro-
vided rectangular hoop and supplementary crosstie reinforce-
ment in accordance with Section A.6.4 of the 1971 ACI
Building Code. This confinement was placed at a spacing of
1.33 in. (34 mm) over the first 6 ft (1.83 m) of the wall.
Ordinary column ties were used over the remaining height of
the wall.

Details of Reinforcement. Reinforcing steel details
for the nine specimens are shown in Fig. A-3 through Fig.
A-16. All reinforcing steel was detailed and fabricated
according to standard practice.[5,14]

Anchorage for the horizontal steel was provided by
embedment in the boundary elements plus a standard 90° hook
around the outer main flexural steel. Additional anchorage
was provided for the horizontal steel in Specimen B5 by
using one 135° hook and one 90° hook as shown in Fig. A-8.
The hooks were alternated end for end.

1 in. = 25.4 mm

(b) Cross Section

(a) Elevation

Fig. A-3 Reinforcement for Specimen Rl

A-5

1 in. = 25.4 mm

(b) Cross Section

(a) Elevation

Fig A-4   Reinforcement for Specimen R2

A-6

1 in. = 25.4 mm

Sym. About C̸

6 mm

5/8" CL

6 mm

1/2"CL

D3

8 #4

(b) Cross Section

C.J.

C.J.

C.J.

C.J.

C.J.

32"

36"

36"

36"

36"

24"

8"

2"

6 mm @ 8" EF

D3 ties @ 8"

#4

6 mm @ 9" EF

C̸

#4
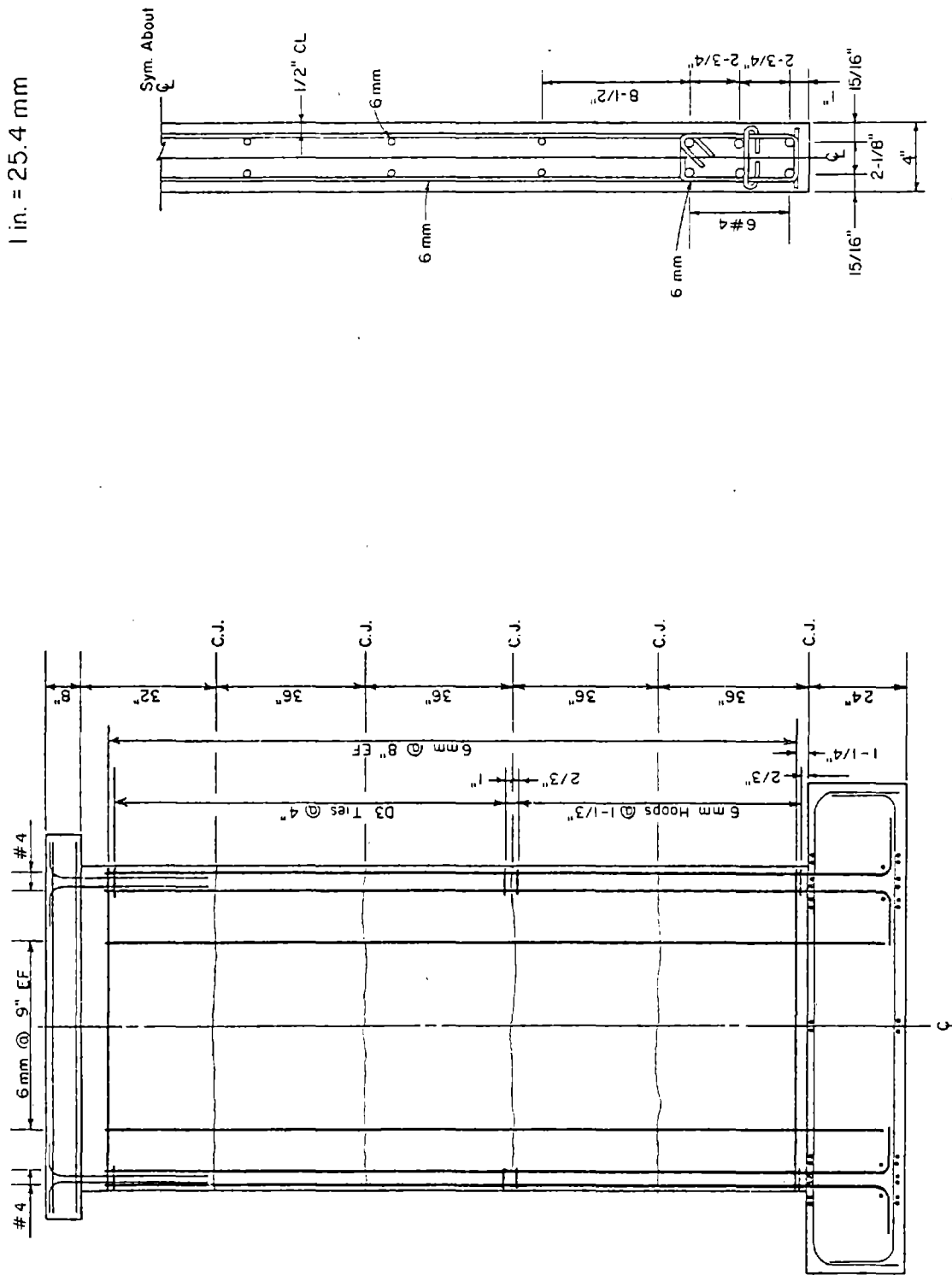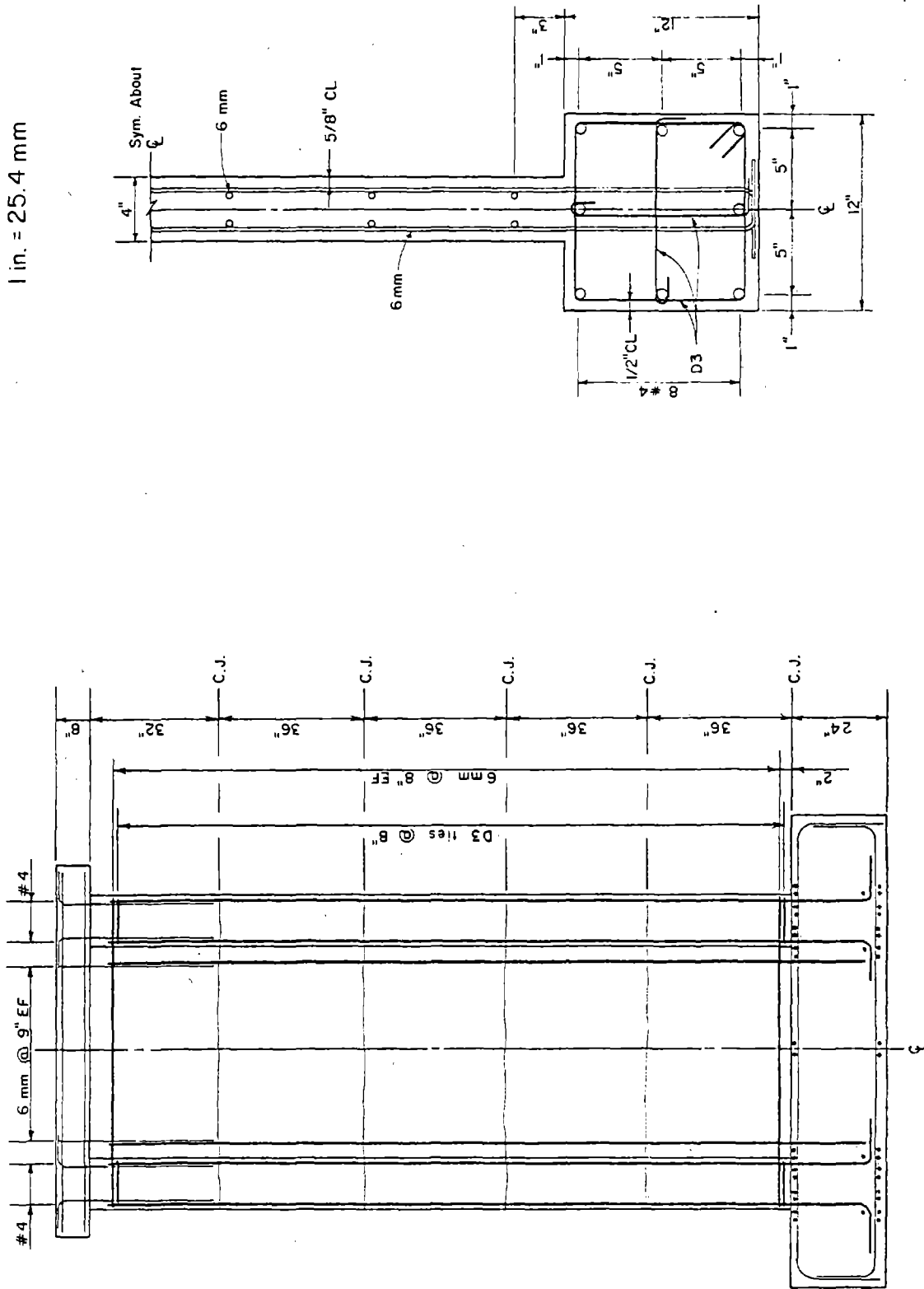
(a) Elevation

Fig. A-5 Reinforcement for Specimen B1

A-7

1 in. = 25.4 mm

(b) Cross Section

(a) Elevation

Fig. A-6 Reinforcement for Specimens B3 and B4

A-8

1 in. = 25.4 mm

Sym. About ℄

6 mm

5/8" CL

6 mm

3/8" CL

D3

12 # 6

(b) Cross Section

Fig. A-7   Reinforcement for Specimen B2

C.J.

C.J.

C.J.

C.J.

C.J.

6 mm @ 4" EF

D3 ties @ 8"

#6

6 mm @ 9" EF

#6

(a) Elevation

A-9
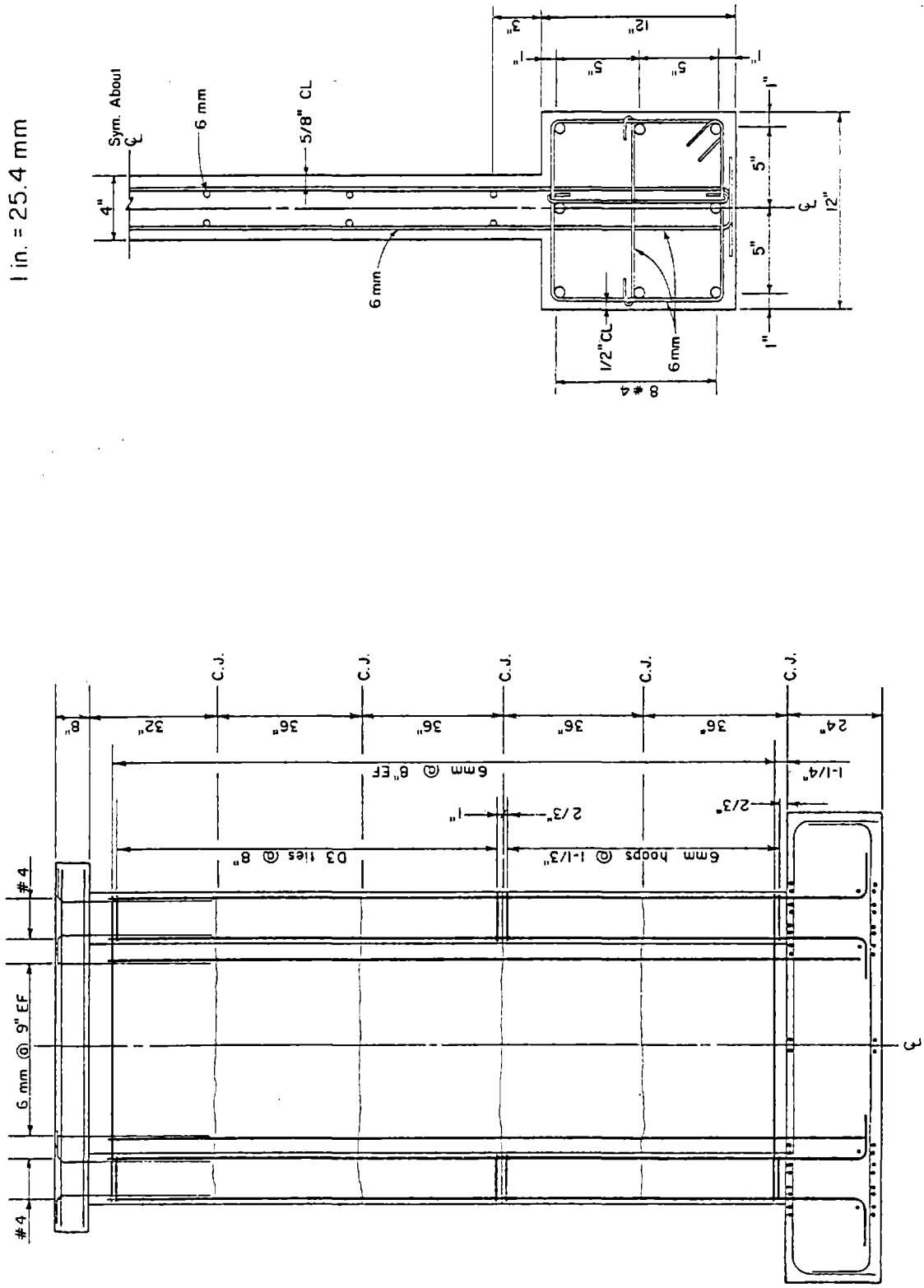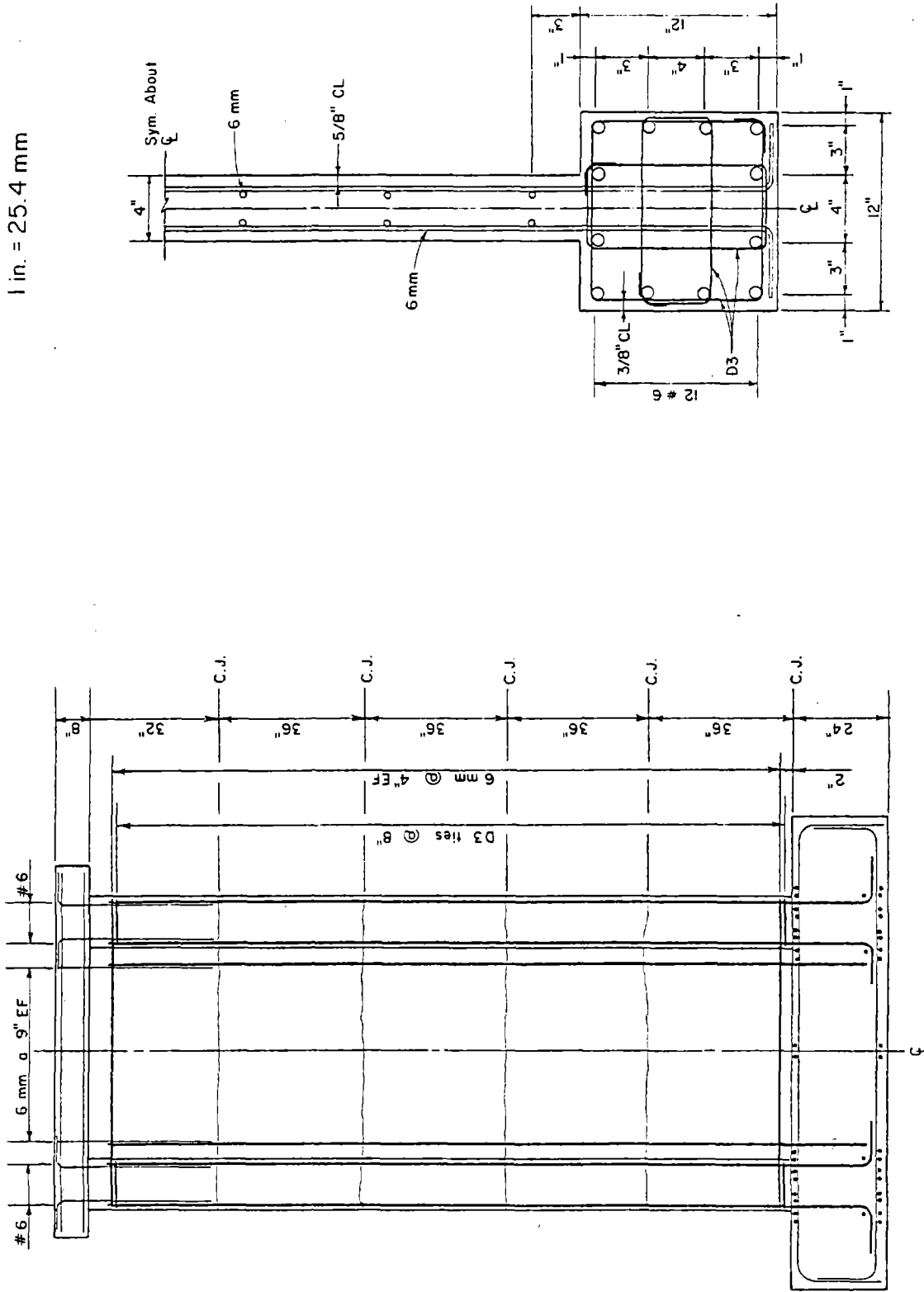
1 in. = 25.4 mm
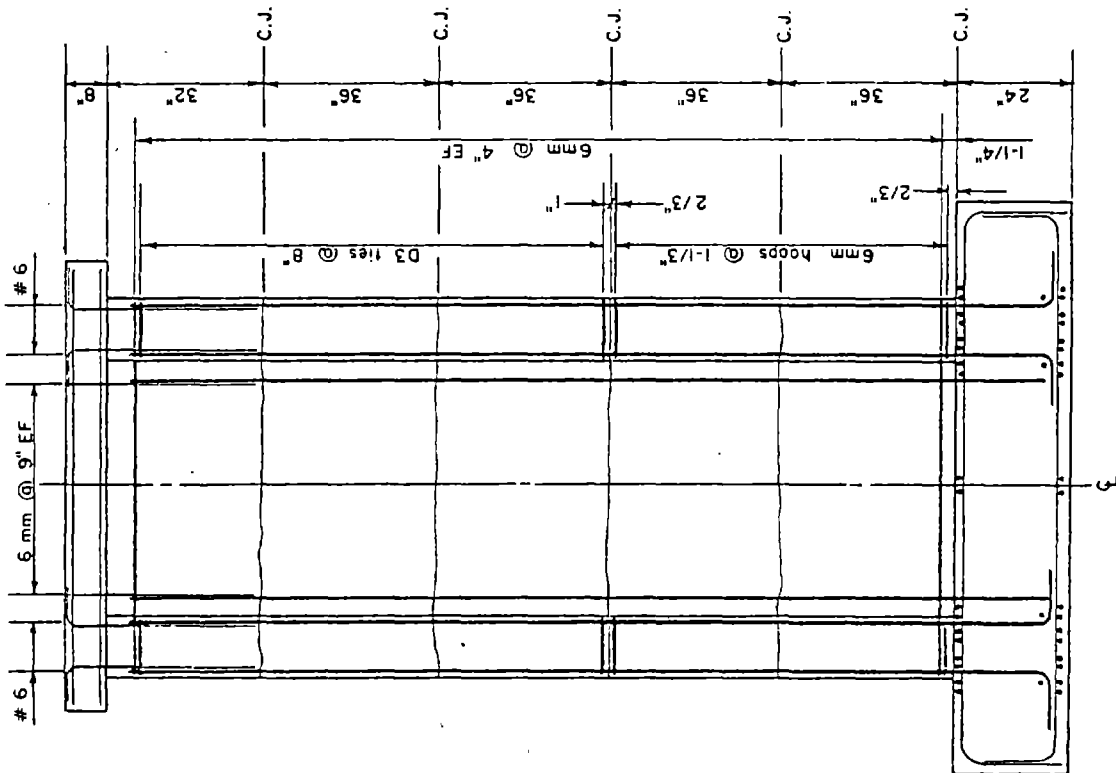
a) Elevation

b) CROSS SECTION AT LEVEL OF 6 mm HORIZONTAL BARS

c) CROSS SECTION AT LEVEL BETWEEN 6 mm HORIZONTAL BARS.

Fig. A-8 Reinforcement for Specimens B5 and B5R

A-10

1 in. = 25.4 mm
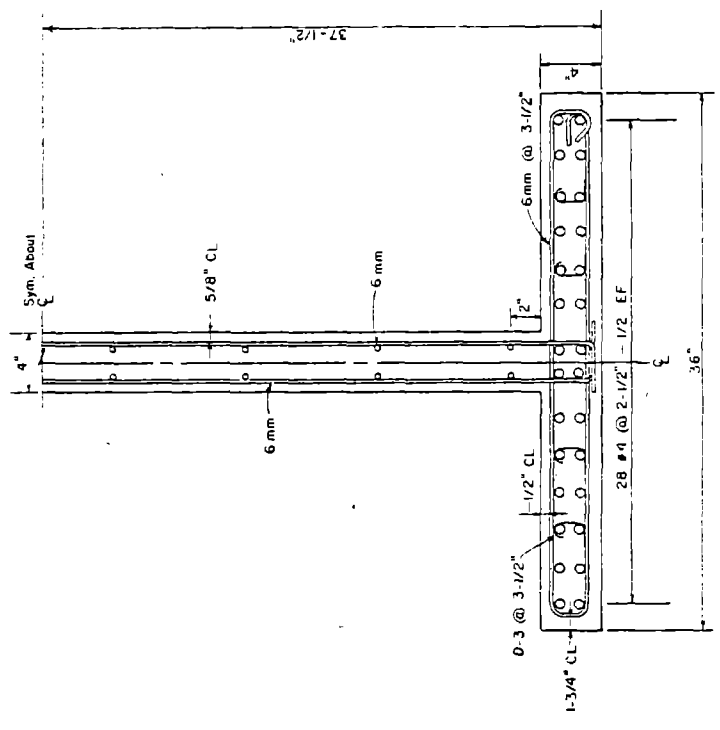
(b) Cross Section

(a) Elevation

Fig. A-9   Reinforcement for Specimen F1

A-11
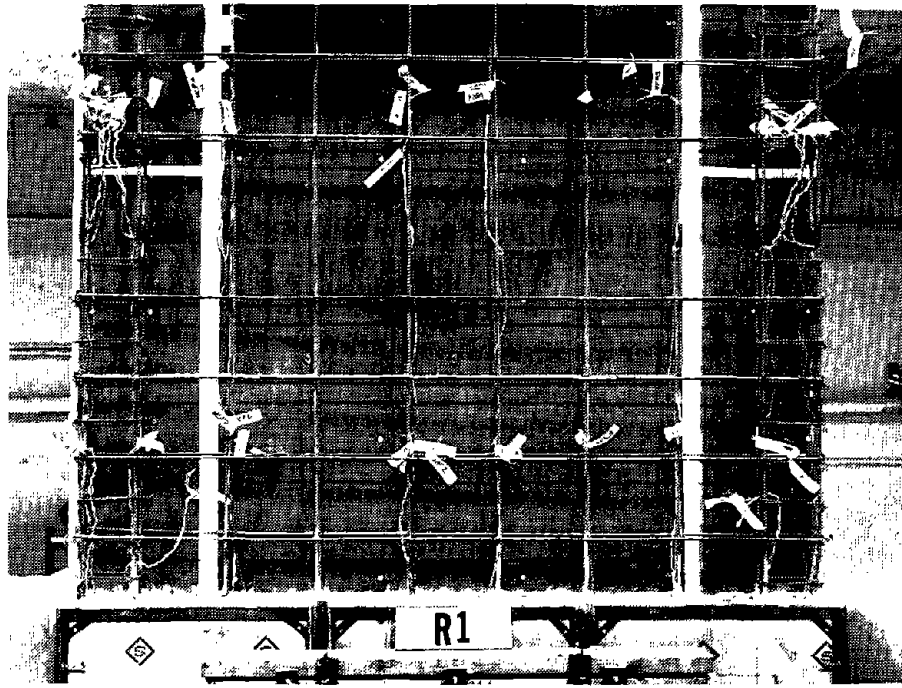
Fig. A-10   Reinforcing for Specimen R1
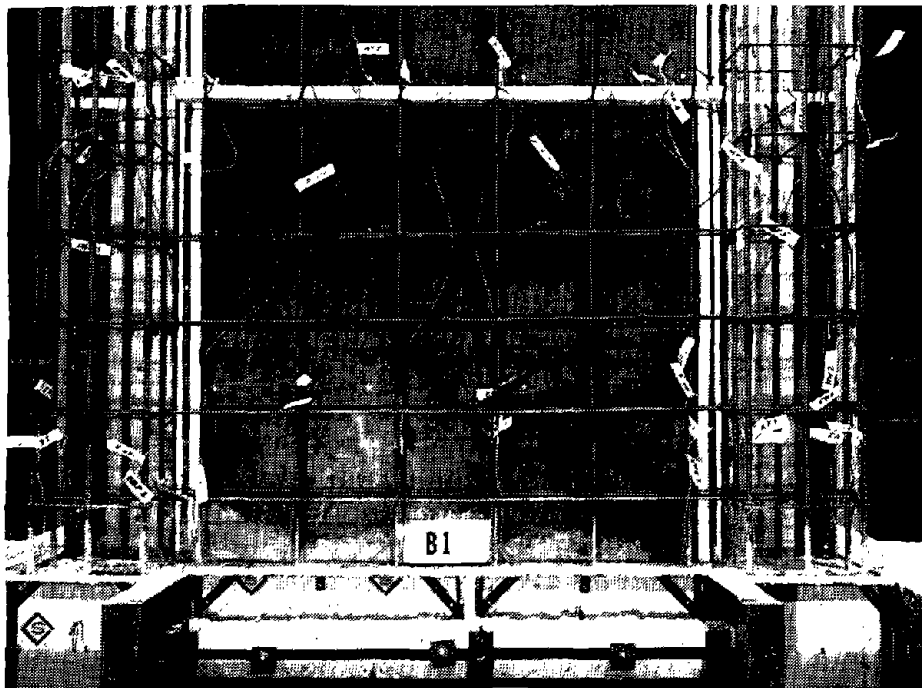
Fig. A-11   Reinforcing for Specimen B1
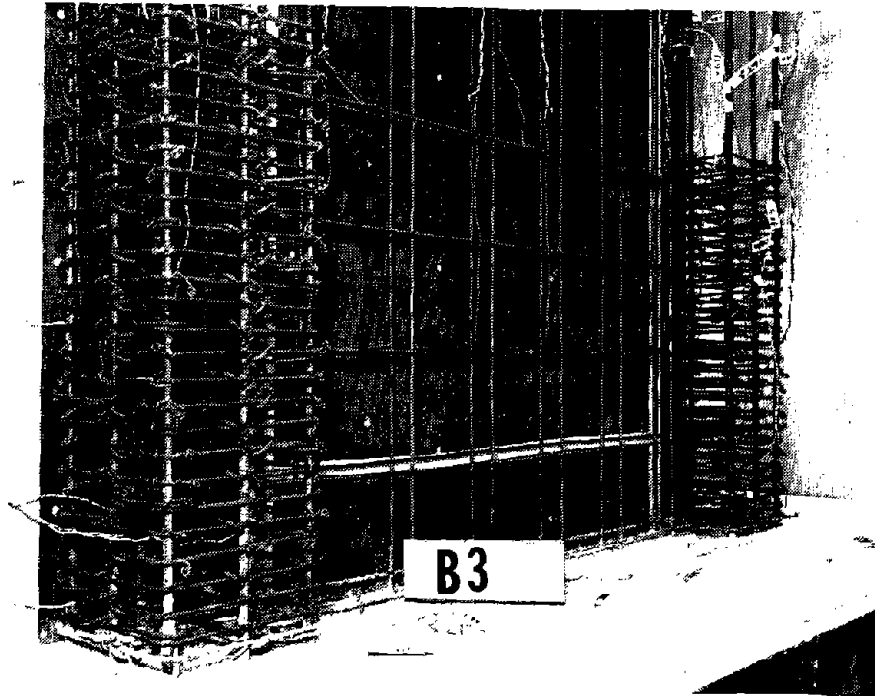
Fig. A-12   Reinforcing for Specimen B3

Fig. A-13   Reinforcing for Specimen B4
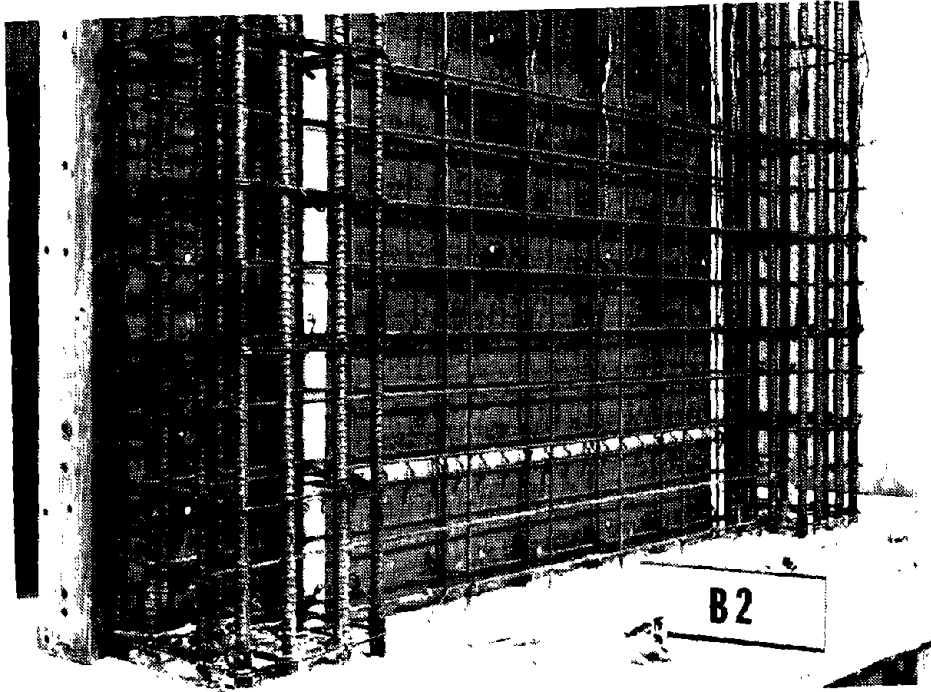
Fig. A-14   Reinforcing for Specimen B2
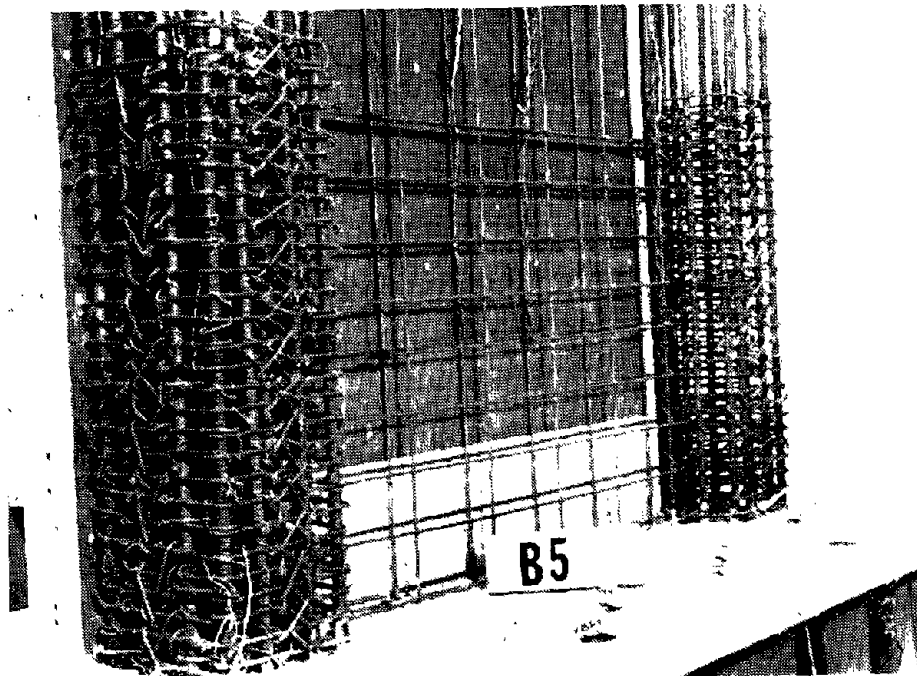
Fig. A-15   Reinforcing for Specimen B5
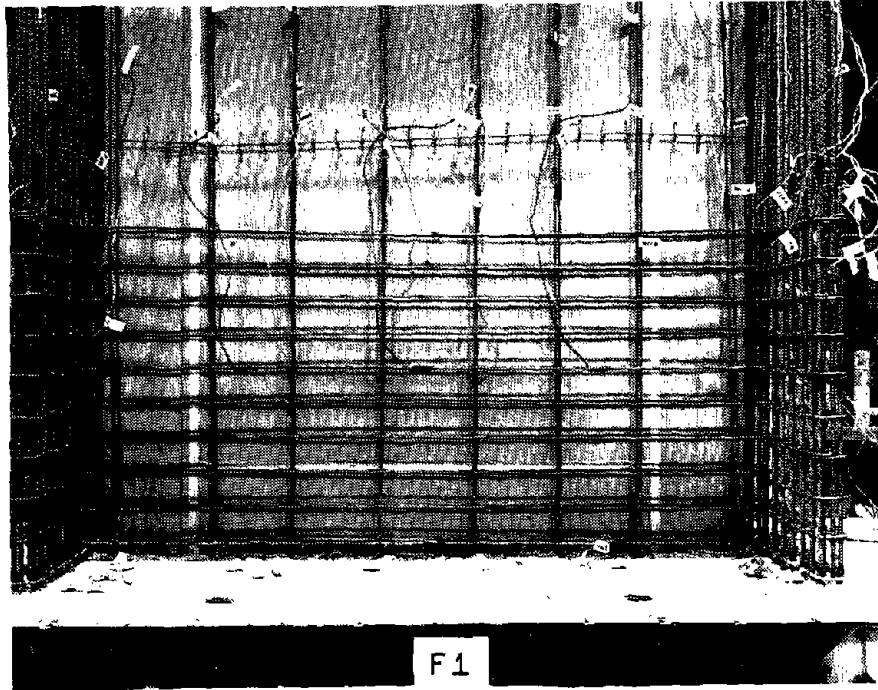
Fig. A-16   Reinforcing for Specimen F1

Confinement reinforcement was detailed according to Section A.6.4.3 of the 1971 ACI Building Code[5] for Specimens R2, B3 and B4. A ten bar diameter extension was used on all confinement steel hooks. Each end of the supplementary crossties had a semicircular hook.

This hoop and crosstie arrangement was found to be difficult to assemble. Each hoop and crosstie set had to be pre-assembled and then slipped over the vertical boundary element steel from the top of the specimen.

To eliminate this assembly problem the supplementary crossties for Specimen B5 were detailed with one 135° hook and one 90° hook as shown in Fig. A-8. This arrangement permitted placement of crossties after the hoop was in place around the vertical steel. Also, supplementary crossties parallel to the plane of the web were not provided at levels where the horizontal web steel tied into the columns. The unsupported length of the hoop used in the calculations for the volumetric ratio was the length from the perpendicular leg of the hoop to a point one-half way between the supplementary crossties.

Material Properties

Concrete. A concrete mix using a maximum aggregate size of 3/8 in. (9.5 mm) was selected for the walls. Type I cement, sand, and coarse aggregate were combined to provide concrete with a slump of 3 ± 1/2 in. (76.2 ± 12.7 mm). Aggregate gradation curves for the sand and coarse aggregate are given in Fig. A-17.
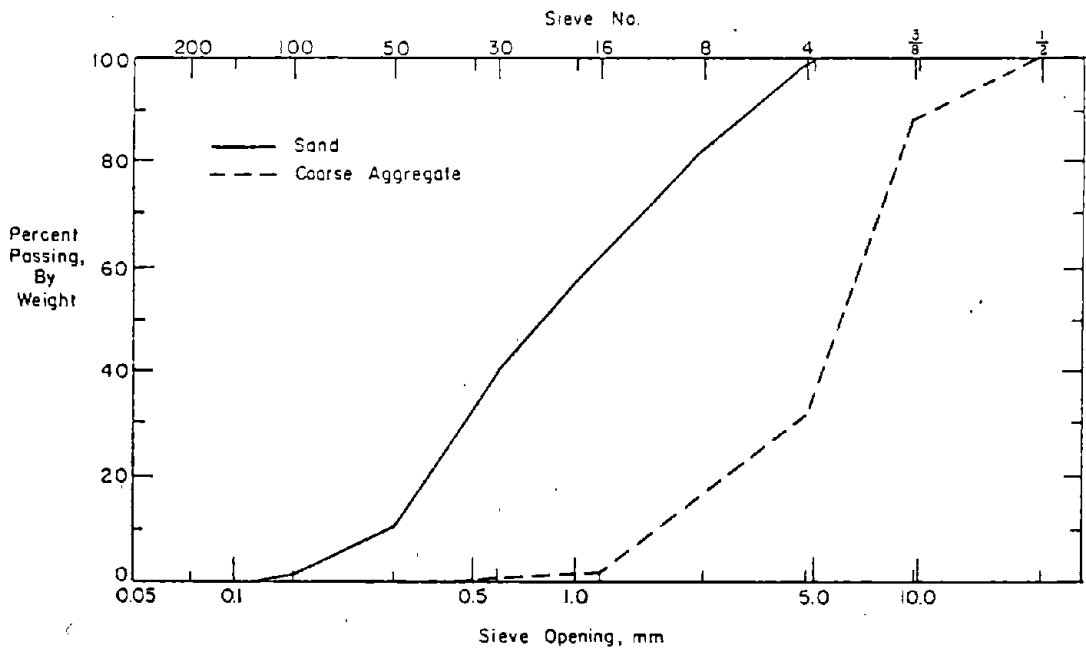
Fig. A-17 Aggregate Gradation Curve
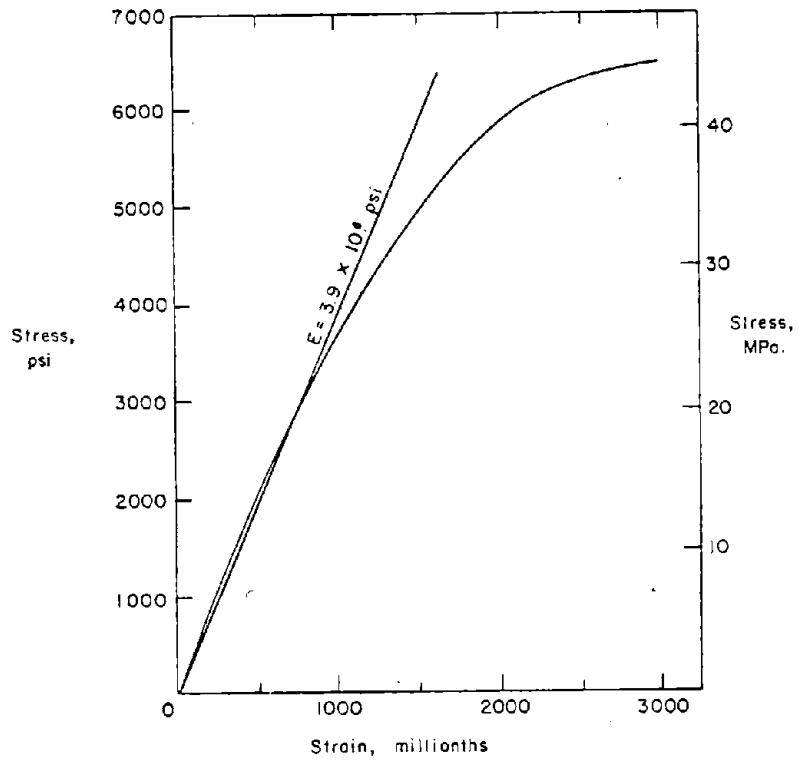
Fig. A-18 Stress versus Strain Relationship
For Concrete

Physical properties of the concrete used in each specimen are given in Table A-1. Compressive strength and modulus of elasticity of the concrete were determined from compressive tests on 6x12-in. (152x305 mm) cylinders. The modulus of rupture was determined from tests on 6x6x30-in. (152x152x762 mm) beams. A representative stress-strain relationship for the concrete is shown in Fig. A-18.

Reinforcement. In the specimens, No. 3, No. 4 and No. 6 bars conforming to ASTM Designation A615 Grade 60 were used as reinforcement. Deformed 6 mm hot rolled bars with properties similar to Grade 60 were also used. Deformed wire, size D-3, was used to represent smaller bar sizes. This wire was heat-treated to obtain stress-strain characteristics similar to those of Grade 60 bars.

The physical properties of the reinforcement used in the test specimens are summarized in Table A-2. Representative stress-strain relationships for the reinforcement are shown in Fig. A-19.

Construction

Test specimens were constructed in the vertical position. Figure A-20 shows Specimen B1 during construction. The formwork system shown in Fig. A-21 was designed to facilitate construction. Stationary formwork served to maintain the vertical position of the specimen. Each wall was cast in six lifts as shown in Fig. A-22.

At the start of construction, a heavy reinforcing cage for the base block was constructed. This cage was placed on

TABLE A-1 CONCRETE PROPERTIES FOR TEST SPECIMENS[1]

Specimen	Age At Test (days)	Compressive Strength f'_c (psi)[2]	Modulus of Rupture f_r (psi)	Modulus of Elasticity E_c (psi x 10^6)
R1	48	6490	655	4.03
R2	54	6735	650	3.89
B1	55	7685	730	4.08
B3	54	6860	635	3.96
B4	68	6530	680	4.10
B2	47	7775	710	4.20
B5	52	6570	625	3.97
B5R[3]	36	6205	525	4.01
F1	68	5575	635	3.69

(1) Average properties for lower 6 ft (1.83 m) of wall
(2) 1000 psi = 1.0 ksi = 6.895 MPa
(3) Average properties for replaced web concrete

TABLE A-2 REINFORCING BAR PROPERTIES FOR TEST SPECIMENS

Size	Properties	Specimen							
		R1	R2	B1	B3	B4	B2	B5	F1
D3*	f_y (ksi)	66.0	70.4	68.7	69.0	73.8	67.1	69.2	69.7
	f_{su} (ksi)	72.0	76.2	75.1	76.8	78.8	74.4	75.4	76.6
	E_s (psi x 10^6)	30.6	28.3	33.0	32.5	28.4	33.8	31.2	32.8
	Elong. (%)	5.9	11.1	11.0	8.9	10.8	9.4	10.1	10.3
6mm**	f_y (ksi)	75.7	77.6	75.5	69.4	73.2	77.2	72.8	76.2
	f_{su} (ksi)	101.5	100.2	100.8	95.5	98.8	101.6	97.4	102.2
	E_s (psi x 10^6)	31.4	32.6	32.5	30.4	31.9	32.1	31.4	31.3
	Elong. (%)	12.2	12.4	10.7	11.7	12.6	10.2	12.1	10.4
No. 3	f_y (ksi)	74.2	--	--	--	--	--	--	--
	f_{su} (ksi)	111.0	--	--	--	--	--	--	--
	E_s (psi x 10^6)	27.8	--	--	--	--	--	--	--
	Elong. (%)	9.8	--	--	--	--	--	--	--
No. 4	f_y (ksi)	--	65.3	65.2	63.5	65.3	--	--	64.5
	f_{su} (ksi)	--	102.7	102.7	101.0	102.5	--	--	102.6
	E_s (psi x 10^6)	--	26.9	28.3	25.9	27.5	--	--	28.1
	Elong. (%)	--	12.3	11.7	10.9	11.8	--	--	11.5
No. 6	f_y (ksi)	--	--	--	--	--	59.5	64.4	--
	f_{su} (ksi)	--	--	--	--	--	100.8	106.4	--
	E_s (psi x 10^6)	--	--	--	--	--	30.2	29.5	--
	Elong. (%)	--	--	--	--	--	13.3	13.2	--

*A = 0.03 sq.in. d_b = 0.195 in.

**A = 0.05 sq.in. d_b = 0.25 in.

1000 psi = 1.0 ksi = 6.895 MPa.
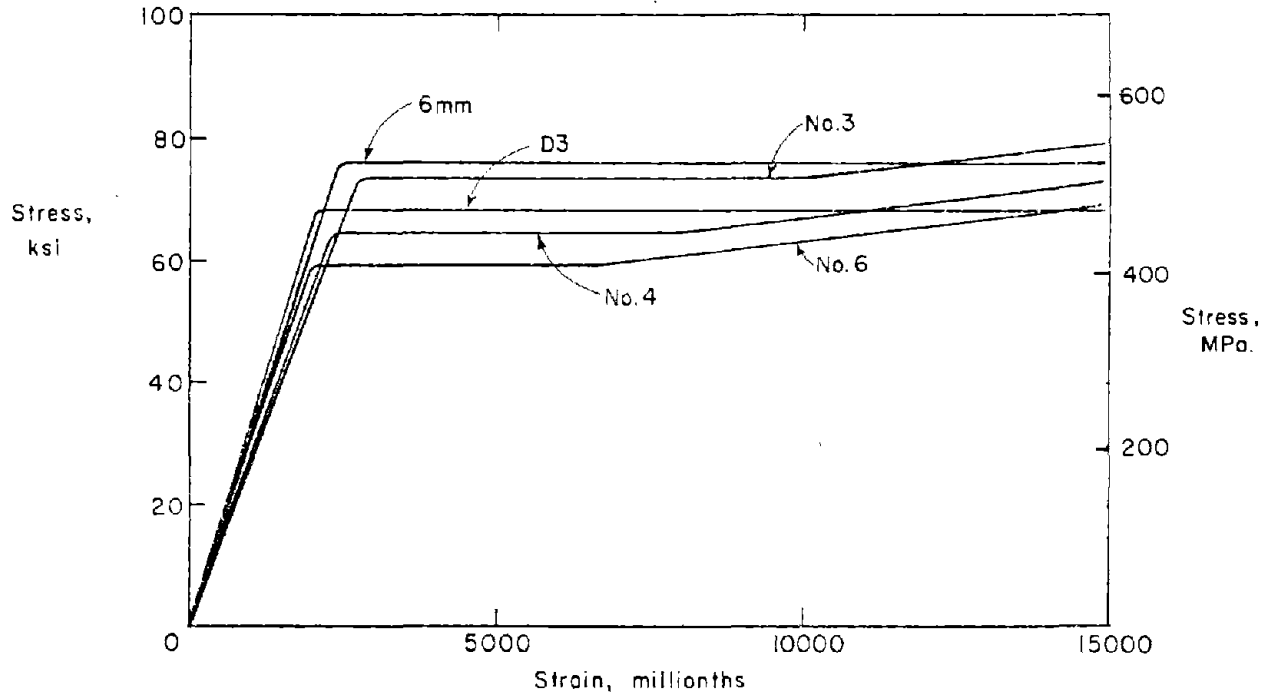
Fig. A-19 Stress Versus Strain Relationship
for Reinforcement
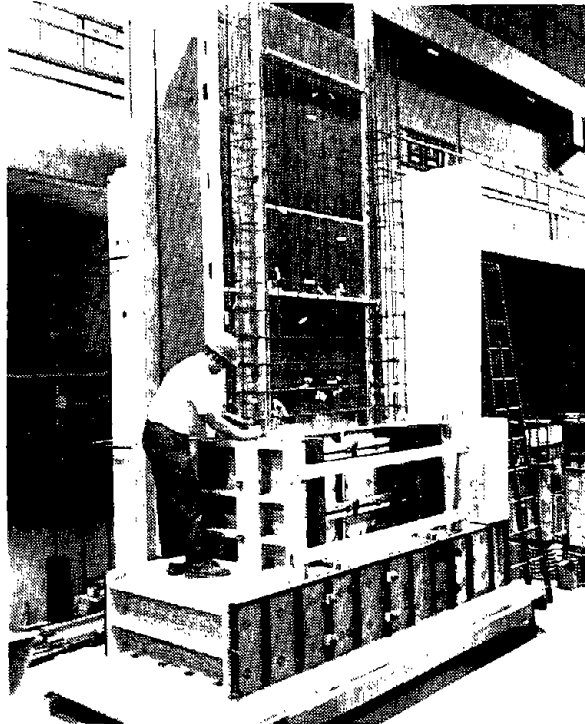
Fig. A-20 Specimen B1 During Construction
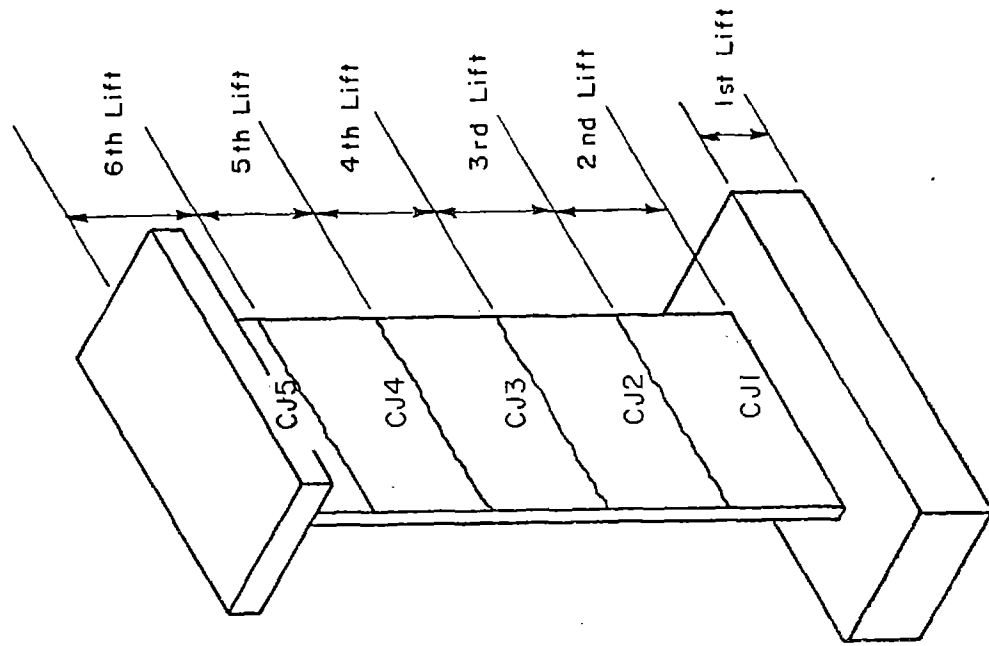
Fig. A-22 Lift Designations for Casting Test Specimens

6th Lift

5th Lift

4th Lift

3rd Lift

2nd Lift

1st Lift

CJ5

CJ4

CJ3

CJ2

CJI

Stationary Formwork

Spine Slab

Hinged Base

Wall Specimen

Removable Formwork

Jack
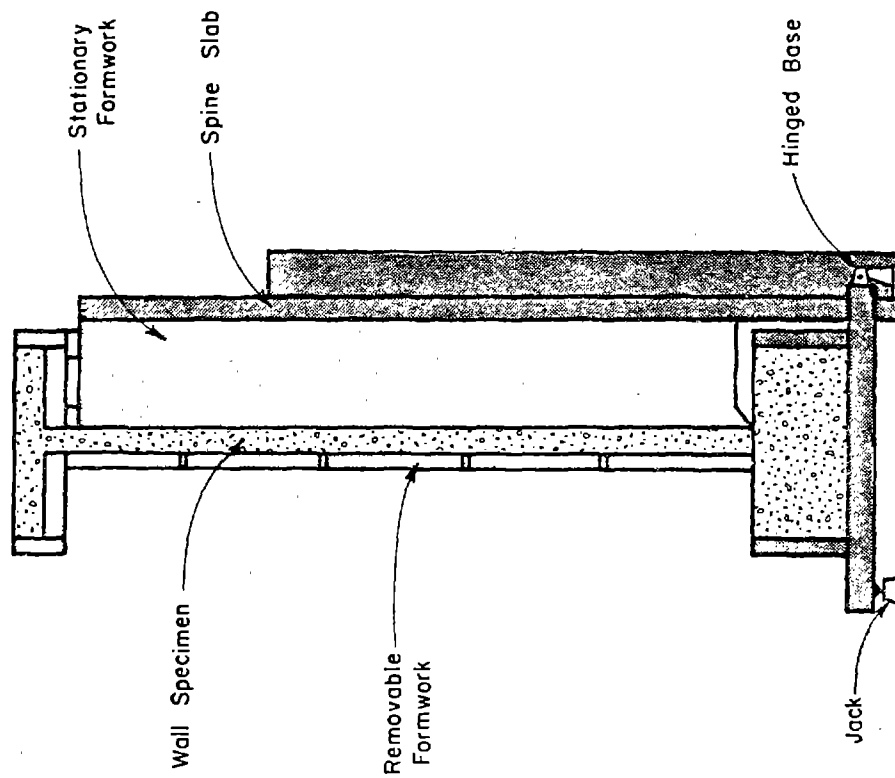
Fig. A-21 Formwork System for Casting Test Specimens

the level base platform of the formwork. The vertical wall reinforcement was then placed in the base cage and supported against the stationary formwork. After the vertical rein- forcement was secured, the base block was cast. This casting was designated Lift 1.

Following casting of the base block, the construction joint was prepared and the horizontal reinforcement for Lift 2 was placed. Then the removable formwork for Lift 2 was set, and Lift 2 was cast. Subsequent wall lifts were con- structed in the same manner. The wall lifts were 36 in. (0.91 m) in height.

Construction joints between lifts were made following standard practice.[15] The surface of the concrete was roughened with a cold chisel, and cleaned of laitance and loose particles prior to placing adjoining concrete. The construction joints are designated CJ1 through CJ5 as shown in Fig. A-22.

The sixth lift was cast in two segments. First, the wall segment was cast in the morning, then the slab segment was cast in the afternoon. The delay between segments was to avoid problems caused by plastic skrinkage.

Approximately two days after casting the sixth lift, the removable formwork was stripped. Following this opera- tion, a special lifting rig was placed on the specimen. This rig allowed the specimen to be lifted through rods attached to the base block. Prior to lifting, the base platform of the formwork was rotated to tilt the specimen away from the stationary formwork; thus essentially stripping

the specimen from the stationary form. The specimen could then be lifted away from the stationary formwork and placed in position on the test floor.

Repaired Specimen

As shown in Fig. A-23, the web of Specimen B5 was considerably damaged after completion of testing. However, the columns were in very good condition. The outer shell had spalled off the lower 3 to 6 in. (76.2 to 152.4 mm) of the compression face of the columns, but the confined cores were intact. The maximum measured crack widths in the columns during testing were 0.075 in. (1.91 mm) on the tension side and 0.023 in. (0.58 mm) on the compression side at peak lateral load. After completion of the test, the average increase in vertical length of the lower 3 ft of wall was 0.49 in. (12.5 mm). The average increase in vertical length of the second 3 ft (0.91 m) of wall was 0.42 in. (10.7 mm). No reinforcing steel had fractured or buckled. It was decided that this specimen could be repaired and retested.

Repair procedures were chosen to provide the simplest and least expensive repair that would restore reasonable strength and ductility to the wall.

As shown in Fig. A-24, the web concrete was removed up to the 8 ft 6 in. (2.6 m) level. The reinforcing steel was left intact. No new steel was added. The columns were rubbed with a soap stone to remove loose particles. The web to base block and web to column joint surfaces were roughened to remove any loose material.
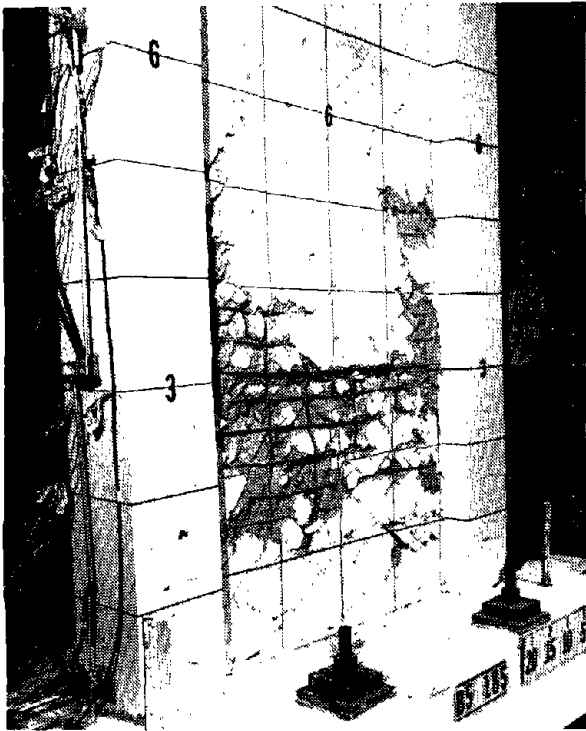
Fig. A-23 Specimen B5 After
Lateral Load Test
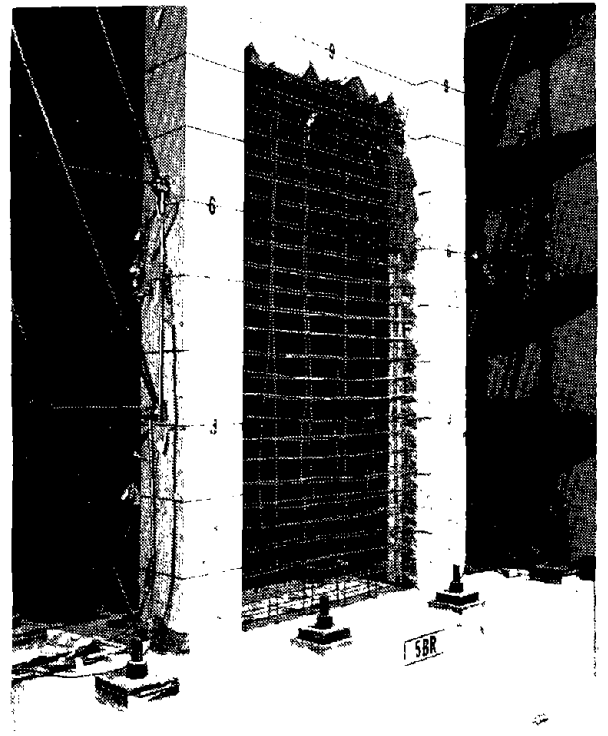
Fig. A-24 Specimen B5R With
Web Concrete Removed
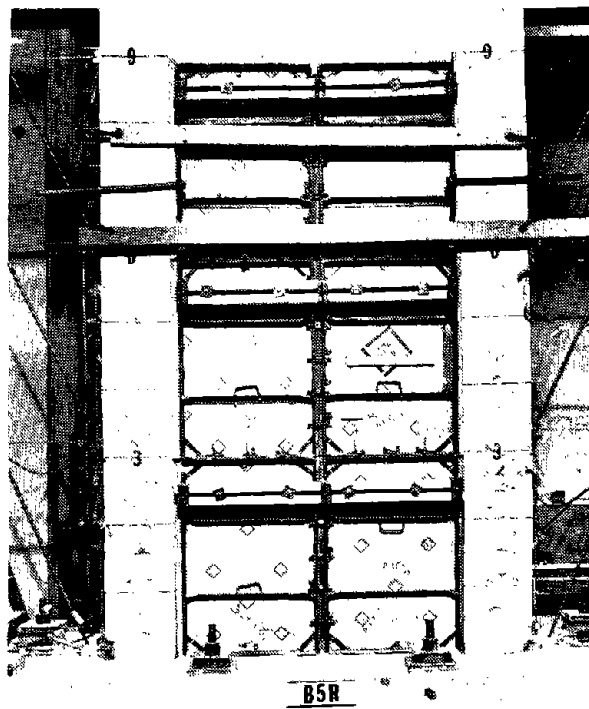
Fig. A-25 Formwork for New Web Concrete

A-25

New web concrete was cast in 3 ft (0.91 m) lifts. The formwork for the web is shown in Fig. A-25. The last several inches near the top joint were hand packed with a stiff mix from one side of the wall. After the forms were stripped, this joint was hand rubbed with a sand-cement mortar.

Although tapping with a hammer indicated that the shell of the columns was loose in several areas, this concrete was not removed. Only the areas shown in Fig. A-26 and Fig. A-27 at the base of the column where the outer shell had crushed were repaired. These areas were roughened to remove loose particles and then a stiff sand-cement mortar was hand packed into place. The remaining areas of the columns were given a cosmetic repair by hand rubbing a neat cement paste over the surface of the cracks.

Figure A-28 shows the Specimen B5R after completion of the repairs.

Lateral Load Test Setup

Loading System

The apparatus for testing the walls is shown in Fig. A-29. A photograph of test set up is shown in Fig. A-30.

Each test specimen was post-tensioned to the floor using eight 1-3/8 in. (34.9 mm) diameter Stressteel bars.

Loads were applied to the specimen as a vertical canti-lever with concentrated forces at the top. Hydraulic rams on each side of the specimen alternately applied force to first one side then the other side of the top slab. Reactions
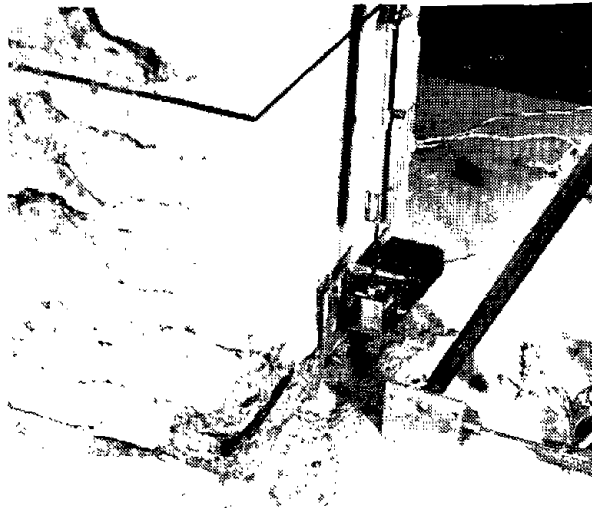
Fig. A-26   Base of Left Column   Fig. A-27   Base of Left Column
            Prior to Repairs   After Repairs

Fig. A-28   Specimen B5R After Completion
            of Repairs

A-27
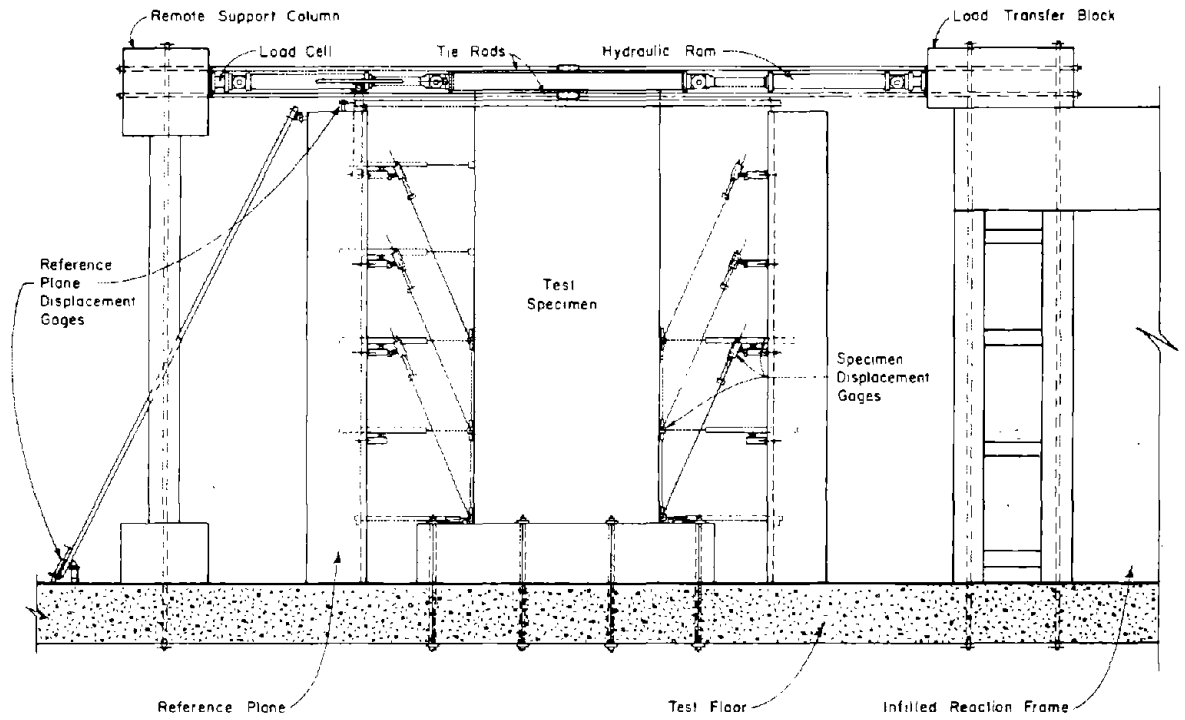
Fig. A-29   Test Apparatus
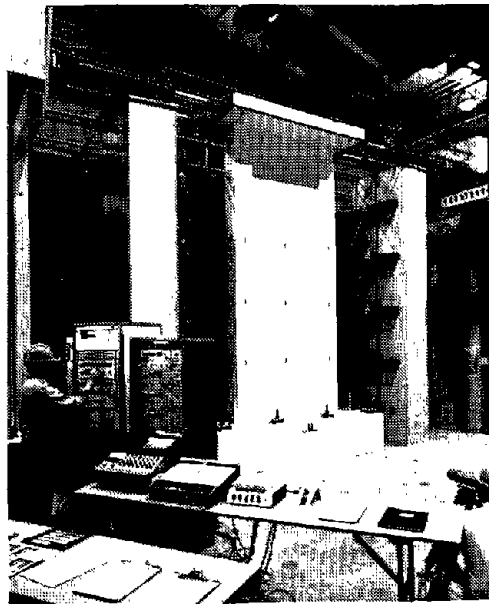
Fig. A-30   Isolated Wall Testing Arrangement

A-28

from the applied loads were transferred to the test floor
through a large infilled reaction frame. This load transfer
occurred directly when the rams closest to the reaction
frame were activated, and indirectly through the remote
support column and tie rods, when the rams farthest from the
reaction frame were activated. A system of one or two rams
on each side of the specimen was used depending on the
anticipated capacity of each specimen. The hydraulic rams
have a capacity of 200 kips (890 kN) and a stroke of 36 in.
(0.91 m). At each end of the ram, a clevis bracket and pin
arrangement formed a link assembly.

Instrumentation

Loads. During each test, the applied lateral load was
measured and recorded by two methods. In the first method,
a load cell was attached to one end of each ram. The load
cell readings were recorded as discrete points at each load
stage during testing. In the second method, pressure cells
were attached to the two hydraulic pressure lines for each
set of rams. A continuous plot of the pressure cell read-
ings versus the top wall deflection was made during testing.

External Instrumentation. A system of external gages
as shown in Fig. A-31 was attached to each specimen.

These gages were mounted on independent reference
planes on each side of the specimen. They were used to
determine deflections, rotations, shear distortions, and
reference plane movement. In addition, 3 dial gages were
mounted on the specimen to determine slip at construction
joints.
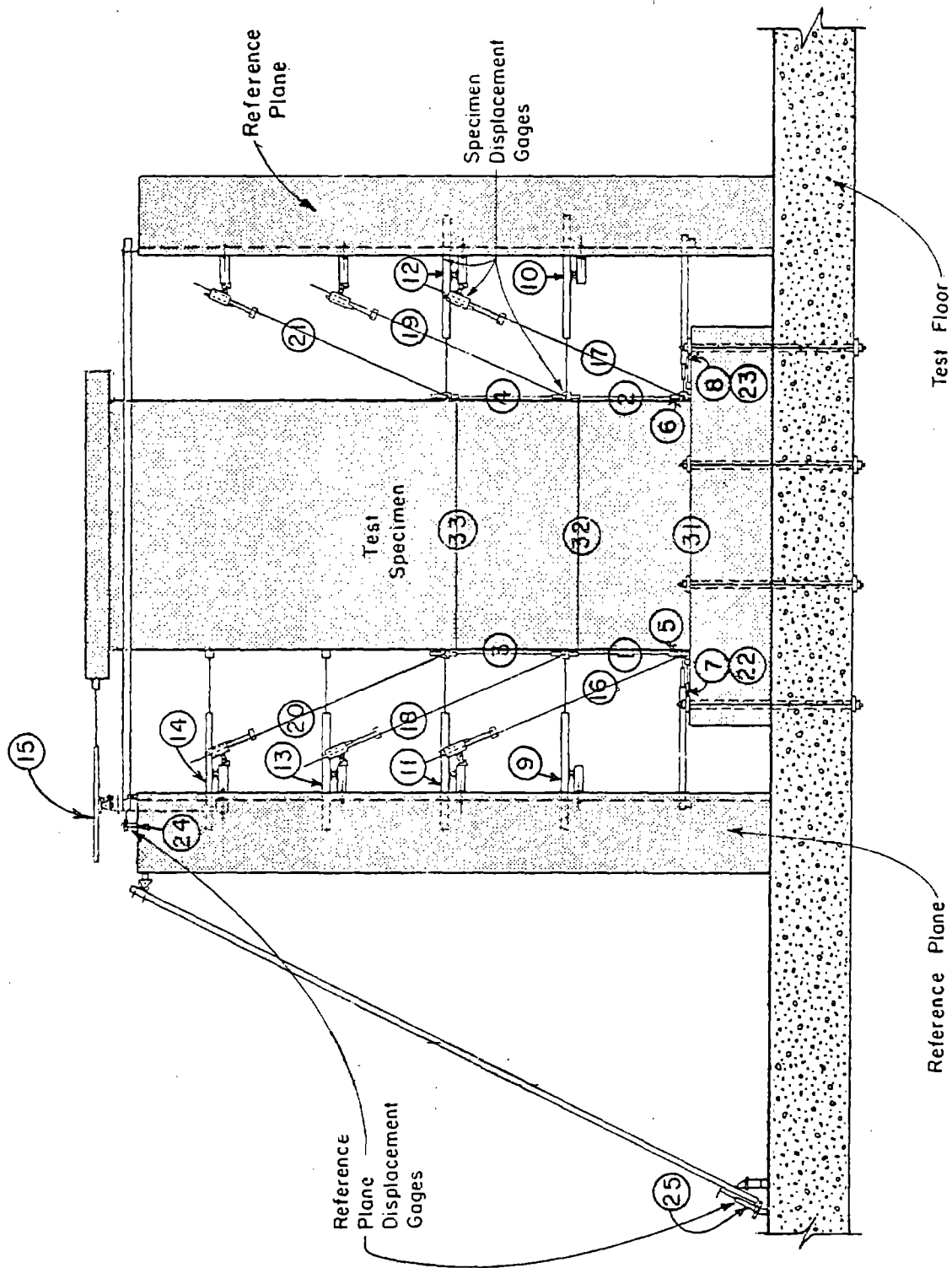
Fig. A-31 External Gages

All horizontal and vertical displacement measurements were made using linear potentiometers and direct current differential transducers (DCDT's). These gages have resolutions from 0.001 in. to 0.003 in. (0.025 mm to 0.076 mm).

Horizontal Displacements. Horizontal displacements are measured at seven levels as shown on Fig. A-31. Gages 7 and 8 measured horizontal movement of the base block. Gages 22, 23, and 9 through 15 measured horizontal movement of the wall. For the lower three levels, measurements were made at each end of the wall.

Rotations. Rotations were measured at four levels on the specimen. The first was the rotation of the top of the base block. This rotation was obtained using triangulation calculations from the output of Gages 7 and 16, and Gages 8 and 17.

Rotations in the lower 6 ft (1.83 m) of the wall were obtained by measuring vertical displacements along each end of the wall. Three sets of measurements were made. The first set was made using Gages 5 and 6 between the top of the base block and the bottom of the wall over a nominal gage length of 3 in. (76.2 mm). The other two sets of measurements were made over nominal gage lengths of 36 in. (0.91 m) using Gages 1 and 2, and Gages 3 and 4. An independent check on the output of Gages 1, 2, 3 and 4 was obtained using triangulation calculations from the output of Gages 9 and 18, 10 and 19, 11 and 20, and Gages 12 and 21.

Movement of the reference planes was monitored using Gages 24 and 25 as shown in Fig. A-31. Gage 24 measured the relative horizontal movement between the tops of the reference planes.

Shear Distortions. An indication of shear distortions was obtained over two zones in the lower 6 ft (1.83 m) of the wall. The first zone was from the top of the base block to the 3 ft (0.91 m) level. The second zone was from the 3 ft level to the 6 ft level.

The horizontal and vertical movement of Points A through F in Fig. A-32 were determined from the displacement gages previously described. From this data, the changes in length of the diagonals d_1 through d_4 were calculated.

It can be seen in Fig. A-33a that the length of the diagonals does not change in an element subjected to pure flexure. Also, as shown in Fig. A-33b, the length change of diagonals is equal and in the same direction for each diagonal in vertical or lateral expansion. For shear distortions, however, the change in length of the diagonals is in opposite directions. As shown in Fig. A-34, their change in length can be related to shear distortions by:

$$\gamma_{avg} = \frac{\gamma_R + \gamma_L}{2} = \frac{\delta_1 d_1 - \delta_2 d_2}{2hl} \qquad (A-1)$$

Shear distortions calculated as described above cannot be considered exact values in a reinforced concrete element. Because of cracking, plane sections not remaining plane, and the existence of a moment gradient across the element, these shear distortions can only be considered as approximate values.

A-32
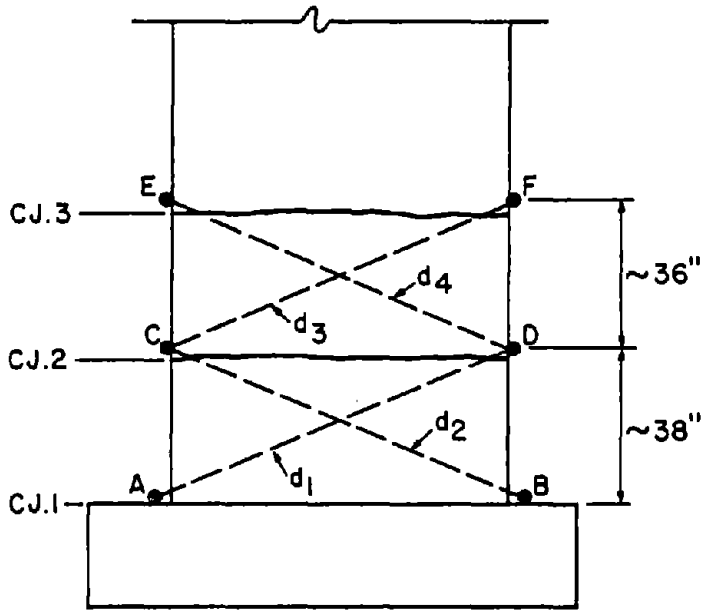
Fig. A-32   Points Measured for
             Shear Distortions

a) Flexure

$d = d'$

b) Expansion

$d_1 = d_2$
$d'_1 = d'_2$
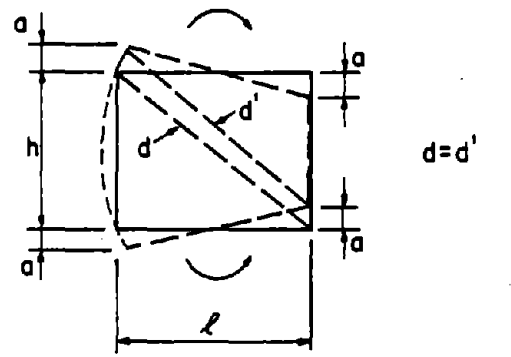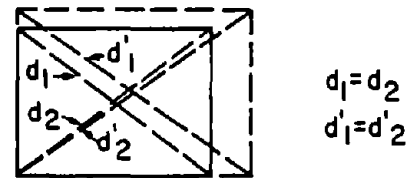
Fig. A-33   Length of Diagonal
             in Element
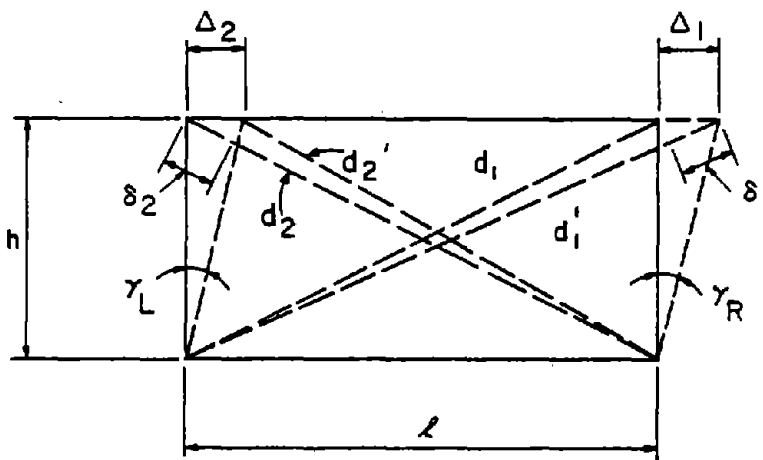
Fig. A-34   Calculation of Shear Distortions

$$\gamma_R = \frac{\Delta_1}{h} \quad , \quad \gamma_L = \frac{\Delta_2}{h}$$

$$\gamma_{Avg.} = \frac{\Delta_1 + \Delta_2}{2h}$$

$$\frac{\Delta_1}{\delta_1} = \frac{d_1}{\ell} \quad , \quad \frac{\Delta_2}{-\delta_2} = \frac{d_2}{\ell}$$

$$\therefore \quad \gamma_{Avg.} = \frac{\delta_1 d_1 - \delta_2 d_2}{2h\ell}$$

As can be seen in Fig. A-32, the shear distortions measured in the lower 3 ft (0.91 m) zone include the slip at construction joints CJ1 and CJ2. The shear distortions in the upper 3 ft zone include the slip at construction joint CJ3.

Slip at Construction Joints. Dial gages 31, 32 and 33 as shown in Fig. A-31 were used to measure relative slip at construction joints CJ1, CJ2 and CJ3. These gages have a sensitivity of 0.001 in. (.025 mm).

Crack Widths. Crack widths were measured during testing across selected cracks in the lower 6 ft (1.83 m) of the web and boundary elements. These measurements were obtained using a hand microscope containing a scale with gradations of 0.001 in. (0.025 mm).

Internal Instrumentation. Strain gages were placed on both vertical and horizontal reinforcement. The basic strain gage layout is shown in Figs. A-35 and A-36. In addition, strains were measured on several of the hoops and supplementary crossties of the confinement reinforcement of Specimens B3, B4 and B5.

Recording Equipment. Output from load cells, potentio-meters, DCDT's and strain gages was recorded as discrete points at each load stage using a VIDAR Digital Data Aquisition System.

Raw test data for Specimens R1, R2, B1, B2, B3 and F1 was stored on printed and punched paper tape. The data was transferred from punched paper tape to disc storage to

Gaged Vertical Bar

Gaged Horizontal Bar

(a) Specimen FI

(b) Specimen BI, B3 & B4

(c) Specimen B2 & B5

(d) Specimen RI & R2

Fig. A-36 Strain Gage Locations In Cross Section of Test Specimens

1 in. = 25.4 mm.

36"   36"   18"   18"   18"   18"   1"

Horizontal Bar Strain Gage

Vertical Bar Strain Gage

⑦ ⑥ ⑤ ④ ③ ② ①
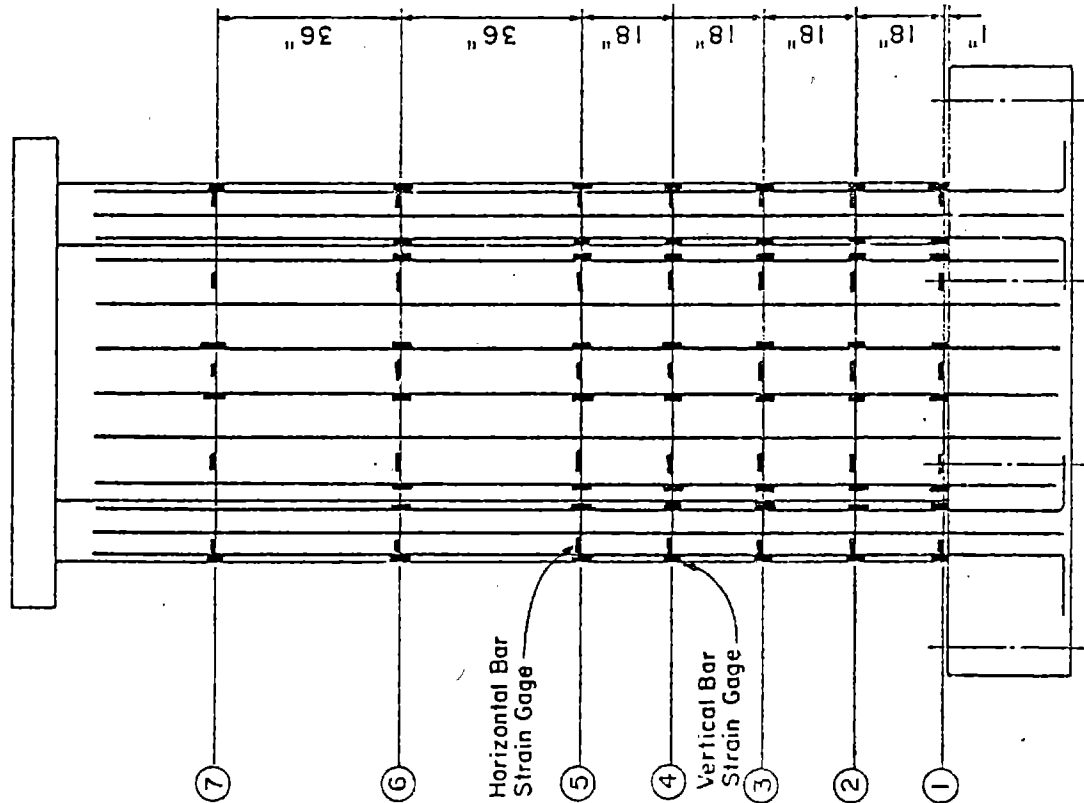
Fig. A-35 Strain Gage Locations in Elevation of Test Specimens

A-35

facilitate reduction using a Meta 4 Digital Computer.
Reduced data was then transferred to magnetic tape cassette
storage for analysis using an HP9830 calculator.

Raw test data for Specimens B4, B5 and B5R was stored
on printed tape and transferred from the VIDAR directly into
an HP9830 calculator for immediate reduction. Reduced data
was then stored on magnetic tape cassettes for later analysis.

Data from the construction joint slip gages and crack
width measurements were hand recorded.

Photographic Equipment. A complete photographic record
was kept for each test. Color slides and black and white
photographs were taken at selected load stages throughout
the testing. In addition, three time-lapse movie cameras
running at one frame per second recorded each cycle of
loading.

Test Procedures

Loading. A loading increment consists of three complete,
reversed cycles at a specific maximum load or deflection.
The second and third cycles were used as a measure of
stability of the specimen performance within a loading
increment.

The specimens were initially loaded in equally increasing
force increments. The increments were determined by dividing
the calculated yield load by three or four so that the first
increment was below the cracking load. After the first
cracking increment was applied, a reduced load increment

equal to the pre-cracking load was applied again. The force
increments were then increased until the yield level was
reached.

Subsequent to yielding, loading was controlled by
increasing deflection increments. The deflection was con-
trolled by manually closing a value in the hydraulic pres-
sure line when the desired deflection was reached. Within
the post yield loading sequence, a reduced load increment
was applied. Deflection increments were increased until
extensive damage was produced and the load capacity was con-
siderably reduced.

Data Recording. Each point at which a VIDAR reading
was taken is termed a load stage. Several load stages were
used in the first cycle of each load increment. A sufficient
number were used in the first cycle to reasonably define the
load versus displacement loops with discrete points. In the
second and third cycles of each increment, load stages occur
only at the zero and peak loading points.

Free Vibration Test Methods

Free vibration tests were conducted at selected stages
as the number and magnitude of the reversed lateral load
cycles applied to the specimen were increased. These tests
were carried out to determine the frequency and damping
characteristics of the specimens.

Tests were performed using two methods. In the first,
specimens were tested using an "initial displacement-sudden
release" method. The force used to displace the wall was
lower than the calculated cracking load. In the second,

small amplitude tests were performed using the impact force of an 8 lb. (3.63 kg) hammer to initiate vibrations. Plots of displacement of the top of the wall versus time were used to compute the natural frequency and logarithmic decrement. The damping coefficient was calculated from the logarithmic decrement.

APPENDIX B - TEST RESULTS

Introduction

In this section the methods used for analysis and presentation of the data from the tests are described in general. The results from each lateral load test are then presented in detail. The specimen behavior during testing is described and the resulting data is presented and discussed. The results of the free vibration tests are not presented separately for each specimen but are summarized at the end of this appendix.

Data Presentation and Analysis

Loading History

Loads and deflections applied to each specimen are plotted versus cycle number. First yield and full yield loads and deflections are indicated on these figures.

First yield load is defined as the first load at which a yield strain was measured in the boundary element tensile reinforcement. It was determined by monitoring specific strain gages during loading.

Full yield load is defined as the load at which all of the main tensile reinforcement in the boundary element had yielded. It was determined from interpolation between measured strains at load stages before and after full yield.

In the specimen loading history, an inelastic cycle is defined as a complete reversed load cycle during which both the load and deflection exceeded the first yield level.

Load-Deflection Relationships

Two continuous load-deflection figures are presented for each test. The first figure shows the initial cycles with first cracking indicated. The second figure shows the cycles for the entire test. Included in these figures are indications of yield loads and failure modes. This is the only figure for each specimen that includes all loading cycles for the specimen. Other load-deformation type figures show only the first cycle of each loading increment. These cycles are numbered on the figures.

Moment-Rotation Relationships

Reversing Load. The reversing moment-rotation data are shown for each specimen at three levels. These are the base level, the 3-ft (0.91 m) level and the 6-ft (1.83 m) level. The fixed body rotation at the top of the base block is subtracted out of the data used for these figures. However, rotations due to slip of the flexural steel anchored within the base block are included in the rotations. The moment plotted in all cases is the moment at the base level.

Monotonic Load. One of the objectives of the experimental program was to compare the behavior of specimens subjected to reversing load with the behavior under monotonic loading. To partially accomplish this, Specimen B4 was constructed similar to Specimen B3 and tested with monotonic loading. Specimen B4 was also similar to Specimen B1, with the exception that B1 did not have confinement reinforcement

in the boundary elements. Therefore, the results for Specimen B4 are included on all plots for Specimens B1 and B3.

Since cost and time prohibited a monotonic test for each of the other types of specimens, a calculated moment-rotation relationship was used to extend the reversed loading versus monotonic loading comparison to other specimens.

To obtain the calculated moment-rotation relationship, a computer analysis of each cross section was performed to obtain a moment-curvature relationship.[16] Analysis of sections was based on satisfying applicable conditions of equilibrium and strain compatibility. A linear distribution of strain over the section was assumed. Measured material properties were used. The analysis considered complete stress-strain relationships for concrete and steel, including strain hardening of the reinforcement and the effect of confinement in the concrete compression block. The Kent and Park[17] relationship was used for the confined concrete stress-strain relationship.

The maximum calculated curvature was determined by either concrete crushing or reinforcing steel fracture. For unconfined concrete, the limiting concrete strain, ε_u, at the compression face was taken as $\varepsilon_u = 0.004$. For confined concrete, the limiting strain for the compression face was determined from an expression developed by W. G. Corley.[18,19]

$$\varepsilon_u = 0.003 + \left(\frac{\rho_s f_y}{15}\right)^2 \tag{B-1}$$

where: ρ_s = the volumetric ratio of confinement reinforcement

f_y = the yield stress of confinement reinforcement in ksi.

Fracture of the reinforcing steel was assumed to occur at a strain equivalent to the measured elongation from reinforcement tension tests.

In reinforced concrete flexural members, inelastic curvature spreads over a hinge length, ℓ_p. Therefore, the theoretical curvature distribution corresponding to the actual moment distribution is not accurate. An effective curvature distribution must be determined. Rotations at a specific level can then be calculated by integrating the effective curvature distribution over the length involved.

Two different methods were used to determine an effective curvature distribution. One method shown in Fig. B-1 was used to include the effect of diagonal shear cracking on the spread of the hinging region. It was used for specimens B1, B2, B3, B4, B5 and F1. A hinge length, ℓ_p, was determined visually from the crack pattern of each specimen. This was the height at which the steepest diagonal crack extending from the base compression zone intercepted the centroid of the tension boundary element as shown in Fig. B-1. Based on equilibrium of the forces in the hinge region, Bachmann[20,21] presented a relationship for determining force in the tensile reinforcement. Using this relationship, the effective moment for flexural steel tension is:
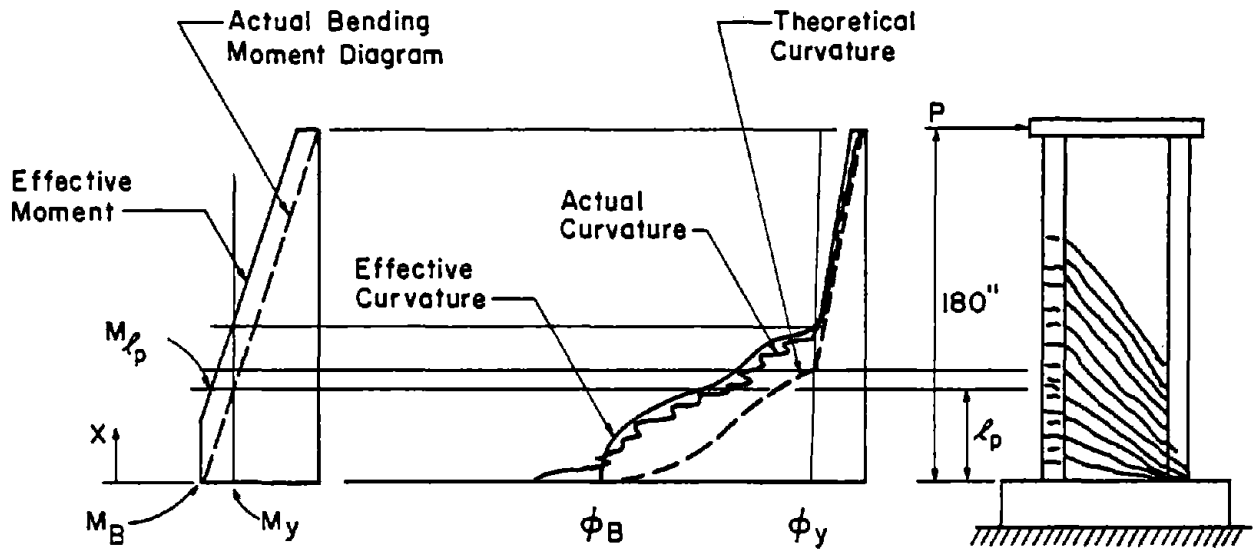
Fig. B-1   Curvature Distribution for Specimens
With Inclined Cracking
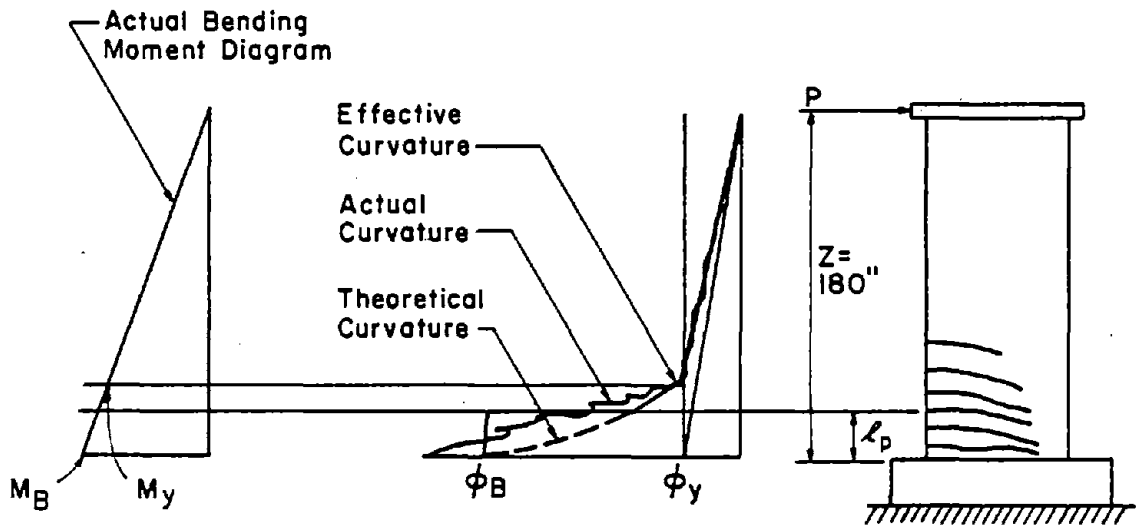
Fig. B-2   Curvature Distribution for Specimens
With Predominantly Flexural Cracking

B-5

For $0 < X \leq \ell_p$

$$M_x = M_B - \frac{x^2 \eta P}{2d} \qquad \text{(B-2)}$$

For $\ell_p < X < 180$ in.

$$M_x = M_{\ell_p} - P(x - \ell_p) \qquad \text{(B-3)}$$

Where: M_B = Moment at the base

M_x = Effective moment at a distance X from the base

M_{ℓ_p} = Effective moment at ℓ_p from the base

$$= M_B - \frac{(\ell_p)^2 \eta P}{2d}$$

P = Total lateral load

η = V_s/P

V_s = Lateral load taken by stirrups across a
      45 degree crack.

The calculated curvature related to this effective moment distribution was used to calculate rotations at each level.

A second method was used for specimens with predominately flexural cracking. This was used for specimens R1 and R2. A hinge length ℓ_p was determined from Mattock's[22] equation:

$$\ell_p = 0.5d + 0.05Z \qquad \text{(B-4)}$$

Where: d = effective depth

Z = distance along the span from section of maximum
      moment to adjacent section of zero moment.

After the yield moment was reached at the base, the effective curvature distribution shown in Fig. B-2 was used to calculate rotations.

The rotation calculations described above were performed only to obtain an estimate of monotonic rotation behavior. In both methods, no attempt was made to include the effects of bond slip and variation of steel strain between cracks. In the method used for diagonally cracked specimens, only the tensile strains are directly related to the effective moment distribution and plane sections do not remain plane. The calculated curvature is only approximately related to the effective moment at a section. Therefore, the calculated monotonic rotations should only be considered approximate values. However, the calculated monotonic strengths should be accurate estimates.

The calculated monotonic rotations for Specimen B4 are compared with the measured rotations in Fig. B-3.

The calculated maximum strength of 74.3 kips (330.5 kN) is in very close agreement with the measured, strength of 75.3 kips (334.9 kN).

The calculated rotation at the base level is considerably lower than the measured. This is as expected since a major portion of the measured rotation at the base is due to the steel strain within the base block. This would be true in all test specimens. Therefore, no further attempt was made to compare calculated and measured rotations at the base level.

Calculated rotations at the 3-ft (0.91 m) and 6-ft (1.83 m) level overestimate the measured rotations. This is the direction of error to be expected considering the assumptions made in the calculations. However, the calculated

a) At 6 ft. Level

b) At 3 ft. Level

c) At Base Level
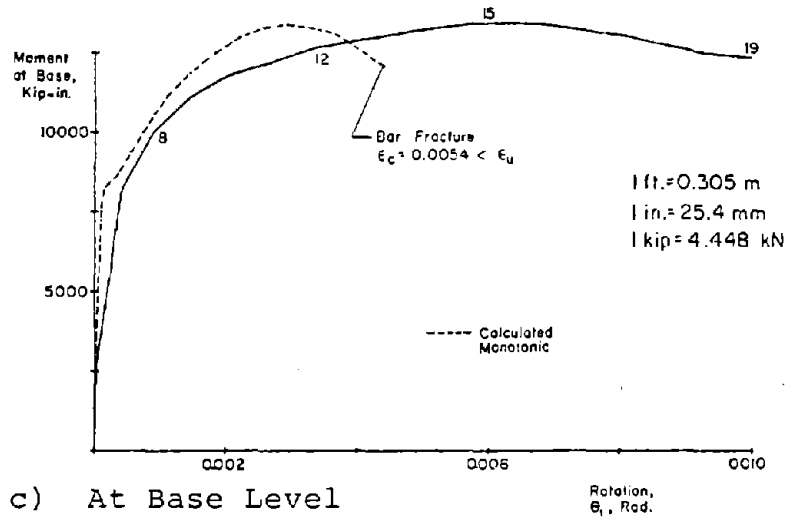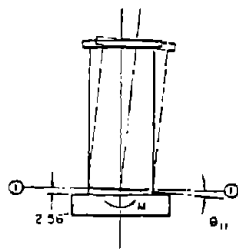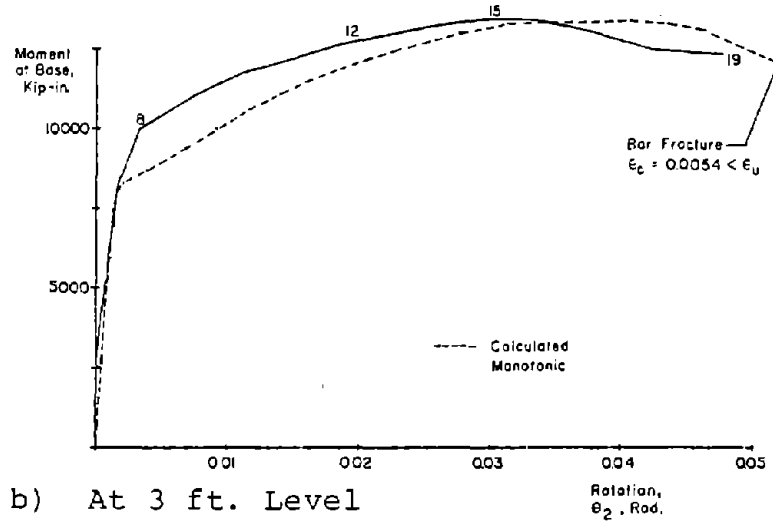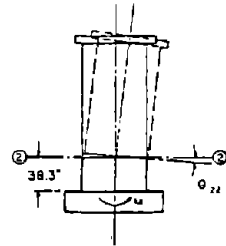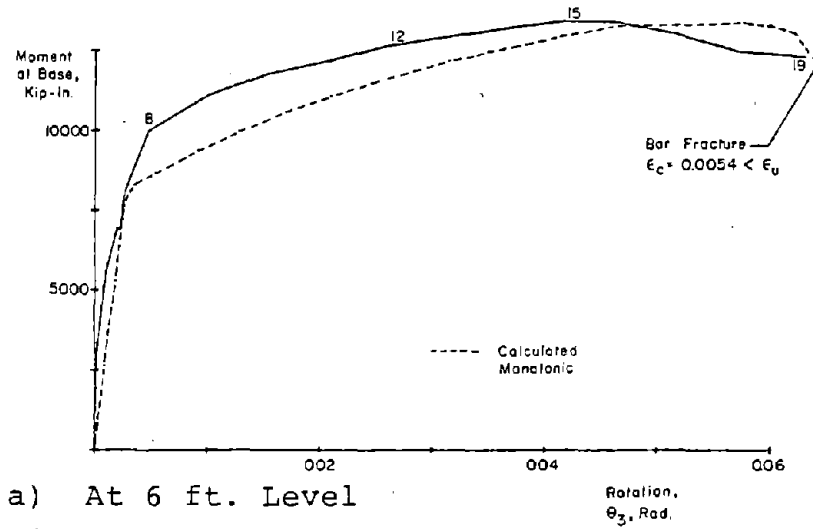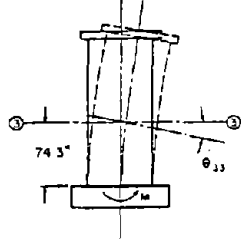
Fig. B-3   Moment at the Base Versus
Rotation for Specimen B4

B-8

maximum rotation is in reasonable agreement with measured at both the 3-ft and 6-ft levels. Therefore, the plots of calculated monotonic rotation at these two levels were superimposed on measured reversed load rotation plots for each specimen.

It should be noted that these calculated rotations are not intended to be an estimate of rotations in specimens under reversed loading. They are intended to be an estimate of rotations under monotonic loading. They are shown on the figures to demonstrate the effects of reversed loading on strength, ductility and rotation.

Shear Distortion Relationships

Shear distortion plots are shown for each specimen over three zones as indicated in Fig. B-4. Zone 1 is from the top of the base block to the 3-ft level. Zone 2 is from the 3-ft level to the 6-ft level. The shear distortions in these two zones were calculated from measured deformations as previously described in the section on instrumentation.

In order to present the average shear distortion over what is considered the hinging region, a third zone is defined. Zone 3 is from the top of the base block to the 6-ft level. Using the notation defined in Fig. B-4 the average shear distortion in Zone 3 was calculated from the distortions in Zones 1 and 2 by:

$$\gamma_3 = \frac{\gamma_1 h_1 + \gamma_2 h_2}{h_1 + h_2} \qquad (B-5)$$
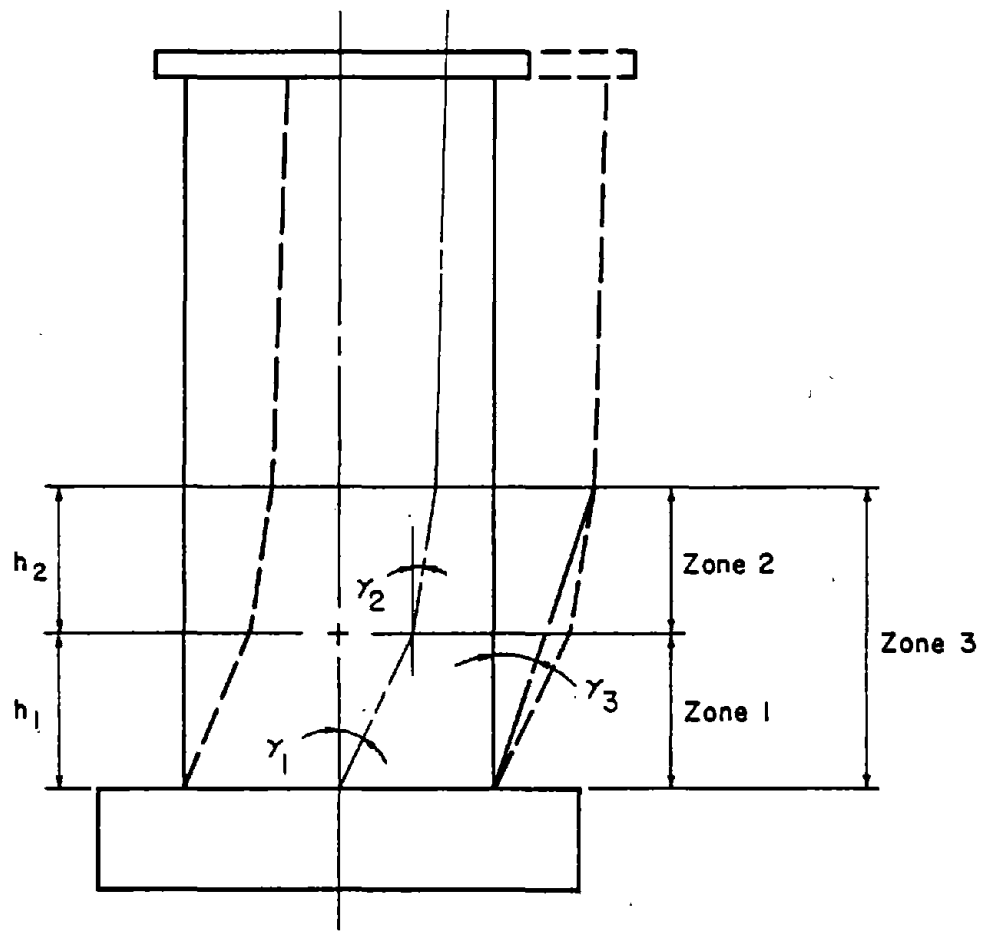
Fig. B-4   Location of Shear Distortion
           Measurements

Slip at Construction Joints

Load versus slip plots are shown for each specimen at
Construction Joints CJ1, CJ2, and CJ3. The base construc-
tion joint data is an accurate representation of slip at the
base joint, CJ1. However, the measurements at CJ2 and CJ3
were often influenced by diagonal cracks passing between the
gage brackets and, therefore, are not always an accurate
representation of construction joint slip. Also, due to
extensive cracking, dial gages often fell off or were
removed from the specimen prior to the end of the test. The
cycle after which no slip data were obtained is noted on
the figures.

Deflections

The total deflection of the specimen at the 3-ft (0.93 m),
6-ft (1.83 m) and top levels were separated into deflections
due to base rotation, flexural rotation and shear distortion.
This data is presented in two types of figures.

The first type of figure shows the separate components
of deflection versus the total deflection at the three
levels. The ordinate is the deflection in inches. The
abscissa is the displacement ductility ratio using the
measured deflection at the full yield load as the yield
deflection. The deflections are shown for the maximum
positive load in the first cycle of each loading increment.
Both axes of these plots are proportioned so that a 45
degree line represents the total measured deflection.

The second type of figure shows the deflected shape of the wall at maximum positive and negative loads in various cycles. One plot shows the total deflected shape from measurements at five levels on the specimen. Two other plots show the deflected shape due to flexural and shear deformations.

Each set of figures includes the deflected shape in the first cycle and the third cycle of a loading increment in the latter stages of the test. This demonstrates the stability of the deflected shape within the loading increment. Also included is the deflected shape immediately before and after significant strength deterioration.

For both types of figures the flexural and shear deflections were calculated from the measured rotations and distortions.

The flexural deflections were calculated assuming the measured rotations over a gage length to be concentrated at the center of that gage length. For the top deflection, the wall between the 6-ft (1.83 m) level and the top was considered rigid. Therefore, using the notation defined in Fig. B-5:

$$\Delta_{F3} = \theta_1\left(h_2 + \frac{h_1}{2}\right) + (\theta_2 - \theta_1)\left(\frac{h_2}{2}\right) \tag{B-6}$$

$$\Delta_{F6} = \theta_1\left(h_3 + h_2 + \frac{h_1}{2}\right) + (\theta_2 - \theta_1)\left(h_3 + \frac{h_2}{2}\right)$$
$$+ (\theta_3 - \theta_2)\left(\frac{h_3}{2}\right) \tag{B-7}$$
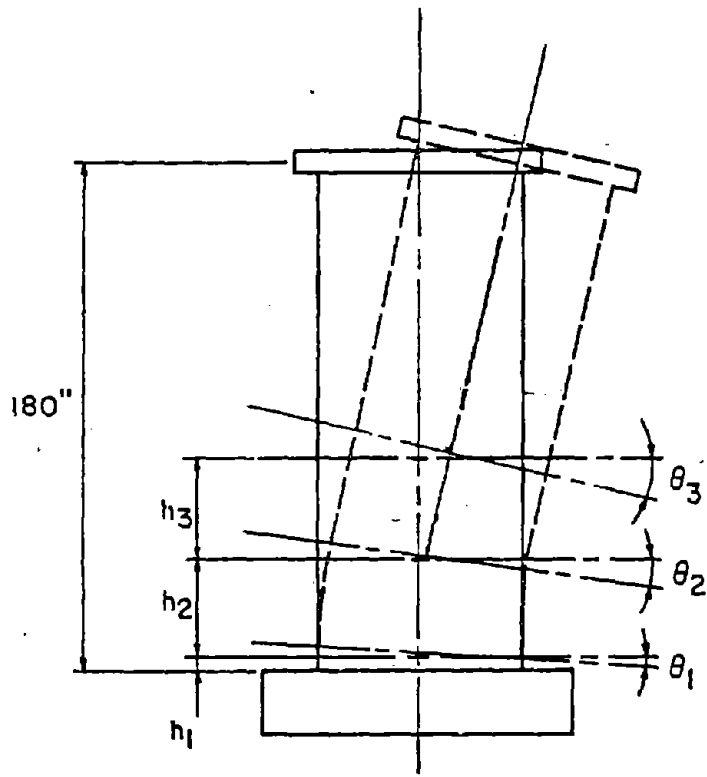
Fig. B-5 Flexural Deformations
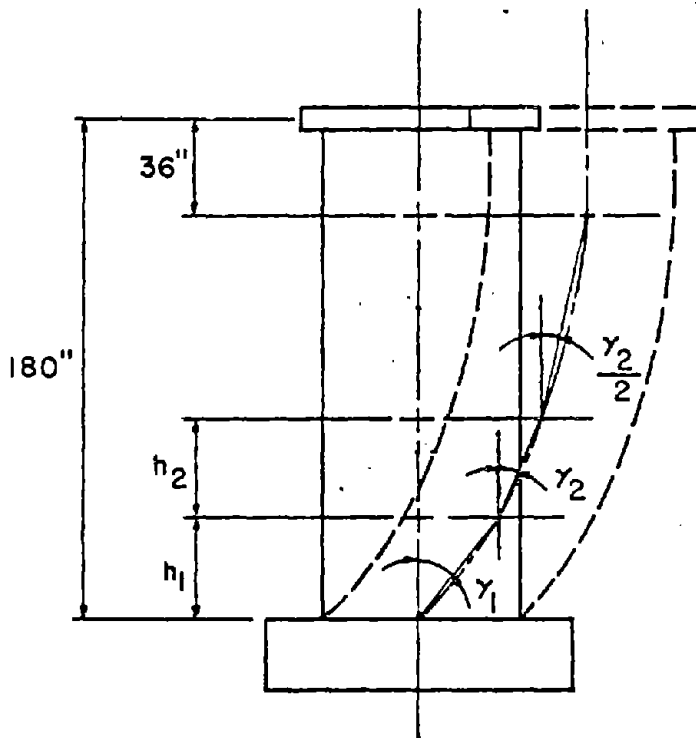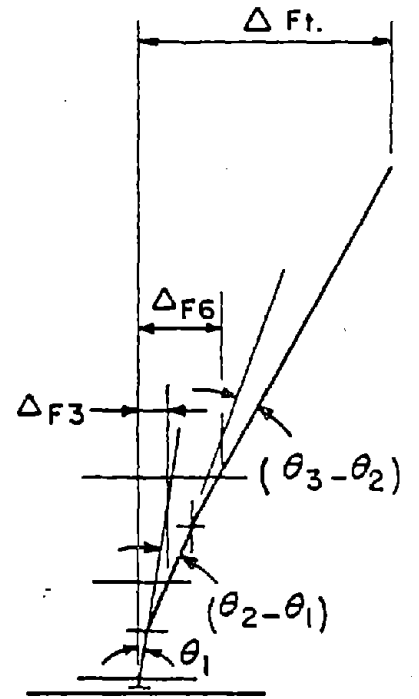
Fig. B-6 Shear Deformations
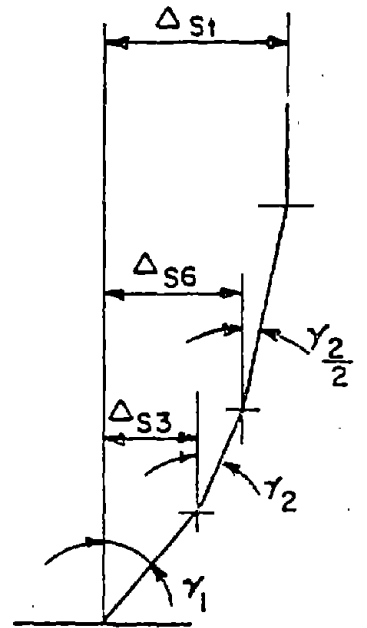
$$\Delta_{Ft} = \theta_1 \left(180 - \frac{h_1}{2}\right) + (\theta_2 - \theta_1)\left[180 - \left(h_1 + \frac{h_2}{2}\right)\right]$$

$$+ (\theta_3 - \theta_2)\left[180 - \left(h_1 + h_2 + \frac{h_3}{2}\right)\right] \quad \text{(B-8)}$$

The shear deflections at the 3-ft and 6-ft (0.91 m and 1.83 m) levels were calculated as described under instrumentation. In calculating the shear deflection at the top of the wall, the shear strain was assumed to be zero at a distance of 36 in. (0.91 m) ($\sim d/2$) from the top. There would actually be some elastic shear deformation in this top segment, however, the magnitude is insignificant. An average shear distortion of $\gamma_2/2$ was assumed over the distance from the 6-ft level up to 36 in. from the top of the wall. Therefore, using the notation defined in Fig. B-6:

$$\Delta_{S3} = \gamma_1 h_1 \quad \text{(B-9)}$$

$$\Delta_{S6} = \gamma_1 h_1 + \gamma_2 h_2 \quad \text{(B-10)}$$

$$\Delta_{St} = \gamma_1 h_1 + \gamma_2 h_2 + \frac{\gamma_2}{2}[180 - (h_1 + h_2 + 36)] \text{(B-11)}$$

The calculated flexural and shear deflections at the 3-ft and 6-ft levels are as accurate as the measured data. The deflection components calculated for the top of the wall are considered approximate values and are presented as extrapolated data.

Base Slip Versus Shear Distortions

In the deflection component analysis described above, no attempt was made to separate the construction joint slip from the shear deflections because of the previously indicated limitation of the slip data. However, since the base

joint slip data is considered accurate, it was separated
from the shear deflection at the 3-ft level. For each
specimen, the base slip is shown on two figures as a per-
centage of the total shear deflection at the 3-ft (0.91 m)
level. The data is presented at the maximum positive and
negative loads in the first cycle of each loading increment.

Reinforcement Strains

Several types of figures showing reinforcing steel
strain data are presented for each specimen.

The first type shows the cyclic load versus strain
relationships for two vertical bars in the boundary element
and for two horizontal bars in the web. The other types of
figures show the strain gradient over the height of the wall
and across horizontal sections at several locations for both
vertical and horizontal reinforcement.

The strain gages used on the reinforcing steel usually
lost bond with the steel between a strain of 0.015 and 0.030.
Therefore, on the majority of figures, the strain scale was
limited to 0.0125. A dashed arrow and cycle number indicate
when a strain gage stopped functioning or the gage reading
went off the scale.

<u>Specimen R1</u>

Test Description

Specimen R1 was a rectangular shaped wall with 1.47% vertical reinforcement concentrated within a distance of 7.5 in. (190.5 mm) from each end. The boundary element had ordinary column ties throughout the height of the specimen.

The test consisted of 30-1/2 loading cycles as seen in Fig. B-7. Figures B-8 and B-9 show the complete load versus top deflection relationship.

Flexural cracking was first observed in Cycle 4 at a load of 12 kips (53.4 kN). First yielding occurred in cycle 10 at a load of 20.1 kips (89.4 kN). The maximum measured crack width at this stage was 0.018 in. (0.46 mm).

Minor spalling and flaking along cracks were first observed at Cycle 14.

The maximum measured load, +26.6 kips (118.3 kN), occurred in Cycle 16 at a +2.0 in. (50.8 mm) deflection. This load corresponded to a nominal shear stress, $v_{max} = 1.4\sqrt{f_c'}$ ($0.12\sqrt{f_c'}$, MPa). The maximum measured crack width at this stage was 0.20 in. (5.1 mm). Cracks in the compression side of the wall remained open with a width of approximately 0.02 in. (0.51 mm).

The cracking pattern in the lower 6 ft (1.83 m) of the wall is shown in Figs. B-10 and B-11. The photographs were taken in Cycle 19 at a top deflections of +3 in. (76.2 mm) and -3 in., respectively. The cracks started in a horizontal

Load, kips

a) Load History

1 in. = 25.4 mm
1 kip = 4.448 kN

Defl., in.
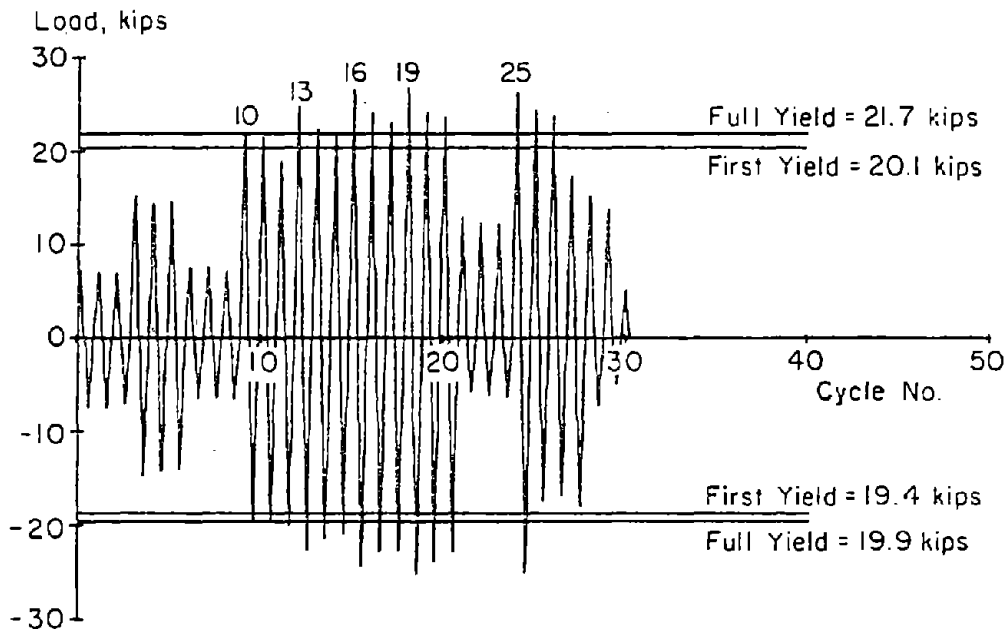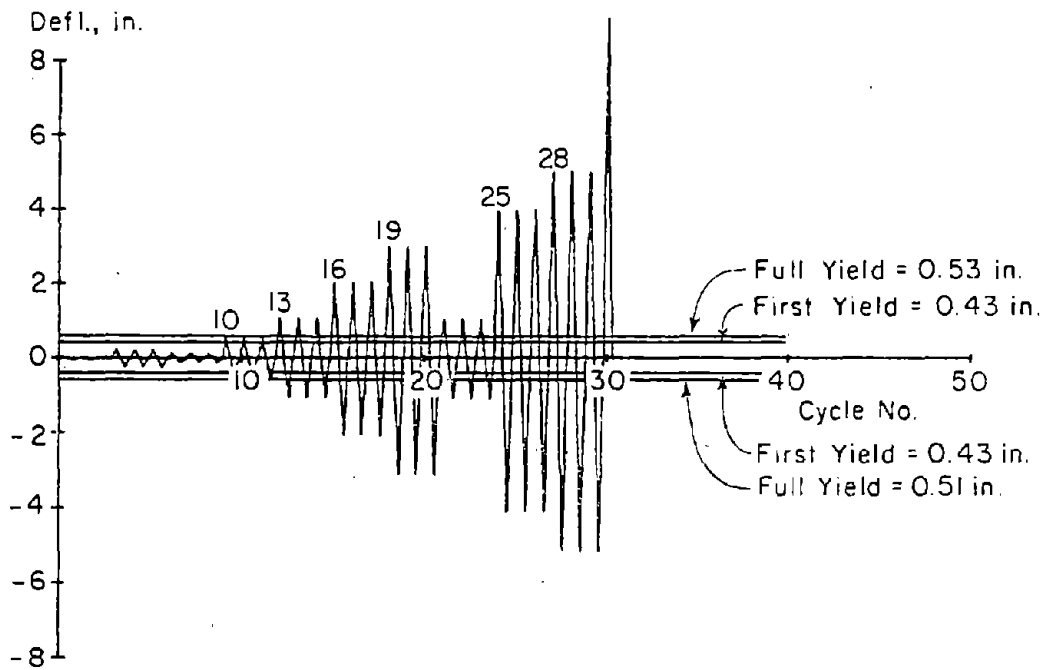
b) Deflection History

Fig. B-7 Loading History for Specimen R1

B-17
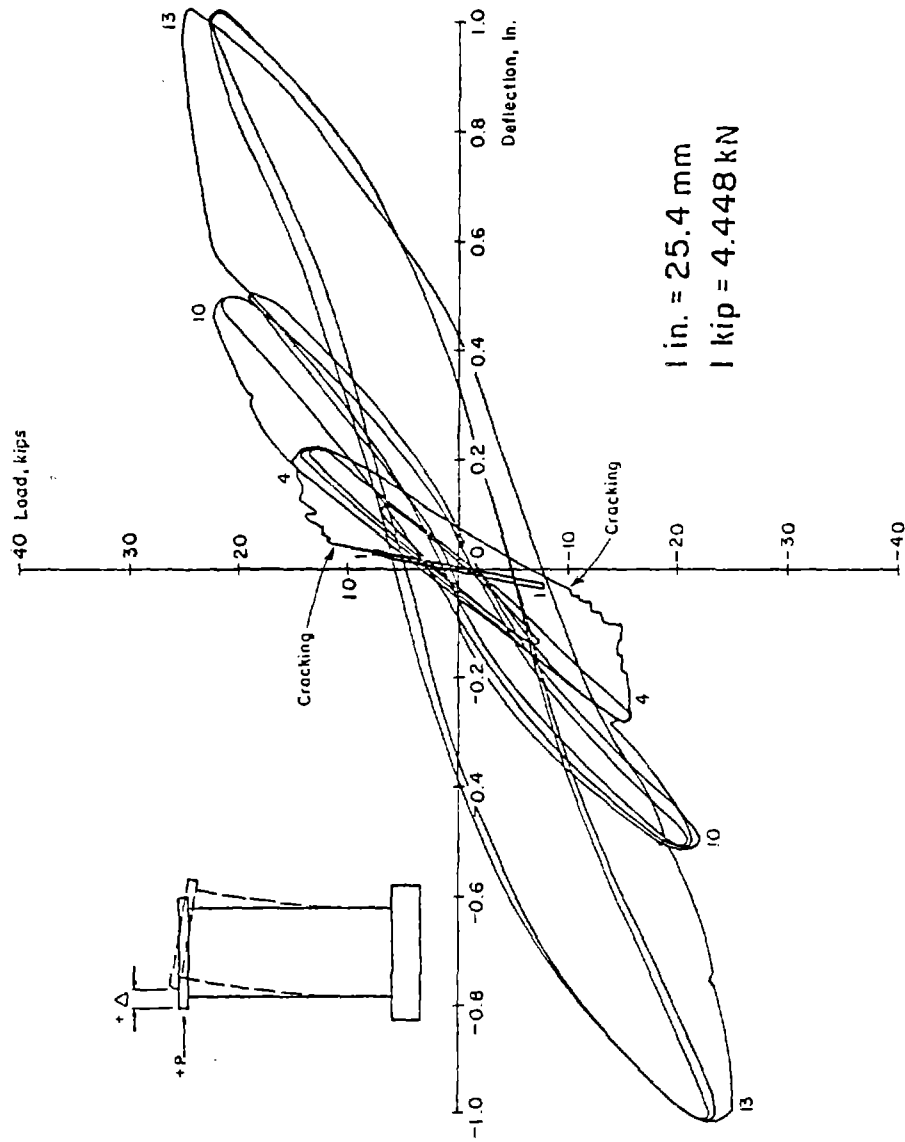
Fig. B-8 Continuous Load-Deflection Plot
for Initial Cycles for Specimen R1
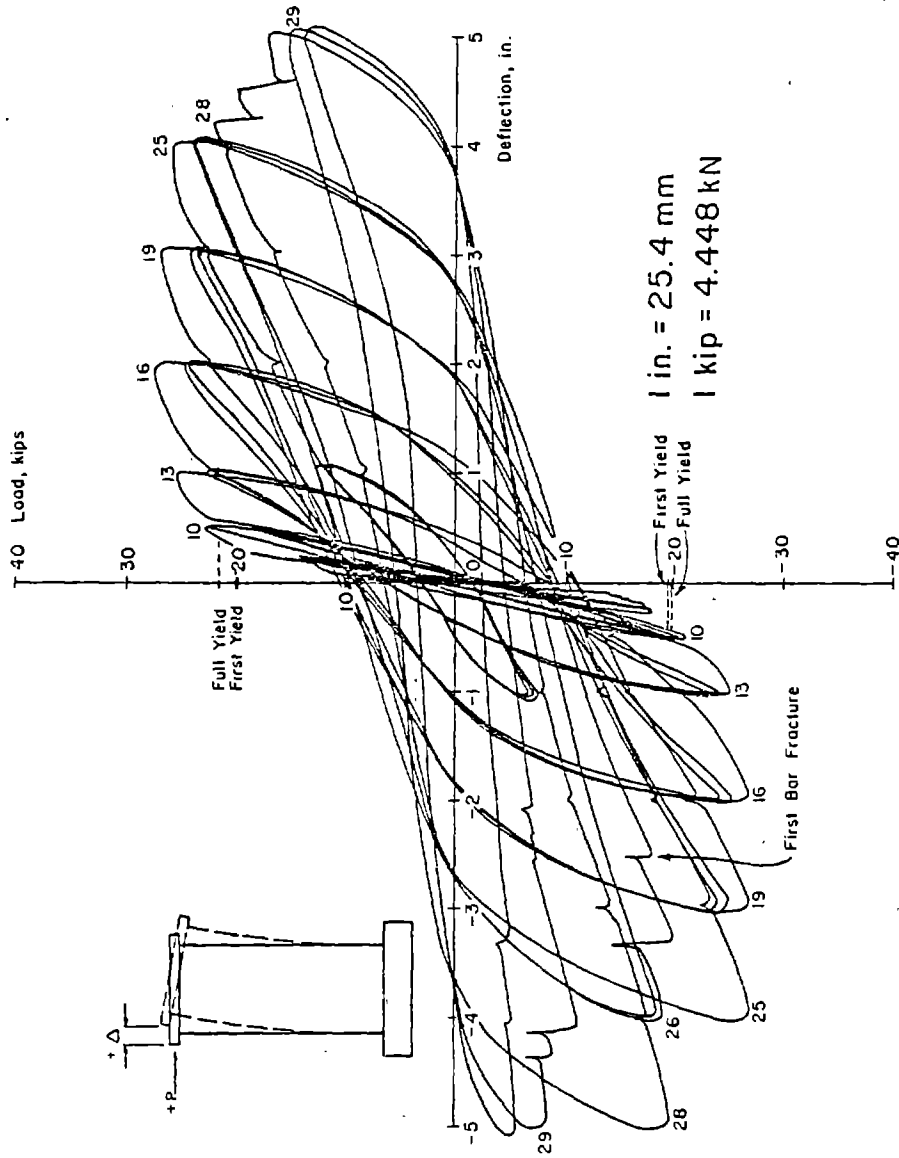
Fig. B-9 Continuous Load-Deflection Plot for Specimen R1
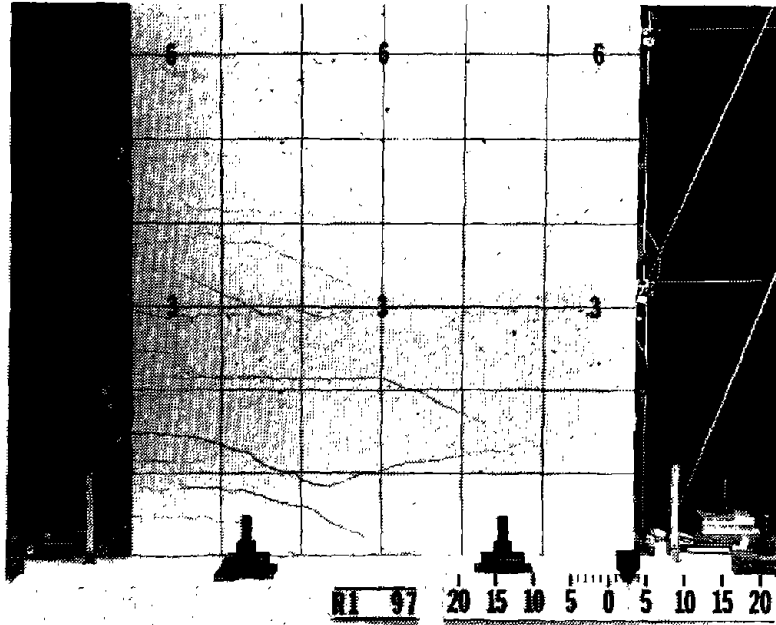
Fig. B-10 Cracking Pattern at +3 in. Deflection
for Specimen R1
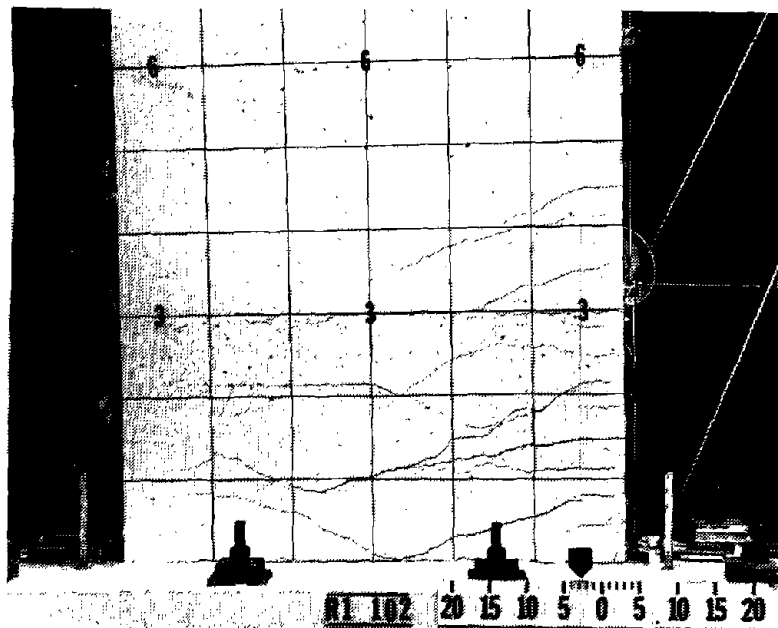
Fig. B-11 Cracking Pattern at -3 in. Deflection
for Specimen R1

direction as flexural cracks. They then inclined until they intercepted cracks from the opposite direction. The lower 3 ft (0.91 m) of wall was completely traversed by several predominately horizontal cracks. Significant spalling and sliding along the horizontal crack at the 3-ft level was noted in Cycle 19.

First buckling of the main flexural reinforcement was observed in Cycle 20, the second cycle at +3 in. deflection. The outer two bars in the compression end of the wall buckled at a location 15 in. (381 mm) above the base. A crack width of 0.05 in. (1.27 mm) had previously been measured when this end was in compression. Subsequent to buckling of the first two bars, ten additional bars buckled during the test.

First bar fracture occurred in Cycle 26. The fractured bars were the two that had buckled first. Six and one-half cycles were applied between first buckling and fracture. Subsequent to the first two bar fractures, nine additional bars fractured during the test. Each bar fracture was associated with a drop in the load resisted by the specimen.

During the latter load increments, concrete in the compression zone was segmented into large pieces. However, since the wall was lightly reinforced in flexure, the concrete did not crush.

The specimen sustained at least 80% of the maximum measured load through 13 complete inelastic cycles. The last inelastic loading increment in which the load was sustained at or above 80% of the maximum for all 3 cycles

was at ±3 in. (±76.2 mm). A photograph of the wall after
the test is shown in Fig. B-12.

Discussion of Results

Moment-Rotation. Moment rotation data for Specimen R1
is shown in Fig. B-13. The maximum measured moment was 91%
of the calculated monotonic maximum. The relationship
between the calculated and measured rotation at the 3-ft
(0.91 m) level is very similar to that at the 6-ft (1.83 m)
level. This indicates that the shape of the assumed effective
curvature distribution was accurate.

The maximum measured loads in each cycle reached a peak
in Cycle 16 and then leveled off exhibiting no "strain
hardening" as the rotations increased.

The loops at all three levels exhibited some pinching.
The base level loops exhibited the most pinching. It should
be noted that there is a discontinuity at the end of each
loop on the negative side. This results from plotting only
every third loop.

Shear-Distortion. The shear-distortion loops for
Specimen R1 are shown in Fig. B-14. Although the wall was
considerably over-reinforced for shear, the specimen ex-
hibited shear "yielding" during approximately the same load
cycles in which flexural yielding occurred.

After shear "yield" the loops exhibit pinching due to a
low shear stiffness over an increasingly wider range of
deflection in the center region of the loops. Pinching was
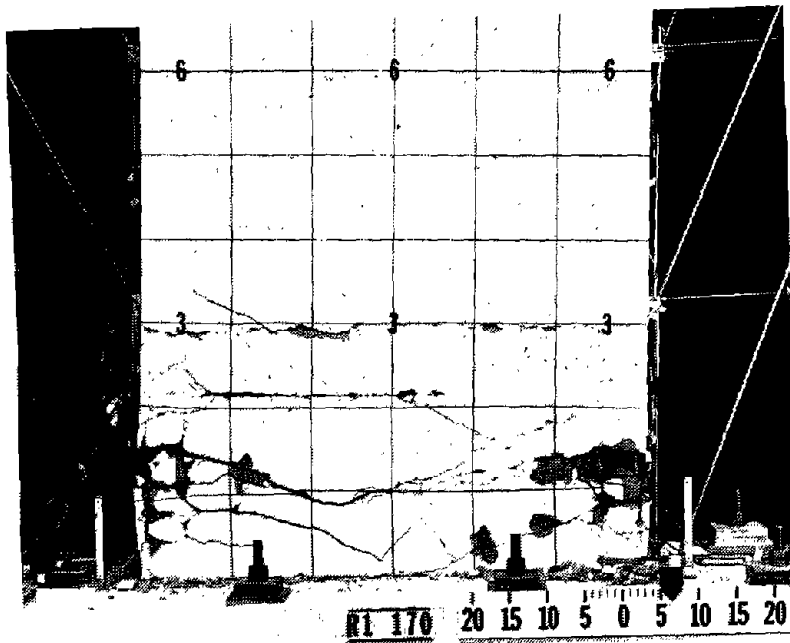
Fig. B-12   Specimen R1 at End of Test

a) At 6 ft. Level
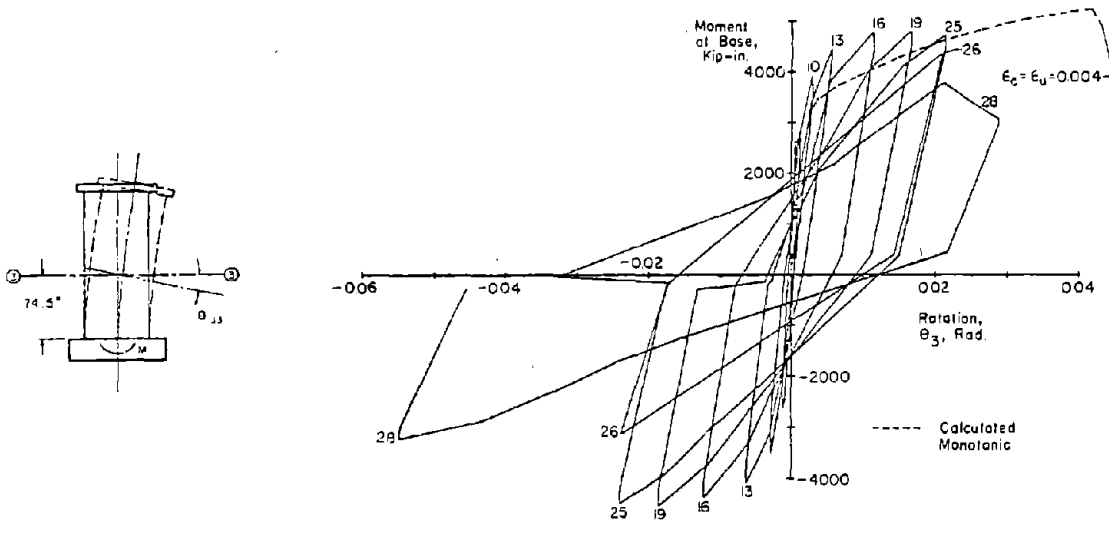
b) At 3 ft. Level
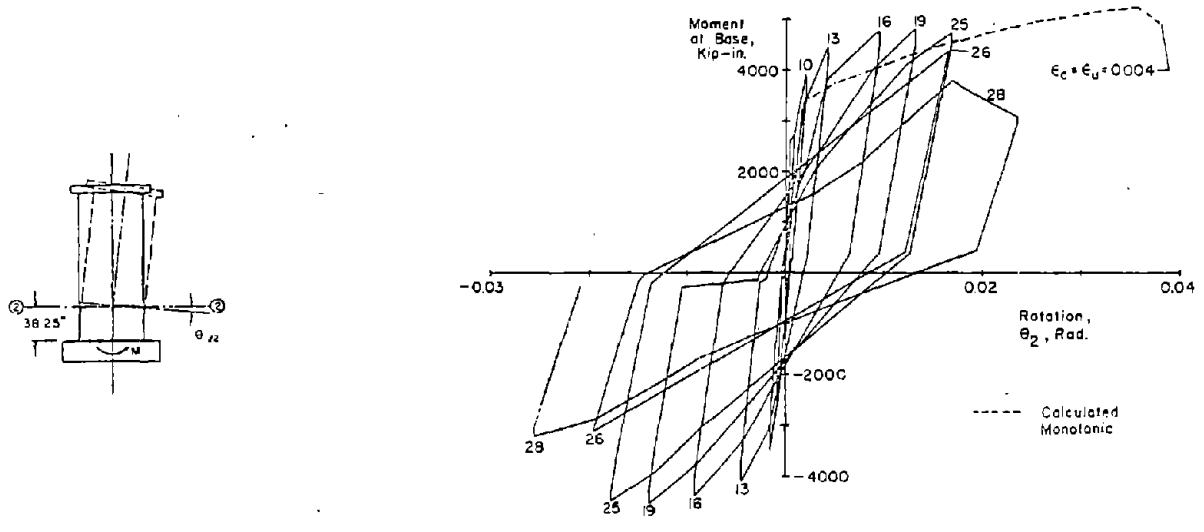
c) At Base Level
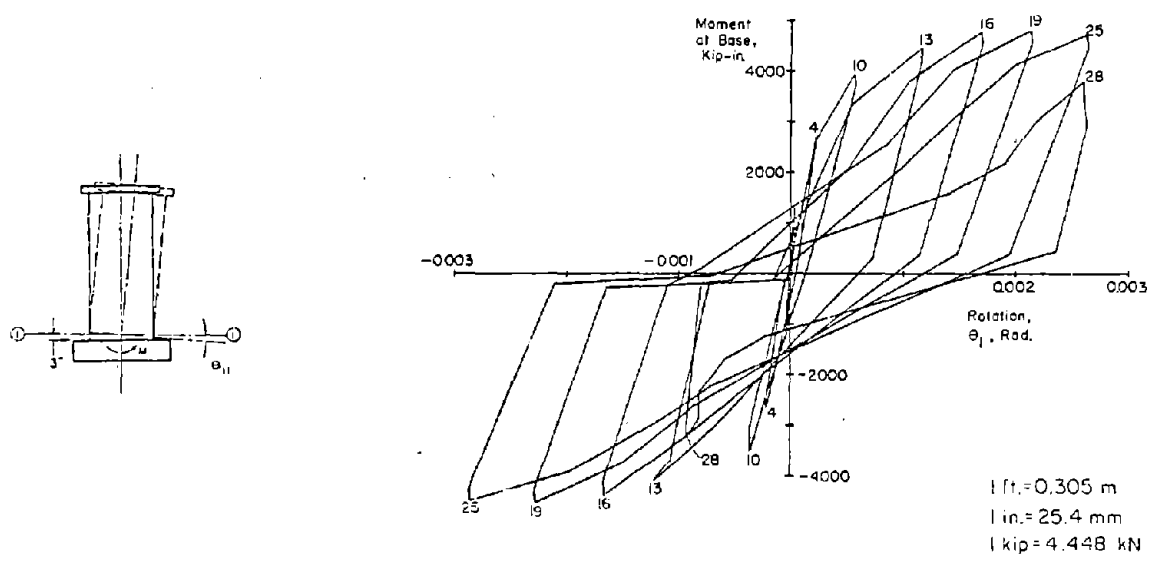
1 ft.=0.305 m
1 in.=25.4 mm
1 kip=4.448 kN

Fig. B-13   Moment at Base versus Rotation
for Specimen R1
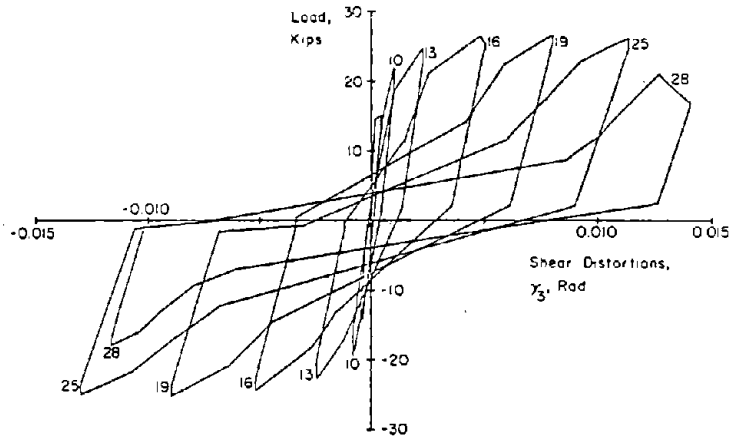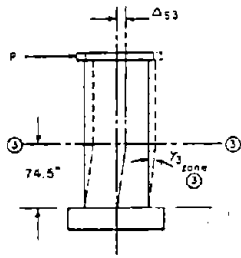
B-24

a)   In Base to 6 ft Level
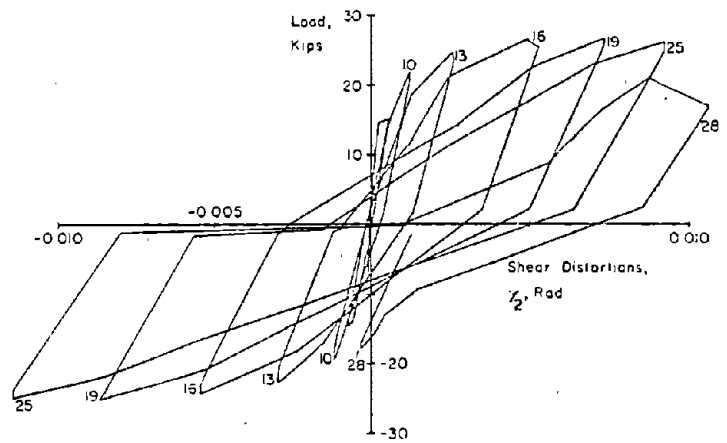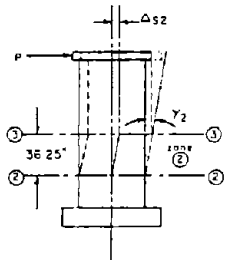
b)   In 3 ft to 6 ft Level
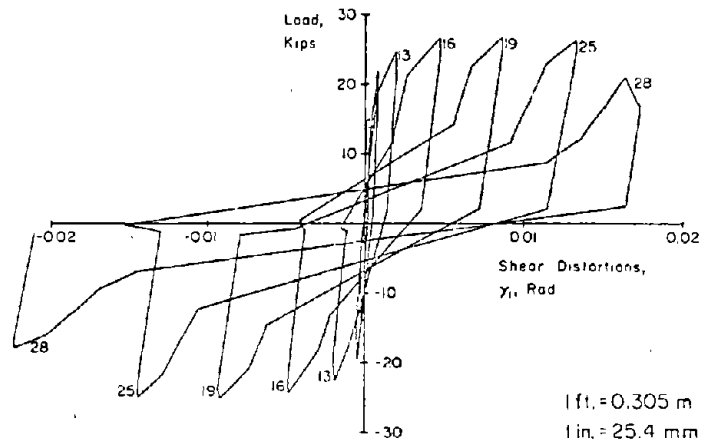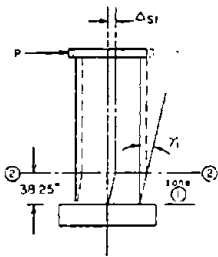
I ft.=0.305 m
I in.= 25.4 mm
I kip= 4.448 kN

c)   In Base to 3 ft Level

Fig. B-14   Load versus Shear Distortion for
              Specimen R1

most evident in Zone 1. The maximum shear distortions in each new increment increased at an approximately constant rate. The magnitude of distortions in Zone 2 were approximately 70% of those in Zone 1. In both zones, the specimen was somewhat stiffer for positive direction loading. This difference can be related to the slip allowed by the crack pattern.

Slip at Construction Joints. The slip at construction joints for Specimen R1 are shown in Fig. B-15. The slip at CJ1 and CJ2 exhibited a "yielding" similar to shear "yielding" at later load increments than flexural yielding occurred. No significant slip was measured at CJ3.

The slip at CJ1 is shown as a percentage of the total shear deflections in Zone 1 in Fig. B-16. Specimen R1 exhibited a larger percentage of slip at CJ1 than did the other eight specimens tested.

Deflections. The deflection components and deflected shapes for R1 are shown in Figs. B-17 and B-18. These figures show that flexural deflections predominated. This is expected for a specimen subjected to low nominal shear stresses. However, shear deflections were a measurable portion of the total and were becoming an increasing portion in the latter load increments. The total deflected shape was nearly a straight line as can be seen in Fig. B-18. The deflected shapes at Cycles 16 and 18 show only a slight shear degradation within the 2-in. (50.8 mm) increment.
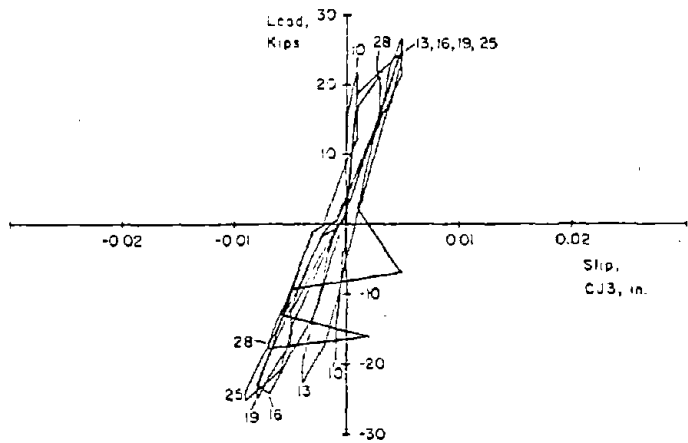
a) At 6 ft. Level
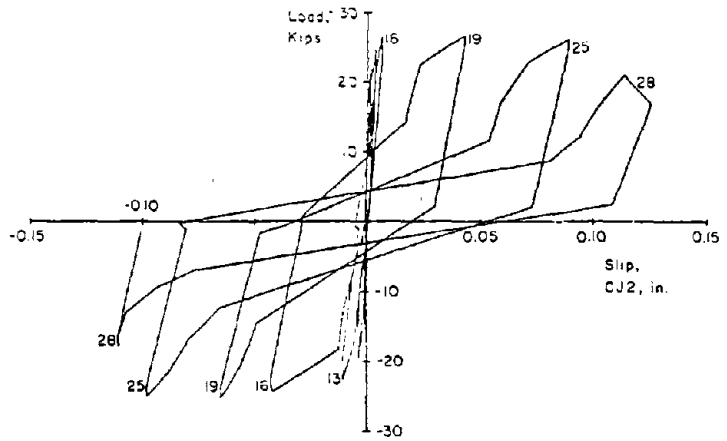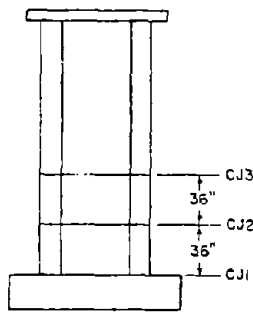
b) At 3 ft. Level
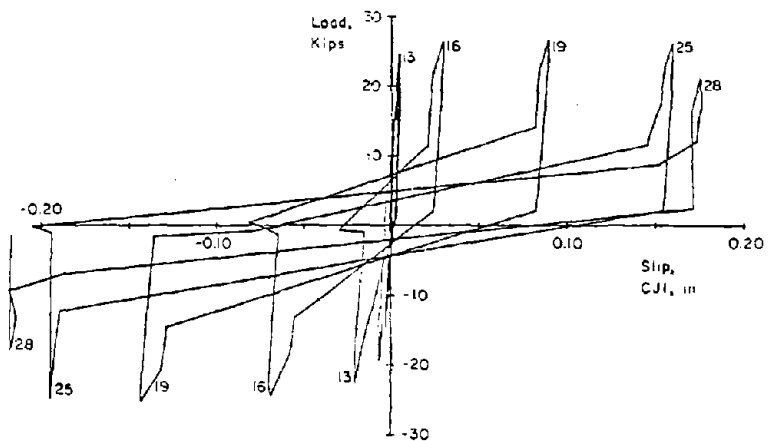
c) At Base Level

1 ft.= 0.305 m
1 in.= 25.4 mm
1 kip= 4.448 kN

Fig. B-15   Load versus Slip at Construction Joints
for Specimen R1

$$\frac{\Delta CJ1}{\Delta \gamma_1}, \%$$

1 in. = 25.4 mm

Shear Deflection, $\Delta \gamma_1$ (in.)

a) At Maximum Positive Loads

$$\frac{\Delta CJ1}{\Delta \gamma_1}, \%$$
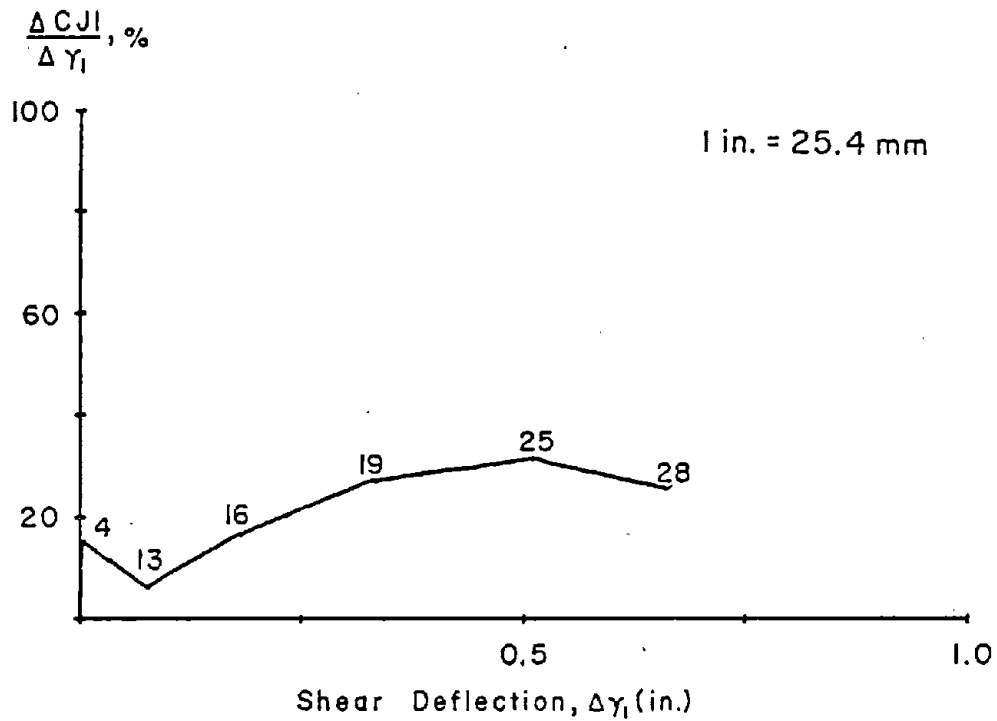
Shear Deflection, $\Delta \gamma_1$ (in.)
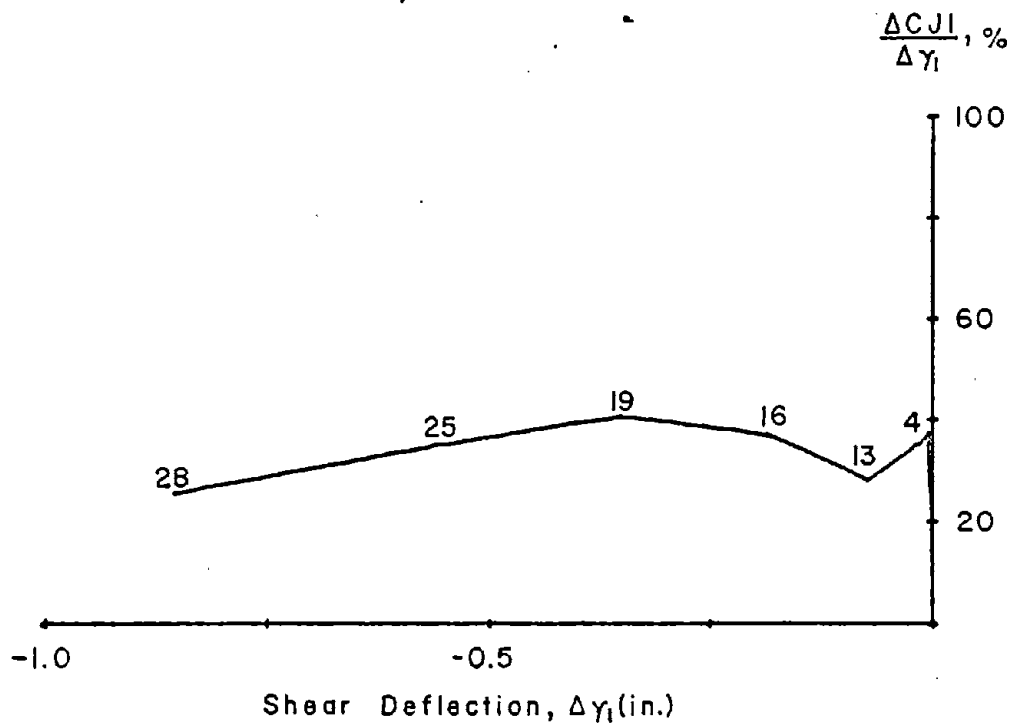
b) At Maximum Negative Loads

Fig. B-16   Slip at Base Construction Joint versus
Shear Deflection in Zone 1 for Specimen R1

a) At Top of Wall
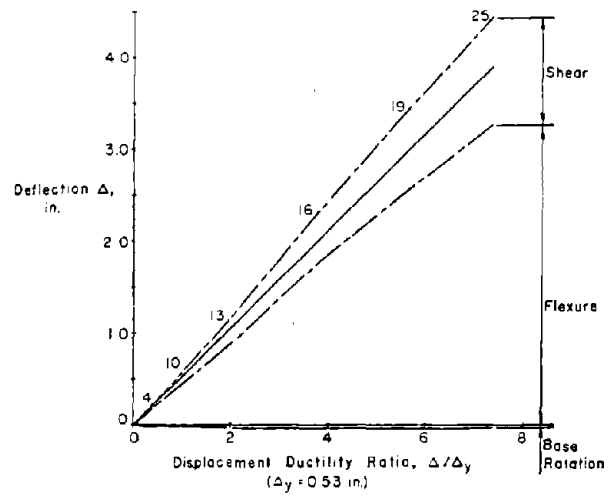
b) At 6 ft. Level
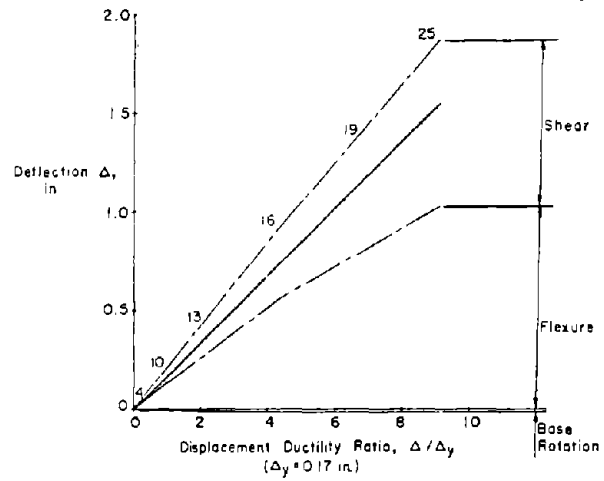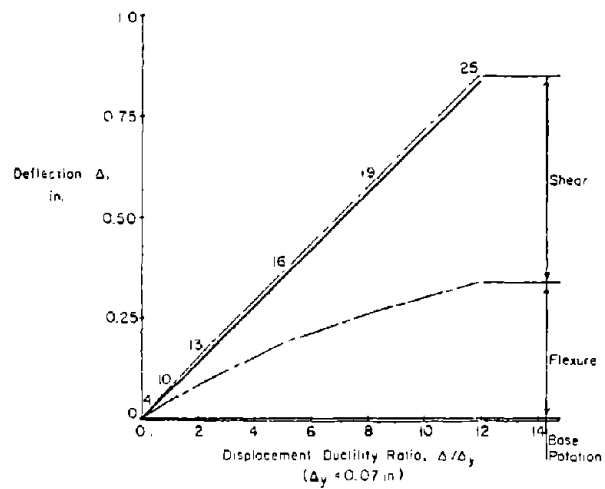
CALCULATED FROM
MEASURED DEFORMATION
EXTRAPOLATED
MEASURED TOTAL

1 in. = 25.4 mm
1 ft. = 0.305 m

c) At 3 ft. Level

Fig. B-17 Component of Deflection for Specimen R1
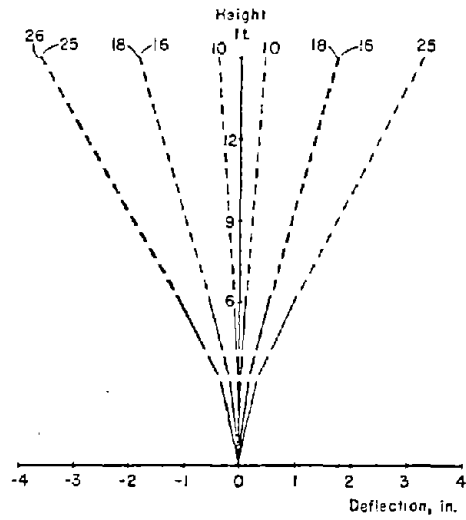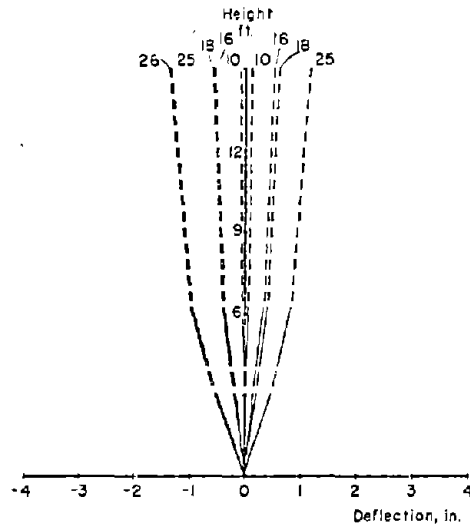
B-29

a) Flexural

b) Shear

CALCULATED FROM
MEASURED DEFORMATION
EXTRAPOLATED
MEASURED TOTAL

1 in. = 25.4 mm
1 ft. = 0.305 m

B.F. — BAR FRACTURE   CYCLE 26
AFTER 1st. B.F.

CYCLE 25 PRIOR
TO 1st. B.F.

c) Total
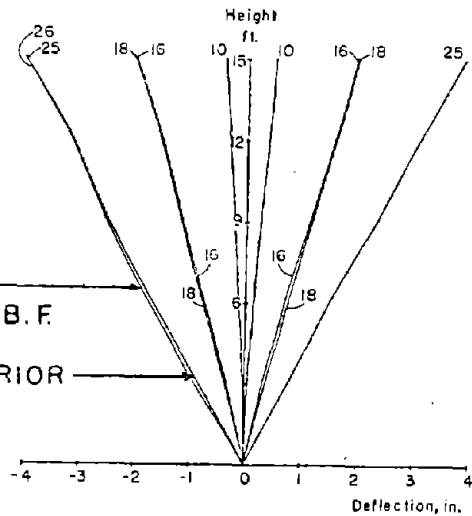
Fig. B-18   Deflected Shape for Specimen R1

B-30

<u>Reinforcement Strains</u>. Figures B-19 through B-27
show reinforcement strains in the specimen at several
stages.

Figure B-20 shows that yielding of the vertical bars
was limited to the lower 6-ft (1.83 m) region. Figure B-22
shows that the left compression element started to grow in
Cycle 13.

Figure B-23 through B-27 show that, even though the
specimen was considerably over-designed for shear and the
maximum measured load corresponded to only $1.4 \sqrt{f'_c}$
($0.12 \sqrt{f'_c}$, MPa), horizontal bars yielded in the lower 6-ft
region during Cycle 16.
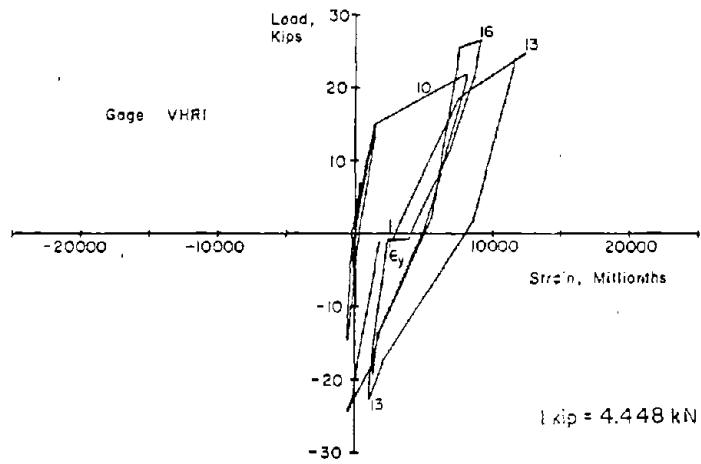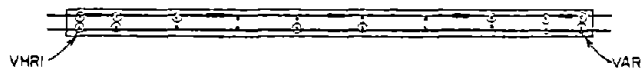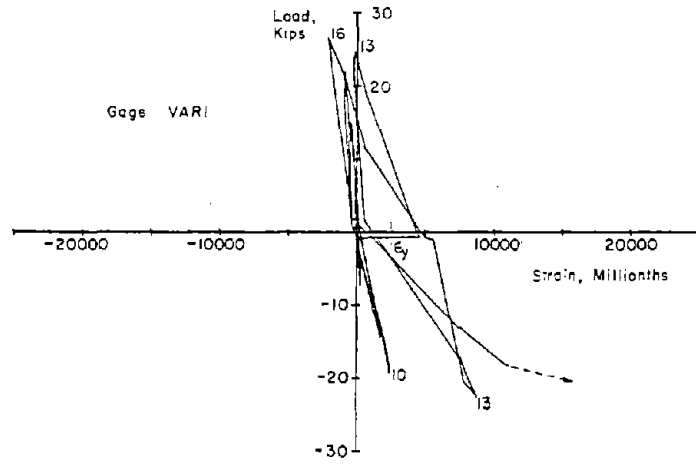
Fig. B-19 Measured Strains at Vertical Reinforcement
at Base of Specimen R1
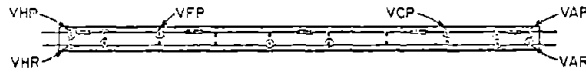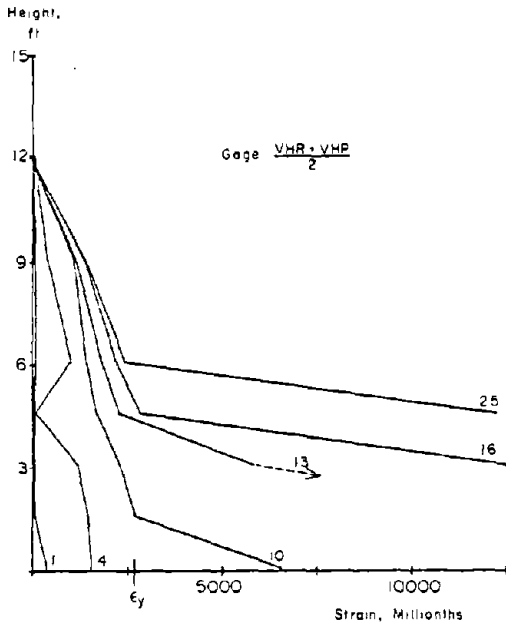
a) Average of VHP & VHR
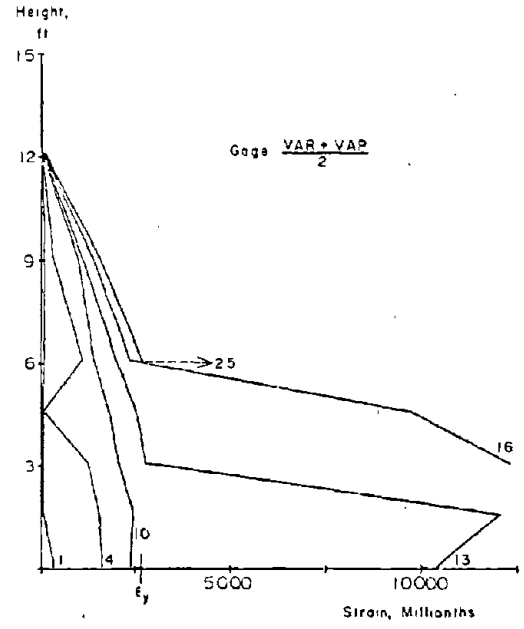
b) Average of VAP & VAR
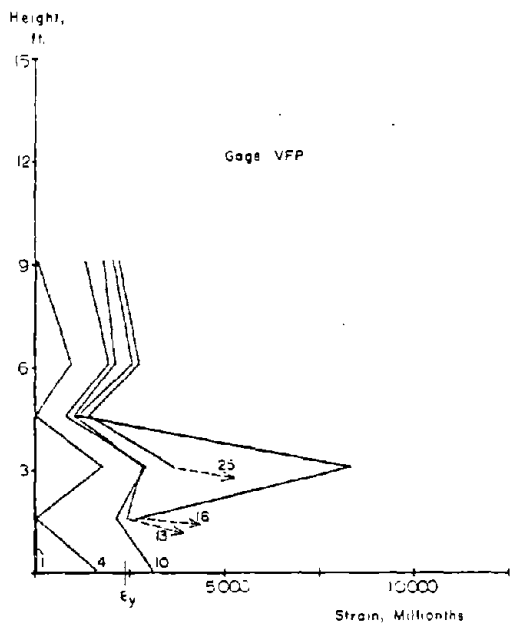
c) Strain Gage VFP
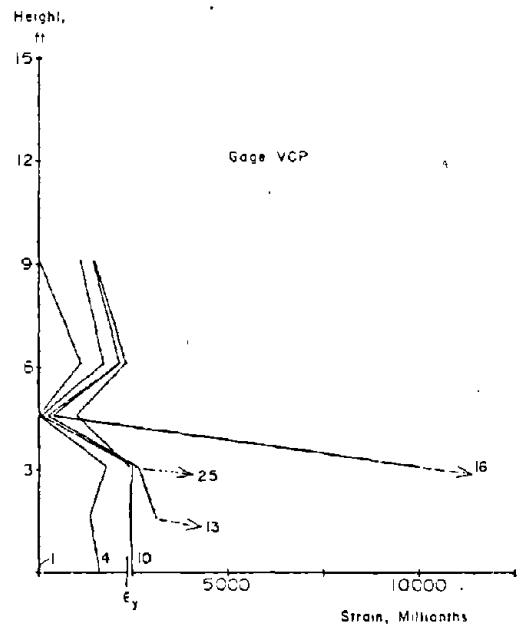
d) Strain Gage VCP

Fig. B-20   Vertical Reinforcement Strains at
Maximum Loads for Specimen Rl
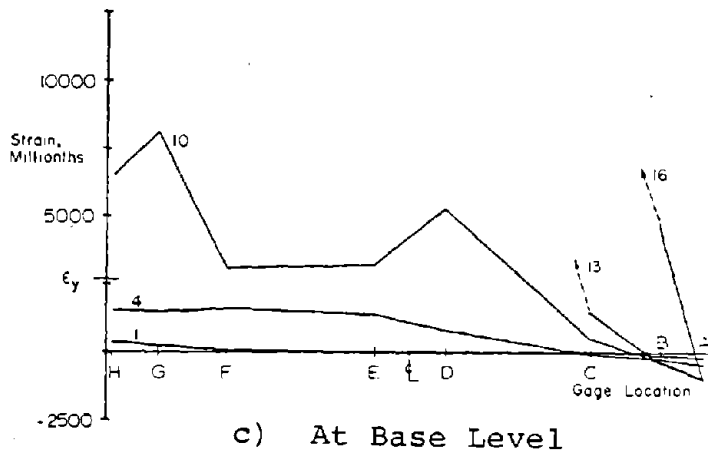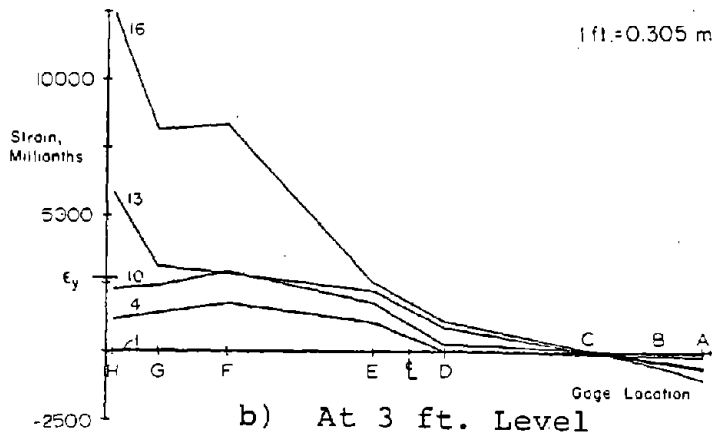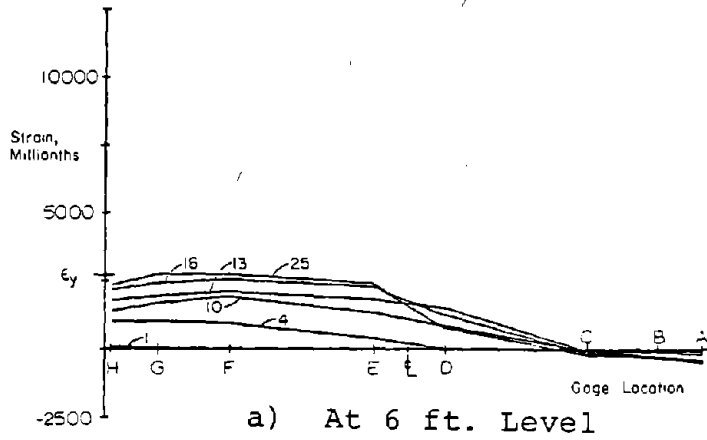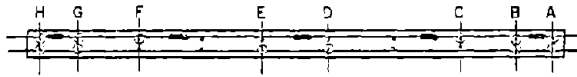
Fig. B-21 Vertical Reinforcement Strains at
Maximum Positive Loads for Specimen R1
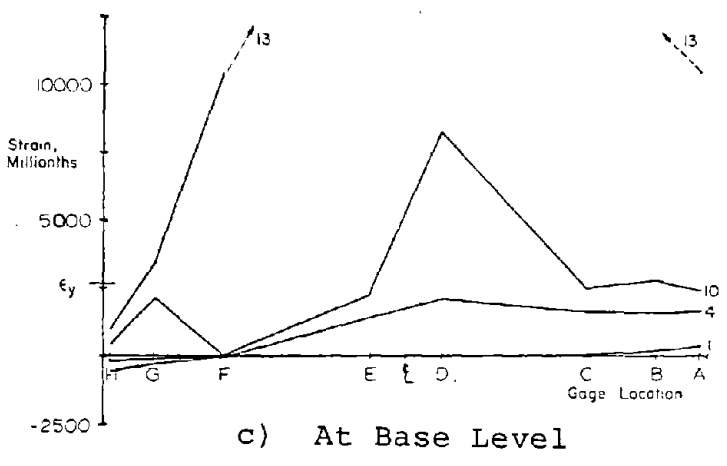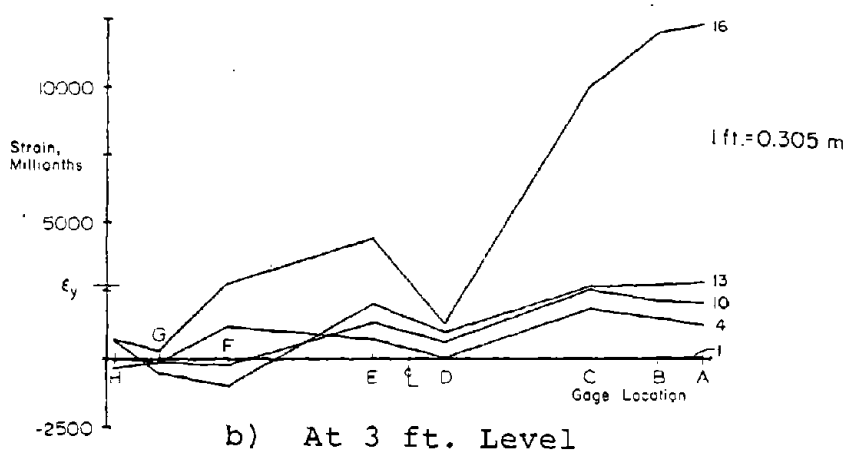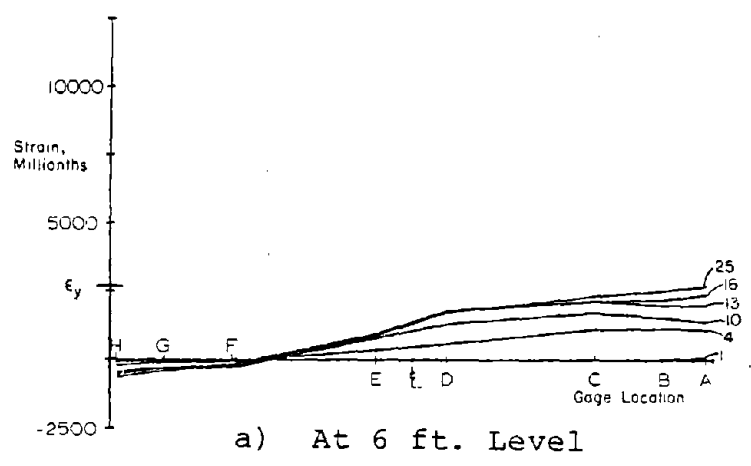
Fig. B-22   Vertical Reinforcement Strains at
            Maximum Negative Loads for Specimen R1

Load, 30
Kips

Gage HE3

1 in. = 25.4 mm
1 kip = 4.448 kN

Strain, Millionths

Load, 30
Kips

Gage HE2

Strain, Millionths
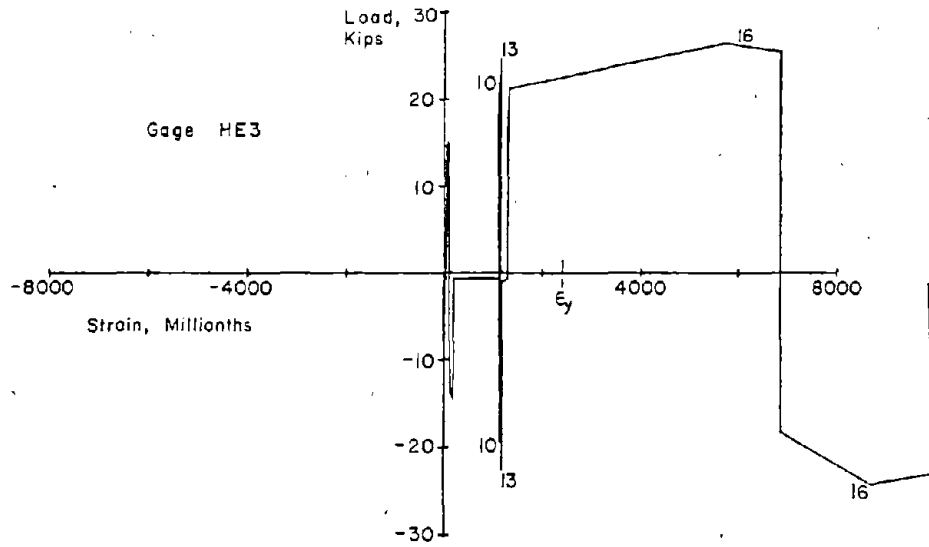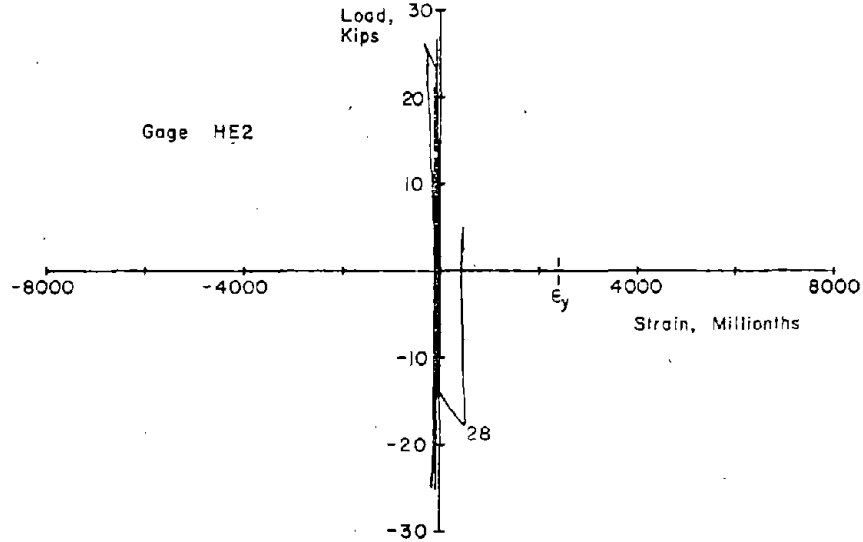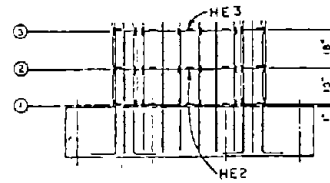
Fig. B-23   Measured Strains on Horizontal Reinforcement
            for Specimen R1
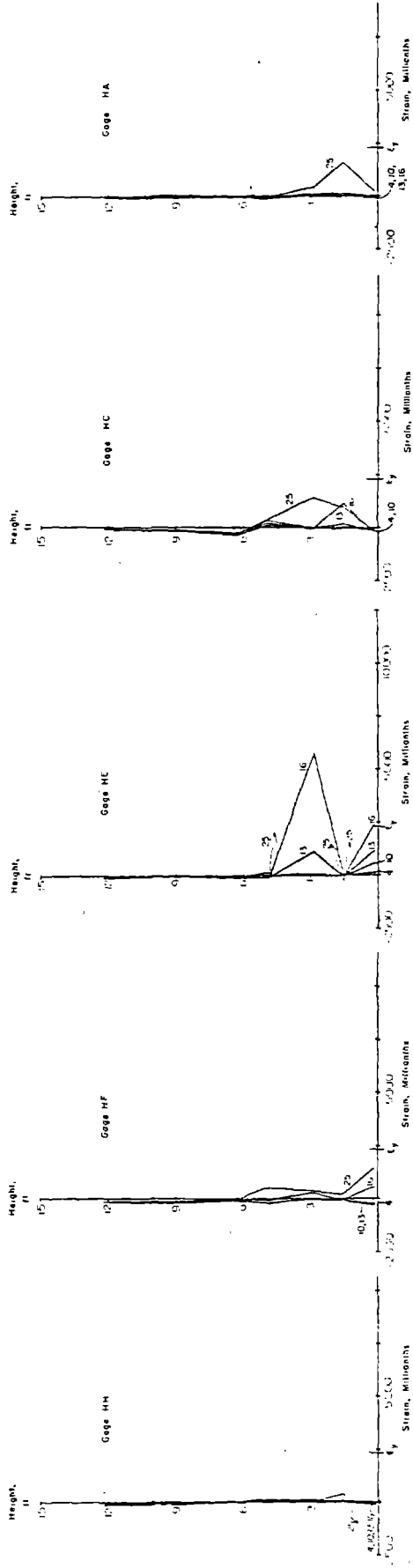
Fig. B-24 Horizontal Reinforcement Strains at
Maximum Positive Loads for Specimen R1
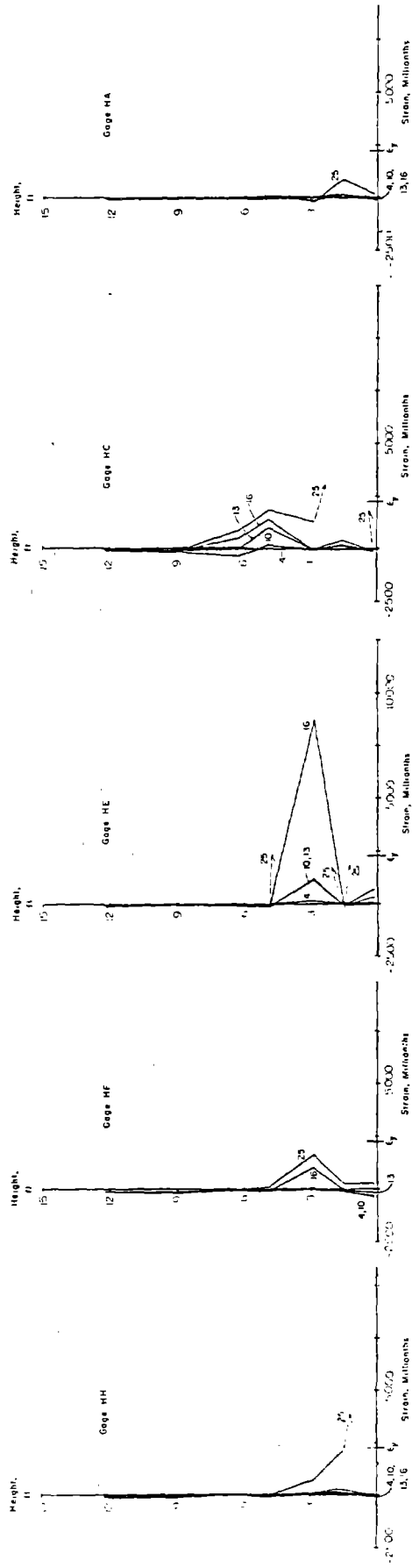
Fig. B-25 Horizontal Reinforcement Strain at
Maximum Negative Loads for Specimen R1
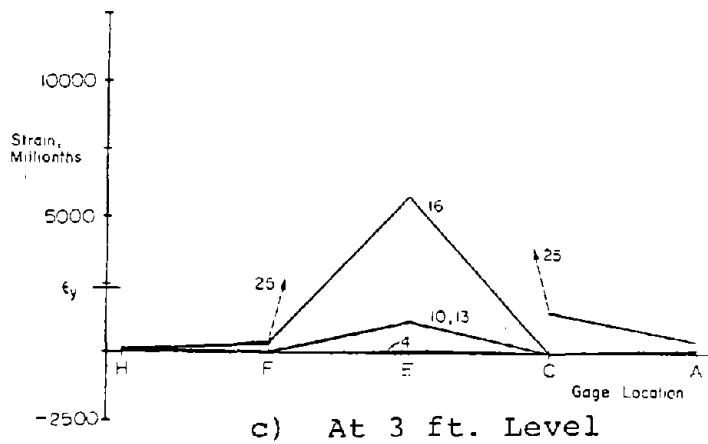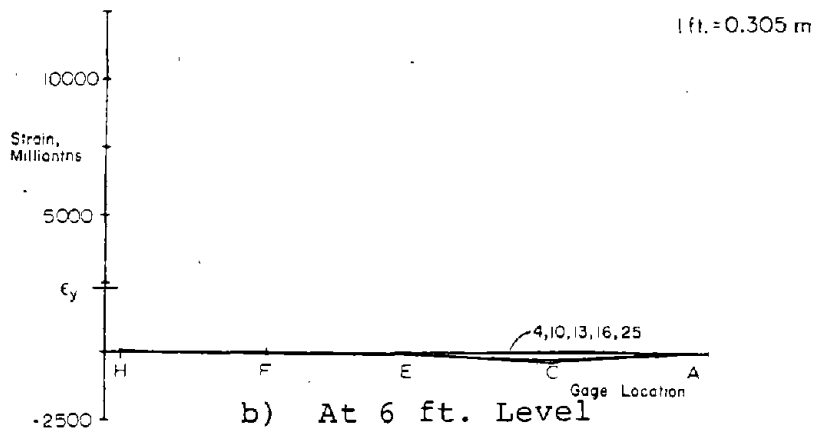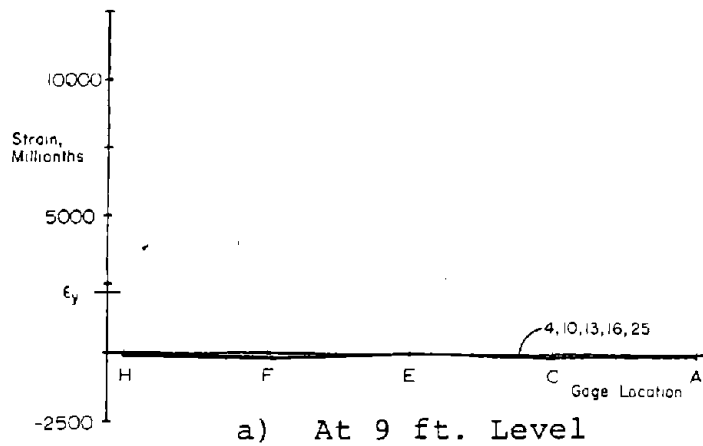
Fig. B-26   Horizontal Reinforcement Strains in Web
at Maximum Positive Loads for Specimen R1
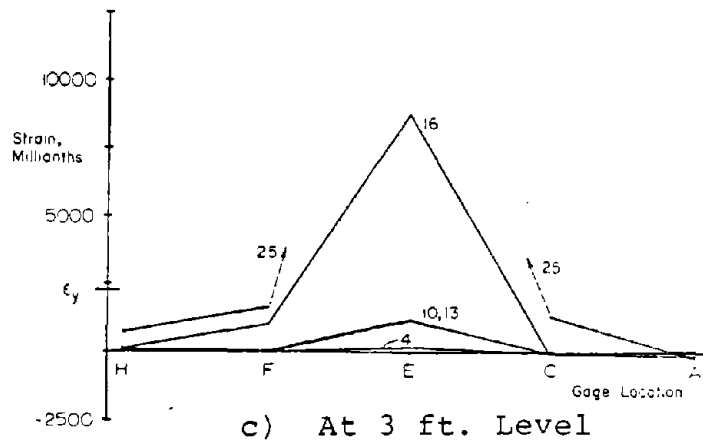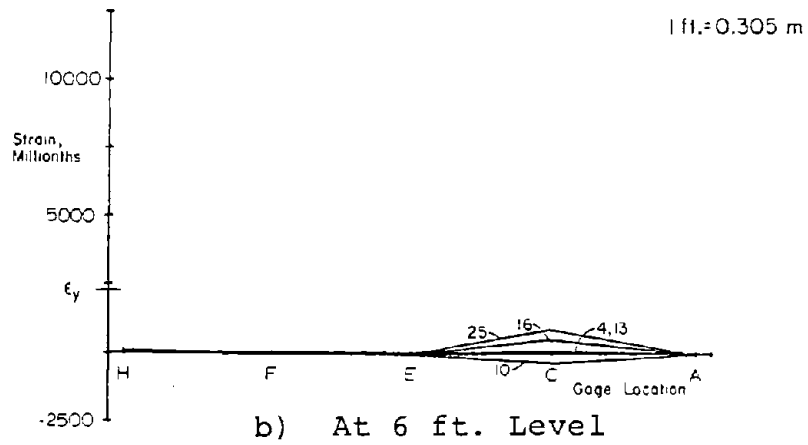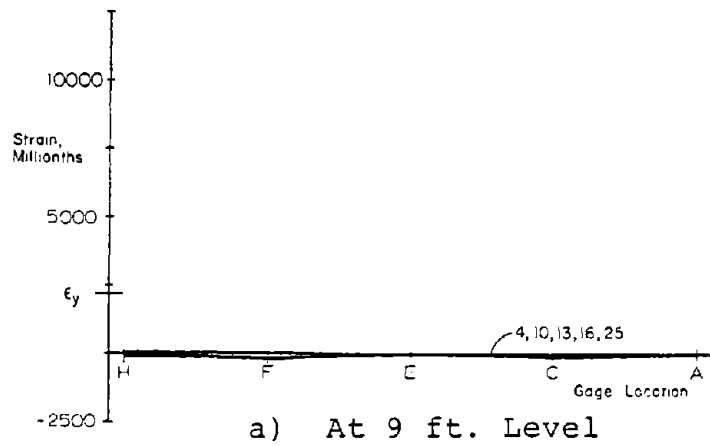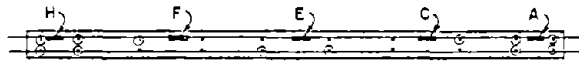
Fig. B-27 Horizontal Reinforcement Strains in Web
at Maximum Negative Loads for Specimen R1

Specimen R2

Test Description

Specimen R2 was a rectangular shaped wall with 4.0%
vertical reinforcement concentrated within a distance of
7.5 in. (190.5 mm) from each end. The boundary element had
confinement reinforcement in the lower 6 ft (1.83 m) of the
boundary elements.

The test consisted of 39 loading cycles as shown in
Fig. B-28. The complete load versus top deflection relation-
ship for the R2 test is shown in Figs. B-29 and B-30.

The first significant flexural cracking occurred in
Cycle 4 at a load of 15 kips (66.7 kN). First yielding
occurred in Cycle 19 at a load of 37.0 kips (164.6 kN). The
maximum measured crack widths at this stage were 0.012 in.
(0.30 mm) in the tension boundary element and 0.019 in.
(0.48 mm) in a diagonal web crack. Minor spalling and
flaking were first noted along horizontal web crack in the
lower 3 ft (0.91 m) in Cycle 19.

The cracking pattern in the lower 6 ft (1.83 m) of the
wall is shown in Figs. B-31 and B-32. These photographs
were taken during Cycle 25 at a top deflection of +3 in.
(76.2 mm) and -3 in., respectively. As these figures show,
the flexural cracking in the end regions was very finely
distributed due to the close spacing of confinement steel.
These flexural cracks progressed into coarsely distributed
diagonal and horizontal cracks in the web. The cracks from

Load, kips

Full Yield = 41.8 kips

First Yield = 37.0 kips

Cycle No.

First Yield = 30.9 kips

Full Yield = 39.7 kips

a) Load History

I in. = 25.4 mm
I kip = 4.448 kN

Defl. in.

Full Yield = 0.85 in.
First Yield = 0.60 in.

Cycle No.

First Yield = 0.56 in.
Full Yield = 0.82 in.
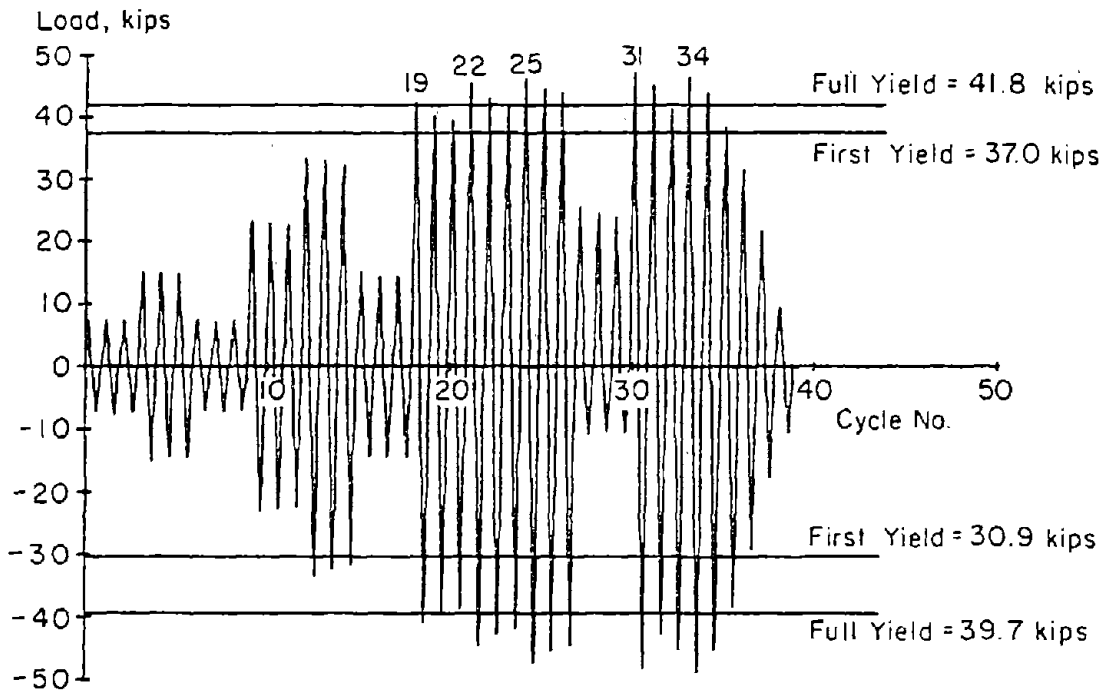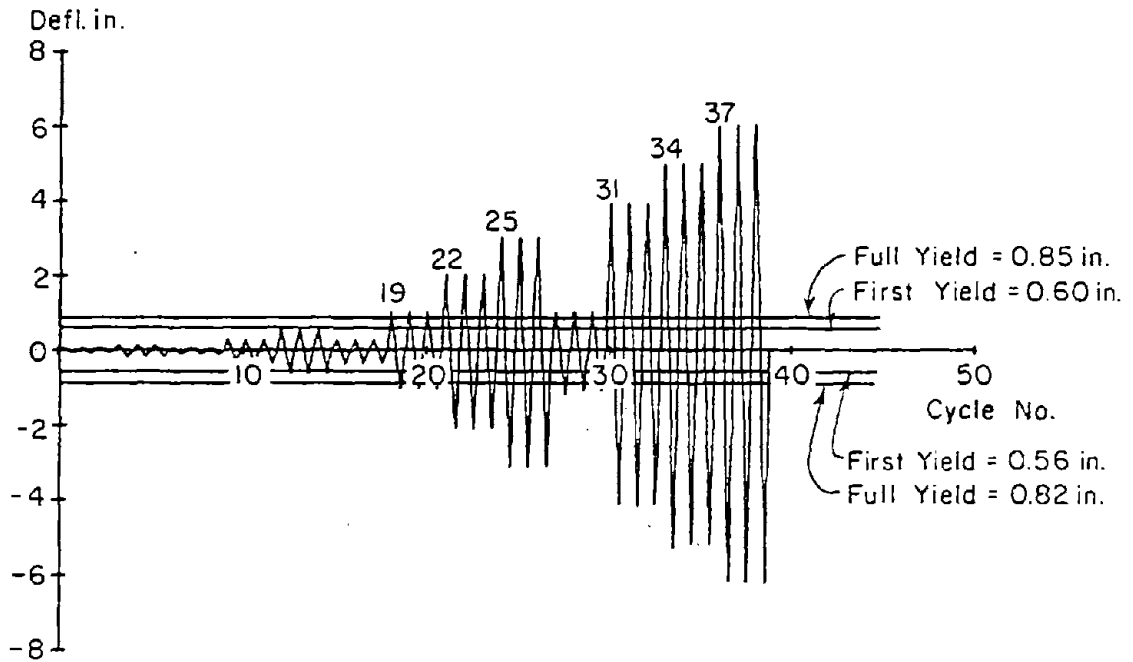
b) Deflection History

Fig. B-28 Loading History for Specimen R2

B-42
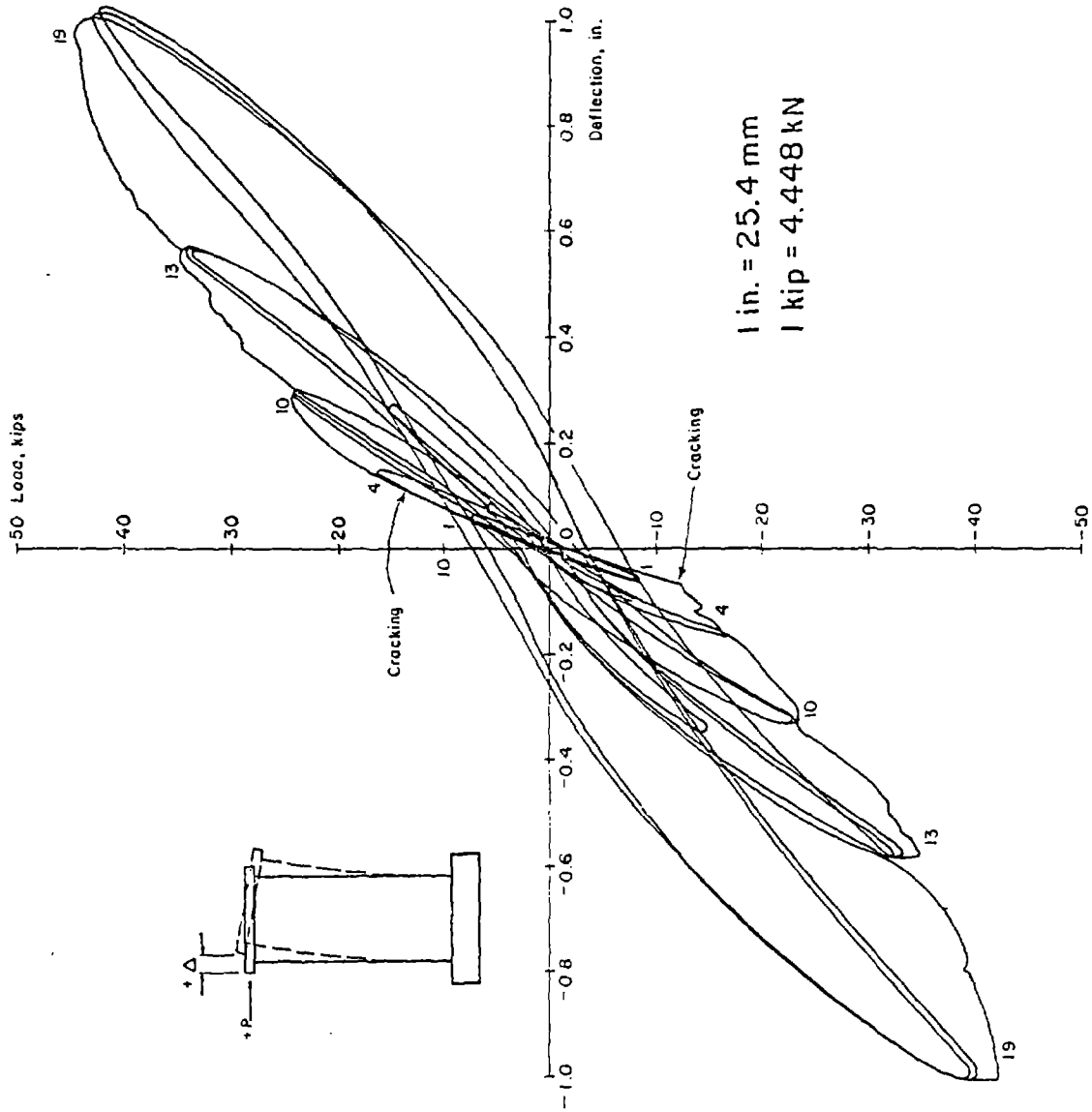
Fig. B-29 Continuous Load-Deflection Plot for Initial Cycles for Specimen R2

1 in. = 25.4 mm
1 kip = 4.448 kN
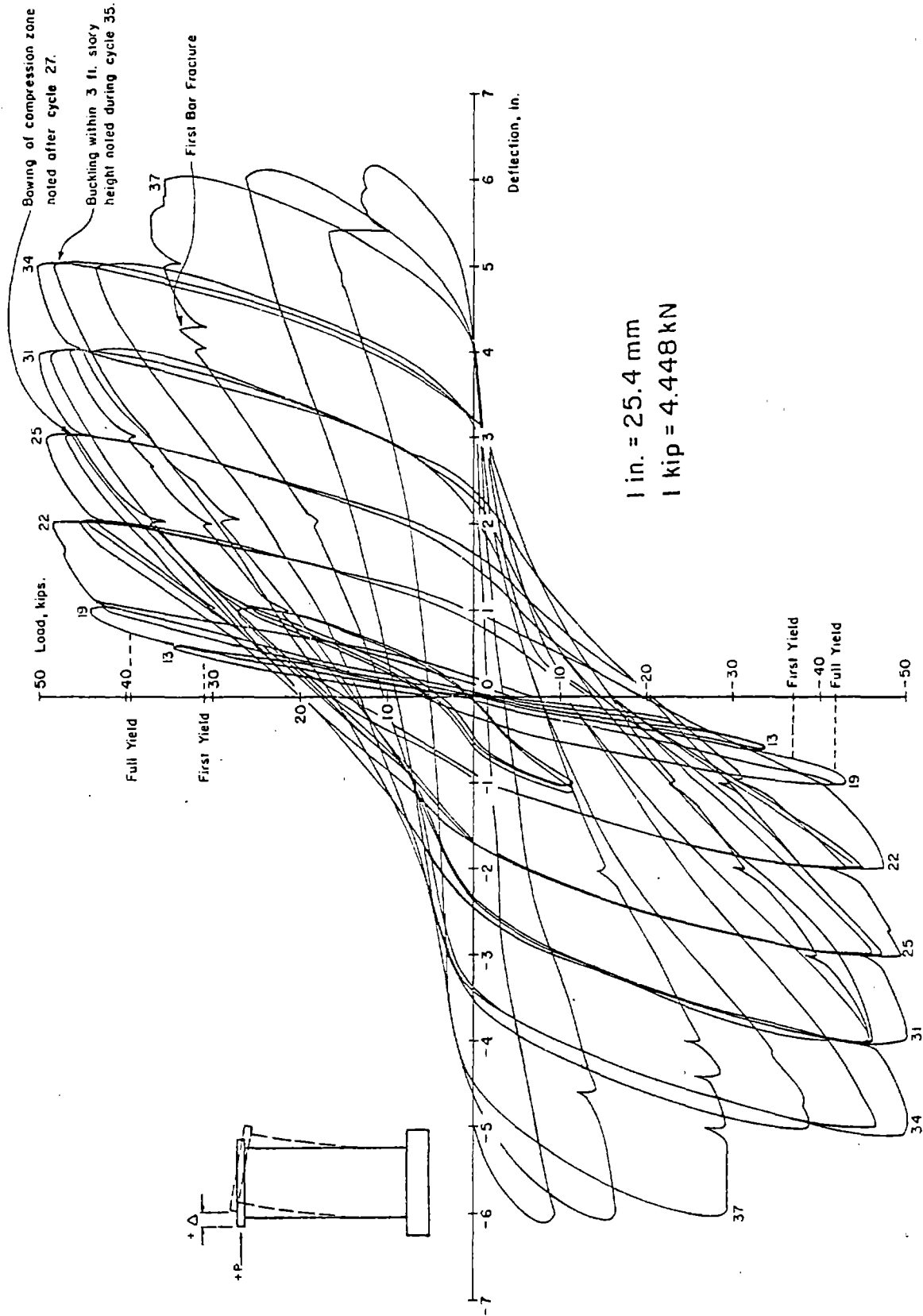
Fig. B-30 Continuous Load-Deflection Plot for Specimen R2

1 in. = 25.4 mm
1 kip = 4.448 kN

Bowing of compression zone noted after cycle 27.

Buckling within 3 ft. story height noted during cycle 35.

First Bar Fracture

Load, kips.
Deflection, in.
First Yield
Full Yield
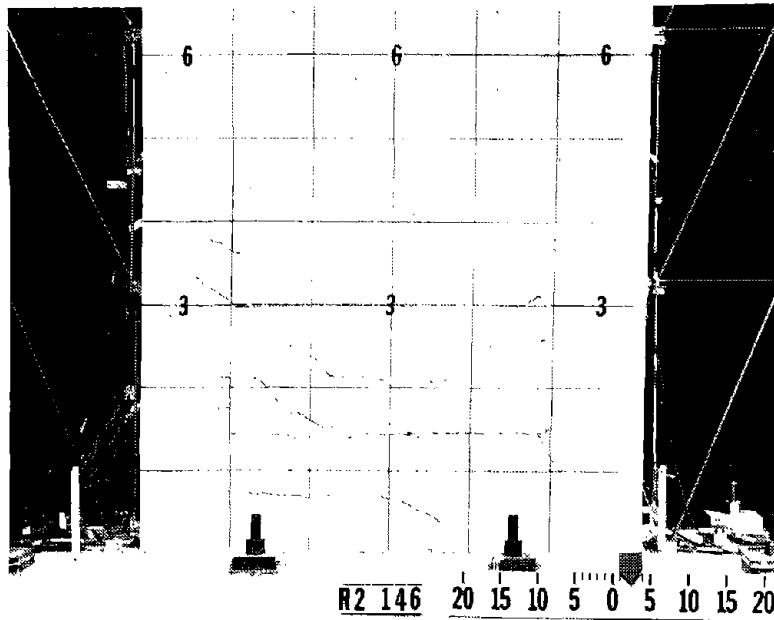
Fig. B-31   Cracking Pattern at +3 in. Deflection
for Specimen R2
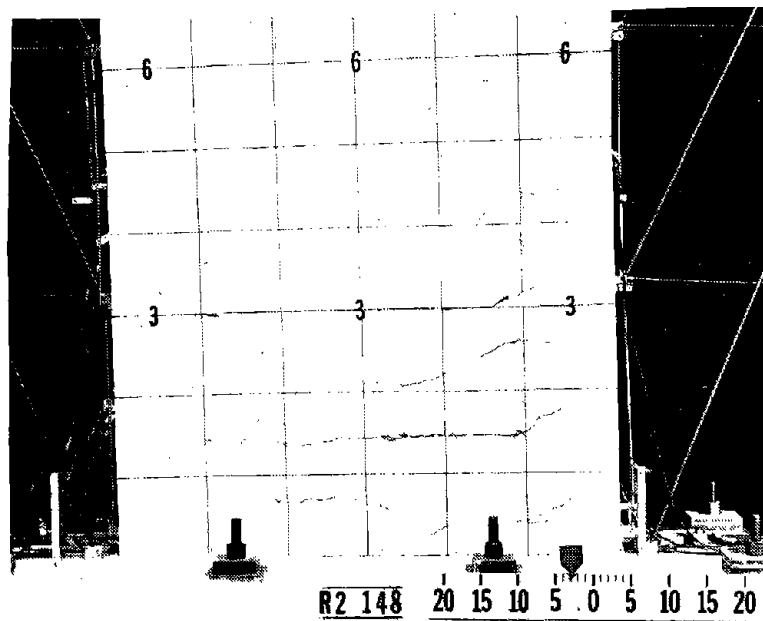
Fig. B-32   Cracking Pattern at -3 in. Deflection
for Specimen R2

the opposite directions of loading intercept each other. These cracks segmented the web into large pieces. Several horizontal cracks completely traversed the width of the wall. The horizontal cracks formed at the levels of the horizontal steel in the web which was at 8 in. (203.2 mm) on center.

In the first 3 in. deflection Cycle 25, it was noted that the cracks in the compression zone remained open 0.003 in. (0.076 mm). First indication of crushing of the outer shell at the base of the wall had been noted in Cycle 22. A significant increase in spalling and flaking along the horizontal cracks was observed during the 3 in. deflection cycles.

During Cycle 28, a 1 in. (25.4 mm) deflection cycle, bowing of the compression end was observed. The compression boundary element was 0.25 in. (6.4 mm) out of plane at a point 3 ft 6 in. (1.1 m) above the base. Although this bowing progressed further with each cycle the load carrying capacity of the wall remained stable. After Cycle 32, the compression end of the wall was 3 in. (76.2 mm) out of plane at a point 3 ft-6 in. above the base. Fig. B-33 shows the specimen after Cycle 32.

The test was stopped after Cycle 32 and lateral bracing was added to the test set-up. An omni-direction ball caster was placed against the face of the each boundary element at a level 3 ft 6 in. above the base. This simulated lateral support at approximately the first story height.
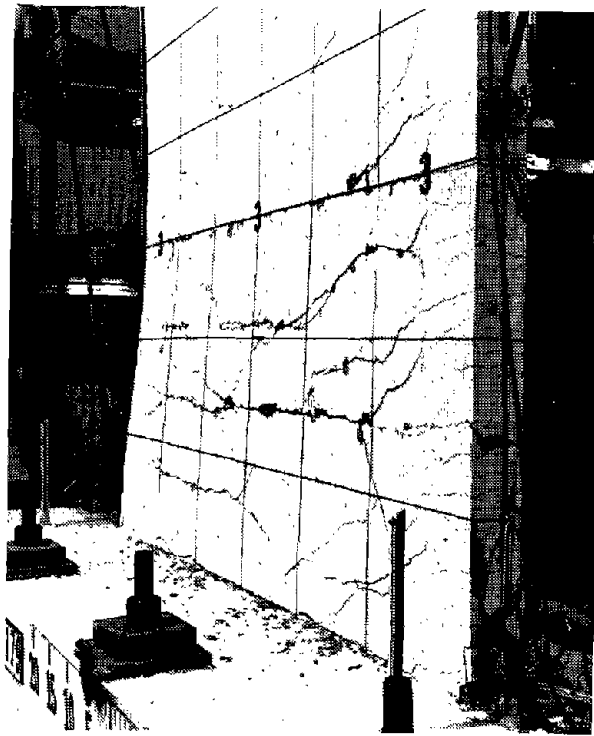
Fig. B-33   Lateral Displacement of Compression Zone
After 4 in. Deflection for Specimen R2
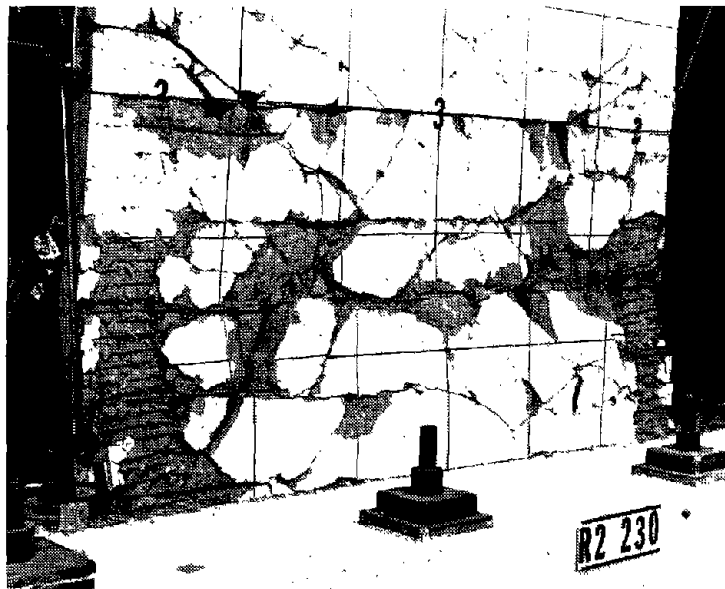
Fig. B-34   Specimen R2 at End of Test

The test was continued with the third 4 in. (101.6 mm) deflection Cycle 33. Considerable grinding and spalling along web cracks occurred during the 4-in. deflection cycles. Also, the end hooks of several horizontal bars started to open during the 4-in. cycles.

The maximum measured load, -48.8 kips (216.6 kN), occurred in Cycle 34 at a -5 in. deflection. This load corresponded to a nominal shear stress, $v_{max} = 2.5\sqrt{f'_c}$ ($0.21\sqrt{f'_c}$, MPa). The maximum measured crack widths at this stage were 0.023 in. (0.58 mm) in the tension boundary element and 0.125 in. (3.18 mm) in a diagonal crack in the web.

In Cycle 35, a large out of plane displacement of the compression zone within the lower 3 ft 6 in. height was observed and the load carrying capacity of the wall decreased. The maximum negative load in the third cycle of the 5 in. (127.0 mm) deflection increment was 79% of the maximum in the first cycle.

Several bars fractured in Cycle 37 and out of plane displacement of the compression zones progressed further. Considerable crushing and loss of concrete occurred in subsequent cycles and the load carrying capacity continued to decrease.

The specimen sustained at least 80% of the maximum measured load through 14 complete inelastic cycles. The last inelastic loading increment in which the load was sustained at or above 80% of the maximum for all 3 cycles

was at ±4 in. (±101.6 mm). A photograph of the wall after testing is shown in Fig. B-34.

The fact that lateral support at the first story level was not present during the major portion of the test probably precipitated an early failure. The reverse curvature out of plane of the boundary element just above the base during the bowing in the 3-in. and 4-in. cycles contributed to premature out of plane displacement within the 3 ft 6 in. height. This out of plane movement may also have contributed to fracture of bars at the base.

Discussion of Results

Moment-Rotation. The moment rotation data for Specimen R2 is shown in Fig. B-35. The measured maximum moment was 85% of the calculated monotonic maximum. The relationship between the calculated and measured rotations at the 3-ft (0.91 m) level is very similar to that relationship at the 6-ft (1.83 m) level. This indicates the shape of the assumed effective curvature distribution was accurate.

The maximum measured loads in each new increment exhibit only slight "strain hardening" as the rotations increase. An envelope through the measured peaks appeared to approach a maximum lower than the maximum calculated for monotonic loading.

The rotation loops at the base level exhibited considerable pinching after Cycle 19. Pinching is only slightly evident in the latter loops at the 3-ft level. No indication of pinching is evident in the stable loops at the 6-ft level.

a) At 6 ft. Level

b) At 3 ft. Level

1 ft. = 0.305 m
1 in. = 25.4 mm
1 kip = 4.448 kN
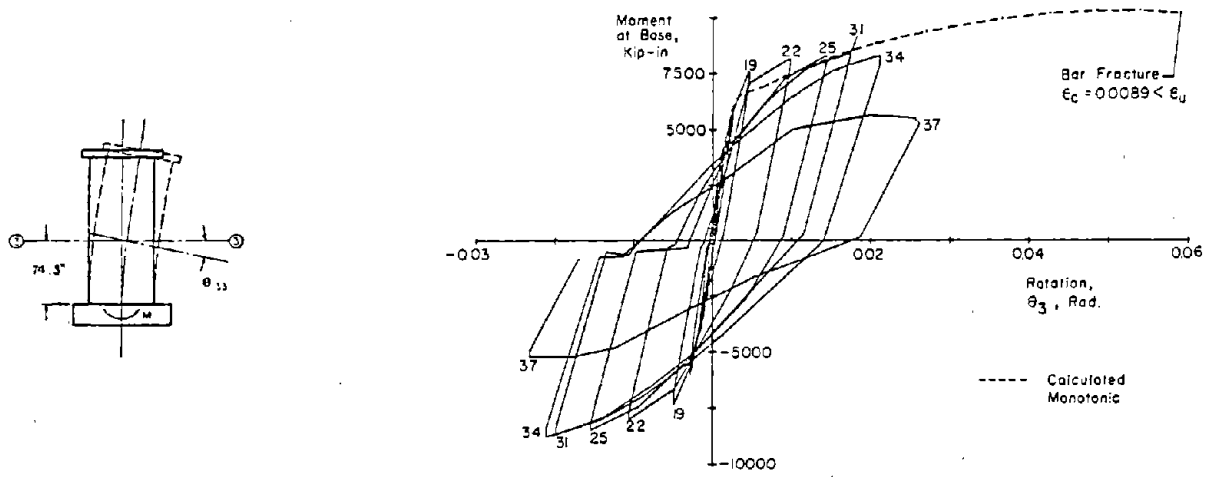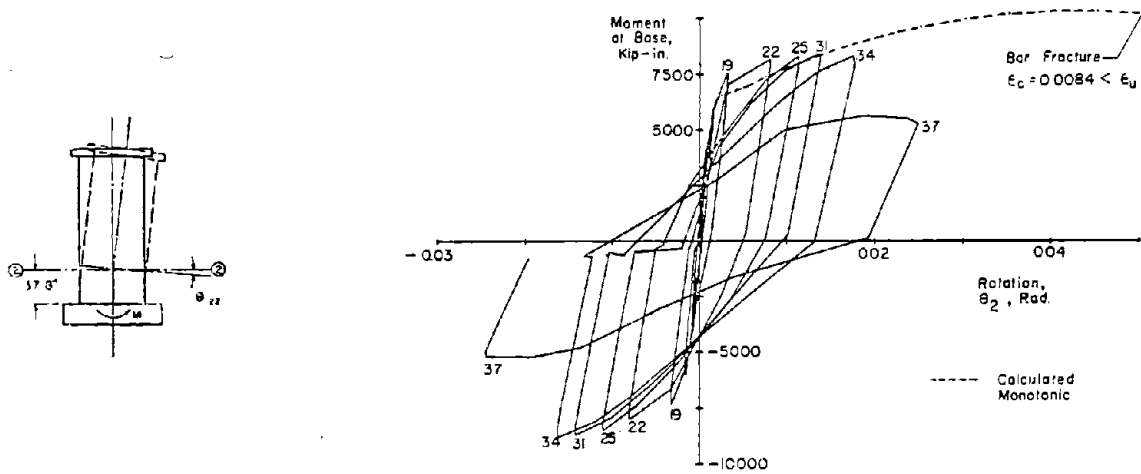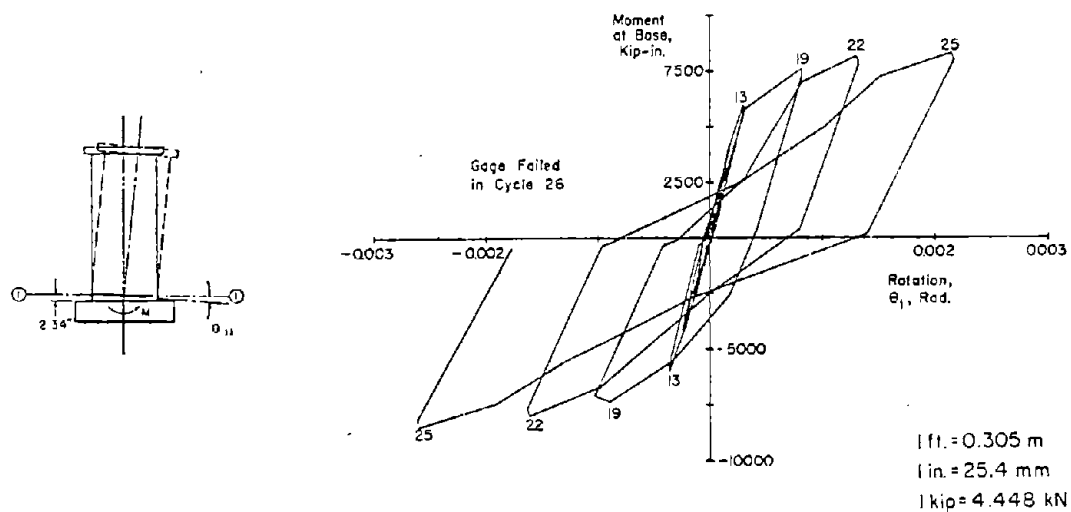
c) At Base Level

Fig. B-35   Moment at Base versus Rotation
for Specimen R2

Shear-Distortion. The shear distortion loops for R2 are shown in Fig. B-36. Although the wall was considerably over-reinforced for shear, the specimen exhibited shear "yielding" during approximately the same load cycles in which flexural yielding occurred.

After shear "yielding" the loops exhibited pinching over an increasingly wide range of deflection. The pinching was more evident in Zone 1. The new maximum shear distortion in each increment became larger at an increasing rate. The magnitude of distortion in Zone 2 was approximately 50% of that in Zone 1.

Slip at Construction Joints. The slip at construction joints in R2 is shown in Fig. B-37. The slip at CJ1 and CJ2 exhibited a "yielding" similar to shear "yielding" at a later load increment than flexural yielding occurred at the corresponding levels. The slip stiffness for CJ1 and CJ2 was larger for positive load. The slip at CJ3 was negligible.

The slip at CJ1 is shown as a percentage of the total shear deflections in Zone 1 in Fig. B-38. With the exception of R1, Specimen R2 exhibited a larger percentage of slip in the negative direction than did the other test specimens.

Deflection. The deflection components and deflected shapes for Specimen R2 are shown in Figs. B-39 and B-40. As in Specimen R1, these figures show that flexure was the larger component of top deflection. However, shear deflections were a significant portion of the total and a somewhat larger portion than in R1. The shear deflections were
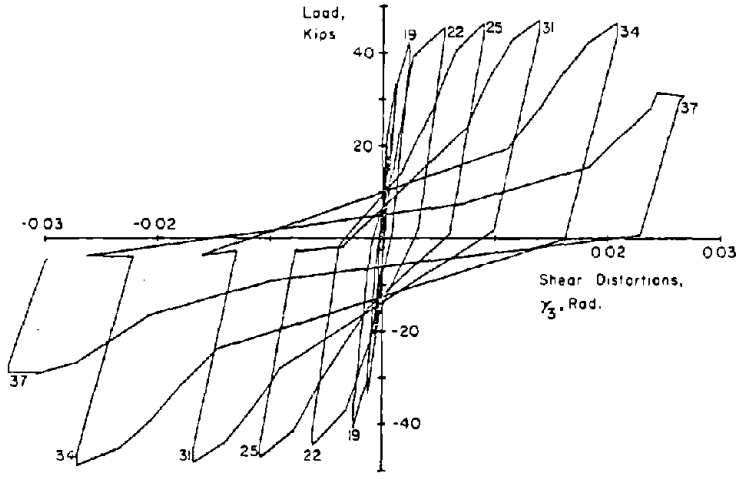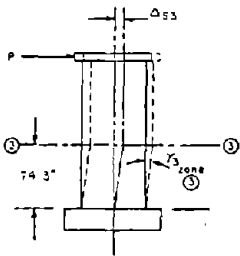
a) In Base to 6 ft Level
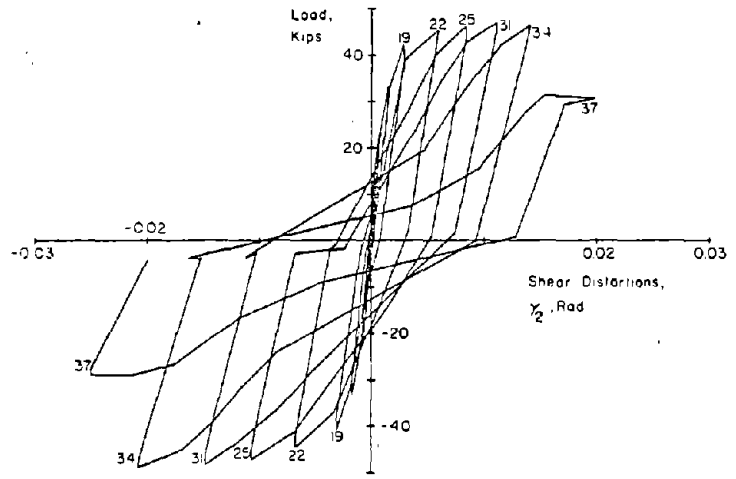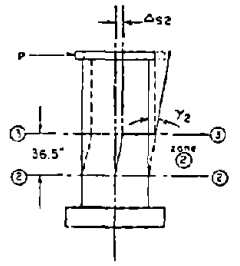
b) In 3 ft to 6 ft Level
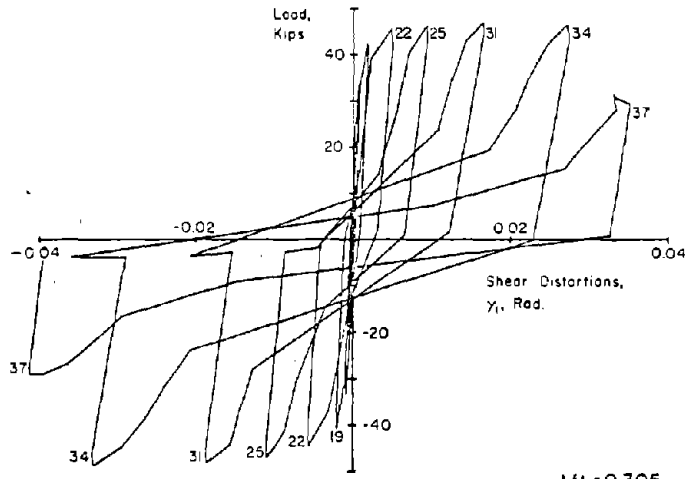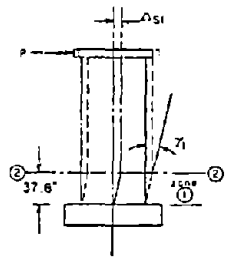
c) In Base to 3 ft Level

1 ft.=0.305 m
1 in.= 25.4 mm
1 kip=4.448 kN

Fig. B-36   Load versus Shear Distortion
for Specimen R2
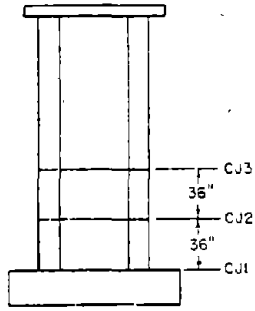
a) At 6 ft. Level
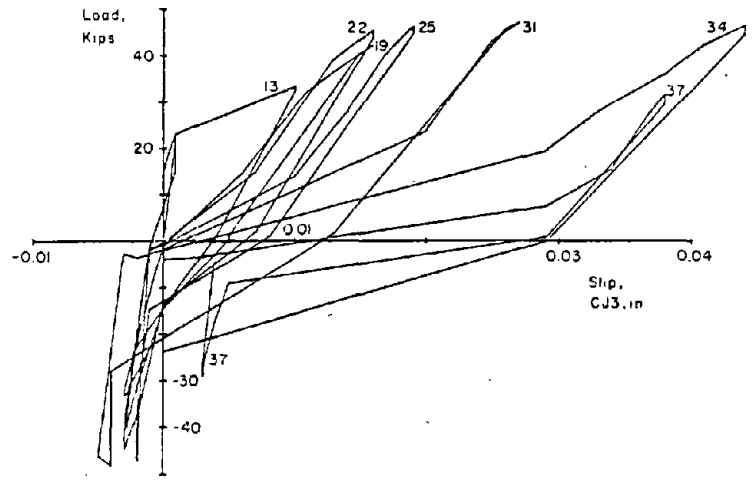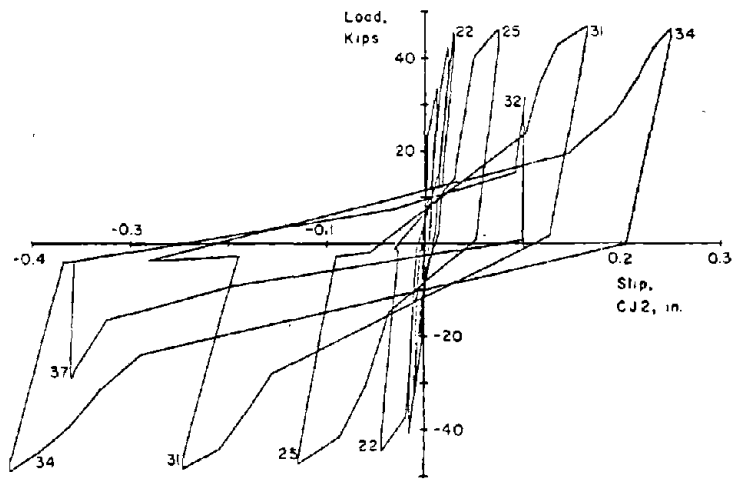
b) At 3 ft. Level

1 ft.=0.305 m
1 in.=25.4 mm
1 kip=4.448 kN

c) At Base Level
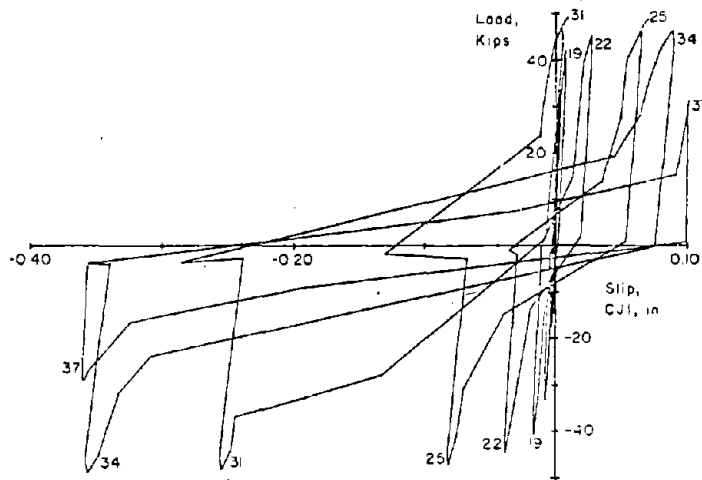
Fig. B-37   Load versus Slip at Construction Joint
For Specimen R2

a) At Maximum Positive Loads

b) At Maximum Negative Loads
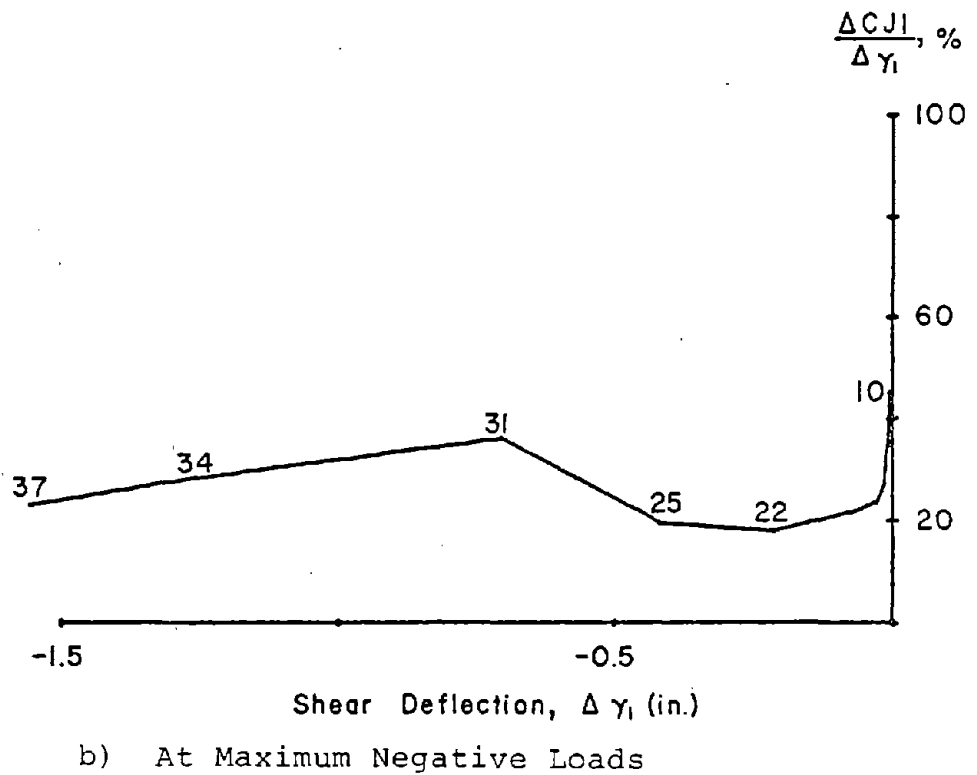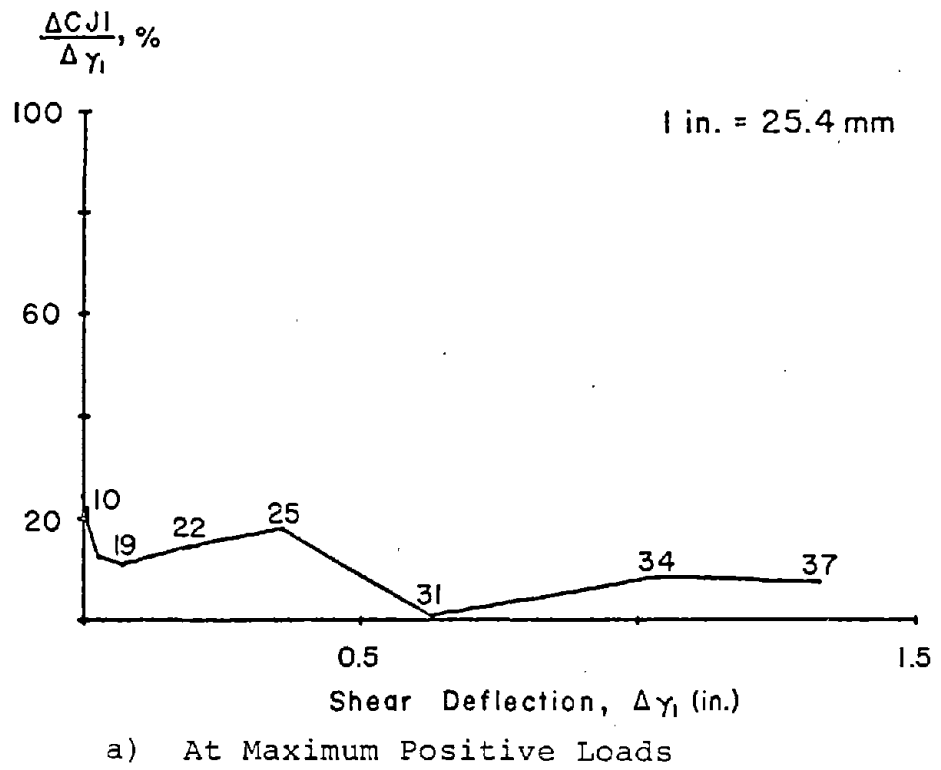
Fig. B-38   Slip at Base Construction Joints versus
Shear Deflection in Zone 1 for Specimen R2

a)   At Top of Wall
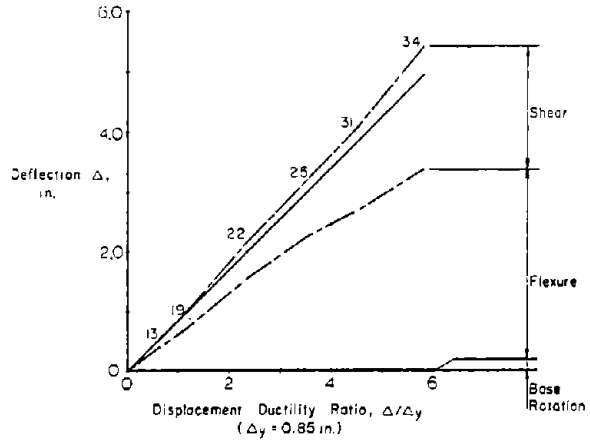
b)   At 6 ft. Level
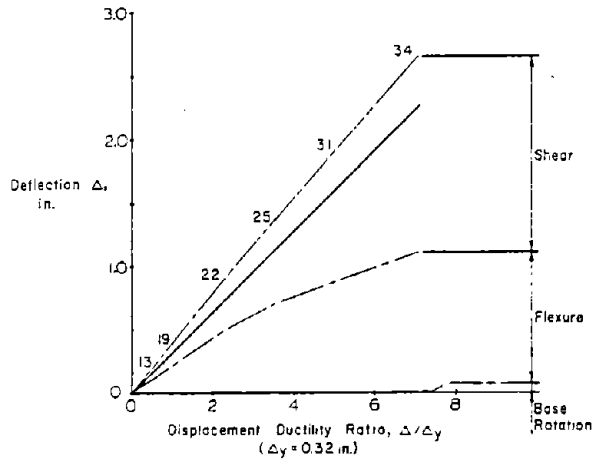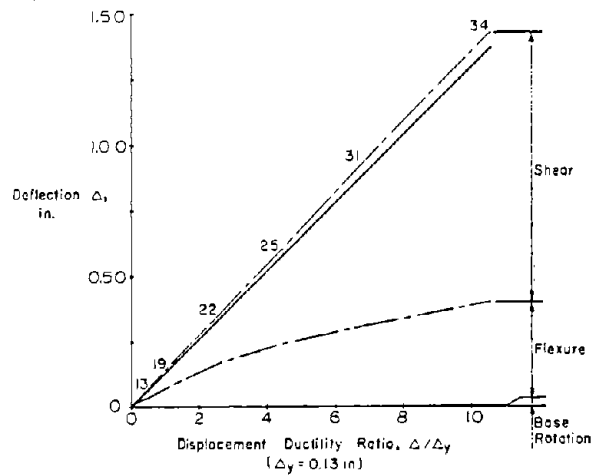
c)   At 3 ft. Level

Fig. B-39   Component of Deflection for Specimen R2

a) Flexural
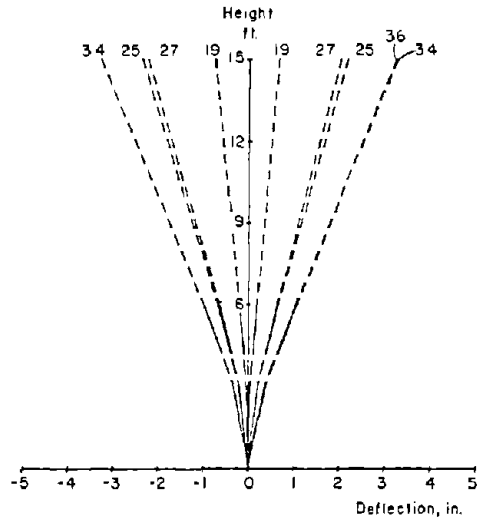
b) Shear
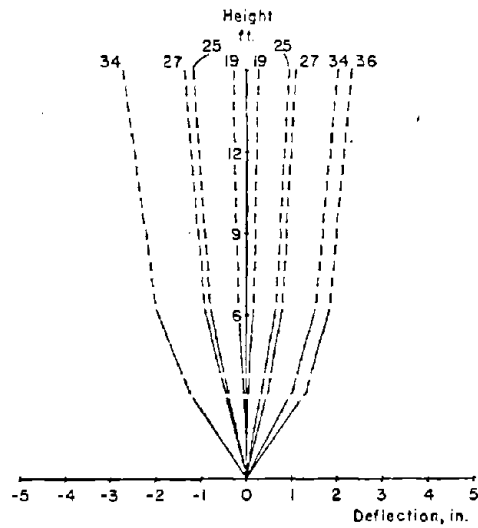
— — — CALCULATED FROM
          MEASURED DEFORMATION
— — — EXTRAPOLATED
———— MEASURED TOTAL

1 in.= 25.4 mm
1 ft.= 0.305 m

CYCLE 36, AFTER
BUCKLING

CYCLE 34, PRIOR
TO BUCKLING
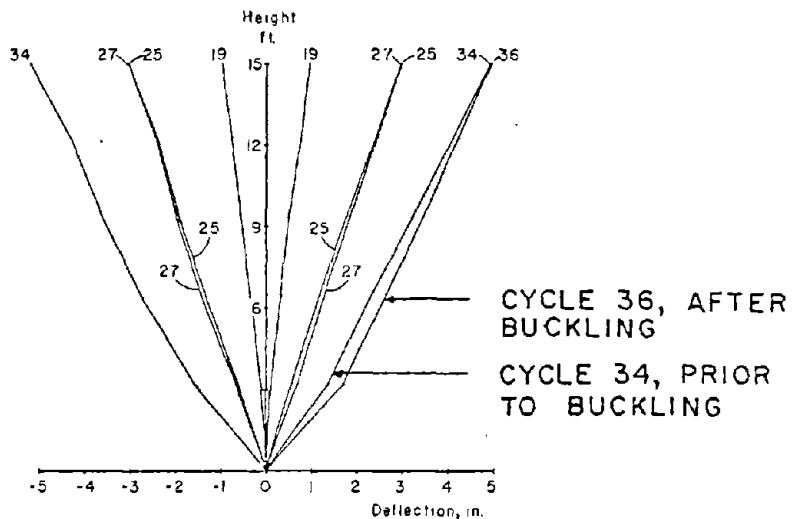
c) Total

Fig. B-40 Deflected Shape for Specimen R2

becoming an increasing portion of the total in the latter load increments, especially in the lower 3 ft (0.91 m). This latter shear deflection was such that the total deflected shape was similar to the deflected shape of a frame. This is shown in Fig. B-40. The deflected shapes at Cycle 25 and 27 showed a small amount of shear degradation within the 3-in. (76.2 mm) increment.

Reinforcement Strains. Figures B-41 through B-49 show reinforcement strains in the specimen at several stages.

Figure B-42 shows that yielding of the vertical bars extended up to the 9-ft (2.74 m) level in Cycle 31. Figure B-44 shows that the left compression element started to grow in Cycle 19.

Figures B-45 through B-49 show that, even though the specimen was over-reinforced for shear, considerable yielding occurred in the horizontal bars in the lower 9 ft of wall. Even the gages near the ends of the horizontal bars, HH and HA, indicated strains at or near yield. This indicates that the end hooks on the horizontal bars were necessary. The strains approached zero at the 12-ft (3.66 m) level.
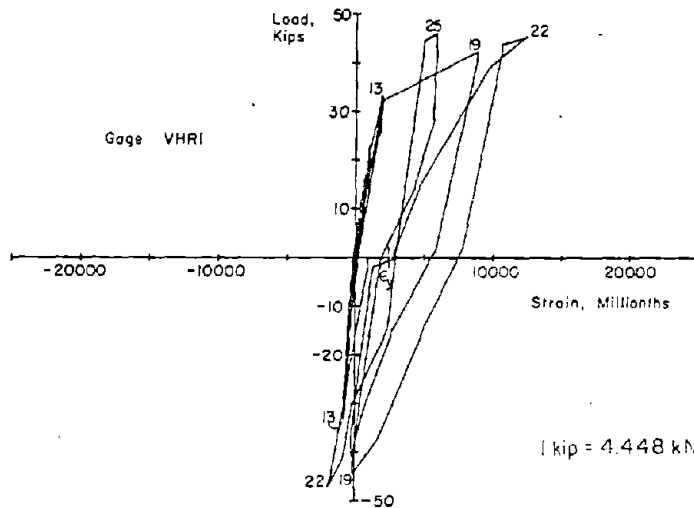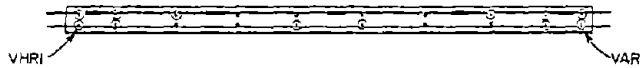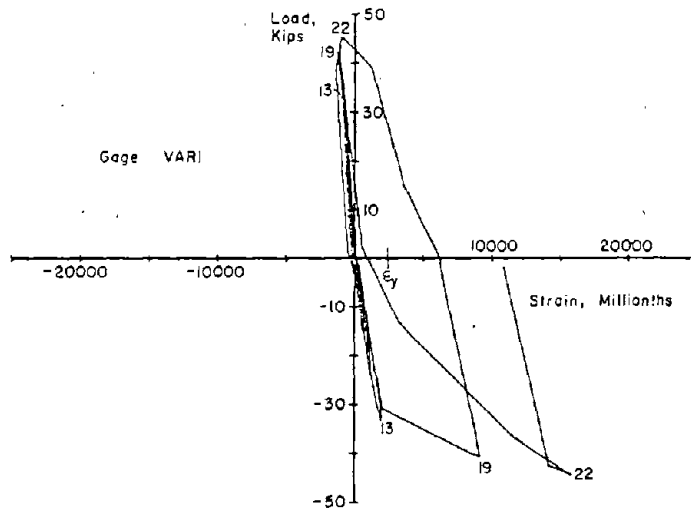
Fig. B-41   Measured Strains at Vertical Reinforcement
at Base of Specimen R2
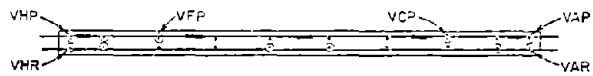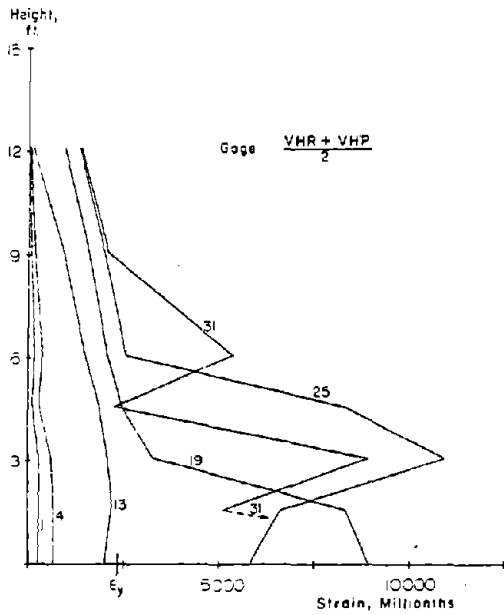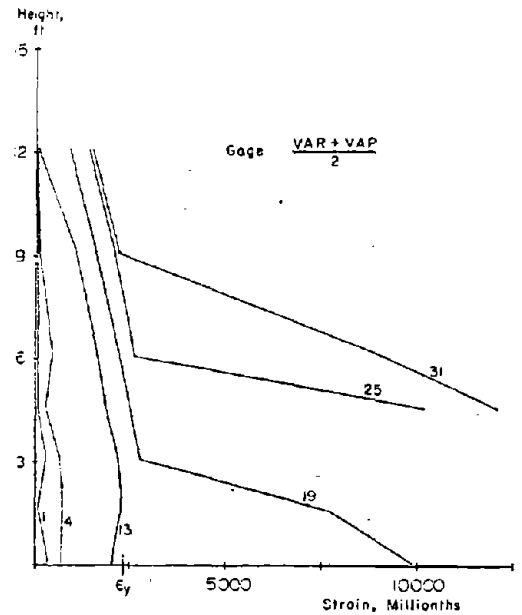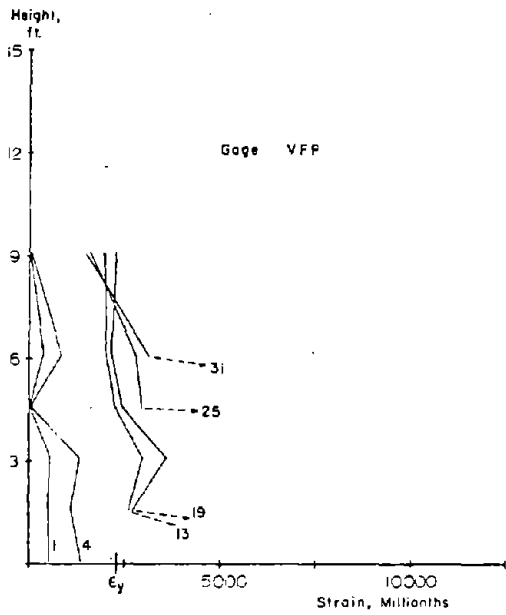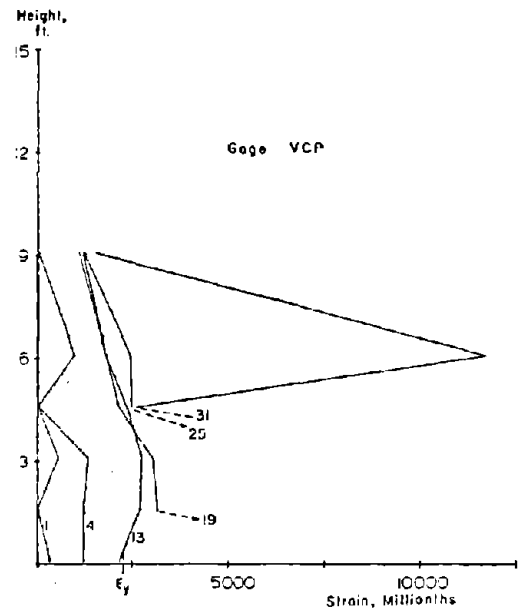
Fig. B-42 Vertical Reinforcement Strains at
Maximum Loads for Specimen R2
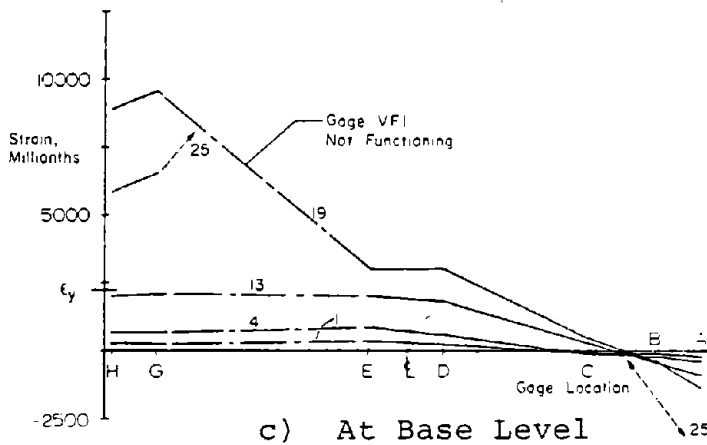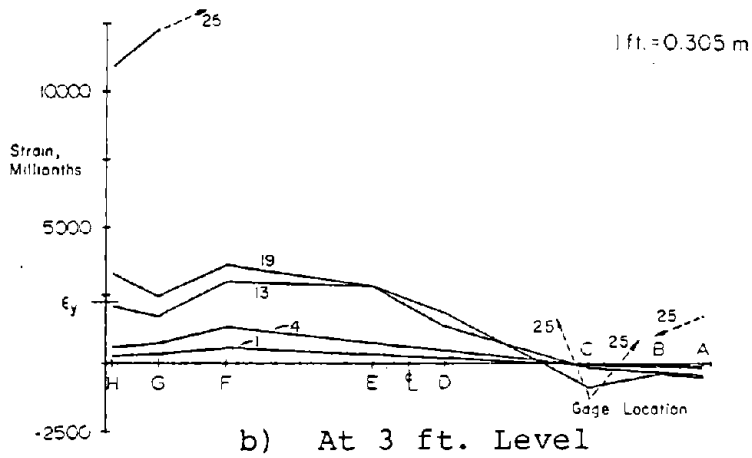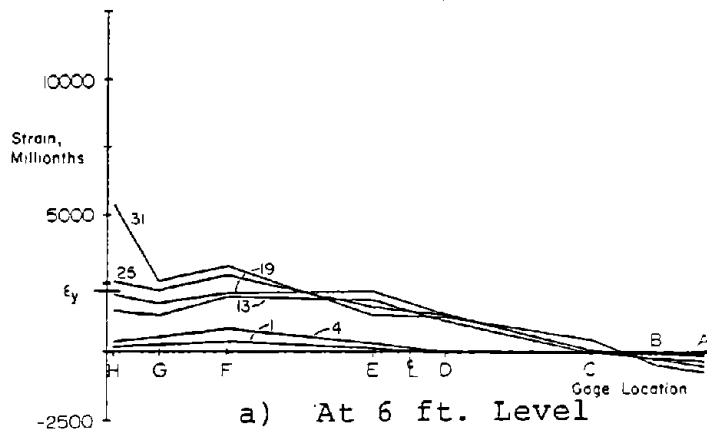
Fig. B-43   Vertical Reinforcement Strains at
            Maximum Positive Loads for Specimen R2

a)   At 6 ft. Level

b)   At 3 ft. Level

c)   At Base Level
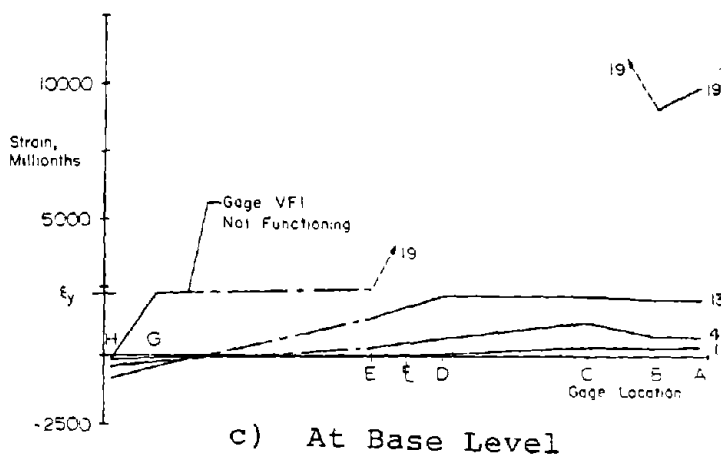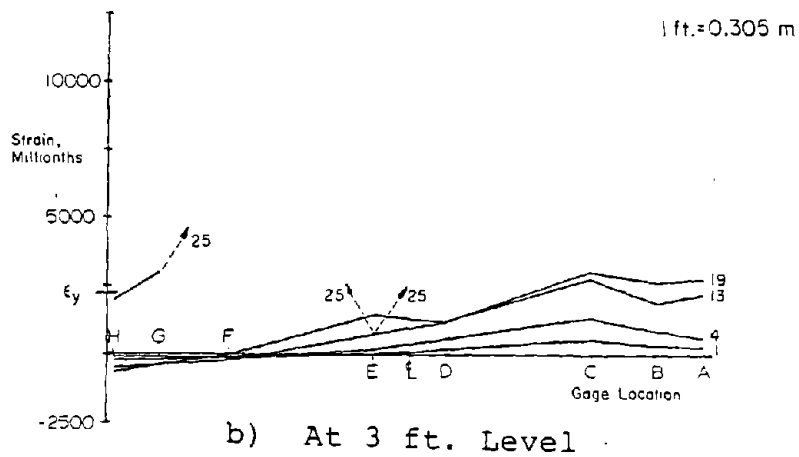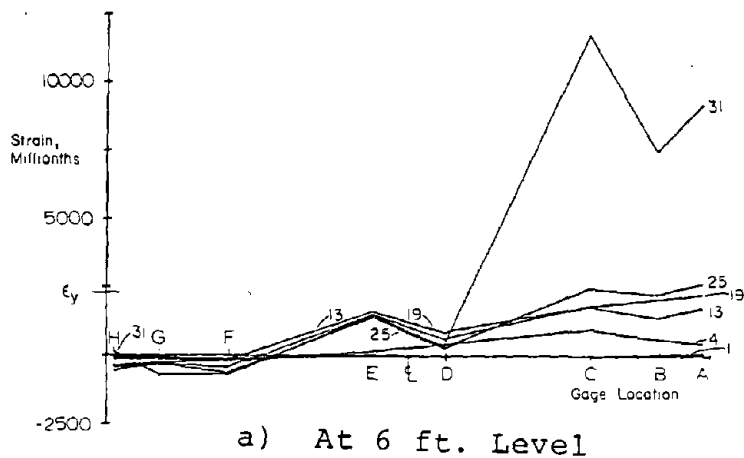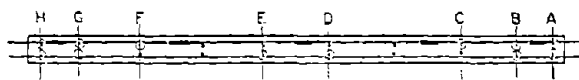
Fig. B-44   Vertical Reinforcement Strains at
Maximum Negative Loads for Specimen R2
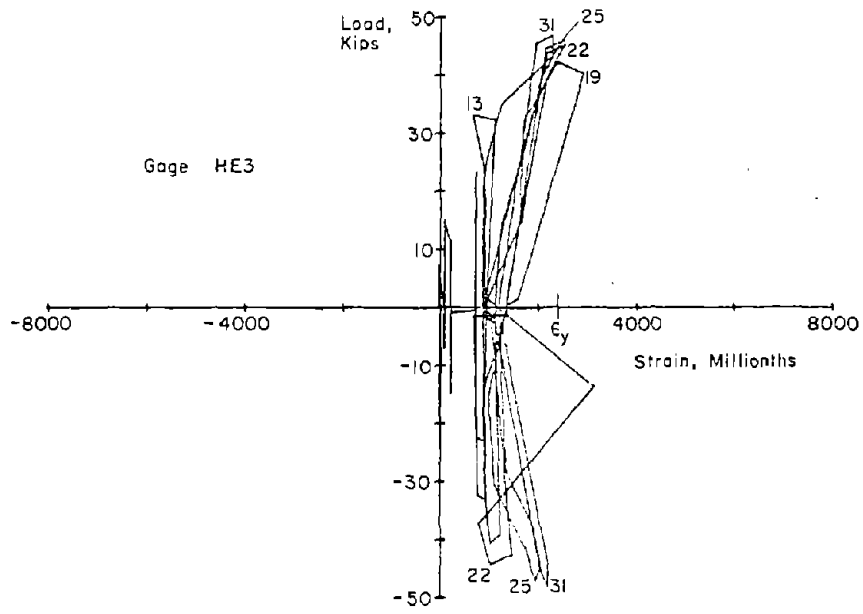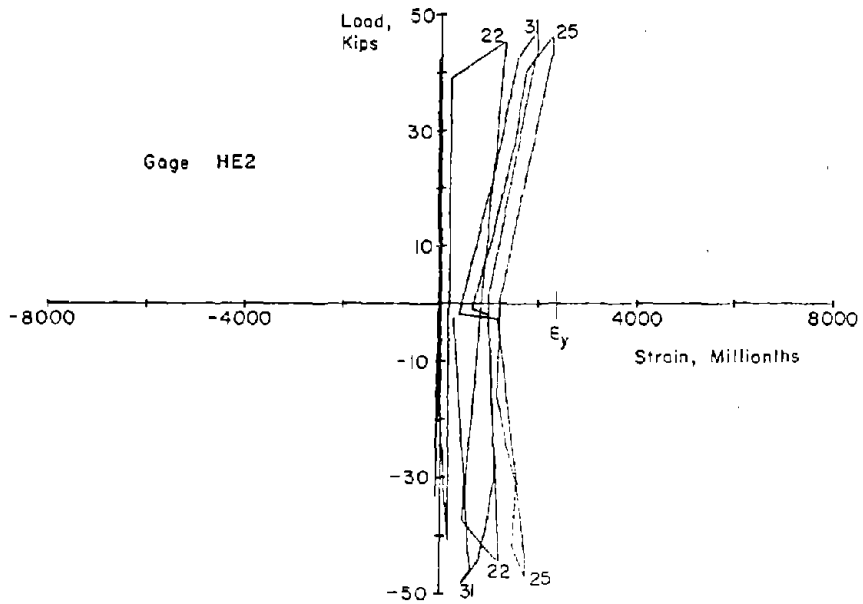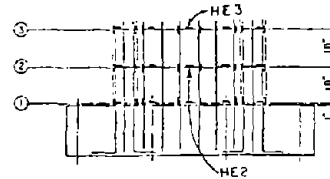
Fig. B-45 Measured Strains on Horizontal Reinforcement
for Specimen R2
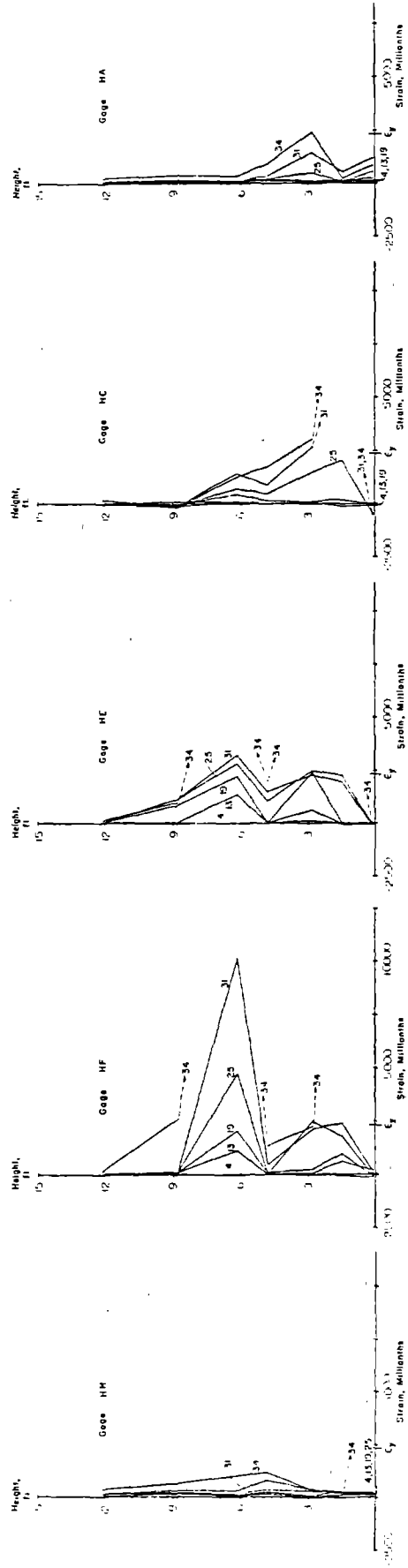
Fig. B-46 Horizontal Reinforcement Strains at
Maximum Positive Loads for Specimen R2
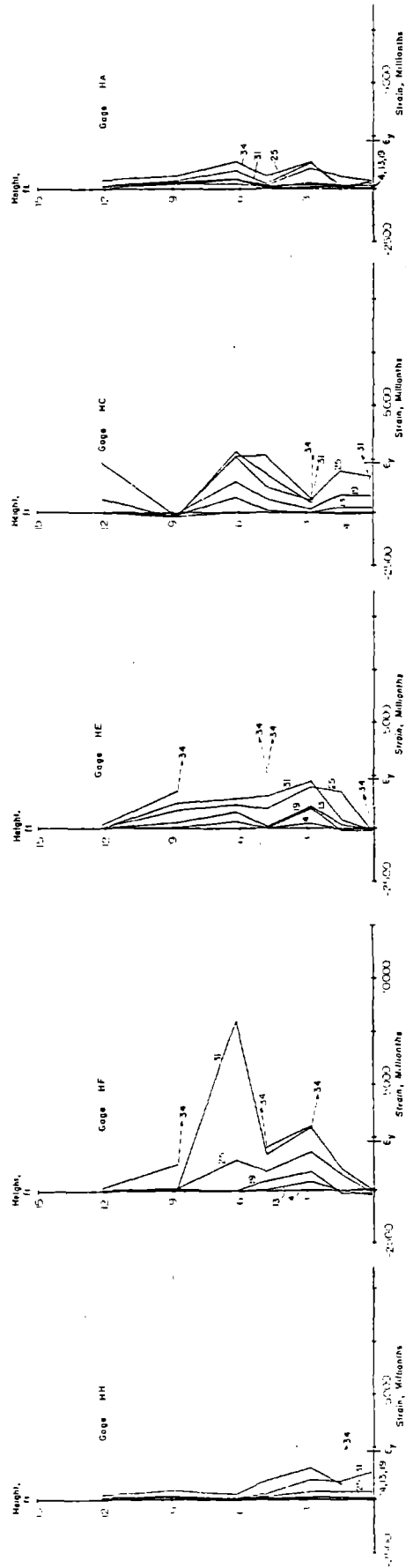
1 ft.=0.305 m

Fig. B-47 Horizontal Reinforcement Strains at
Maximum Negative Loads for Specimen R2
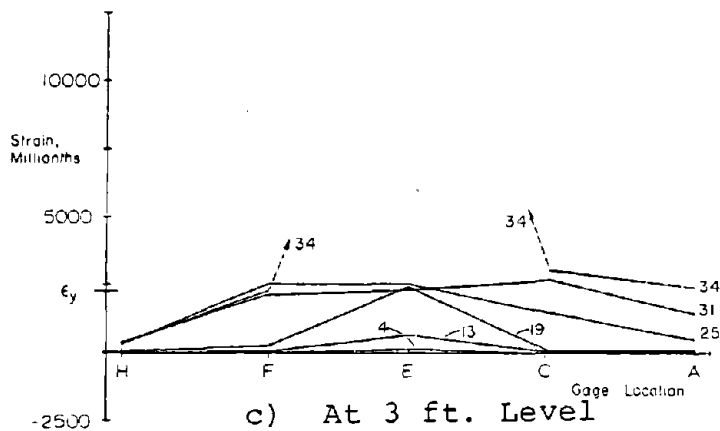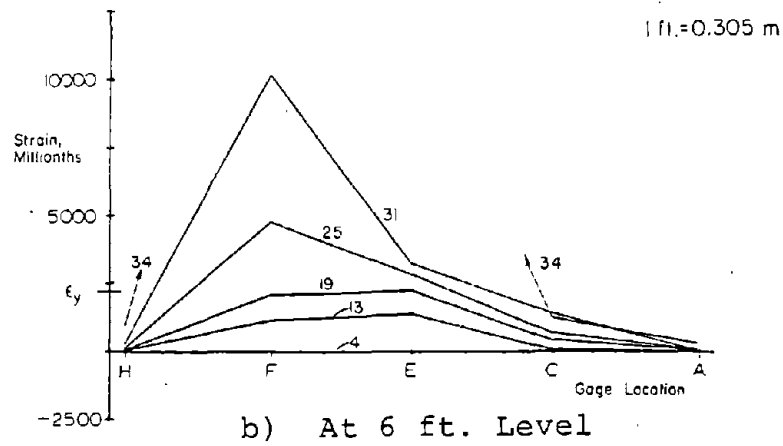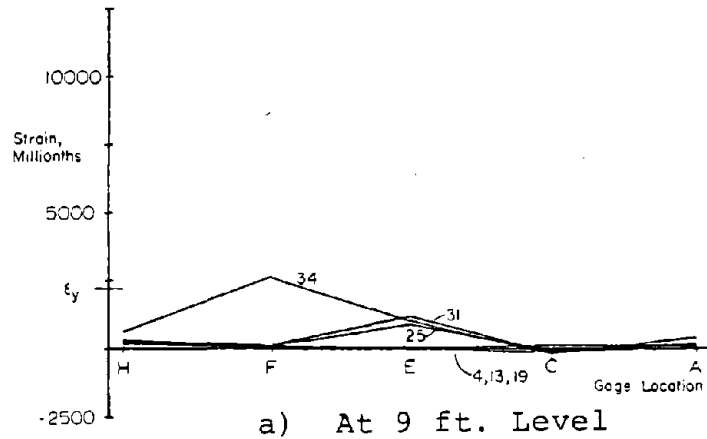
1 ft. = 0.305 m

a) At 9 ft. Level

I ft.=0.305 m

b) At 6 ft. Level

c) At 3 ft. Level

Fig. B-48   Horizontal Reinforcement Strains in Web
at Maximum Positive Loads for Specimen R2

a) At 9 ft. Level

b) At 6 ft. Level

c) At 3 ft. Level
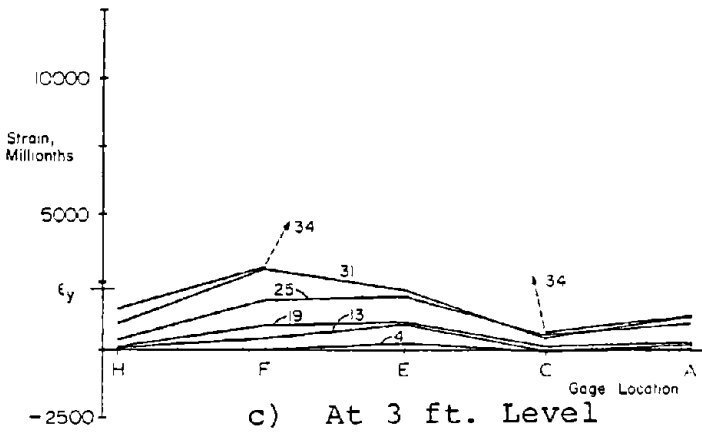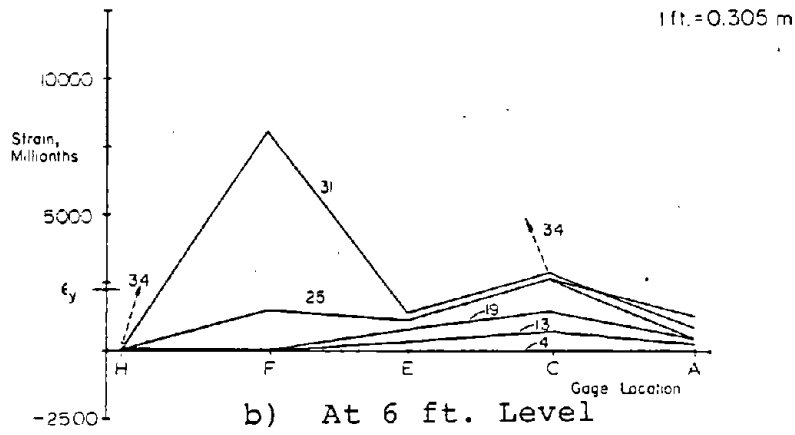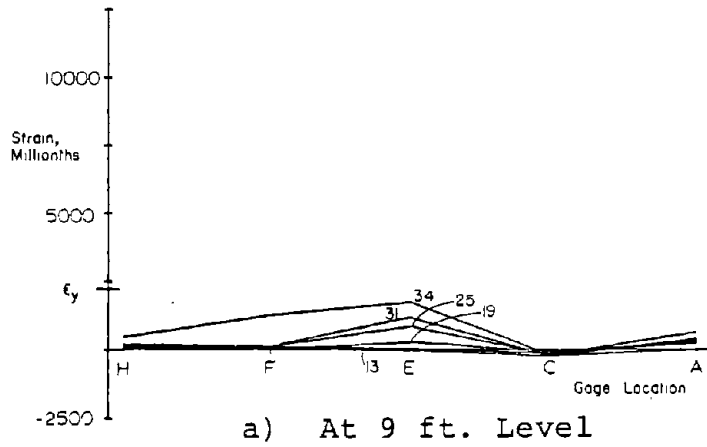
Fig. B-49   Horizontal Reinforcement Strains in Web
           at Maximum Negative Loads for Specimen R2

B-66

Specimen Bl

Test Description

Specimen Bl had column boundary elements with 1.11%
vertical reinforcement in each column. Ordinary column ties
at 8 in. (203.2 mm) on center were used throughout the
height of the boundary element.

The test consisted of 36 loading cycles as seen in Fig.
B-50. Figures B-51 and B-52 show the complete load versus
top deflection relationship for Specimen Bl. Initial flexural
cracking was observed in Cycle 4 at a load of 26 kips
(115.7 kN). First yielding occurred in Cycle 10 at a load
of 45.1 kips (200.6 kN). The maximum measured crack widths
at this stage were 0.009 in. (0.23 mm) in the tension column
and 0.014 in. (0.36 mm) across a diagonal cracks in the web.

The crack pattern that developed started with horizontal
flexural cracks in the columns that progressed into diagonal
shear cracks in the web. The angle of the diagonal cracks
was steeper than the cracking in the rectangular section
specimens. However, web cracks were intercepted by cracks
from the opposite direction loading. The specimen was
eventually traversed across the entire width by several
predominantly straight horizontal cracks. The crack pattern
is shown in Figs. B-53 and B-54 at + 3 in. (76.2 mm) and
-3 in. deflections, respectively.

Minor spalling and flaking along the web cracks was
first noted in Cycle 14. There was a significant increase
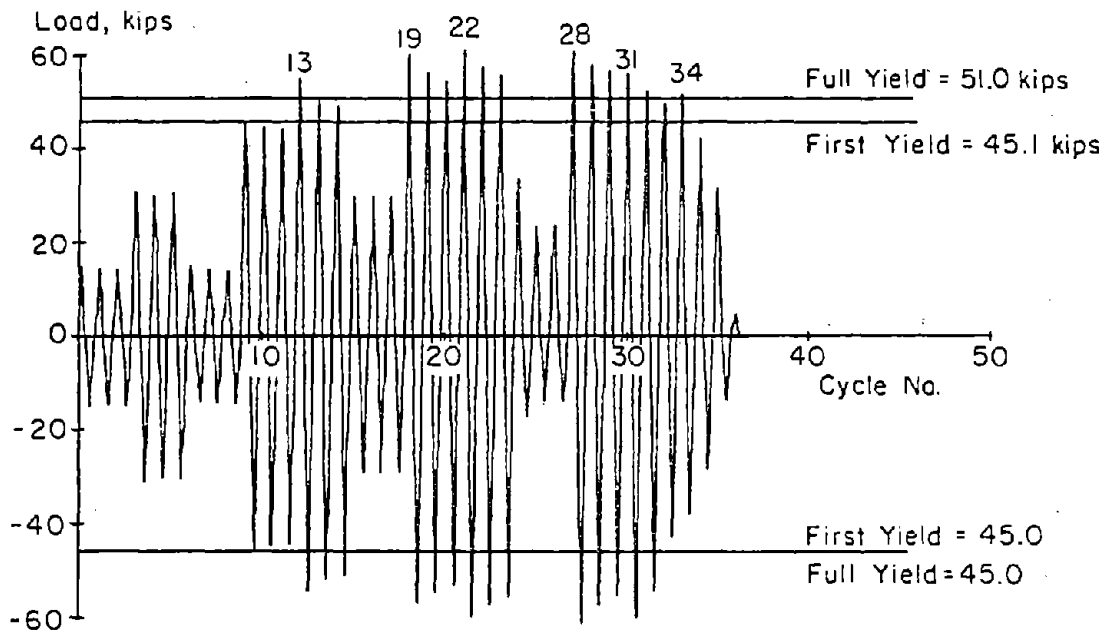
a) Load History

1 in. = 25.4 mm
1 kip = 4.448 kN
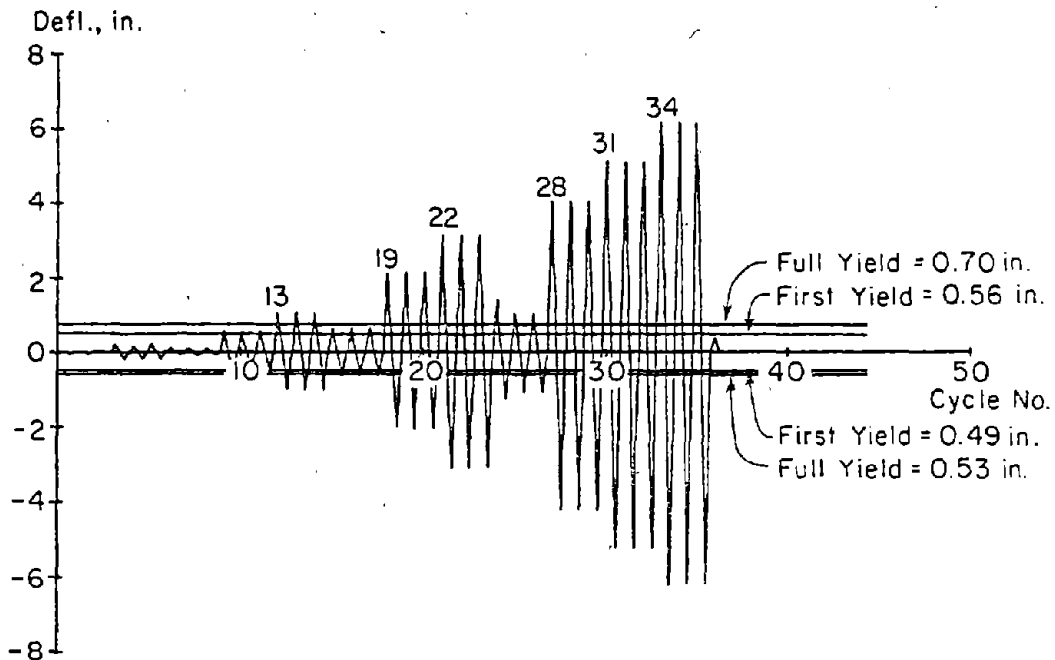
b) Deflection History

Fig. B-50 Loading History for Specimen B1

B-68
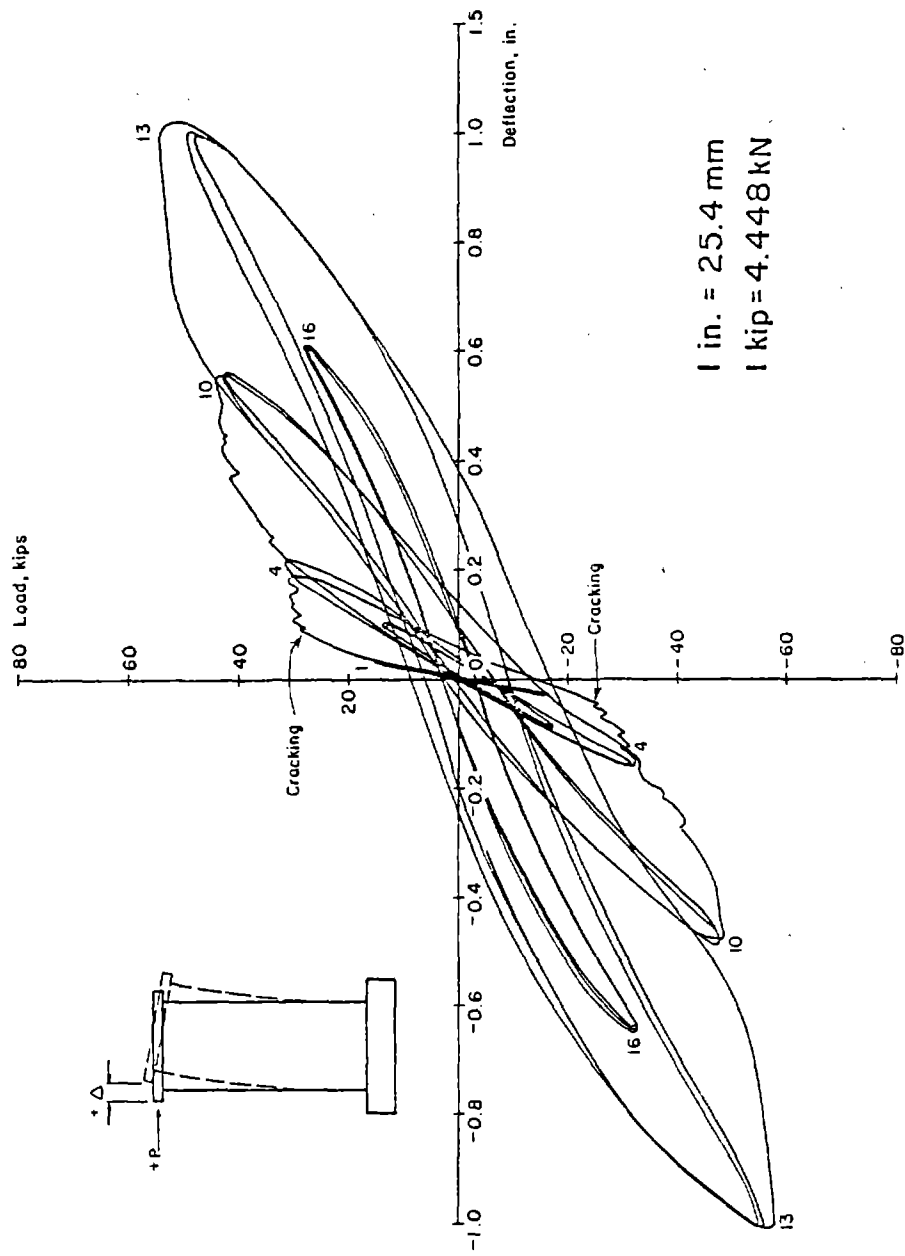
Fig. B-51 Continuous Load-Deflection Plot for Initial Cycles for Specimen B1
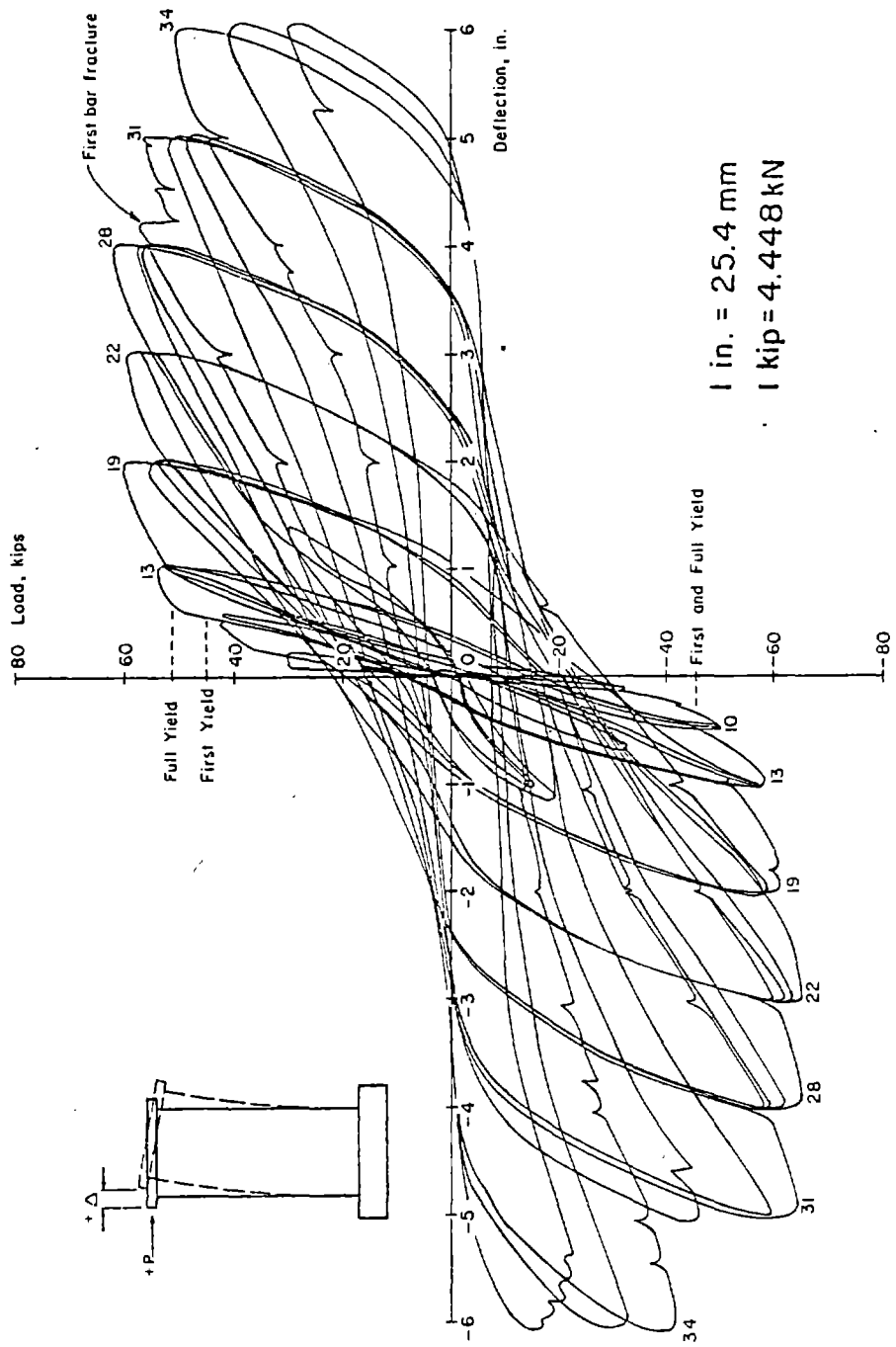
Fig. B-52 Continuous Load-Deflection Plot for Specimen B1
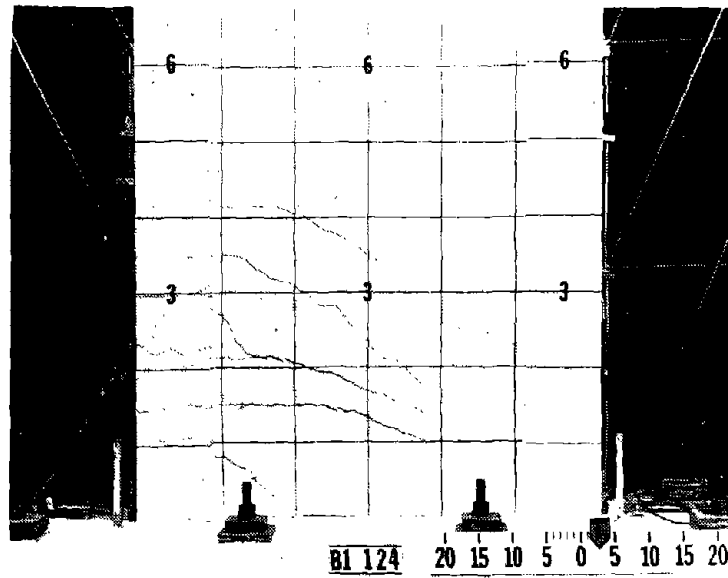
Fig. B-53   Cracking Pattern at +3 in. Deflection
            For Specimen Bl
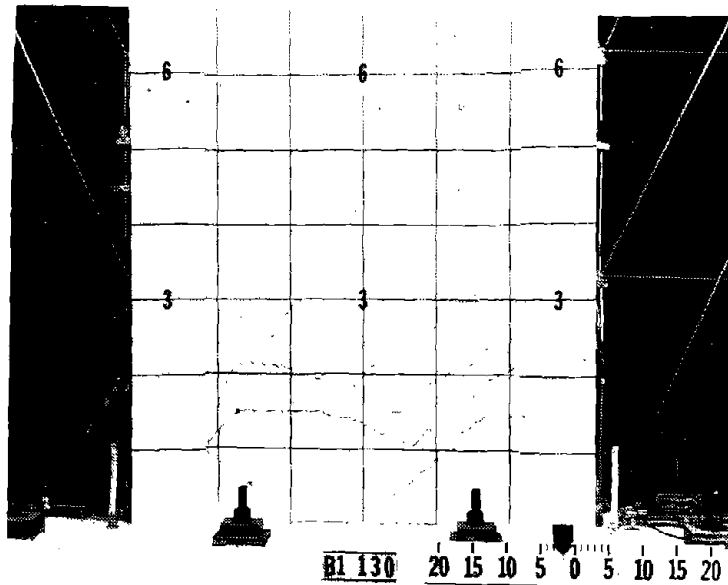
Fig. B-54   Cracking Pattern at -3 in. Deflection
            for Specimen Bl

in this spalling and flaking in Cycle 19. During Cycle 19,
it was first noted that cracks appeared to remain open in
the compression column approximately 0.005 in. (0.13 mm).
Also, it was first noted in Cycle 19 that the boundary
elements had a slight reverse curvature occurring in the
lower 3 ft (0.91 m) of height.

It should be noted that the crack at the base joint
always remained open a considerably greater width in the
center region of the web than in the end boundary elements.
This was a typical behavior observed in all specimens.

First indication of crushing of the concrete at the
base of the wall occurred in Cycle 22, the first 3 in.
deflection cycle. Also, during Cycle 22, the first flexural
bar buckling occurred. A corner bar near the outer face of
a boundary element bowed out between ties near the base. In
subsequent cycles, 13 other bars buckled, some at two or
three levels. A photograph of some of the buckled bars is
shown in Fig. B-55.

After first buckling of flexural bars, the boundary
elements started to deteriorate. The outer shell spalled
off and small pieces of concrete would fall out of the core
when the element was in tension. However, the load carrying
capacity did not reduce during several additional cycles.
The maximum load measured, 61.0 kips (271.3 kN), occurred in
Cycle 28 at a -4-in. (101.6 mm) deflection. This load
corresponded to a nominal shear stress. $v_{max} = 2.9\sqrt{f_c'}$
($0.24\sqrt{f_c'}$, MPa). The end hooks of the horizontal steel
started to open during Cycle 28.
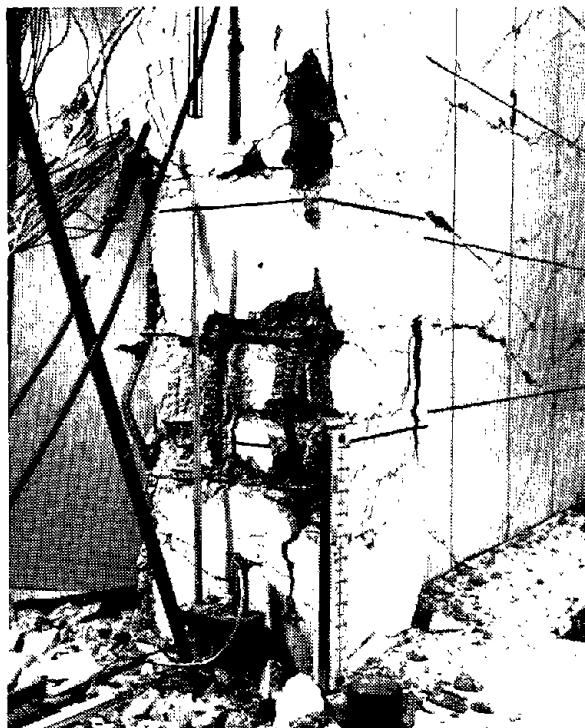
Fig. B-55   Buckling of Reinforcing Bars for Specimen B1
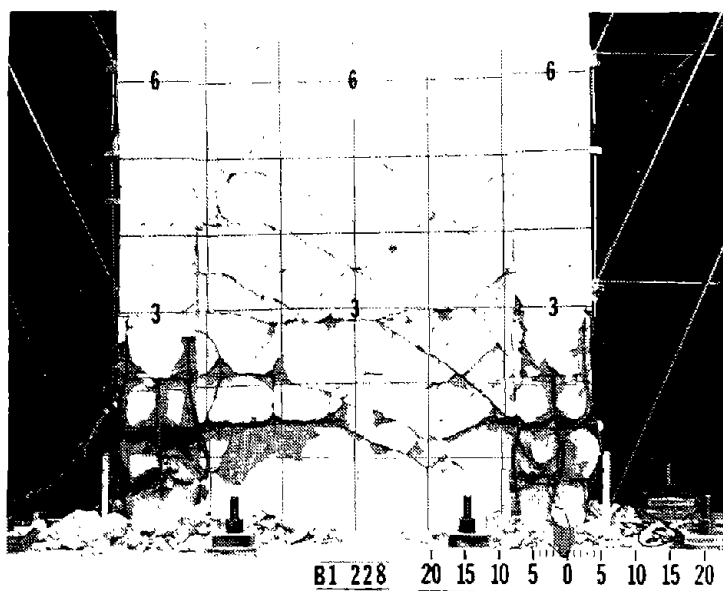
Fig. B-56   Specimen B1 at End of Test

First bar fracture occurred in Cycle 31. The bar that had buckled first was the first to fracture after sustaining 8-1/2 cycles. Subsequently, 3 other bars fractured, however, the load carrying capacity remained above 80% of maximum until the negative half of Cycle 33, the last 5-in. (127.0 mm) deflection cycle. The load at this stage was 70% of the maximum load.

The boundary element deteriorated significantly in the latter cycles of the test with large pieces of concrete falling out when the element was in tension. Finally the concrete in one of the columns was completely lost and the web of the wall was crushed by compressive forces which could not be carried by the column.

The specimen sustained at least 80% of the maximum measured load capacity through 14 inelastic cycles. The last inelastic loading increment in which the load was sustained at or above 80% of the maximum for all 3 cycles was at ±4 in. (101.6 mm) A photograph of the wall after testing is shown in Fig. B-56.

Discussion of Results

Moment-Rotation. Moment rotation data for Specimen B1 is shown in Fig. B-57. The measured maximum moment was 85% of the calculated monotonic maximum. The relationship between the calculated monotic and measured rotations at the 3-ft (0.91 m) level is similar to that relationship at the

a) At 6 ft. Level

b) At 3 ft. Level

c) At Base Level

1 ft. = 0.305 m
1 in. = 25.4 mm
1 kip = 4.448 kN
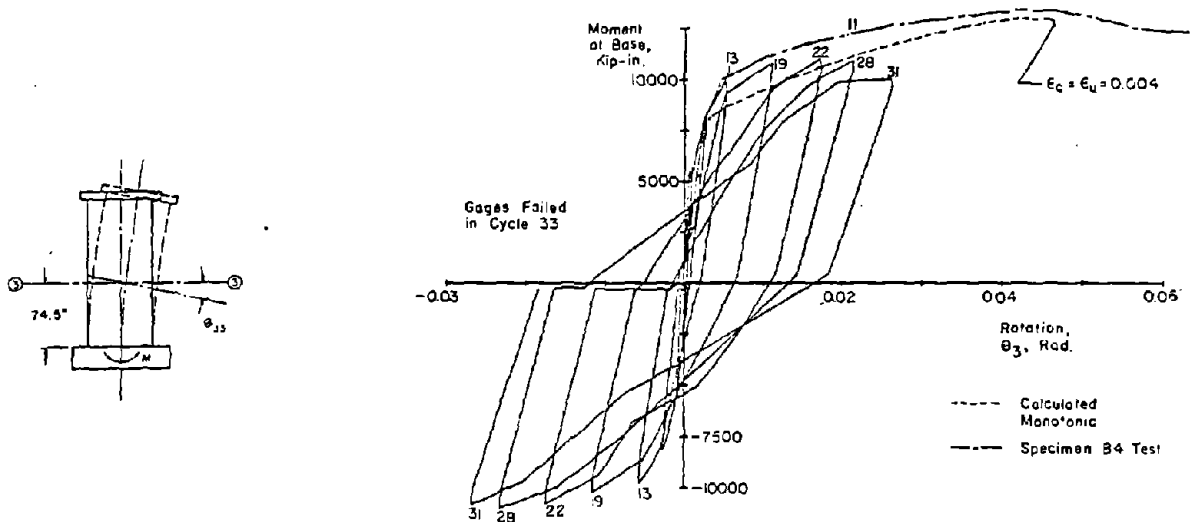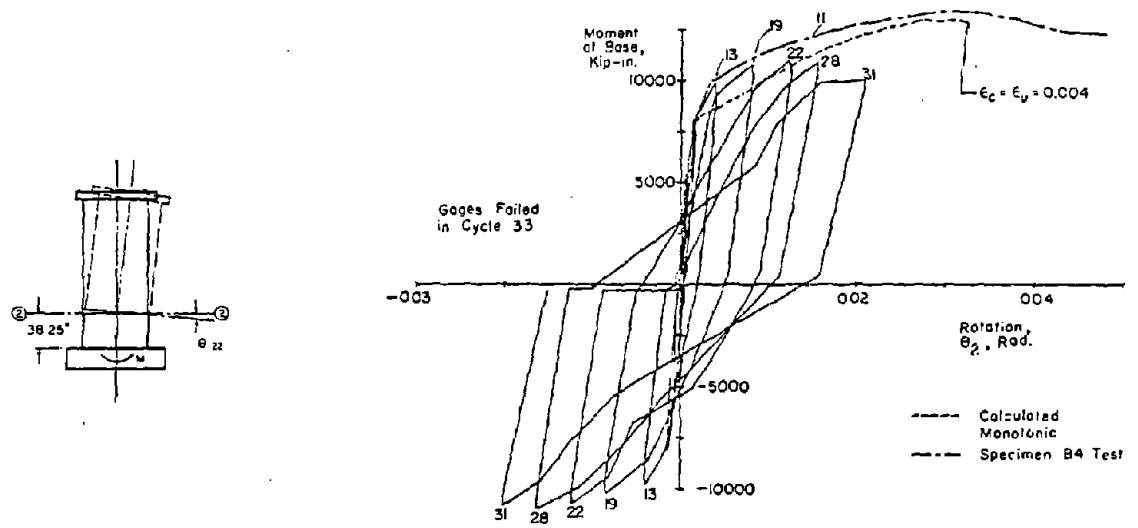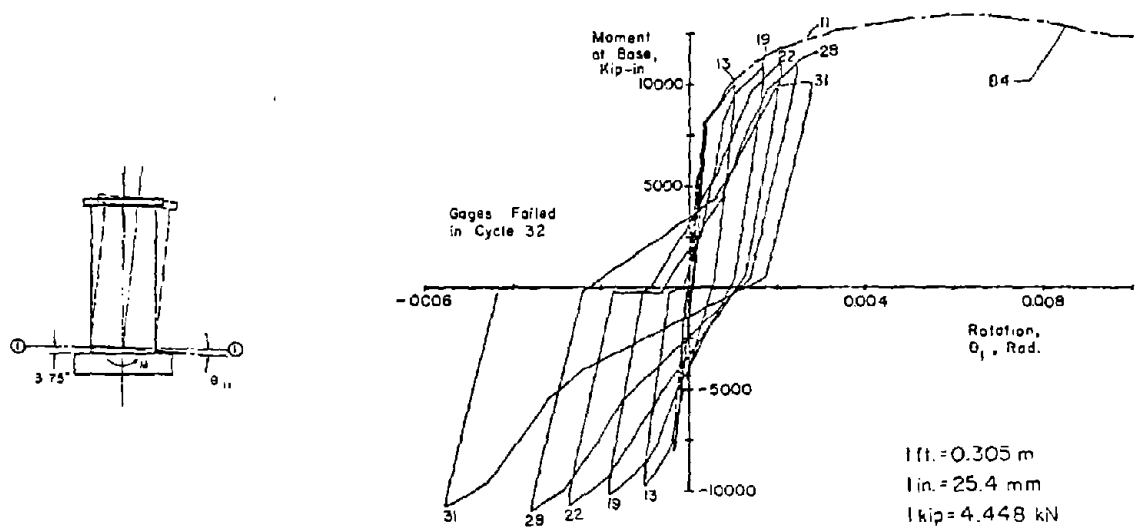
Fig. B-57   Moment at Base versus Rotation
for Specimen B1

B-75

6-ft (1.83 m) level. This indicates the shape of the assumed effective curvature distribution was accurate.

Cycle 28 for Specimen B1 and Load Stage 11 for Specimen B4 correspond to a top deflection of 4 in. (101.6 mm). As seen in Fig. B-57, the rotations in B1 are very close to the rotations in B4 at this stage. However, the load is significantly different.

The maximum measured loads in each new cycle reach a peak level in Cycle 19 and exhibited no "strain hardening" as the rotations increase.

The loops at all three levels exhibited some pinching. The base level rotation exhibited the most pinching.

Shear-Distortion. The shear distortion loops for Specimen B1 are shown in Fig. B-58. As in the rectangular specimen, with over-reinforcement for shear, the specimen exhibited shear "yielding" during approximately the same load cycles in which flexural yielding occurred.

The pinching in the loops was more evident in Zone 1. The maximum shear distortions in each new increment became larger at a slightly increasing rate. The magnitudes of distortion in Zones 1 and 2 were approximately equal at each load increment. The specimen was slightly stiffer for positive loading.

As shown in Fig. B-58, the maximum shear distortion in Cycle 28 was only slightly larger then that in B4 at Load Stage 11. This indicated only negligible shear degradation had occurred due to reversed loads at this stage.
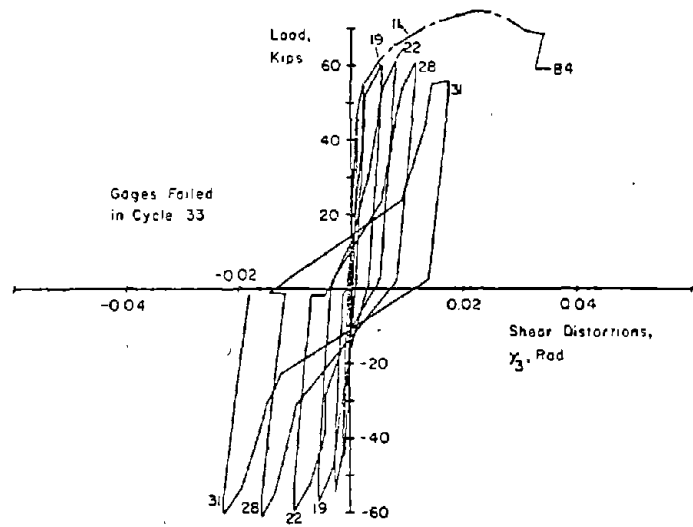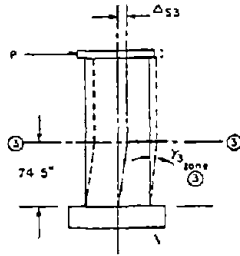
a.) In Base to 6 ft Level
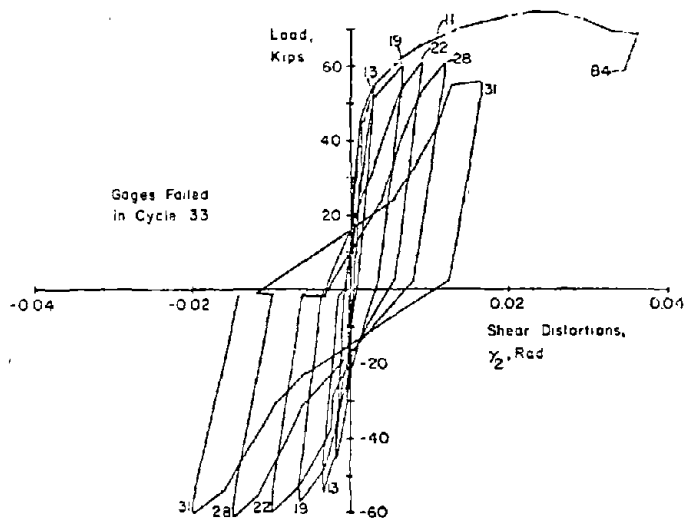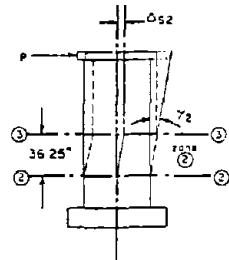
b) In 3 ft to 6 ft Level
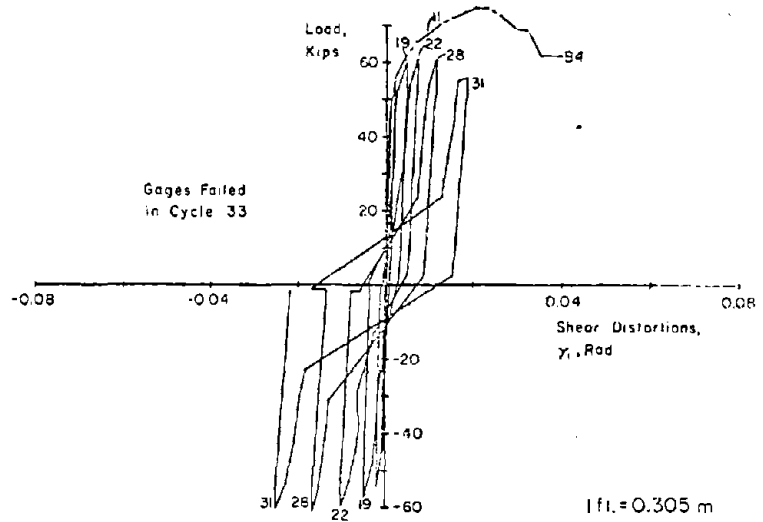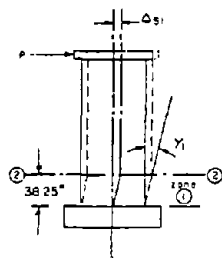
1 ft.= 0.305 m
1 in.= 25.4 mm
1 kip= 4.448 kN

c) In Base to 3 ft Level

Fig. B-58   Load versus Shear Distortion
for Specimen B1

B-77

Slip at Construction Joints. The slip at construction
joints in B1 is shown in Fig. B-59. The slip at CJ1
exhibited a "yield" at the load increment after the incre-
ment in which flexural yielding occurred at the base. The
maximum slip in B1 during Cycle 28 was more than twice the
slip at Load Stage 11. This is one source for the difference
in total shear distortions between B1 and B4.

The slip in CJ1 is shown as a percentage of the total
shear deflections in Zone 1 in Fig. B-60. After yield, the
slip remained a relatively constant at 20% to 25% of the
total shear deflection in Zone 1. It will be shown later
that the slip at CJ1 in Specimen B4 is only about 10% of the
total in Zone 1.

The measured slip at CJ2 is erratic and was probably
influenced by a diagonal crack. The slip measured at CJ3
was considerably less than the slip at CJ3 in Specimen B4.

Deflections. The deflection components and deflected
shapes are shown in Figs. B-61 and B-62. As in the rectan-
gular specimens, these figures show that although flexure
was the larger component of top deflection, shear was
becoming an increasingly major portion of the total in the
latter load increments. A comparison of the deflection
components for Specimen B1 and R2 indicates that although
the shear stress was somewhat higher in B1, the shear
deflections were a smaller portion of the total at equal
displacement ductilities.
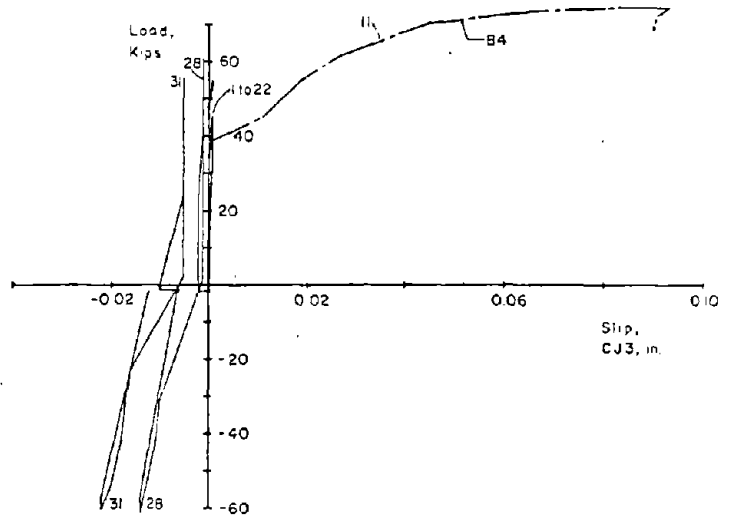
a) At 6 ft. Level
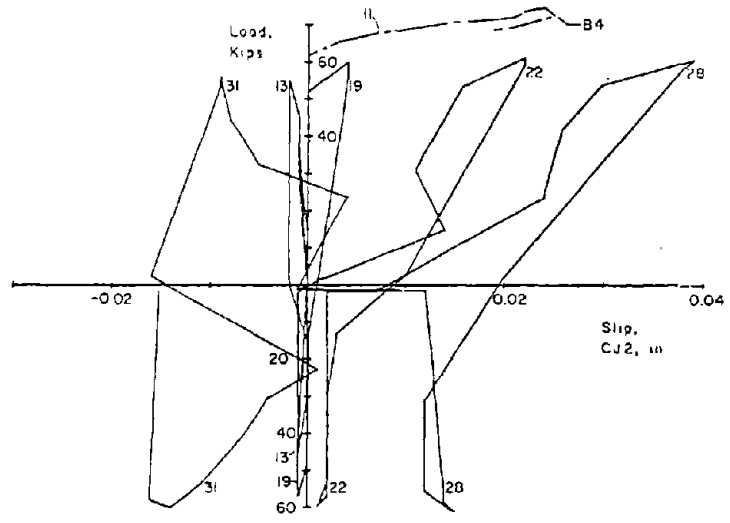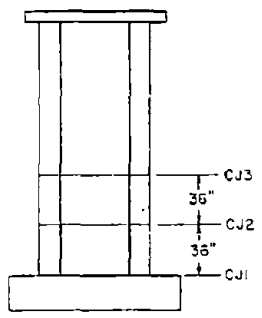
b) At 3 ft. Level
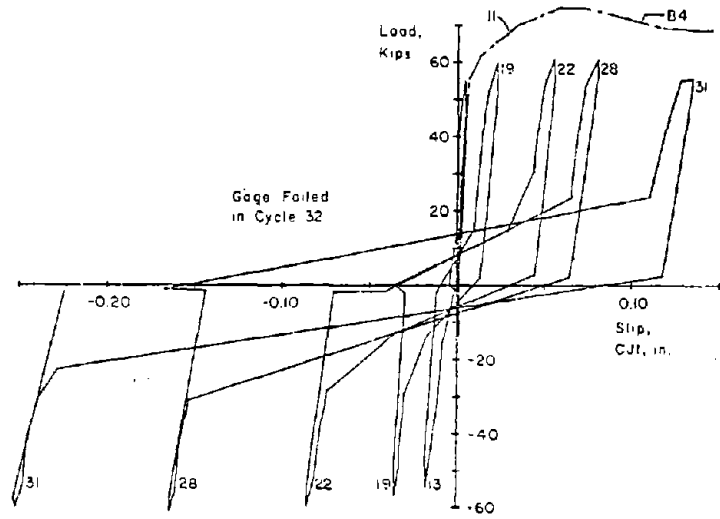
c) At Base Level

1 ft.= 0.305 m
1 in.= 25.4 mm
1 kip= 4.448 kN

Fig. B-59   Load versus Slip at Construction Joints
for Specimen B1
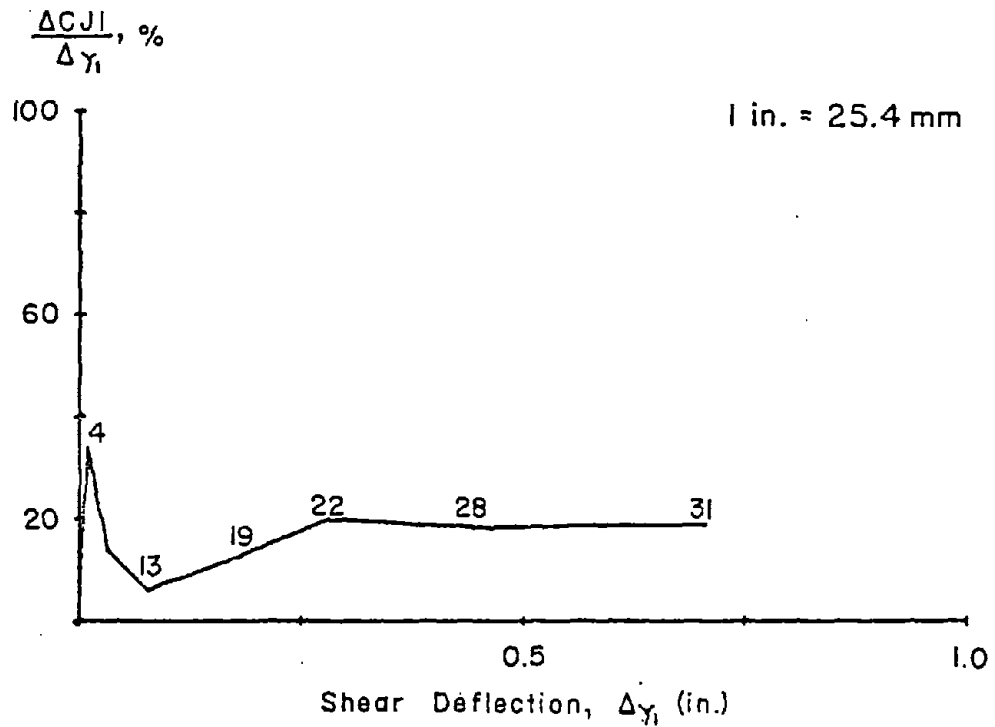
a) At Maximum Positive Loads
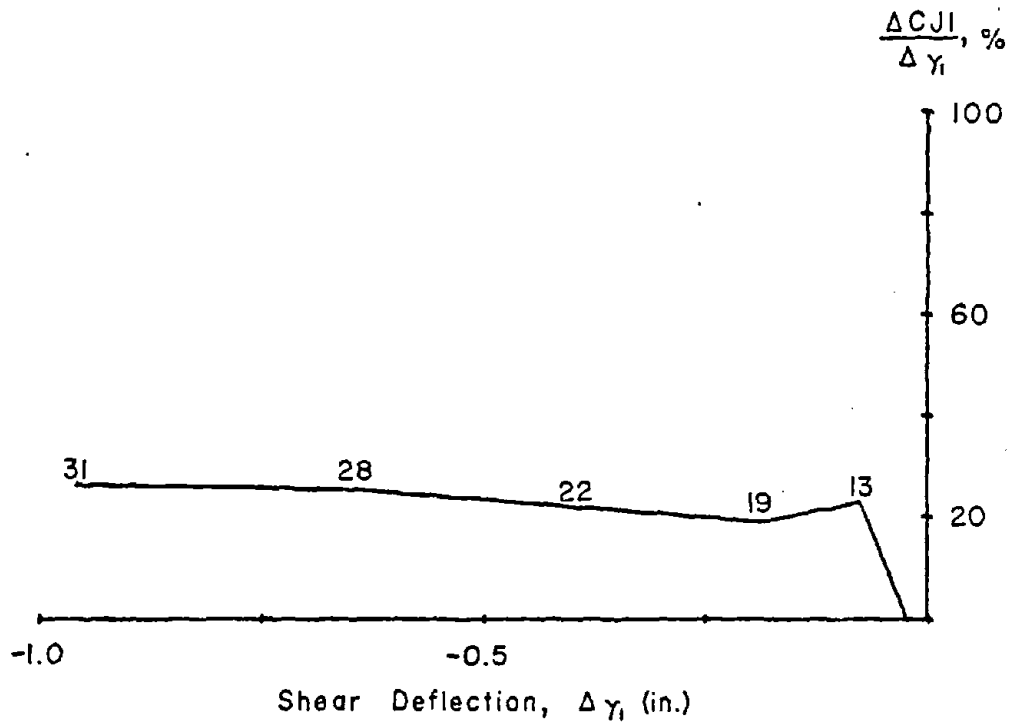
b) At Maximum Negative Loads

Fig. B-60   Slip at Base Construction Joints versus
             Shear Deflection in Zone 1 for Specimen B1

a)   At Top of Wall
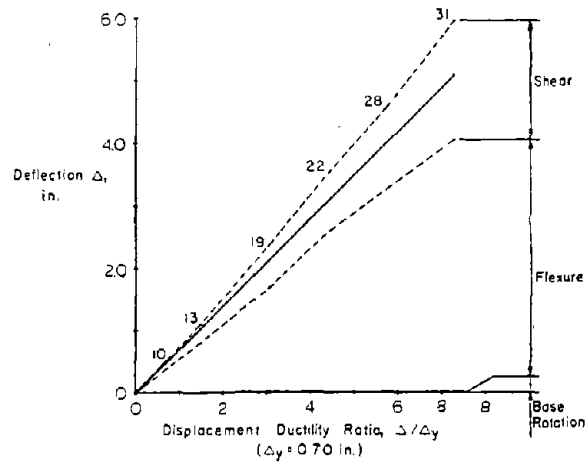
b)   At 6 ft. Level
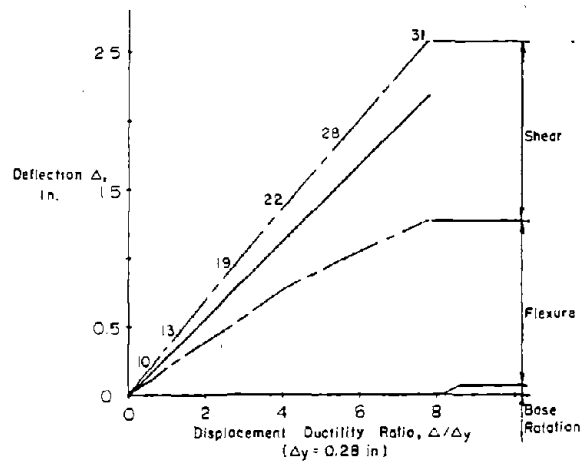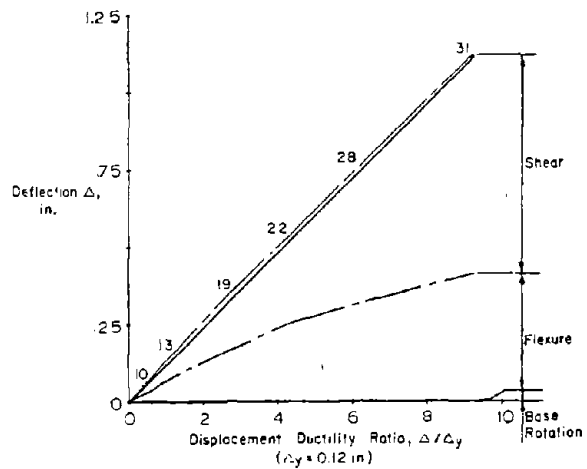
CALCULATED FROM
     MEASURED DEFOMATION
---- EXTRAPOLATED
—— MEASURED TOTAL

1 in = 25.4 mm
1 ft = 0.305 m

c)   At 3 ft. Level

Fig. B-61   Compenent of Deflection for Specimen B1

B-81

a) Flexural

b) Shear

— · — CALCULATED FROM
      MEASURED DEFORMATION
— — — EXTRAPOLATED
———— MEASURED TOTAL

1 in.= 25.4 mm
1 ft.= 0.305 m

B. F. — BAR FRACTURE

c) Total

AFTER 1st. B.F.
PRIOR TO 1st. B.F.
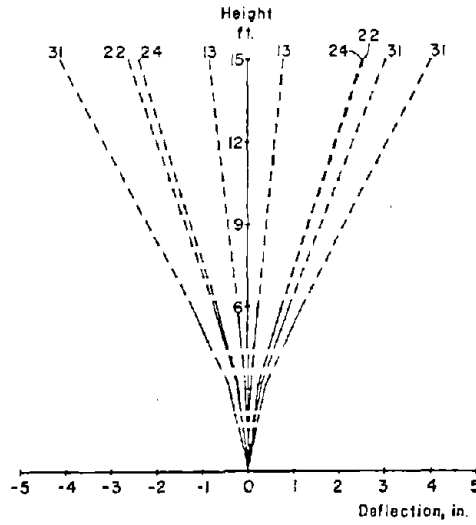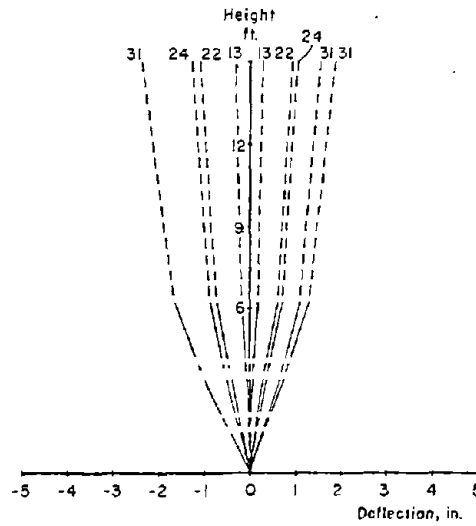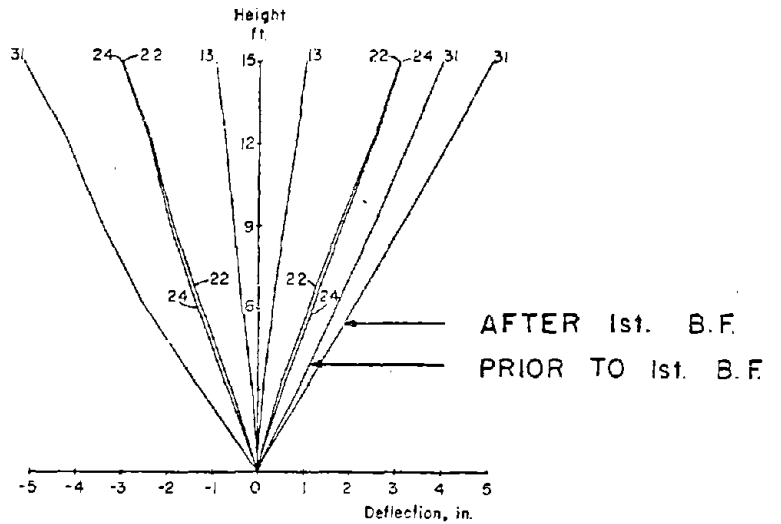
Fig. B-62 Deflected Shape for Specimen B1

As can be seen in Fig. B-62, the total deflected shape was nearly a straight line. The deflected shapes at Cycle 22 and 24 show a small shear degradation within the 3-in. (76.2 mm) increment.

Reinforcement Strains. Figures B-63 through B-71 show reinforcement strains in the specimen at various stages.

Figure B-63 indicates the columns started to grow after Cycle 10.

Figure B-64 indicates that yielding of the vertical bars extended up to the 9-ft (2.74 m) level in Cycle 22.

Figures B-65 and B-66 show that the strains in the web vertical bars were somewhat larger than the strains in the tension column at the base level. This corresponds with the observation that the base crack was always wider in the center region. This is due to the low percentage of vertical steel in the web. Also, the reversal of the strain gradient in the compression column during the latter load stages can be seen at the 3-ft (0.91 m) and 6-ft (1.83 m) levels in Figs. B-65 and B-66.

Figures B-67 through B-71 show that, even though the specimen was over-reinforced for shear, considerable yielding occurred in the horizontal bars in the lower 9 ft (2.74 m) of wall. Also, gages near the ends of the bars, HH and HA, show strains at approximately 50% of yield indicating the end hooks were necessary. The strains approached zero at the 12-ft (3.66 m) level.
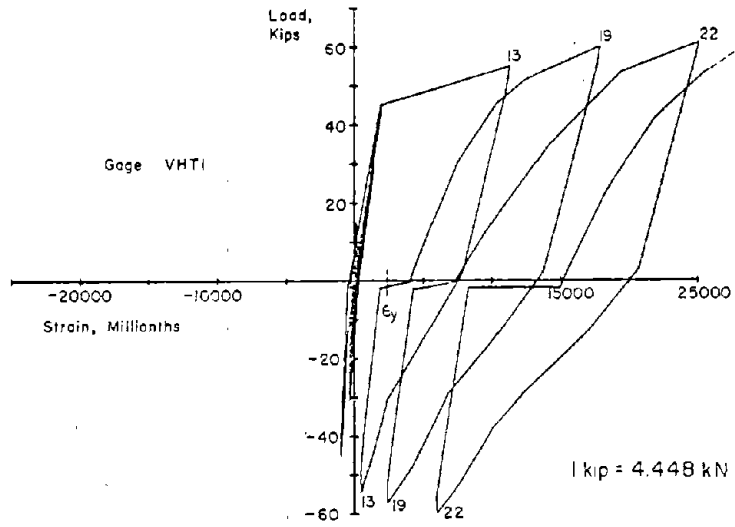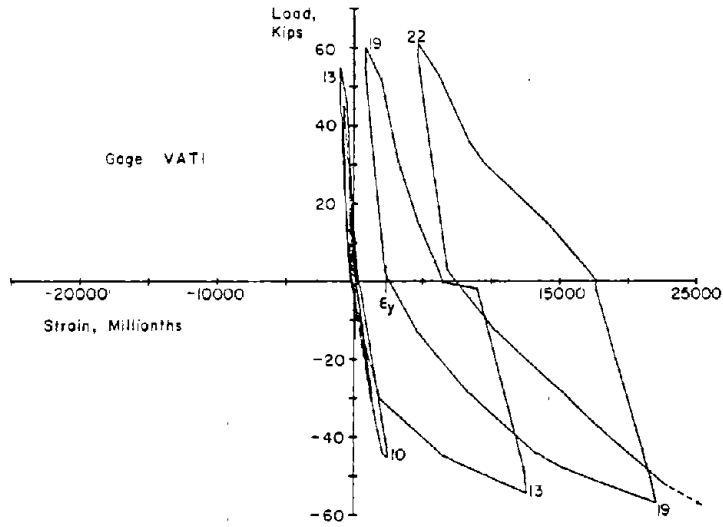
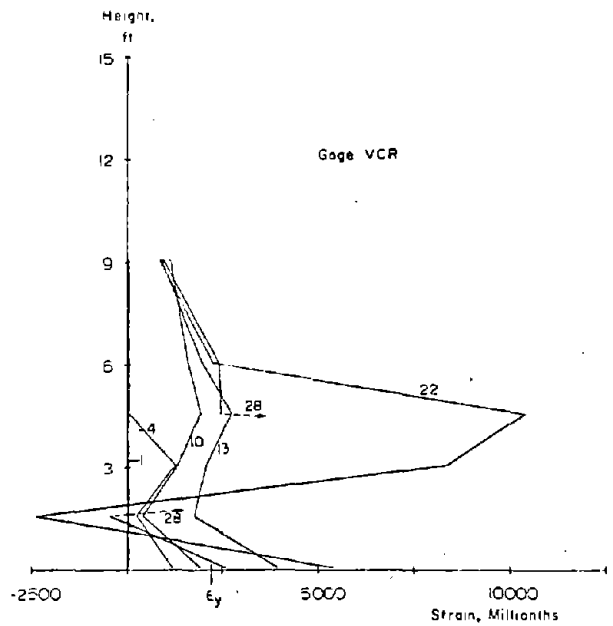Fig. B-63 Measured Strains on Vertical Reinforcement
at Base of Specimen B1
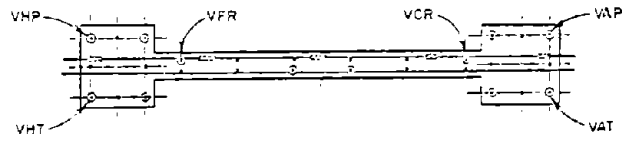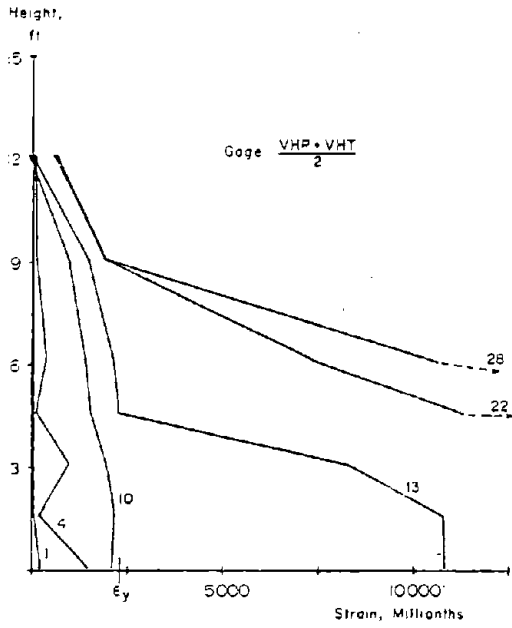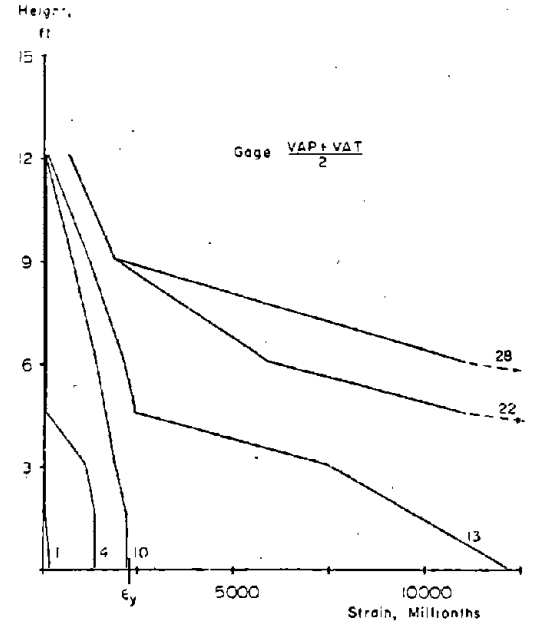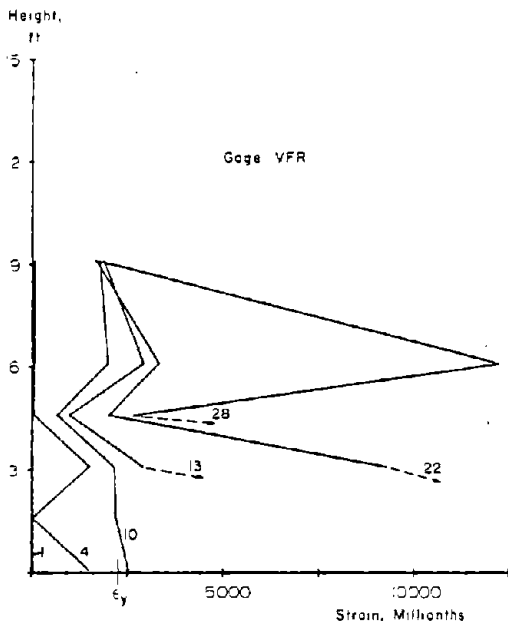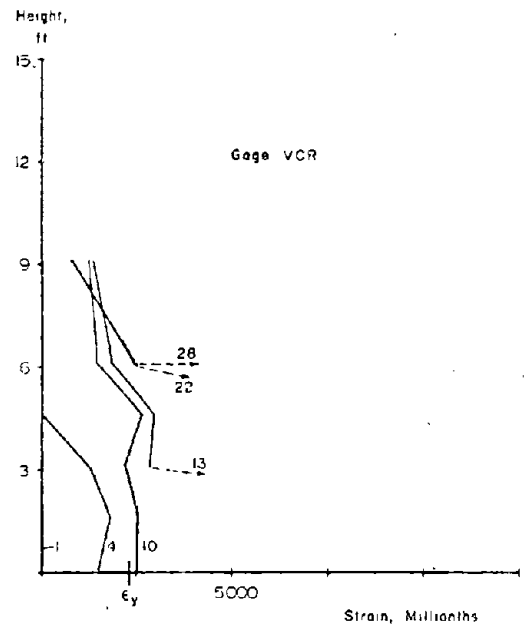
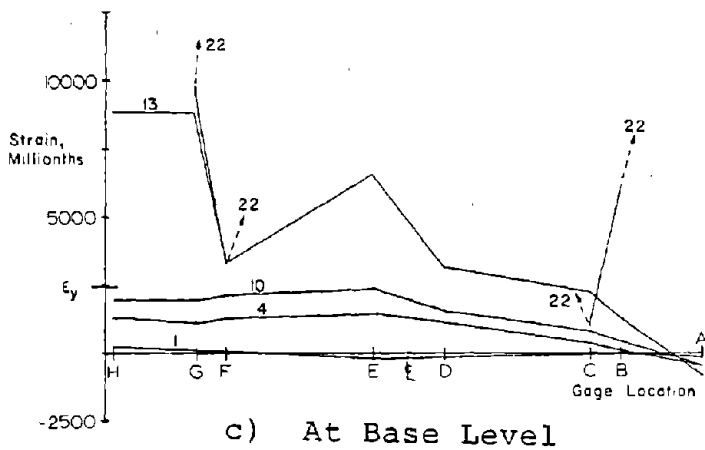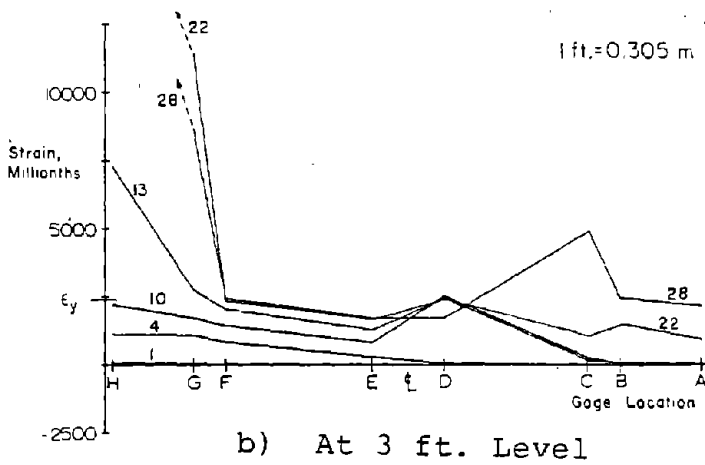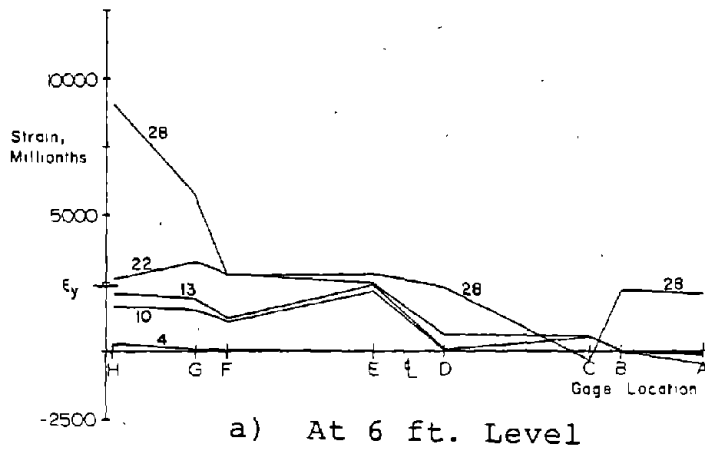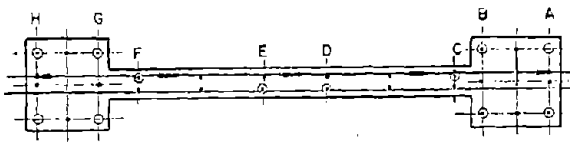Fig. B-64 Vertical Reinforcement Strains at
Maximum Loads for Specimen Bl
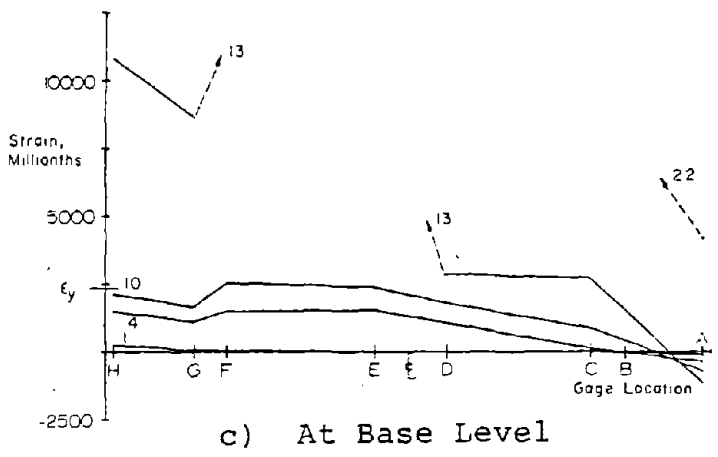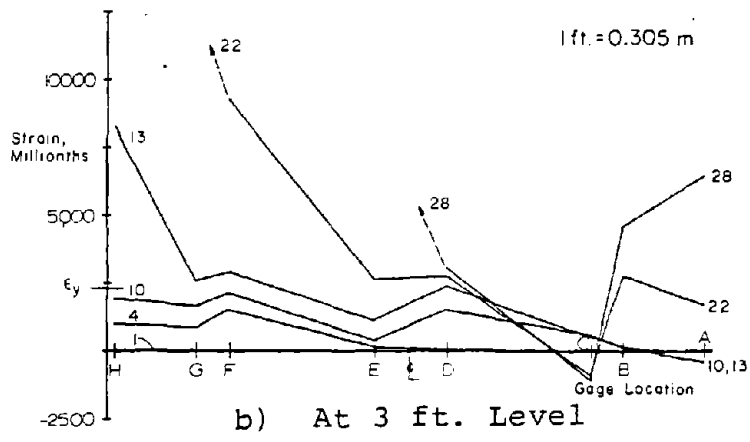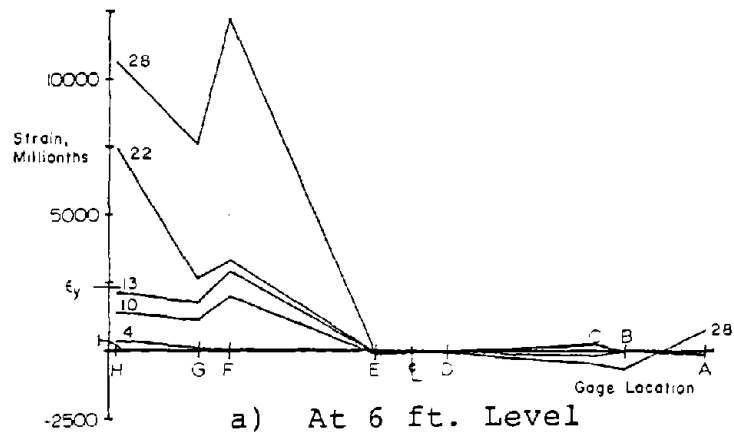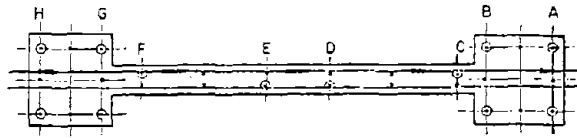
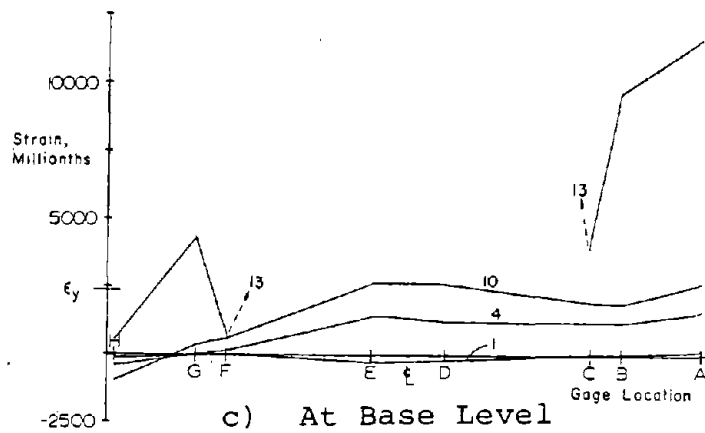Fig. B-65 Vertical Reinforcement Strains at
Maximum Positive Loads for Specimen Bl
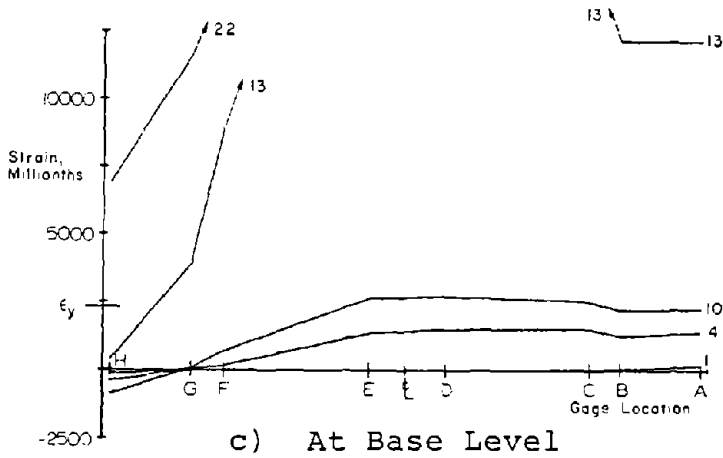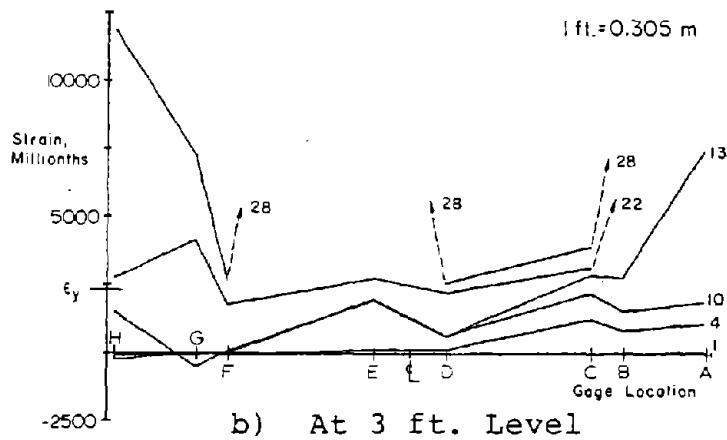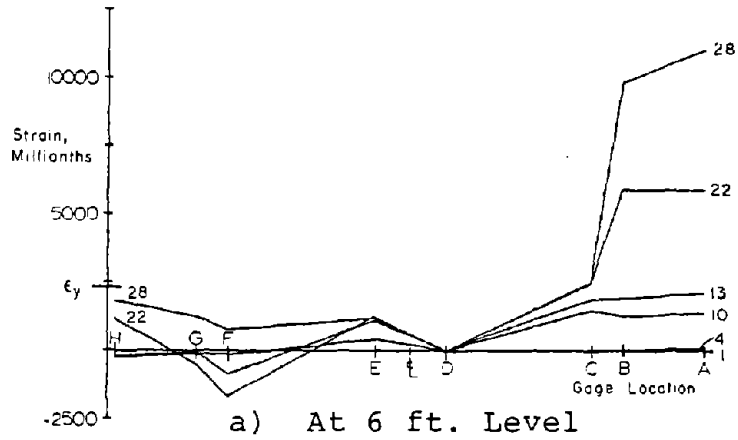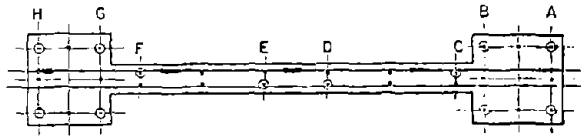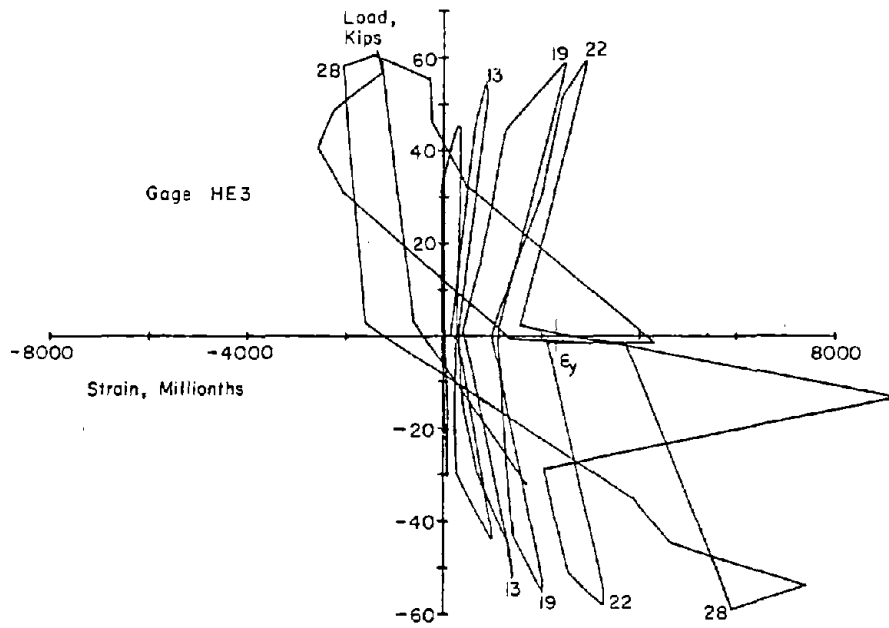
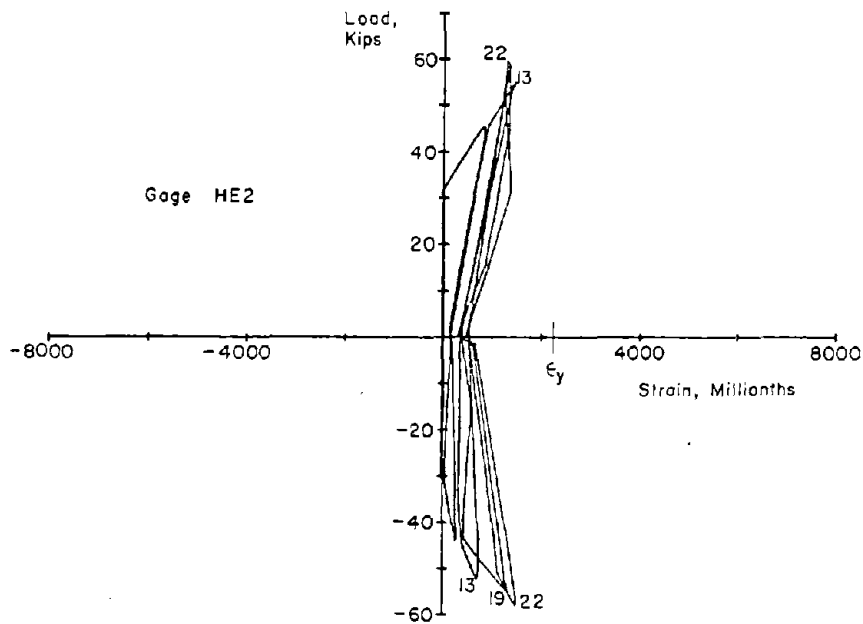Fig. B-66   Vertical Reinforcement Strains at
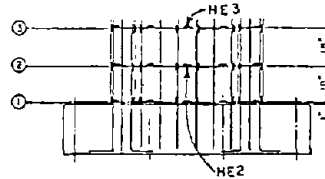Maximum Negative Loads for Specimen Bl
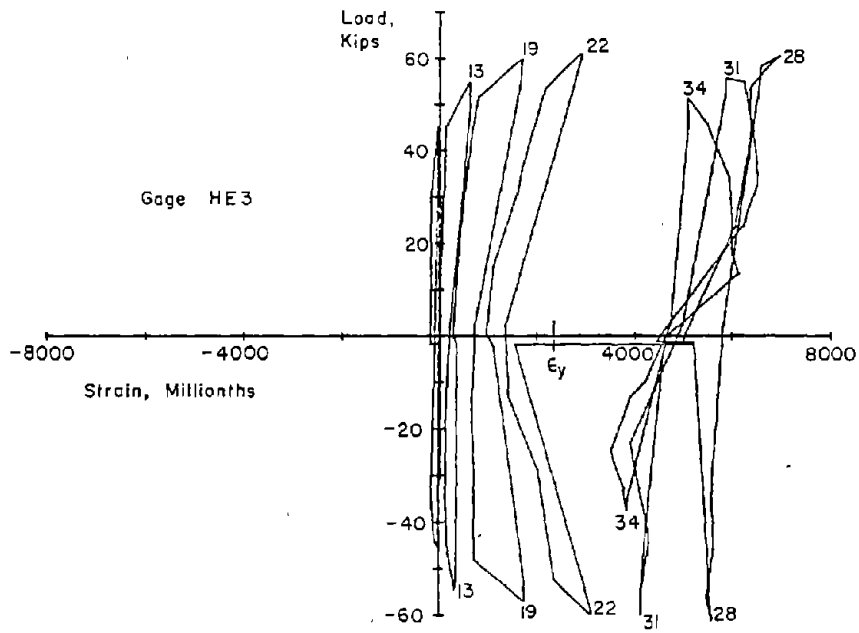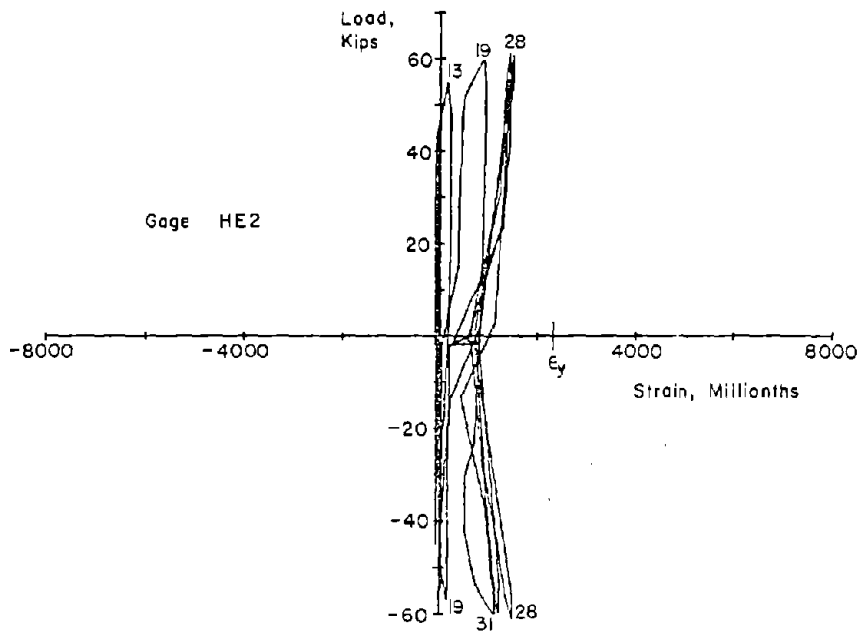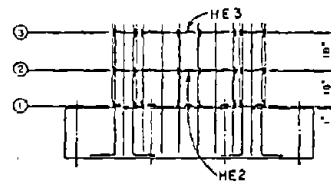
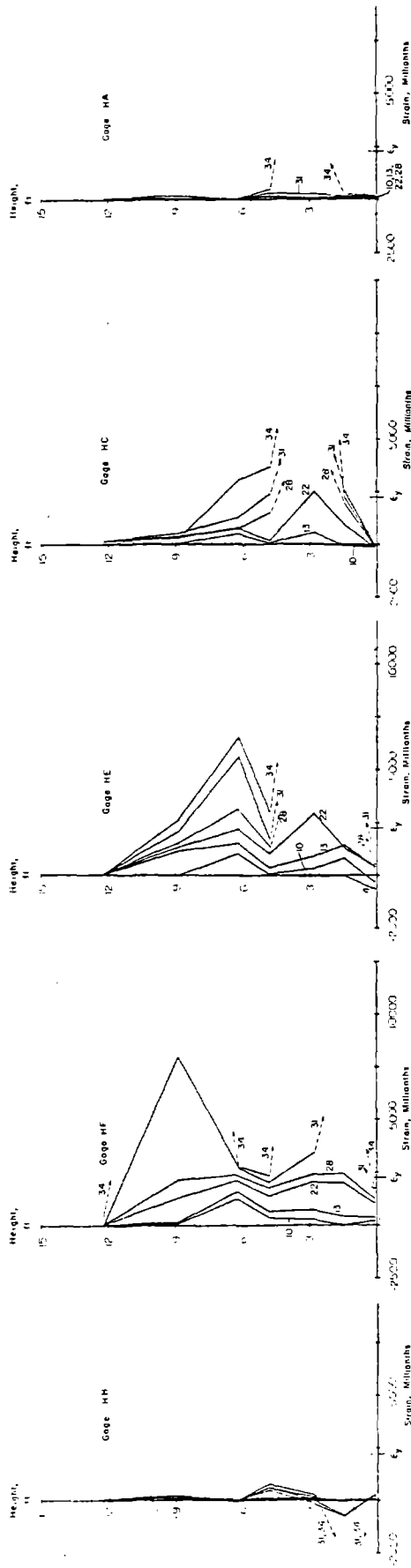Fig. B-67   Measured Strains on Horizontal Reinforcement
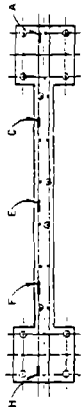for Specimen Bl
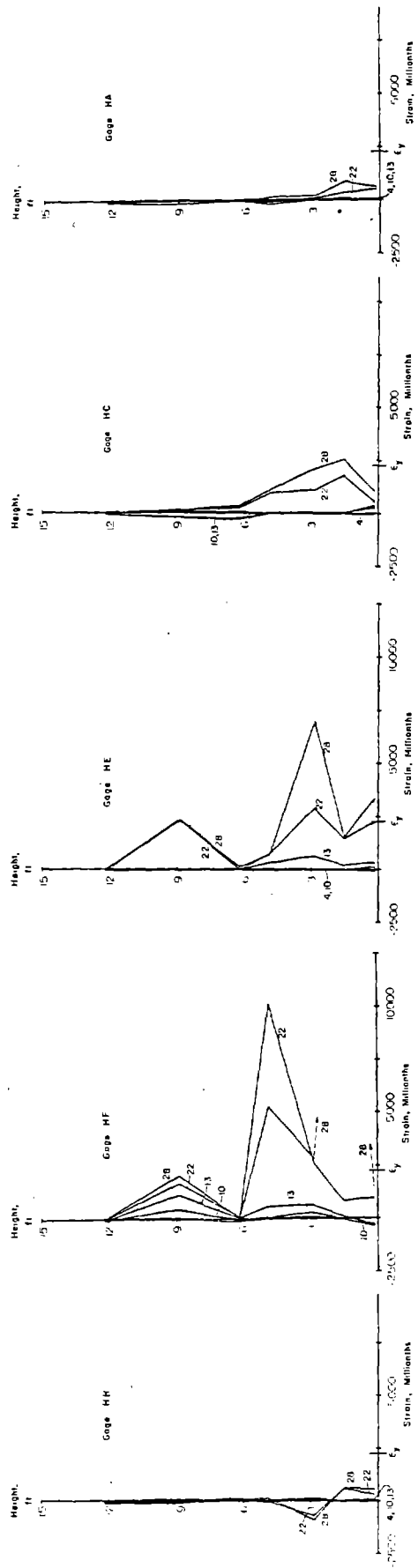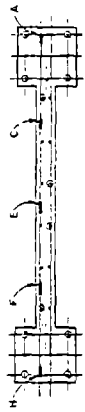
Fig. B-68 Horizontal Reinforcement Strains at
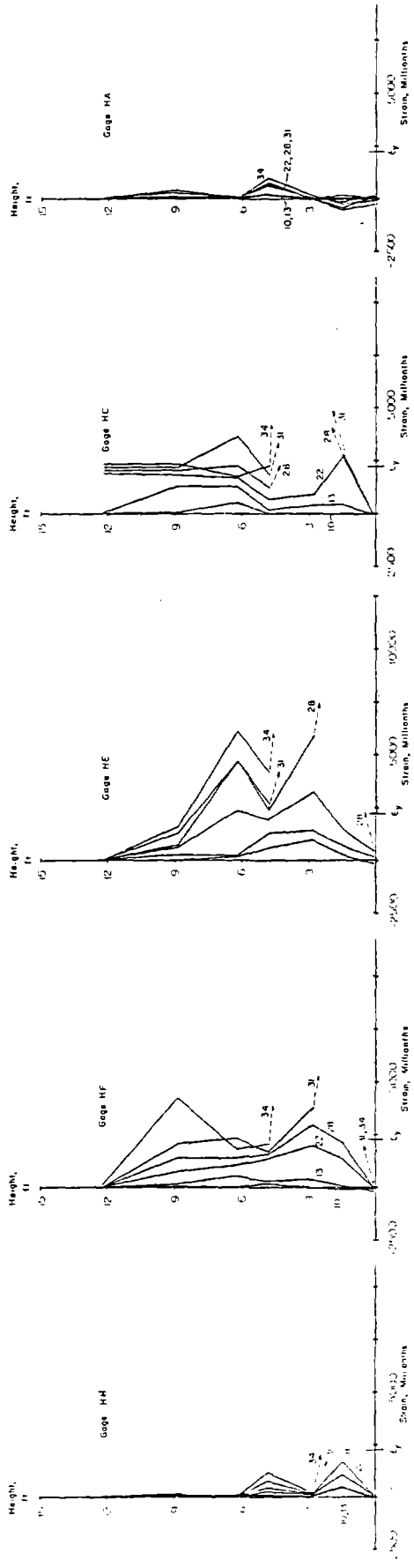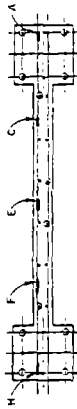Maximum Positive Loads for Specimen B1
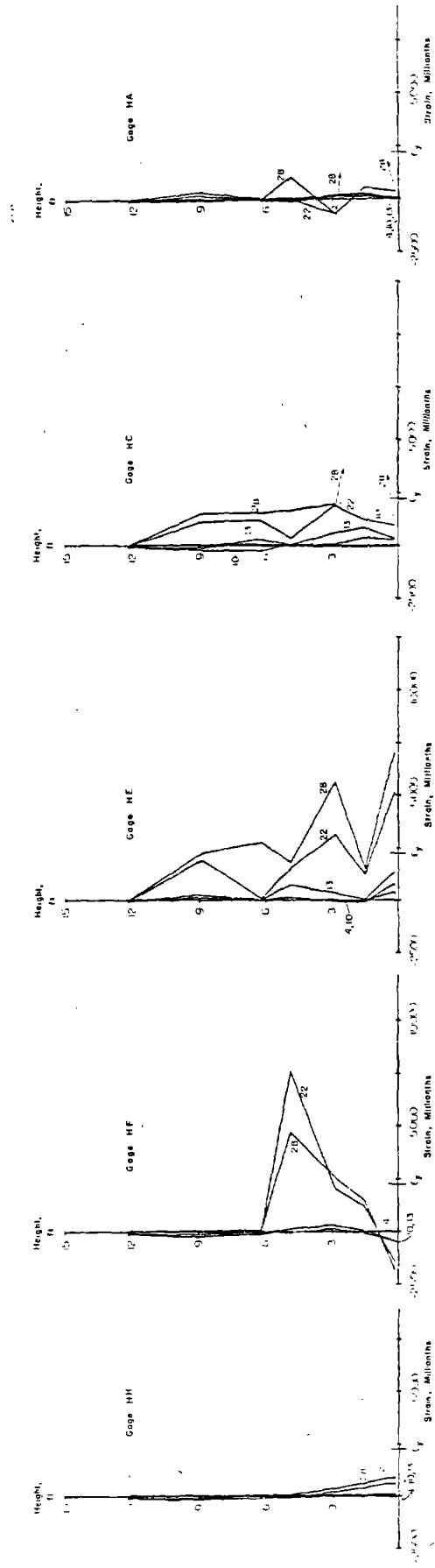
1 ft = 0.305 m

Fig. B-69 Horizontal Reinforcement Strains at
Maximum Negative Loads for Specimen B1
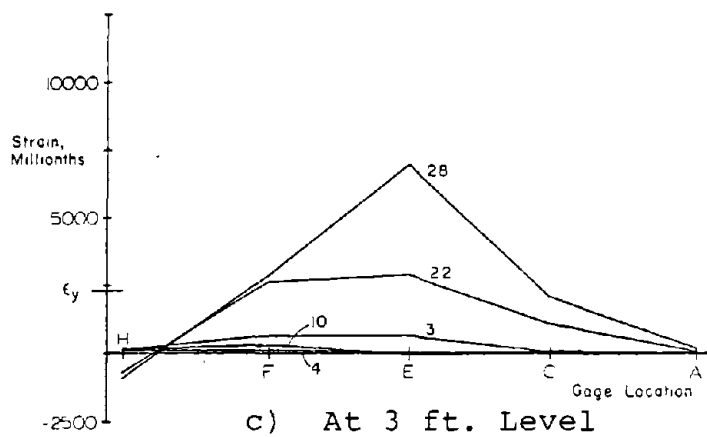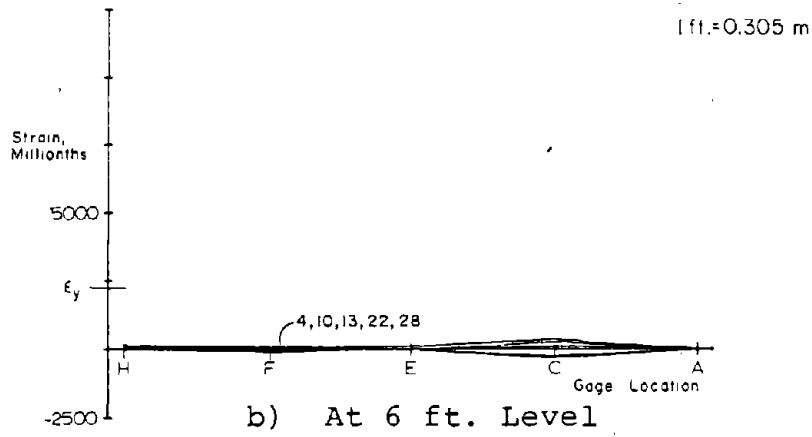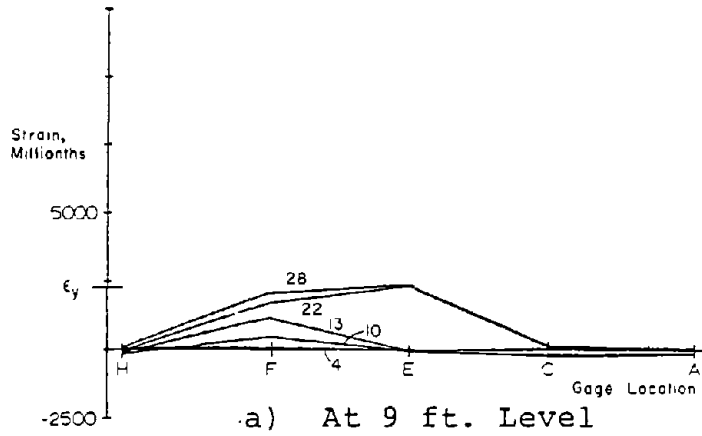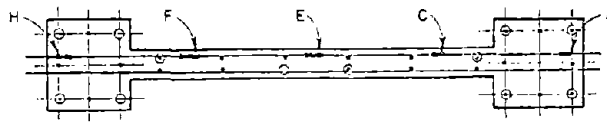
1ft.=0.305 m

a) At 9 ft. Level

1 ft.=0.305 m

b) At 6 ft. Level

c) At 3 ft. Level

Fig. B-70   Horizontal Reinforcement Strains in Web
at Maximum Positive Loads for Specimen B1

B-91

a) At 9 ft. Level

1 ft. = 0.305 m

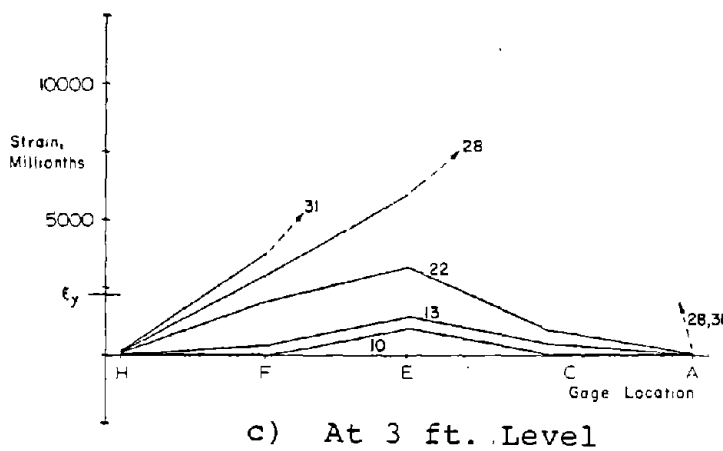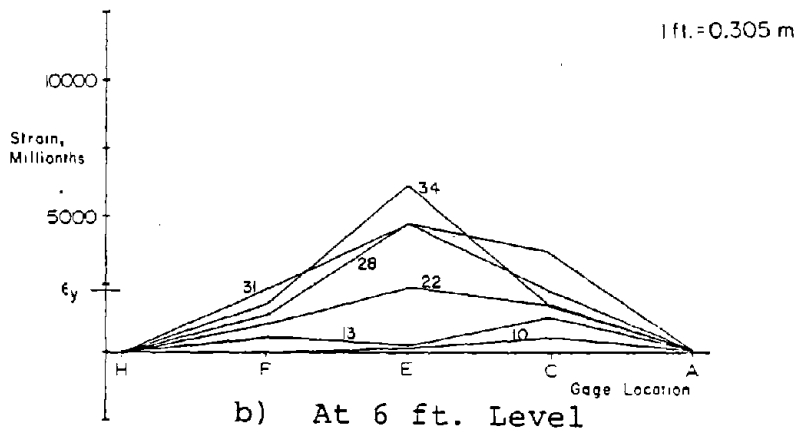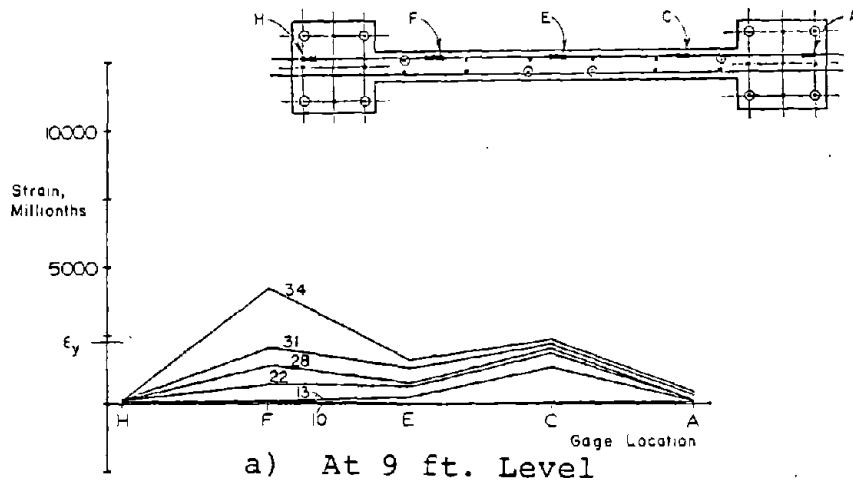b) At 6 ft. Level

c) At 3 ft. Level
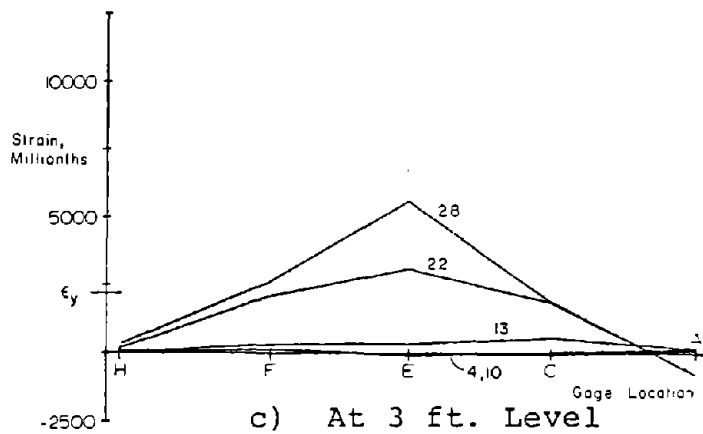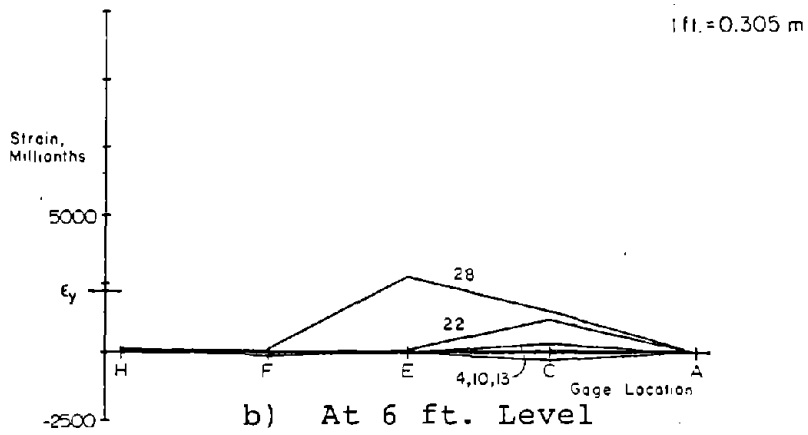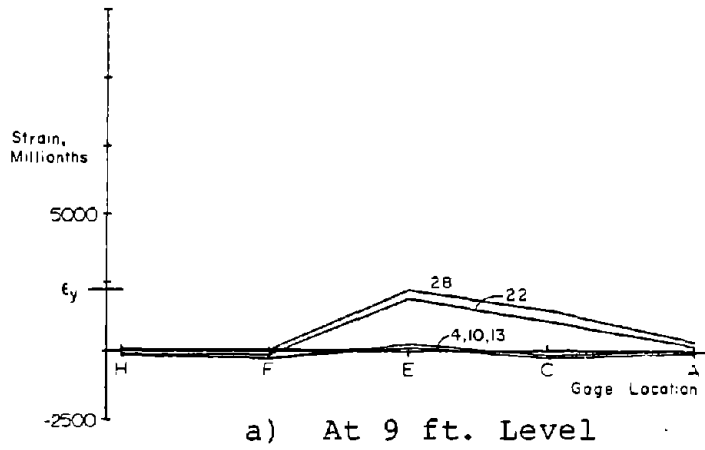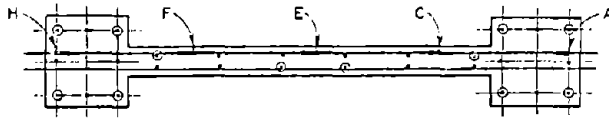
Fig. B-71   Horizontal Reinforcement Strains in Web
at Maximum Negative Loads for Specimen B1

Specimen B3

Test description

Specimen B3 was similar to Specimen B1 with 1.11% vertical reinforcement in each column. However, B3 had confinement reinforcement in the lower 6 ft (1.83 m) of the boundary elements.

The test consisted of 42 loading cycles as seen in Fig. B-72. The complete load versus top deflection relationship for the B3 test is shown in Figs. B-73 and B-74.

Initial flexural cracking was observed in Cycle 4 at a load of 28.0 kips (124.5 kN). First yielding occurred in Cycle 10 at a load of 45.2 kips (201.0 kN). The maximum measured crack widths at this stage were 0.012 in. (0.30 mm) in the tension column and 0.025 in. (0.54 mm) across a diagonal crack in the web.

The crack pattern that developed was very similar to the crack pattern in B1. The crack pattern at +3 in. (76.2 mm) and -3 in. deflection is shown in Figs. B-75 and B-76, respectively.

The behavior of Specimen B3 was very similar to the behavior of B1 through the first 21 cycles. However, where as flexural buckling of vertical bars occurred in Cycle 22 for B1, no significant distress was observed in the boundary elements of B3 until Cycle 38. Significant crushing and grinding progressively deteriorated the web concrete after Cycle 28. However, the confinement hoops in the columns
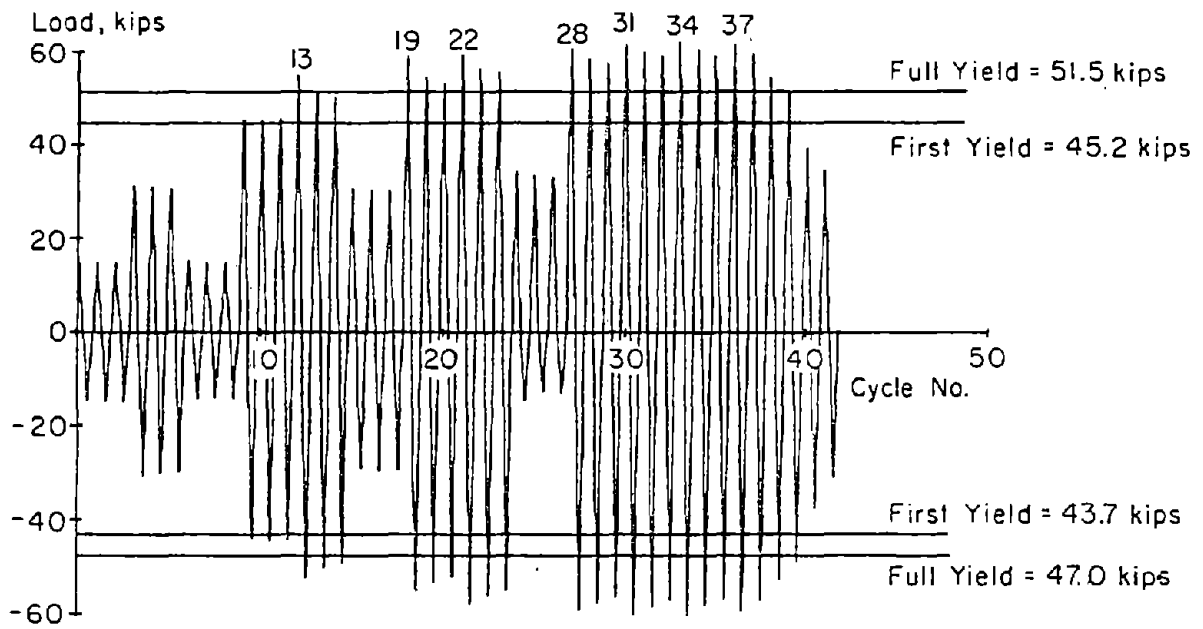
a) Load History

1 in. = 25.4 mm
1 kip = 4.448 kN
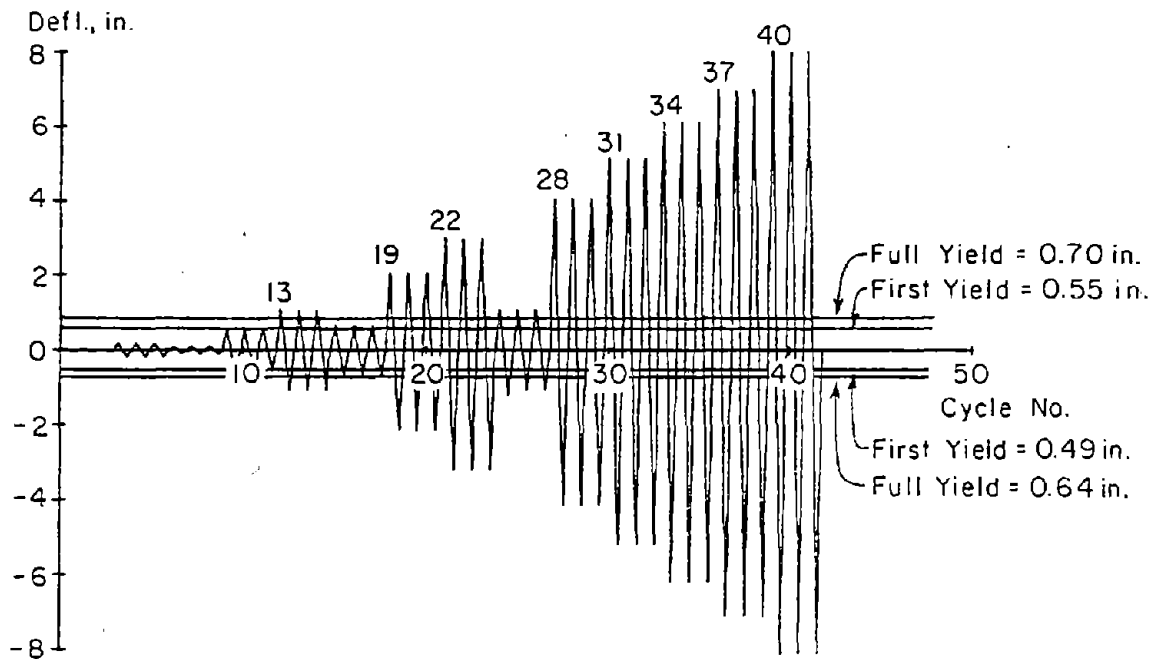
b) Deflection History

Fig. B-72   Loading History for Specimen B3

B-94
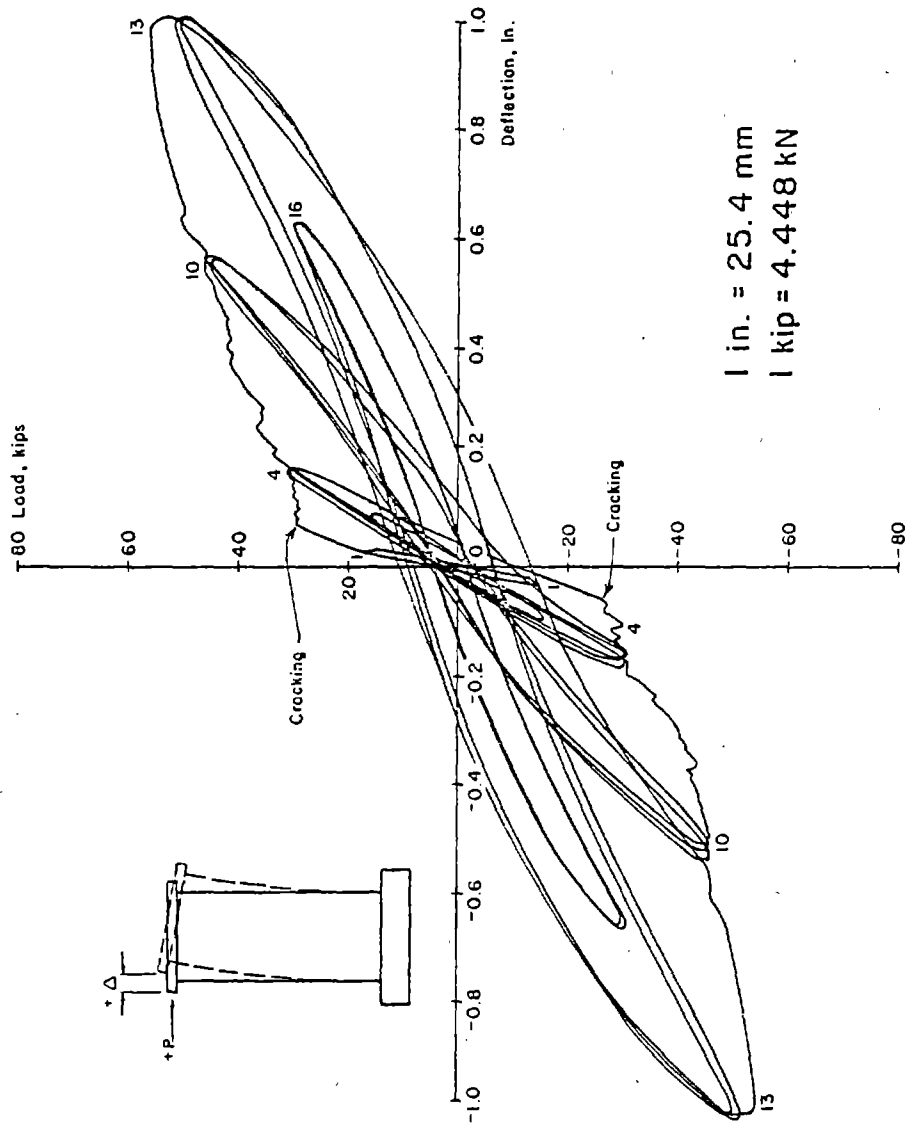
Fig. B-73 Continuous Load-Deflection Plot for Initial Cycles for Specimen B3

B-95
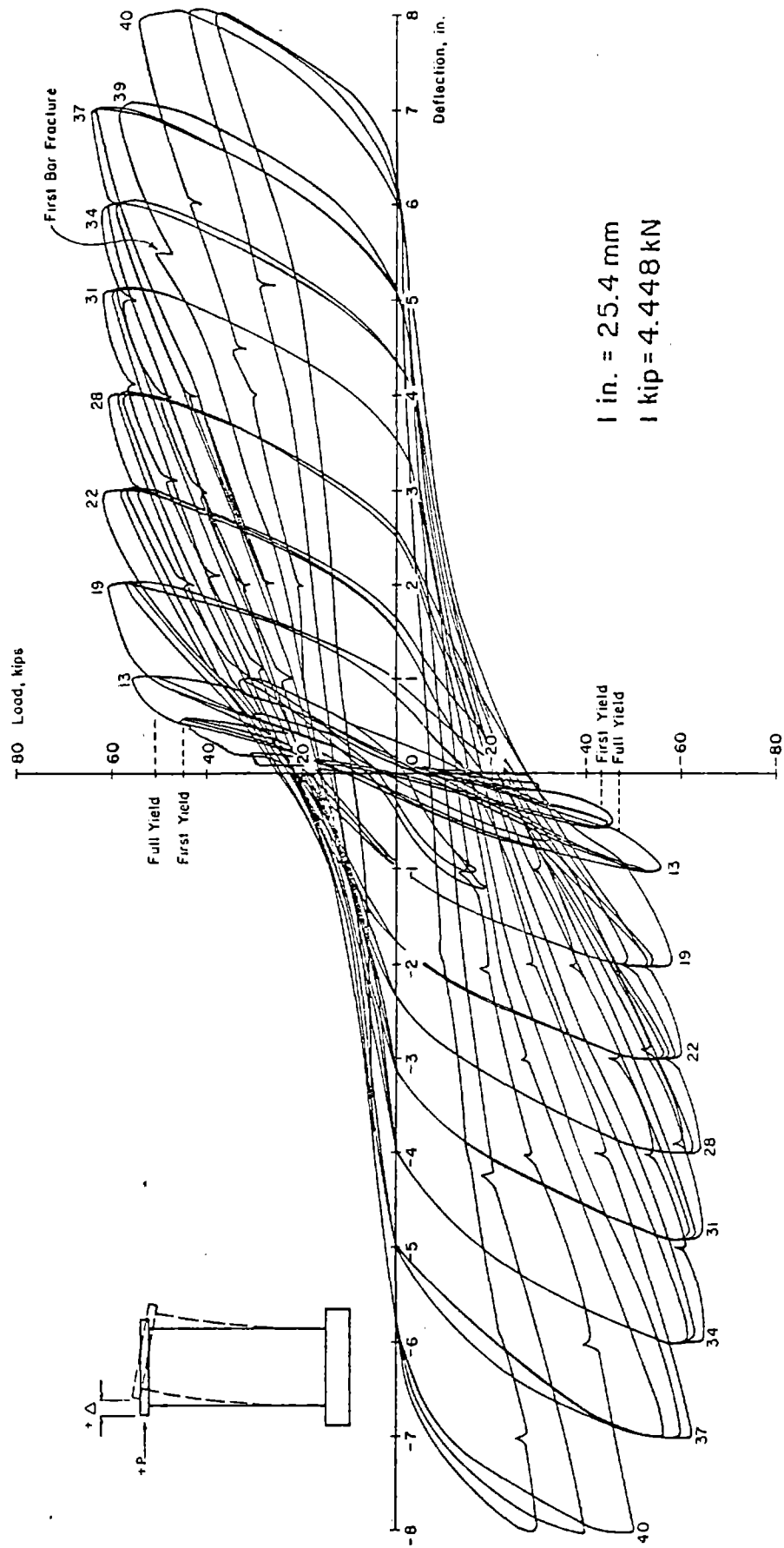
Fig. B-74 Continuous Load-Deflection Plot for Specimen B3

1 in. = 25.4 mm
1 kip = 4.448 kN
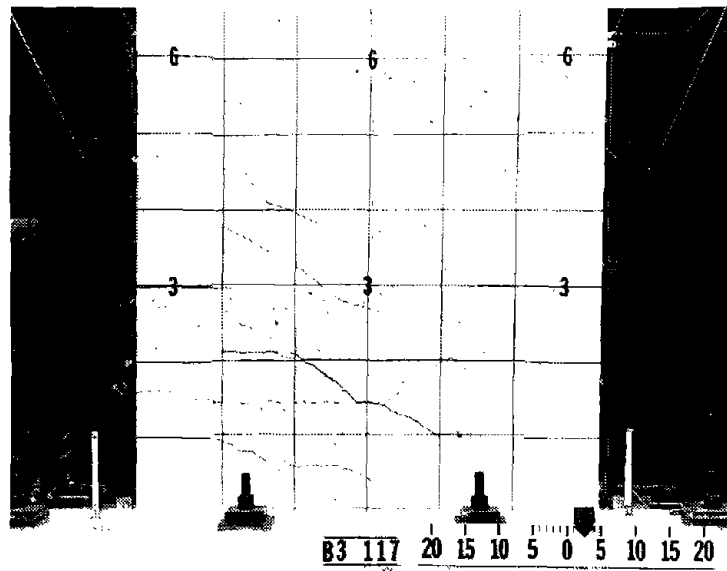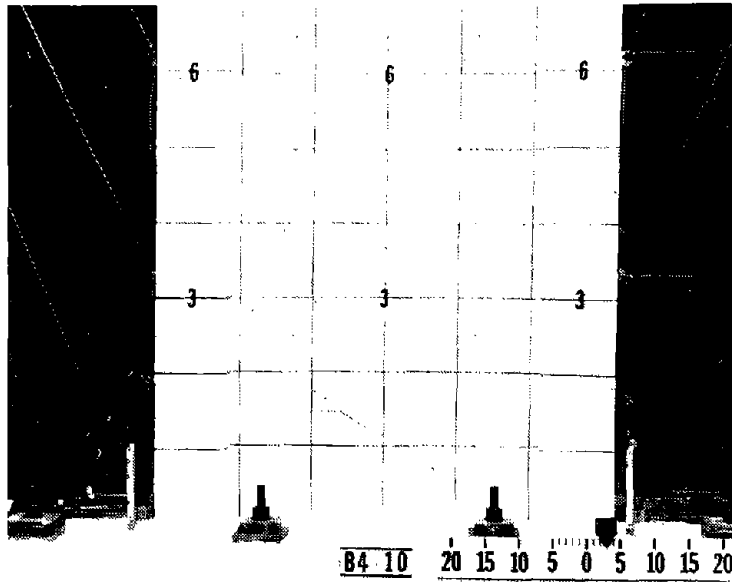
Fig. B-75   Cracking Pattern at +3 in. Deflection
             for Specimen B3
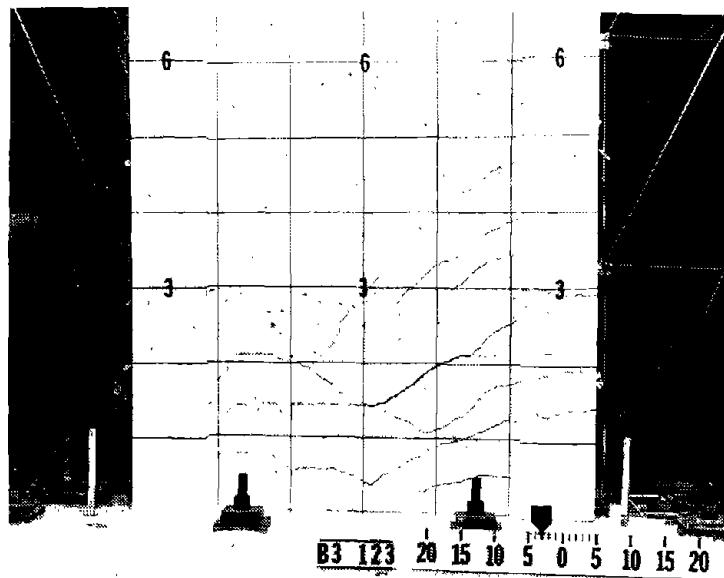
Fig. B-76   Cracking Pattern at -3 in. Deflection
             for Specimen B3

contained the boundary element concrete and helped to prevent
bar buckling. The maximum load measured, 62.0 kips, (275.8 kN),
occurred in Cycle 34 at a +6 in. deflection. This load
corresponded to a nominal shear stress, $v_{max} = 3.1\sqrt{f'_c}$
$(0.26\sqrt{f'_c}$, MPa). The maximum measured crack widths at this
stage were 0.125 in. (3.18 mm) in the column and 0.170 in.
(4.32 mm) across a diagonal crack in the web. The specimen
maintained a nearly constant load capacity through to Cycle
39.

In Cycles 25 through 27, a 1 in. (25.4 mm) deflection
loading increment, a considerably different stiffness of the
wall was observed for the two loading directions. This can
be attributed to the crack pattern. As shown in Figs. B-75
and B-76, when the wall is loaded in the negative direction
there are several straight horizontal cracks (in the com-
pression side) for the wall to slip across. However, when
loaded in the positive direction the crack pattern in the
compression side is crisscrossed. Therefore, the specimen
is stiffer in this direction.

In Cycle 38, the compression boundary element appeared
to shear through, although the load capacity remained rela-
tively constant. The specimen is shown at this stage in
Fig. B-77.

In Cycle 39, a vertical bar fractured at the base while
loading the specimen to +7-in. (177.8 mm) deflection. The
fractured bar still had concrete cover and no evidence of
previous distress, such as buckling, was present. While
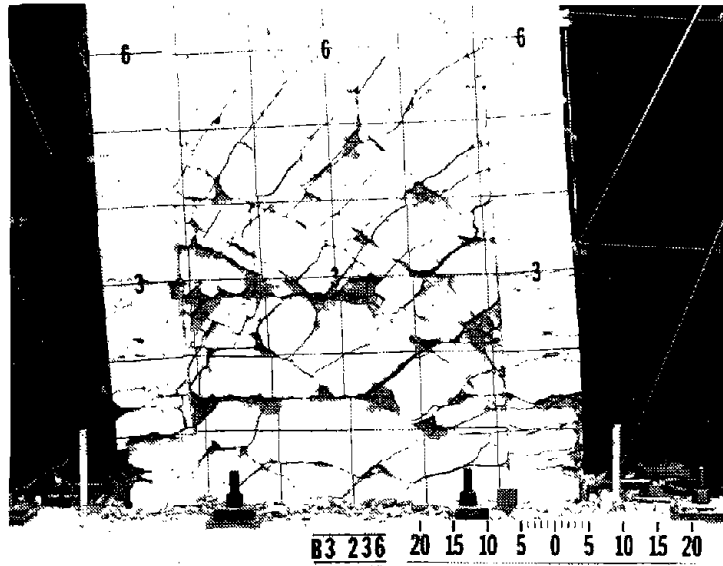
Fig. B-77   Specimen B3 Prior to Bar Fracture
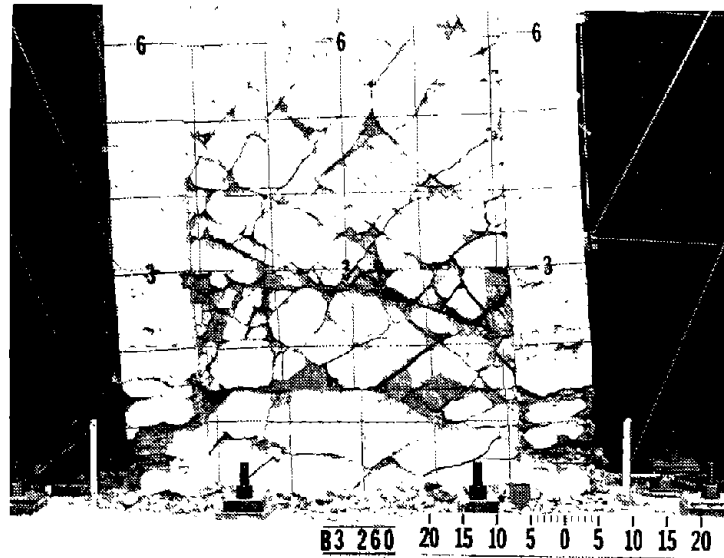
Fig. B-78   Specimen B3 at End of Test

B-99

loading the specimen in Cycle 39 to -7-in. deflection, a bar
in the opposite column fractured. This bar was visible and
it was evident that the bar had previously buckled between
the confinement hoops. The load capacity at this stage was
85% of the measured maximum. In subsequent cycles, buckling
was noted in 7 main flexural bars and 5 of these fractured
1/2 to 1-1/2 cycles after buckling. The buckling of these
bars was associated with a shear displacement of the compres-
sion columns.

All of the small vertical bars in the web buckled in
Cycles 39 and 40, but only one fractured.

The specimen sustained its load carrying capacity
through 21 inelastic cycles. The last inelastic loading
increment in which the load was sustained at or above 80% of
the maximum for all 3 cycles was at $\pm$7 in. A photograph of
the wall after testing is shown in Fig. B-78.

Discussion of Results

Moment-Rotation. Moment rotation data for Specimen B3
is shown in Fig. B-79. The measured maximum moment was 84%
of the calculated monotonic maximum. The maximum rotations
during Cycle 37 in B3 was approximately 1.4 times that
during Cycle 28 in B1 at the 3-ft (0.91 m) level and 1.25
times that in B1, Cycle 28, at the 6-ft (1.83 m) level.

The relationship between the calculated monotonic and
measured rotations at the 3-ft level differs only slightly
from that relationship at the 6-ft. level. The difference
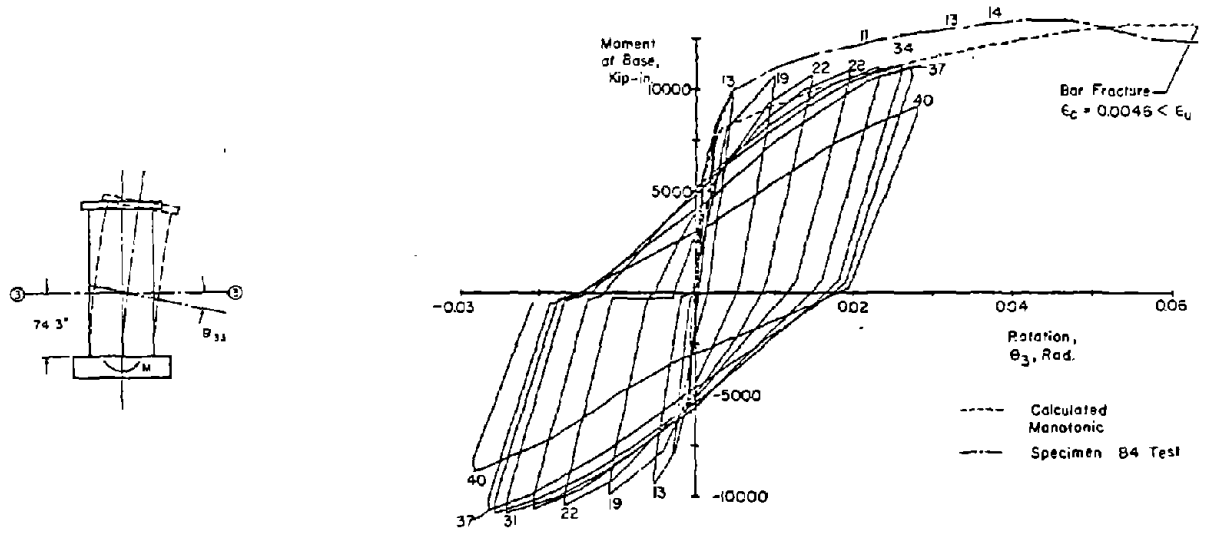
a) At 6 ft. Level
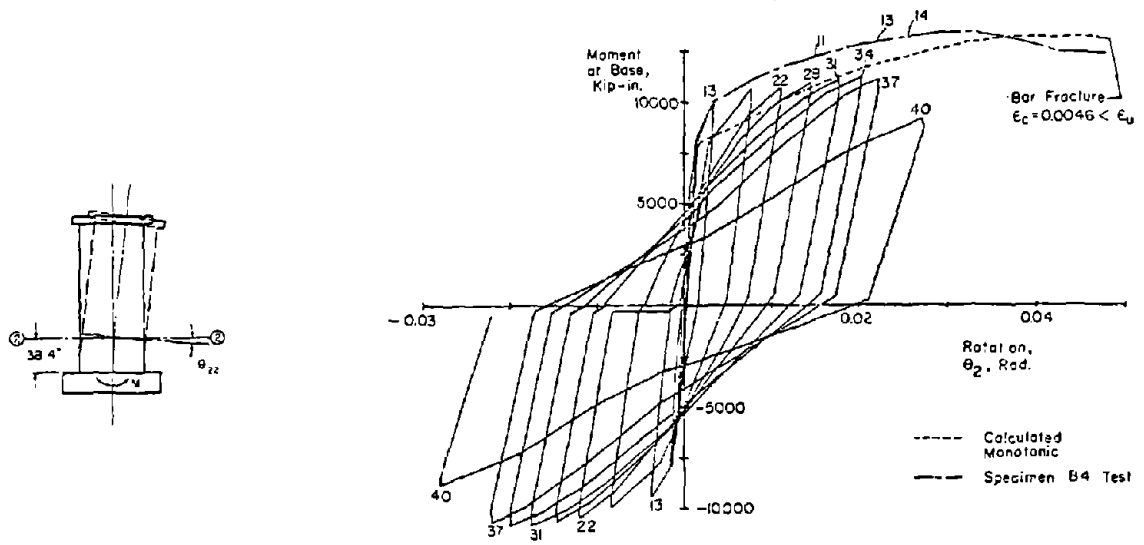
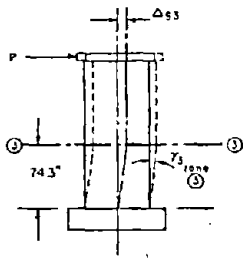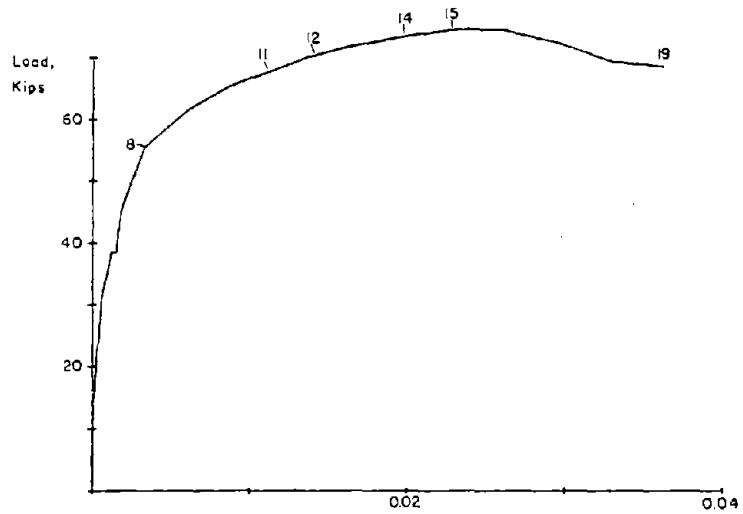b) At 3 ft. Level
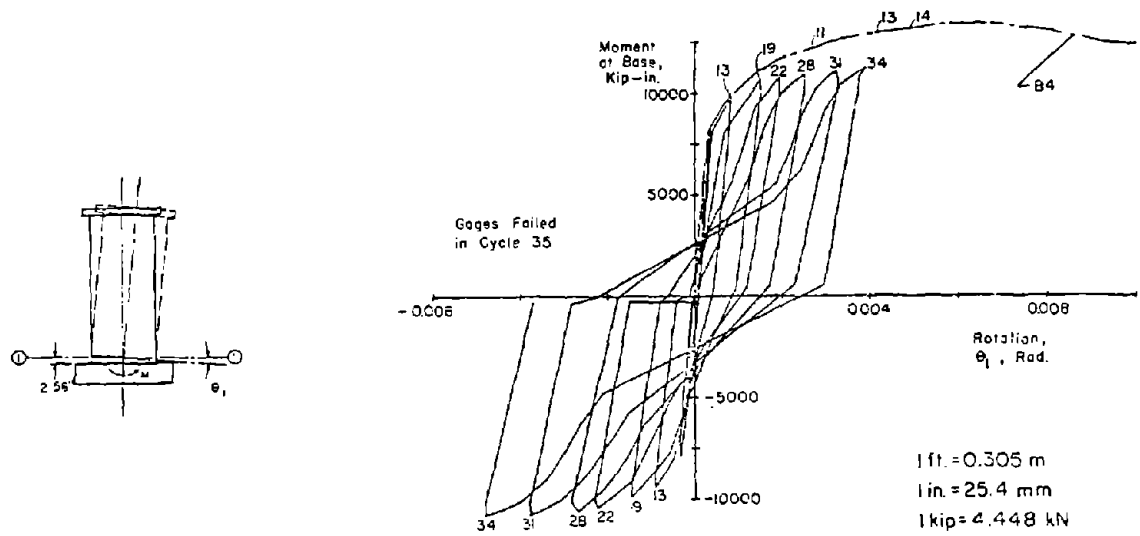
c) At Base Level

Fig. B-79   Moment at Base versus Rotation
for Specimen B3

B-101

indicates that a slightly larger portion of the assumed curvature distribution should have been concentrated in the lower 3-ft of wall.

Cycle 28 in B3 and Load Stage 11 in B4 correspond to a 4-in. (101.6 mm) top deflection. Cycle 37 in B3 and Load Stage 14 in B4 correspond to a 7 in. (177.8 mm) top deflection. As shown in Fig. B-79, the maximum rotations in B3 at the 4-in. deflection were only slightly less than the rotation in B4. However, at the 7-in. deflection the difference between B3 and B4 had increased significantly. The rate of increase of maximum rotation in new load increments reduced after Cycle 28. This indicated that shear degradation was occurring.

The maximum measured loads in each new increment exhibit some "strain hardening" as the rotations increase. However, an envelope through the measured peaks approached a maximum lower than the maximum for monotonic loading.

The rotation loops at the base level exhibited considerable pinching after Cycle 19. Pinching was only slightly evident in Cycles 34 and 37 at the 3-ft and 6-ft levels.

Shear-Distortion. Shear distortion loops for Specimen B3 are shown in Fig. B-80. As in the previously described tests of specimens over-reinforced for shear, B3 exhibited shear "yielding" during the same load cycles in which flexural yielding occurred.

The pinching in the loops was more evident in Zone 1. The new maximum shear distortions in Zone 1 in each new
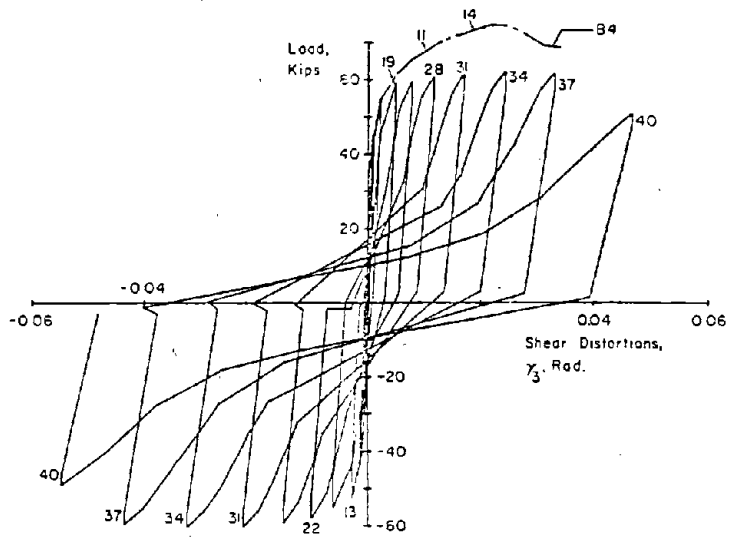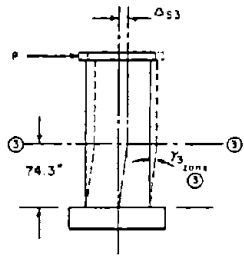
a) In Base to 6 ft Level
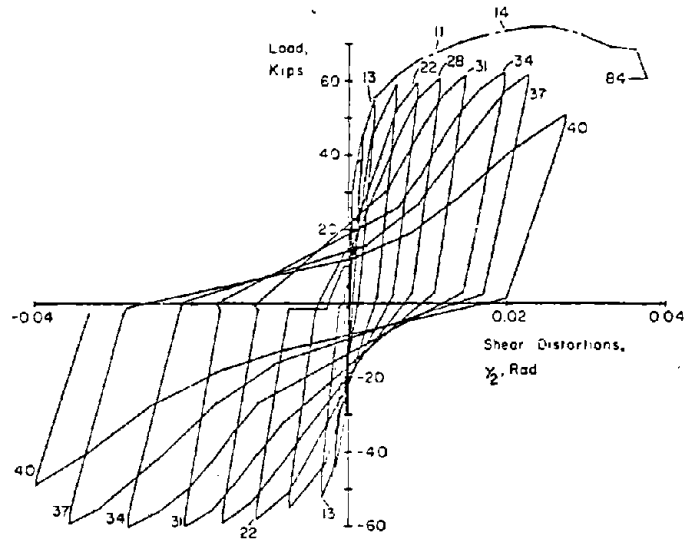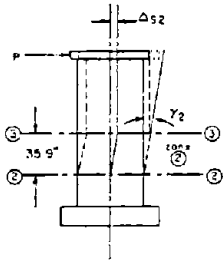
b) In 3 ft to 6 ft Level
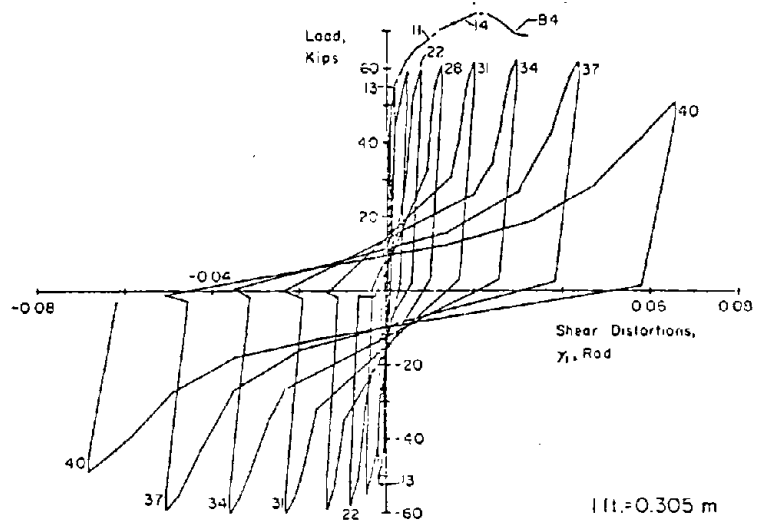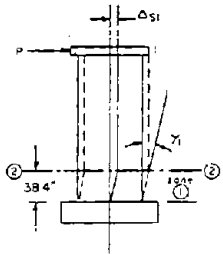
c) In Base to 3 ft Level

1 ft.=0.305 m
1 in.=25.4 mm
1 kip=4.448 kN

Fig. B-80   Load versus Shear Distortion
             for Specimen B3

B-103

increment became larger at an increasing rate. The magnitude of distortions in Zones 1 and 2 were approximately equal in Cycle 28. However, by Cycle 37, the distortions in Zone 1 were twice the distortions in Zone 2.

The distortions during Cycle 28 were only slightly larger than the distortions at Load Stage 11 in B4. However, the distortions in Zone 1 during Cycle 37 were more than twice the distortions at Load Stage 14 in B4. This indicated considerable shear degradation in the lower 3 ft (0.91 m) of wall due to reversed loading after Cycle 28.

Slip at Construction Joints. The slip at construction joints in B3 is shown in Fig. B-81. The slip at CJ1 exhibited "yield" similar to shear "yielding" at a load increment slightly later than that in which flexural yielding occurred. The gage at CJ1 failed in Cycle 31. Up to this cycle the slip in B3 was less than that measured in B1 and more than that measured in B4 at equivalent top deflections.

The slip in CJ1 is shown as a percentage of the total shear deflection in Zone 1 in Fig. B-82. After yield, the slip remained a relatively constant 10 to 15% of the total. This is significantly smaller than the percentage in Specimen B1 and slightly higher than that in Specimen B4.

The measured slip at CJ2 and CJ3 was small compared to that in B4.

Deflections. Deflection components and deflected shapes are shown in Figs. B-83 and B-84. These figures show that prior to Cycle 31 the deflection components and deflected
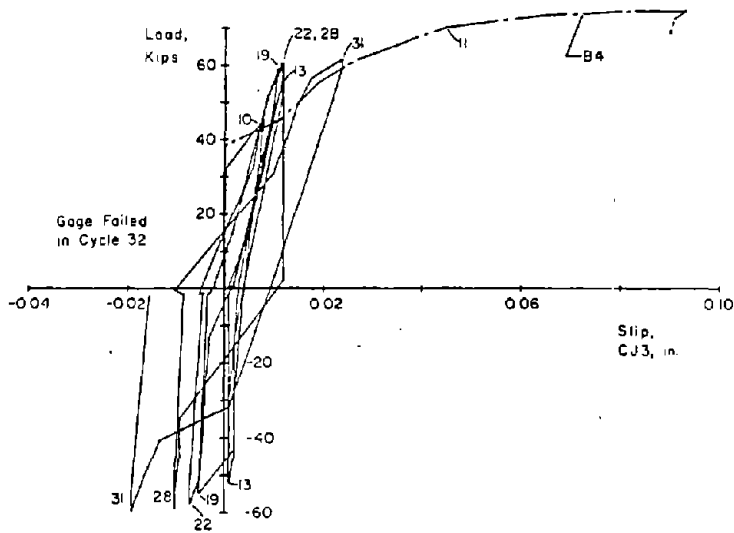
a) At 6 ft. Level
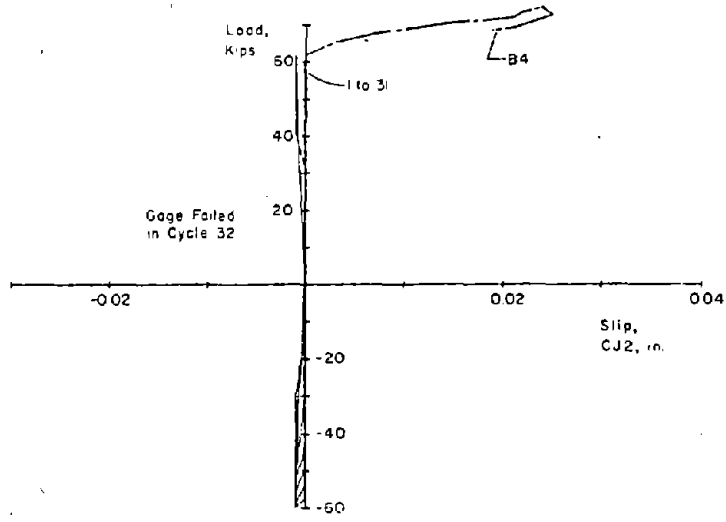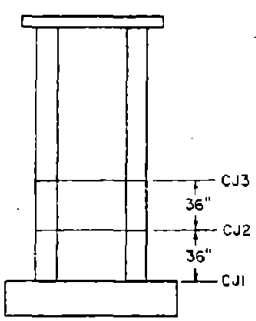
b) At 3 ft. Level
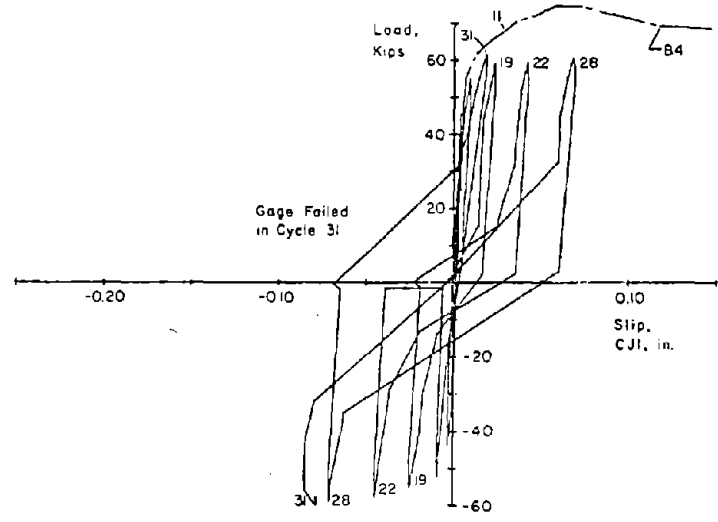
c) At Base Level

1 ft. = 0.305 m
1 in. = 25.4 mm
1 kip = 4.448 kN

Fig. B-81   Load Versus Slip at Construction Joints
for Specimen B3
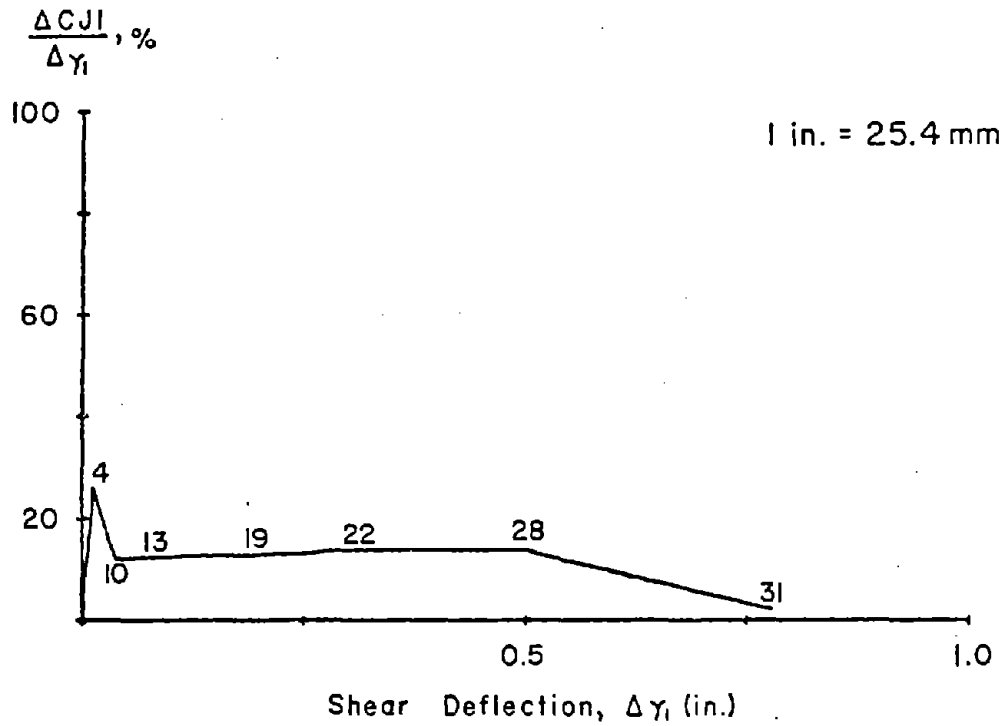
a) At Maximum Positive Loads
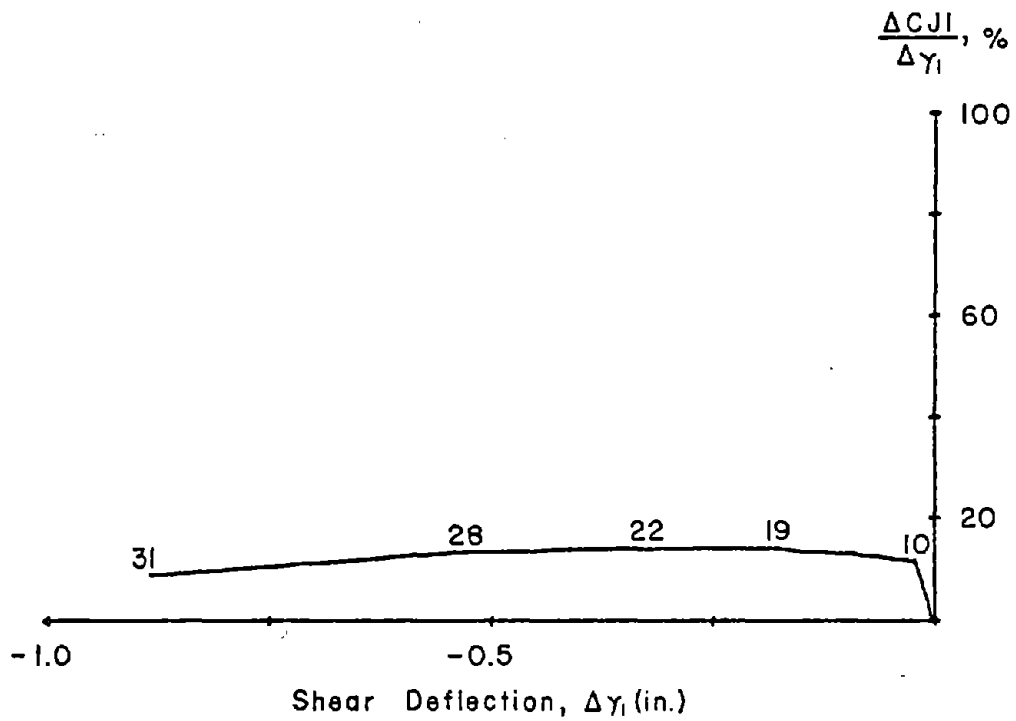

b) At Maximum Negative Loads

Fig. B-82   Slip at Base Construction Joint versus
            Shear Deflection in Zone 1 for Specimen B3
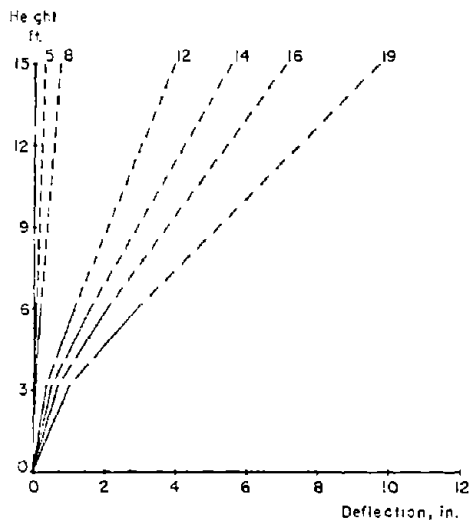
a)   At Top of Wall
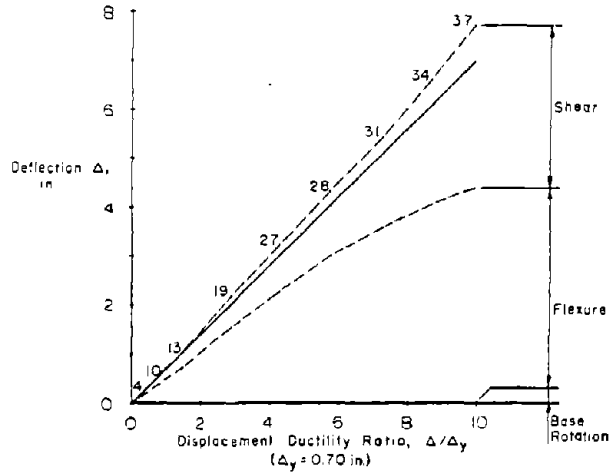
b)   At 6 ft. Level
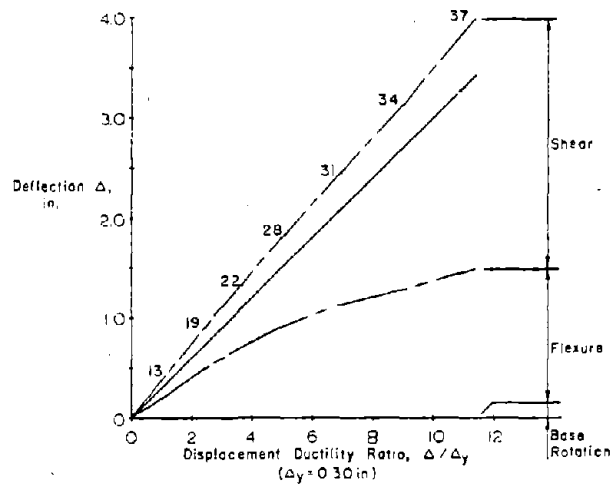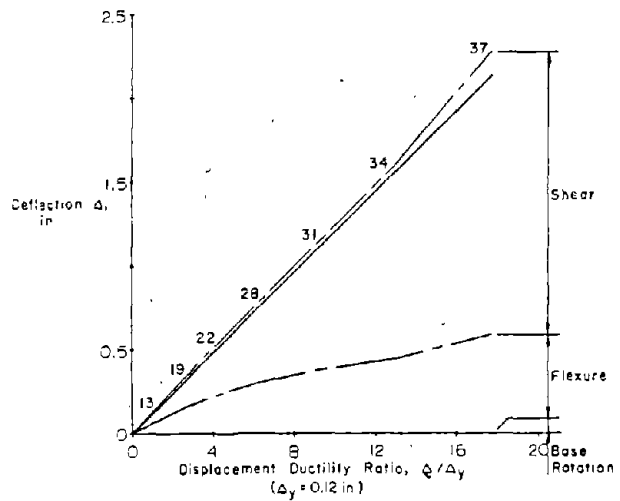
CALCULATED FROM
MEASURED DEFORMATION
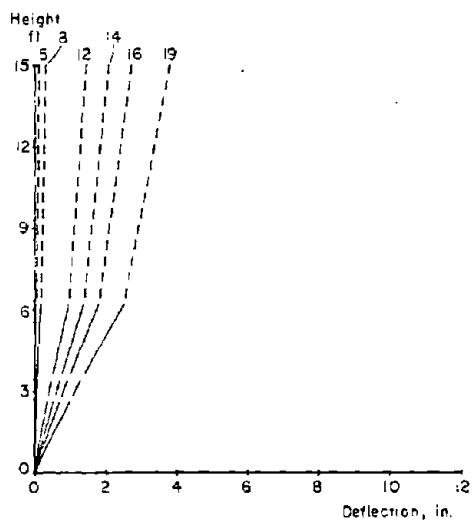EXTRAPOLATED
MEASURED TOTAL

1 in = 25.4 mm
1 ft. = 0.305 m

c)   At 3 ft. Level

Fig. B-83   Component of Deflection for Specimen B3
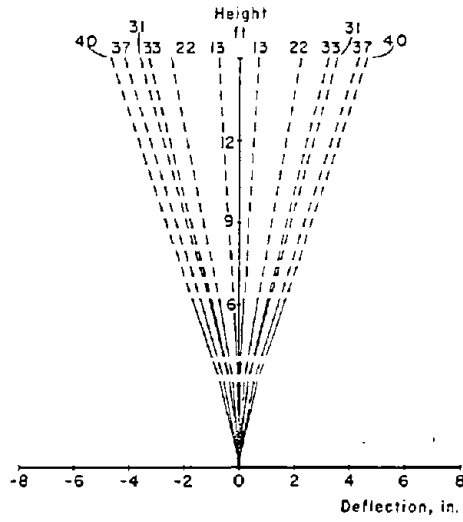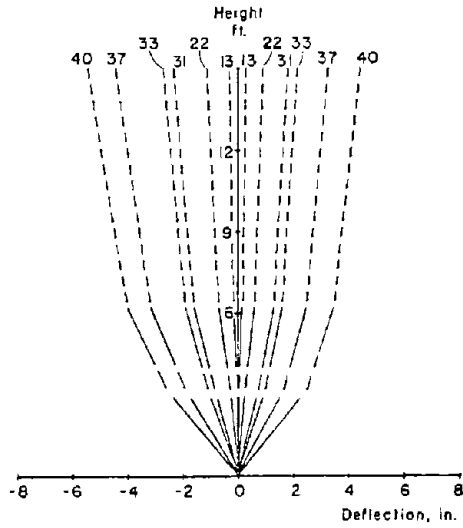
B-107

a) Flexural

b) Shear

—··— CALCULATED FROM
MEASURED DEFORMATION
———— EXTRAPOLATED
——— MEASURED TOTAL

I in.= 25.4 mm
I ft.= 0.305 m

B.F. – BAR FRACTURE

CYCLE 40, AFTER
SEVERAL B.F.

CYCLE 37, PRIOR
TO 1st. B.F.
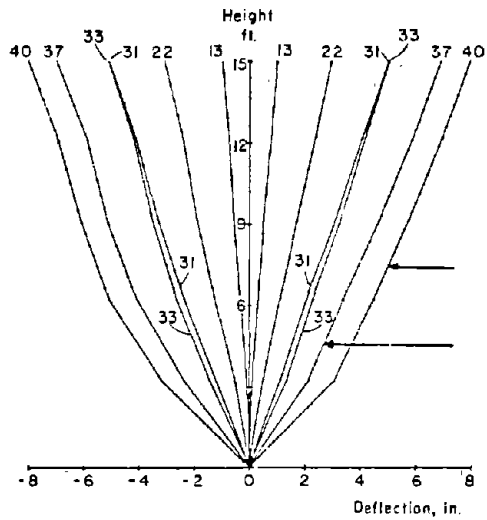
c) Total

Fig. B-84 Deflected Shape for Specimen B3

shapes in B3 were very similar to those in B1. After cycle 31 shear deflections increased. At the latter load increments the total deflected shape of the wall was similar to the deflected shape of a frame.

The deflected shapes at Cycle 31 and 33 showed an approximate 20% increase in shear deflection at the top of the wall within the 5-in. increment. The deflected shapes at Cycles 37 and 40 show the stiffness degradation due to several bar fractures. It is interesting to note that fracture of the vertical steel affected the shear deflections more than it did the flexural deflections.

Reinforcement Strains. Figures B-85 through B-93 show reinforcement strains in the specimen at various stages.

Since the majority of the vertical strain gages were either not functioning or off scale after Cycle 28, The strain gage figures are very similar to the strain gage figures for Specimen B1.

The horizontal gages functioned for a few more cycles than did the vertical gages. Therefore, Figs. B-89 through B-93 show more extensive yielding in the horizontal web bars than do Figs. B-67 through B-71 for Specimen B1. The horizontal strains approach zero at the 12-ft level.

Load,
Kips

Gage VAT1

Strain, Millionths

Gage VHT1

Strain, Millionths

1 kip = 4.448 kN
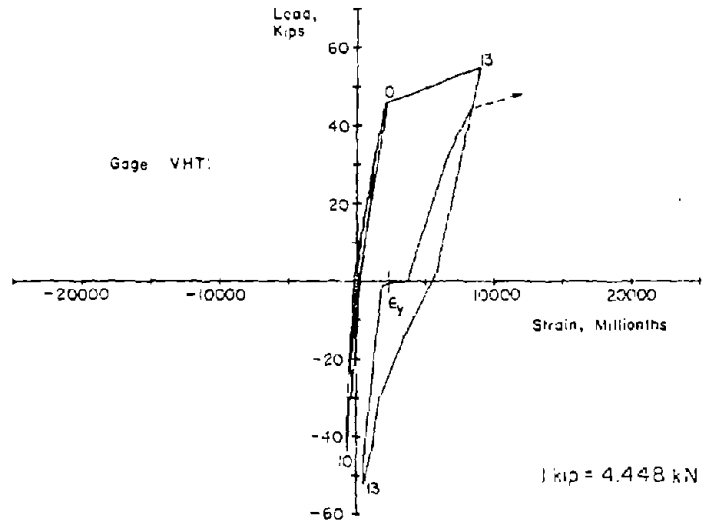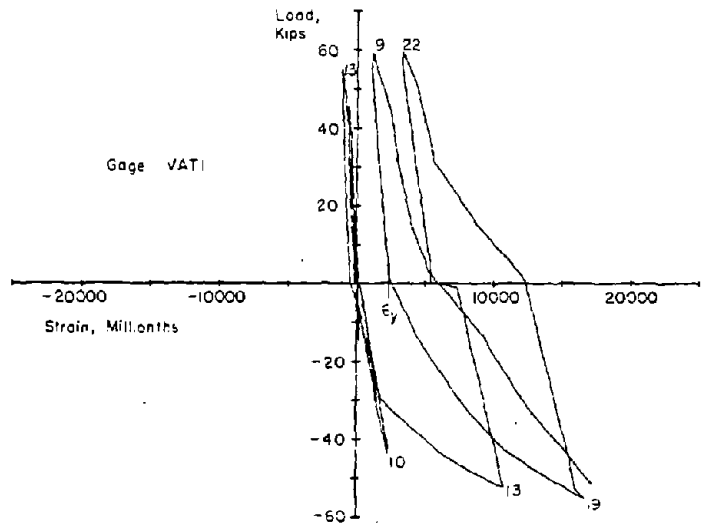
Fig. B-85   Measured Strains on Vertical Reinforcement
at Base of Specimen B3
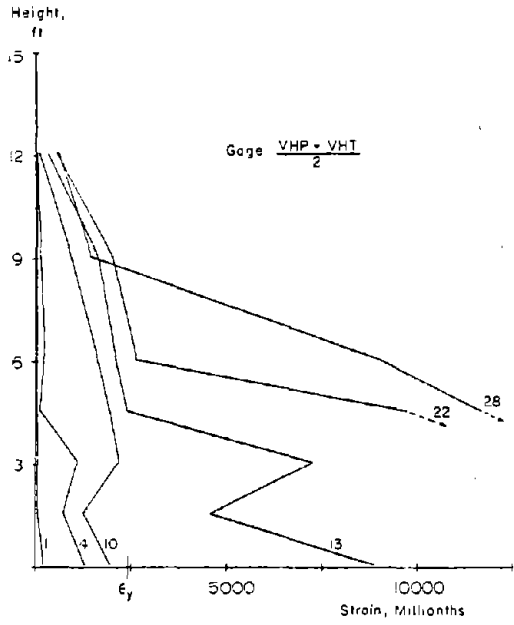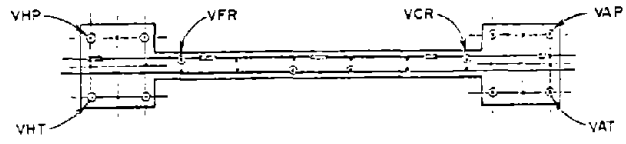
a) Average of VHP & VHT
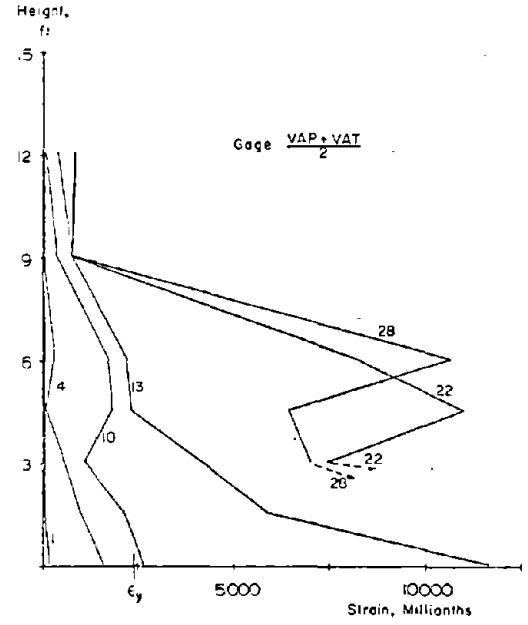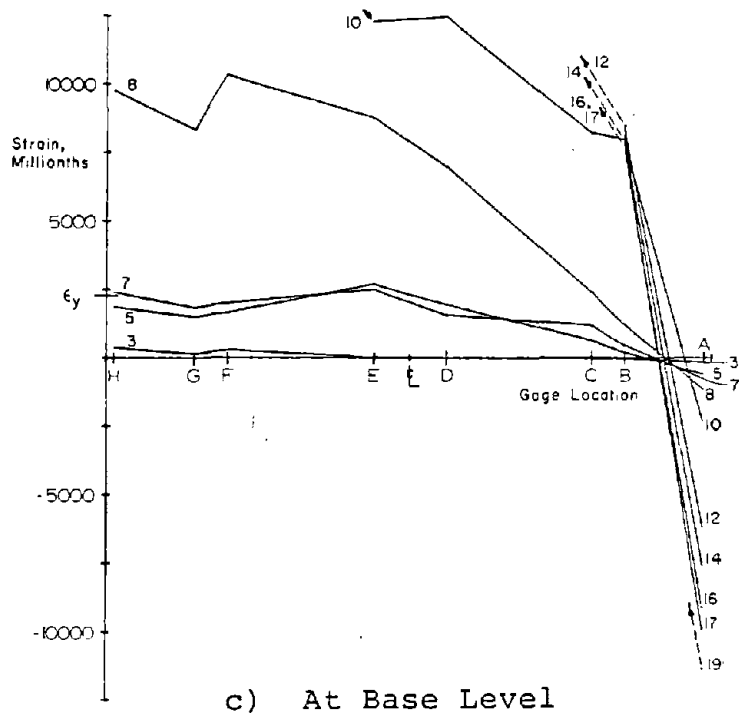
b) Average of VAP & VAT
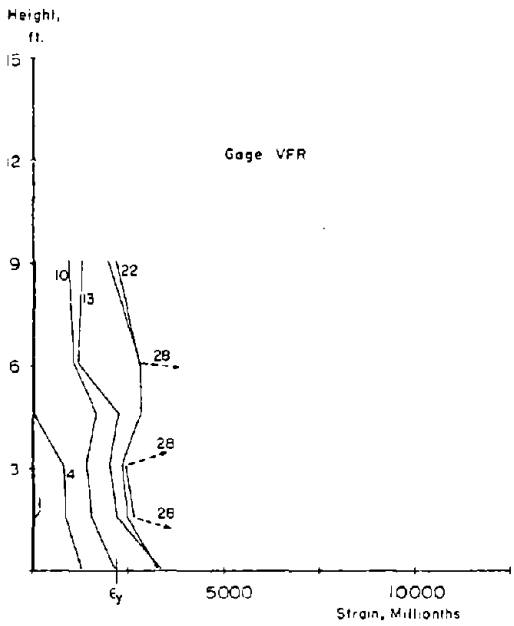
c) Strain Gage VFR

d) Strain Gage VCR

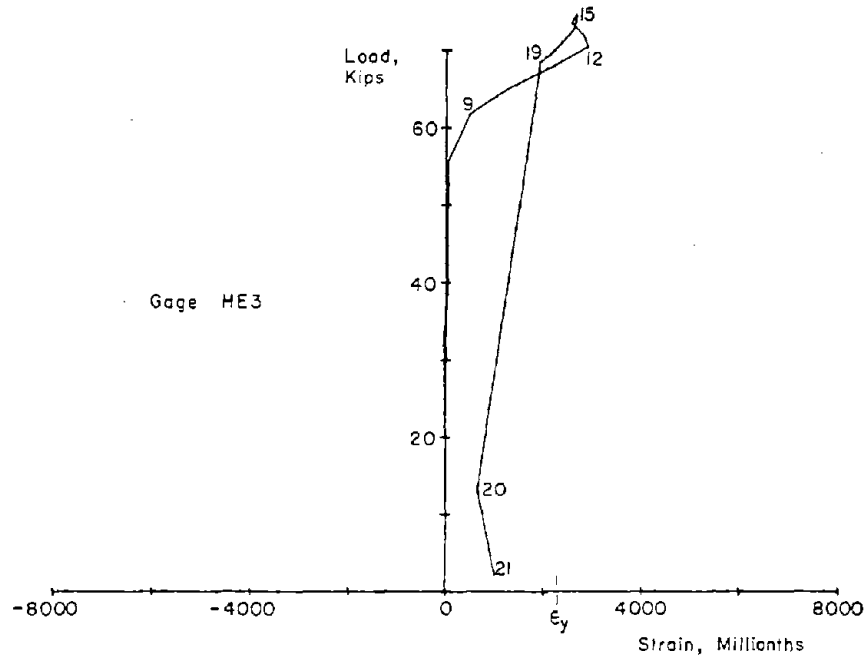Fig. B-86 Vertical Reinforcement Strains at
Maximum Loads for Specimen B3

Fig. B-87   Vertical Reinforcement Strains at
Maximum Positive Loads for Specimen B3
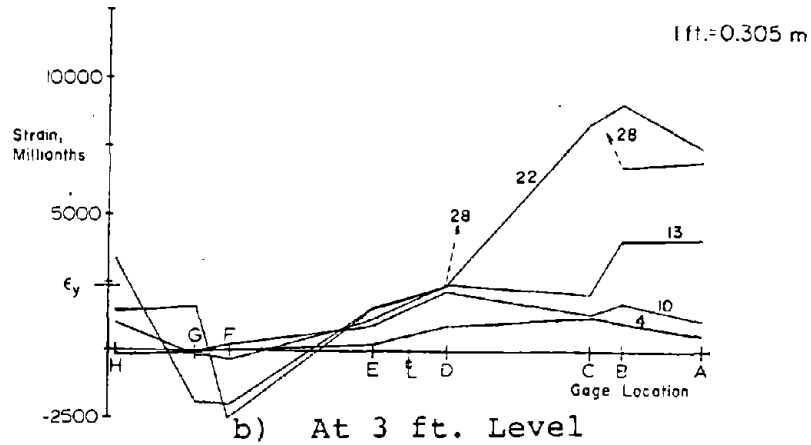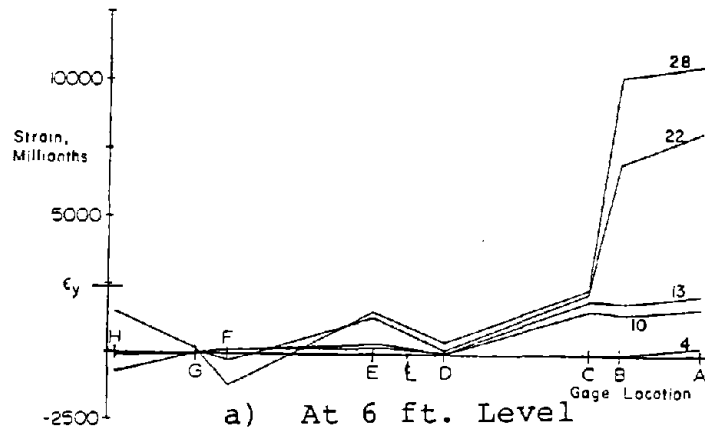
Fig. B-88   Vertical Reinforcement Strains at
            Maximum Negative Loads for Specimen B3

B-113

Load,
Kips

Gage HE3

28   60

19 22

13

40

20

-8000   -4000   ε_y   8000

Strain, Millionths

-20

-40

13   19   22   28

-60

1 in. = 25.4 mm
1 kip = 4.448 kN

HE3

HE2

Load,
Kips

Gage HE2

60   22 13

40

20

-8000   -4000   ε_y   4000   8000

Strain, Millionths

-20

-40

13   19 22

-60

Fig. B-89   Measured Strains on Horizontal Reinforcement
for Specimen B3

B-114

Fig. B-90 Horizontal Reinforcement Strains at
Maximum Positive Load for Specimen B3

1 ft. = 0.305 m

Fig. B-91 Horizontal Reinforcement Strains at
Maximum Negative Loads for Specimen B3

1 ft = 0.305 m
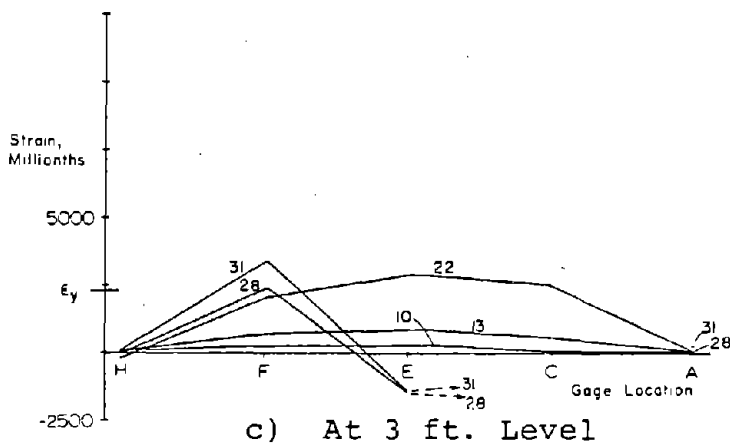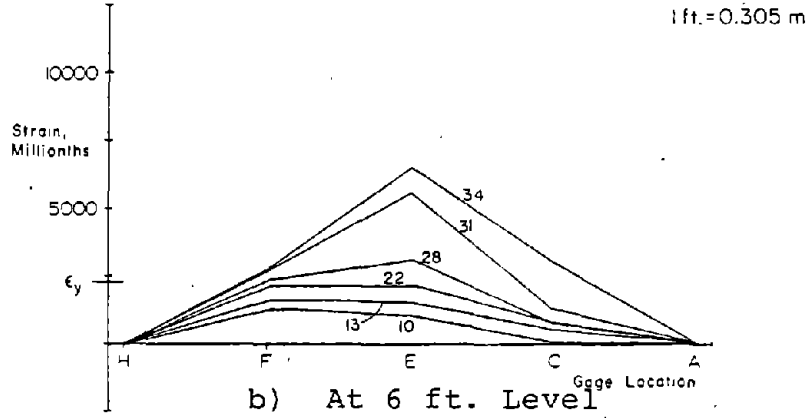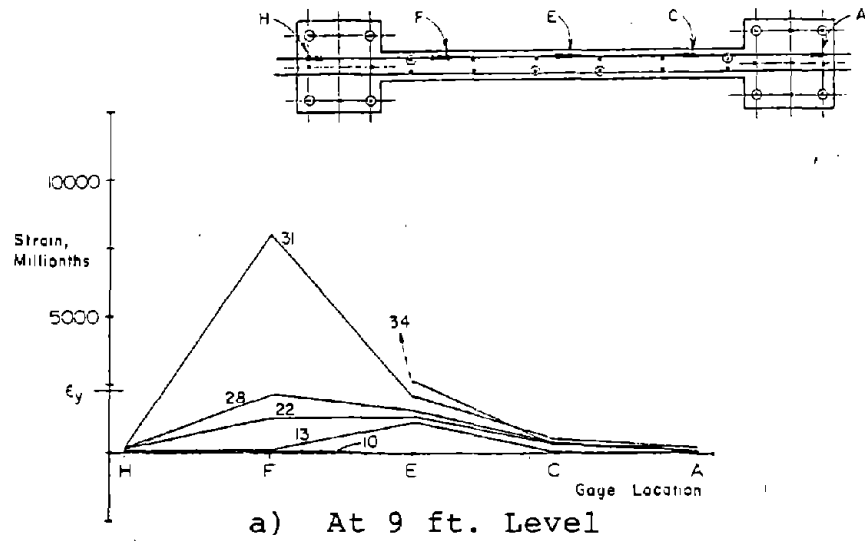
a) At 9 ft. Level

b) At 6 ft. Level

1 ft.=0.305 m

c) At 3 ft. Level

Fig. B-92   Horizontal Reinforcement Strains in Web
at Maximum Positive Loads for Specimen B3

B-117

a) At 9 ft. Level

1 ft.=0.305 m

b) At 6 ft. Level

c) At 3 ft. Level

Fig. B-93   Horizontal Reinforcement Strains in Web
at Maximum Negative Loads for Specimen B3

B-118

Specimen B4

Test Description

Specimen B4 was similar to Specimen B3 with 1.11% vertical reinforcement in each column and confinement in the lower 6 ft (1.83 m) of the column. B4 was loaded monotonically for comparison with B3.

The test consisted of 20 load stages as shown in Fig. B-94. First cracking was observed between Load Stages 3 and 4 at a load of 26 kips (115.6 kN). First yielding occurred at Load Stage 7 at a load of 45.3 kips (201.5 kN). The maximum measured crack widths at this stage were 0.010 in. (0.25 mm) in the tension column and 0.020 in. (0.51 mm) across a diagonal crack in the web.

The crack pattern that developed in the lower 6 ft is shown in Figs. B-95 through B-98. Figure B-95 shows the crack pattern at 3 in. (76.2 mm) top deflection. Figure B-96 shows the specimen at 8 in. (203.2 mm) top deflection when the load was near the maximum. Figure B-97 shows the specimen at 12 in. (304.8 mm) in. top deflection just before the end of the test. Figure B-98 shows the specimen just after the end of the test.

Slight crushing in the outer shell of the compression face was first noted at Load Stage 9. This crushing progressively increased throughout the test.

After Load Stage 10, one diagonal crack started to predominate. As seen in Fig. B-96, this crack extended from
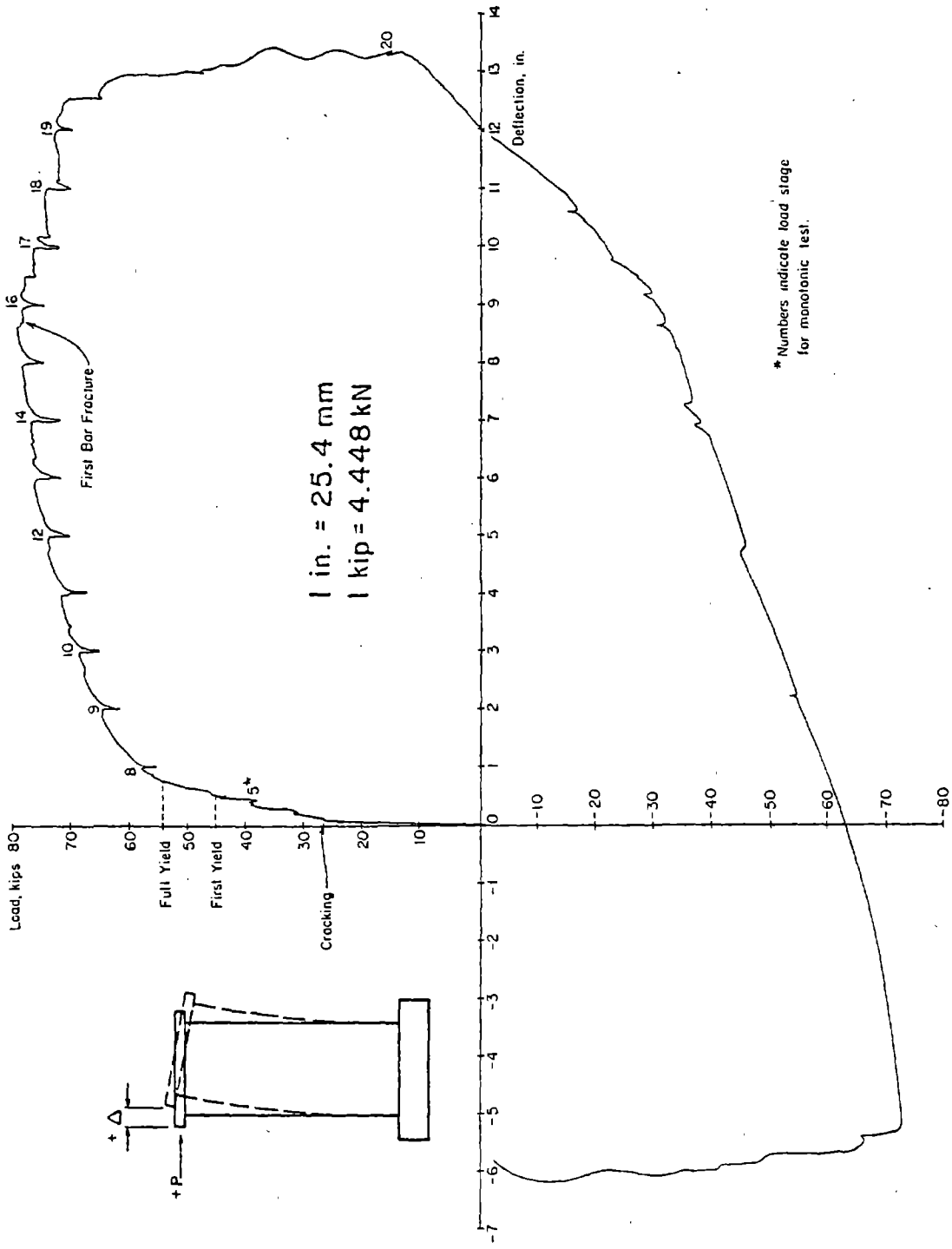
Fig. B-94 Continuous Load-Deflection Plot for Specimen B4

1 in. = 25.4 mm
1 kip = 4.448 kN

* Numbers indicate load stage
  for monotonic test.

B-120

Fig. B-95   Cracking Pattern at +3 in. Deflection
            for Specimen B4
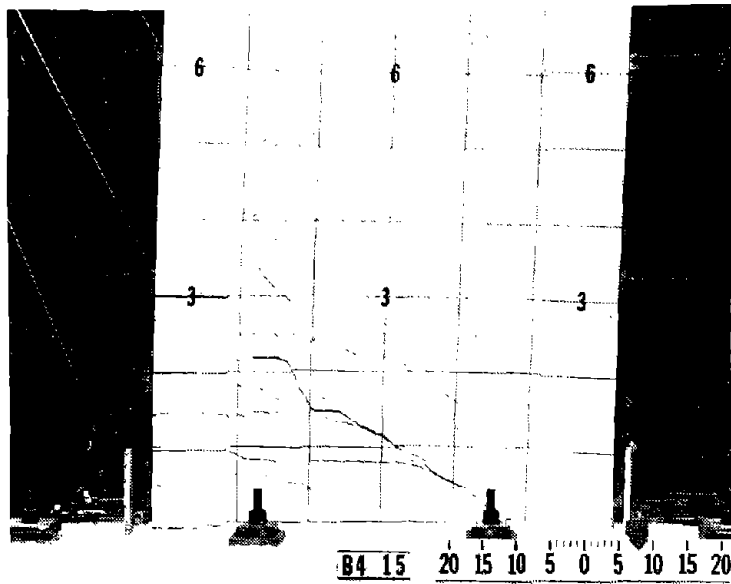
Fig. B-96   Cracking Pattern at +8 in. Deflection
            for Specimen B4

B-121
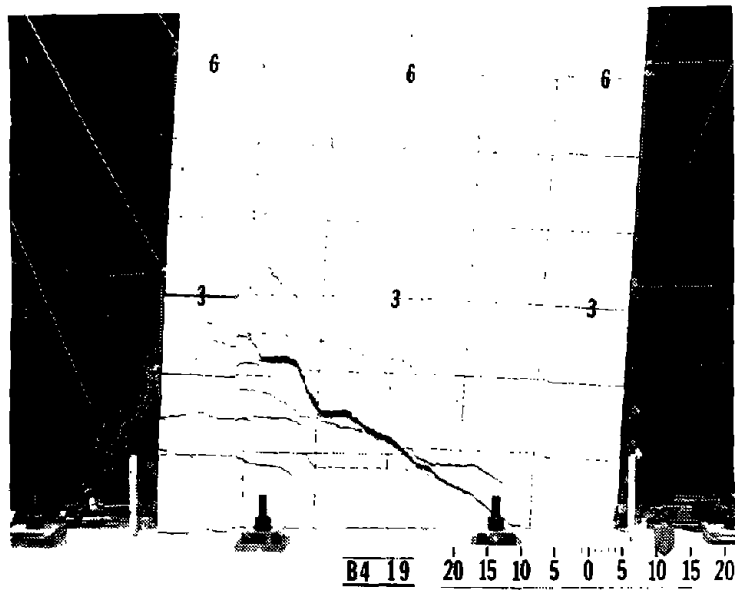
Fig. B-97   Specimen B4 Prior to End of Test
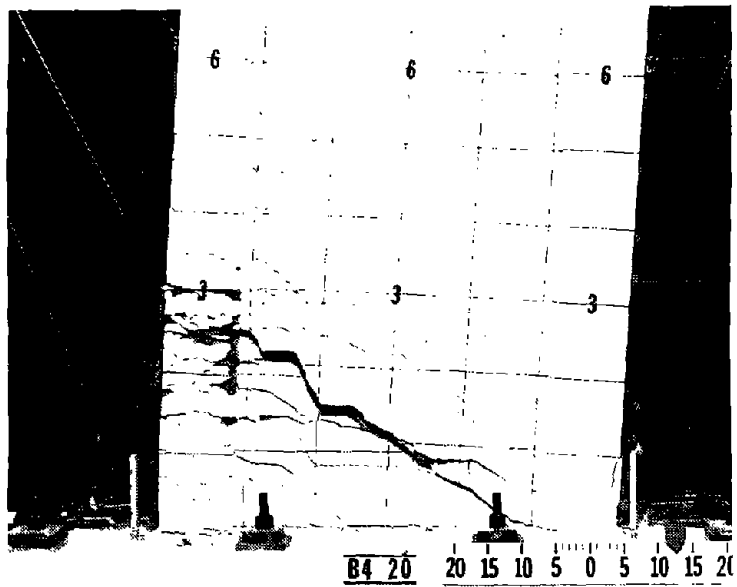
Fig. B-98   Specimen B4 at End of Test

B-122

the base compression column to the tension column approximately 2 ft 6 in. (0.76 m) above the base.

The maximum load measured, 75.3 kips (334.9 kN), occurred at a top deflection of 8.5 in. (215.9 mm). This load correspond to a nominal shear stress, $v_{max} = 3.9\sqrt{f'_c}$ ($0.32\sqrt{f'_c}$, MPa), between Load Stages 15 and 16. At this point one of the smaller diameter vertical bars in the web region fractured. The measured crack widths at this stage in the column ranged from 0.075 to 0.125 in. (1.90 to 3.18 mm). The measured width across the large diagonal crack was 0.44 in. (11.2 mm) other measured web crack widths ranged from 0.07 to 0.10 in. (1.78 to 2.54 mm).

Between Load Stages 16 to 19, 4 more small diameter vertical bars in the web fractured. A small decrease in load was associated with each of these bar fractures. At Load Stage 19, the width across the large diagonal crack was 1.0 in. (25.4 m).

Between load stages 19 and 20 at a top deflection 12.5 in. (317.5 mm), all 8 tension column bars and 4 additional vertical web bars fractured simultaneously. The 8 column bars fractured at a level where the large diagonal crack intercepted the tension column 2 ft 6 in. above the base. The load reduction was very sudden and nearly complete.

Since very little load capacity remained in the wall for loads in the positive direction, the wall was loading in the negative direction. The wall reached a maximum load of 72.5 kips (322.5 kN) at -5.3 in. (134.6 mm) top deflection

before a sudden failure occurred when all the remaining bars
fractured.

Discussion of Results

Moment-Rotation. Moment rotation data for Specimen B4
is shown in Fig. B-99. As described previously in the data
analysis and presentation section, the calculated maximum
strength agreed closely with the measured. The calculated
rotation at the base level differed considerably from the
measured due to strains in the steel anchored in the base
block. However, the calculated maximum rotations at the
3-ft and 6-ft (0.91 m and 1.83 m) levels are in reasonable
agreement with the measured.

Shear-Distortion. The shear-distortion data for B4 are
shown in Fig. B-100. As in the previously described tests,
shear "yielding" occurred at the same load stage in which
flexural yield occurred. The distortions in Zone 1 were
approximately equal to those in Zone 2. The distortions
increased at an approximately constant rate with each new
1 in. deflection increment.

Slip at Construction Joints The slip at construction
joints in B4 is shown in Fig. B-101. The slip at CJ1 ex-
hibited a "yielding" similar to shear "yielding" at the same
stage that flexural yield occurred. Slip at CJ2 "yielded"
one load stage after flexural yield. Slip at CJ3 "yielded"
one load stage before flexural yield.
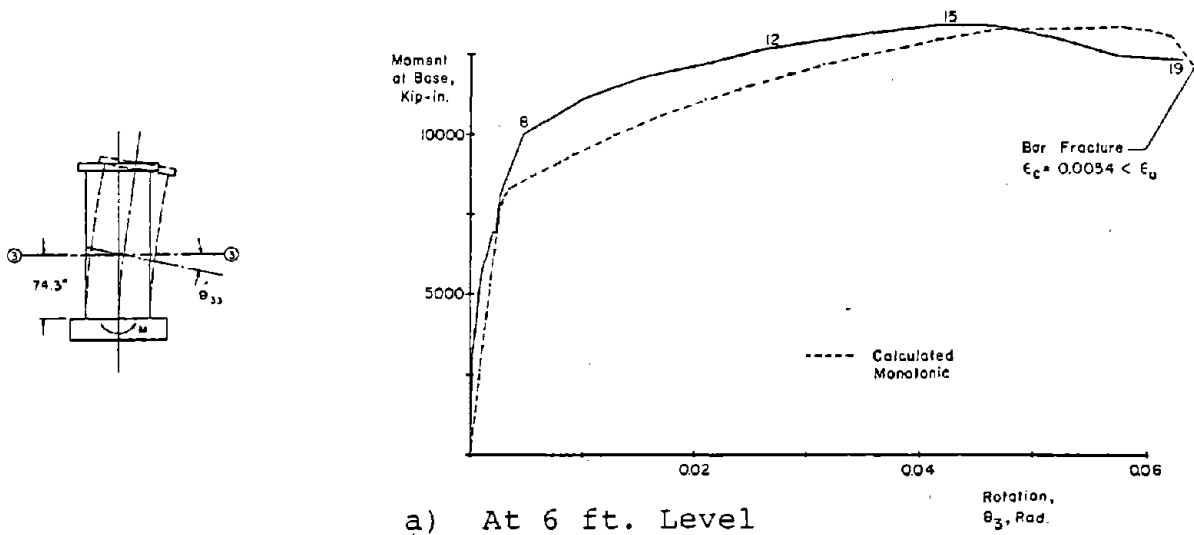
a) At 6 ft. Level
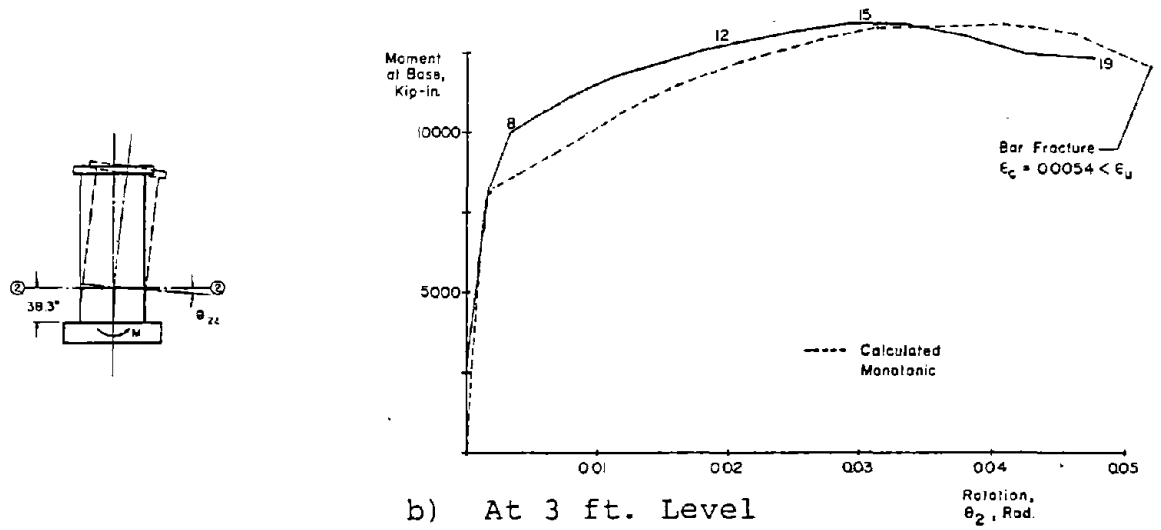
b) At 3 ft. Level
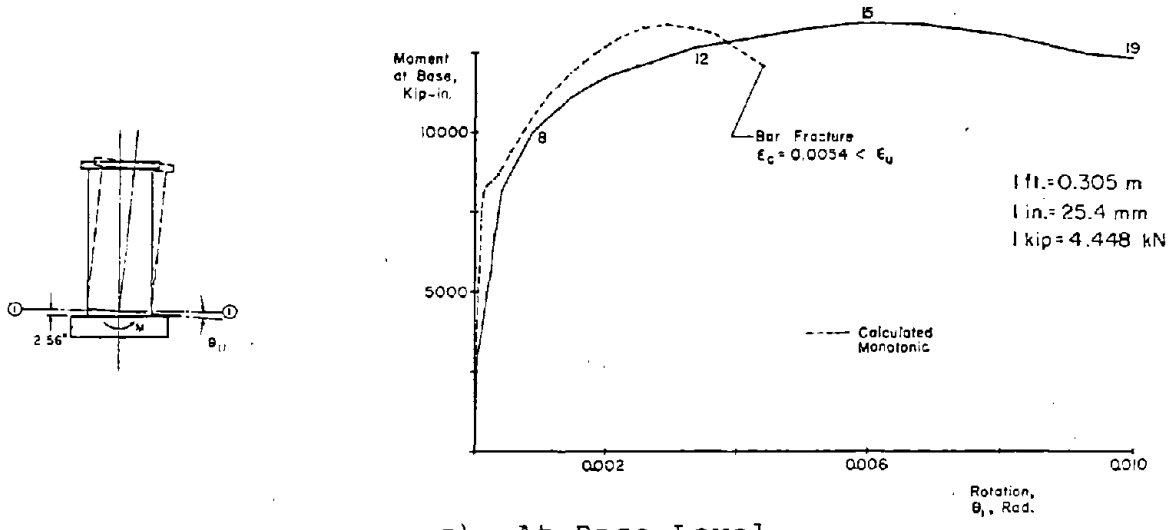
c) At Base Level

Fig. B-99   Moment at Base Level versus Rotation
            for Specimen B4
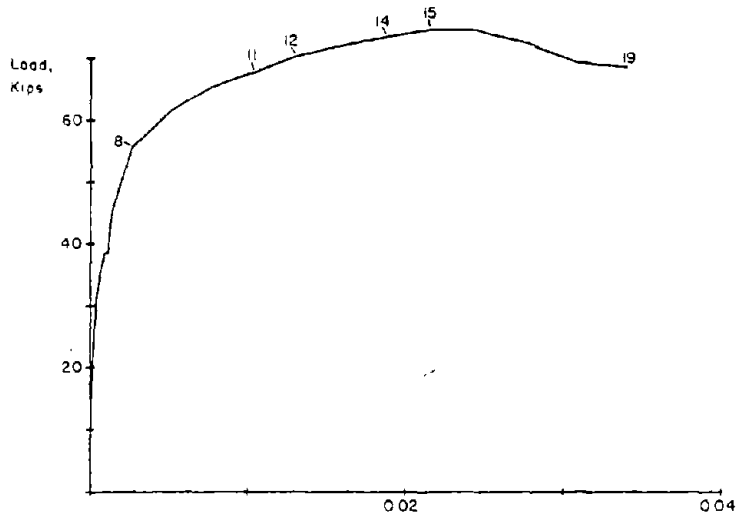
a) In Base to 6 ft Level
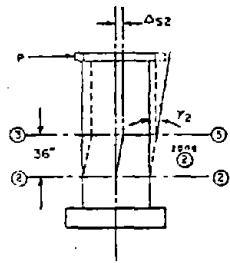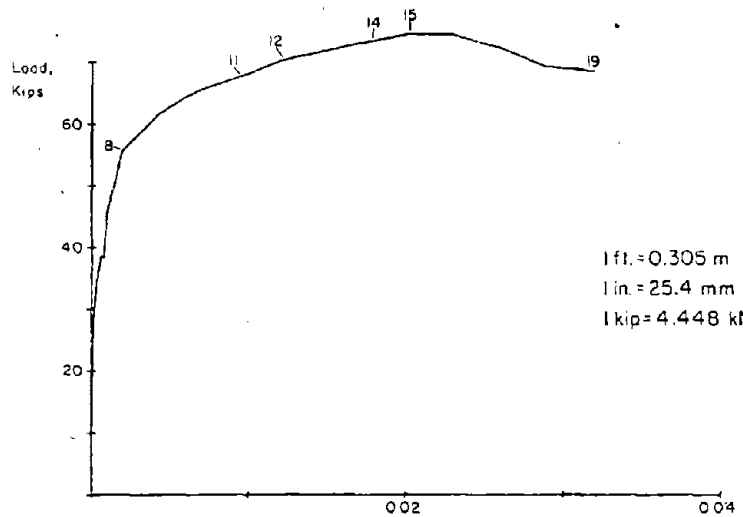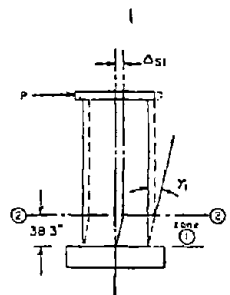
b) In 3 ft to 6 ft Level

1 ft. = 0.305 m
1 in. = 25.4 mm
1 kip = 4.448 kN

c) In Base to 3 ft Level

Fig. B-100   Load versus Shear Distortions for
                Specimen B4

a) At 6 ft. Level

b) At 3 ft. Level

1 ft.=0.305 m
1 in.=25.4 mm
1 kip=4.448 kN

c) At Base Level
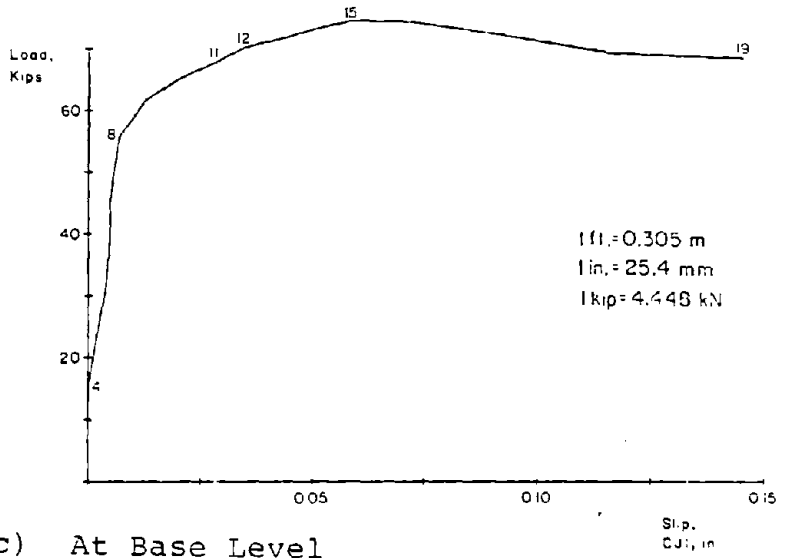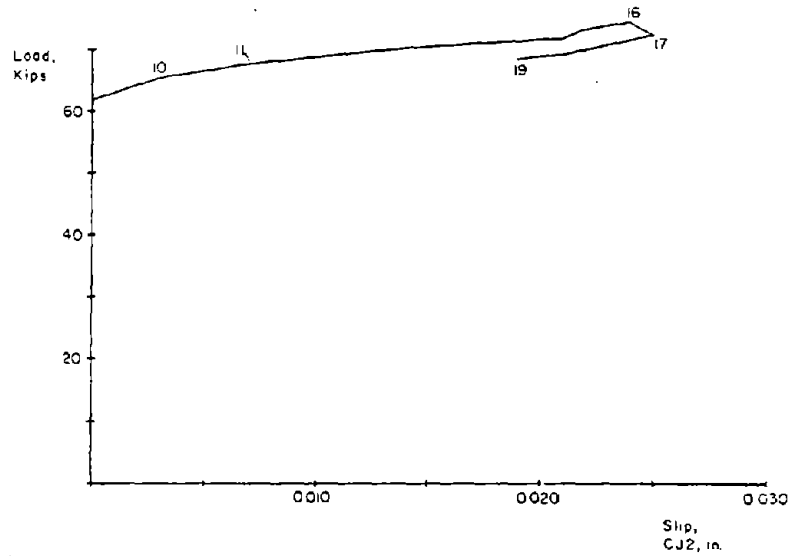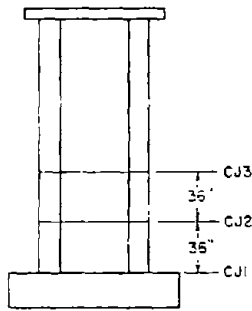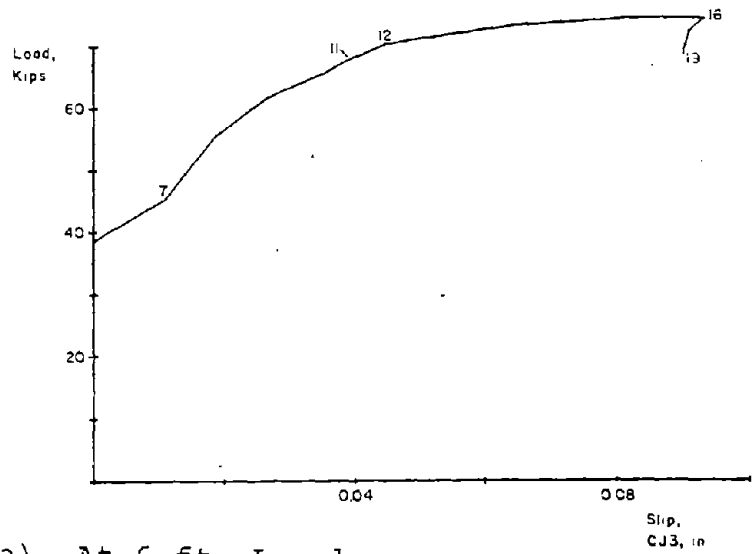
Fig. B-101   Load versus Slip at Construction Joints
             for Specimen B4

As shown in Fig. B-102, the slip at CJl was a relatively constant 8 to 10% of the total shear deflection in the lower 3 ft of the wall.

Deflections. The deflection components and deflected shapes are shown in Figs. B-103 and B-104. While flexural deflections predominated, shear deflections were approximately 30% of the total top deflection. The relationship between shear and flexural deflections remained constant through the test.

Reinforcement Strains. Figures B-105 through B-110 show reinforcement strains in the specimen at various load stages. The strain gradient figures for B4 appear similar to those for B1 and B3. Figure B-107 shows that the neutral axis at the base moved toward the compression face until Load Stage 10. The neutral axis then moved away from the compression face until the end of the test. Figures B-109 and B-110 show that yielding occurred in the vertical and horizontal bars up to the 9-ft (2.74 m) level.
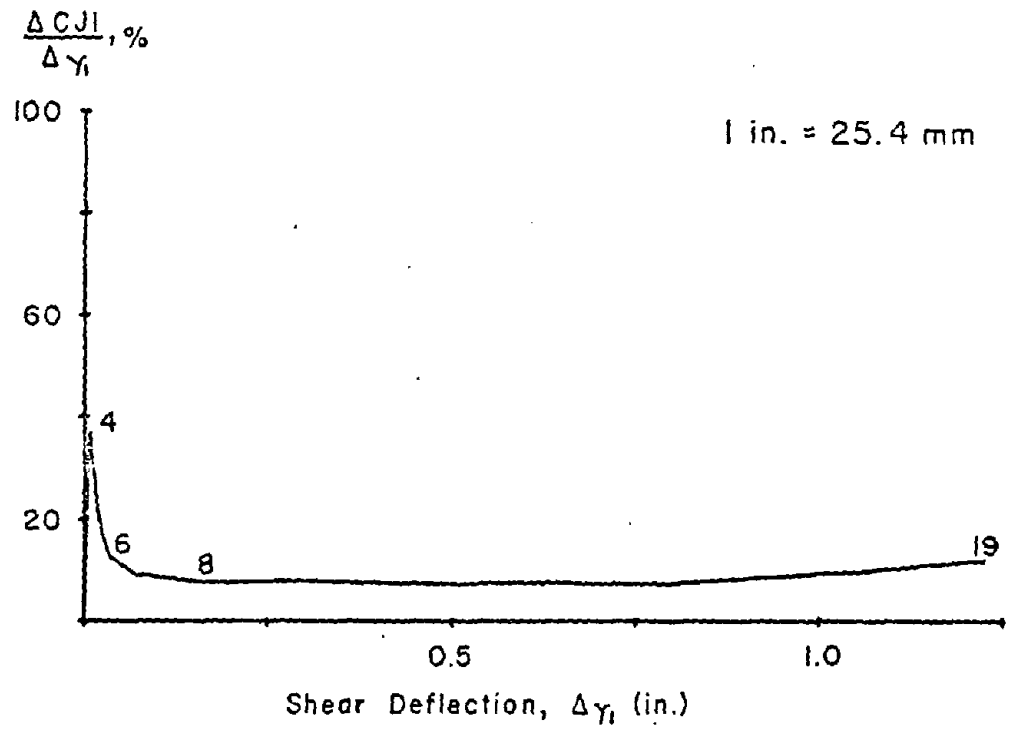
Fig. B-102   Slip at Base Construction Joints versus
              Shear Deflection in Zone 1 for Specimen B4
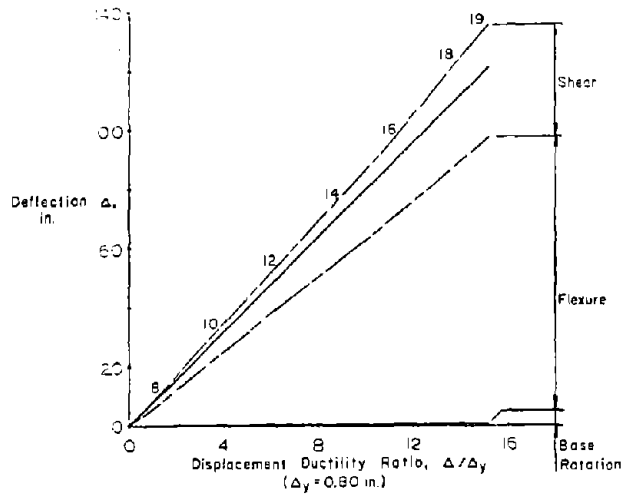
a) At Top of Wall
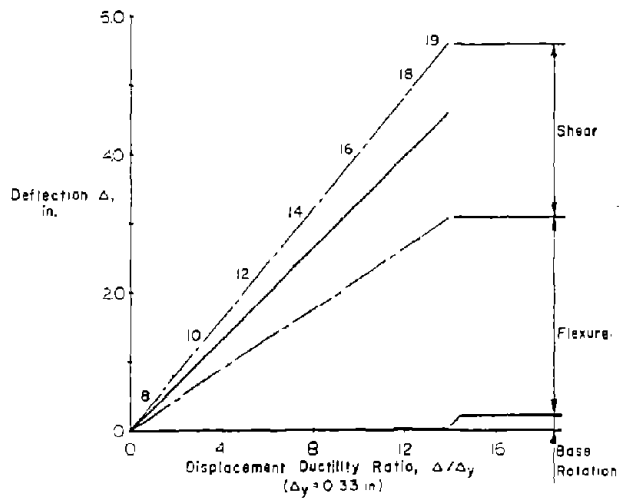
b) A 6 ft. Level
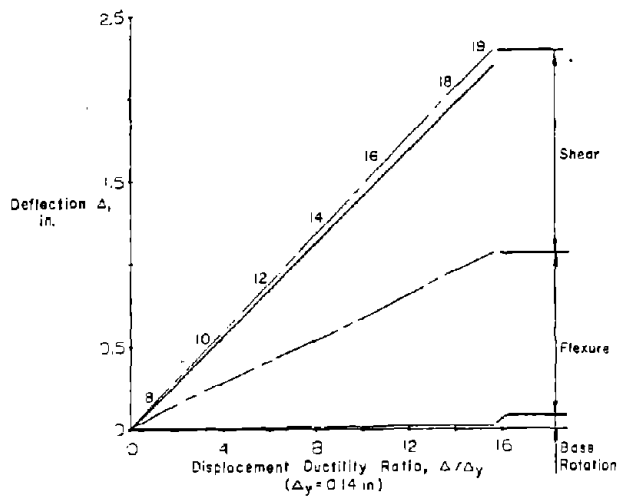
CALCULATED FROM
MEASURED DEFORMATION
EXTRAPOLATED
MEASURED TOTAL

I in = 25.4 mm
I ft = 0 305 m

c) At 3 ft. Level

Fig. B-103 Component of Deflection for Specimen B4

a) Flexural

b) Shear

— — — CALCULATED FROM
        MEASURED DEFORMATION
— — — EXTRAPOLATED
———— MEASURED TOTAL

1 in.= 25.4 mm
1 ft.= 0.305 m

c) Total
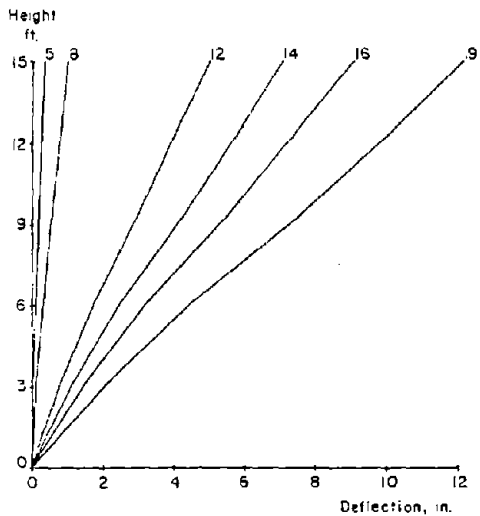
Fig. B-104 Deflected Shape for Specimen B4
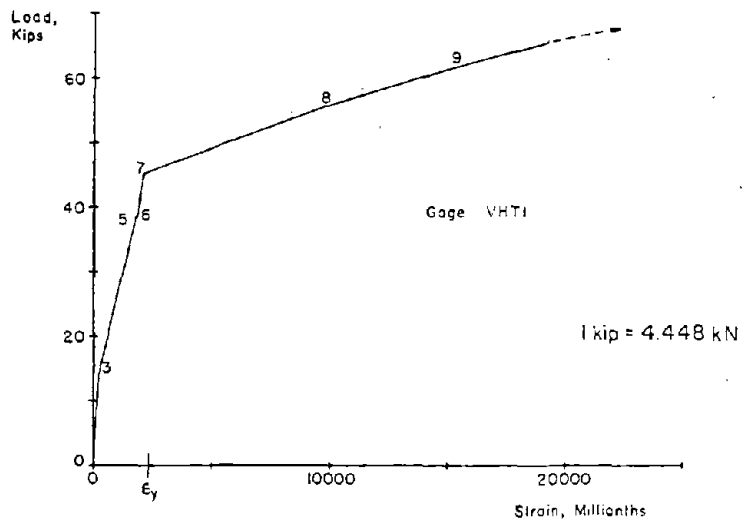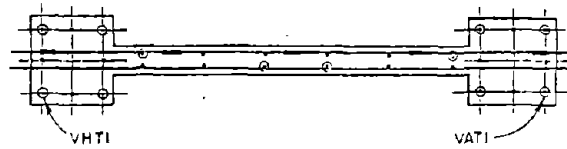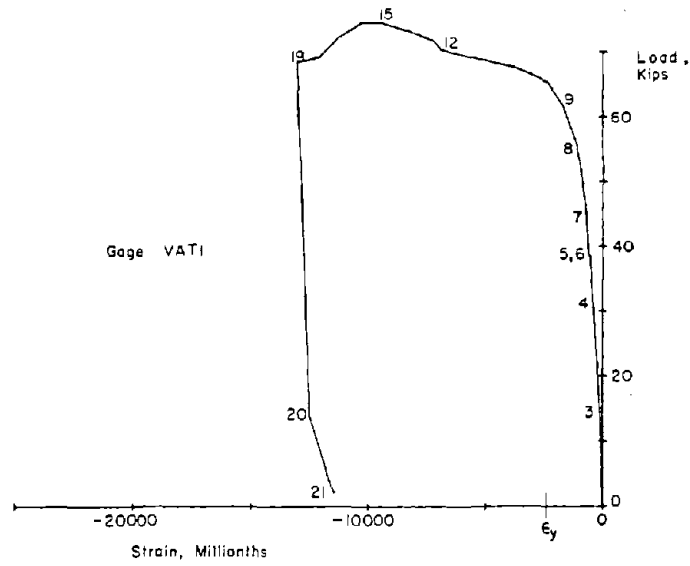
Fig. B-105 Measured Strains on Vertical Reinforcement
at Base of Specimen B4

1 ft.= 0.305 m
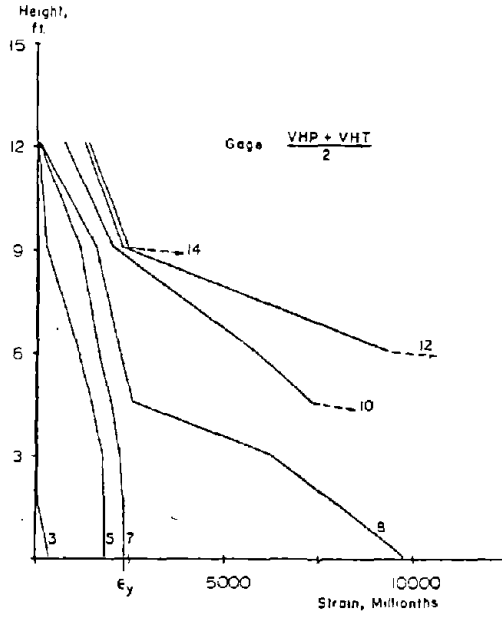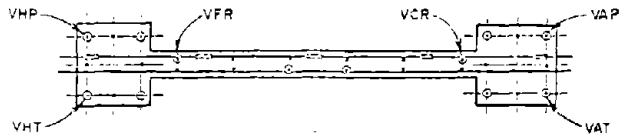
a) Average of VHP & VHT
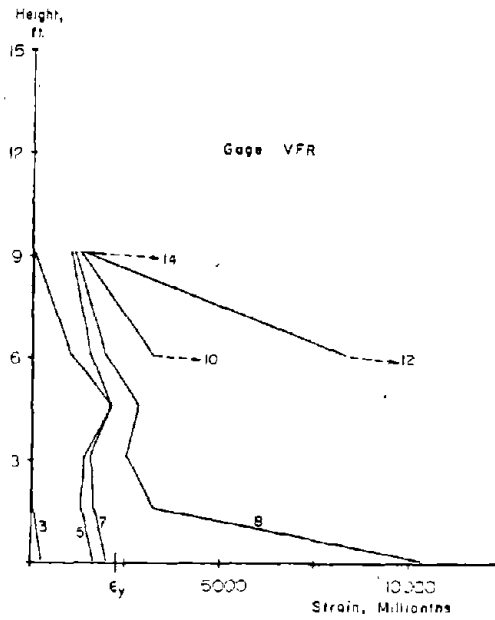
b) Strain Gage VFR

Fig. B-106   Vertical Reinforcement Strains at
Maximum Loads for Specimen B4

B-133
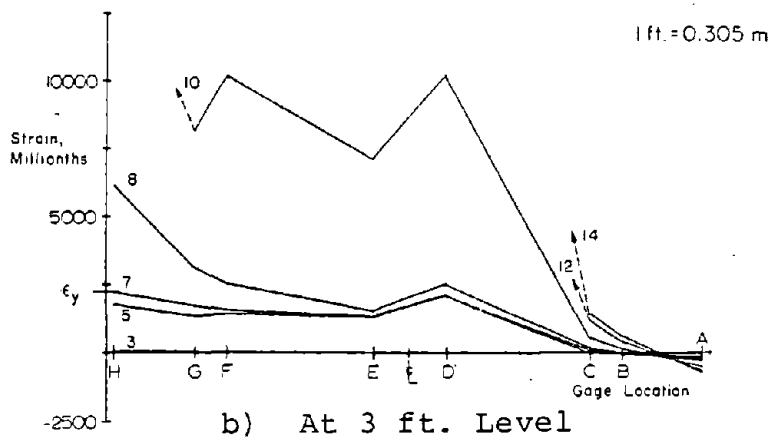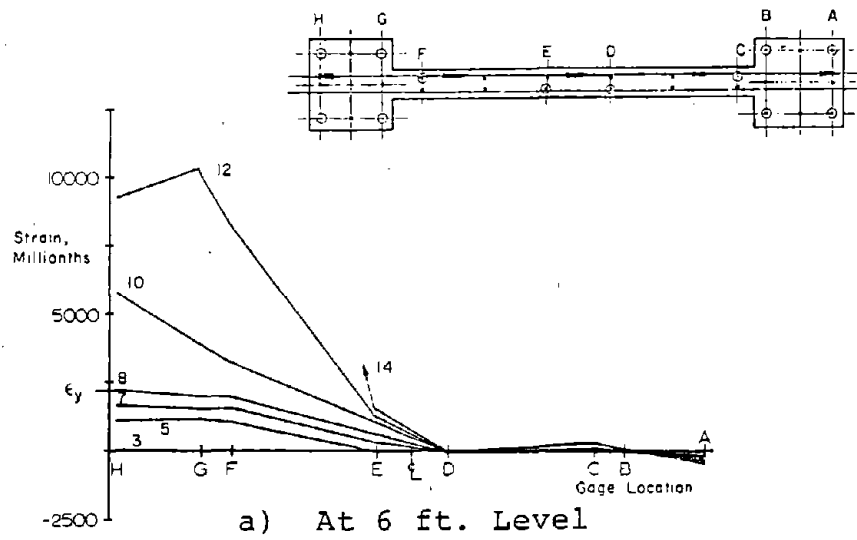
Fig. B-107 Vertical Reinforcement Strains at Maximum Loads for Specimen B4

Load,
Kips

15

19   12

9

60

Gage HE3

40

20

20

21

-8000   -4000   0 ϵ_y 4000   8000

Strain, Millionths

1 in. = 25.4 mm
1 kip = 4.448 kN

Load,
Kips

15

19

9

60

Gage   HE2

40

20

20

21

-8000   -4000   0 ϵ_y 4000   8000

Strain, Millionths
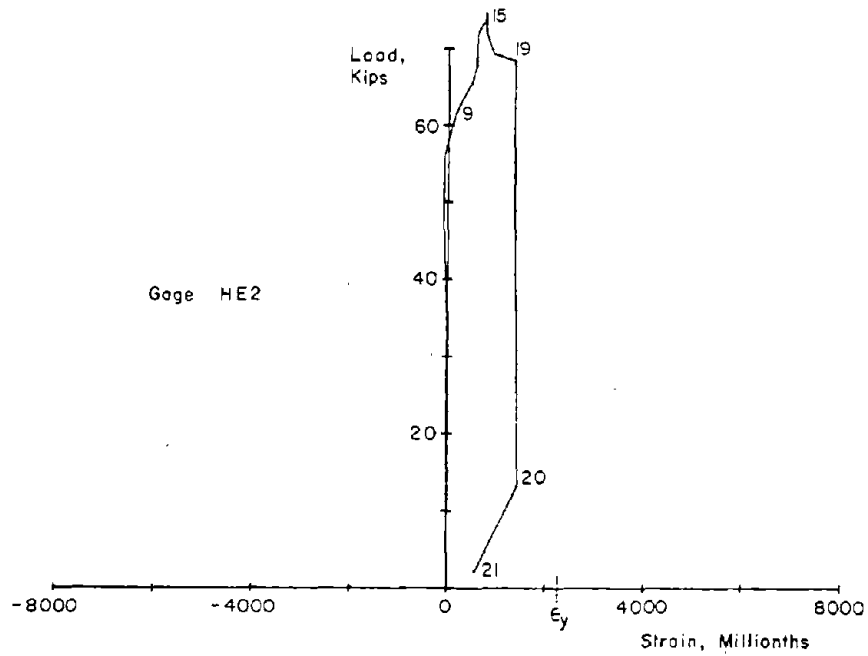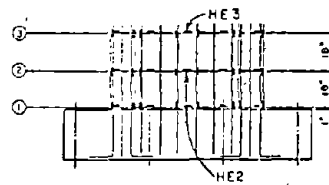
Fig. B-108   Measured Strains on Horizontal Reinforcement
for Specimen B4
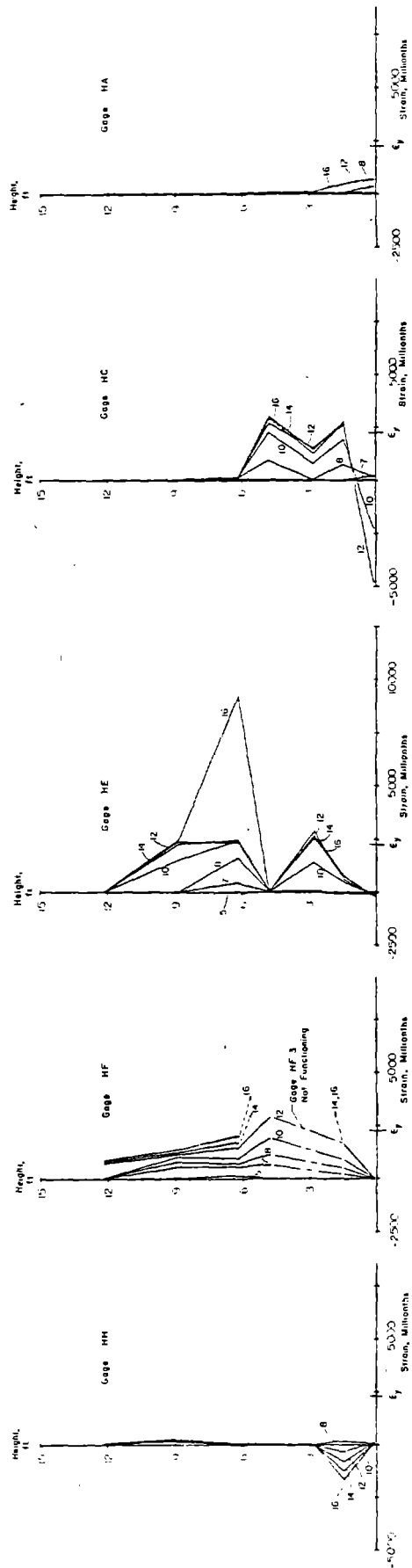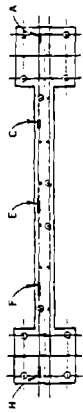
Fig. B-109 Horizontal Reinforcement Strains at
Maximum Loads for Specimen B4

1ft.=0.305 m

a) At 9 ft. Level

b) At 6 ft. Level

1 ft.=0.305 m

c) At 3 ft. Level
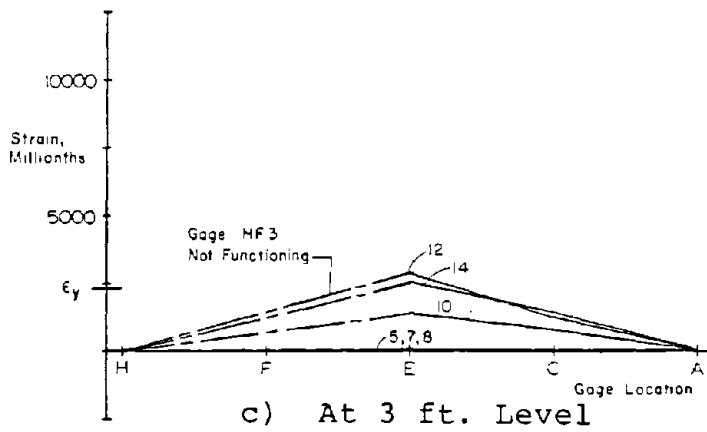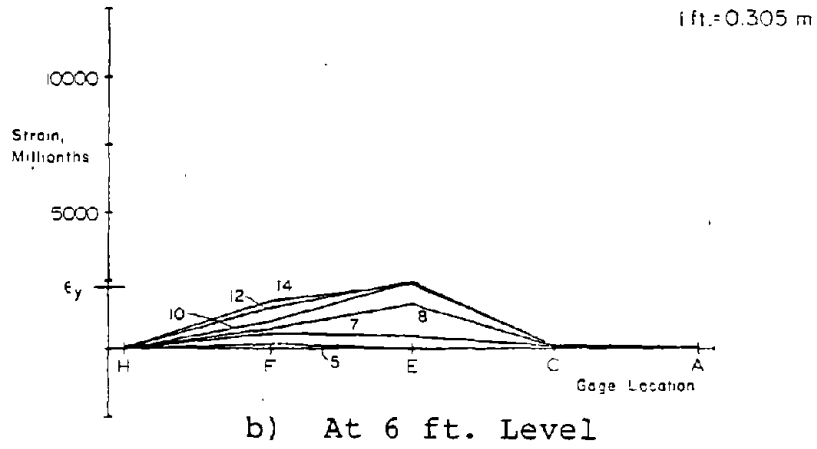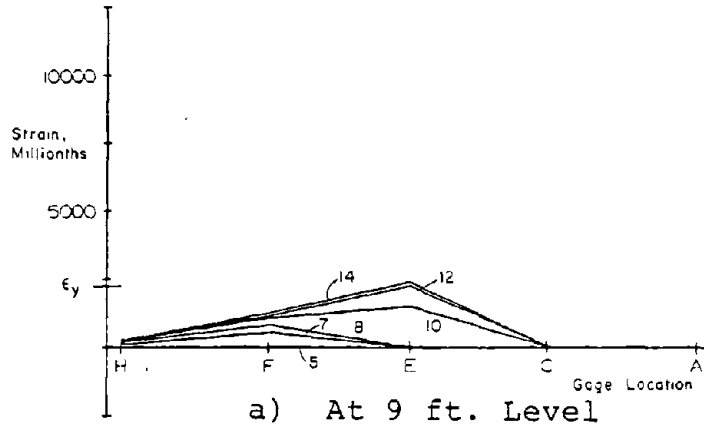
Fig. B-110   Horizontal Reinforcement Strains in Web
at Maximum Loads for Specimen B4

Specimen B2

Test Description

Specimen B2 had column boundary elements with 3.67%
vertical reinforcement in each column. Ordinary column ties
at 8 in. on center were used throughout the height of the
boundary elements.

The test consisted of 30-1/2 loading cycles as shown in
Fig. B-111. The complete load versus top deflection relation-
ship for Specimen B2 is shown in Figs. B-112 and B-113.

The first significant cracking was observed in Cycle 4
at a load of 30 kips (133.4 kN). First yielding occurred in
Cycle 13 at a load of 119.7 kips (532.4 kN). The maximum
measured crack widths at this stage were 0.005 in. (0.13 mm)
in the tension column and 0.017 in. (0.43 mm) across a
diagonal crack in the web.

The crack pattern that developed started with horizontal
cracks in the columns that progressed into diagonal shear
cracks in the web. The angle of the diagonal cracks was
steeper than those in the lighter reinforced barbell section.
Also, the diagonal cracks were not affected by cracks from
the opposite direction of loading. The diagonal cracks
crisscrossed the web forming compression strut systems for
each direction of loading. Each compression strut was
segmented by cracks from the opposite direction loading and
the specimen was completely traversed by numerous cracks.
However, the crack pattern across horizontal planes was
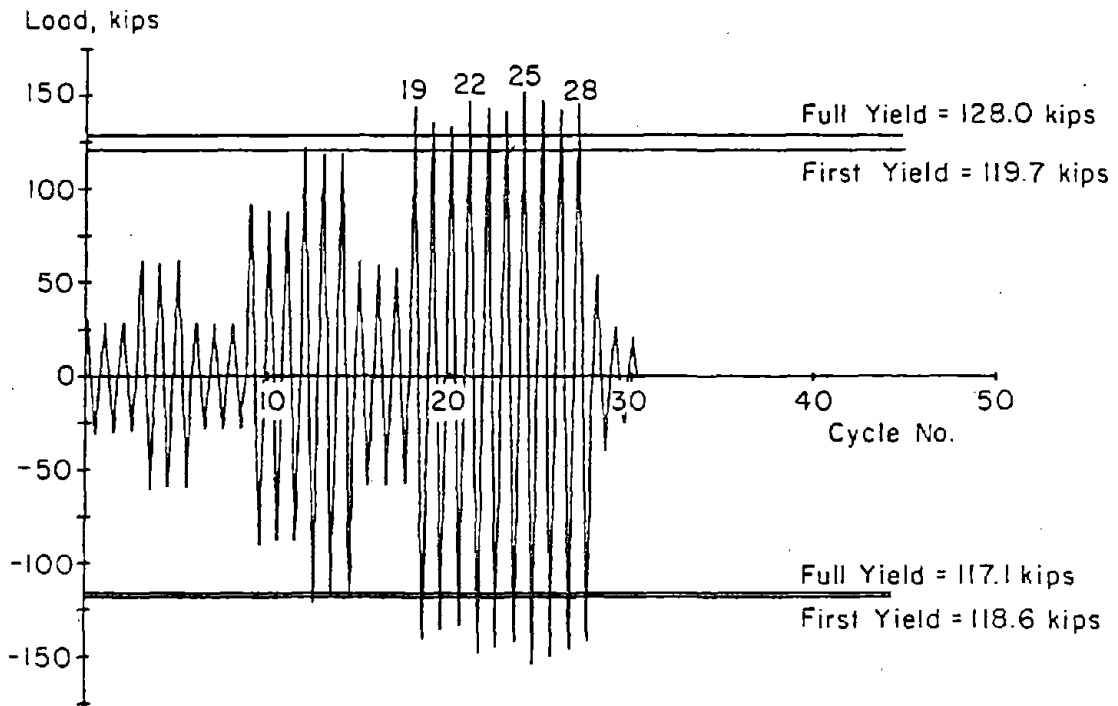
a) Load History

1 in. = 25.4 mm
1 kip = 4.448 kN
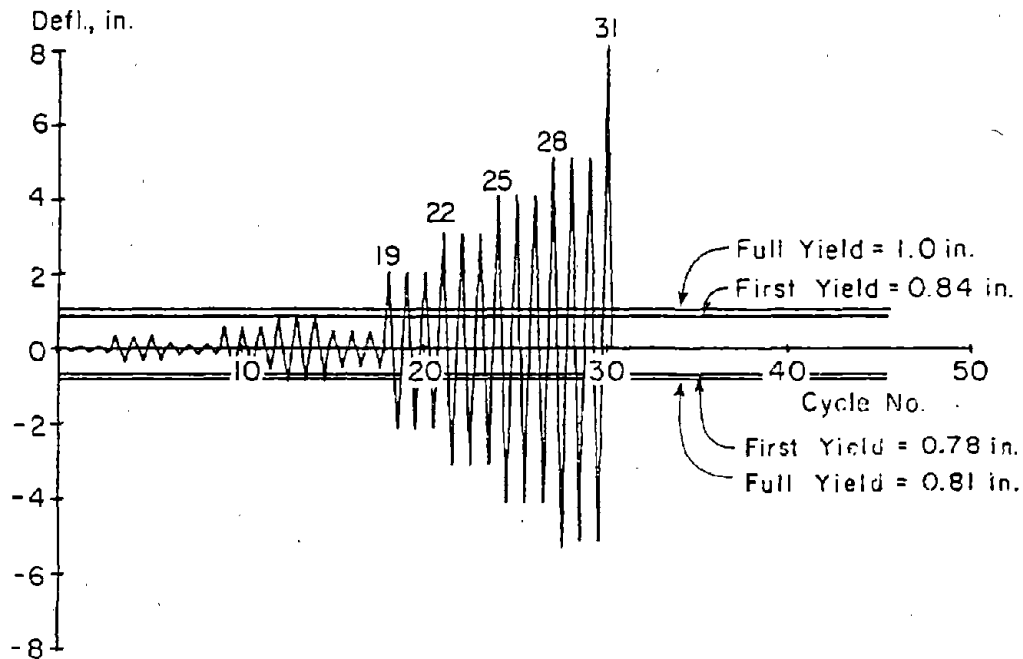
b) Deflection History

Fig. B-111 Loading History for Specimen B2

B-139
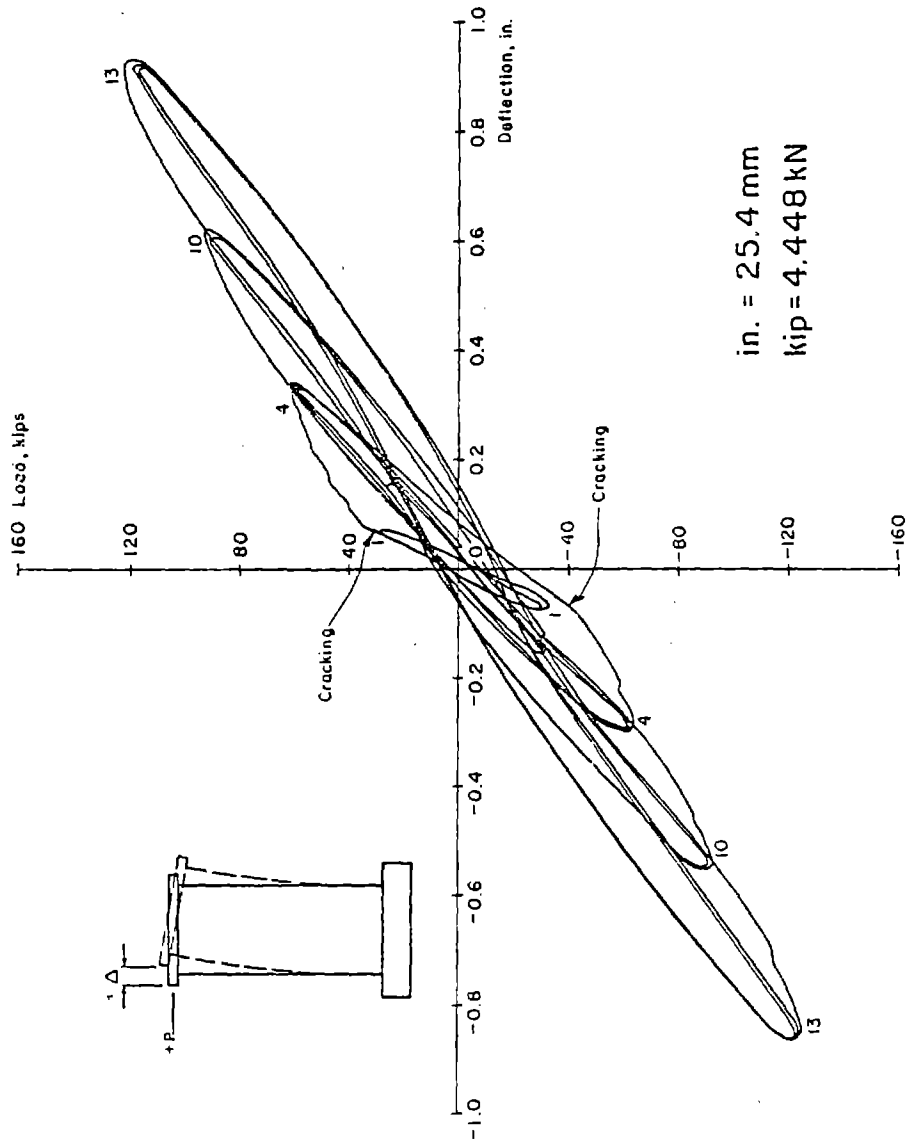
Fig. B-112 Continuous Load-Deflection Plot for
Initial Cycles for Specimen B2

in. = 25.4 mm
kip = 4.448 kN

B-140
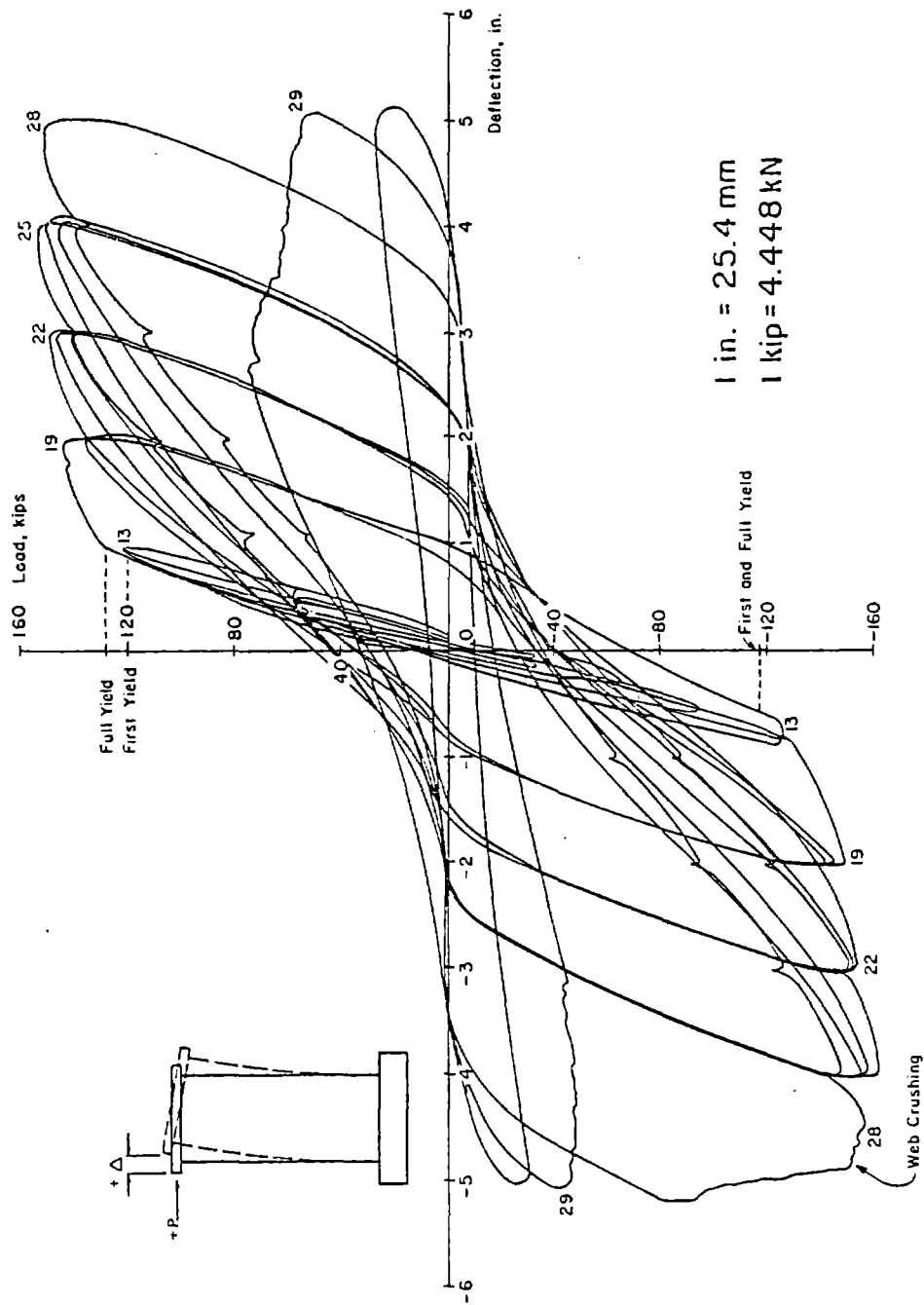
Fig. B-113 Continuous Load-Deflection Plot for Specimen B2

B-141

sawtooth shaped. The crack pattern is shown in Figs. B-114 and B-115 at +3-in. (76.2 mm) and -3-in. deflections, respectively.

First indication of spalling and flaking along the diagonal cracks was noted in Cycle 14. During Cycle 19 it was noted that the cracks in compression columns appeared to remain open approximately 0.003 in. (0.08 m). First indication of crushing concrete at the outer compression face occurred in Cycle 22.

The maximum measured load, 152.8 kips (703.7 kN), occurred in Cycle 25 at a -4-in. (101.6 mm) deflection. This load corresponded to a nominal shear stress, v_{max} = $7.2\sqrt{f_c'}$ ($0.60\sqrt{f_c'}$, MPa). Crushing at the base of the columns increased significantly and first indication of a reverse curvature in the lower 3 ft (0.91 m) of the columns was noted in Cycle 25.

During Cycle 26, two bars buckled in the lower 1 ft (0.30 m) of the compression column under positive load. In subsequent cycles, 10 more bars buckled so that the outer six bars in each column buckled. Also considerable spalling and flaking occurred in the web during Cycles 25 through 27. However, the load capacity did not decrease at this stage.

In Cycle 28, while loading the specimen to a -5-in. (127.0 mm) deflection, a sudden web failure occurred. The highest compression strut that intercepted the base of the column crushed and slipped along an existing crack at a point 2 ft 1 in. (0.63 m) above the base. The load from
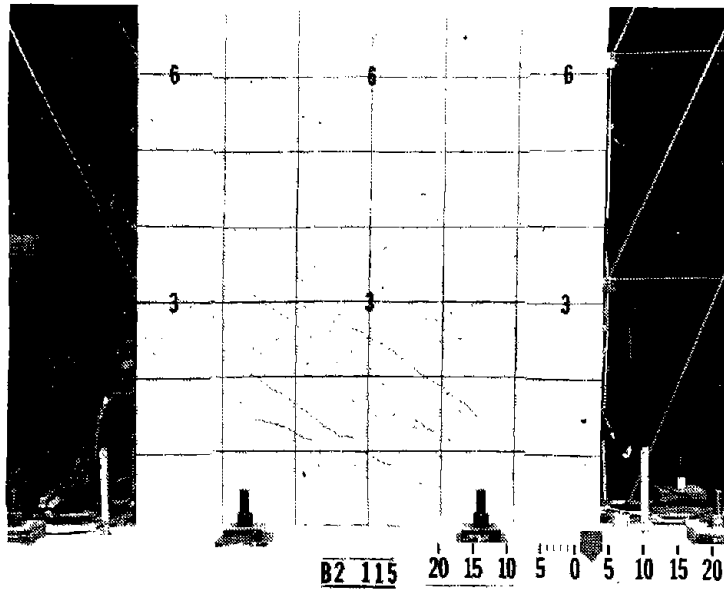
Fig. B-114   Cracking Pattern at +3 in. Deflection
            for Specimen B2
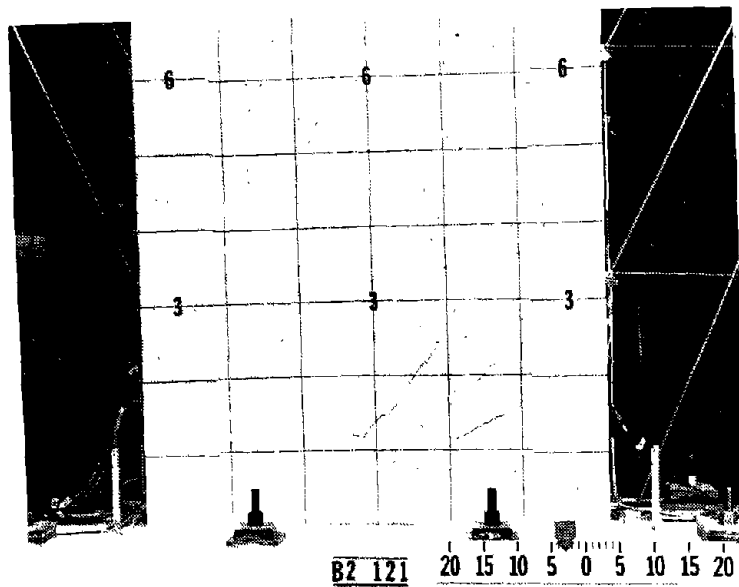
Fig. B-115   Cracking Pattern at -3 in. Deflection
            for Specimen B2

this strut was transferred to higher and lower struts. The additional load in the higher struts immediately sheared the compression column 1 ft (0.30 m) above the base. With all the load now in the lower struts, all of these struts then sheared through simultaneously along a horizontal plane 1 ft 2 in. (0.36 m) above the base. As the load capacity was dropping the specimen was "caught" by closing the deflection control valve in the hydraulic system. The measured load at this stage had decreased to 59% of the maximum measured load. Figures B-116 and B-117 show the specimen immediately prior to and after web crushing.

The specimen sustained at least 80% of the maximum measured load capacity through 9 inelastic cycles. The last inelastic loading increment in which the load was sustained at or above 80% of the maximum for all 3 cycles was at ±4 in. (101.6 mm).

Discussion of Results

Moment-Rotation. The moment-rotation data for B2 is shown in Fig. B-118. The measured maximum moment was 89% of the calculated monotonic maximum.

The relationship between the calculated monotonic and measured rotations at the 3-ft (0.91 m) level differed slightly from that relationship at the 6-ft (1.83 m) level. The difference indicates that the actual curvature had a larger portion concentrated in the lower 3 ft of wall than assumed.
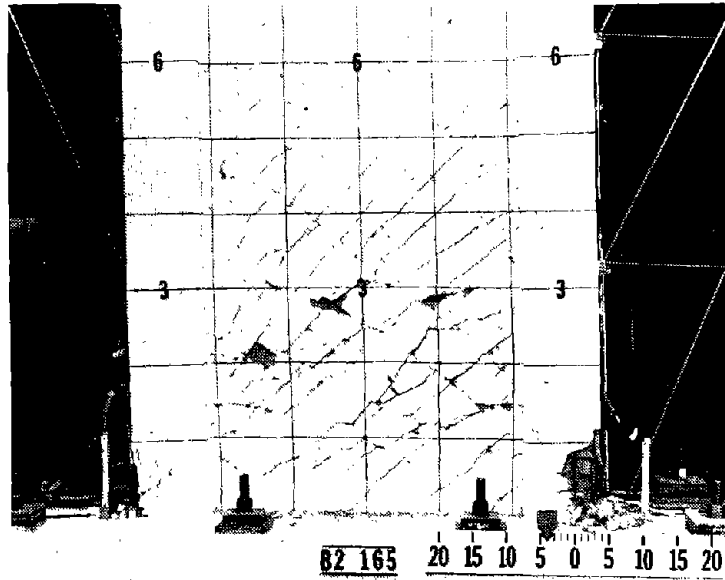
Fig. B-116   Specimen B2 Prior to Web Crushing
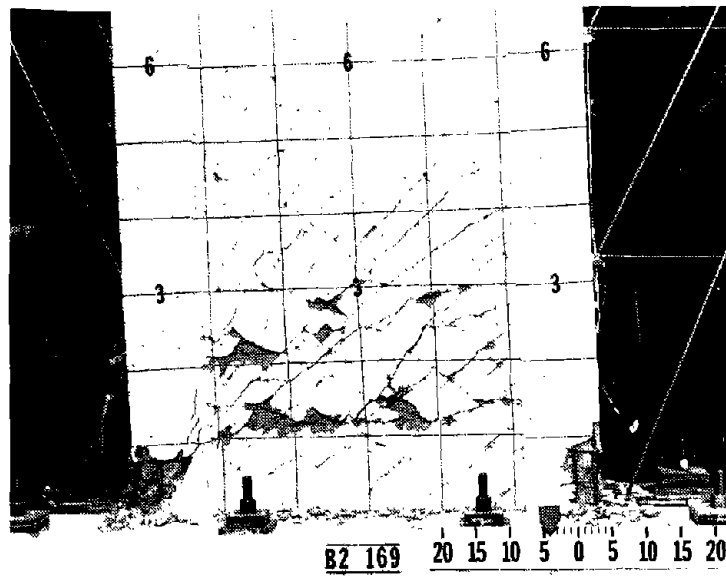
Fig. B-117   Specimen B2 After Web Crushing

B-145
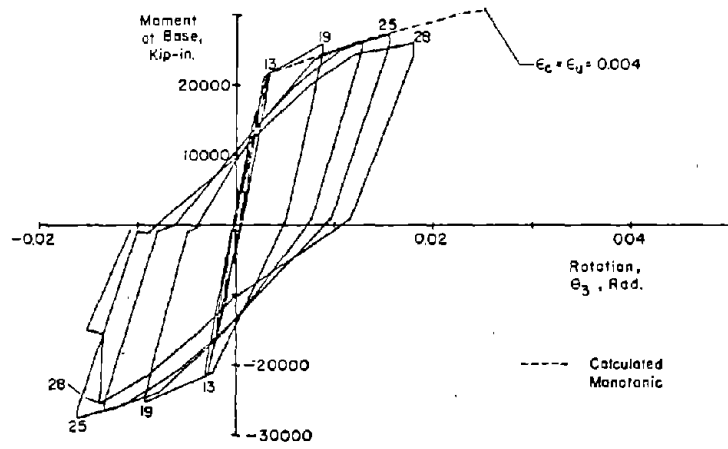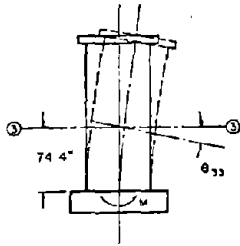
a) At 6 ft. Level
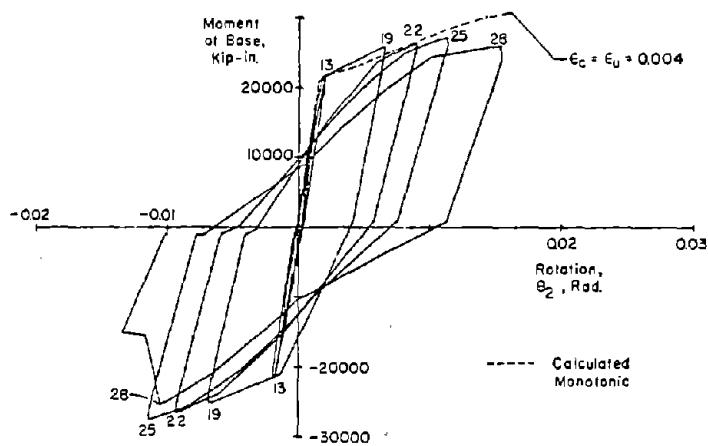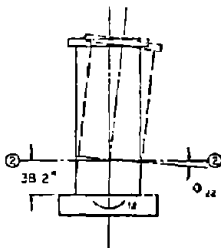
b) At 3 ft. Level
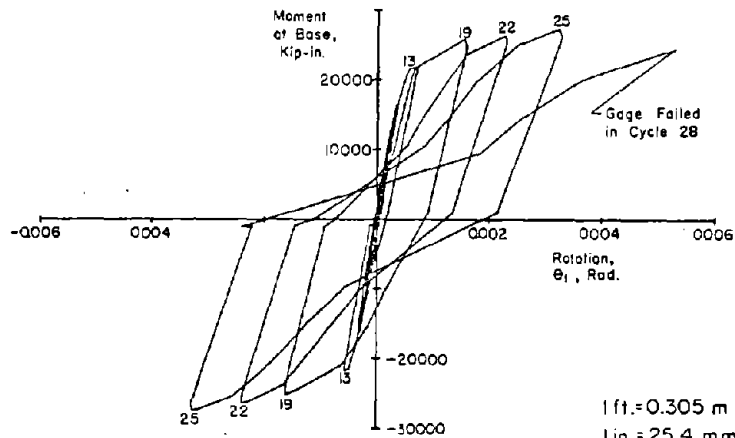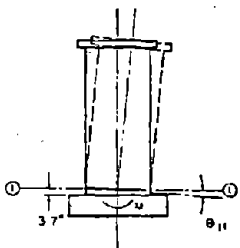
c) At Base Level

1 ft.=0.305 m
1 in.= 25.4 mm
1 kip= 4.448 kN

Fig. B-118   Moment at Base versus Rotation
             for Specimen B2

The measured rotation at the 3 and 6-ft (0.91 and 1.83 m) levels in B2 was approximately 75% of the measured rotation in B1 during the 4-in. (101.6 m) top deflection increment.

The maximum measured loads in each new increment exhibit "strain hardening" as the rotations increase.

The rotation loops at the base level exhibited considerable pinching after Cycle 19. Pinching is not evident in the other two levels until cycle 28.

Shear-Distortion. The shear-distortion loops for B2 are shown in Fig. B-119. As in the other specimens, shear "yielding" occurred during the same cycle in which flexural yielding occurred.

It should be noted that while the maximum load corresponded to a shear stress of $7.2\sqrt{f_c'}$ ($0.60\sqrt{f_c'}$, MPa), the design shear stress was $6.0\sqrt{f_c'}$ ($0.50\sqrt{f_c'}$, MPa). This design allowed $2\sqrt{f_c'}$ ($0.17\sqrt{f_c'}$, MPa) in the concrete with the steel taking $4.0\sqrt{f_c'}$ ($0.33\sqrt{f_c'}$, MPa) at 60 ksi. Even assuming the horizontal steel at an ultimate stress of 100 ksi, the steel shear capacity would only have been $6.7\sqrt{f_c'}$ ($0.04\sqrt{f_c'}$, MPa). This indicated that the concrete contribution must have been at least $0.5\sqrt{f_c'}$ ($0.04\sqrt{f_c'}$, MPa) shear stress at maximum load.

Pinching in the loops was more evident in Zone 1. The new maximum shear distortions in each new increment became larger at an increasing rate. The magnitude of distortions in Zone 1 and 2 were approximately equal and the plots are relatively symmetrical.
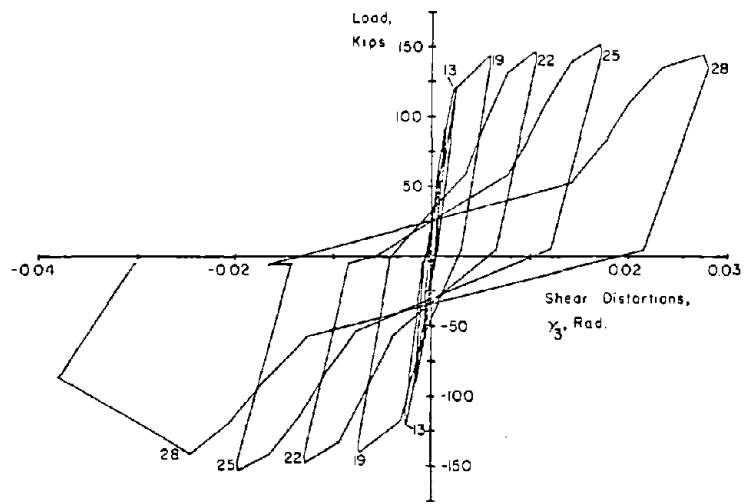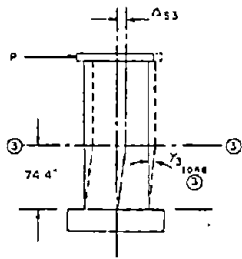
a) In Base to 6 ft Level
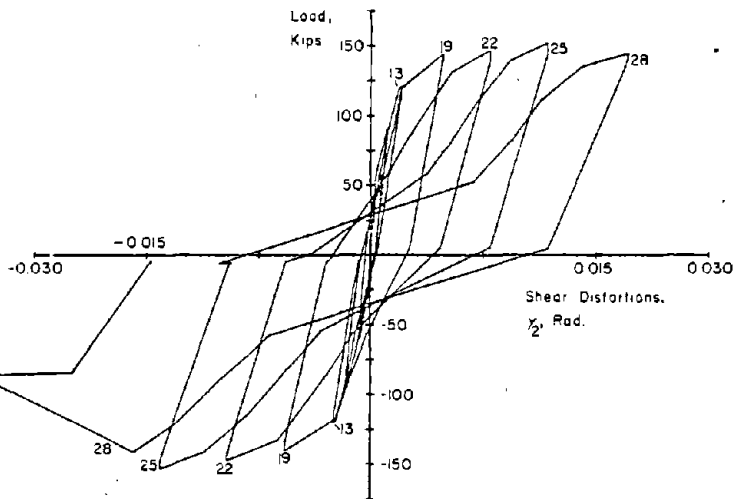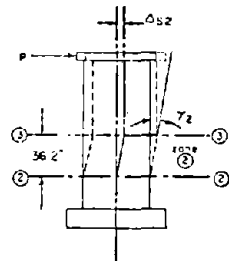
b) In 3 ft to 6 ft Level
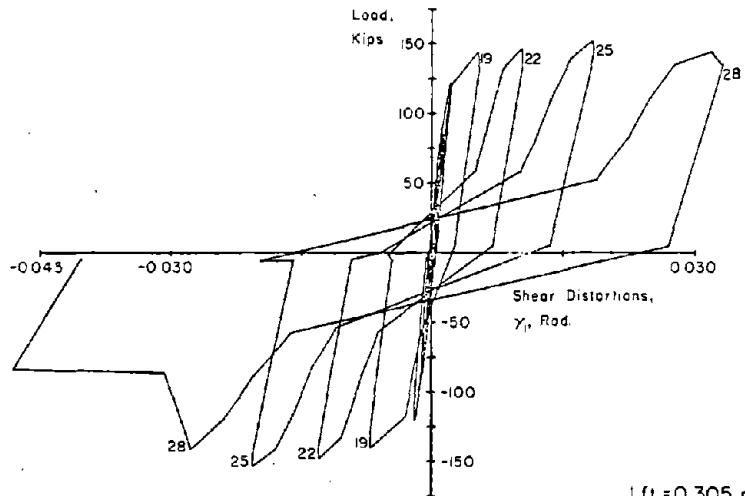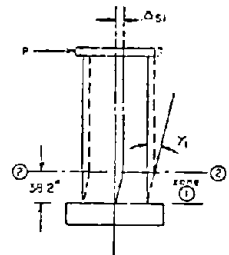
c) In Base to 3 ft Level

1 ft.=0.305 m
1 in.= 25.4 mm
1 kip= 4.448 kN

Fig. B-119   Load versus Shear Distortion
for Specimen B2

Slip at Construction Joints. The slip at construction joints in B2 is shown in Fig. B-120. The slip at CJ1 exhibited "yielding" similar to shear "yielding" during the same cycle in which flexural yielding occurred. As shown in Fig. B-121, the slip in CJ1 was a relatively constant 15% to 20% of the total shear deflection in the lower 3 ft (0.91 m).

The slip plots for CJ2 and CJ3 are unsymmetrical and the measured slip was probably affected by diagonal cracking.

Deflections. The deflection components and deflected shapes are shown in Figs. B-122 and B-123. These figures show that shear deflections were a larger percentage of the total than they were in the previously described specimens with low nominal shear stress.

The deflected shapes for Cycles 22 and 24 show an average 20% increase in shear deflection at the top of the wall within the 3-in. (76.2 mm) increment.

Reinforcement Strains. Figures B-124 through B-132 show reinforcement strains in the specimen at various stages.

Figure B-124 shows that the specimen started to grow after Cycle 19. Figure B-125 shows that yielding of the vertical bars occurred up to the 9-ft (2.74 m) level in Cycle 28. Figure B-126 shows the reversed strain gradient in the compression column in Cycle 28.

Figures B-128 through B-132 show the strain gradients in the horizontal bars. Although the figures show considerable yielding up to the 9-ft (2.74 m) level, the plots
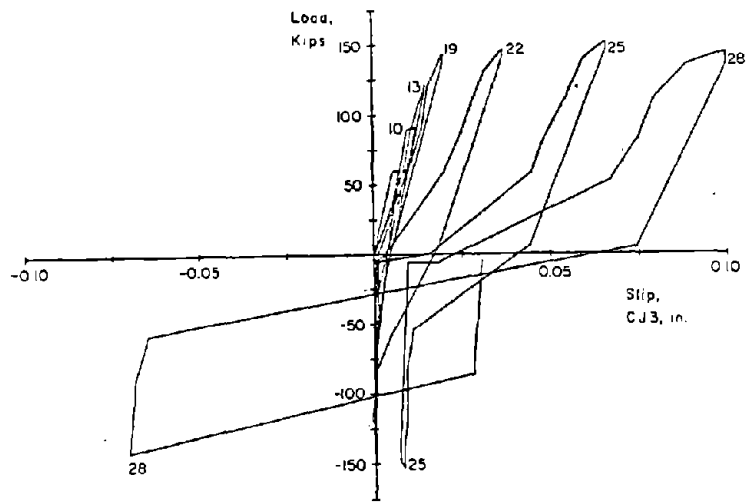
a) At 6 ft. Level
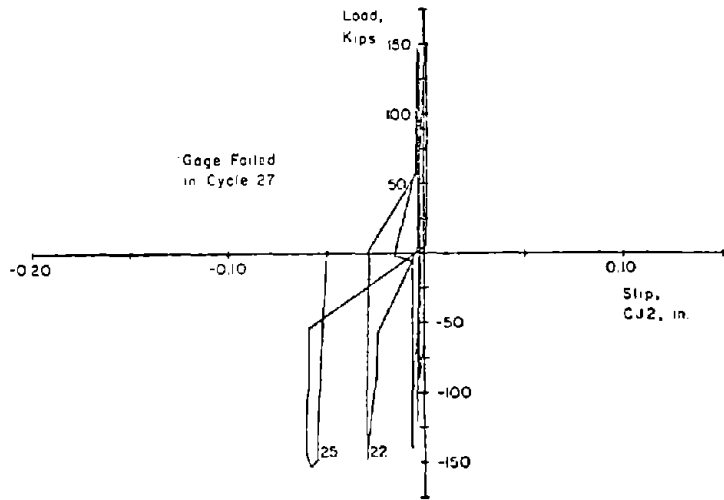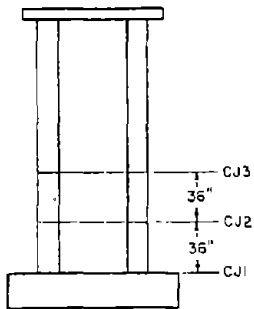
b) At 3 ft. Level
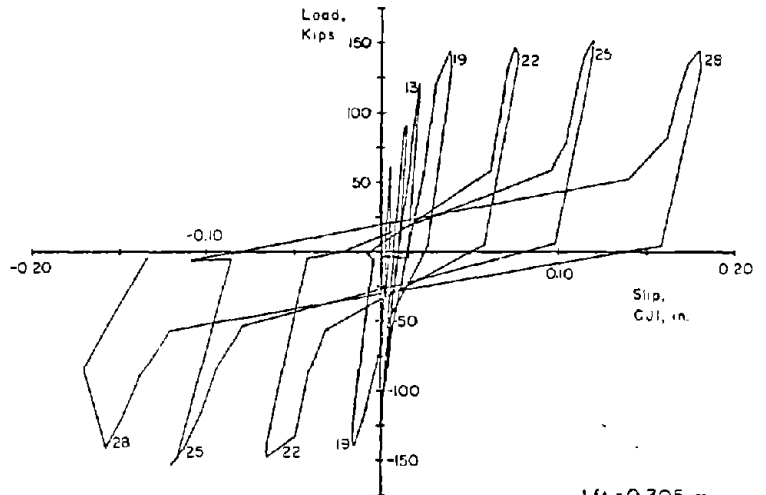
c) At Base Level

1 ft.=0.305 m
1 in.=25.4 mm
1 kip=4.448 kN

Fig. B-120   Load versus Slip at Construction Joints
for Specimen B2
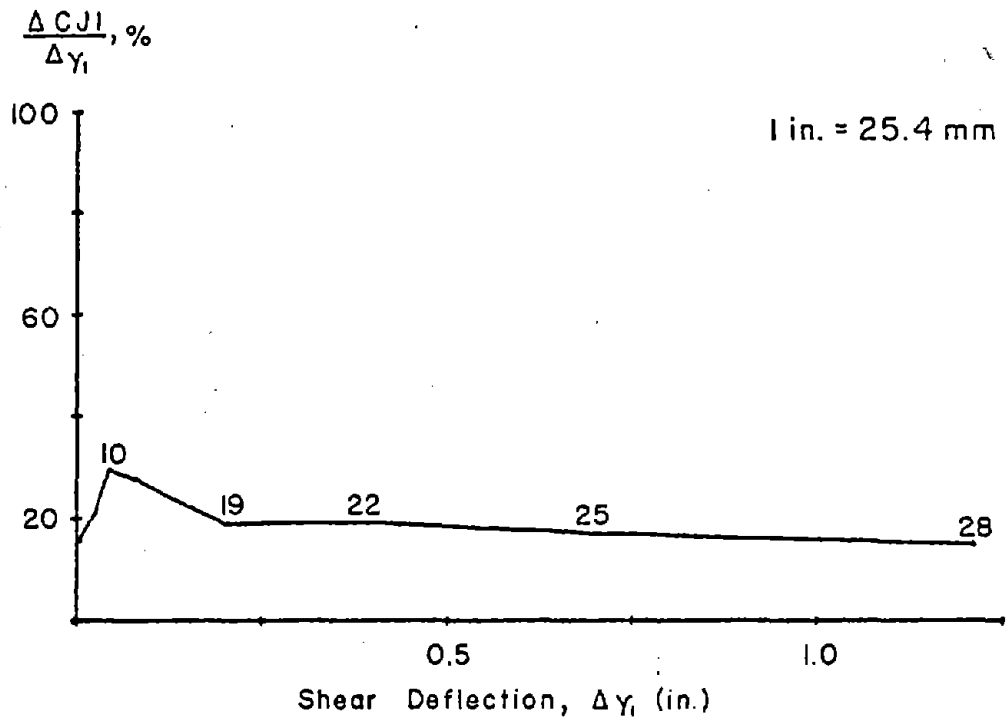
a) At Maximum Positive Load
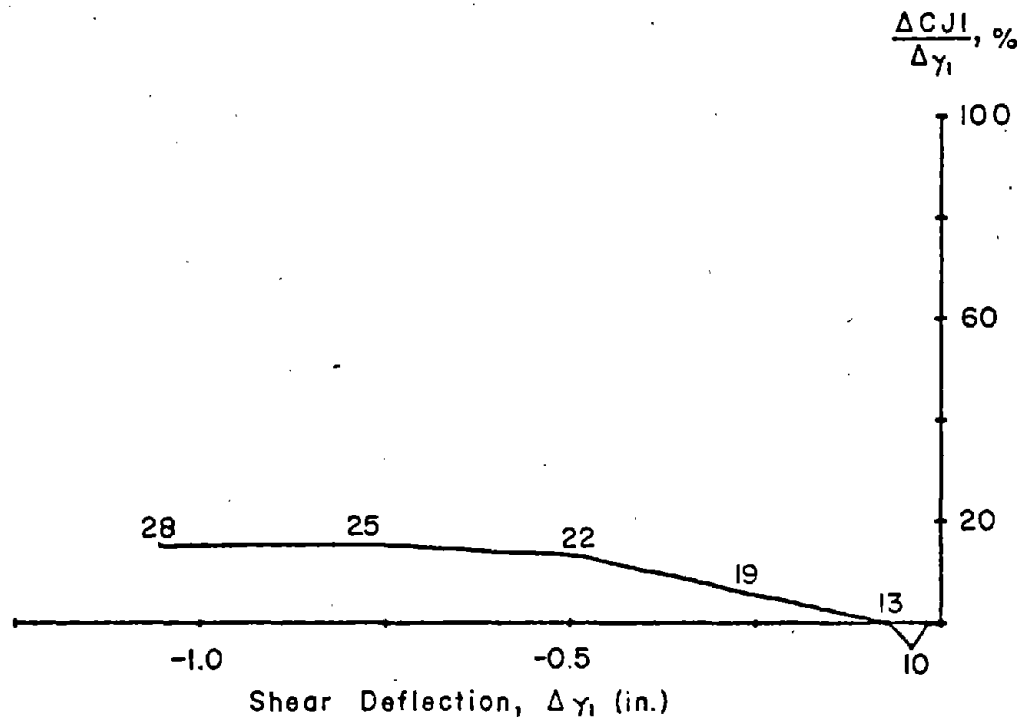
b) At Maximum Negative Load

Fig. B-121   Slip at Base Construction Join versus
             Shear Deflection in Zone 1 for Specimen B2

a) At Top of Wall
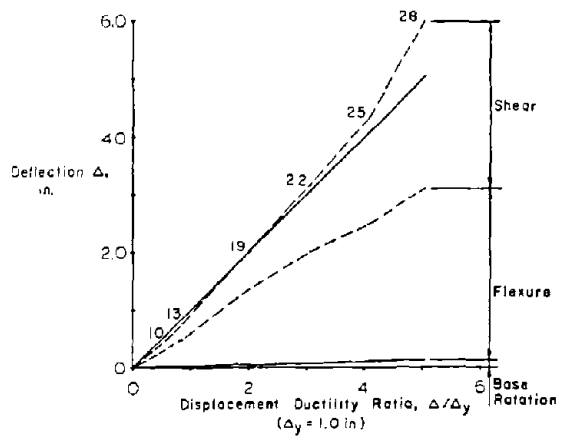
b) At 6 ft. Level
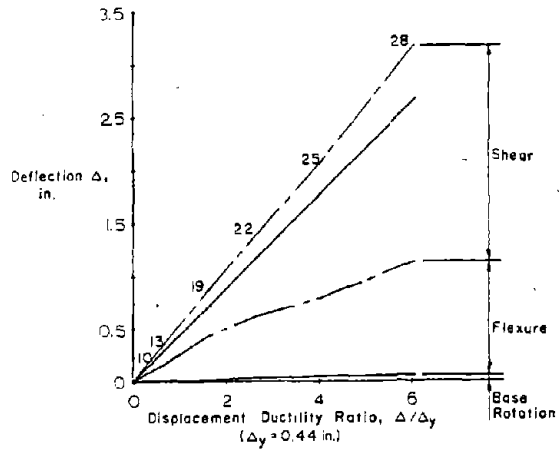
c) At 3 ft. Level
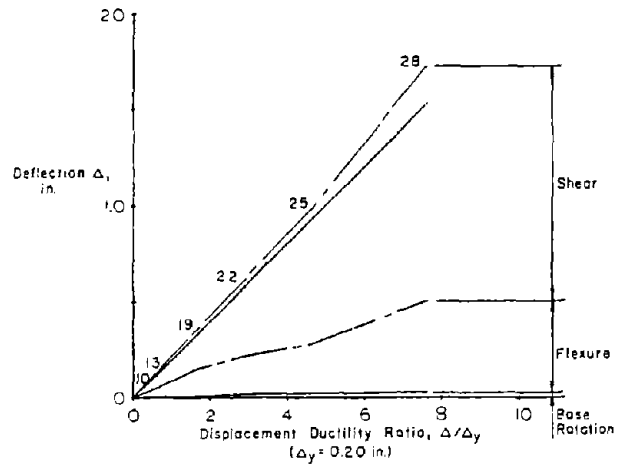
Fig. B-122   Component of Deflection for Specimen B2

a)   Flexural
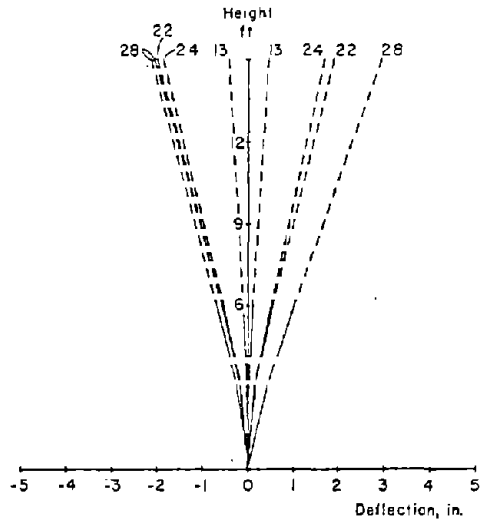
b)   Shear
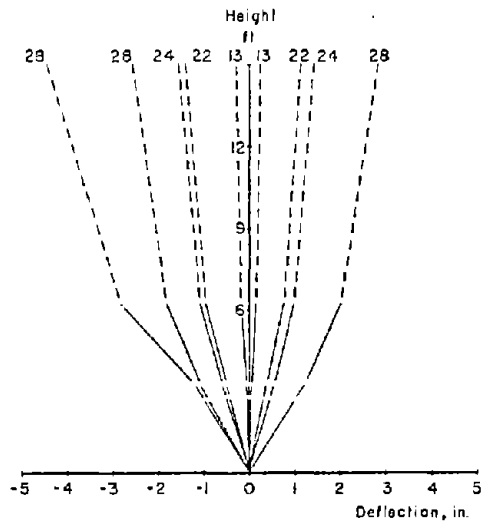
- - —   CALCULATED   FROM
          MEASURED   DEFORMATION
- - - -   EXTRAPOLATED
———   MEASURED   TOTAL

1 in.= 25.4 mm
1 ft.= 0.305 m

W.C. — WEB   CRUSHING

AFTER   W. C.

PRIOR   TO   W.C.

c)   Total
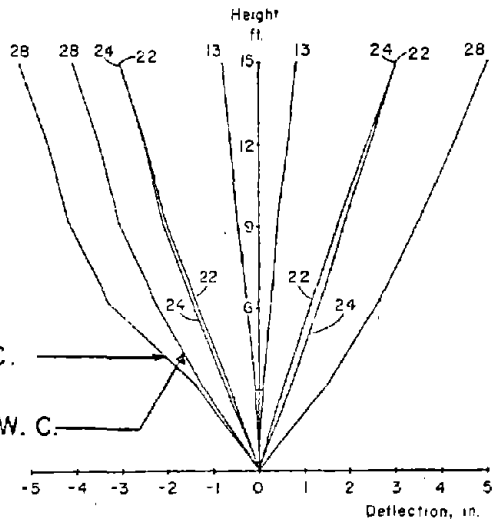
Fig. B-123   Deflected Shape for Specimen B2
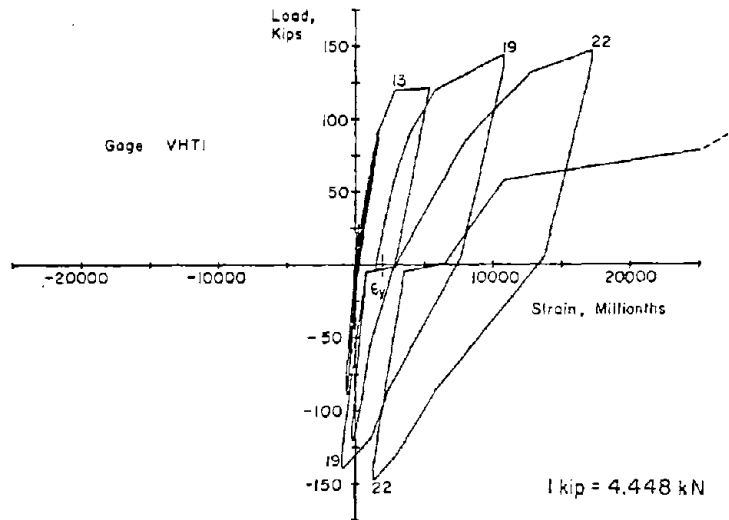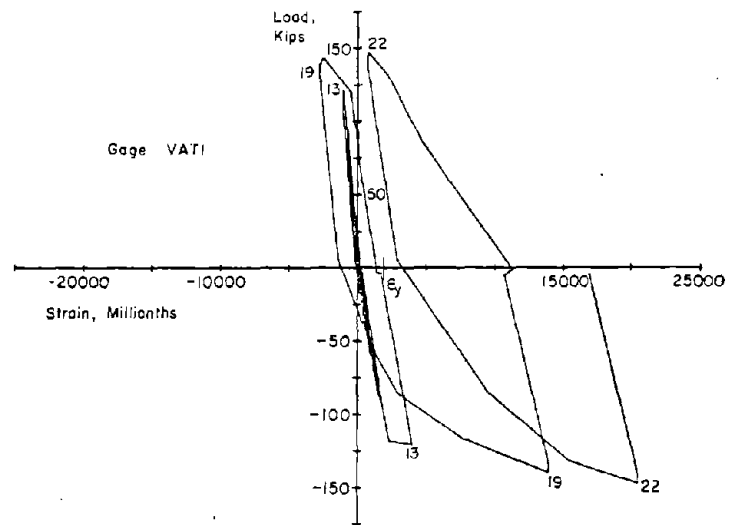
Fig. B-124 Measured Strains on Vertical Reinforcement at Base of Specimen B2
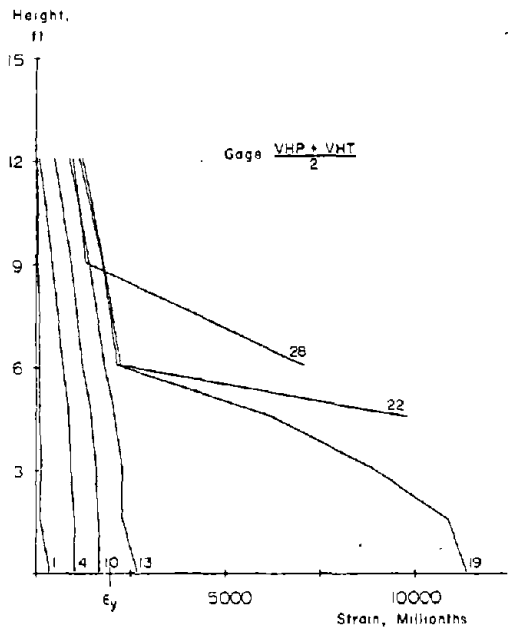
a) Average of VHP & VAT
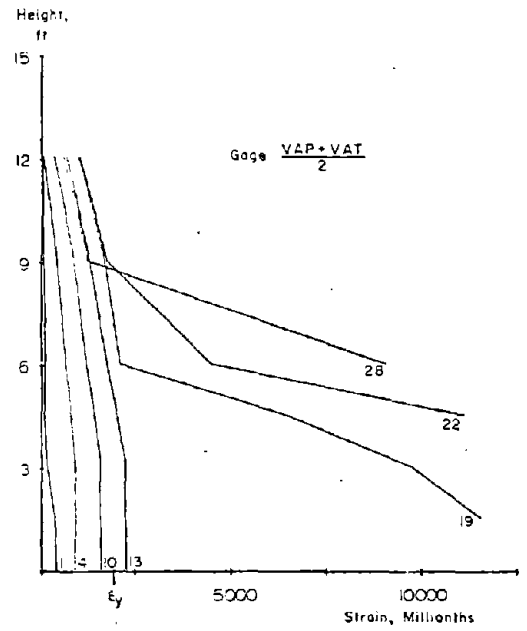
b) Average of VAP & VAT
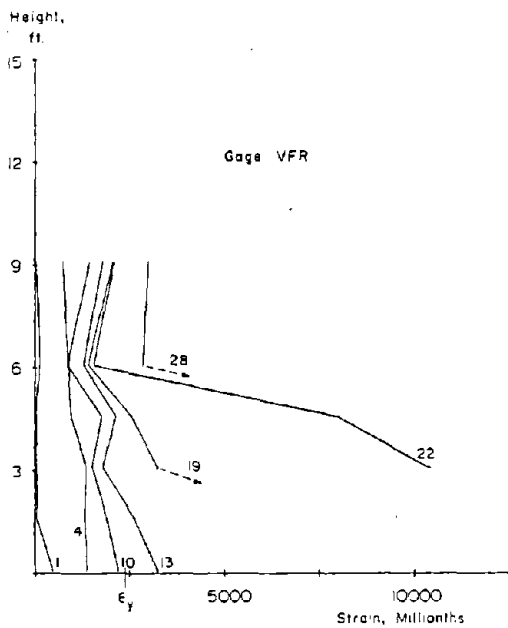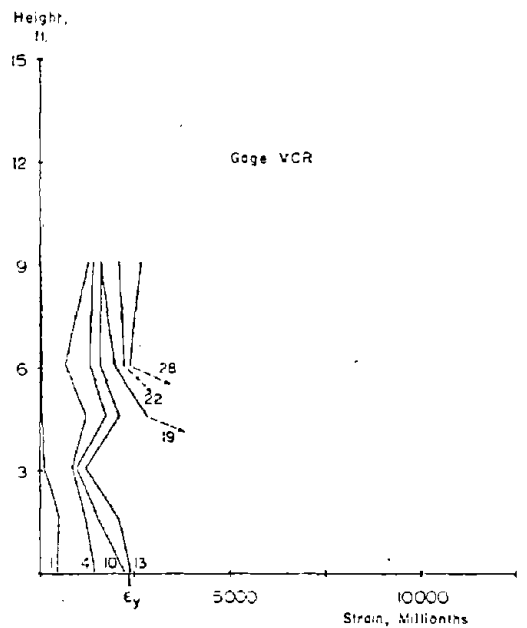
c) Strain Gage VFR

d) Strain Gage VCR

Fig. B-125   Vertical Reinforcement Strains at
Maximum Loads for Specimen B2

a) At 6 ft. Level

b) At 3 ft. Level

c) At Base Level
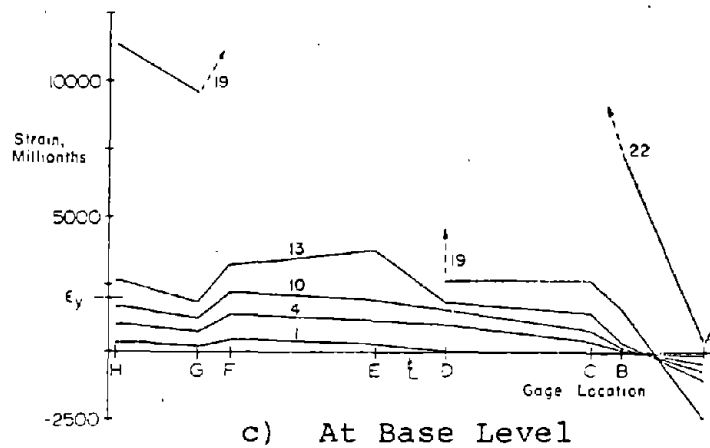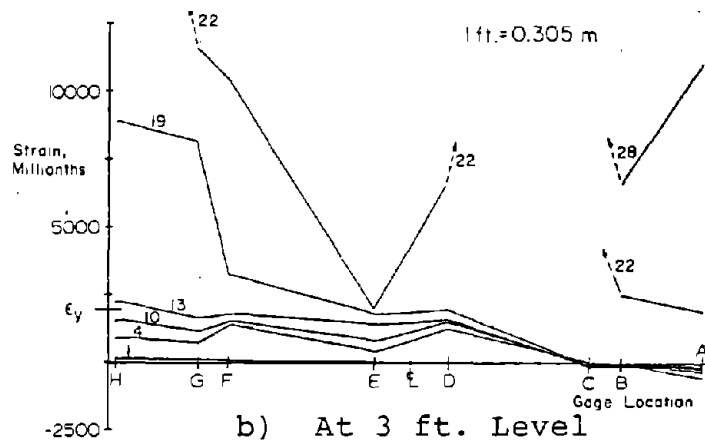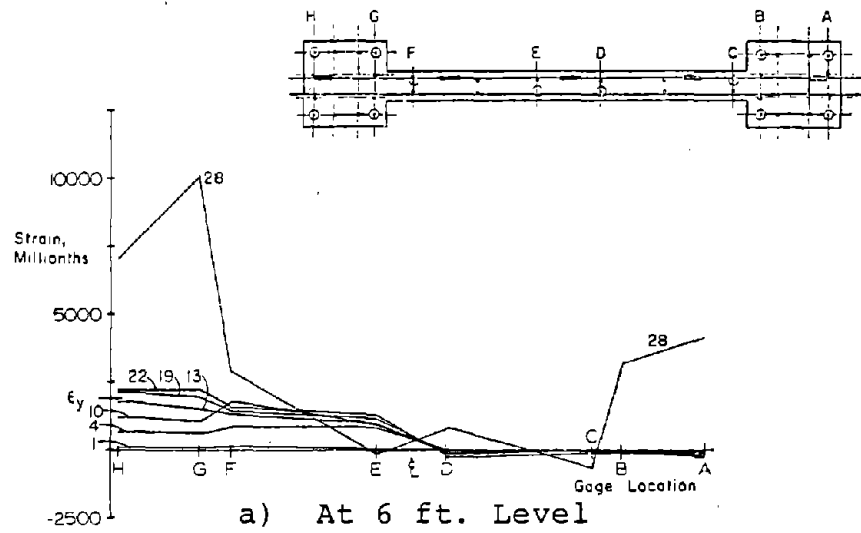
Fig. B-126 Vertical Reinforcement Strains at
Maximum Positive Loads for Specimen B2
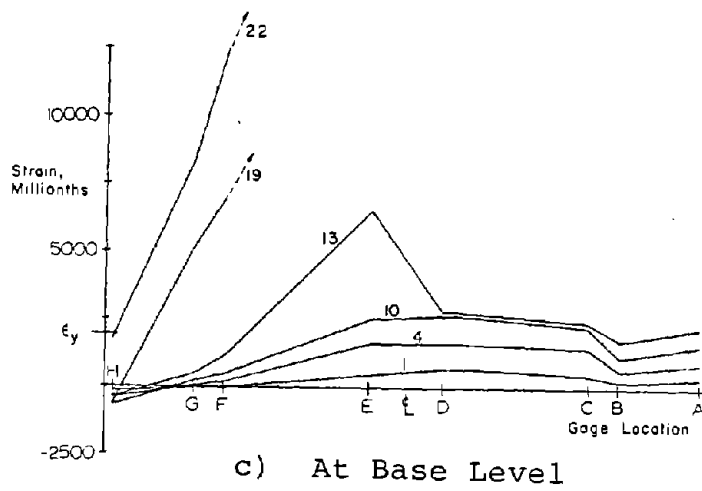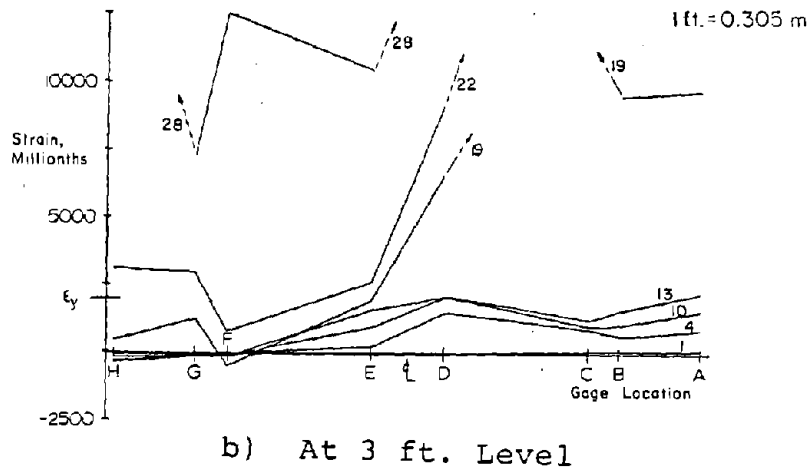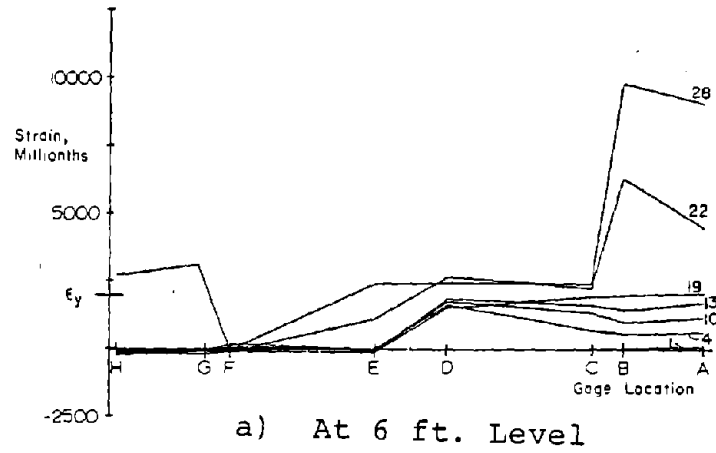
Fig. B-127   Vertical Reinforcement Strains at
Maximum Negative Loads for Specimen B2
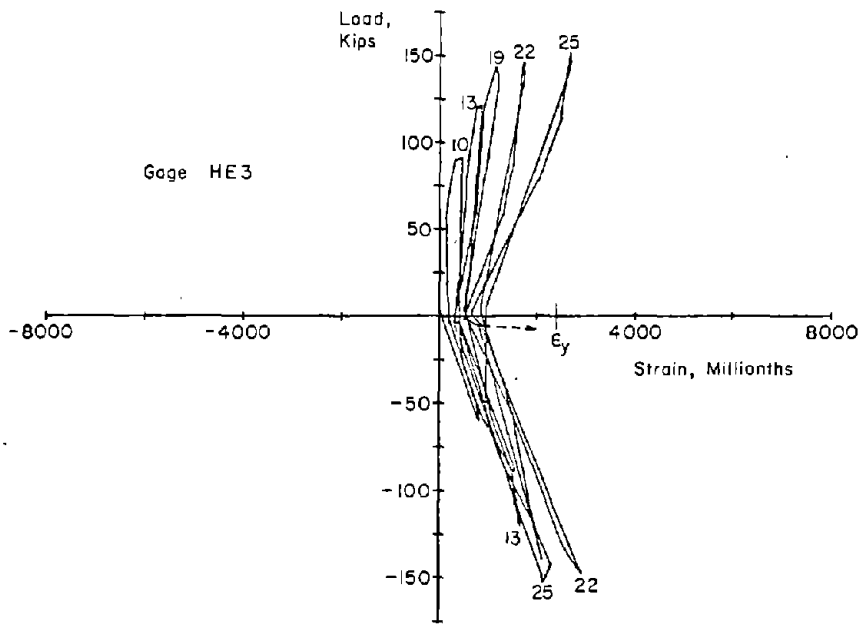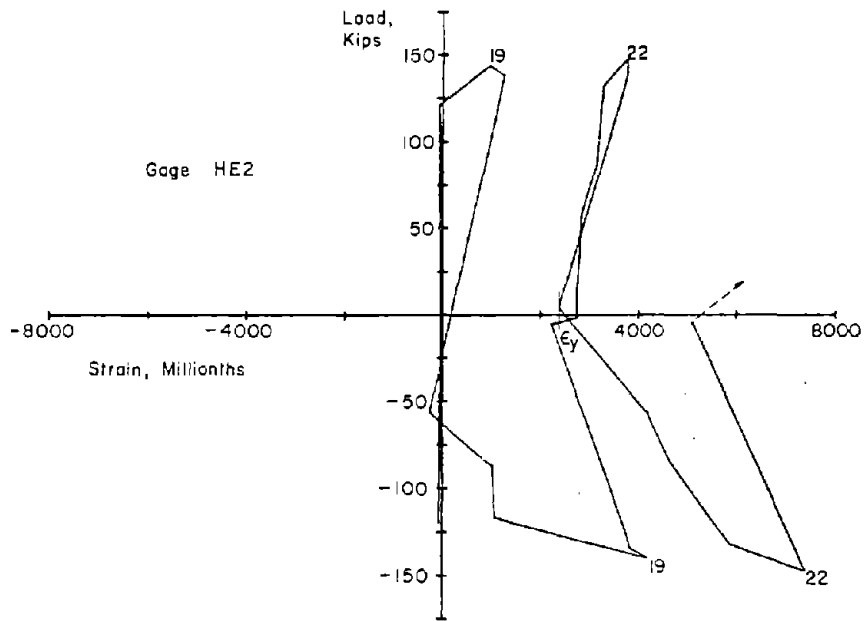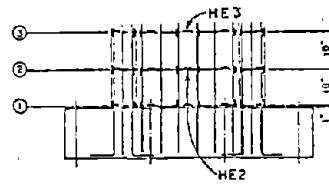
Fig. B-128   Measured Strains on Horizontal Reinforcement
for Specimen B2
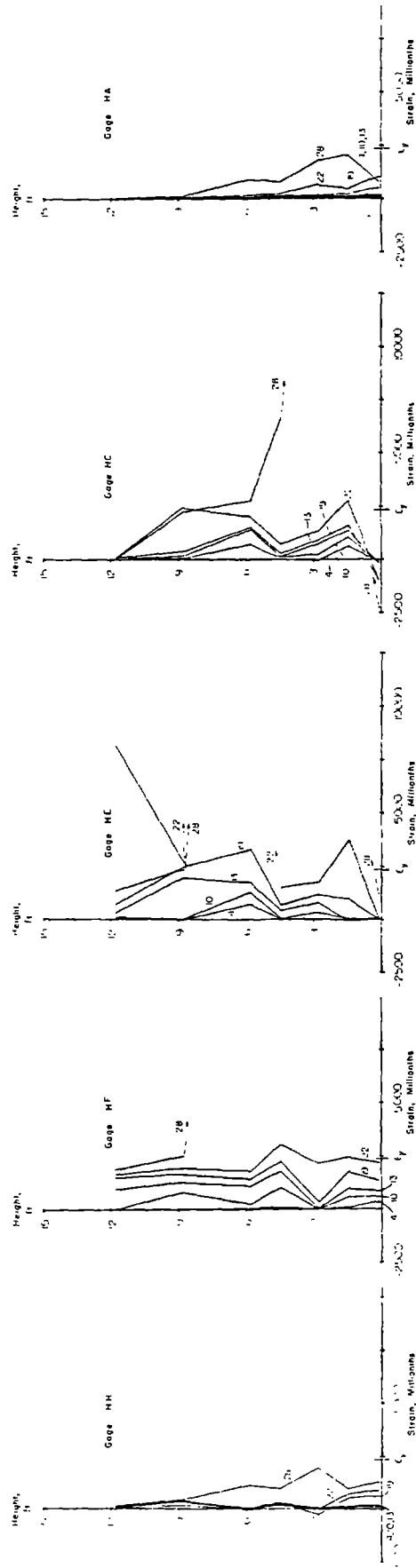
Fig. B-129 Horizontal Reinforcement Strains at
Maximum Positive Loads for Specimen B2
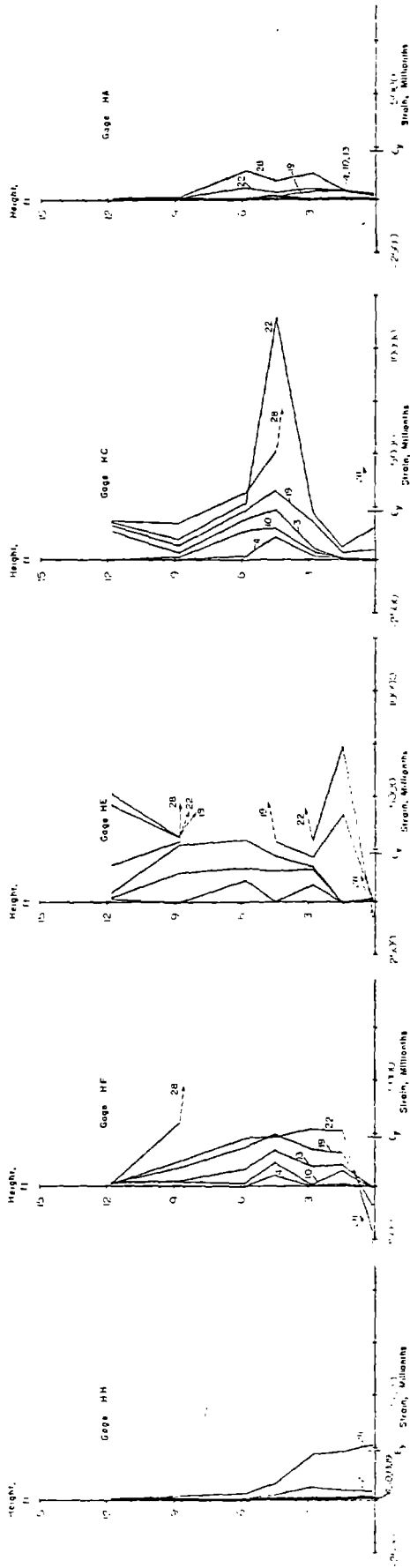
Fig. B-130 Horizontal Reinforcement Strains at
Maximum Negative Loads for Specimen B2

a) At 9 ft. Level

b) At 6 ft. Level

1 ft.=0.305 m

c) At 3 ft. Level
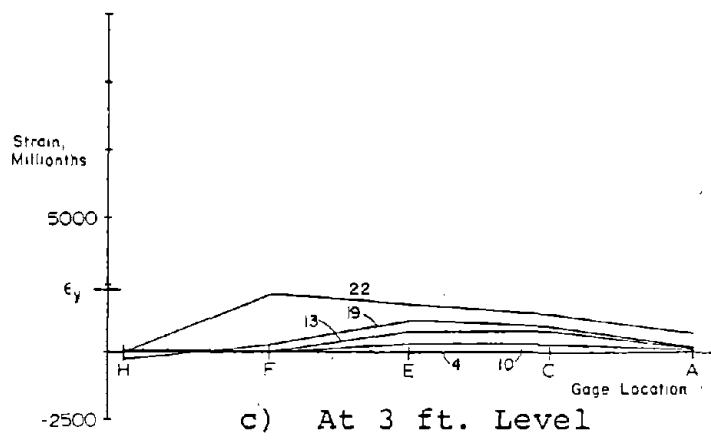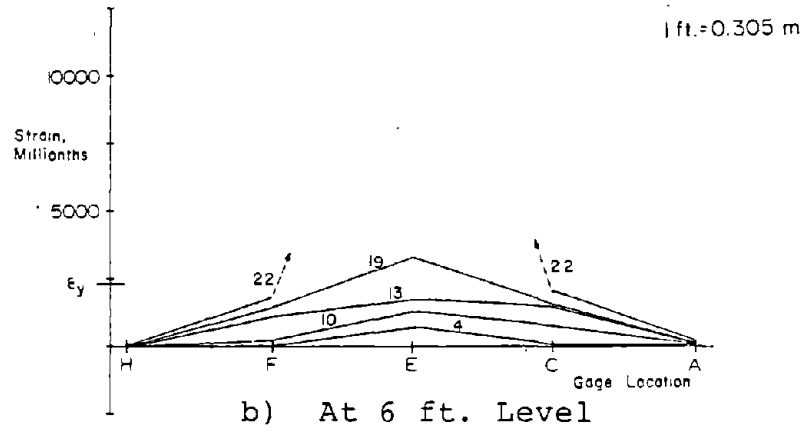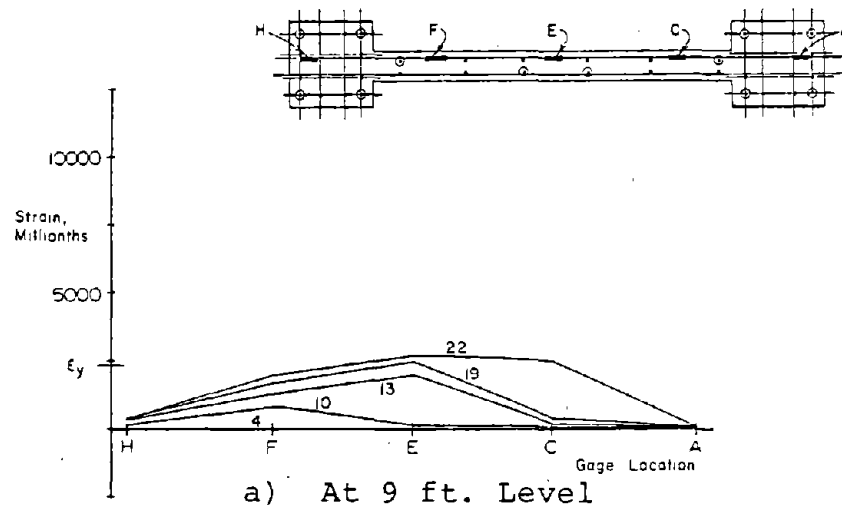
Fig. B-131   Horizontal Reinforcement Strains in Web
at Maximum Positive Loads for Specimen B2

a) At 9 ft. Level

1 ft.=0.305 m

b) At 6 ft. Level

c) At 3 ft. Level
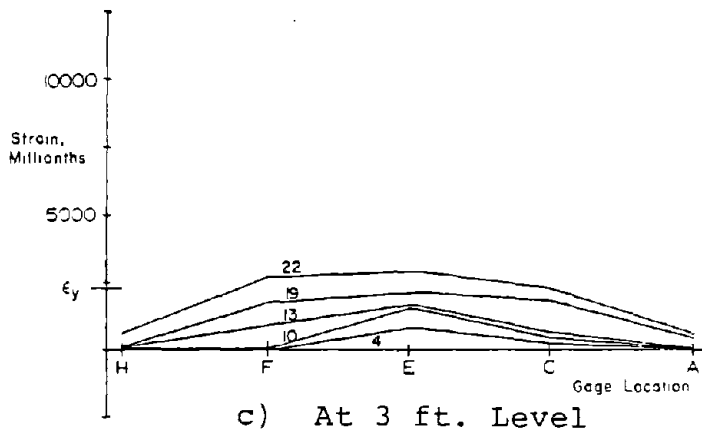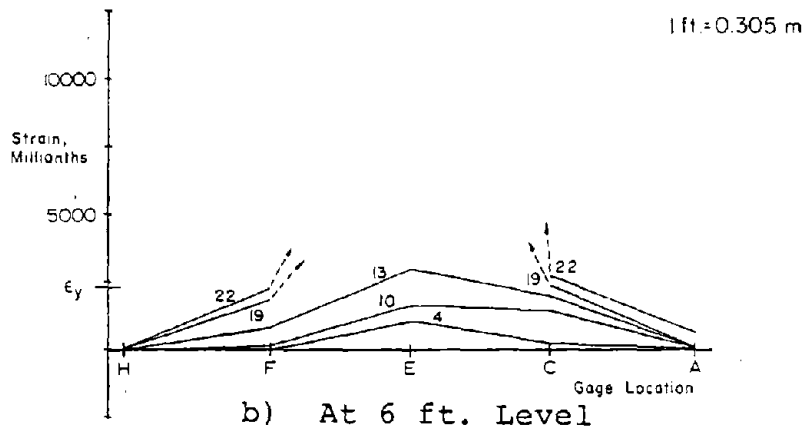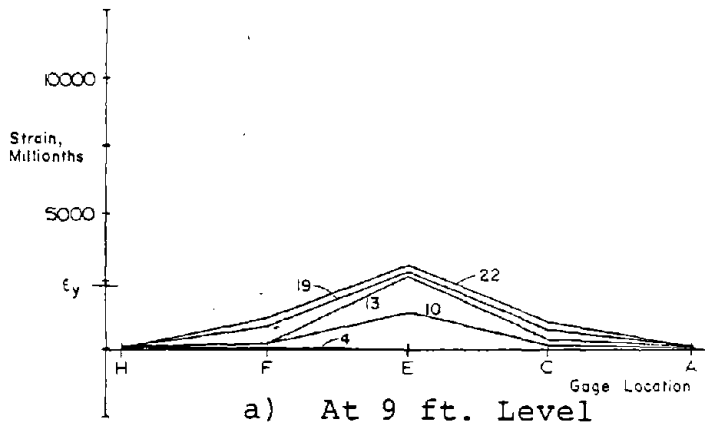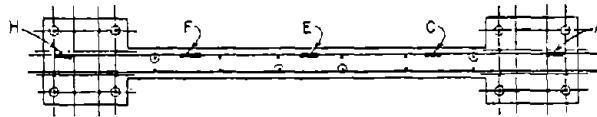
Fig. B-132   Horizontal Reinforcement Strains in Web
at Maximum Negative Loads for Specimen B2

are not significantly different from the equivalent plots

for previously described specimens with low nominal shear

stress.

Specimen B5

Test Description

Specimen B5 was similar to Specimen B2 with 3.67% vertical reinforcement in each column. However, B5 had confinement reinforcement in the lower 6 ft (1.83 m) of the boundary columns.

The test consisted of 30 loading cycles as shown in Fig. B-133. The complete load versus top deflection relationship for Specimen B5 is shown in Figs. B-134 and B-135.

The first significant cracking was observed in cycle 4 at a load of 30 kips (133.4 kN). First yielding occurred in Cycle 13 at a load of 112.3 kips (449.5 kN). The maximum measured crack widths at this stage were 0.007 in. (0.18 mm) in the tension column and 0.025 in. (0.64 mm) across a diagonal crack in the web.

The crack pattern that developed was very similar to the crack pattern in B2. The crack pattern at +3-in. (76.2 mm) and -3-in. deflection is shown in Figs. B-136 and B-137.

The behavior of Specimen B5 differed from the behavior of B2 after the first yield cycles in that the measured load in Specimen B5 was significantly higher than the load in B2 for equal top deflections. This difference can be attributed to the flexural steel yield stresses. The yield stress was 59.5 ksi in B2 and 64.4 ksi in B5.

First indication of spalling and flaking along diagonal cracks occurred in Cycle 16. First indication of crushing
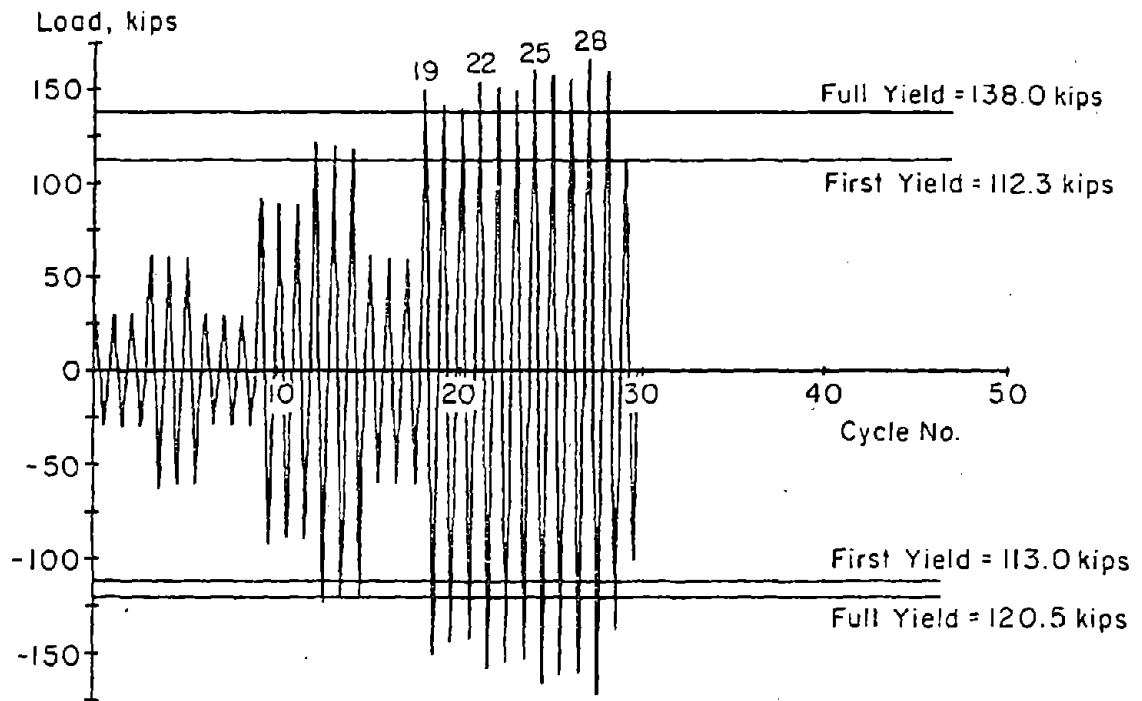
a) Load History

1 in. = 25.4 mm
1 kip = 4.448 kN
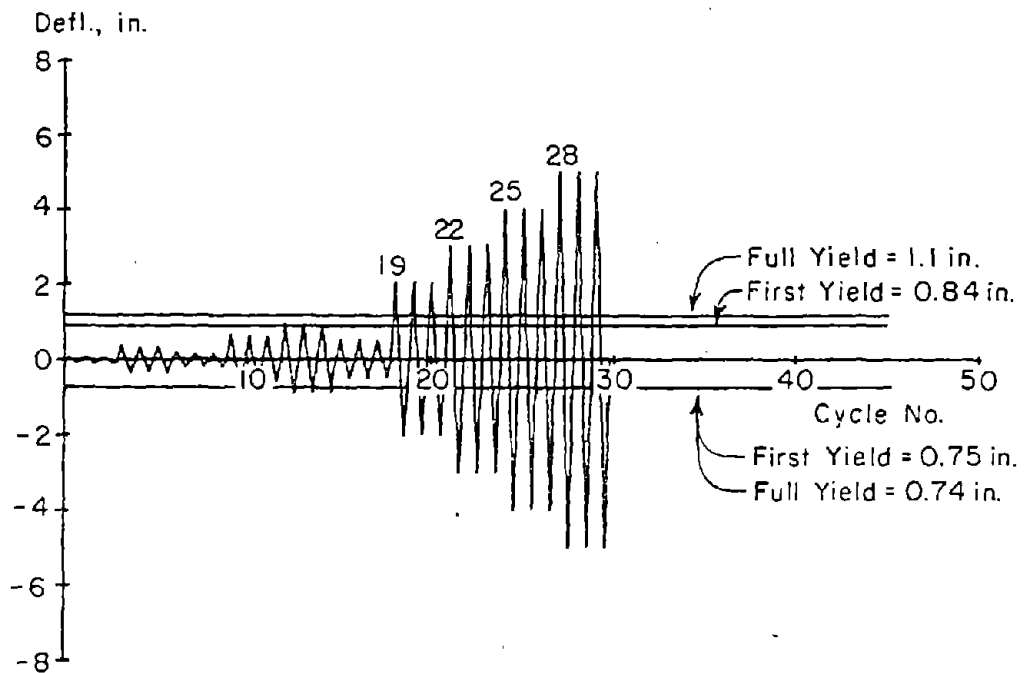
b) Deflection History

Fig. B-133 Loading History for Specimen B5
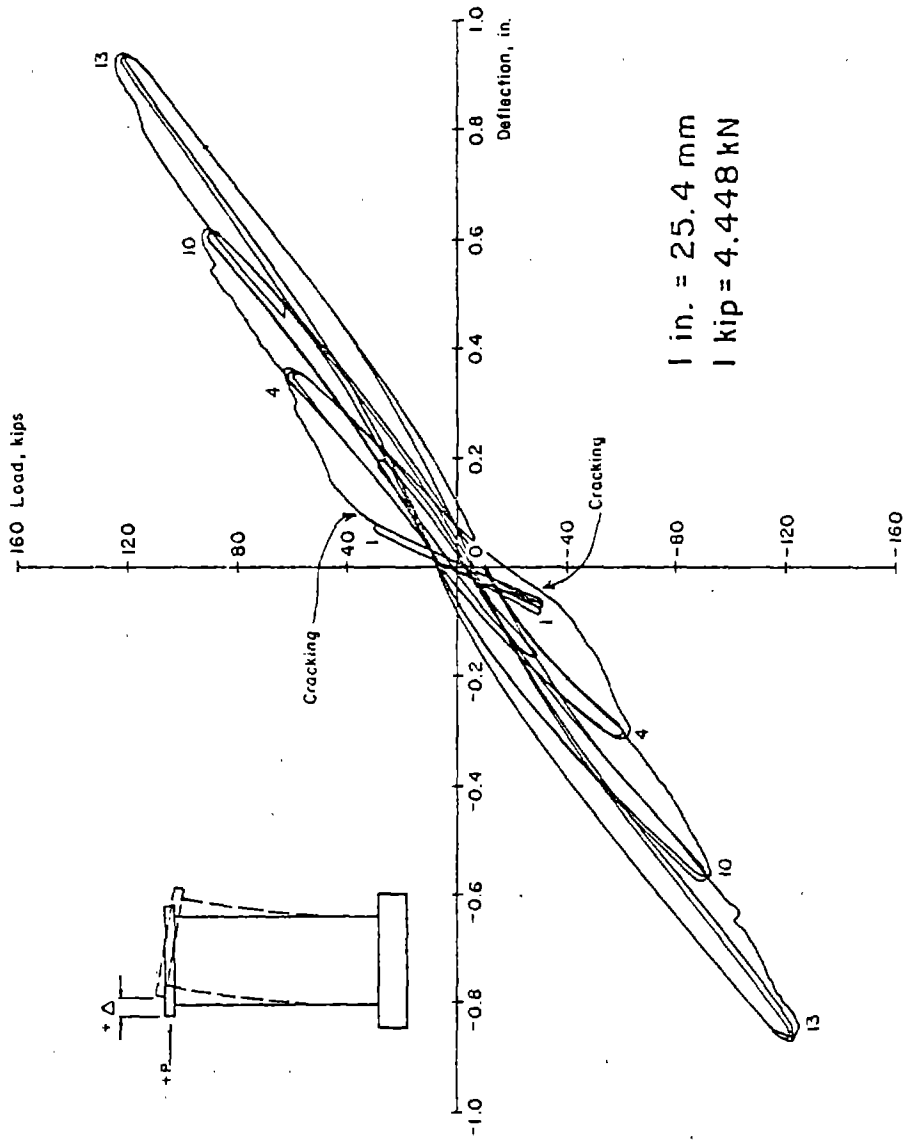
Fig. B-134   Continuous Load-Deflection Plot for Initial Cycles for Specimen B5

1 in. = 25.4 mm
1 kip = 4.448 kN
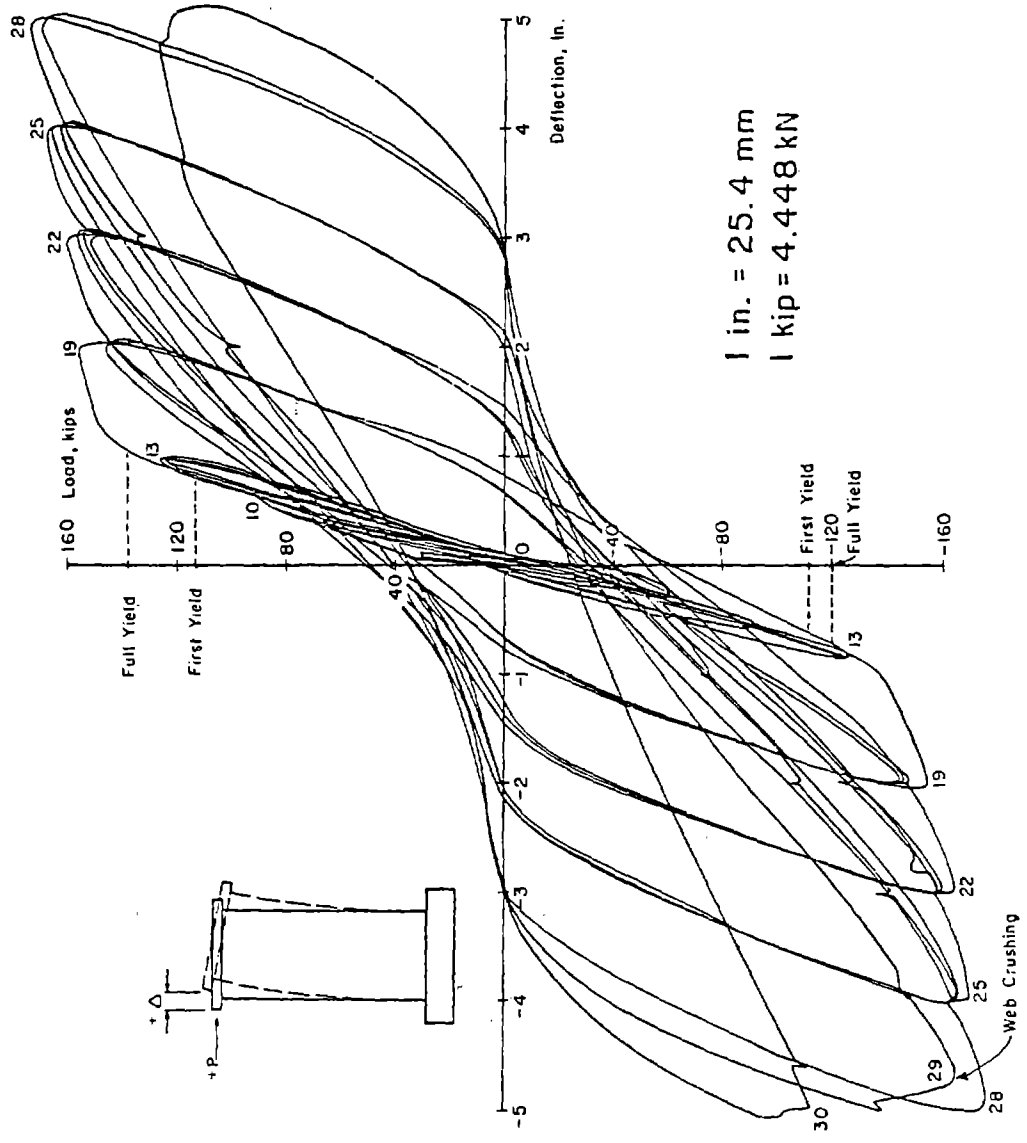
Fig. B-135 Continuous Load-Deflection Plot for Specimen B5
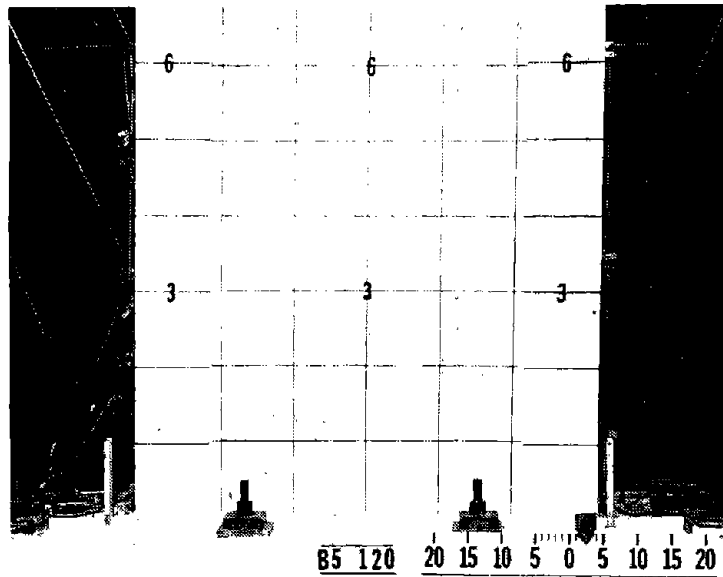
Fig. B-136   Cracking Pattern at +3 in. Deflection
             for Specimen B5
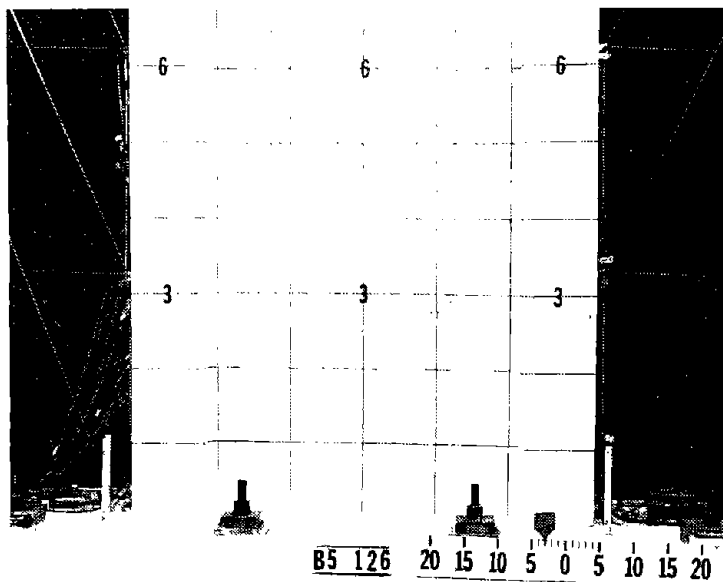
Fig. B-137   Cracking Pattern at -3 in. Deflection
             for Specimen B5

B-168

of the outer compression face was noted in Cycle 19. It was noted that the compression column cracks appeared to remain open approximately 0.005 in. (0.13 mm) in Cycle 22.

During Cycle 22, significant spalling and crushing along the right half of the construction joint at the 3-ft (0.91 m) level was observed. The joint deterioration was caused by previous cracking in the outer surface of the web below the joint. The previous cracking was due to damage to the edge of the joint when it was roughened with a chisel during the specimen construction.

The joint progressively deteriorated during each load cycle. The deterioration was probably amplified by a scale effect in the model wall. A full size wall would not have been damaged as extensively by this improper joint preparation. As shown in Fig. B-138, the deteriorated portion of the joint intersected the two steepest compression struts extending from the base for negative direction loading. The load from these struts had to be taken by higher and lower struts which increased the rate of deterioration of the web. However, the load capacity continued to increase in each new loading increment.

A noticeable reverse curvature developed in the lower 3 ft 8 in. (1.12 m) of both columns during Cycle 25.

The maximum load measured, 171.3 kips (761.9 kN), occurred in Cycle 28 at a -5-in. (127.0 mm) deflection. This load corresponds to a nominal shear stress, v_{max} = 8.8 $\sqrt{f_c'}$ (0.73 $\sqrt{f_c'}$, MPa). As the specimen was being loaded to a -5-in. deflection in Cycle 29, several compression
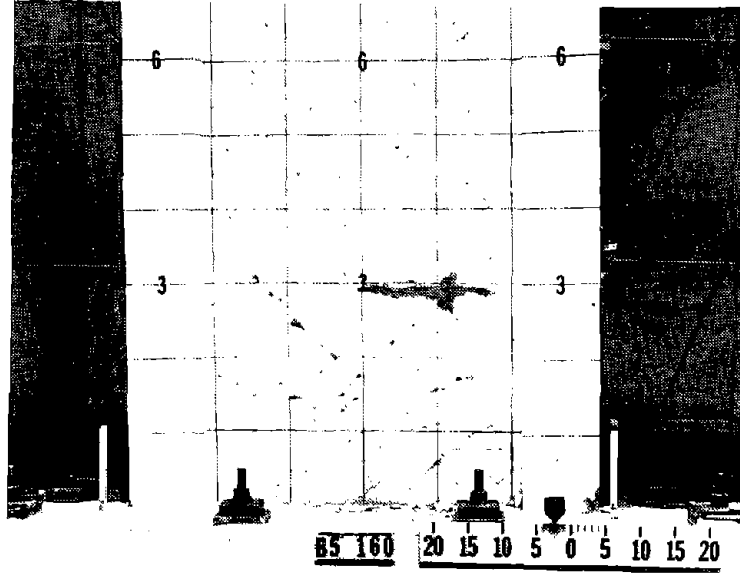
Fig. B-138   Deterioration of Construction Joint
             at the 3 ft. Level for Specimen B5
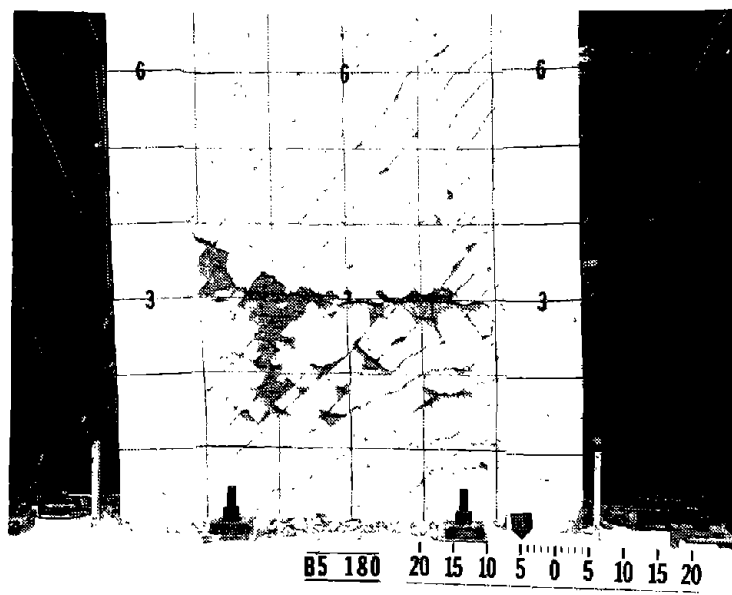
Fig B-139   Specimen B5 After Web Crushing

struts crushed simultaneously. The crushing occurred in the struts immediately above the struts that were intercepted by the deteriorated construction joint. This construction joint probably precipitated an early web crushing in the specimen. Figure B-139 shows the specimen immediately after the web crushing.

As the web crushing occurred, the specimen was "caught" by closing the deflection control valve in the hydraulic system. The measured load at this stage had decreased to 76% of the maximum measured load. The specimen was loaded with one more 5-in. (127.0 mm) deflection and the load capacity reduced to 63% of the maximum measured load.

The specimen sustained at least 80% of the maximum measured load capacity through 10 inelastic cycles. The last inelastic loading increment in which the load was sustained at or above 80% of the maximum for all 3 cycles was at ±4 in. (101.6 mm).

Although the first 6 ft (1.83 m) of the web was con-siderably damaged after the test, the columns were in good condition. The close confinement hoops had prevented bar buckling and maintained the shear integrity of the columns. It was decided that this specimen could be repaired and retested.

Discussion of Results

Moment-Rotation. Moment-rotation data for Specimen B5 is shown in Fig. B-140. The measured maximum moment was 80% of the calculated monotonic maximum.

a) At 6 ft. Level

b) At 3 ft. Level

1 ft. = 0.305 m
1 in. = 25.4 mm
1 kip = 4.448 kN
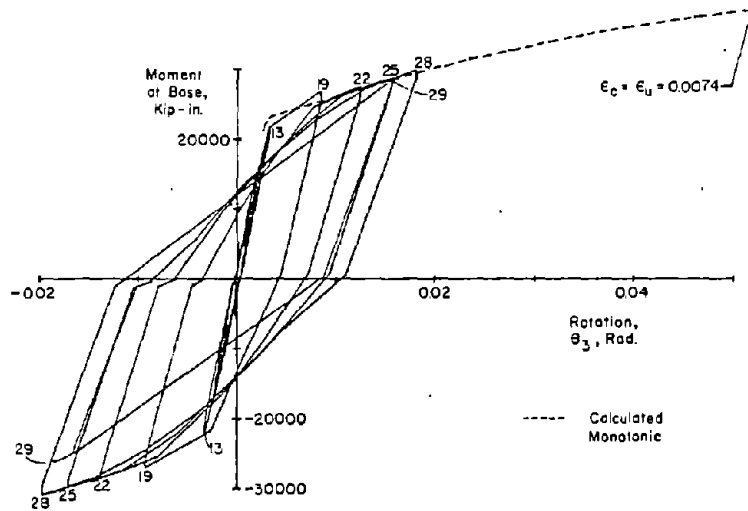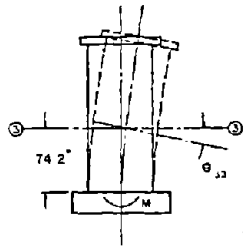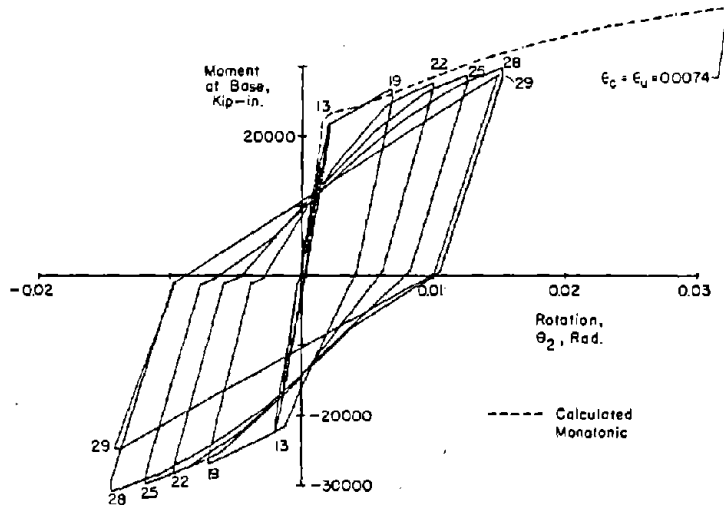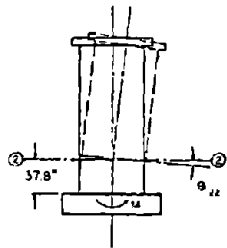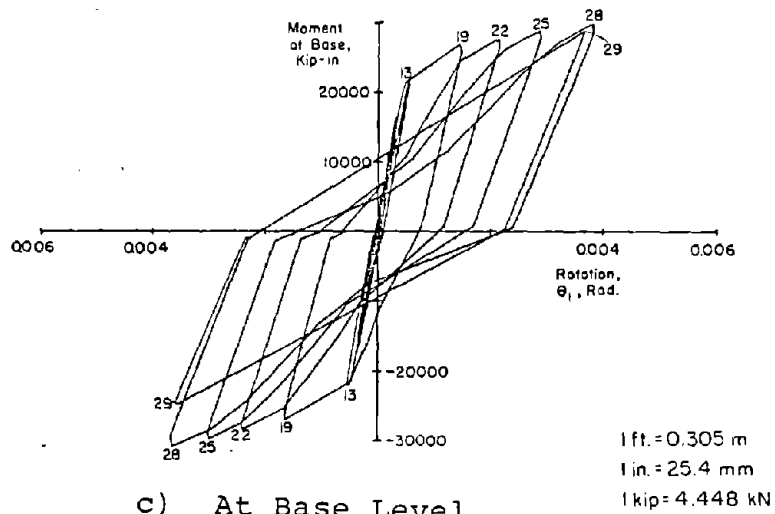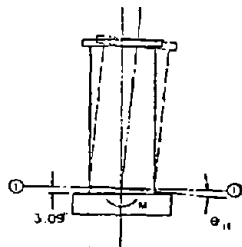
c) At Base Level

Fig. B-140   Moment at Base versus Rotation
for Specimen B5

The moment-rotation data for B5 was very similar to that for B2 through Cycle 25. The magnitudes of rotation are nearly equal for equal top deflection. The ratio of the maximum measured loads in Cycle 25 for B2 and B5 is equal to the ratio of the yield stresses for the reinforcing steel used in each. The relationships between the measured and the calculated monotonic at both the 3-ft (0.91 m) and the 6-ft (1.83 m) levels in B5 were very similar to those relationships in B2. The difference between B2 and B5 was that the confinement maintained the integrity of the columns through Cycle 28 allowing the load to increase to 171.3 kips (761.9 kN), which was 12% higher than the maximum load in B2.

Shear-Distortions. The shear distortion loops for B5 are shown in Fig. B-141. This data for B5 is similar to the shear-distortion data for B2 with the exception that the distortions in B5 were approximately 15% less than those in B2 for equal top deflections.

There is no indication of increased distortions caused by the previously described deterioration of CJ2. The deterioration was first noted visually in Cycle 22.

The maximum measured load in B5 corresponded to a shear stress of $8.8\sqrt{f_c'}$ ($0.73\sqrt{f_c'}$, MPa). With a shear reinforcement design similar to that of B2, assuming an ultimate stress of 100 ksi in the horizontal steel, the steel shear capacity would only be $7.5\sqrt{f_c'}$ ($0.62\sqrt{f_c'}$, MPa). This indicated that the concrete contribution must have been at least $1.3\sqrt{f_c'}$ ($0.11\sqrt{f_c'}$, MPa) shear stress at maximum load.
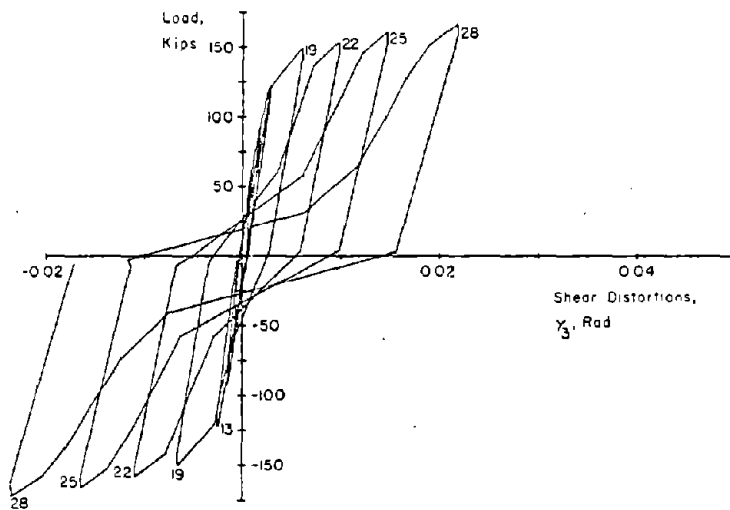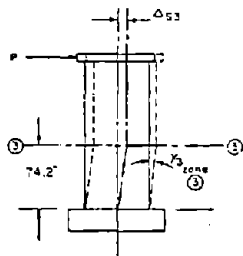
a) In Base to 6 ft Level
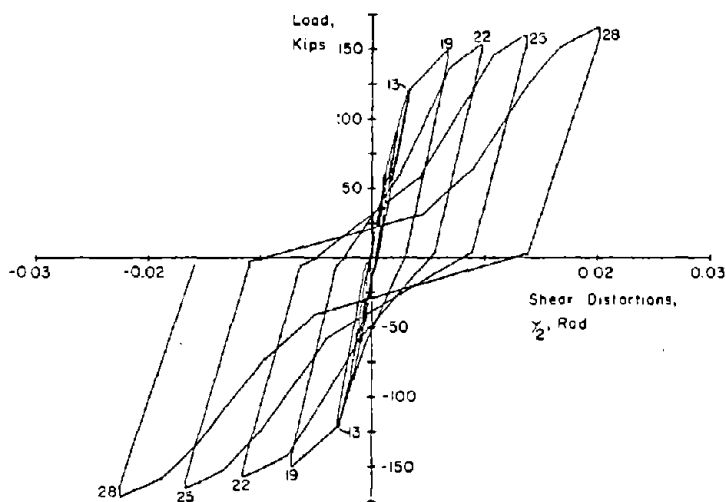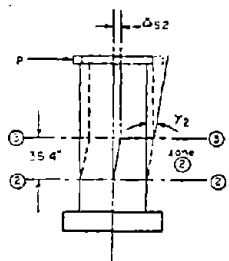
b) In 3 ft to 6 ft Level
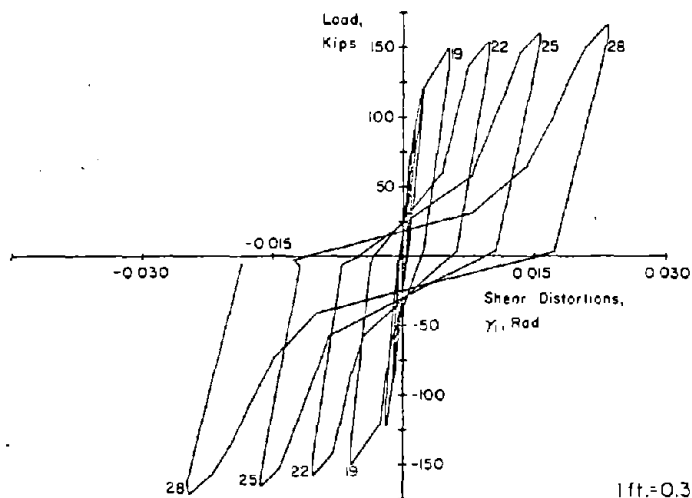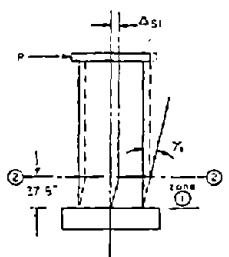
1 ft.=0.305 m
1 in.=25.4 mm
1 kip=4.448 kN

c) In Base to 3 ft Level

Fig. B-141   Load versus Shear Distortion
for Specimen B5

Slip at Construction Joints. The slip at construction
joints in B5 is shown in Fig. B-142. The slip at CJ1 is
similar to that in B2 except that the magnitude in B5 is
approximately 30% lower than that in B2 for equal top
deflections. As shown in Fig. B-143, the slip at CJ1 was a
relatively constant 15% of the total shear deflection in the
lower 3 ft (0.91 m) This is a slightly lower percentage
than that in B2.

The gage at CJ2 failed after the first half of Cycle 22.
The data exhibited a "yielding" for positive load in Cycle 22.
However, there was no further data to quantify the visually
observed deterioration of CJ2 after Cycle 22.

The slip at CJ3 was probably affected by diagonal
cracking.

Deflections. The deflection components and deflected
shapes are shown in Figs. B-144 and B-145. These figures
show that deflections in B5 were very similar to deflections
in B2 with the following exceptions. The shear deflections
are slightly smaller in B5. Also, the average increase in
shear deflection between Cycle 22 and 24 was 15% as compared
to 20% in B2.

Reinforcement Strains. Figures B-146 through B-154
show reinforcement strains in the specimen at various
stages. These figures are very similar to the equivalent
figures for Specimen B2 with the following exception. The
gages on the ends of the horizontal bar in B5 indicated a
lower stress level near the end hooks than in B2.
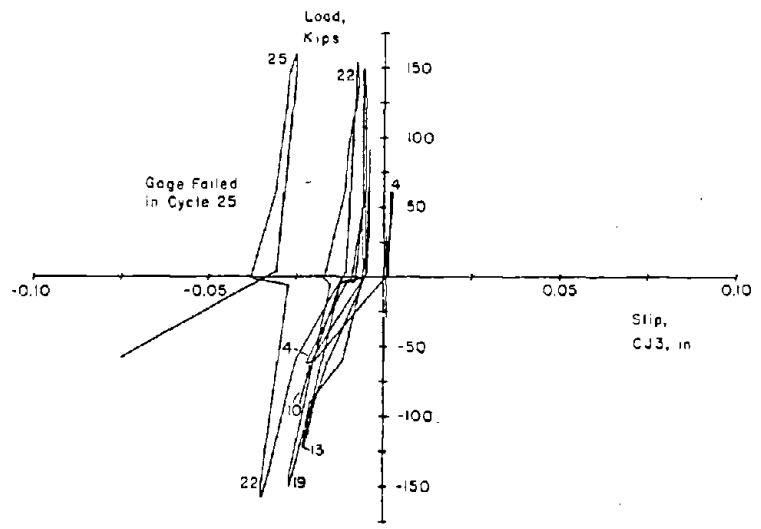
a) At 6 ft. Level
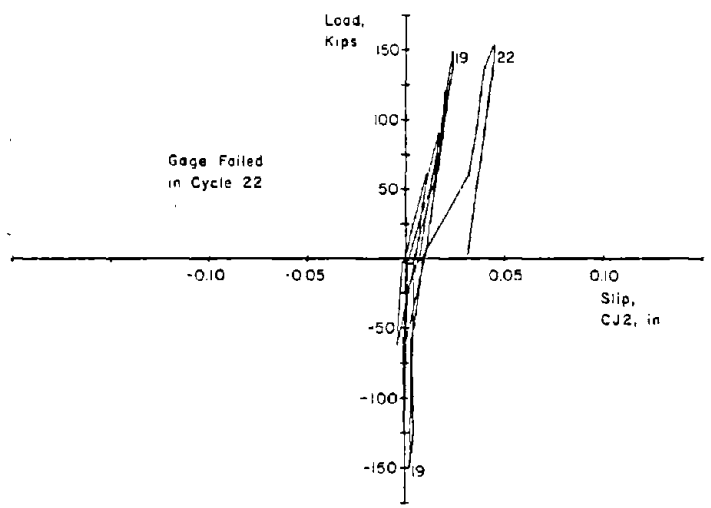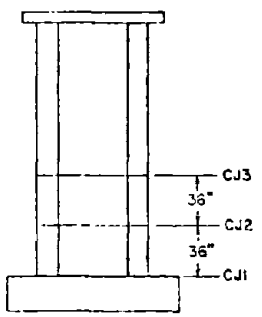
b) At 3 ft. Level
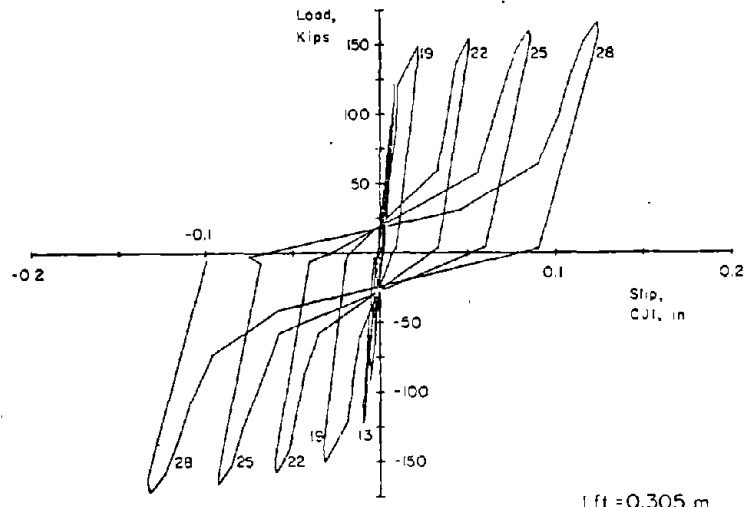
c) At Base Level

1 ft.=0.305 m
1 in.=25.4 mm
1 kip=4.448 kN

Fig. B-142   Load versus Slip at Construction Joints
for Specimen B5

$\dfrac{\Delta CJ1}{\Delta \gamma_1}$, %

100

60

20

I in. = 25.4 mm

4

13

19

22

25

28

0.5

1.0

Shear   Deflection, $\Delta \gamma_1$ (in.)

a)   At Maximum Positive Loads

$\dfrac{\Delta CJ1}{\Delta \gamma_1}$, %

100

60

20

28

25

22

19

13   4

1

-1.0

-0.5
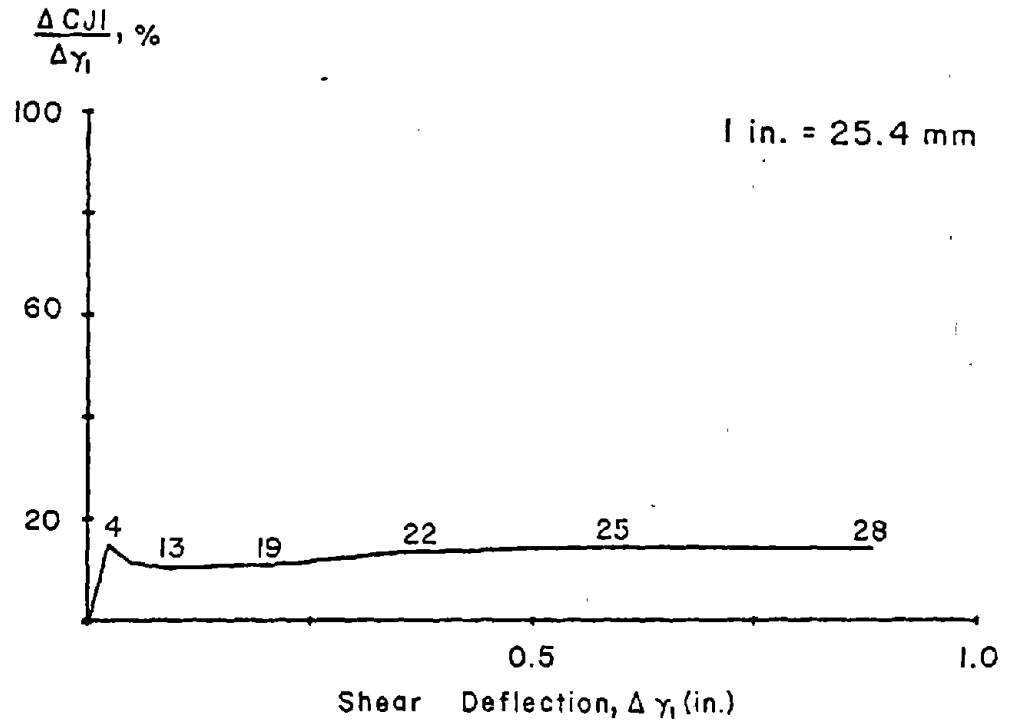
Shear   Deflection, $\Delta \gamma_1$ (in.)
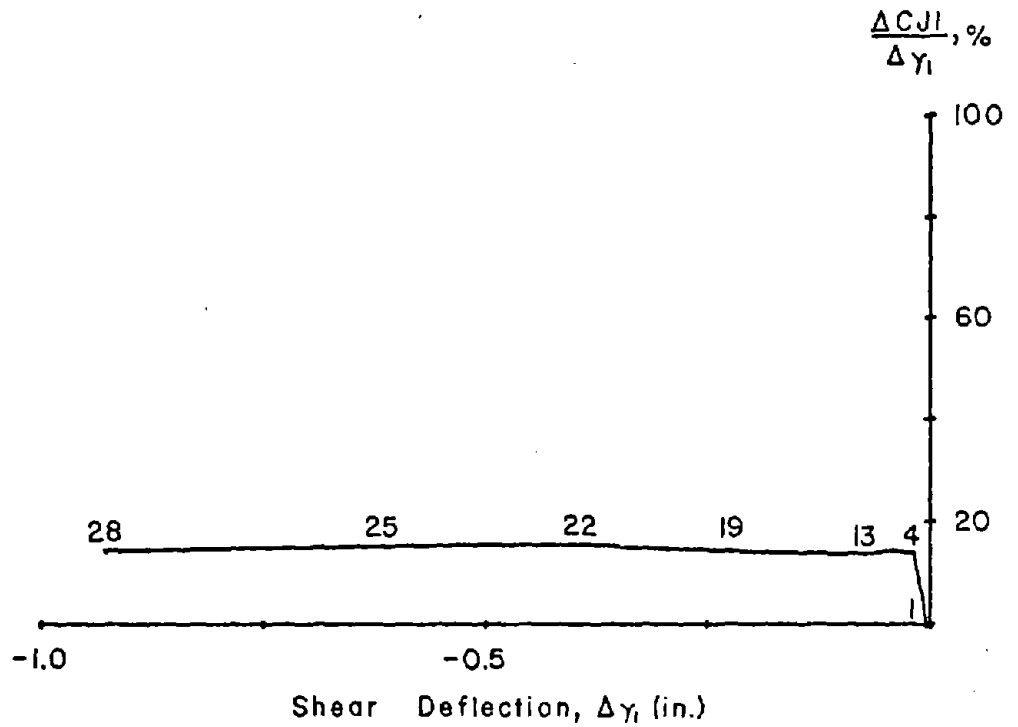
b)   At Maximum Negative Loads

Fig. B-143   Slip at Base Construction Joints versus
Shear Deflection in Zone 1 for Specimen B5

a) At Top of Wall
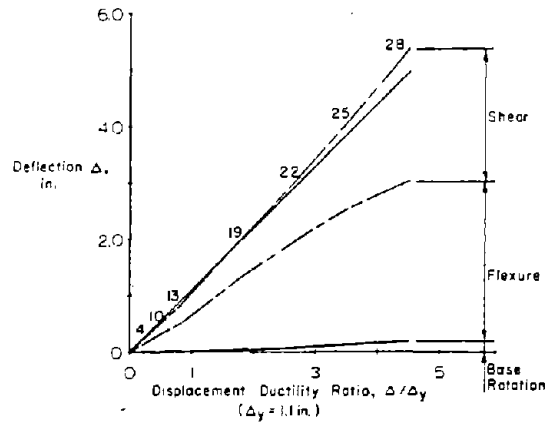
b) A 6 ft. Level
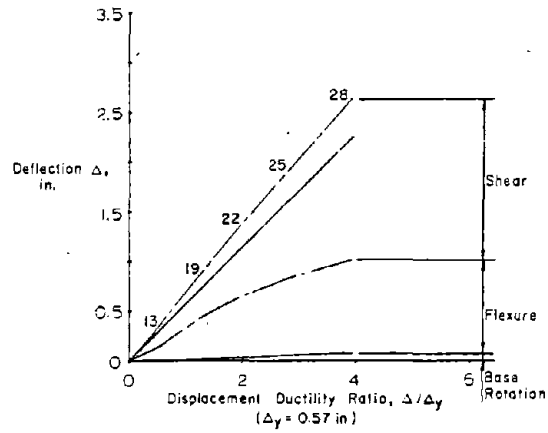
c) At 3 ft. Level
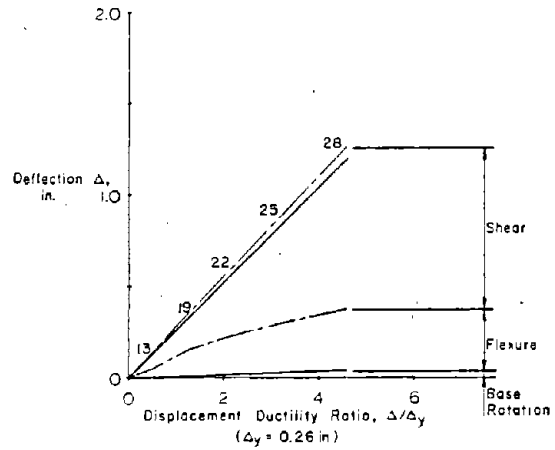
Fig. B-144 Component of Deflection for Specimen B5
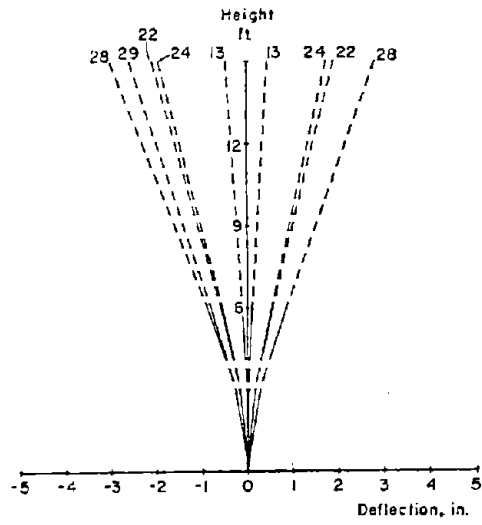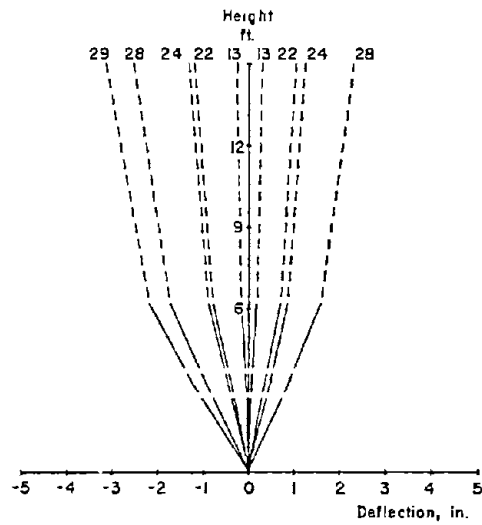
B-178

a) Flexural

b) Shear

— - — CALCULATED FROM
        MEASURED DEFORMATION
— - — - EXTRAPOLATED
——— MEASURED TOTAL

1 in.= 25.4 mm
1 ft.= 0.305 m

W.C.— WEB CRUSHING

CYCLE 29
AFTER W.C.

CYCLE 28
PRIOR TO W.C.

c) Total
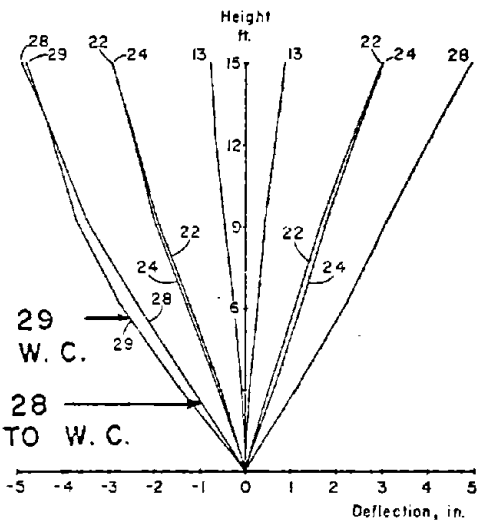
Fig. B-145 Deflected Shape for Specimen B5
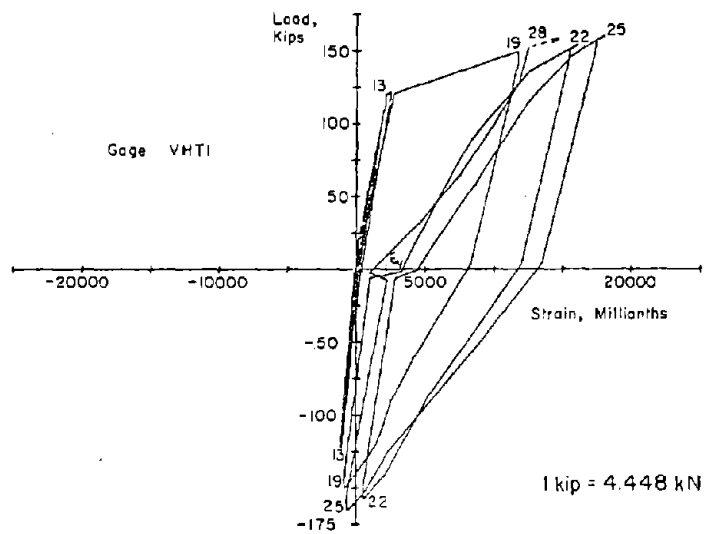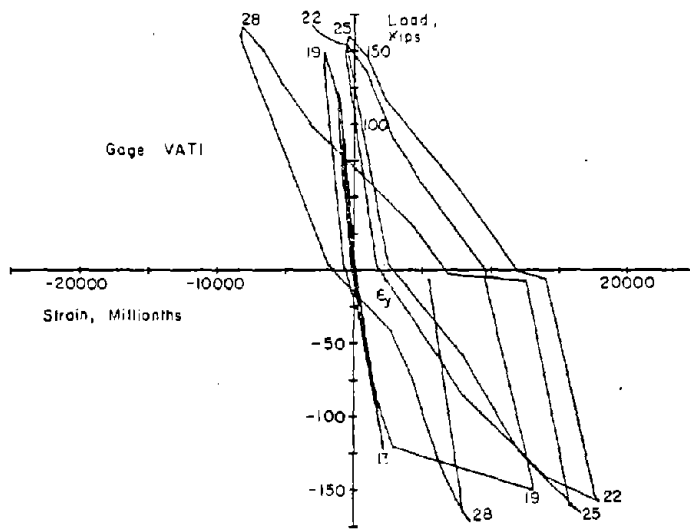
Fig. B-146   Measured Strains on Vertical Reinforcement
             at Base of Specimen B5
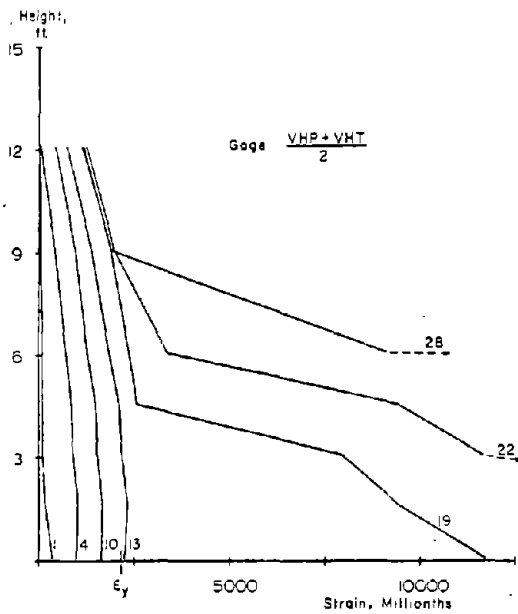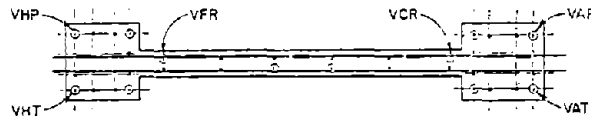
a) Average of VHP & VHT
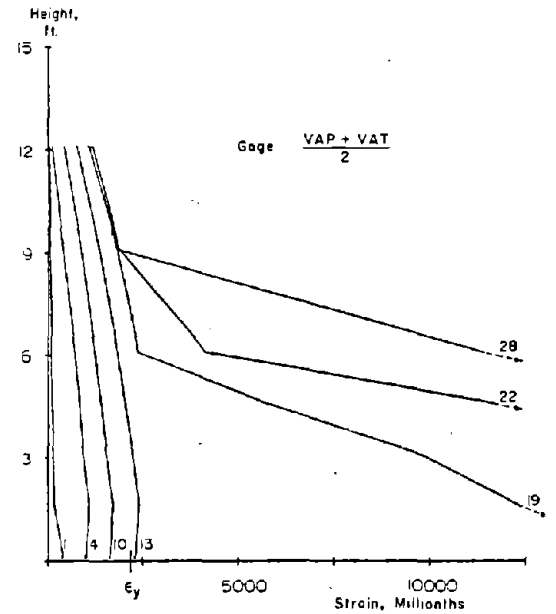
b) Average of VAP & VAT
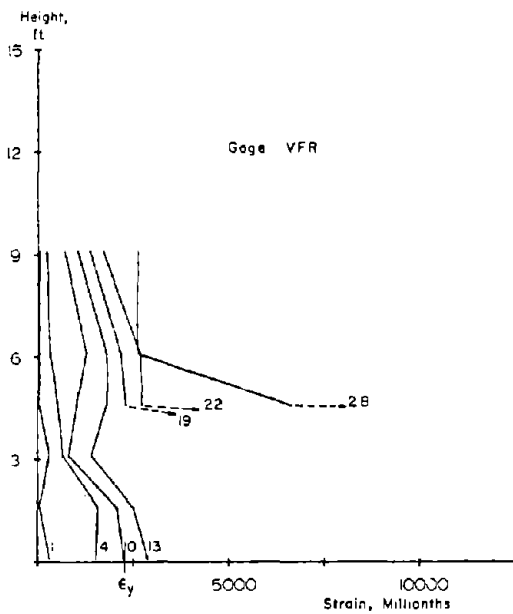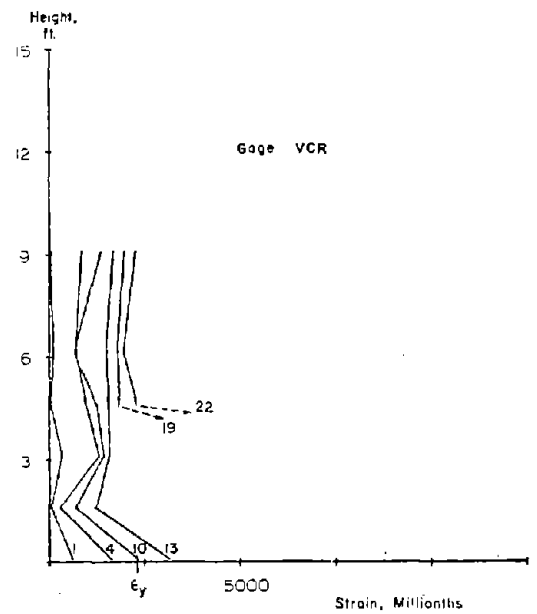
c) Strain Gage VFR

d) Strain Gage VCR

Fig. B-147 Vertical Reinforcement Strains at
Maximum Loads for Specimen B5

B-181

a) At 6 ft. Level

b) At 3 ft. Level

1 ft.=0.305 m

c) At Base Level
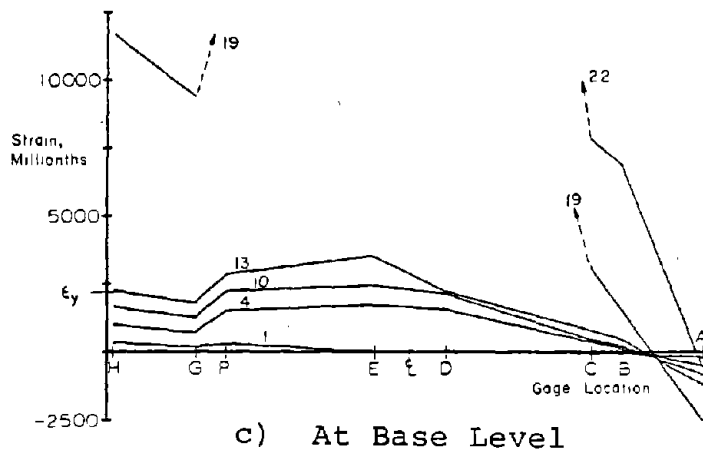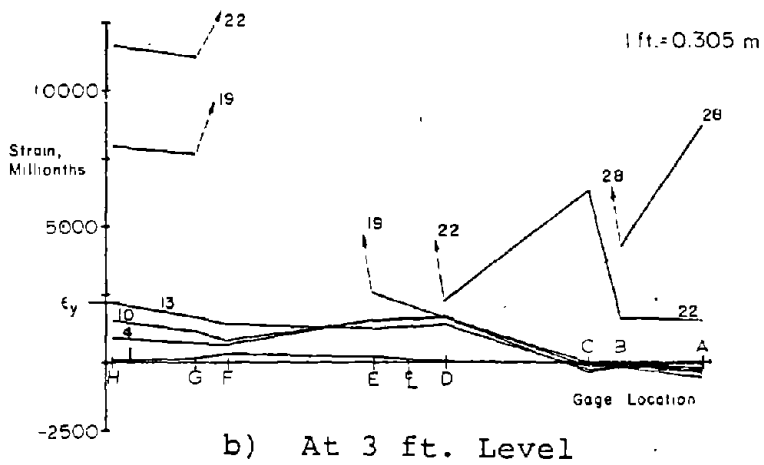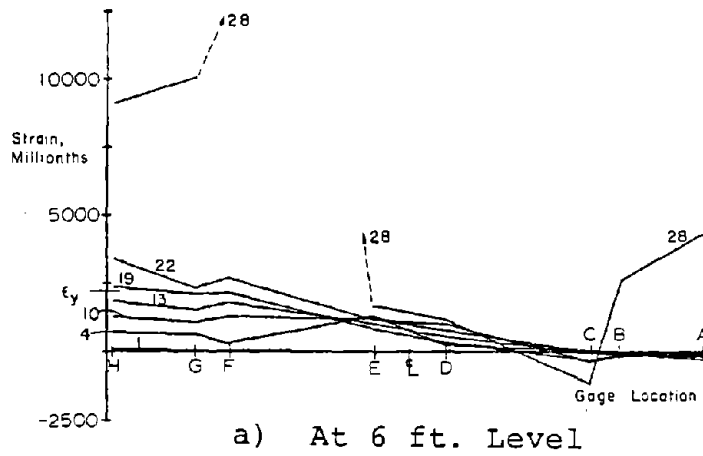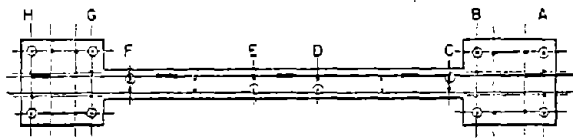
Fig. B-148 Vertical Reinforcement Strains at
Maximum Positive Loads for Specimen B5
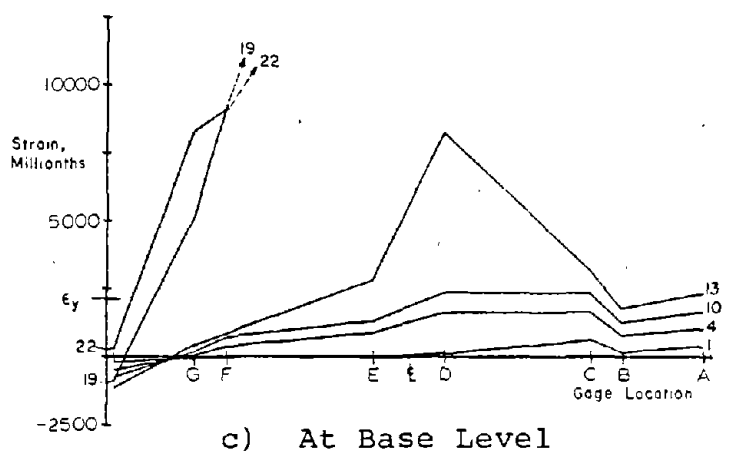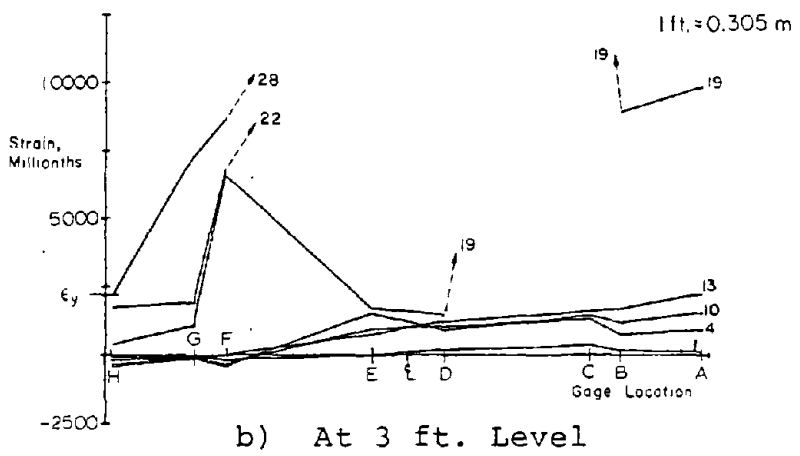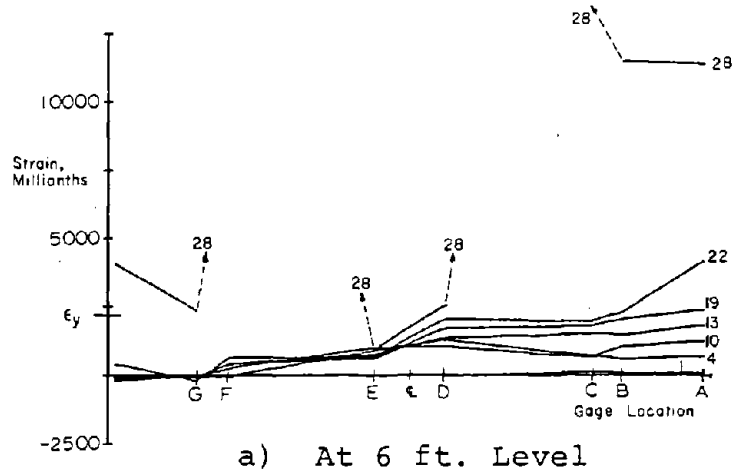
Fig. B-149 Vertical Reinforcment Strains at
Maximum Negative Loads for Specimen B5
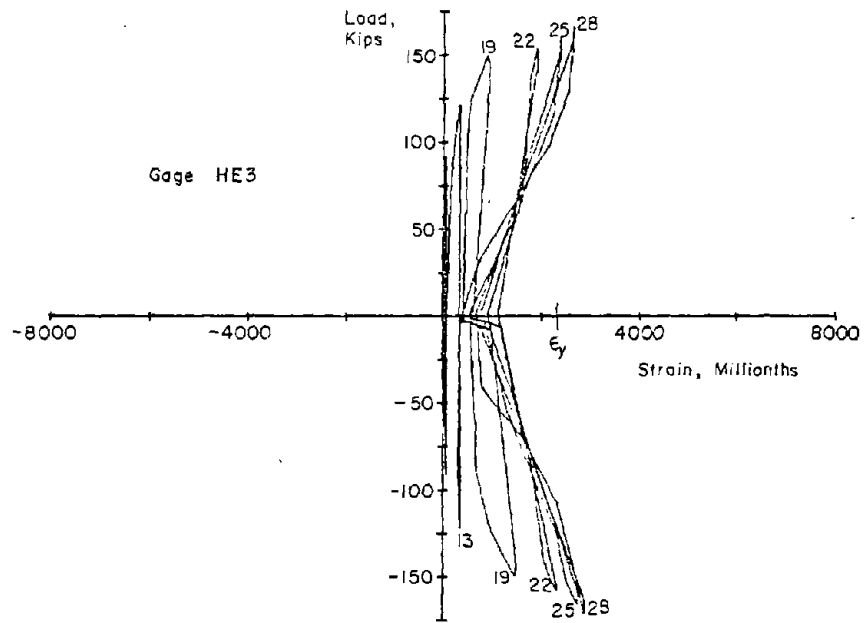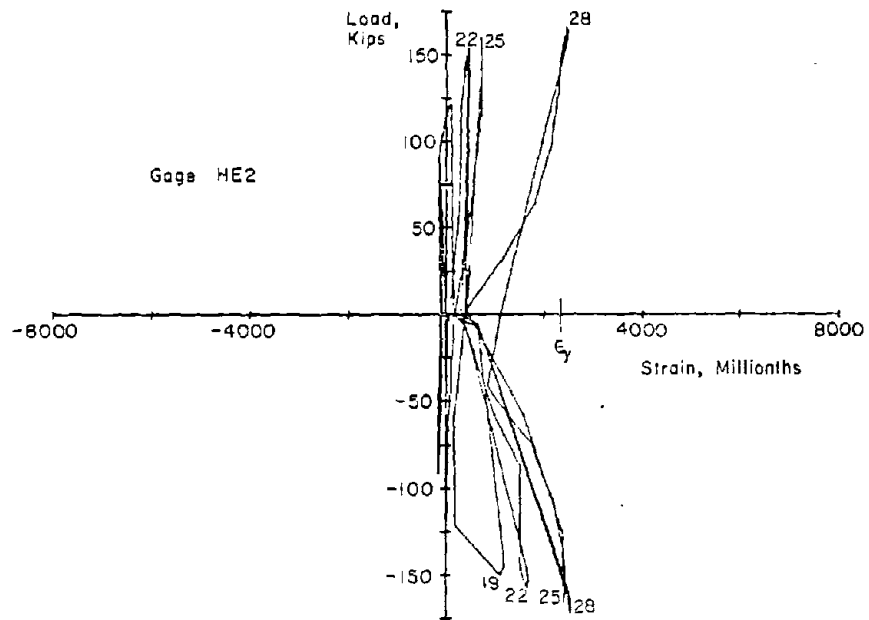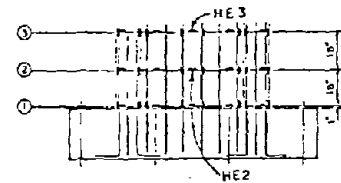
Fig. B-150   Measured Strains on Horizontal Reinforcement
              for Specimen B5

B-184
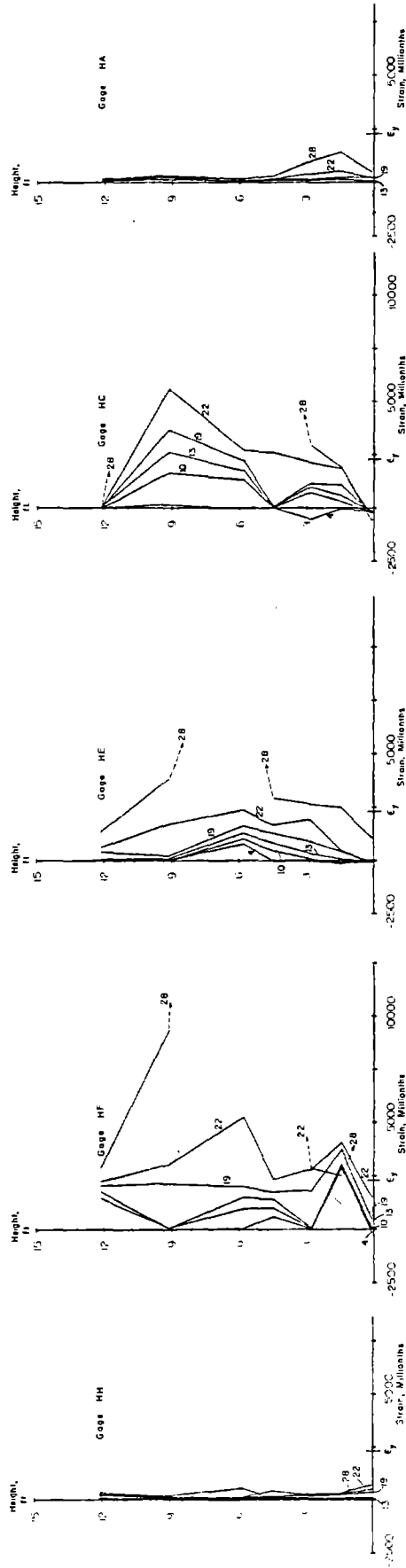
Fig. B-151 Horizontal Reinforcement Strains at
Maximum Positive Loads for Specimen B5

1 ft.=0.305 m
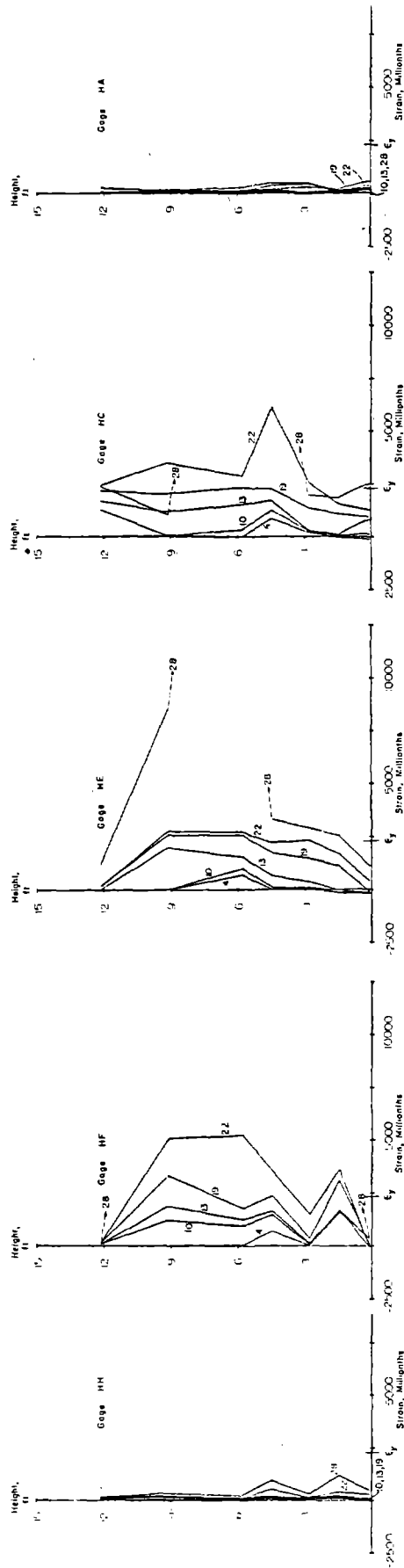
Fig. B-152 Horizontal Reinforcement Strains at Maximum Negative Loads for Specimen B5

1 ft.=0.305 m

B-186
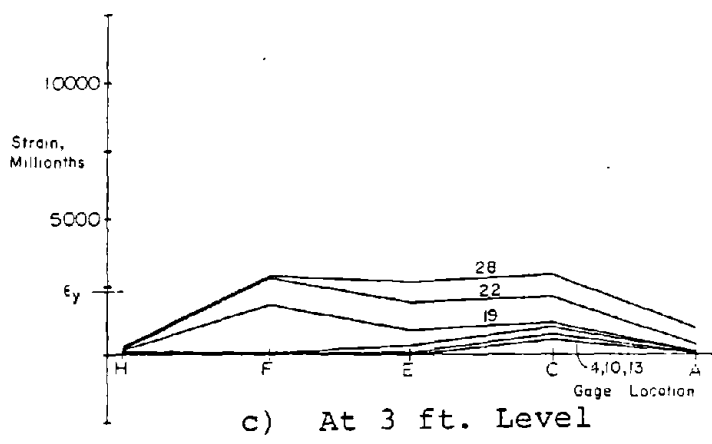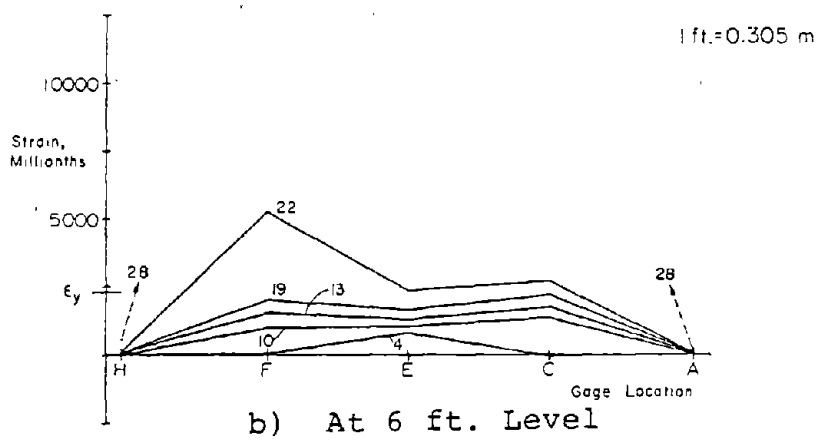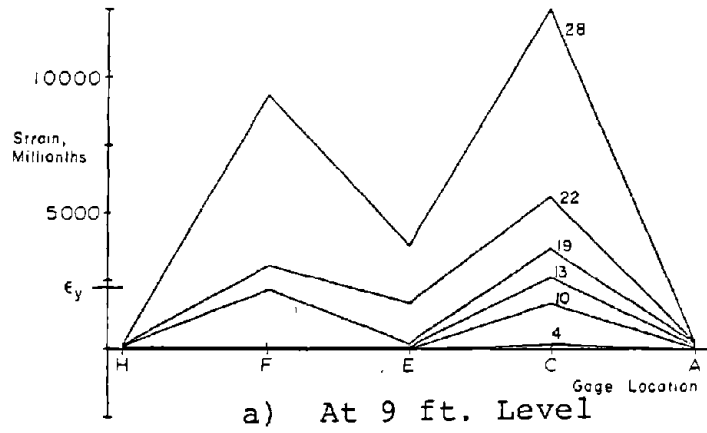
Fig. B-153 Horizontal Reinforcement Strains in Web
at Maximum Positive Loads for Specimen B5

a) At 9 ft. Level

b) At 6 ft. Level

1 ft.=0.305 m

c) At 3 ft. Level
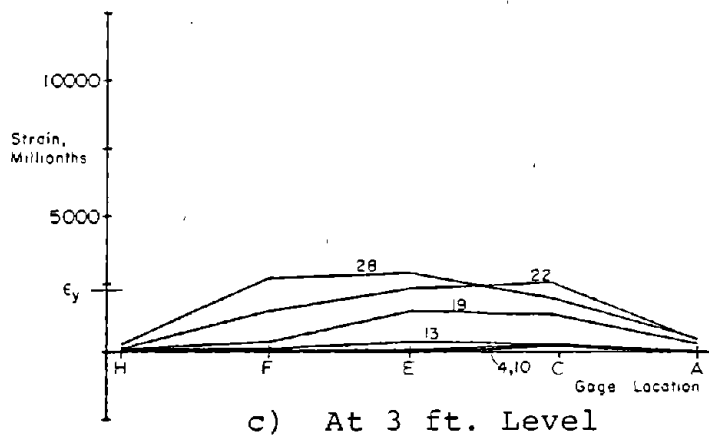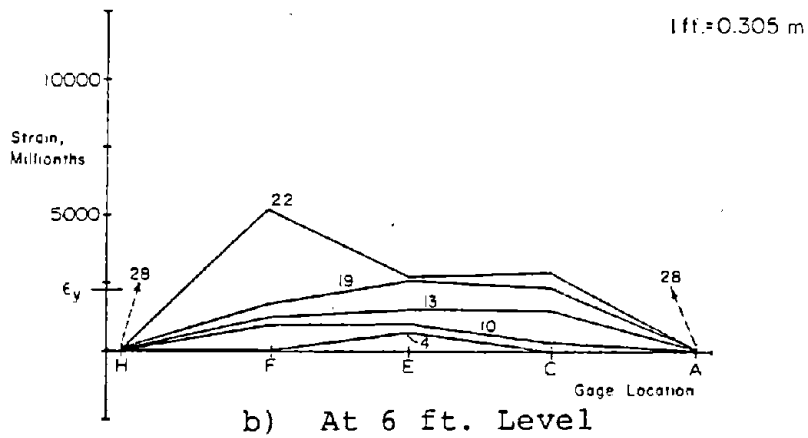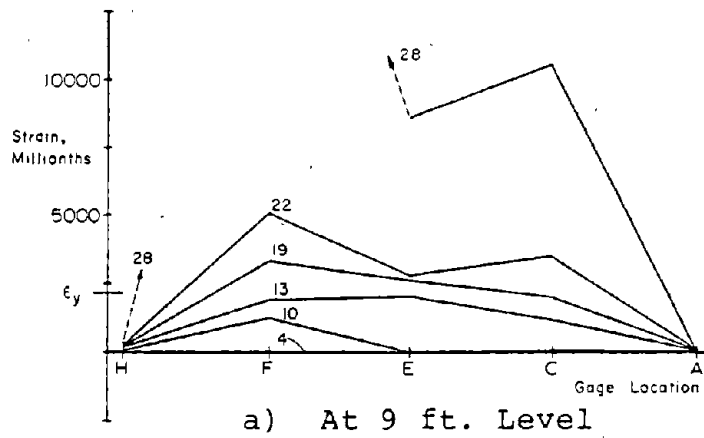
Fig. B-154   Horizontal Reinforcement Strains in Web
at Maximum Negative Loads for Specimen B5

<u>Specimen B5R</u>

Test Description

Specimen B5R was a repair of B5 as described in the experimental program section. The lateral load test for B5R was conducted similar to the test of Specimen B5. The only exception was that since nearly all strain gages were inoperative at the end of the B5 test, no steel strains were monitored or recorded during the B5R test.

The test consisted of 30 loading cycles as shown in Fig. B-155. The complete load versus top deflection relationship for the test is shown in Figs. B-156 and B-157. Since the reinforcing steel had already yielded in the test of B5, the yield loads for B5R were defined as those loads measured for B5. The yield deflections were then taken as the deflections occurring in B5R when these yield loads were first reached.

First significant cracking in the web occurred in Cycle 4 at a load of approximately 30 kips (133.4 kN). The first yield load level was reached in Cycle 13. The maximum measured crack width in the web at this stage was 0.025 in. (0.64 mm) The corresponding deflections indicated that the lateral top displacement stiffness of B5R was about half that of B5 at the yield level. The crack pattern that developed was similar to that in B2 and B5 with the following exception. Several diagonal cracks that intersected the construction joint at the 3-ft (0.91 m) level turned and

Load, kips

150 — Full Yield = 138 kips*

100 — First Yield = 112.3 kips*

50

0

10 20 30 40 50 Cycle No.

-50

-100 — First Yield = 113.0 kips*

Full Yield = 120.5 kips*

-150

* Yield loads observed during B5 test.

a) Load History

1 in. = 25.4 mm
1 kip = 4.448 kN

Defl., in.

8

6

4

2 Full Yield = 2.5 in.

0 First Yield = 1.55 in.

10 20 30 40 50 Cycle No.

-2 First Yield = 1.38 in.

-4 Full Yield = 1.5 in.

-6

-8

b) Deflection History
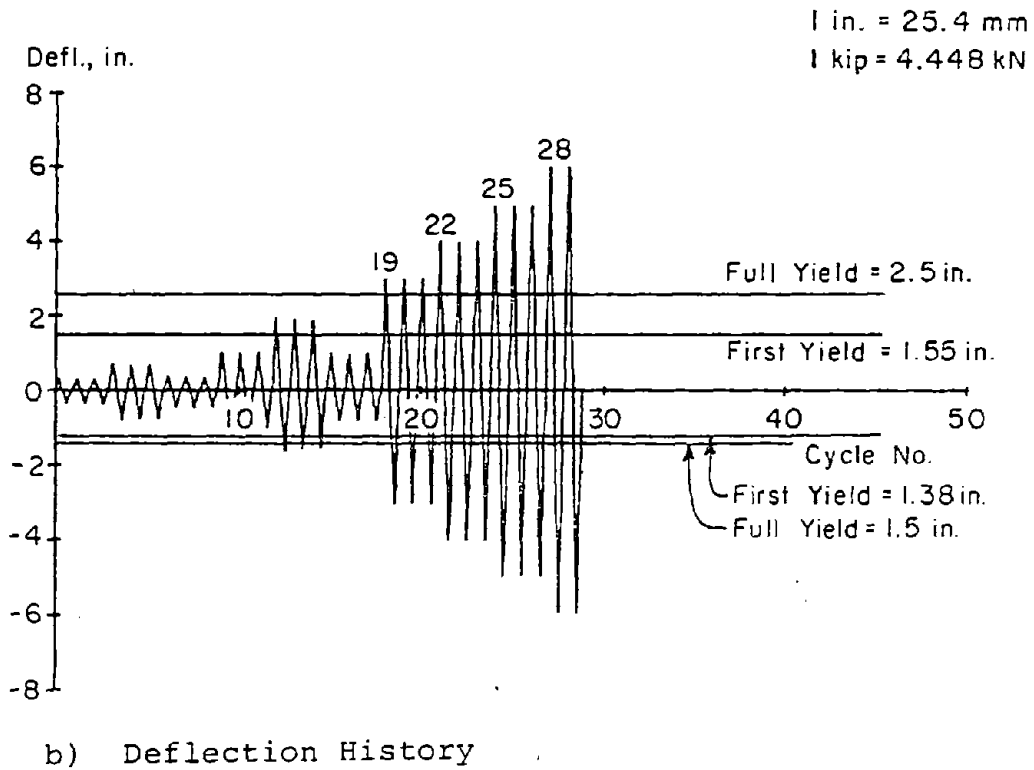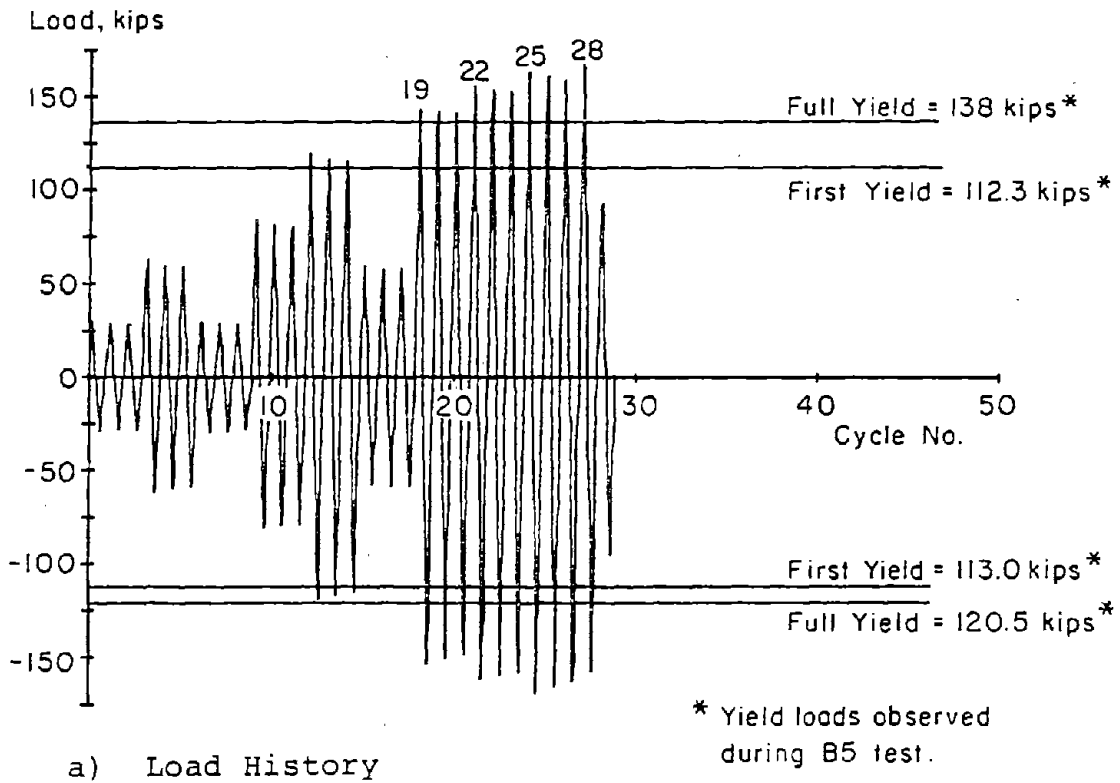
Fig. B-155   Loading History for Specimen B5R

B-190
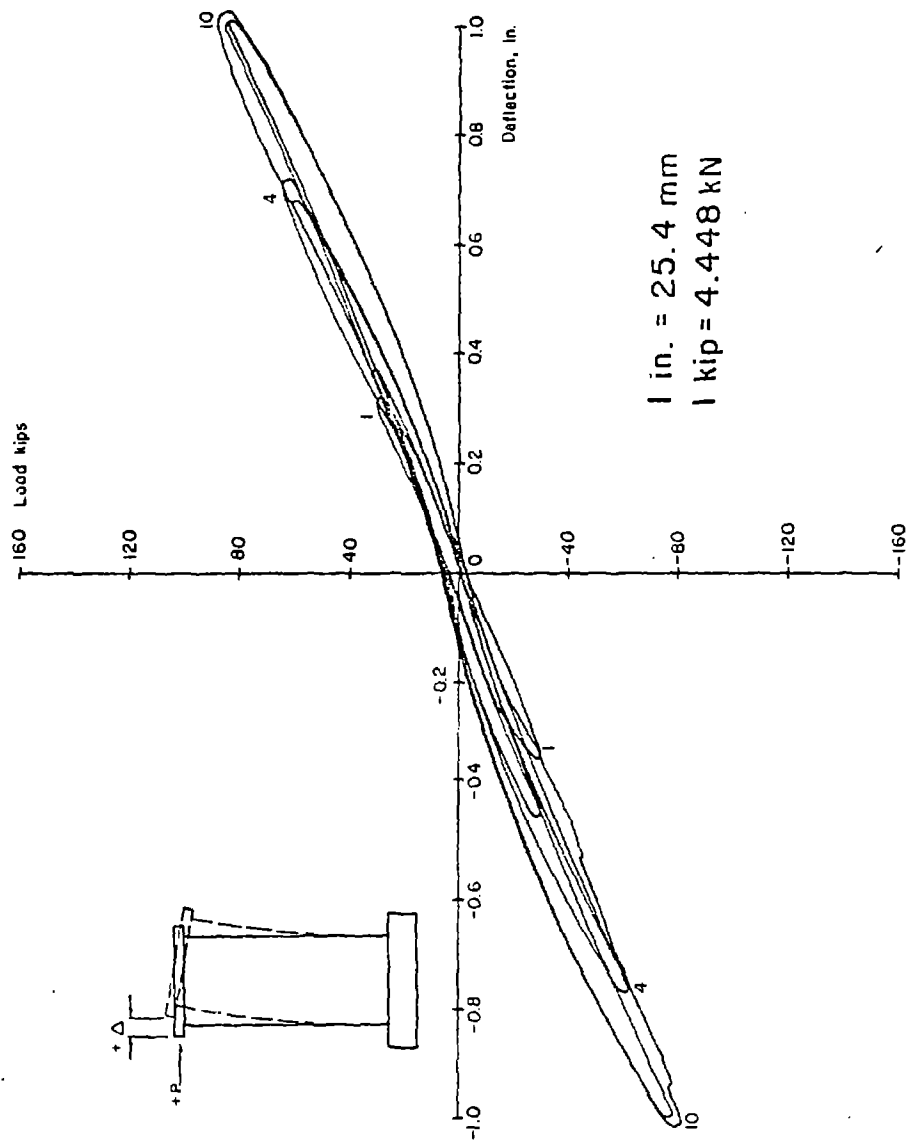
Fig. B-156. Continuous Load-Deflection Plot for
Initial Cycles for Specimen B5R
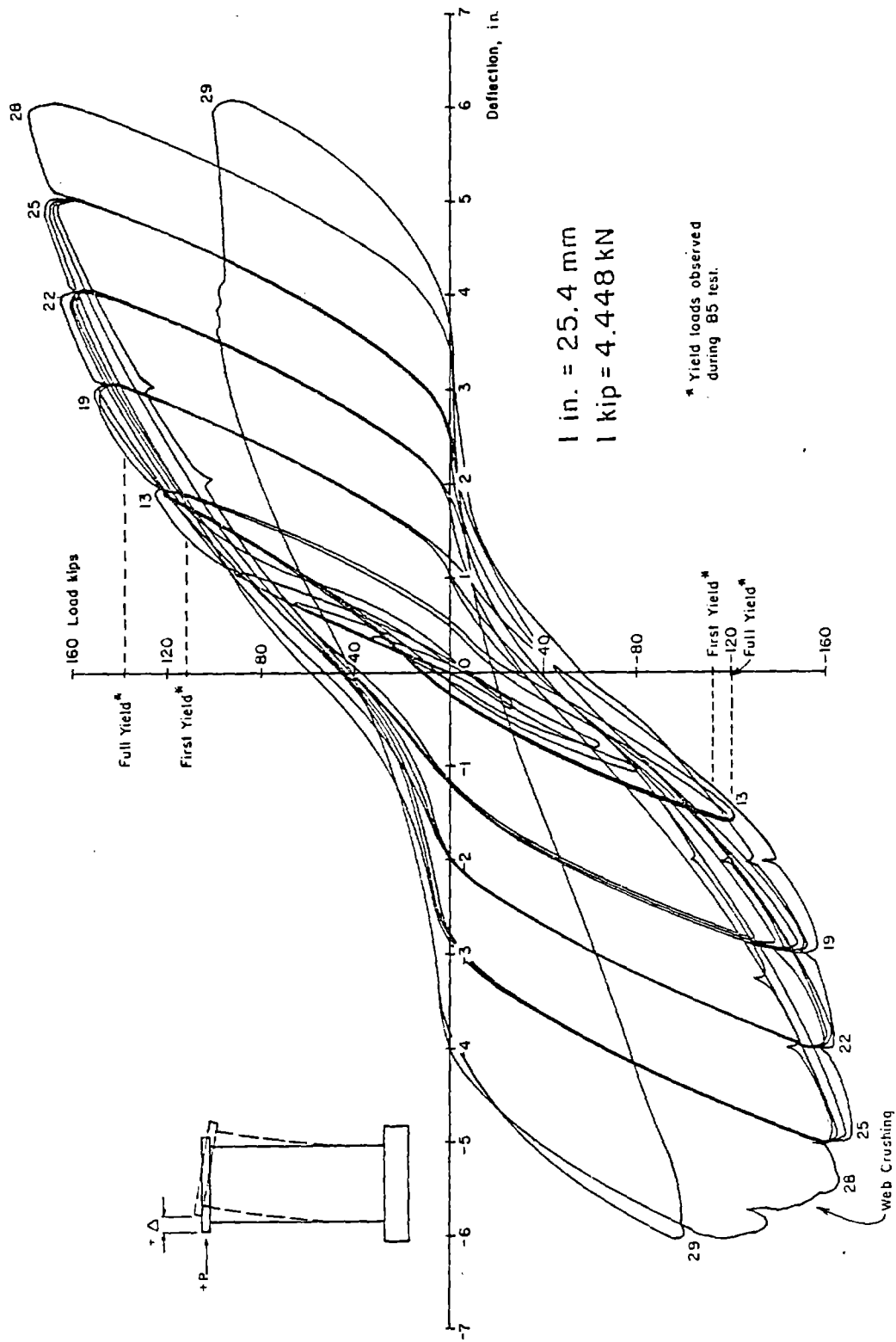
Fig. B-157 Continuous Load-Deflection Plot for Specimen B5R

progressed horizontally along the joint for several inches, then inclined down and continued diagonally toward the base. The angle of these cracks was slightly steeper and focused toward a lower point than the cracks in B5. Figures B-158 and B-159 show the crack pattern at +5-in. (127.0 mm) and -5-in. deflection, respectively.

Crushing of the repair patches at the base of the outer column faces was noted in Cycle 13. The first indication of spalling and flaking along diagonal web cracks occurred in Cycle 16. The neat cement paste which had been rubbed over column cracks started spalling and flaking in Cycle 19. The spalling and crushing in the web and columns had increased significantly by Cycle 24.

A significant increase in the reverse curvature in the columns was noted in Cycle 25. The columns appeared to be kinking at the 3-ft level. Also, in Cycle 25 it was noted that the offsets in the diagonal cracks at the 3-ft level construction joint had combined to form a complete straight horizontal crack across the entire section.

As the concrete was spalling and grinding in Cycles 16 through 28 the maximum measured load in each new increment continued to increase. The maximum measured load, 167.8 kips (746.8 kN), occurred in Cycle 28 at a +6-in. (152.4 mm) deflection. This load was 98% of the maximum measured load in the test of B5. It corresponds to a nominal shear stress, $v_{max} = 8.9\sqrt{f_c'}$ ($0.74\sqrt{f_c'}$, MPa).
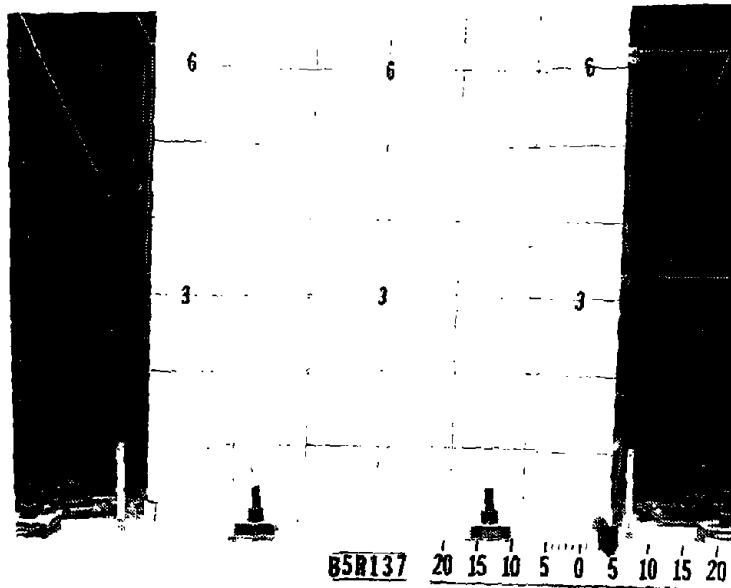
Fig. B-158 Cracking Pattern at +5 in. Deflection
for Specimen B5R
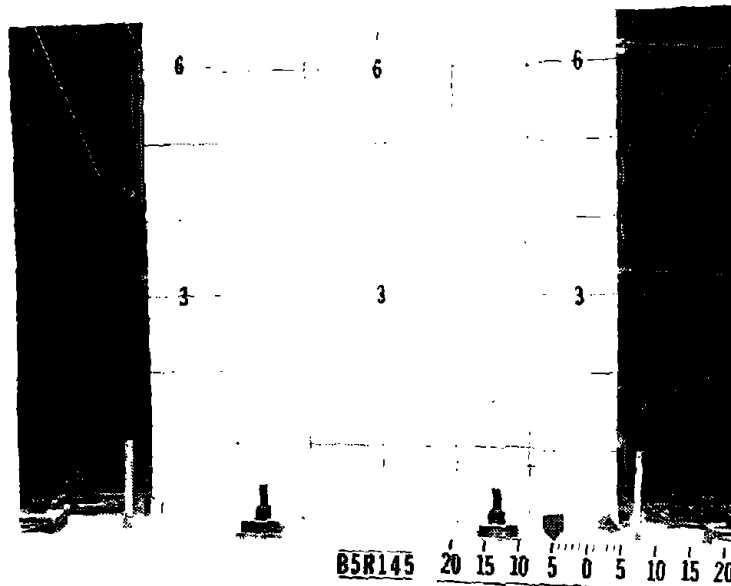
Fig. B-159 Cracking Pattern at -5 in. Deflection
for Specimen B5R

B-194

As the specimen was being loaded to -6-in. (152.4 mm) deflection in Cycle 28, all of the compression struts crossing the 3-ft (0.91 m) level construction joint failed progressively starting near the right side. Each strut failed in a combined sliding crushing mode. Figures B-160 and B-161 show the specimen immediately prior to and after the web failure.

The specimen was "caught" as the load reduced by closing the deflection control valve. The load had decreased to 77% of the previous maximum measured load.

The specimen sustained at least 80% of the maximum measured load capacity through 9 inelastic cycles. The last inelastic loading increment in which the load was sustained at or above 80% of the maximum for all 3 cycles was at ±5 in. (127.0 mm).

Discussion of Results

Moment-Rotation. The moment-rotation data for B5R is shown in Fig. B-162. The measured maximum moment was 79% of the calculated monotonic maximum for Specimen B5 and 98% of the maximum measured load in B5.

A comparison of moment-rotation data for B5R and B5 indicates that, for positive direction loading the stiffness of B5R was considerably lower than that of B5 in the initial cycles. However, the difference became small during the latter load increments. It should be pointed out that equal cycle numbers in B5 and B5R do not correspond to the same
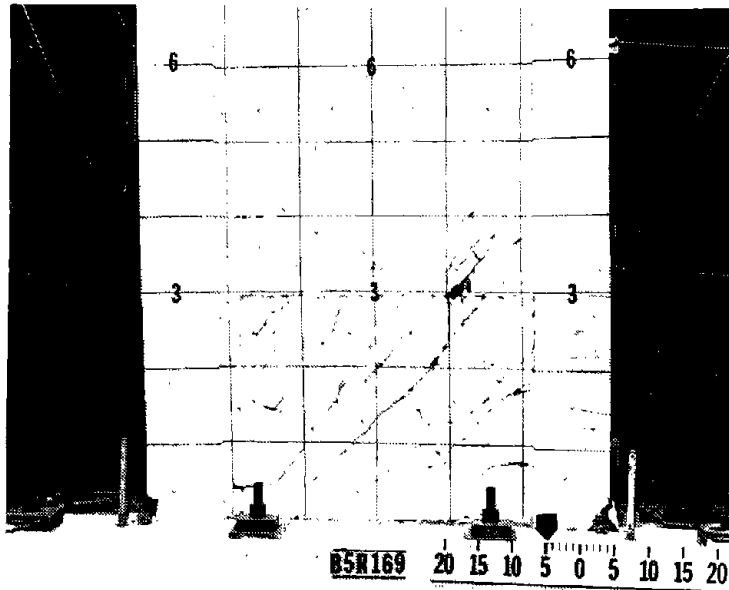
Fig. B-160   Specimen B5R Prior to Web Crushing
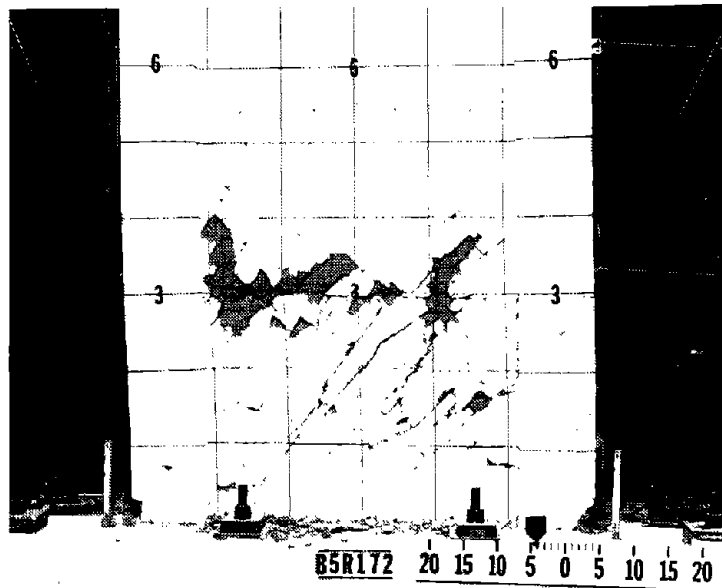
Fig. B-161   Specimen B5R After Web Crushing

B-196

a)   At 6 ft. Level

b)   At 3 ft. Level

c)   At Base Level

1 ft.=0.305 m
1 in.=25.4 mm
1 kip=4.448 kN
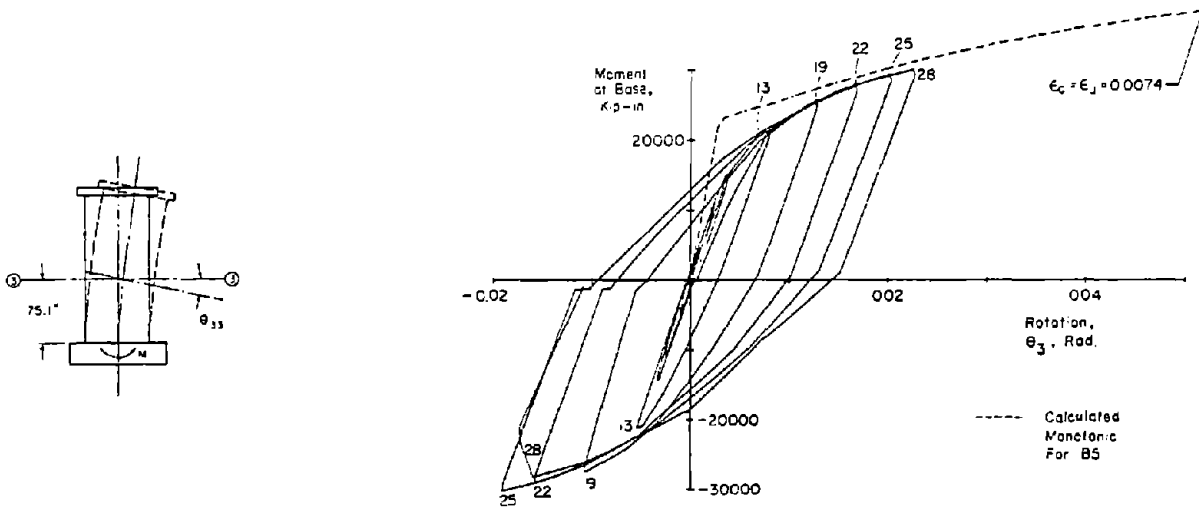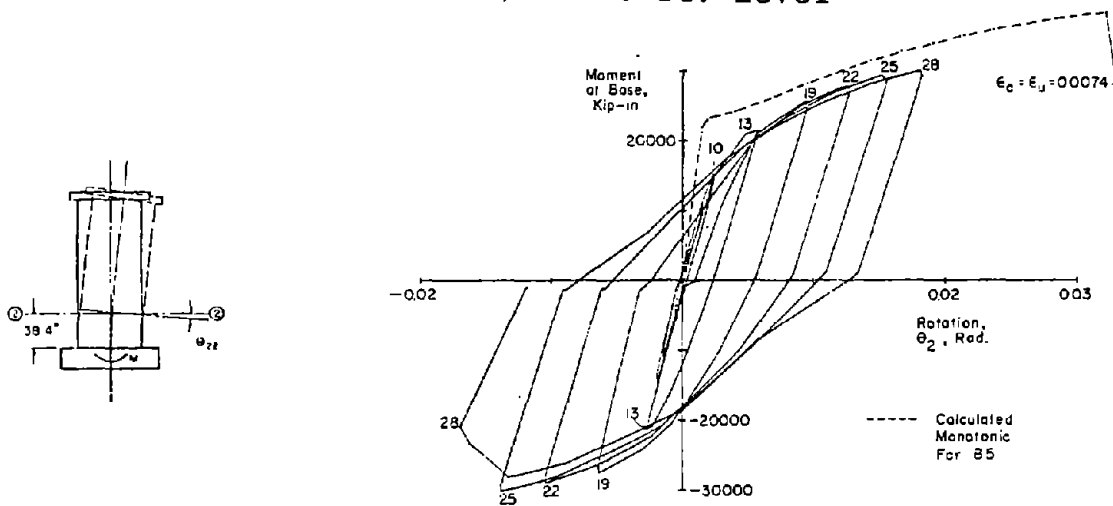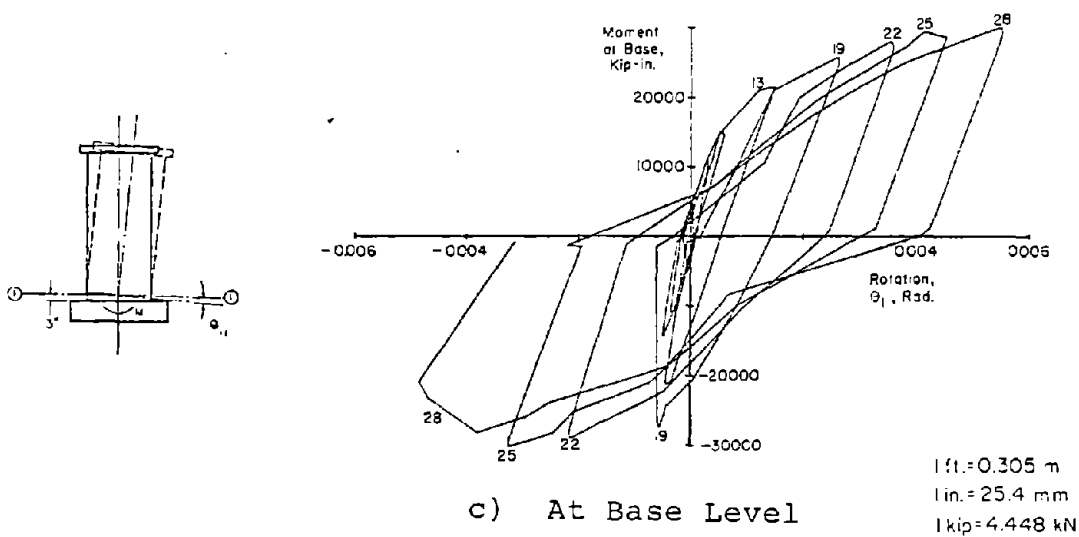
Fig. B-162   Moment at Base versus Rotation
               for Specimen B5R

B-197

top deflection. Cycle 25 in B5R and Cycle 28 in B5 correspond
to the 5-in. (127.0 mm) deflection increment.

For negative direction loading the stiffness in B5R was
very similar to that in B5. The initial stiffness was
somewhat lower. However, after Cycle 19, an envelope
through the peak points of the negative halves of the loops
for B5R was nearly identical to a similar envelope for B5.
Also, there was noticeably less pinching in the negative
half of the loops in B5R compared to those in B5.

Shear-Distortion. The shear distortion loops for B5R
are shown in Fig. B-163. A comparison of shear-distortion
data for B5R and B5 shows that the initial stiffness in B5R
was considerably lower. In the latter inelastic cycles, the
shear distortions in B5R were considerably lower than those
in B5 for equal top deflections. However, the shear distor-
tions in B5R and B5 were approximately equal for equal cycle
numbers. There was, however, noticeably less pinching in
the shear-distortion loops for B5R as compared to those for
B5.

Slip at Construction Joints. The slip at construction
joints in B5R is shown in Fig. B-164. A comparison of the
slip data for B5R and B5 shows that, in the inelastic cycles,
the slip at CJ1 in B5R is considerably greater than that in
B5. This is true whether the comparison was made by equal
top deflection or equal cycle numbers. Also, there was
noticeably less pinching in the B5R loops as compared to
that in B5. As shown in Fig. B-165, the slip at CJ1 was an
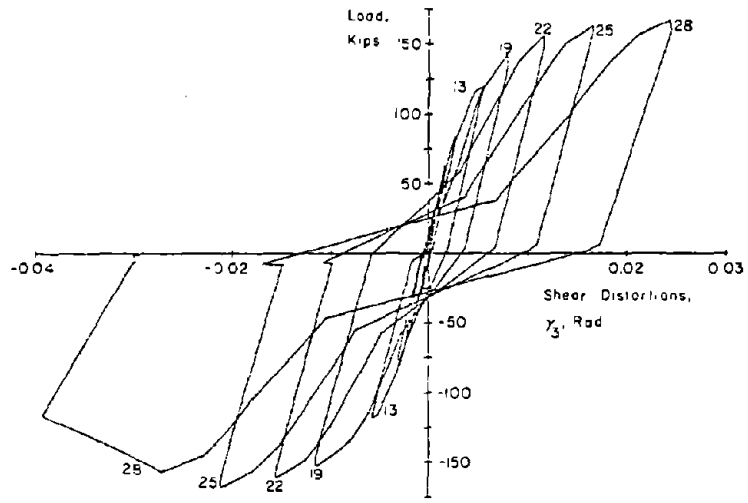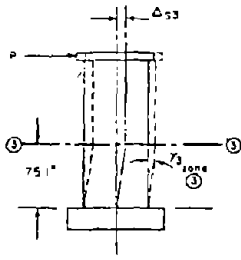
a) In Base to 6 ft Level
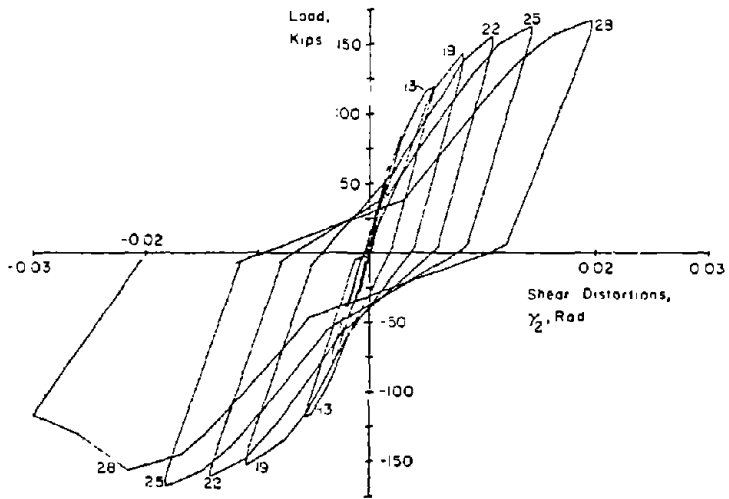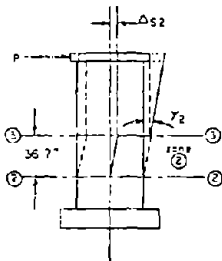
b) In 3 ft to 6 ft Level
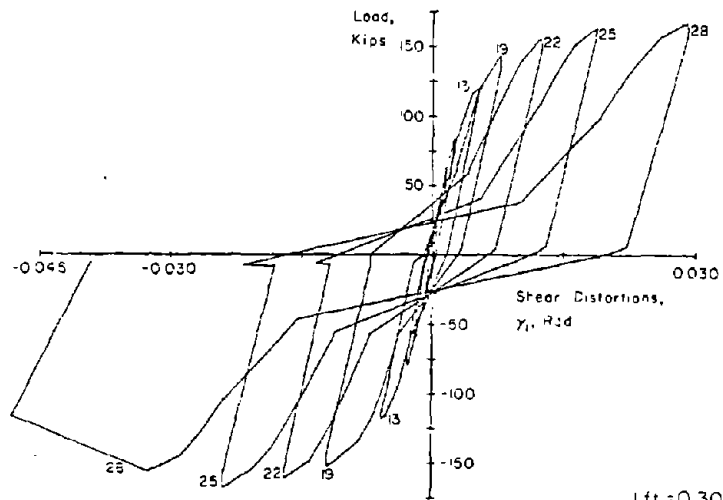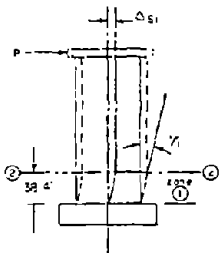
c) In Base to 3 ft Level

1 ft.=0.305 m
1 in.=25.4 mm
1 kip=4.448 kN

Fig. B-163   Load versus Shear Distortion
             for Specimen B5R
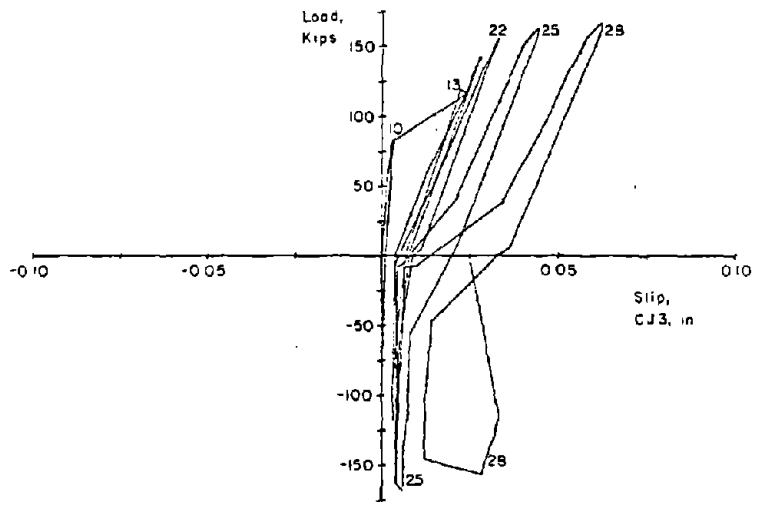
a)   At 6 ft. Level
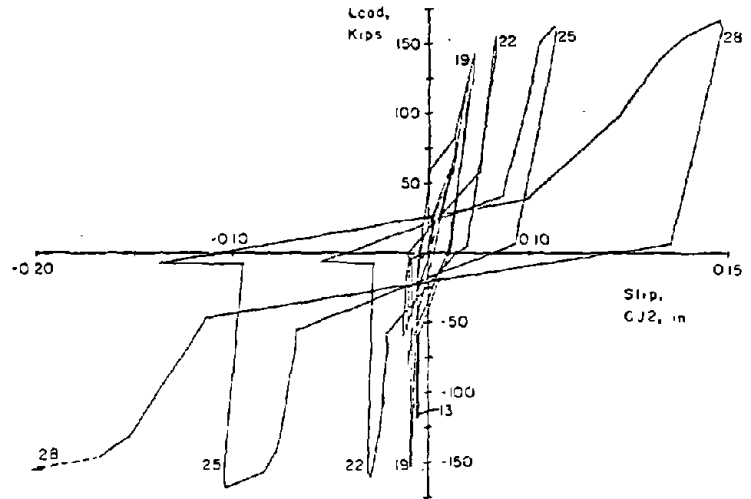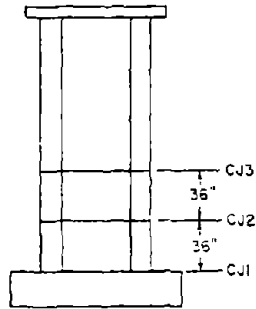
b)   At 3 ft. Level
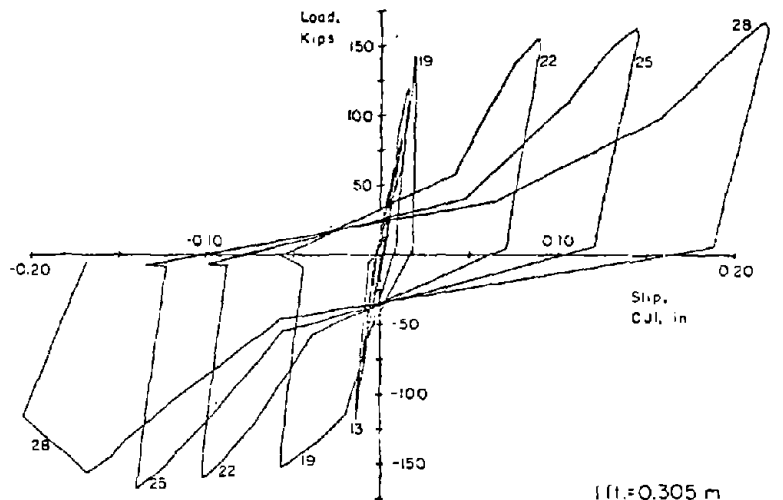
c)   At Base Level

1 ft.=0.305 m
1 in.=25.4 mm
1 kip=4.448 kN

Fig. B-164   Load versus Slip at Construction Joints
             for Specimen B5R
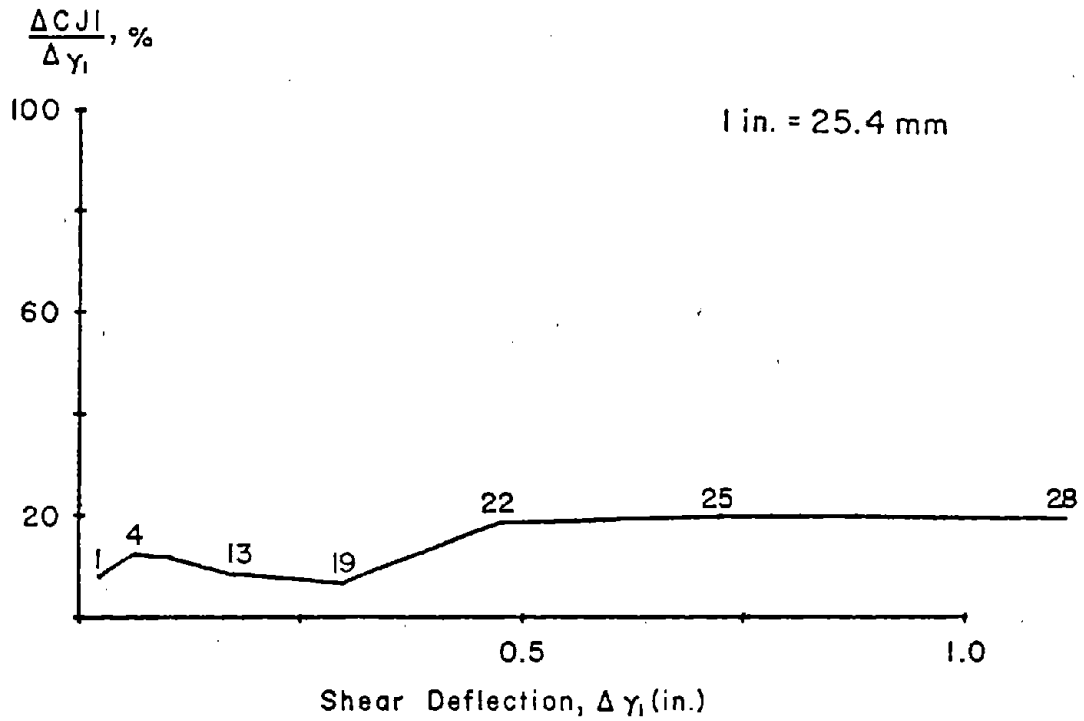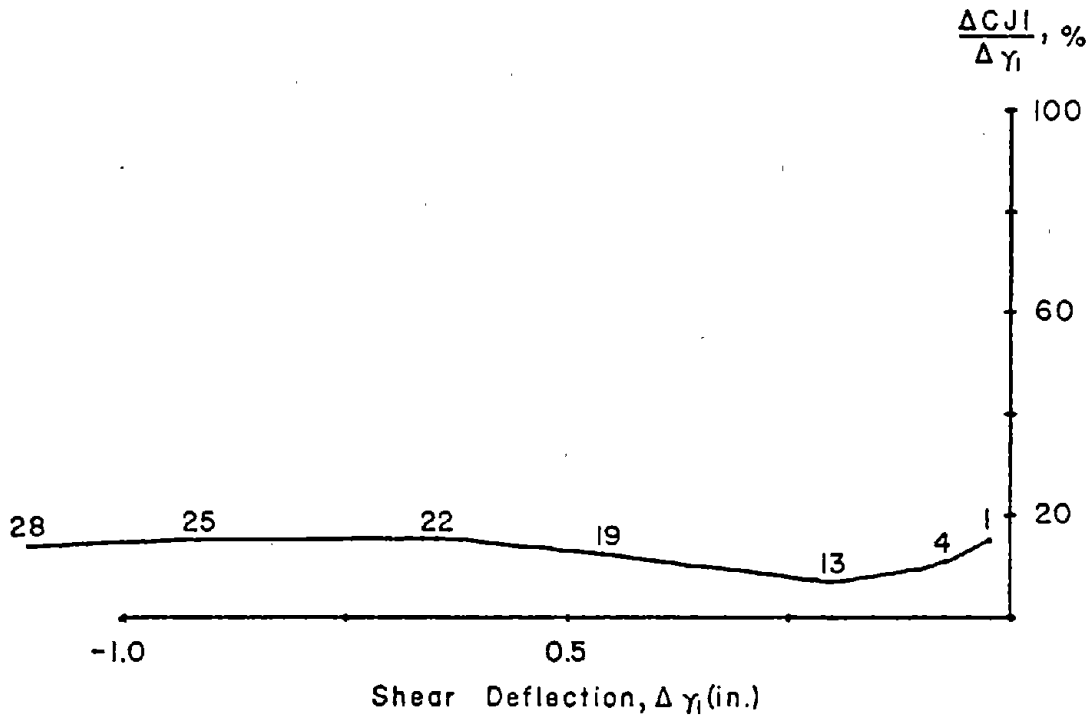
Fig. B-165   Slip at Base Construction Joints versus
             Shear Deflection in Zone 1 for Specimen B5R

approximately constant 20% of the total shear deflection in the lower 3 ft (0.91 m).

The data at CJ2 for B5R indicated considerable slip occurring after Cycle 19. This corresponded with the cracking and joint deterioration noted visually during the test.

Deflections. The deflection components and deflected shapes are shown in Figs. B-166 and B-167. These figures show that deflections in B5R were similar to deflections in B5.

The average increase in shear deflection between Cycle 22 and 24 was 10% in B5R as compared to 15% in B5.

a)   At Top of Wall

b)   At 6 ft. Level

CALCULATED FROM
        MEASURED DEFORMATION
---- EXTRAPOLATED
—— MEASURED TOTAL
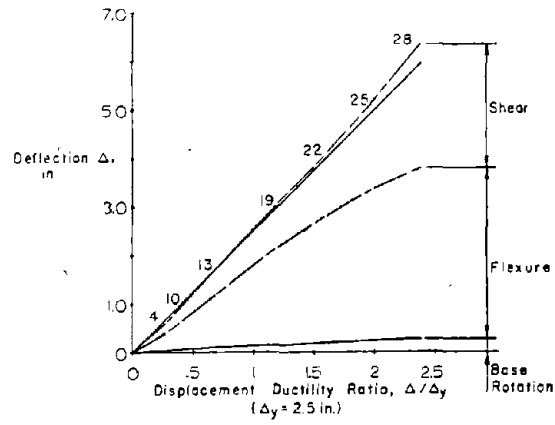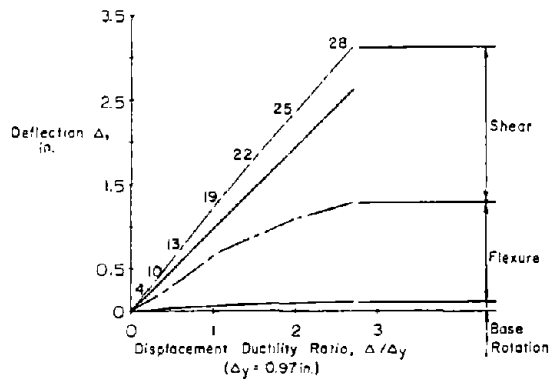
1 in. = 25.4 mm
1 ft = 0.305 m

c)   At 3 ft. Level
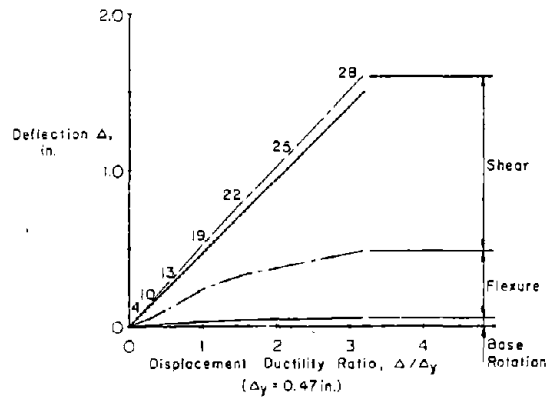
Fig. B-166   Component of Deflection for Specimen B5R

a) Flexural
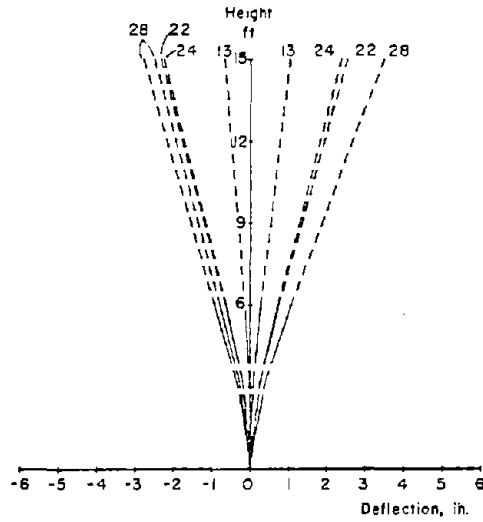
b) Shear
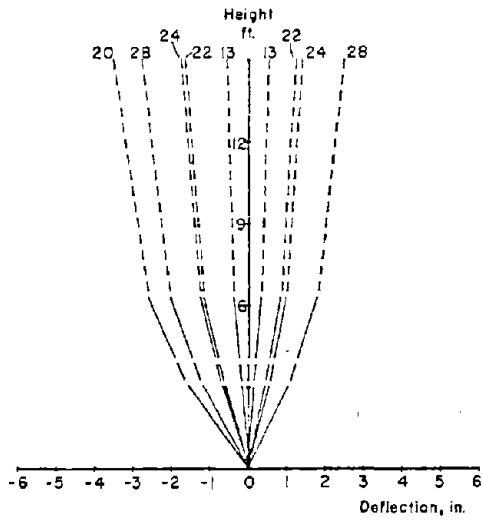
CALCULATED FROM
MEASURED DEFORMATION
EXTRAPOLATED
MEASURED TOTAL

1 in.= 25.4 mm
1 ft.= 0.305 m

W. C. – WEB CRUSHING

AFTER W. C.

PRIOR TO W.C.

c) Total
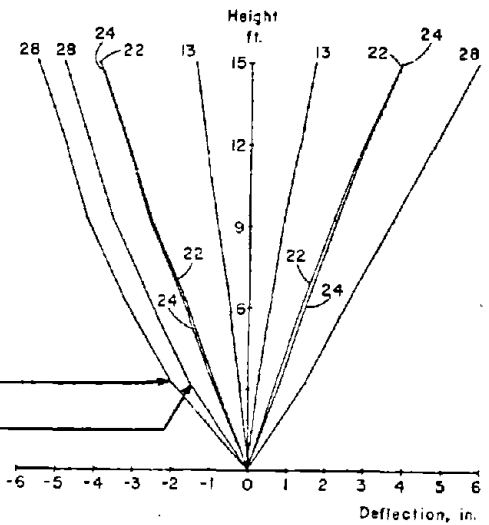
Fig. B-167 Deflected Shape for Specimen B5R

Sepcimen F1

◊ Test Description

Specimen F1 had a flanged cross-section with 3.89% reinforcement in each flange. The flange was considered the boundary element and detailed as a compression column. The lateral tie arrangement was not designed as or intended to be confinement reinforcement. However, due to the close spacing of both the vertical and horizontal bars, considerable confinement or at least containment of the concrete was provided by this tie arrangement.

The test consisted of 25 loading cycles as shown in Fig. B-168. The complete load versus top deflection relationship for F1 is shown in Figs. B-169 and B-170.

First significant cracking was observed in Cycle 4 at a load of 39 kips (173.5 kN). First yielding occurred in Cycle 13 at a load of 150.6 kips (669.9 kN). The maximum measured crack width in the web at this stage was 0.018 in. (0.46 mm).

The crack pattern that developed in the lower 6 ft (1.83 m) was similar to the patterns in B2, B5 and B5R with the following exception. The focal point of the "fan" pattern was slightly lower in F1. Also, the cracks in F1 converged closer together in the 4-in. (101.6 mm) web near the base than did the cracks in the barbell sections. The crack pattern is shown in Figs. B-171 and B-172 at +3-in. (76.2 mm) and -3-in. deflection, respectively.

a)   Load History

1 in. = 25.4 mm
1 kip = 4.448 kN
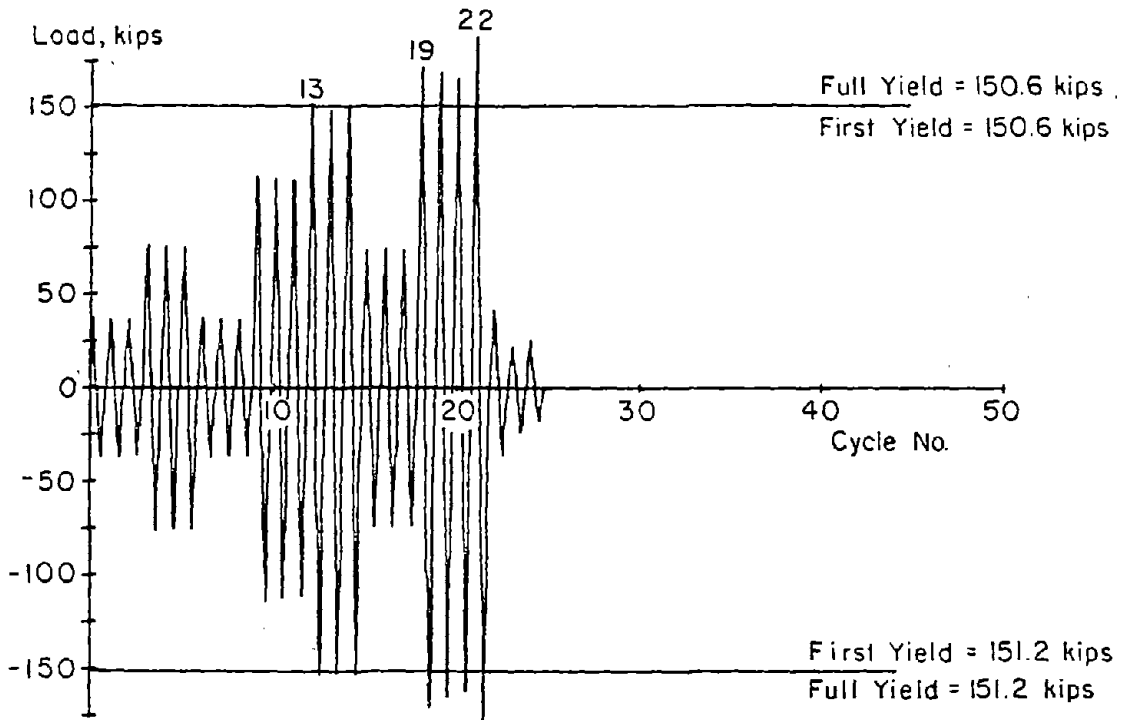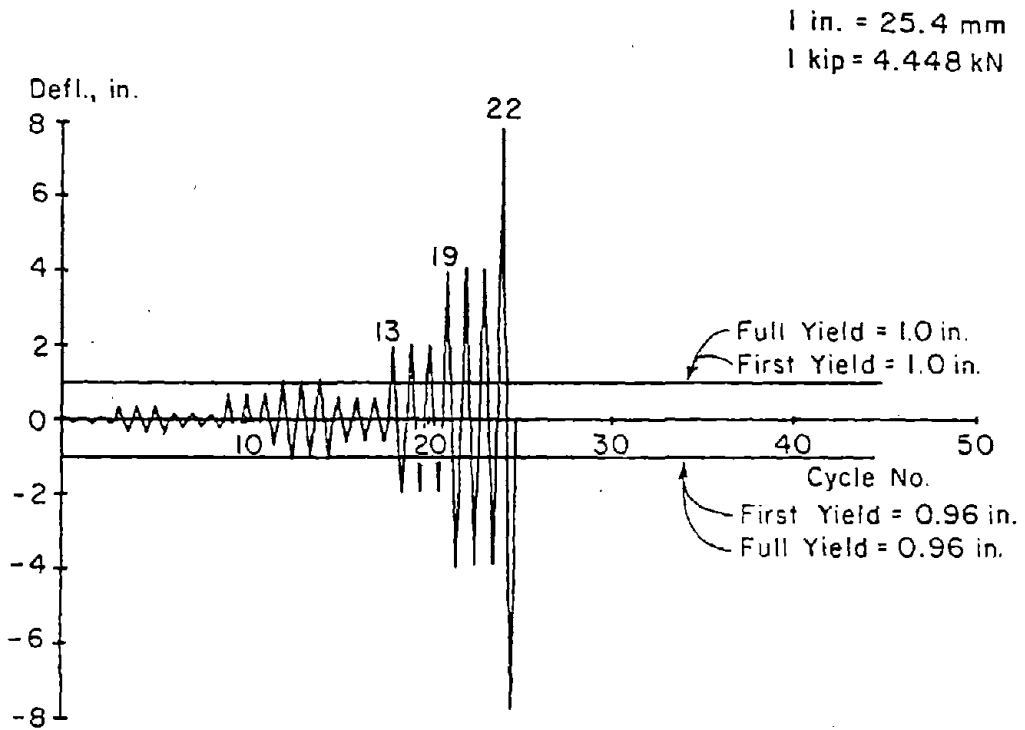
b)   Deflection History

Fig. B-168   Loading History for Specimen F1

B-206
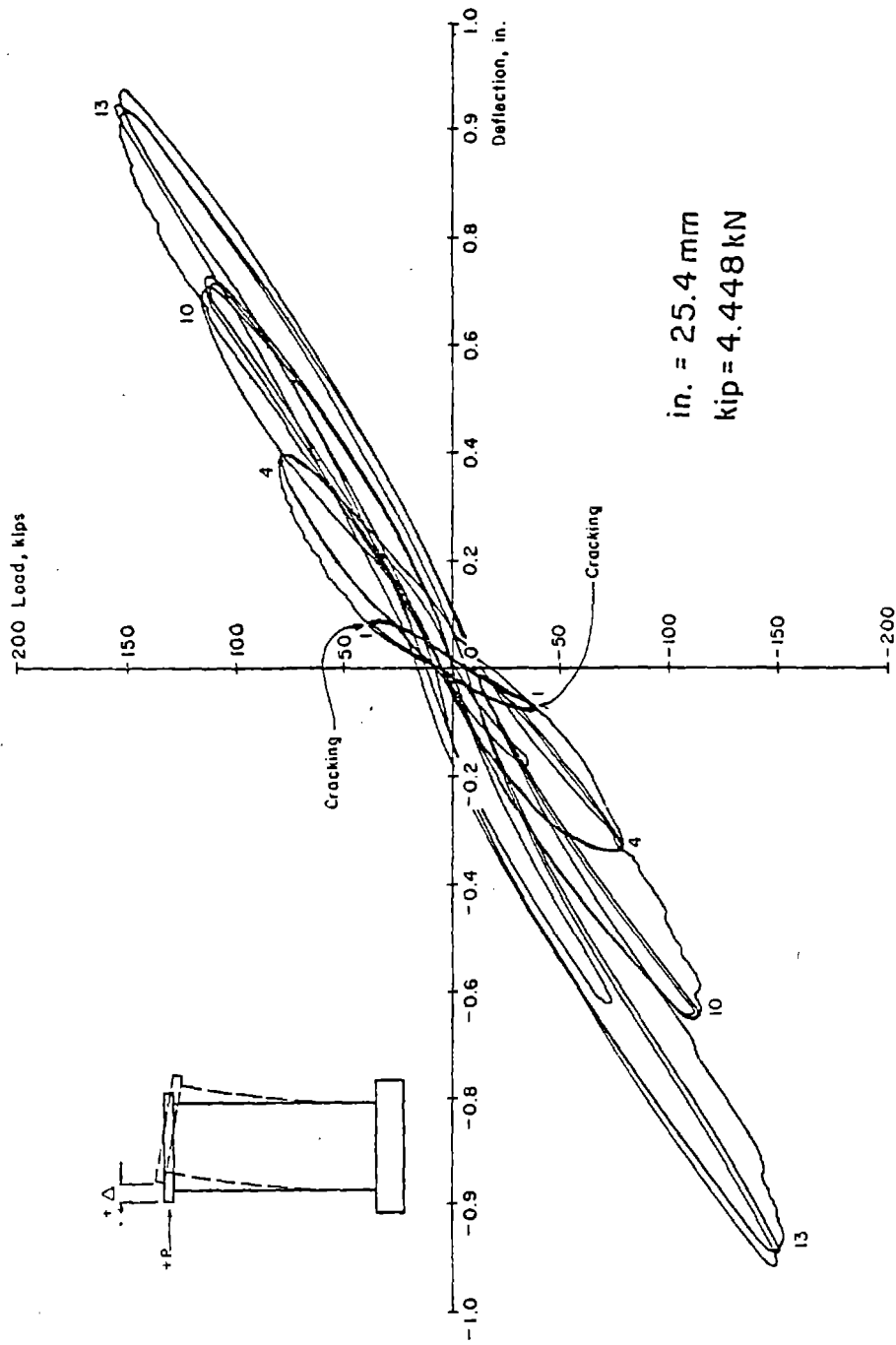
Fig. B-169 Continuous Load-Deflection Plot for
Initial Cycles for Specimen F1
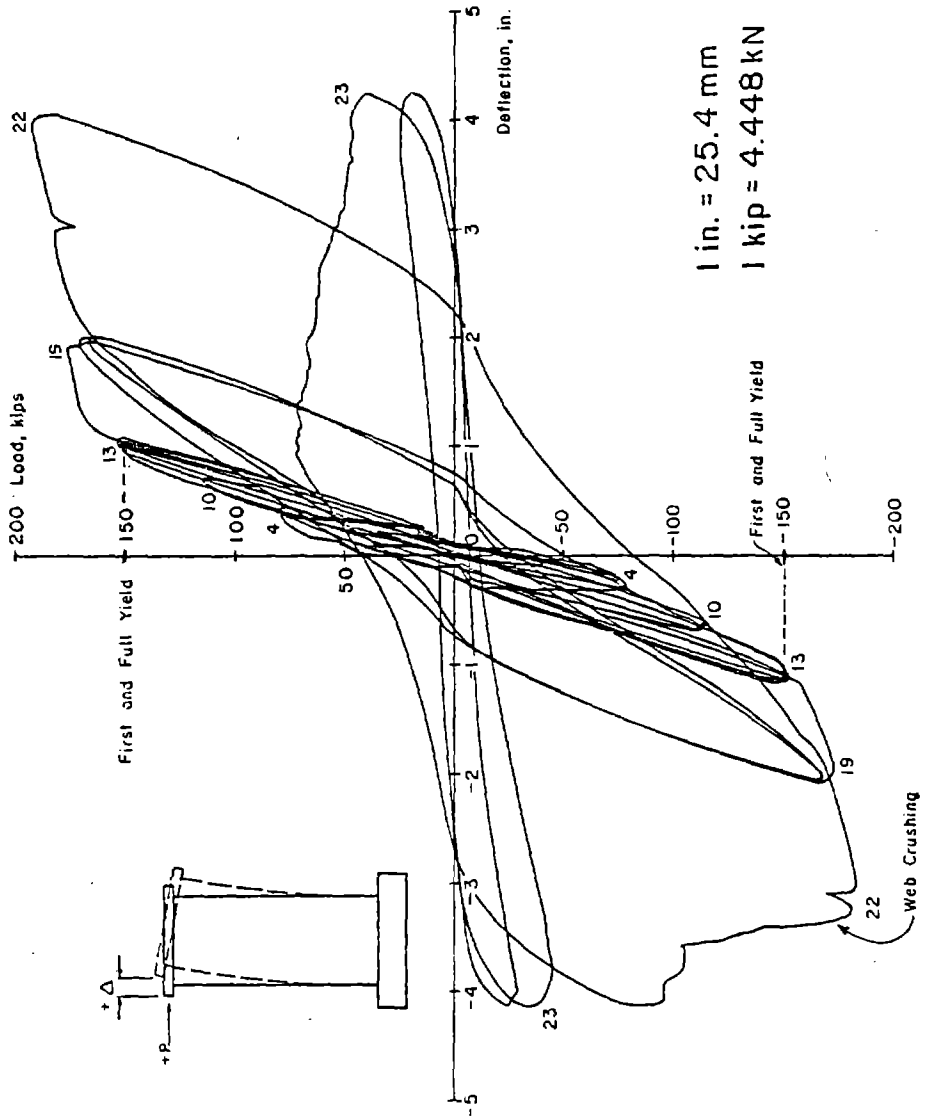
Fig. B-170 Continuous Load-Deflection Plot for Specimen F1
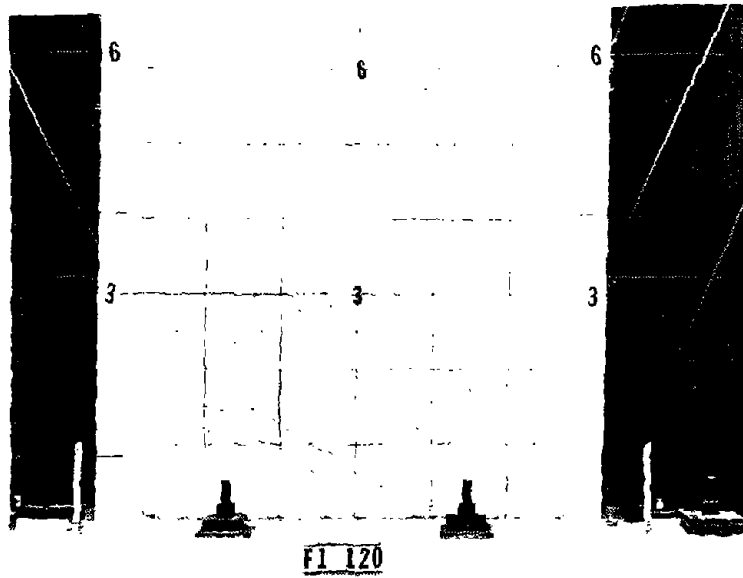
Fig. B-171   Cracking Pattern at +3 in. Deflection
             for Specimen Fl
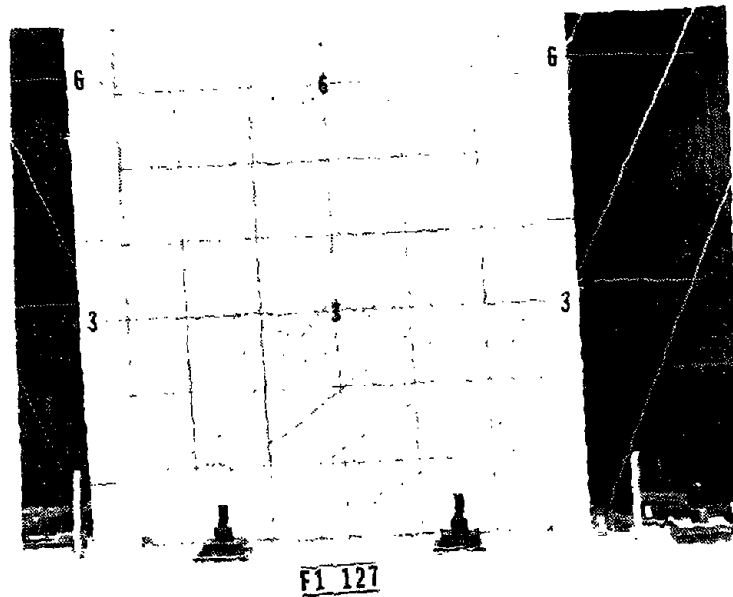
Fig. B-172   Cracking Pattern at -3 in. Deflection
             for Specimen Fl

Spalling and flaking along the construction joints and diagonal cracks in the lower 3 ft (0.91 m) were noted in Cycle 20, the second 2-in. (50.8 mm) deflection cycle. Also in Cycle 20, horizontal movement of the web caused a bowing of the flanges in a horizontal plane from 1 to 2 ft (0.30 to 0.61 m) above the base. This bowing caused the vertical cracking in the outer faces of the flange shown in Fig. B-173.

Specimen F1 was the first specimen tested in the experimental program. The original load history included increasing the deflection increments by 2 in. (50.8 mm) in each new increment. Therefore, after the ± 2 in. loading increment, the specimen was loaded to 4 in. (101.6 mm).

The maximum load measured, 187.9 kips (835.8 kN), occurred in Cycle 22 at a +4-in. deflection. This corresponds to a nominal shear stress, $v_{max} = 10.5\sqrt{f_c'}$ ($0.87\sqrt{f_c'}$, MPa). The maximum measured crack width in the web at this stage was 0.125 in. (3.18 mm).

While loading the specimen to a -4-in. deflection, the steepest diagonal strut that intercepted the base crushed and slipped along a crack from the opposite direction loading at a point 1 ft (0.30 m) above the base. The flange hinged to allow this slip. This immediately transferred additional load to lower struts. These struts then simultaneously slipped and crushed along a horizontal plane 1 ft above the base. The wall immediately before and after web crushing is shown in Figs. B-172 and B-174.

Fig. B-173   Cracking Pattern in Flange
of Specimen F1

F1 129
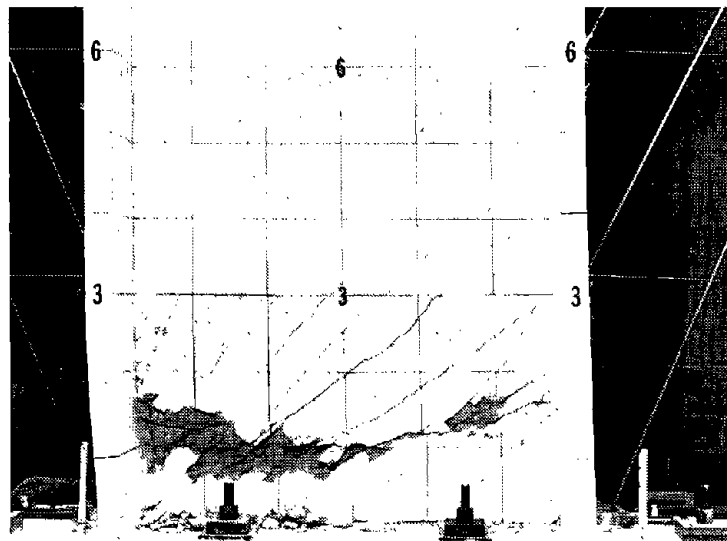
Fig. B-174   Specimen F1 After Web Crushing

The specimen sustained at least 80% of the maximum measured load capacity through 6 inelastic cycles. The last inelastic load increment in which the load was sustained at or above 80% of the maximum for all 3 cycles was at ± 2 in.

Within the final 4-in. deflection cycle the specimen sustained the load through the +3-in. and -3-in. deflections. It is suspected that the specimen would have maintained the load capacity through a ± 3-in. deflection increment.

Discussion of Results

Moment-Rotation. The moment-rotation data for F1 is shown in Fig. B-175. The measured maximum moment was 77% of the calculated monotonic.

The relationship between the calculated monotonic and measured rotations at the 3-ft (0.91 m) level differs slightly from that relationship at the 6-ft (1.83 m) level. The difference indicates that a larger portion than the assumed effective distribution of curvature should have been concentrated in the lower 3 ft of the wall.

The maximum measured loads in Cycles 13, 19 and 22 exhibit "strain hardening" after yield.

The rotation data for Cycle 22 at the base level exhibits pinching while the data at the 3-ft and 6-ft levels do not.

Shear-distortion. The shear distortion loops for F1 are shown in Fig. B-176. As in the other specimens, shear
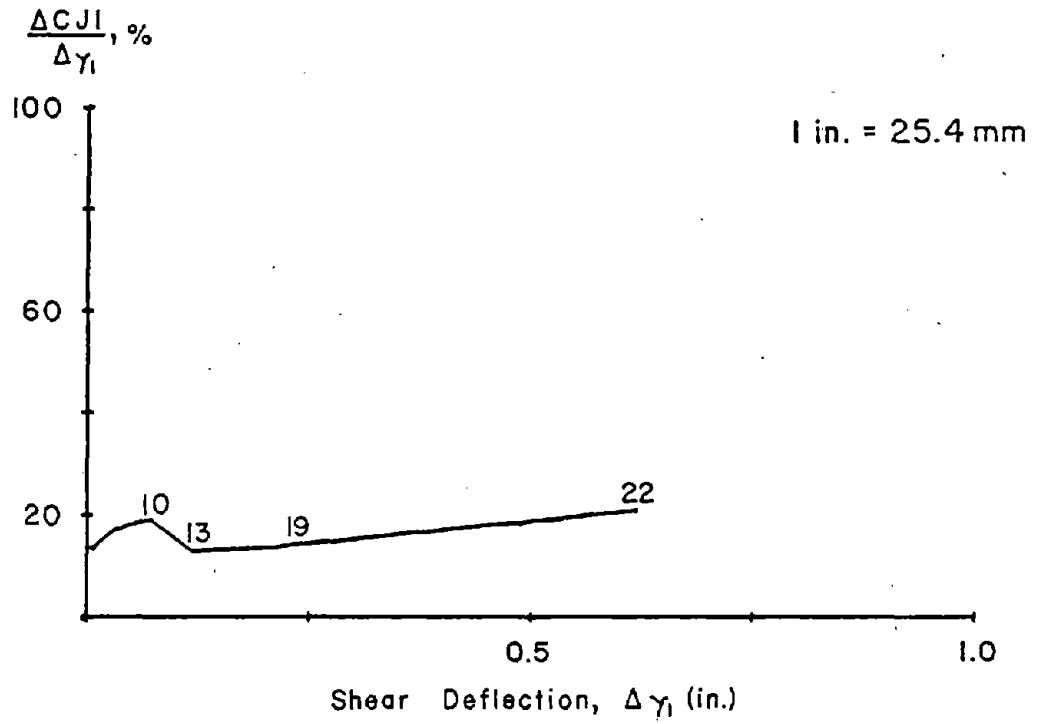
a) At 6 ft. Level
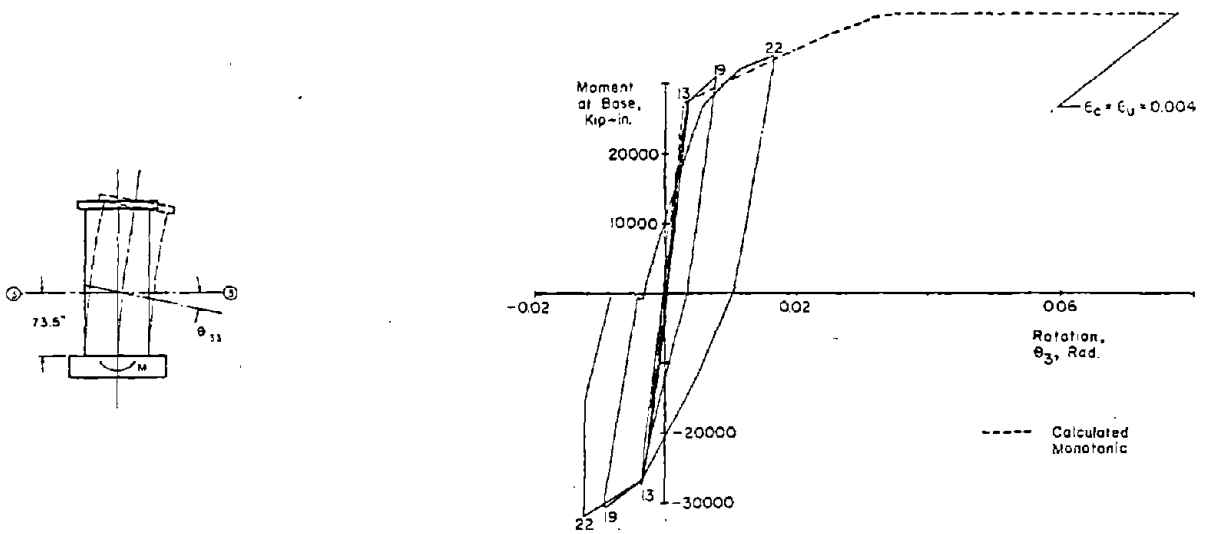
b) At 3 ft. Level
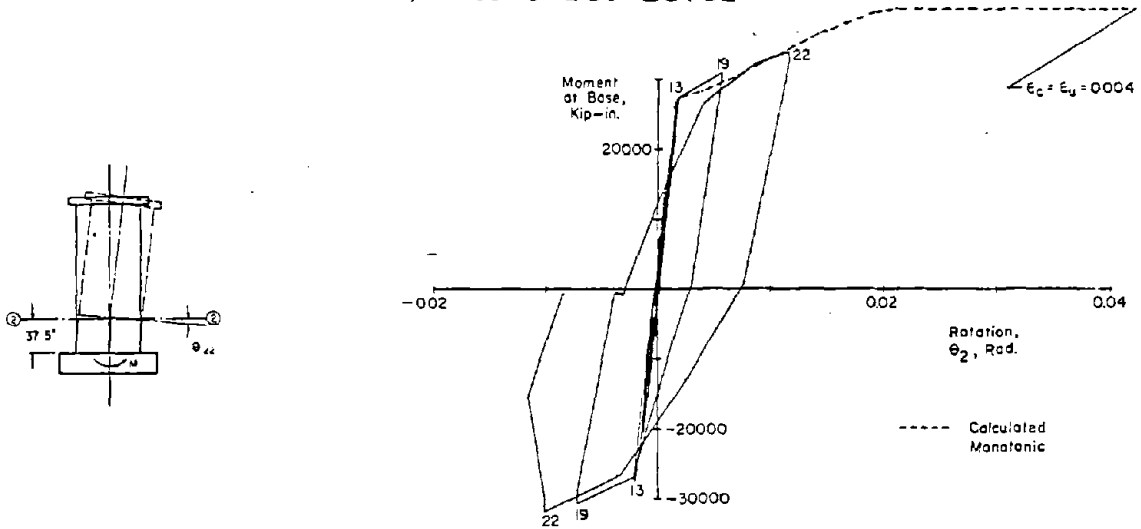
c) At Base Level
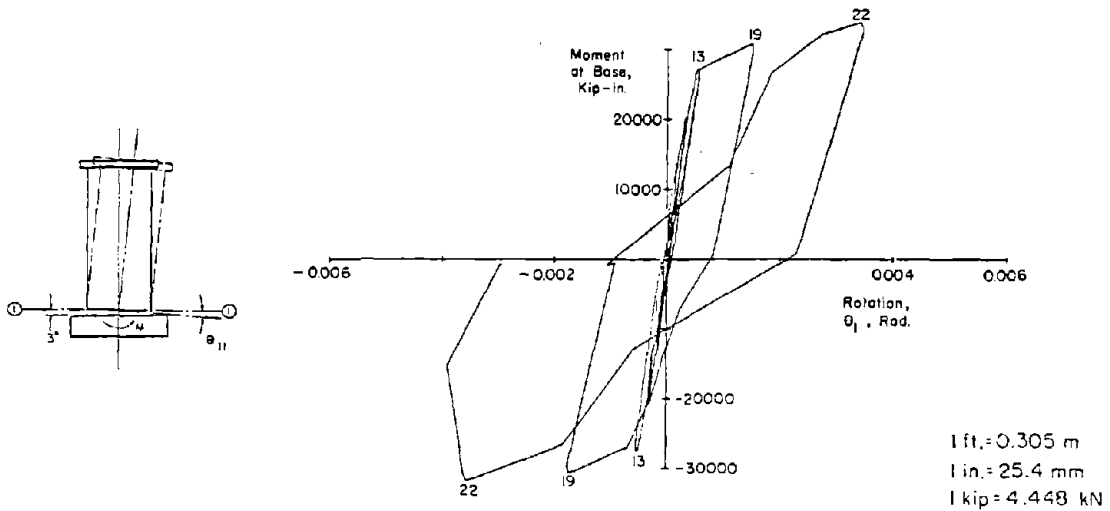
1 ft.= 0.305 m
1 in.= 25.4 mm
1 kip = 4.448 kN

Fig. B-175   Moment at Base versus Rotation
for Specimen F1
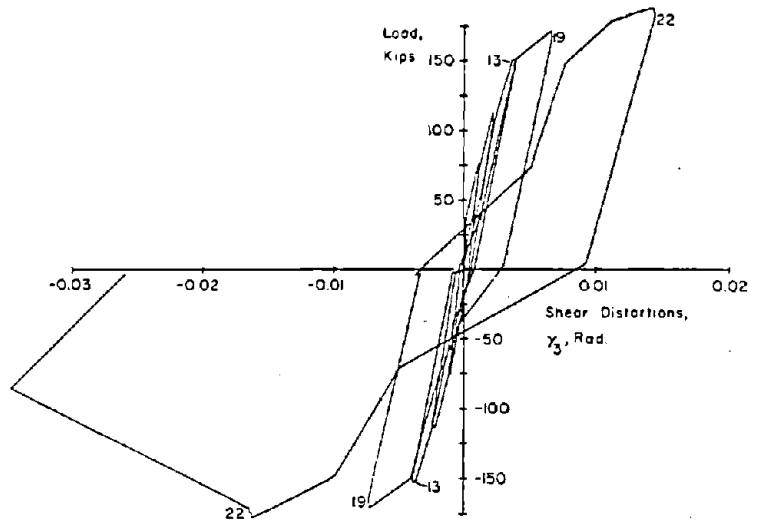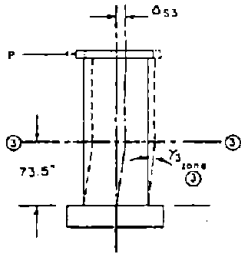
B-213

a) In Base to 6 ft LEVEL
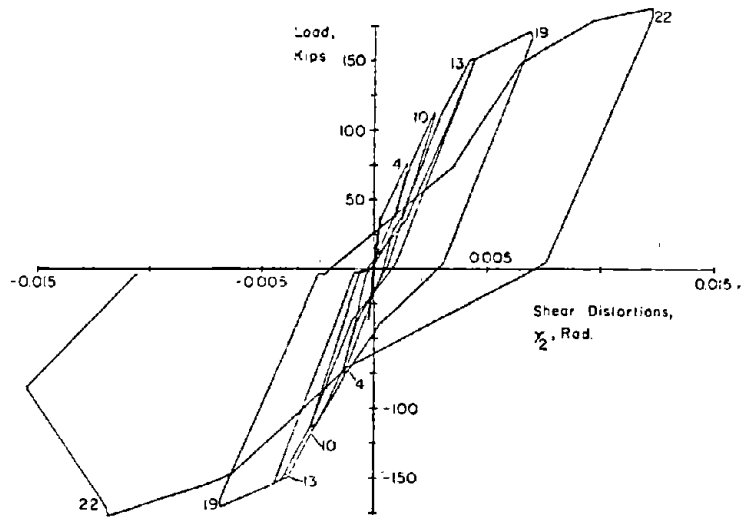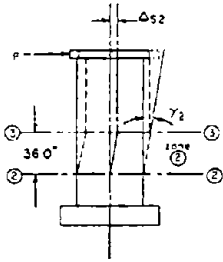
b) In 3 ft to 6 ft Level
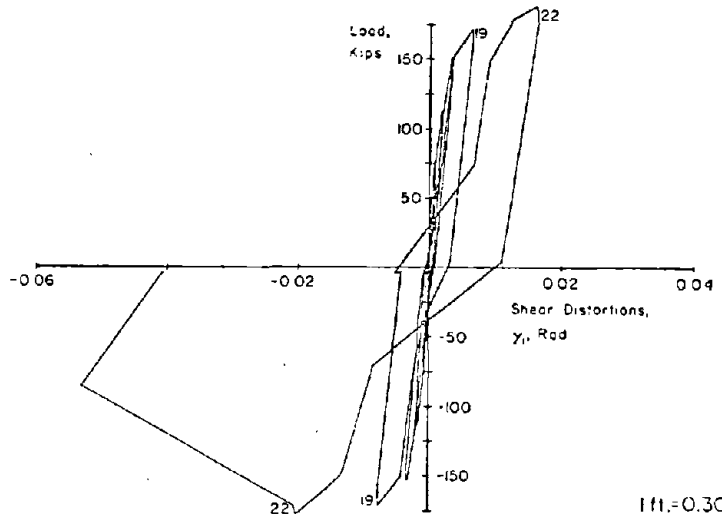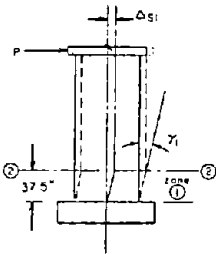
1 ft.=0.305 m
1 in.=25.4 mm
1 kip=4.448 kN

c) In Base to 3 ft Level

Fig. B-176   Load versus Shear Distortion
              for Specimen F1

"yielding" occurred during the same cycle in which flexural yielding occurred.

The maximum measured load in F1 corresponded to a shear stress of $10.5\sqrt{f'_c}$ ($0.87\sqrt{f'_c}$, MPa). With a shear reinforcement design similar to B2, assuming an ultimate stress of 100 ksi in the horizontal steel, the steel shear capacity would be only $9.7\sqrt{f'_c}$ ($0.80\sqrt{f'_c}$, MPa). This indicates that the concrete contribution must have been <u>at least</u> $0.8\sqrt{f'_c}$ ($0.07\sqrt{f'_c}$, MPa) shear at maximum load.

The pinching of the loops was more evident in Zone 1.

<u>Slip at Construction joints</u>. The slip at construction joints in F1 is shown in Fig. B-177. The slip at CJ1 exhibited a "yielding" during the same cycle in which flexural yielding occurred. As shown in Fig. B-178, the slip at CJ1 is between 15% and 25% of the total shear deflection in the lower 3 ft (0.91 m). This percentage was increasing with the numbers of inelastic cycles.

The slip at CJ2 was somewhat erratic and probably was affected by diagonal cracks. The slip at CJ3 was negligible.

<u>Deflections</u>. The deflection components and deflected shapes are shown in B-179 and B-180. These figures show that shear deflections were approximately the same percentage of the total as they were in B2 and B5 at equivalent displacement ductilities. The deflected shapes for Cycles 19 and 21 showed a small increase in shear deflections during the 2-in. (50.8 mm) increment.
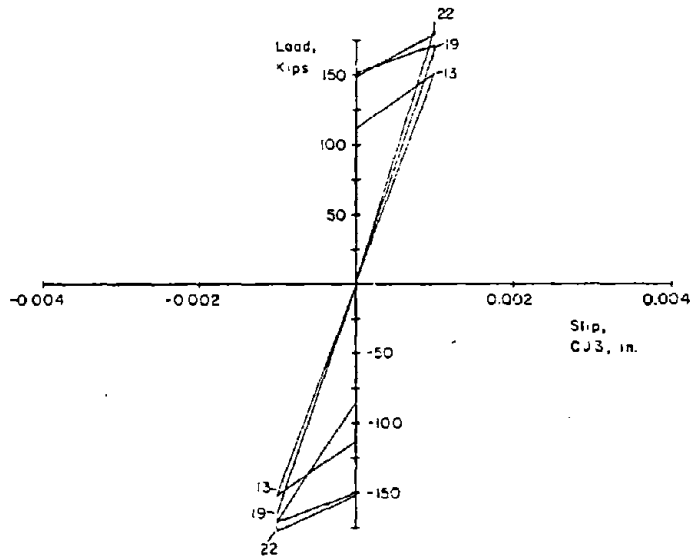
a)   At 6 ft. Level
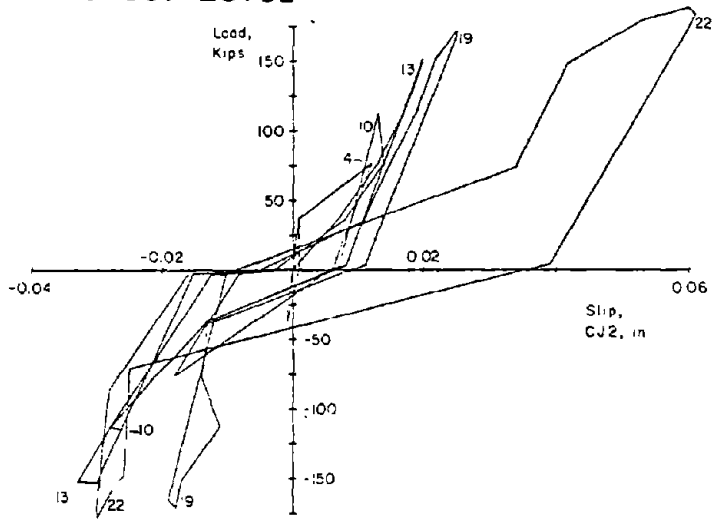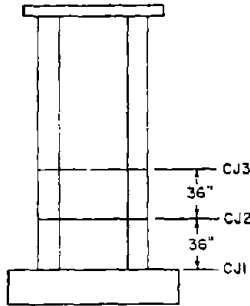
b)   At 3 ft. Level
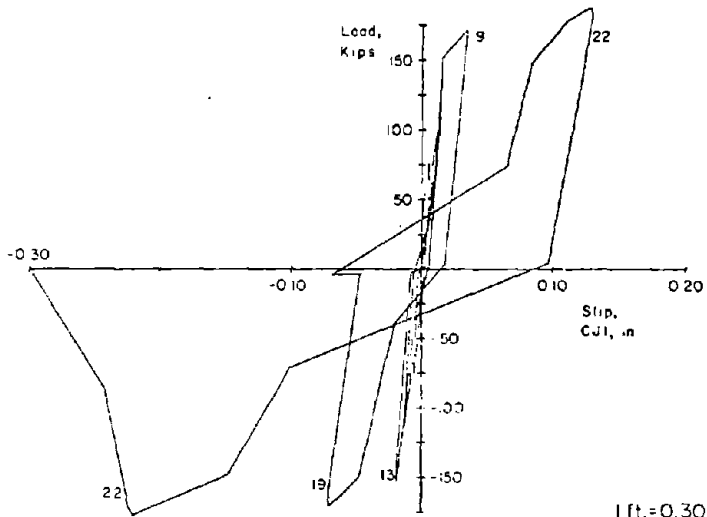
c)   At Base Level

1 ft.= 0.305 m
1 in.= 25.4 mm
1 kip= 4.448 kN

Fig. B-177   Load versus Slip at Construction Joints
             for Specimen F1

a) At Maximum Positive Loads
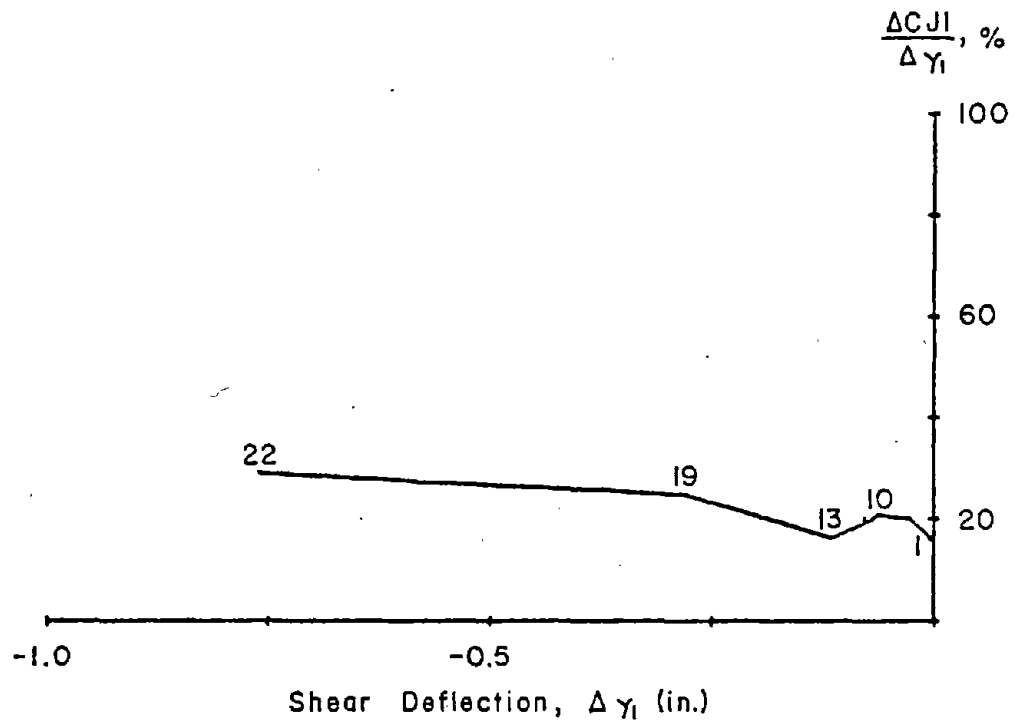
b) At Maximum Negative Loads

Fig. B-178   Slip at Base Construction Joint versus
             Shear Deflection in Zone 1 for Specimen F1

a) At Top of Wall
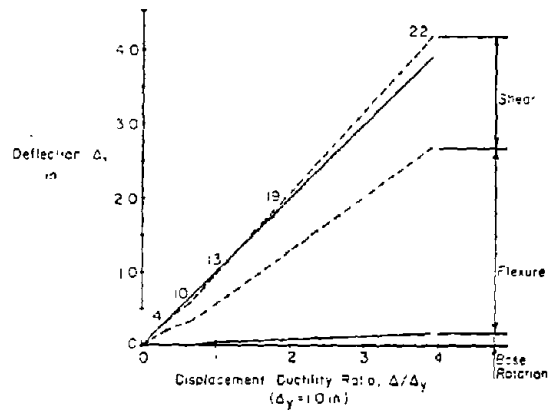
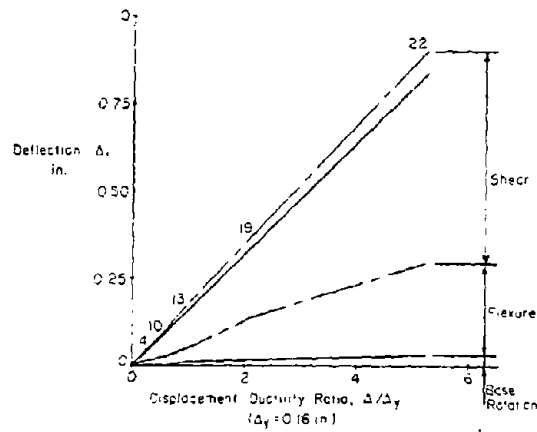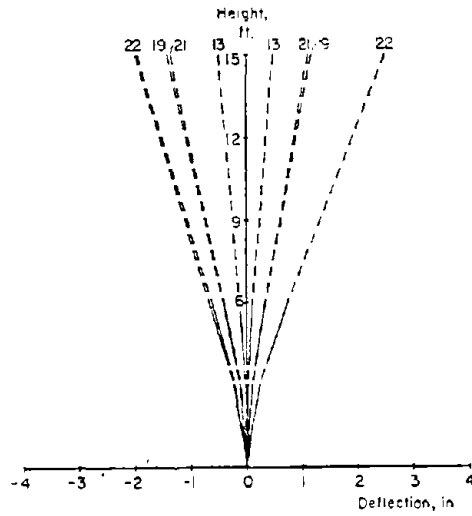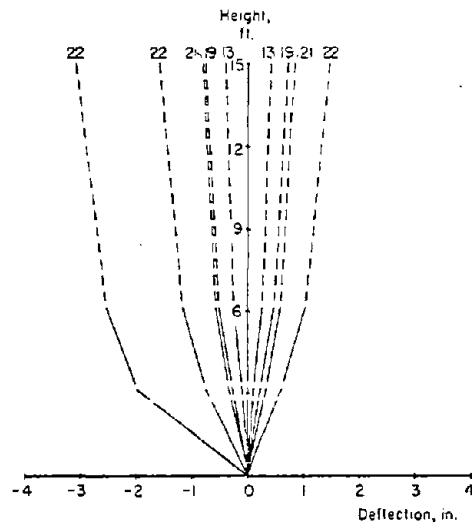b) At 6 ft. Level
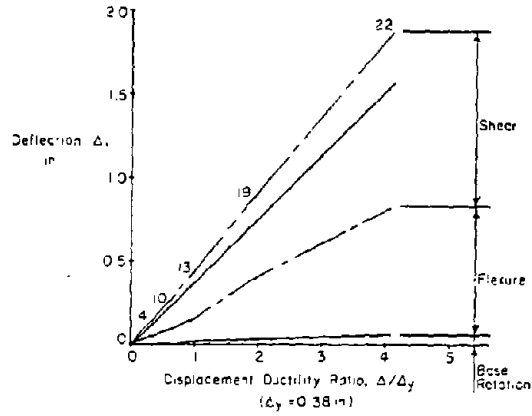
c) At 3 ft. Level

Fig. B-179 Component of Deflection for Specimen F1

a) Flexural

b) Shear

— - — CALCULATED FROM
         MEASURED DEFORMATION
— — — EXTRAPOLATED
———— MEASURED TOTAL

1 in. = 25.4 mm
1 ft. = 0.305 m

W. C. – WEB CRUSHING

AFTER W. C.

PRIOR TO W. C.

c) Total
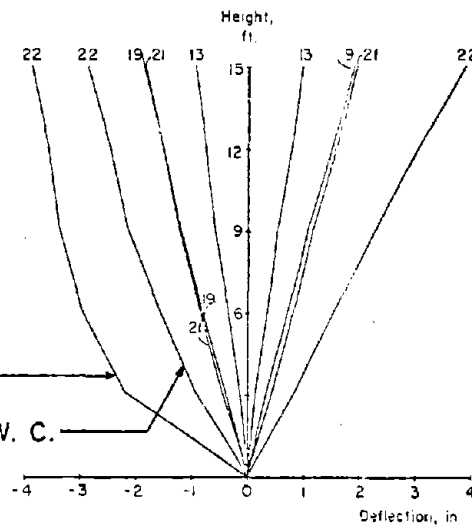
Fig. B-180 Deflected Shape for Specimen F1

Reinforcement Strains. Figures B-181 through B-191
show reinforcement strains in the specimen at various stages.

Figure B-181 shows that the flanges started growing
between Cycles 13 and 22. Figure B-182 shows that yielding
in the vertical bars had extended to the 6-ft (1.83 m) level
in Cycle 22.

Figures B-186 and B-187 show that horizontal bar strains
did not significantly exceed the yield strain until Cycle 22.
In Cycle 22, the strains only reach high levels in the 3-ft
(0.91 m) region.

Figures B-190 and B-191 show that prior to yielding,
the vertical bar strains in the tension flanges exhibited no
evidence of shear lag across the flange.
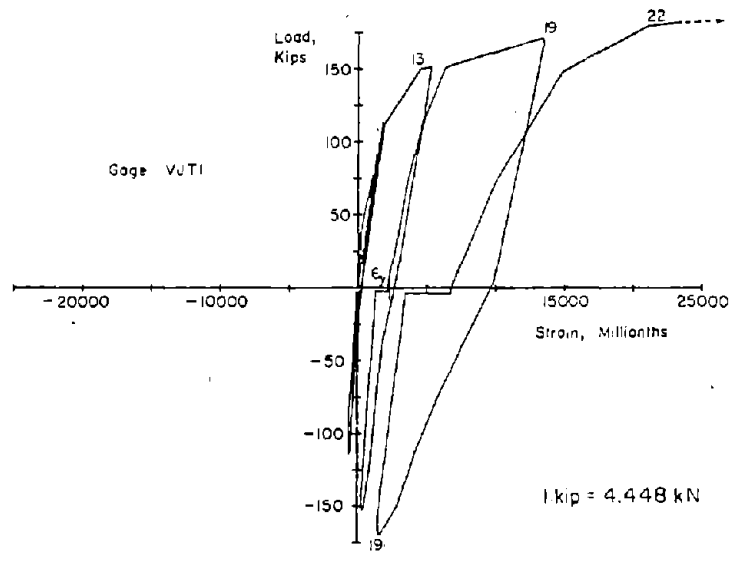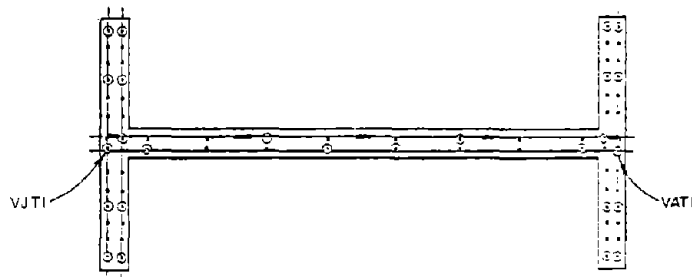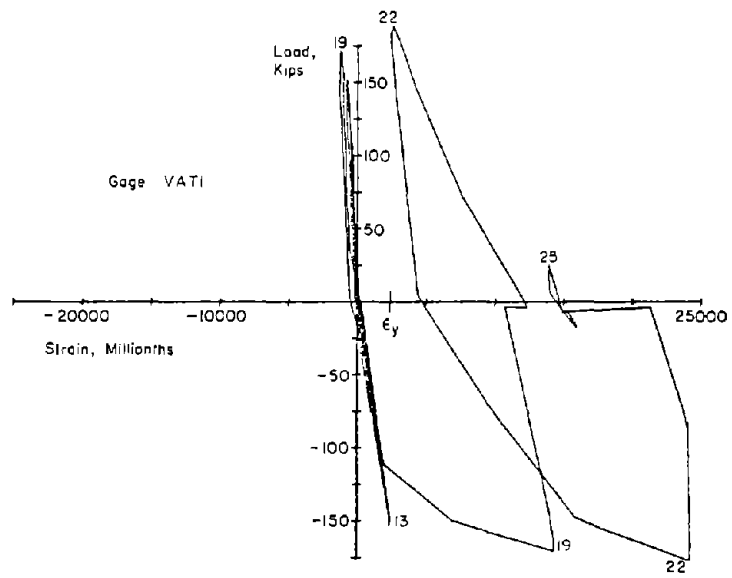
Fig. B-181   Measured Strain on Vertical Reinforcement
at Base of Specimen F1
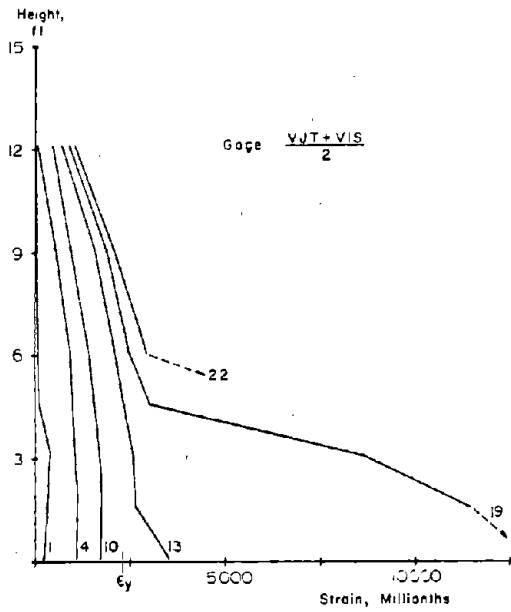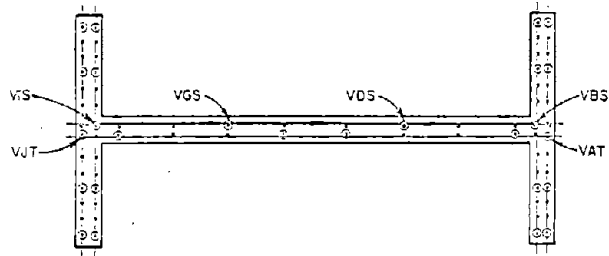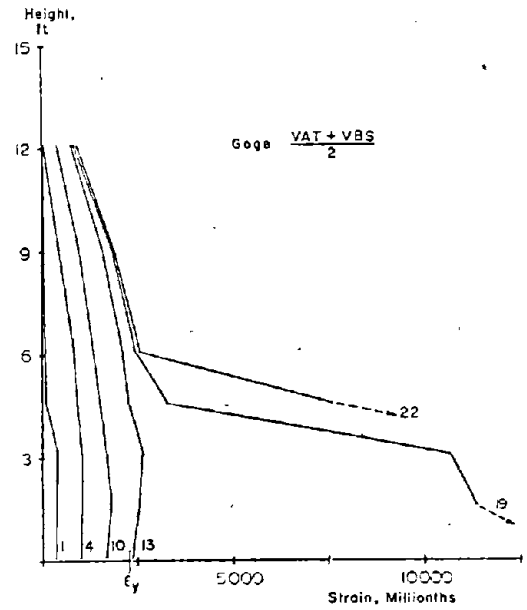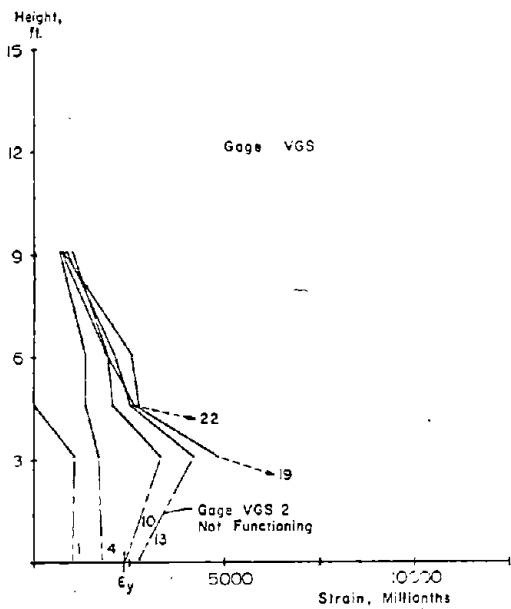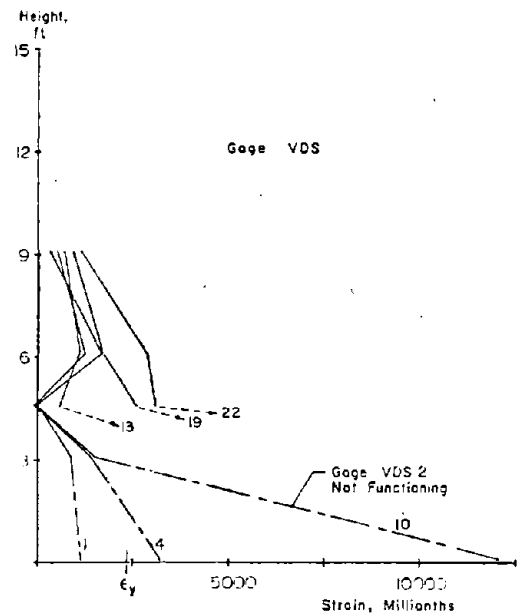
Fig. B-182 Vertical Reinforcement Strains at
Maximum Loads for Specimen Fl

a)   At 6 ft. Level

1 ft.=0.305 m

b)   At 3 ft. Level
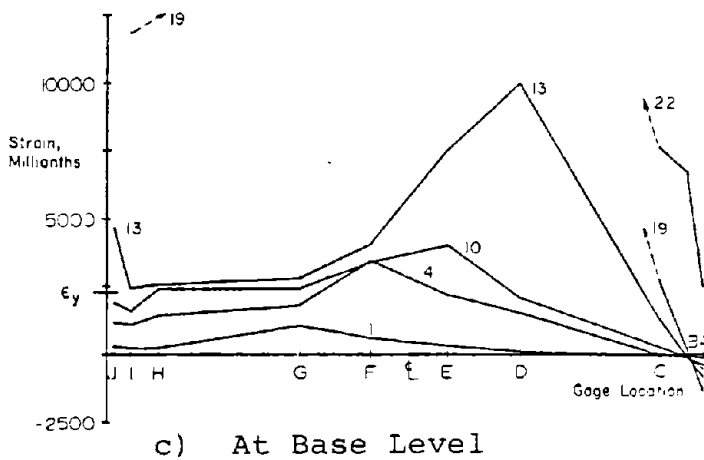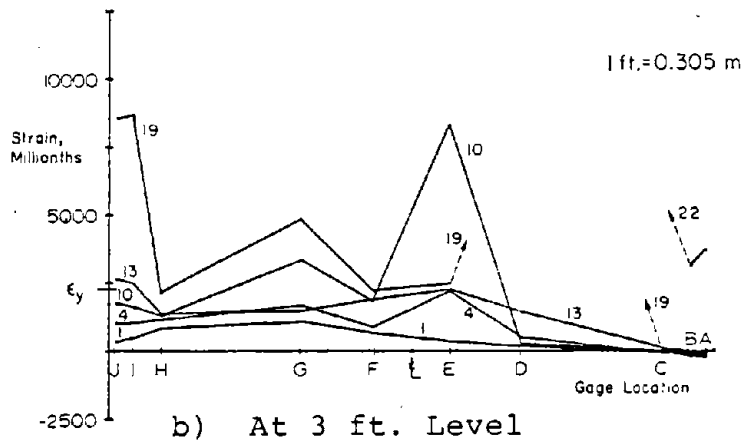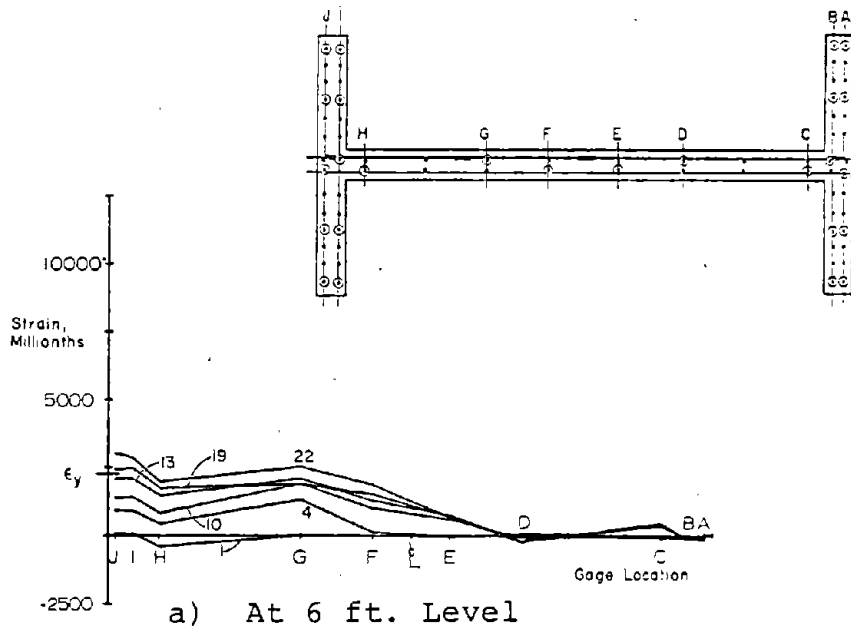
c)   At Base Level

Fig. B-183   Vertical Reinforcement Strains at
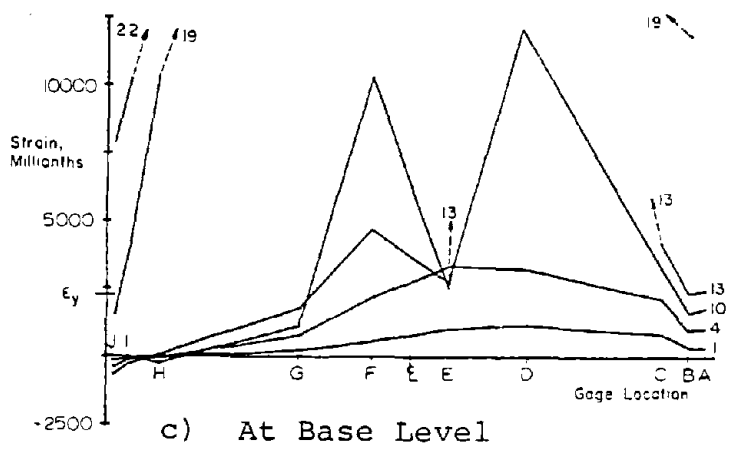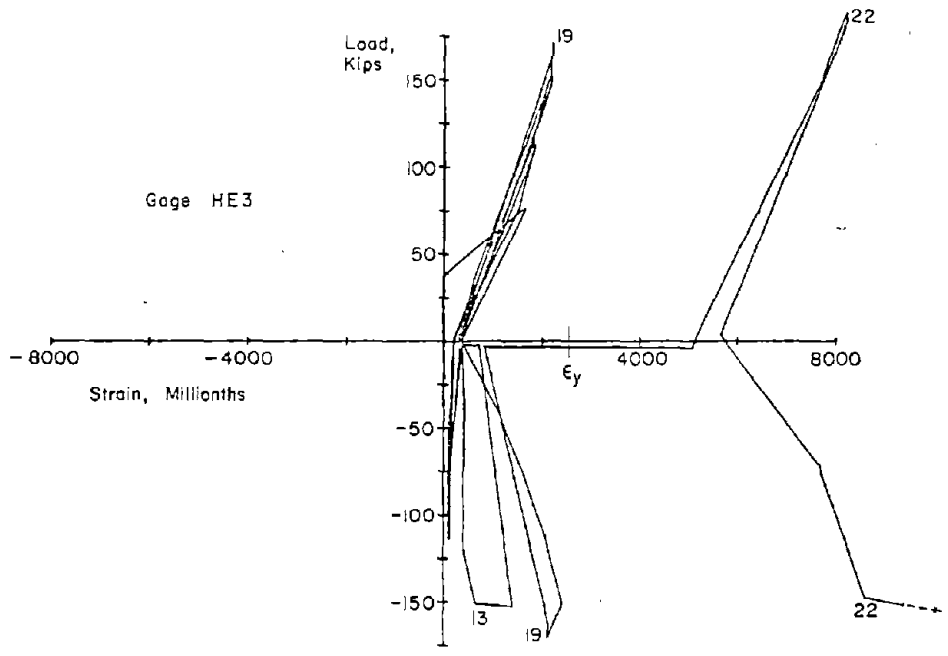Maximum Positive Loads for Specimen F1

B-223
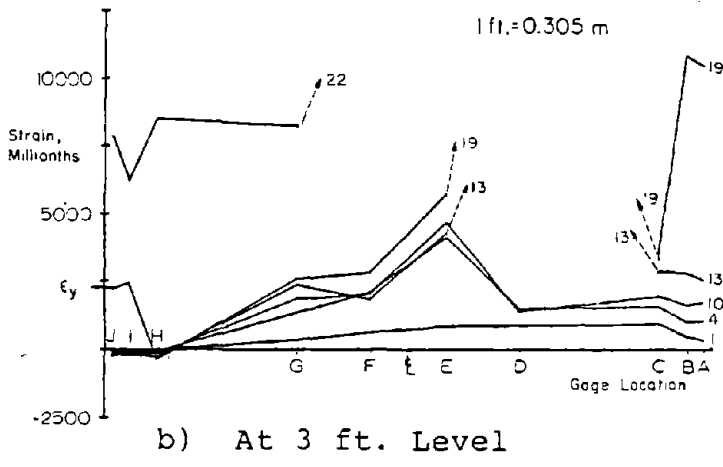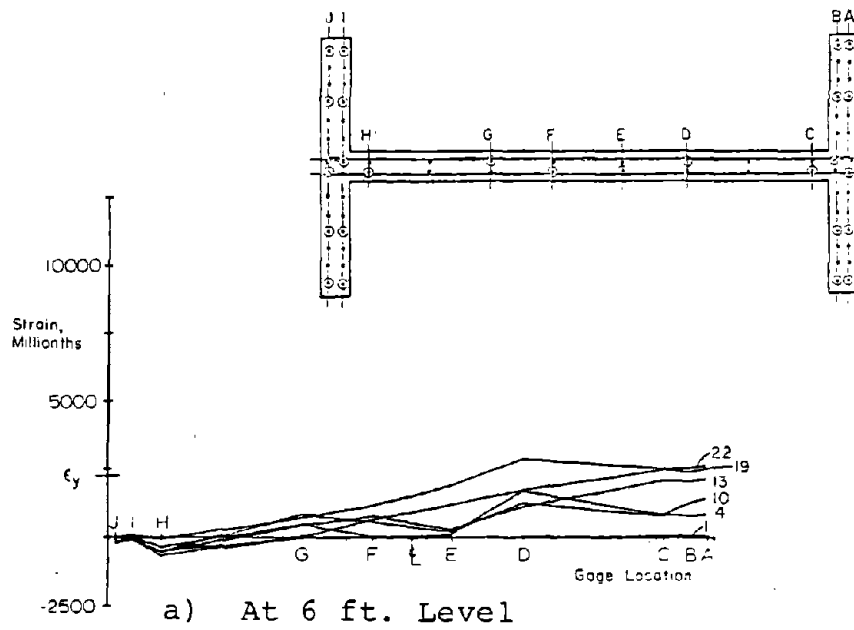
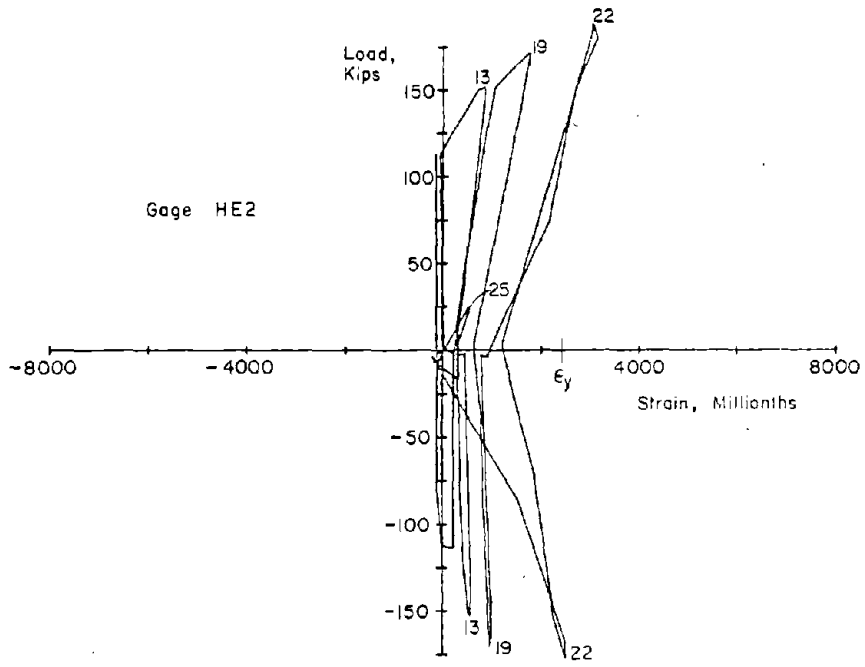Fig. B-184 Vertical Reinforcement Strains at
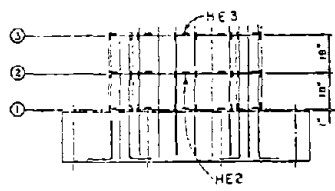Maximum Negative Loads for Specimen Fl

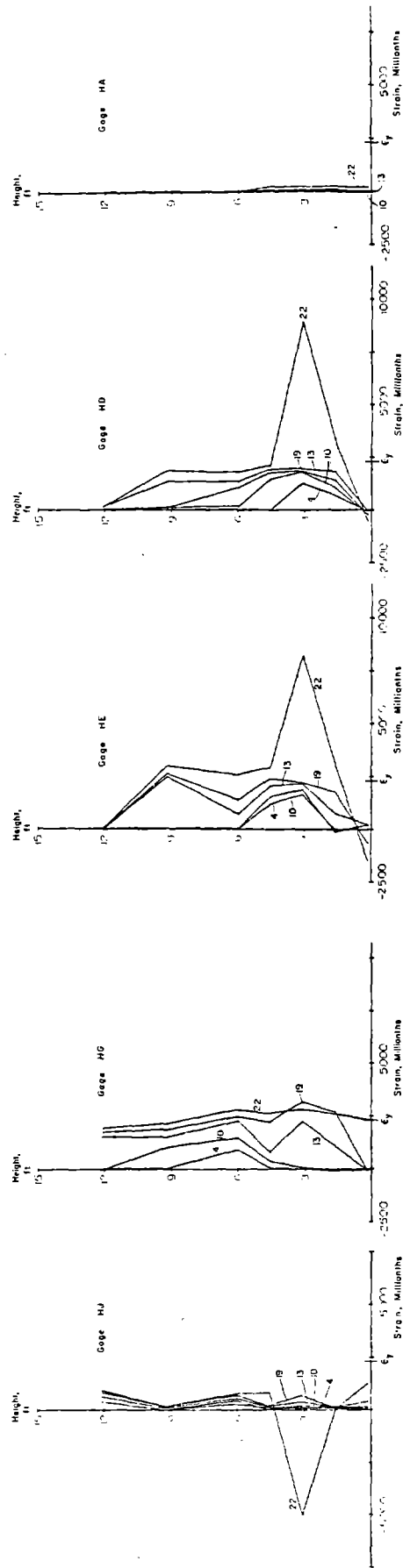Fig. B-185 Measured Strains on Horizontal Reinforcement for Specimen Fl
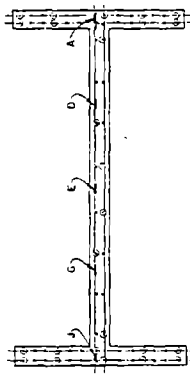
Fig. B-186 Horizontal Reinforcement Strains at
Maximum Positive Loads for Specimen F1

1 ft = 0.305 m

Fig. B-187 Horizontal Reinforcement Strains at
Maximum Negative Loads for Specimen F1

1 ft. = 0.305 m

B-227

a) At 9 ft. Level

1 ft.=0.305 m

b) At 9 ft. Level

c) At 3 ft. Level

Fig. B-188   Horizontal Reinforcement Strains in Web
at Maximum Positive Loads from Specimen Fl

B-228

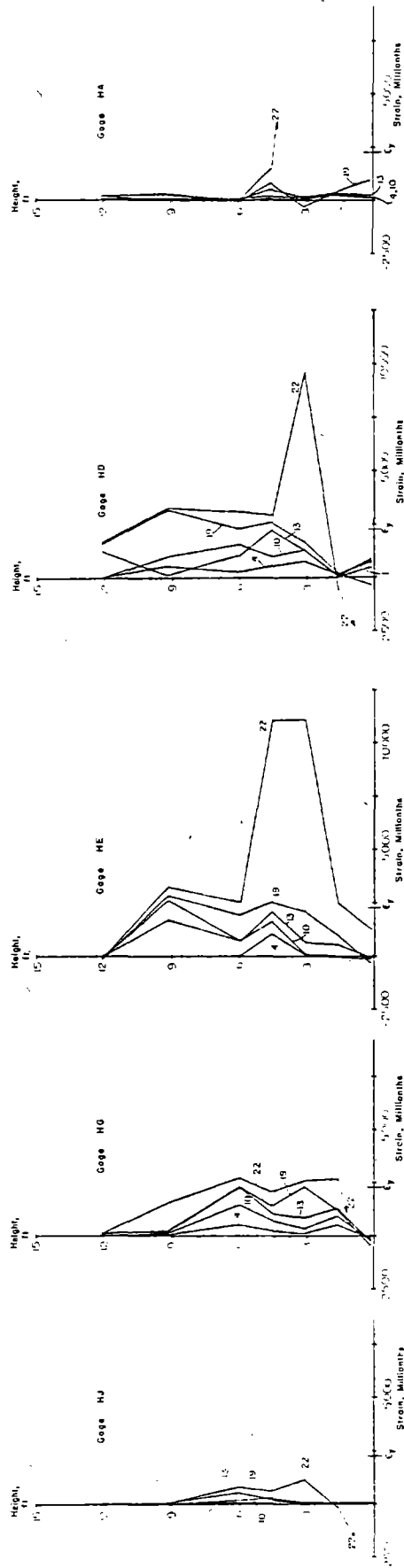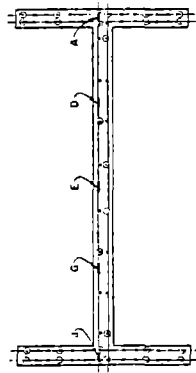a) At 9 ft. Level

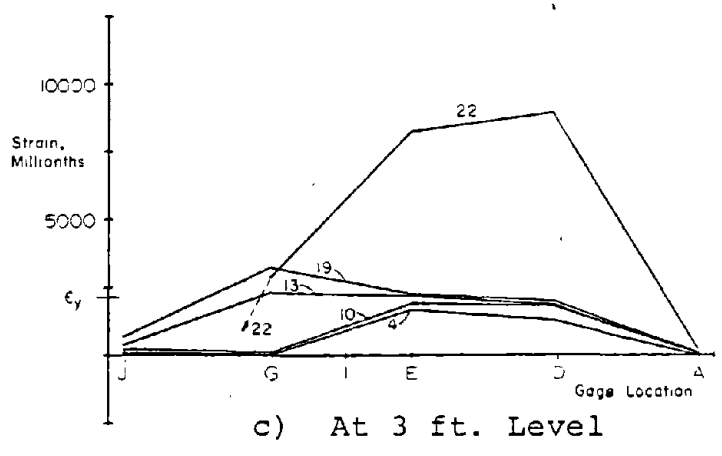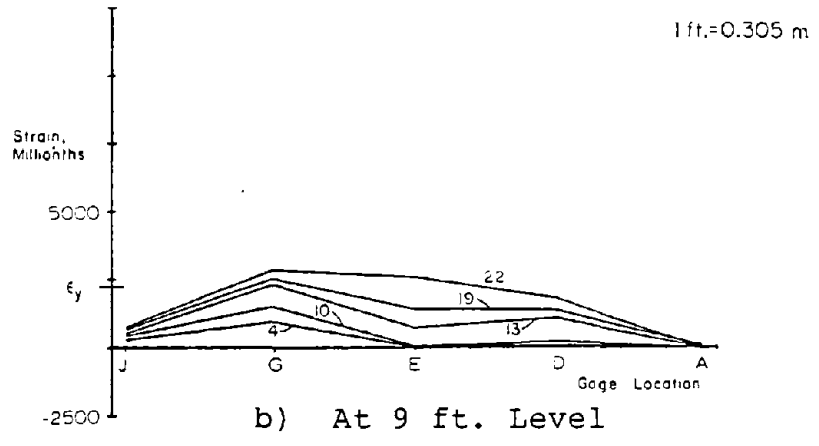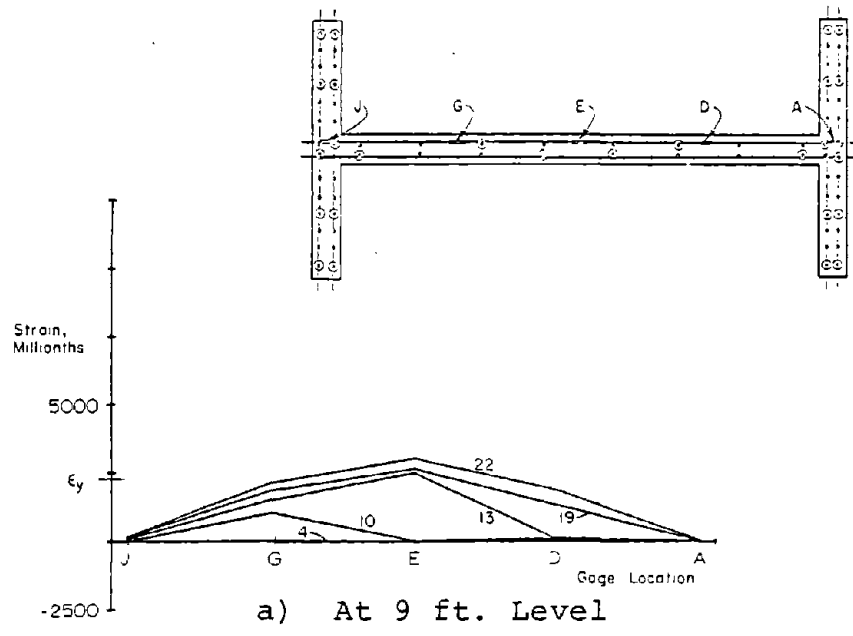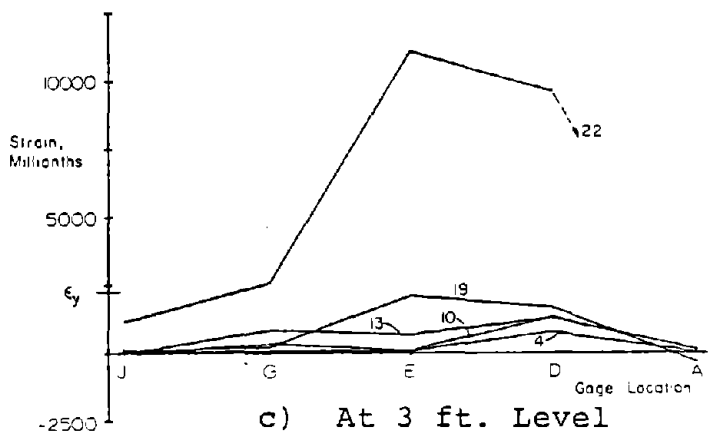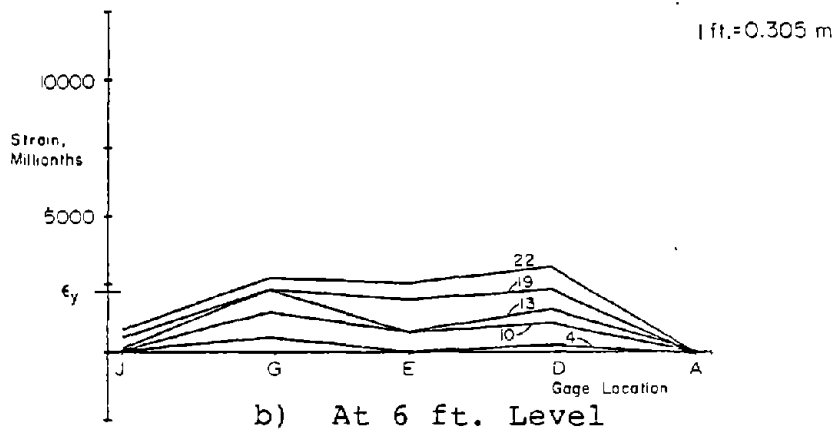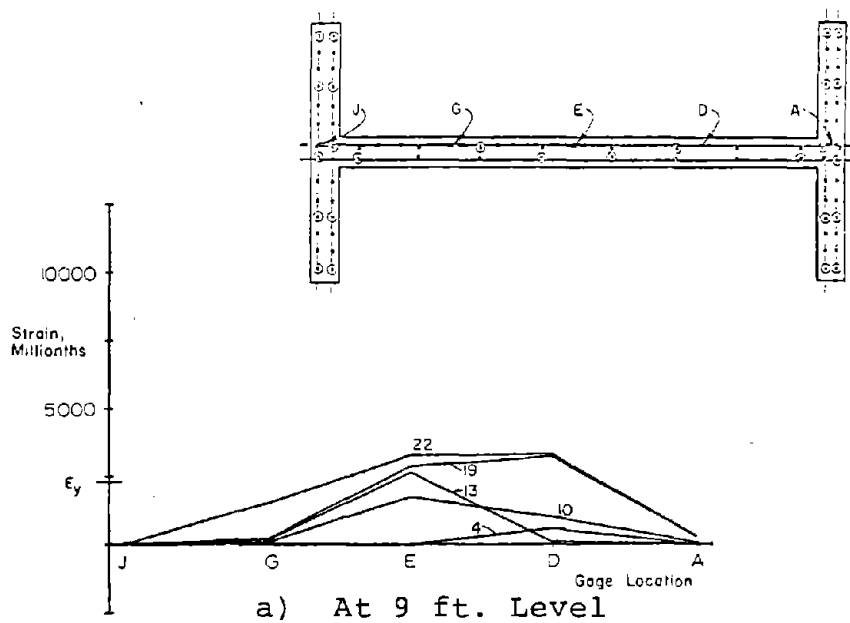b) At 6 ft. Level

c) At 3 ft. Level

Fig. B-189   Horizontal Reinforcement Strains in Web
at Maximum Negative Loads for Specimen F1

a)   At 6 ft. Level
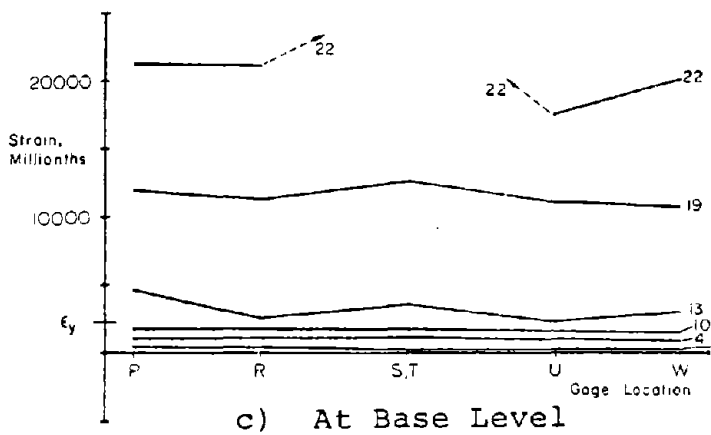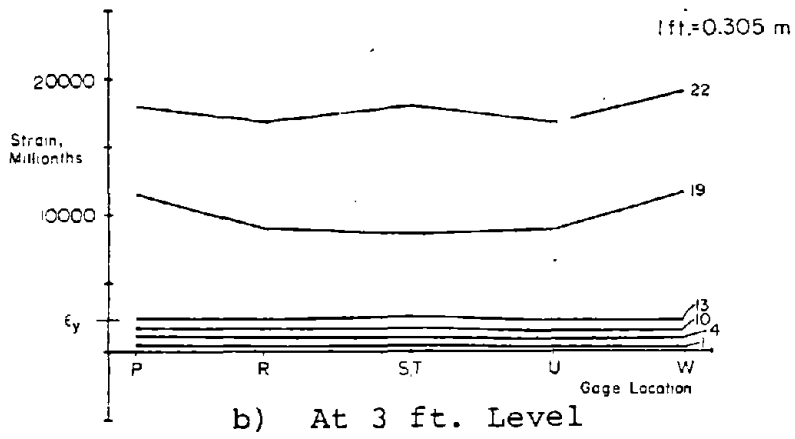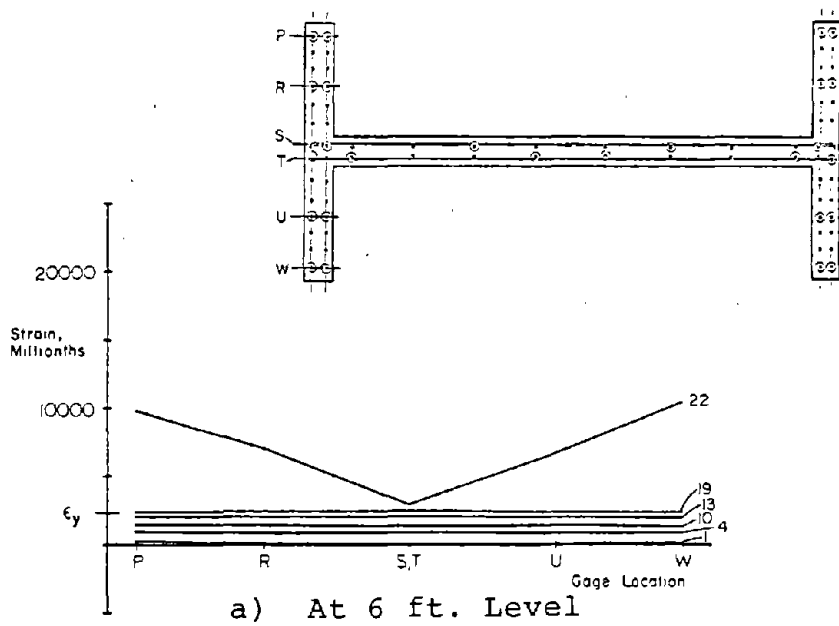
1ft.=0.305 m

b)   At 3 ft. Level

c)   At Base Level

Fig. B-190   Vertical Reinforcement Strains in Flange
at Maximum Positive Loads for Specimen F1
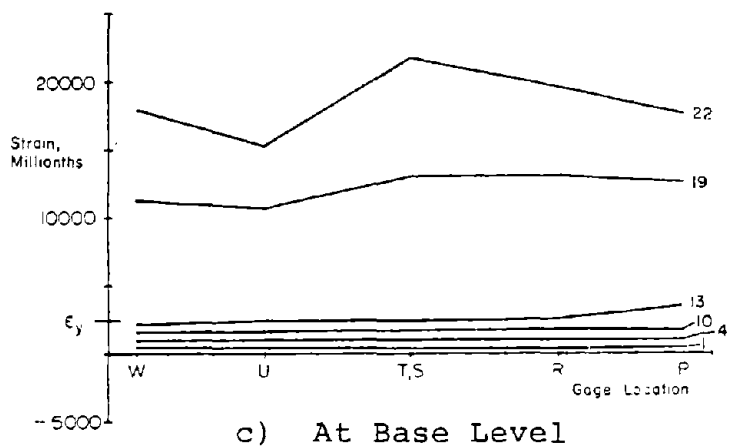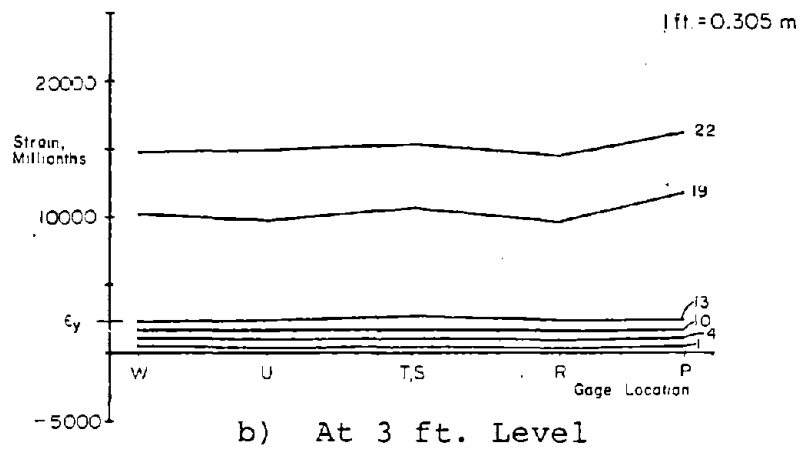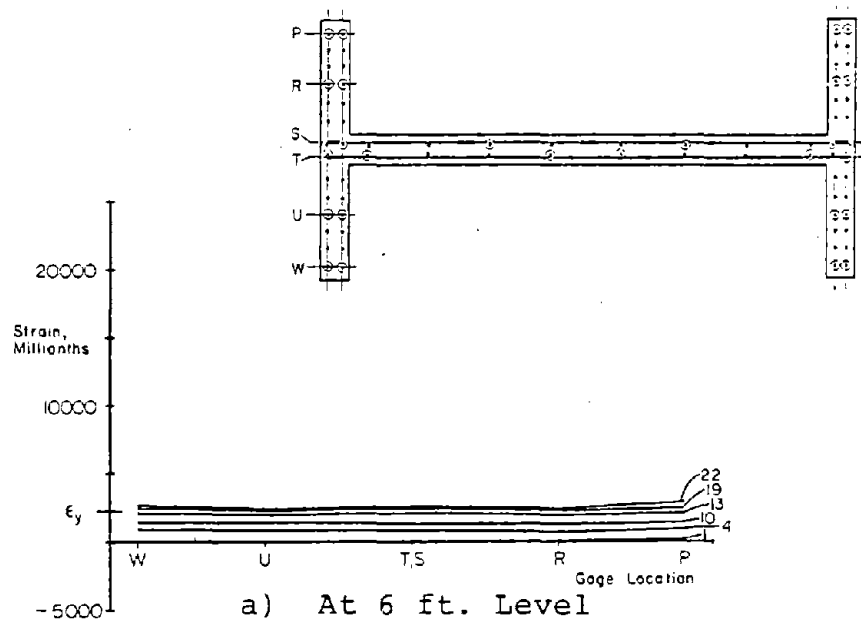
Fig. B-191 Vertical Reinforcement Strains in Flange
at Maximum Negative Loads for Specimen Fl

Free Vibration Test Results

The results of the tests are presented in Table B-1. Frequency measured prior to the application of lateral load ranged from 64% to 82% of the frequency calculated based on uncracked section properties. The differences are attributed to the existence of micro-cracks caused by shrinkage and handling.

The measured frequency decreased by an average factor of 2.2 from the initial tests to the tests carried out after application of lateral load cycles near yield. For the same conditions, the average damping coefficient changed from 3.4% to 8.5% of critical.

"Initial displacement-sudden release" tests on specimens that previously had been cycled well beyond yield indicated that the frequency decreased considerably after yielding. However, the damping did not change significantly. Hammer impact tests for the same conditiions for Specimen B5 indicated that the damping decreased significantly. In general, smaller amplitude hammer tests gave higher frequencies and lower damping coefficients than "initial displacement-sudden release" tests. This can be attributed to the differences in crack closure resulting from the magnitude of the initial displacement.

Specimen	Loading History		Excitation		Calculated Frequency (Hertz)	Measured Frequency (Hertz)	Measured Damping % of Critical
	Prior No. of Load Cycles	Prior $\frac{\Delta_{max}}{\Delta_y}$	$\frac{P_i}{P_y}$	Initial Amplitude (in.)			
R1	0 6	- 0.5	0.36 0.36	0.026 0.095	26.6 -	21.8 10.5	3.4 6.7
R2	0 15	- 1.0	0.17 0.17	0.045 0.121	27.8 -	17.8 8.8	5.5 6.8
B1	0 12 24	- 1.0 5.6	0.17 0.17 0.17	0.016 0.098 0.681	38.9 - -	30.0 11.1 3.9	2.2 8.5 9.1
B3	0 12 24 36	- 1.0 5.8 11.2	0.17 0.17 0.17 H.I.T.	0.015 0.106 0.598 (1)	38.0 - - -	29.7 10.9 4.3 5.2	2.7 9.6 8.1 9.0
B4[2]	0 0 0	- - -	H.I.T. 0.13 0.20	(1) 0.018 0.023	38.7 38.7 38.7	29.4 29.4 28.8	2.8 2.4 2.7
B2	0 15 24	- 1.0 3.7	0.07 0.07 0.07	0.014 0.065 0.350	40.9 - -	29.4 13.0 3.9	3.6 10.0 14.5
B5	0 0 6 6 15 15 24 24	- - 0.4 0.4 1.1 1.1 3.6 3.6	H.I.T. 0.07 H.I.T. 0.07 H.I.T. 0.07 H.I.T. 0.05	0.004 0.026 0.004 0.062 0.004 0.090 0.004 0.290	41.0 41.0 - - - - - -	30.6 29.5 20.4 15.2 18.2 12.0 11.3 6.4	2.9 4.0 9.2 9.5 11.2 12.0 3.2 14.5
B5R[3]	0 0 6 6 15 15	- - 0.4 0.4 1.1 1.1	H.I.T. 0.07 H.I.T. 0.07 H.I.T. 0.07	0.005 0.075 0.005 0.110 0.007 0.151	- - - - - -	16.0 13.3 13.2 10.8 11.9 8.3	3.1 4.0 4.0 5.7 3.6 11.0
F1	0 12	- 0.7	0.05 0.05	0.017 0.054	45.6 -	33.8 13.0	2.0 9.8

WHERE: Δ_{max} = Maximum deflection of top of wall during prior lateral load cycles.

Δ_y = Deflection of top of wall at which first yielding of main flexural steel was observed during lateral load tests.

P_i = Load applied at top of wall to initiate vibrations

P_y = Load applied at top of wall corresponding to Δ_y.

H.I.T. = Hammer Impact Test

1 in. = 25.4 mm

NOTES: (1) Initial amplitude not measured.

(2) Specimen B4 tested with monotonic lateral load.

(3) Specimen B5R was a repair of Specimen B5. Yielding in B5R was assumed to occur at the same load, P_y, for B5.